DESIGN OF MICROWAVE FILTERS, IMPEDANCE-MATCHING NETWORKS, AND COUPLING STRUCTURES

VOLUME I

Prepared for:

U.S. ARMY ELECTRONICS RESEARCH AND DEVELOPMENT LABORATORY
FORT MONMOUTH, NEW JERSEY

CONTRACT DA 36-039 SC-87398
DA PROJECT 3A99-15-002-02-02-06

By. *G. L. Matthaei* *Leo Young* *E. M. T. Jones*

STANFORD RESEARCH INSTITUTE

MENLO PARK, CALIFORNIA

January 1963

DESIGN OF MICROWAVE FILTERS, IMPEDANCE-MATCHING NETWORKS, AND COUPLING STRUCTURES

VOLUME I

Prepared for:

U.S. ARMY ELECTRONICS RESEARCH AND DEVELOPMENT LABORATORY
FORT MONMOUTH, NEW JERSEY

CONTRACT DA 36-039 SC-87398
FILE NO. 40663-PM-61-93-93
DA PROJECT 3A99-15-002-02-02-06
SCL-2101N (14 JULY 1961)

By: *G. L. Matthaei* *Leo Young* *E. M. T. Jones*

SRI Project No. 3527

Objective: To advance the state of the art in the field of microwave filters and coupling structures through applied research and development.

Approved:

G. L. Matthaei

G. L. MATTHAEI, MANAGER ELECTROMAGNETIC TECHNIQUES LABORATORY

D. R. SCHEUCH, DIRECTOR ELECTRONICS AND RADIO SCIENCES DIVISION

Copy No.....1...

ABSTRACT OF VOLUMES I AND II

This book presents design techniques for a wide variety of low-pass, band-pass, high-pass, and band-stop microwave filters; for multiplexers; and for certain kinds of directional couplers. The material is organized to be used by the designer who needs to work out a specific design quickly, with a minimum of reading, as well as by the engineer who wants a deeper understanding of the design techniques used, so that he can apply them to new and unusual situations.

Most of the design procedures described make use of either a lumped-element low-pass prototype filter or a step-transformer prototype as a basis for design. Using these prototypes, microwave filters can be obtained which derive response characteristics (such as a Tchebyscheff attenuation ripples in the pass band) from their prototype. Prototype filter designs are tabulated, and data is given relevant to the use of prototype filters as a basis for the design of impedance-matching networks and time-delay networks. Design formulas and tables for step-transformer prototypes are also given.

The design of microwave filter structures to serve as impedance-matching networks is discussed, and examples are presented. The techniques described should find application in the design of impedance-matching networks for use in microwave devices such as tubes, parametric devices, antennas, etc., in order to achieve efficient broad-band operation. The design of microwave filters to achieve various time-delay (or slow-wave) properties is also discussed.

Various equations, graphs, and tables are collected together relevant to the design of coaxial lines, strip-lines, waveguides, parallel-coupled lines between common ground planes, arrays of lines between ground planes, coupling and junction discontinuities, and resonators. Techniques for measuring the Q's of resonators and the coupling coefficients between resonators are also discussed, along with procedures for tuning filters. Equations and principles useful in the analysis of filters are collected

together for easy reference and to aid the reader whose background for the subject matter of this book may contain some gaps.

Directional filters have special advantages for certain applications, and are treated in detail in a separate chapter, as are high-power filters. Tunable filters of the kind that might be desired for preselector applications are also treated. Both mechanically tunable filters and filters using ferrimagnetic resonators, which can be tuned by varying a biasing magnetic field, are discussed.

PREFACE TO VOLUMES I AND II

The organization of this book has three general objectives. The first objective is to present fundamental concepts, techniques, and data that are of general use in the design of the wide range of microwave structures discussed in this book. The second objective is to present specialized data in more or less handbook form so that a designer can work out practical designs for structures having certain specific configurations, without having to recreate the design theory or the derivation of the equations. (However, the operation of most of the devices discussed herein is sufficiently complex that knowledge of some of the basic concepts and techniques is usually important.) The third objective is to present the theory upon which the various design procedures are based, so that the designer can adapt the various design techniques to new and unusual situations, and so that researchers in the field of microwave devices may use some of this information as a basis for deriving additional techniques. The presentation of the material so that it can be adapted to new and unusual situations is important because many of the microwave filter techniques described in this book are potentially useful for the design of microwave devices not ordinarily thought of as having anything to do with filters. Some examples are tubes, parametric devices, and antennas, where filter structures can serve as efficient impedance-matching networks for achieving broad-band operation. Filter structures are also useful as slow-wave structures or time-delay structures. In addition, microwave filter techniques can be applied to other devices not operating in the microwave band of frequencies, as for instance to infrared and optical filters.

The three objectives above are not listed in any order of importance, nor is this book entirely separated into parts according to these objectives. However, in certain chapters where the material lends itself to such organization, the first section or the first few sections discuss general principles which a designer should understand in order to make best use of the design data in the chapter, then come sections giving design data

for specific types of structures, and the end of the chapter discusses the derivations of the various design equations. Also, at numerous places cross references are made to other portions of the book where information useful for the design of the particular structure under consideration can be found. For example, Chapter 11 describes procedures for measuring the unloaded Q and external Q of resonators, and for measuring the coupling coefficients between resonators. Such procedures have wide application in the practical development of many types of band-pass filters and impedance-matching networks.

Chapter 1 of this book describes the broad range of applications for which microwave filter structures are potentially useful. Chapters 2 through 6 contain reference data and background information for the rest of the book. Chapter 2 summarizes various concepts and equations that are particularly useful in the analysis of filter structures. Although the image point of view for filter design is made use of only at certain points in this book, some knowledge of image design methods is desirable. Chapter 3 gives a brief summary of the image design concepts which are particularly useful for the purposes of this book. Chapters 1 to 3 should be especially helpful to readers whose background for the material of this book may have some gaps.

Most of the filter and impedance-matching network design techniques described later in the book make use of a low-pass prototype filter as a basis for design. Chapter 4 discusses various types of lumped-element, low-pass, prototype filters, presents tables of element values for such filters, discusses their time-delay properties, their impedance-matching properties, and the effects of dissipation loss upon their responses. In later chapters these low-pass prototype filters and their various properties are employed in the design of low-pass, high-pass, band-pass, and band-stop microwave filters, and also in the design of microwave impedance-matching networks, and time-delay networks.

Various equations, graphs, and tables relevant to the design of coaxial line, strip-line, waveguide, and a variety of resonators, coupling structures, and discontinuities, are summarized for easy reference in Chapter 5. Chapter 6 discusses the design of step transformers and presents tables of designs for certain cases. The step transformers in Chapter 6 are not only for use in conventional impedance-transformer

applications, but also for use as prototypes for certain types of band-pass or pseudo high-pass filters discussed in Chapter 9.

Design of low-pass filters and high-pass filters from the semi-lumped-element point of view are treated in Chapter 7. Chapters 8, 9, and 10 discuss band-pass or pseudo-high-pass filter design using three different design approaches. Which approach is best depends on the type of filter structure to be used and the bandwidth required. A tabulation of the various filter structures discussed in all three chapters, a summary of the properties of the various filter structures, and the section number where design data for the various structures can be found, are presented at the beginning of Chapter 8.

Chapter 11 describes various additional techniques which are useful to the practical development of microwave band-pass filters, impedance-matching networks, and time-delay networks. These techniques are quite general in their application and can be used in conjunction with the filter structures and techniques discussed in Chapters 8, 9, and 10, and elsewhere in the book.

Chapter 12 discusses band-stop filters, while Chapter 13 treats certain types of directional couplers. The TEM-mode, coupled-transmission-line, directional couplers discussed in Chapter 13 are related to certain types of directional filters discussed in Chapter 14, while the branch-guide directional couplers can be designed using the step-transformer prototypes in Chapter 6. Both waveguide and strip-line directional filters are discussed in Chapter 14, while high-power filters are treated in Chapter 15. Chapter 16 treats multiplexers and diplexers, and Chapter 17 deals with filters that can be tuned either mechanically or by varying a biasing magnetic field.

It is hoped that this book will fill a need (which has become increasingly apparent in the last few years) for a reference book on design data, practical development techniques, and design theory, in a field of engineering which has been evolving rapidly.

ACKNOWLEDGMENTS

The preparation of this book was largely supported by the Signal Corps, under Contract DA 36-039 SC-87398; its preparation was also partially supported by Stanford Research Institute, and by off-work time contributed by the authors. Many of the design techniques described in this book are the result of research programs sponsored by the Signal Corps under Contracts DA 36-039 SC-63232, DA 36-039 SC-64625, DA 36-039 SC-74862, and DA 36-039 SC-87398.

Mr. Nathan Lipetz of the U.S. Army Electronics Research Laboratory, Ft. Monmouth, N. J., because of his belief in the importance of research work in the area of microwave filters and coupling structures, and in the potential value of a book such as this, did much to make this book possible. Mr. John P. Agrios and Mr. William P. Dattilo, both of the U.S. Army Electronics Research Laboratory also were of great help. Mr. Agrios maintained a close interest in this project throughout the preparation of this book, as did Mr. Dattilo, who reviewed all of the chapters as they were prepared. He made numerous suggestions which have resulted in valuable improvement in the clarity and usefulness of this book.

Dr. S. B. Cohn, formerly of Stanford Research Institute and presently of the Rantec Corporation, led the microwave filter and coupling structure research at Stanford Research Institute during the earlier Signal Corps filter programs at SRI. In many places this book presents research results, or reflects points of view, which are due to him.

The authors' colleagues at SRI, and numerous researchers elsewhere have made many valuable contributions to the subject area of this book, and many results of their work have been incorporated into this book.

The authors thank the various journals, book publishers, and electronics firms who have given permission for the use of numerous figures and tables.

And finally, the authors thank the many people at SRI who took a special interest in the huge job of preparing this book. Mrs. Edith Chambers spent countless painstaking hours supervising the preparation of the staggering number of illustrations in this book, and helped greatly in insuring illustrations of high quality and clarity. Mrs. Mary F. Armstrong supervised the Varityping of the text. The authors' thanks also go to the editors, secretaries, and report production staff at SRI who all were very cooperative in the production of this book.

CONTENTS

VOLUME 1

CONTENTS

CHAPTER 1

SOME GENERAL APPLICATIONS OF FILTER STRUCTURES IN MICROWAVE ENGINEERING

SEC. 1.01, INTRODUCTION

Most readers will be familiar with the use of filters as discussed in Sec. 1.02 below. However, the potential applications of the material in this book goes much beyond these classical filter applications to cover many other microwave engineering problems which involve filter-type structures but are not always thought of as being filter problems.

Thus, the purpose of this chapter is to make clear to the reader that this book is not addressed only to filter design specialists, but also to antenna engineers who may need a broadband antenna feed, to microwave tube engineers who may need to obtain broadband impedance matches in and out of microwave tubes, to system engineers who may need a microwave time-delay network, and to numerous others having other special microwave circuit design problems.

SEC. 1.02, USE OF FILTERS FOR THE SEPARATION OR SUMMING OF SIGNALS

The most obvious application of filter structures, of course, is for the rejection of unwanted signal frequencies while permitting good transmission of wanted frequencies. The most common filters of this sort are designed for either low-pass, high-pass, band-pass or band-stop attenuation characteristics such as those shown in Fig. 1.02-1. Of course, in the case of practical filters for the microwave or any other frequency range, these characteristics are only achieved approximately, since there is a high-frequency limit for any given practical filter structure above which its characteristics will deteriorate due to junction effects, resonances within the elements, etc.

Filters are also commonly used for separating frequencies in diplexers or multiplexers. Figure 1.02-2 shows a multiplexer which segregates signals within the 2.0 to 4.0 Gc band into three separate

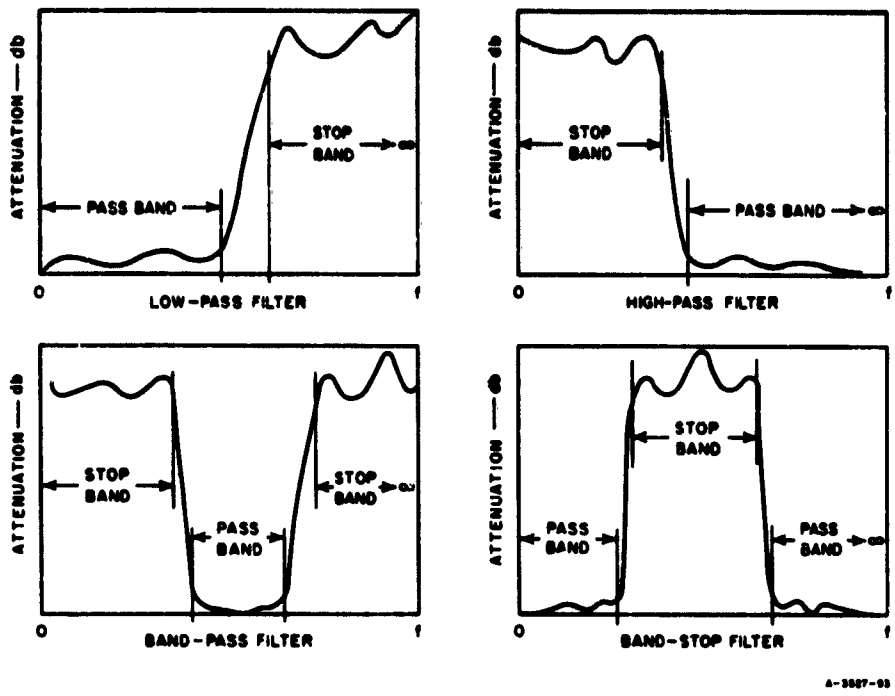

FIG. 1.02-1 FOUR COMMON TYPES OF FILTER CHARACTERISTICS

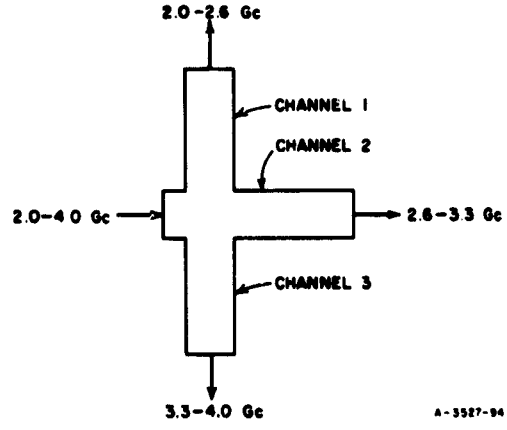

FIG. 1.02-2 A THREE-CHANNEL MULTIPLEXING FILTER GROUP

channels according to their frequencies. A well designed multiplexer of this sort would have very low VSWR at the input port across the 2.0 to 4.0 Gc input band. To achieve this result the individual filters must be designed specially for this purpose along with a special junction-matching network.

Another way that diplexers or multiplexers are often used is in the summing of signals having different frequencies. Supposing that the signal-flow arrowheads in Fig. 1.02-2 are reversed; in this event, signals entering at the various channels can all be joined together with negligible reflection or leakage of energy so that all of the signals will be superimposed on a single output line. If signals in these various channel frequency ranges were summed by a simple junction of transmission lines (*i.e.*, without a multiplexer), the loss in energy at the single output line would, of course, be considerable, as a result of reflections and of leakage out of lines other than the intended output line.

SEC. 1.03, IMPEDANCE-MATCHING NETWORKS

Bode[1] first showed what the physical limitations were on the broadband impedance matching of loads consisting of a reactive element and a resistor in series or in parallel. Later, Fano[2] presented the general limitations on the impedance matching of any load. Fano's work shows that efficiency of transmission and bandwidth are exchangeable quantities in the impedance matching of any load having a reactive component.

To illustrate the theoretical limitations which exist on broadband impedance matching, consider the example shown in Fig. 1.03-1 where the load to be matched consists of a capacitor C_1 and a resistor R_0 in parallel. A lossless impedance-matching network is to be inserted between the generator and the load, and the reflection coefficient between the generator and the impedance-matching network is

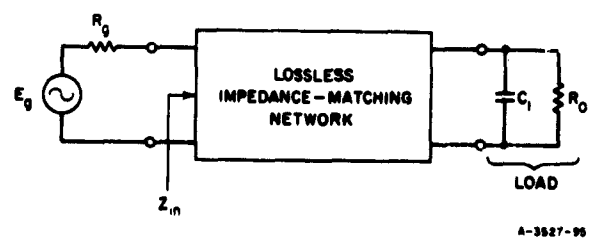

FIG. 1.03-1 EXAMPLE OF AN IMPEDANCE-MATCHING PROBLEM

$$\Gamma = \frac{Z_{in} - R_g}{Z_{in} + R_g} \qquad (1.03\text{-}1)$$

The work of Bode[1] and that of Fano[2] shows that there is a physical limitation on what Γ can be as a function of frequency. The *best possible* results are limited as indicated by the relation*

$$\int_0^\infty ln \left|\frac{1}{\Gamma}\right| d\omega = \frac{\pi}{R_0 C_1} \qquad (1.03\text{-}2)$$

Recall that for a passive circuit $0 \leq |\Gamma| \leq 1$, for total reflection $|\Gamma| = 1$, and that for perfect transmission $|\Gamma| = 0$. Thus, the larger $ln\ |1/\Gamma|$ is the better the transmission will be. But Eq. (1.03-2) says that the area under the curve of $ln\ |1/\Gamma|$ *vs* ω can be no greater than $\pi/(R_0 C_1)$.

If a good impedance match is desired from frequency ω_a to ω_b, best results can be obtained if $|\Gamma| = 1$ at all frequencies except in the band from ω_a to ω_b. Then $ln\ |1/\Gamma| = 0$ at all frequencies except in the ω_a to ω_b band, and the available area under the $ln\ |1/\Gamma|$ curve can all be concentrated in the region where it does the most good. With this specification, Eq. (1.03-2) becomes

$$\int_{\omega_a}^{\omega_b} ln \left|\frac{1}{\Gamma}\right| d\omega = \frac{\pi}{R_0 C_1} \qquad (1.03.3)$$

and if $|\Gamma|$ is assumed to be constant across the band of impedance match, $|\Gamma|$ as a function of frequency becomes

$$|\Gamma| = e^{\frac{-\pi}{(\omega_b - \omega_a) R_0 C_1}} \quad \text{for} \quad \omega_a \leq \omega \leq \omega_b$$
$$|\Gamma| = 1 \quad \text{for} \quad 0 \leq \omega \leq \omega_a \quad \text{and} \quad \omega_b \leq \omega \leq \infty \qquad (1.03\text{-}4)$$

---

* This relation holds if the impedance matching network is designed so that the reflection coefficient between R_0 and the circuit to the left of * in Fig. 1.03-1 has all of its zeros in the left half plane.[1,2]

Equation (1.03-4) says that an ideal impedance-matching network for the load in Fig. 1.03-1 would be a band-pass filter structure which would cut off sharply at the edges of the band of impedance match. The curves in Fig. 1.03-2 show how the $|\Gamma|$ *vs* ω curve for practical band-pass impedance-matching filters might look. The curve marked Case 1 is for the impedance matching of a given load over the relatively narrow band from ω_a to ω_b, while the curve marked Case 2 is for the impedance matching of the same load over the wider band from ω_c to ω_d using the same number of elements in the impedance-matching network. The rectangular $|\Gamma|$ characteristic indicated by Eq. (1.03-4) is that which would be achieved by an optimum band-pass matching filter with an infinite number of elements.*

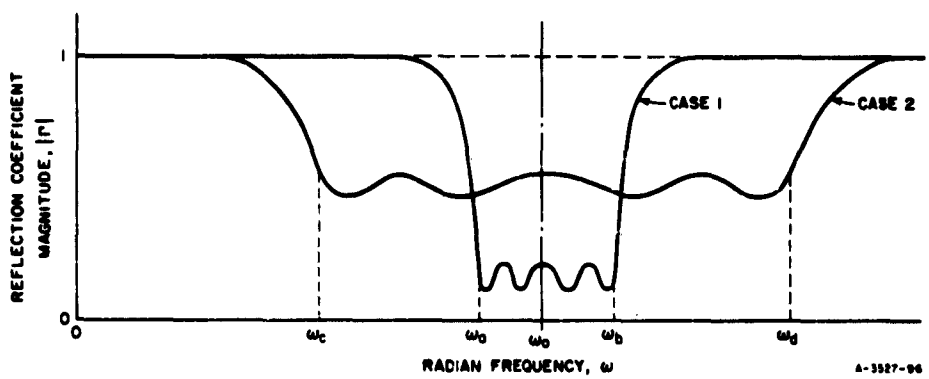

FIG. 1.03-2 CURVES ILLUSTRATING RELATION BETWEEN BANDWIDTH AND DEGREE OF IMPEDANCE MATCH POSSIBLE FOR A GIVEN LOAD HAVING A REACTIVE COMPONENT

The work of Fano[2] shows that similar conditions apply no matter what the nature of the load (as long as the load is not a pure resistance). *Thus, for this very fundamental reason, efficient broadband impedance-matching structures are necessarily filter structures.* In this book methods will be given for designing impedance-matching networks using the various microwave filter structures to be treated herein.

---

* Simple matching networks can give very great improvements in impedance match, and as the number of matching elements is increased the improvement per additional element rapidly becomes smaller and smaller. For this reason fairly simple matching networks can give performance which comes close to the theoretically optimum performance for an infinite number of impedance-matching elements.

SEC. 1.04, COUPLING NETWORKS FOR TUBES AND NEGATIVE-RESISTANCE AMPLIFIERS

A pentode vacuum tube can often be simulated at its output as an infinite-impedance current generator with a capacitor shunted across the terminals. Broadband output circuits for such tubes can be designed as a filter to be driven by an infinite-impedance current generator at one end with only one resistor termination (located at the other end of the filter). Then the output capacitance of the tube is utilized as one of the elements required for the filter, and in this way the deleterious effects of the shunt capacitance are controlled.[3] Data presented later in this book will provide convenient means for designing microwave broadband coupling circuits for possible microwave situations of a similar character where the driving source may be regarded as a current or voltage generator plus a reactive element.

In some cases the input or output impedances of an oscillator or an amplifying device may be represented as a resistance along with one or two reactive elements. In such cases impedance-matching filters as discussed in the preceding section are necessary if optimum broadband performance is to be approached.

Negative-resistance amplifiers are yet another class of devices which require filter structures for optimum broadband operation. Consider the circuit in Fig. 1.04-1, where we shall define the reflection coefficient at the left as

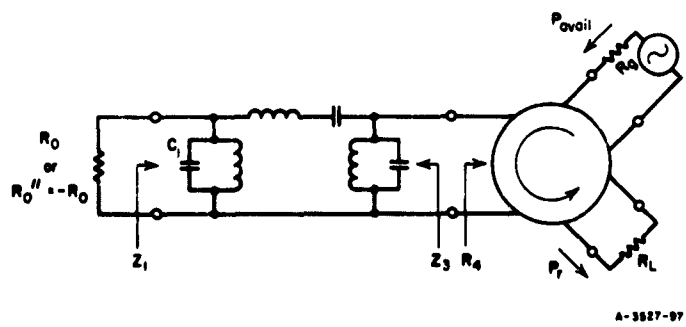

FIG. 1.04-1 CIRCUIT ILLUSTRATING THE USE OF FILTER STRUCTURES IN THE DESIGN OF NEGATIVE-RESISTANCE AMPLIFIERS

$$\Gamma_1 = \frac{Z_1 - R_0}{Z_1 + R_0} \qquad (1.04\text{-}1)$$

and that at the right as

$$\Gamma_3 = \frac{Z_3 - R_4}{Z_3 + R_4} \qquad (1.04\text{-}2)$$

Since the intervening band-pass filter circuit is dissipationless,

$$|\Gamma_1| = |\Gamma_3| \qquad (1.04\text{-}3)$$

though the phases of Γ_1 and Γ_3 are not necessarily the same. The available power entering the circulator on the right is directed into the filter network, and part of it is reflected back to the circulator where it is finally absorbed in the termination R_L. The transducer gain from the generator to R_L is

$$\frac{P_r}{P_{avail}} = |\Gamma_3|^2 \qquad (1.04\text{-}4)$$

where P_{avail} is the available power of the generator and P_r is the power reflected back from the filter network.

If the resistor R_0 on the left in Fig. 1.04-1 is positive, the transducer gain characteristic might be as indicated by the Case 1 curve in Fig. 1.04-2. In this case the gain is low in the pass band of the filter since $|\Gamma_1| = |\Gamma_3|$ is small then. However, if R_0 is replaced by a negative resistance $R_0'' = -R_0$, then the reflection coefficient at the left becomes

$$\Gamma_1'' = \frac{Z_1 - R_0''}{Z_1 + R_0''} = \frac{Z_1 + R_0}{Z_1 - R_0} \qquad (1.04\text{-}5)$$

As a result we then have

$$|\Gamma_3''| = |\Gamma_1''| = \frac{1}{|\Gamma_1|} \qquad (1.04\text{-}6)$$

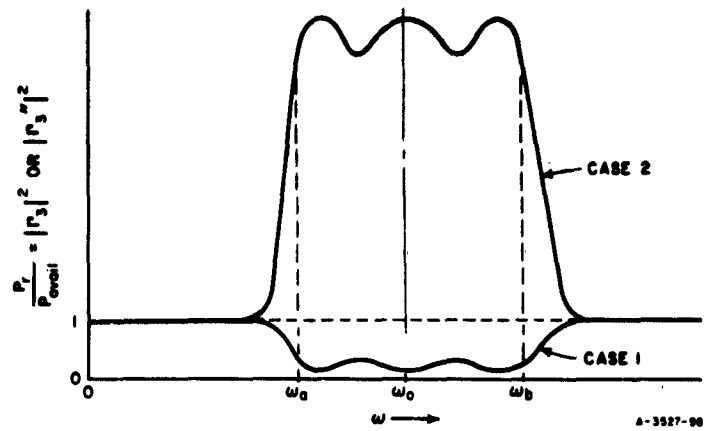

FIG. 1.04-2 TRANSDUCER GAIN BETWEEN GENERATOR IN FIG. 1.04-1 AND THE CIRCULATOR OUTPUT
Case 1 is for R_0 Positive while Case 2 is for R_0 Replaced by $R_0'' = -R_0$

Thus, replacing R_0 by its negative corresponds to $|\Gamma_3|$ being replaced by $|\Gamma_3''| = 1/|\Gamma_3|$, and the transducer gain is as indicated by the curve marked Case 2 in Fig. 1.04-2. Under these circumstances the output power greatly exceeds the available power of the generator for frequencies within the pass band of the filter.

With the aid of Eqs. (1.04-1) and (1.04-6) coupling networks for negative-resistance amplifiers are easily designed using impedance-matching filter design techniques. Practical negative-resistance elements such as tunnel diodes are not simple negative resistances, since they also have reactive elements in their equivalent circuit. In the case of tunnel diodes the dominant reactive element is a relatively large capacitance in parallel with the negative resistance. With this large capacitance present satisfactory operation is impossible at microwave frequencies unless some special coupling network is used to compensate for its effects. In Fig. 1.04-1, C_1 and R_0'' on the left can be defined as the tunnel-diode capacitance and negative resistance, and the remainder of the band-pass filter circuit serves as a broadband coupling network.

Similar principles also apply in the design of broadband coupling networks for masers and parametric amplifiers. In the case of parametric amplifiers, however, the design of the coupling filters is complicated somewhat by the relatively complex impedance transforming effects of the time-varying element.[4]

The coupling network shown in Fig. 1.04-1 is in a lumped-element form which is not very practical to construct at microwave frequencies. However, techniques which are suitable for designing practical microwave filter structures for such applications will be given in later chapters.

SEC. 1.05, TIME-DELAY NETWORKS AND SLOW-WAVE STRUCTURES

Consider the low-pass filter network in Fig. 1.05-1(a) which has a voltage transfer function E_0/E_6. The transmission phase is defined as

$$\varphi = \arg \frac{E_0}{E_6} \quad \text{radians} \quad . \tag{1.05-1}$$

The *phase delay* of this network at any given frequency ω is

$$t_p = \frac{\varphi}{\omega} \quad \text{seconds} \tag{1.05-2}$$

while its *group delay* is

$$t_d = \frac{d\varphi}{d\omega} \quad \text{seconds} \tag{1.05-3}$$

where φ is in radians and ω is in radians per second. Under different circumstances either phase or group delay may be important, but it is

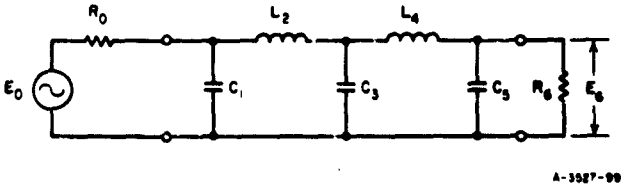

FIG. 1.05-1(a) LOW-PASS FILTER DISCUSSED IN SEC. 1.05

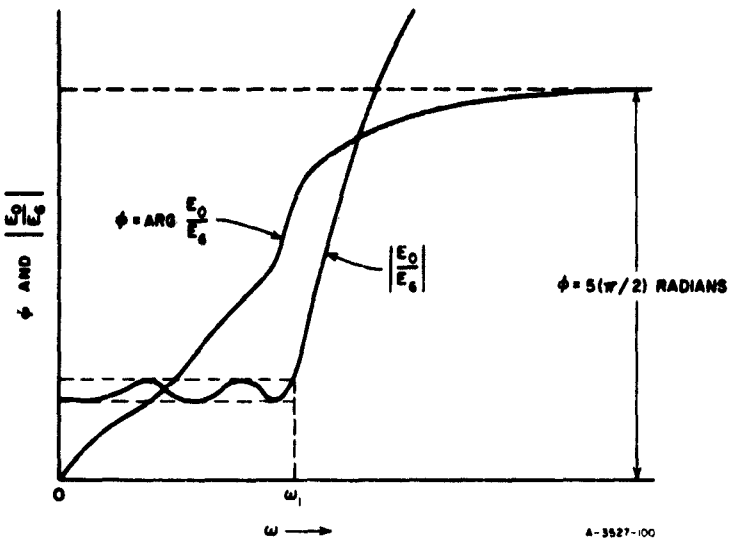

FIG. 1.05-1(b) A POSSIBLE $|E_0/E_6|$ CHARACTERISTIC FOR THE FILTER IN FIG. 1.05-1(a), AND AN APPROXIMATE CORRESPONDING PHASE CHARACTERISTIC

group delay which determines the time required for a signal to pass through a circuit.[5,6] *

Low-pass ladder networks of the form in Fig. 1.05-1(a) have zero transmission phase for $\omega = 0$, and as ω becomes large

$$\varphi\Big|_{\omega\to\infty} \to \frac{n\pi}{2} \quad \text{radians} \qquad (1.05\text{-}4)$$

where n is the number of reactive elements in the circuit. Figure 1.05-1(b) shows a possible $|E_0/E_6|$ characteristic for the filter in Fig. 1.05-1(a) along with the approximate corresponding phase characteristic. Note that most of the phase shift takes place within the pass band $\omega = 0$ to $\omega = \omega_1$. This is normally the case, hence a rough estimate of the group time delay in the pass band of filters of the form in Fig. 1.05-1(a) can be obtained from

* That is, if there is no amplitude distortion and $d\phi/d\omega$ is constant across the frequency band of the signal, then the output signal will be an exact replica of the input signal but displaced in time by t_d seconds.

$$t_d \approx \frac{n\pi}{\omega_1 2} \quad \text{seconds} \qquad (1.05\text{-}5)$$

where n is again the number of reactive elements in the filter. Of course, in some cases t_d may vary appreciably within the pass band, and Eq. (1.05-5) is very approximate.

Figure 1.05-2(a) shows a five-resonator band-pass filter while Fig. 1.05-2(b) shows a possible phase characteristic for this filter. In this case the total phase shift from $\omega = 0$ to $\omega = \infty$ is $n\pi$ radians,

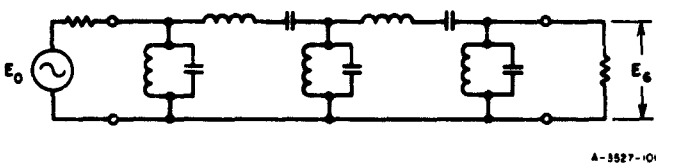

FIG. 1.05-2(a) A BAND-PASS FILTER CORRESPONDING TO THE LOW-PASS FILTER IN FIG. 1.05-1(a)

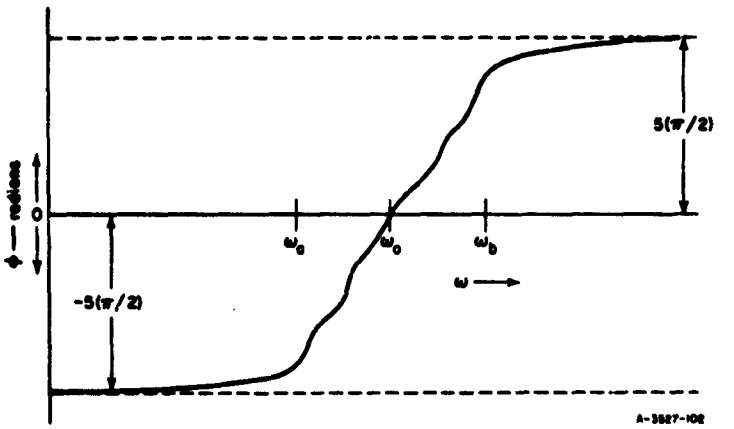

FIG. 1.05-2(b) A POSSIBLE PHASE CHARACTERISTIC FOR THE FILTER IN FIG. 1.05-2(a)

where n is the number of resonators, and a rough estimate of the pass-band group time delay is

$$t_d = \frac{n\pi}{\omega_b - \omega_a} \quad \text{seconds} \tag{1.05-6}$$

where ω_a and ω_b are the radian frequencies of the pass-band edges.

In later chapters more precise information on the time delay characteristics of filters will be presented. Equations (1.05-5) and (1.05-6) are introduced here simply because they are helpful for giving a feel for the general time delay properties of filters. Suppose that for some system application it is desired to delay pulses of S-band energy 0.05 microseconds, and that an operating bandwidth of 50 Mc is desired to accommodate the signal spectrum and to permit some variation of carrier frequency. If this delay were to be achieved with an air-filled coaxial line, 49 feet of line would be required. Equation (1.05-6) indicates that this delay could be achieved with a five-resonator filter having 50 Mc bandwidth. An S-band filter designed for this purpose would typically be less than a foot in length and could be made to be quite light.

In slow-wave structures usually *phase velocity*

$$v_p = \frac{l}{t_p} \tag{1.05-7}$$

or *group velocity*

$$v_g = \frac{l}{t_d} \tag{1.05-8}$$

is of interest, where l is the length of the structure and t_p and t_d are as defined in Eqs. (1.05-2) and (1.05-3). Not all structures used as slow-wave structures are filters, but very many of them are. Some examples of slow-wave structures which are basically filter structures are waveguides periodically loaded with capacitive or inductive irises, interdigital lines, and comb lines. The methods of this book should be quite helpful in the design of such slow-wave structures which are basically filters.

SEC. 1.06, GENERAL USE OF FILTER PRINCIPLES IN THE DESIGN OF MICROWAVE COMPONENTS

As can be readily seen by extrapolating from the discussions in preceding sections, microwave filter design techniques when used in their most general way are fundamental to the efficient design of a wide variety of microwave components. In general, these techniques are basic to precision design when selecting, rejecting, or channeling of energy of different frequencies is important; when achieving energy transfer with low reflection over a wide band is important; or when achieving a controlled time delay is important. The possible specific practical situations where such considerations arise are too numerous and varied to permit any attempt to treat them individually herein. However, a reader who is familiar with the principles to be treated in this book will usually have little trouble in adapting them for use in the many special design situations he will encounter.

REFERENCES

1. H. W. Bode, *Network Analysis and Feedback Amplifier Design*, pp. 360-371 (D. Van Nostrand Co. New York, N.Y., 1945).

2. R. M. Fano, "Theoretical Limitations on the Broadband Matching of Arbitrary Impedances," *Journal of the Franklin Institute*, Vol. 249, pp. 57-84 and 139-154 (January-February 1950).

3. G. E. Valley and H. Wallman, *Vacuum Tube Amplifiers*, Chapters 2 and 4 (McGraw-Hill Book Co., New York, N.Y., 1948).

4. G. L. Matthaei, "A Study of the Optimum Design of Wide-Band Parametric Amplifiers and Up-Converters," *IRE Trans. PGMTT*-9, pp. 23-38 (January 1961).

5. E. A. Guillemin, *Communication Networks*, Vol. 2, pp. 99-106 and 490-498 (John Wiley and Sons, Inc., New York, N.Y., 1935).

6. M. J. Di Toro, "Phase and Amplitude Distortion in Linear Networks," *Proc. IRE*, Vol. 36, pp. 24-36 (January 1948).

CHAPTER 2

SOME USEFUL CIRCUIT CONCEPTS AND EQUATIONS

SEC. 2.01. INTRODUCTION

The purpose of this chapter is to summarize various circuit theory concepts and equations which are useful for the analysis of filters. Though much of this material will be familiar to many readers, it appears desirable to gather it together for easy reference. In addition, there will undoubtedly be topics with which some readers will be unfamiliar. In such cases the discussion given here should provide a brief introduction which should be adequate for the purposes of this book.

SEC. 2.02. COMPLEX FREQUENCY AND POLES AND ZEROS

A "sinusoidal" voltage

$$e(t) = |E_a| \cos(\omega t + \phi) \qquad (2.02\text{-}1)$$

may also be defined in the form

$$e(t) = \mathrm{Re}\,[E_a e^{j\omega t}] \qquad (2.02\text{-}2)$$

where t is the time in seconds, ω is frequency in radians per second, and $E_a = |E_a| e^{j\phi}$ is the complex amplitude of the voltage. The quantity E_a, of course, is related to the root-mean-square voltage E by the relation $E = E_a/\sqrt{2}$.

Sinusoidal waveforms are a special case of the more general waveform

$$e(t) = |E_a| e^{\sigma t} \cos(\omega t + \phi) \qquad (2.02\text{-}3)$$

$$= R_e[E_a e^{pt}] \qquad (2.02\text{-}4)$$

where $E_a = |E_a| e^{j\phi}$ is again the complex amplitude. In this case

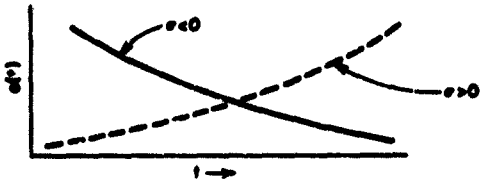

FIG. 2.02-1(a) SHAPE OF COMPLEX-FREQUENCY WAVEFORM WHEN $p = \sigma + j0$

$$p = \sigma + j\omega \qquad (2.02\text{-}5)$$

is the *complex frequency*. In this general case the waveform may be a pure exponential function as illustrated in Fig. 2.02-1(a), it may be an exponentially-varying sinusoid as illustrated in Fig. 2.02-1(b), or it may be a pure sinusoid if $p = j\omega$.

In linear, time-invariant circuits such as are discussed in this book complex-frequency waveforms have fundamental significance not shared by other types of waveforms. Their basic importance is exemplified by the following properties of linear, time-invariant circuits:

(1) If a "steady-state" driving voltage or current of complex frequency p is applied to a circuit the steady-state response seen at any point in the circuit* will also have a complex-frequency waveform with the same frequency p. The amplitude and phase angle will, in general, be different at different points throughout the circuit. But at any given point in the circuit the response amplitude and the phase angle are both linear functions of the driving-signal amplitude and phase.

(2) The various possible natural modes of vibration of the circuit will have complex-frequency waveforms. (The natural modes are current and voltage vibrations which can exist after all driving signals are removed.)

The concepts of impedance and transfer functions result from the first property listed above, since these two functions represent ratios between the complex amplitudes of the driving signal and the response. As a result of Property (2), the transient response of a network will contain a superposition of the complex-frequency waveforms of the various natural modes of vibration of the circuit.

The impedance of a circuit as a function of complex frequency p will take the form

* Unless stated otherwise, a linear, time-invariant circuit will be understood.

$$Z(p) = \frac{E_n}{I_n} = \frac{E}{I} = \frac{a_n p^n + a_{n-1} p^{n-1} + \ldots + a_1 p + a_0}{b_n p^n + b_{n-1} p^{n-1} + \ldots + b_1 p + b_0} \quad (2.02\text{-}6)$$

By factoring the numerator and denominator polynomials this may be written as

$$Z(p) = \left(\frac{a_n}{b_n}\right) \frac{(p - p_1)(p - p_3)(p - p_5) \ldots}{(p - p_2)(p - p_4)(p - p_6) \ldots} \quad (2.02\text{-}7)$$

At the frequencies $p = p_1, p_3, p_5, \ldots$ etc., where the numerator polynomial goes to zero the impedance function will be zero; these frequencies are thus known as the *zeros* of the function. At the frequencies $p = p_2, p_4, p_6, \ldots$, etc., where the denominator polynomial is zero the impedance function will be infinite; these frequencies are known as the *poles* of the function. The poles and zeros of a transfer function are defined in a similar fashion.

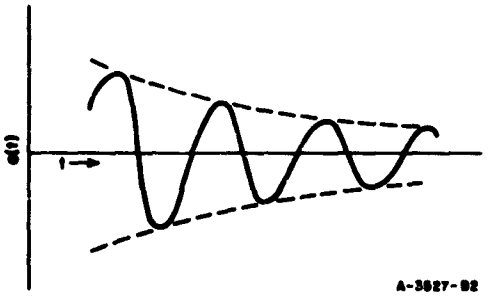

FIG. 2.02-1(b) SHAPE OF COMPLEX-FREQUENCY WAVEFORM WHEN $p = \sigma + j\omega$ AND $\sigma < 0$

A circuit with a finite number of lumped, reactive elements will have a finite number of poles and zeros. However, a circuit involving *distributed elements* (which may be represented as an infinite number of infinitesimal lumped-elements) will have an infinite number of poles and zeros. Thus, circuits involving transmission lines will have impedance functions that are transcendental, *i.e.*, when expressed in the form in Eq. (2.02-7) they will be infinite-product expansions. For example, the input impedance to a lossless, short-circuited transmission line which is one-quarter wavelength long at frequency ω_0 may be expressed as

$$Z(p) = Z_0 \tanh\left(\frac{\pi p}{2\omega_0}\right)$$

$$= Z_0 \frac{\pi p}{2\omega_0} \prod_{k=1}^{\infty} \left(\frac{2k-1}{2k}\right)^2 \frac{[p + j2k\omega_0][p - j2k\omega_0]}{[p + j(2k-1)\omega_0][p - j(2k-1)\omega_0]} \quad (2.02\text{-}8)$$

where Z_0 is the characteristic impedance of the line. This circuit is seen to have poles at $p = \pm j(2k - 1)\omega_0$ and zeros at $p = 0$ and $\pm j2k\omega_0$, where $k = 1, 2, 3, \ldots, \infty$.

Regarding frequency as the more general $p = \sigma + j\omega$ variable instead of the unnecessarily restrictive $j\omega$ variable permits a much broader point of view in circuit analysis and design. Impedance and transfer functions become functions of a complex variable (*i.e.*, they become functions of the variable $p = \sigma + j\omega$) and all of the powerful tools in the mathematical theory of functions of a complex variable become available. It becomes very helpful to define the properties of an impedance or transfer function in terms of the locations of their poles and zeros, and these poles and zeros are often plotted in the *complex-frequency plane* or *p-plane*. The poles are indicated by crosses and the zeros by circles. Figure 2.02-2(a) shows such a plot for the lossless transmission line input impedance in Eq. (2.02-8) while Fig. 2.02-2(b) shows a sketch of the shape of the magnitude of this function for $p = j\omega$. The figure also shows what happens to the poles and zeros if the line has loss: the poles and zeros are all moved to the left of the $j\omega$ axis, and the $|Z(j\omega)|$ characteristic becomes rounded off.

The concepts of complex frequency and poles and zeros are very helpful in network analysis and design. Discussions from this point of view will be found in numerous books on network analysis and synthesis, including those listed in References 1 to 5. Poles and zeros also have an electrostatic analogy which relates the magnitude and phase of an impedance or transfer function to the potential and flux, respectively, of an analogous electrostatic problem. This analogy is useful both as a tool for mathematical reasoning and as a means for determining magnitude and phase by measurements on an analog setup. Some of these matters are discussed in References 2, 3, 6, and 7. Further use of the concepts of complex frequency and poles and zeros will be discussed in the next two sections.

SEC. 2.03, NATURAL MODES OF VIBRATION AND THEIR RELATION TO INPUT-IMPEDANCE POLES AND ZEROS

The natural modes of vibration of a circuit are complex frequencies at which the voltages and currents in the circuit can "vibrate" if the circuit is disturbed. These vibrations can continue even after all driving signals have been set to zero. It should be noted that here the

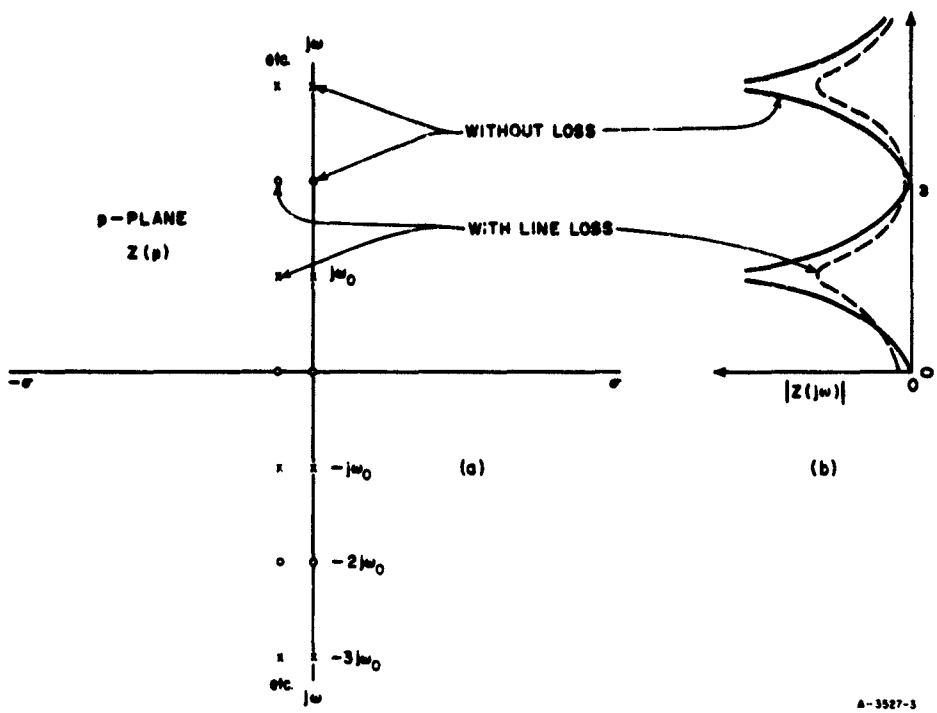

FIG. 2.02-2 THE LOCATIONS OF THE POLES AND ZEROS OF A SHORT-CIRCUITED TRANSMISSION LINE WHICH IS A QUARTER-WAVELENGTH LONG WHEN $p = j\omega_0$
The Magnitude of the Input Impedance for Frequencies $p = j\omega$ is also Sketched

word *vibration* is used to include natural modes having exponential waveforms of frequency $p = \sigma$ as well as oscillatory waveforms of frequency $p = \sigma + j\omega$.

Suppose that the input impedance of a circuit is given by the function

$$Z(p) = \frac{E}{I} = \frac{(p - p_1)(p - p_3)(p - p_5) \ldots}{(p - p_2)(p - p_4)(p - p_6) \ldots} \quad . \qquad (2.03\text{-}1)$$

Rearranging Eq. (2.03-1),

$$\angle = I\,Z(p) \quad . \qquad (2.03\text{-}2)$$

If the input terminals of this circuit are open-circuited and the circuit is vibrating at one of its natural frequencies, there will be a complex-frequency voltage across $Z(p)$ even though $I = 0$. By Eq. (2.03-2) it is seen that the only way in which the voltage E can be non-zero while $I = 0$ is for $Z(p)$ to be infinite. Thus, if $Z(p)$ is open-circuited, natural vibration can be observed only at the frequencies p_2, p_4, p_6, etc., which are the poles of the input impedance function $Z(p)$. Also, by analogous reasoning it is seen that if $Z(p)$ is short-circuited, the natural frequencies of vibration will be the frequencies of the *zeros* of $Z(p)$.

Except for special cases where one or more natural modes may be stifled at certain points in a circuit, if any natural modes are excited in any part of the circuit, they will be observed in the voltages and currents throughout the entire circuit. The frequency $p_n = \sigma_n + j\omega_n$ of each natural mode must lie in the left half of the complex-frequency plane, or on the $j\omega$ axis. If this were not so the vibrations would be of exponentially increasing magnitude and energy, a condition which is impossible in a passive circuit. Since under open-circuit or short-circuit conditions the poles or the zeros, respectively, of an impedance function are natural frequencies of vibration, any impedance of a linear, passive circuit must have all of its poles and zeros in the left half plane or on the $j\omega$ axis.

SEC. 2.04, FUNDAMENTAL PROPERTIES OF TRANSFER FUNCTIONS

Let us define the *voltage attenuation function* E_g/E_L for the network in Fig. 2.04-1 as

$$T(p) = \frac{E_g}{E_L} = \frac{c(p - p_1)(p - p_3)(p - p_5) \cdots}{(p - p_2)(p - p_4)(p - p_6) \cdots} \qquad (2.04\text{-}1)$$

FIG. 2.04-1 NETWORK DISCUSSED IN SECTION 2.04

where c is a real constant and p is the complex-frequency variable. We shall now briefly summarize some important general properties of linear, passive circuits in terms of this transfer function and Fig. 2.04-1.

(1) The zeros of $T(p)$, *i.e.*, p_1, p_3, p_5, ... are all frequencies of natural modes of vibration for the circuit. They are influenced by all of the elements in the circuit so that, for example, if the value for R_g or R_L were changed, generally the frequencies of all the natural modes will change also.

(2) The poles of $T(p)$, *i.e.*, p_2, p_4, p_6, ..., along with any poles of $T(p)$ at $p = 0$ and $p = \infty$ are all *frequencies of infinite attenuation*, or "poles of attenuation." They are properties of the network alone and will not be changed if R_g or R_L is changed. Except for certain degenerate cases, if two networks are connected in cascade, the resultant over-all response will have the poles of attenuation of both component networks.

(3) In a ladder network, a pole of attenuation is created when a *series* branch has *infinite* impedance, or when a *shunt* branch has *zero* impedance. If at a given frequency, infinite impedance occurs in series branches simultaneously with zero impedance in shunt branches, a higher-order pole of attenuation will result.

(4) In circuits where there are two or more transmission channels in parallel, poles of attenuation are created at frequencies where the outputs from the parallel channels have the proper magnitude and phase to cancel each other out. This can happen, for example, in bridged-T, lattice, and parallel-ladder structures.

(5) The natural modes [zeros of $T(p)$] must lie in the left half of the p-plane (or on the $j\omega$ axis if there are no loss elements).

(6) The poles of attenuation can occur anywhere in the p-plane.

(7) If E_g is a zero impedance voltage generator, the zeros of Z_{in} in Fig. 2.04-1 will be the natural frequencies of vibration of the circuit. These zeros must therefore correspond to the zeros of the attenuation function $T(p)$. (Occasionally this fact is obscured because in some special cases cancellations can be carried out between coincident poles and zeros of $T(p)$ or of Z_{in}. Assuming that no such cancellations have been carried out even when they are possible, the above statement always holds.)

(8) If the zero impedance voltage generator E_g were replaced by an infinite impedance current generator I_g, then the natural frequencies of vibration would correspond to the *poles* of Z_{in}. Redefining $T(p)$ as $T'(p) = I_g/E_L$, the zeros of $T'(p)$ would in this case still be the natural frequencies of vibration but they would in this case be the same as the *poles* of Z_{in}.

Let us now consider some examples of how some of the concepts in the statements itemized above may be applied. Suppose that the box in Fig. 2.04-1 contains a lossless transmission line which is one-quarter wavelength long at the frequency ω_0. Let us suppose further that $R_g = R_L \neq Z_0$, where Z_0 is the characteristic impedance of the line. Under these conditions the voltage attenuation function $T(p)$ would have a p-plane plot as indicated in Fig. 2.04-2(a). Since the transmission line is a distributed circuit there are an infinite number of natural

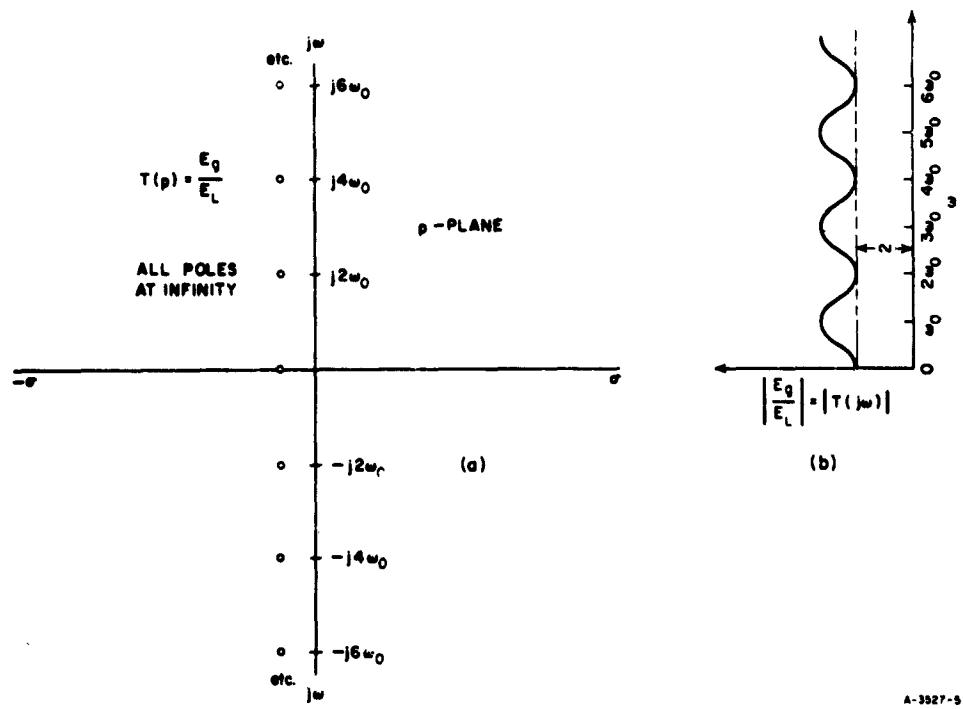

FIG. 2.04-2 TRANSFER FUNCTION OF THE CIRCUIT IN FIG. 2.04-1 IF THE BOX CONTAINS A LOSSLESS TRANSMISSION LINE λ/4 LONG AT ω_0 WITH A CHARACTERISTIC IMPEDANCE $Z_0 \neq R_g = R_L$

modes of vibration, and, hence there are an infinite array of zeros to $T(p)$. In all impedance and transfer functions the number of poles and zeros must be equal if the point at $p = \infty$ is included. In this case there are no poles of attenuation on the finite plane; they are all clustered at infinity. As a result of the periodic array of zeros, $|T(j\omega)|$ has an oscillatory behavior *vs* ω as indicated in Fig. 2.04-2(b). As the value of $R_g = R_L$ is made to approach that of Z_0, the zeros of $T(p)$ will move to the left, the poles will stay fixed at infinity, and the variations in $|T(j\omega)|$ will become smaller in amplitude. When $R_g = R_L = Z_0$, the zeros will have moved toward the left to minus infinity, and the transfer function becomes simply

$$\frac{E_g}{E_L} = T(p) = 2e^{\pi p/2\omega_0} \qquad (2.04\text{-}2)$$

which has $|T(j\omega)|$ equal to two for all $p = j\omega$.

From the preceding example it is seen that the transcendental function e^p has an infinite number of poles and zeros which are all clustered at infinity. The poles are clustered closest to the $p = +\sigma$ axis so that if we approach infinity in that direction e^p becomes infinite. If we approach infinity via the $p = -\sigma$ axis e^p goes to zero. On the other hand, if we approach infinity along the $p = j\omega$ axis, e^p will always have unit magnitude but its phase will vary. This unit magnitude results from the fact that the amplitude effects of the poles and zeros counter balance each other along the $p = j\omega$ axis. The infinite cluster of poles and zeros at infinity forms what is called an *essential singularity*.

Figure 2.04-3 shows a band-pass filter using three transmission-line resonators which are a quarter-wavelength long at the frequency ω_0, and Fig. 2.04-4(a) shows a typical transfer function for this filter. In the example in Fig. 2.04-4, the response is periodic and has an infinite number of poles and zeros. The natural modes of vibration [*i.e.*, zeros of $T(p)$] are clustered near the $j\omega$ axis near the frequencies $j\omega_0$, $j3\omega_0$, $j5\omega_0$, etc., for which the lines are an odd number of quarter wavelengths long. At $p = 0$, and the frequencies $p = j2\omega_0$, $j4\omega_0$, $j6\omega_0$, etc., for which the lines are an even number of quarter-wavelengths long, the circuit functions like a short-circuit, followed by an open-circuit, and then another short-circuit. In accordance with Property (3) above, this creates *third-order* poles of attenuation as indicated in Fig. 2.04-4(a).

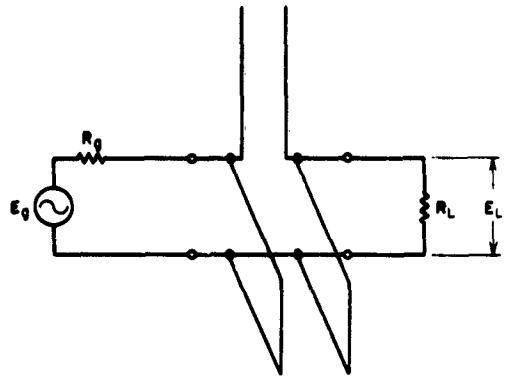

FIG. 2.04-3 A THREE-RESONATOR, BAND-PASS FILTER USING RESONATORS CONSISTING OF AN OPEN-CIRCUITED STUB IN SERIES AND TWO SHORT-CIRCUITED STUBS IN SHUNT

The approximate shape of $|T(j\omega)|$ is indicated in Fig. 2.04-4(b). If the termination values R_g and R_L were changed, the positions of the natural modes [zeros of $T(p)$] would shift and the shape of the pass bands would be altered. However, the positions of the poles of attenuation would be unaffected [see Property (2)].

The circuit in Fig. 2.04-3 is not very practical because the open-circuited series stub in the middle is difficult to construct in a shielded structure. The filter structure shown in Fig. 2.04-5 is much more common and easy to build. It uses short-circuited shunt stubs with connecting lines, the stubs and lines all being one-quarter wavelength long at frequency ω_0. This circuit has the same number of natural modes as does the circuit in Fig. 2.04-3, and can give similar pass-band responses for frequencies in the vicinity of $p = j\omega_0$, $j3\omega_0$, etc. However, at $p = 0$, $j2\omega_0$, $j4\omega_0$, etc., the circuit operates like three short circuits in parallel (which are equivalent to one short-circuit), and as a result the poles of attenuation at these frequencies are *first-order poles* only. It can thus be seen that this filter will not have as fast a rate of cutoff as will the filter in Fig. 2.04-3 whose poles on the $j\omega$ axis are *third*-order poles. The connecting lines between shunt stubs introduce poles of attenuation also, but as for the case in Fig. 2.04-2, the poles they introduce are all at infinity where they do little good as far as creating a fast rate of cutoff is concerned since there are an equal number of zeros (*i.e.*, natural modes) which are much closer, hence more influential.

These examples give brief illustrations of how the natural modes and frequencies of infinite attenuation occur in filters which involve transmission-line elements. Reasoning from the viewpoints discussed above can often be very helpful in deducing what the behavior of a given filter structure will be.

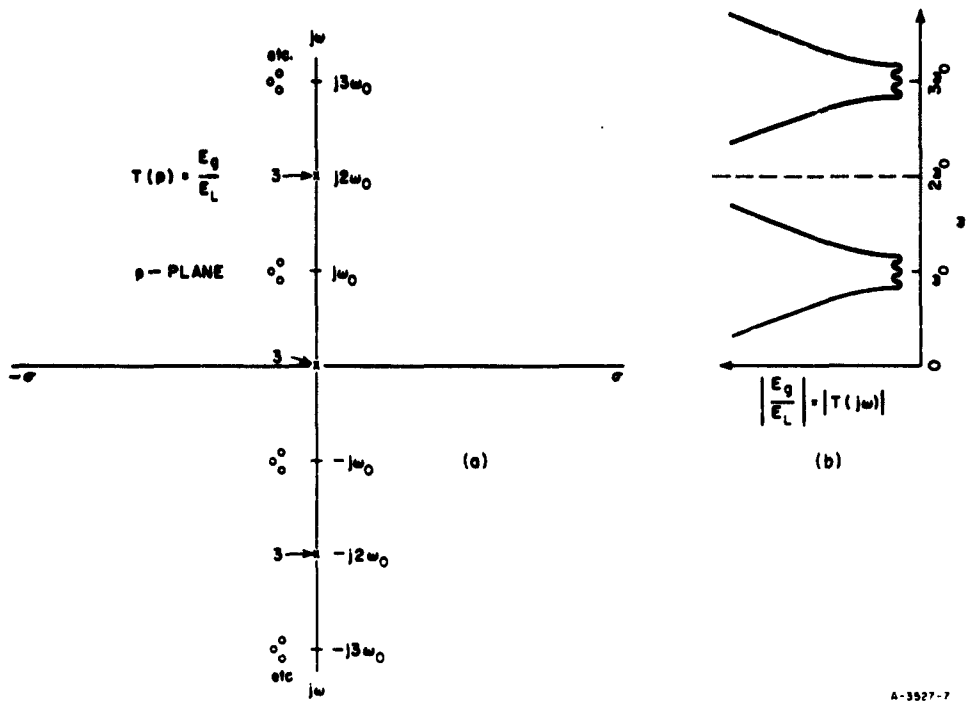

FIG. 2.04-4 VOLTAGE ATTENUATION FUNCTION PROPERTIES FOR THE FILTER IN FIG. 2.04-3
The Stubs are One-Quarter Wavelength Long at Frequency ω_0

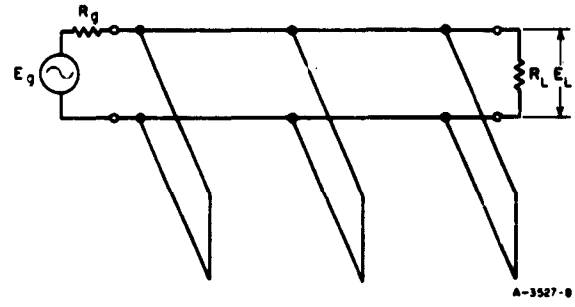

FIG. 2.04-5 A BAND-PASS FILTER CIRCUIT USING SHORT-CIRCUITED STUBS WITH CONNECTING LINES ALL OF WHICH ARE A QUARTER-WAVELENGTH LONG AT THE MIDBAND FREQUENCY ω_0

SEC. 2.05, GENERAL CIRCUIT PARAMETERS

In terms of Fig. 2.05-1, the *general circuit parameters* are defined by the equations

$$\begin{aligned} E_1 &= AE_2 + B(-I_2) \\ I_1 &= CE_2 + D(-I_2) \end{aligned} \tag{2.05-1}$$

or in matrix notation

$$\begin{bmatrix} E_1 \\ I_1 \end{bmatrix} = \begin{bmatrix} A & B \\ C & D \end{bmatrix} \begin{bmatrix} E_2 \\ -I_2 \end{bmatrix} \tag{2.05-2}$$

These parameters are particularly useful in relating the performance of cascaded networks to their performance when operated individually. The general circuit parameters for the two cascaded networks in Fig. 2.05-2 are given by

$$\begin{bmatrix} A & B \\ C & D \end{bmatrix} = \begin{bmatrix} A_a & B_a \\ C_a & D_a \end{bmatrix} \begin{bmatrix} A_b & B_b \\ C_b & D_b \end{bmatrix}$$

$$= \begin{bmatrix} (A_aA_b + B_aC_b) & (A_aB_b + B_aD_b) \\ (C_aA_b + D_aC_b) & (C_aB_b + D_aD_b) \end{bmatrix} \tag{2.05-3}$$

FIG. 2.05-1 DEFINITION OF CURRENTS AND VOLTAGES FOR TWO-PORT NETWORKS

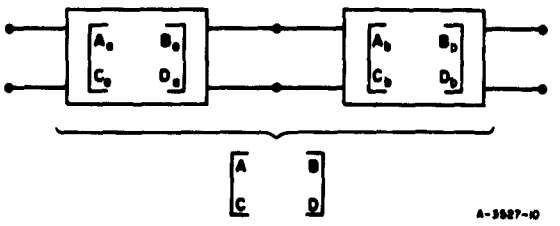

FIG. 2.05-2 CASCADED TWO-PORT NETWORKS

By repeated application of this operation the general circuit parameters can be computed for any number of two-port networks in cascade. Figure 2.05-3 gives the general circuit parameters for a number of common structures.

Under certain conditions the general circuit parameters are interrelated in the following special ways: If the network is reciprocal

$$AD - BC = 1 \quad . \tag{2.05-4}$$

If the network is symmetrical

$$A = D \quad . \tag{2.05-5}$$

If the network is lossless (i.e., without dissipative elements), then for frequencies $p = j\omega$, A and D will be purely real while B and C will be purely imaginary.

If the network in Fig. 2.05-1 is turned around, then the square matrix in Eq. (2.05-2) is

$$\begin{bmatrix} A_t & B_t \\ C_t & D_t \end{bmatrix} = \begin{bmatrix} D & B \\ C & A \end{bmatrix} \tag{2.05-6}$$

where the parameters with t subscripts are for the network when turned around, and the parameters without subscripts are for the network with its original orientation. In both cases, E_1 and I_1 are at the terminals at the left and E_2 and I_2 are at the terminals at the right.

By use of Eqs. (2.05-6), (2.05-3), and (2.05-4), if the parameters A', B', C', D' are for the left half of a reciprocal symmetrical network, the general circuit parameters for the entire network are

$$\begin{bmatrix} A & B \\ C & D \end{bmatrix} = \begin{bmatrix} (1 + 2B'C')(2A'B') \\ (2C'D')(1 + 2B'C') \end{bmatrix} \quad . \tag{2.05-7}$$

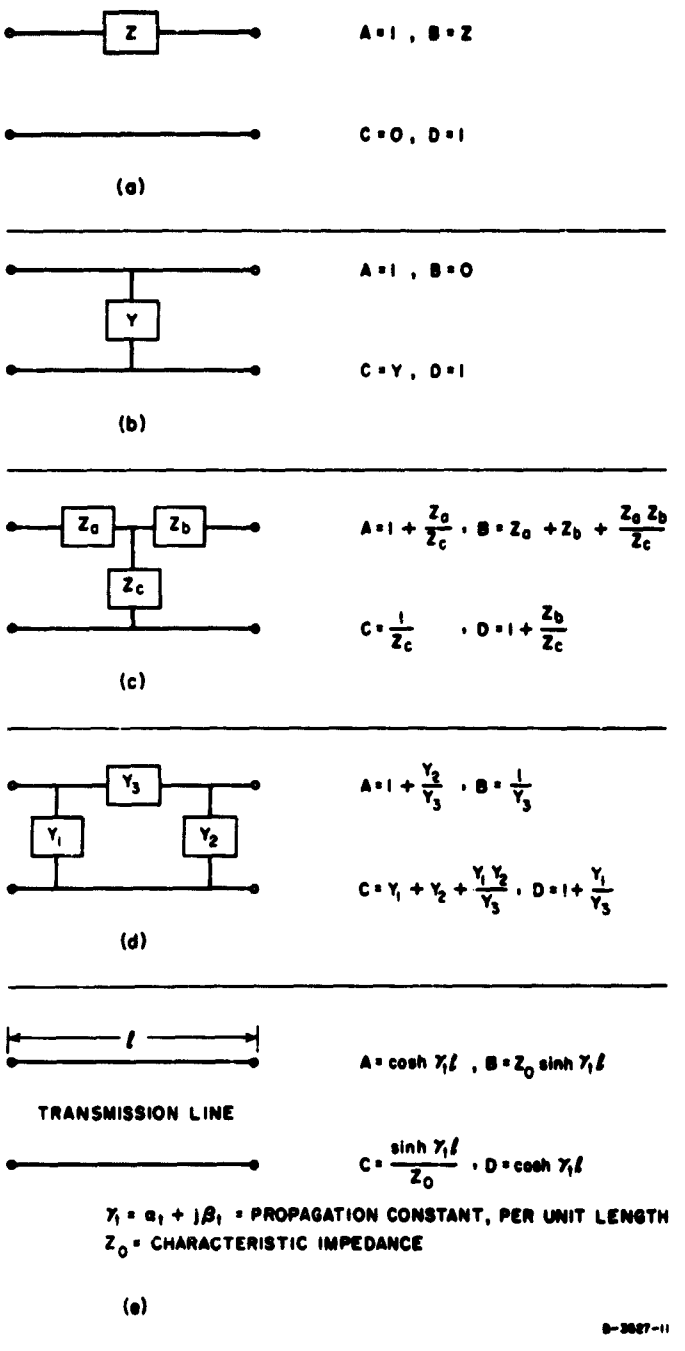

FIG. 2.05-3 GENERAL CIRCUIT PARAMETERS OF SOME COMMON STRUCTURES

SEC. 2.06, OPEN-CIRCUIT IMPEDANCES AND SHORT-CIRCUIT ADMITTANCES

In terms of Fig. 2.05-1, the *open-circuit impedances* of a two-port network may be defined by the equations

$$\begin{aligned} z_{11}I_1 + z_{12}I_2 &= E_1 \\ z_{21}I_1 + z_{22}I_2 &= E_2 \end{aligned} \qquad (2.06\text{-}1)$$

Physically, z_{11} is the input impedance at End 1 when End 2 is open-circuited. The quantity z_{12} could be measured as the ratio of the voltage E_1 I_2 when End 1 is open-circuited and current I_2 is flowing in End 2. The parameters z_{21} and z_{22} may be interpreted analogously.

In a similar fashion, the *short-circuit admittances* may be defined in terms of Fig. 2.05-1 and the equations

$$\begin{aligned} y_{11}E_1 + y_{12}E_2 &= I_1 \\ y_{21}E_1 + y_{22}E_2 &= I_2 \end{aligned} \qquad (2.06\text{-}2)$$

In this case y_{11} is the admittance at End 1 when End 2 is short-circuited. The parameter y_{12} could be computed as the ratio I_1 / E_2 when End 1 is short-circuited and a voltage E_2 is applied at End 2.

Figure 2.06-1 shows the open-circuit impedances and short-circuit admittances for a number of common structures. For reciprocal networks $z_{12} = z_{21}$ and $y_{12} = y_{21}$. For a lossless network (*i.e.*, one composed of reactances), the open-circuit impedances and the short-circuit admittances are all purely imaginary for all $p = j\omega$.

SEC. 2.07, RELATIONS BETWEEN GENERAL CIRCUIT PARAMETERS AND OPEN- AND SHORT-CIRCUIT PARAMETERS

The relationships between the general circuit parameters, the open-circuit impedances, and the short-circuit admittances defined in Secs. 2.05 and 2.06 are as follows:

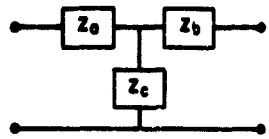

$$z_{11} = (Z_a + Z_c) \quad , \quad z_{12} = Z_c$$

$$z_{21} = Z_c \quad , \quad z_{22} = (Z_c + Z_b)$$

$$\Delta_z = Z_a Z_b + Z_b Z_c + Z_c Z_a$$

(a)

$$y_{11} = \frac{Z_b + Z_c}{\Delta_z} \quad , \quad y_{12} = \frac{-Z_c}{\Delta_z}$$

$$y_{21} = \frac{-Z_c}{\Delta_z} \quad , \quad y_{22} = \frac{Z_a + Z_c}{\Delta_z}$$

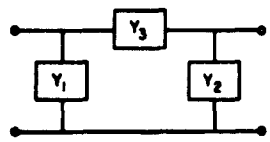

$$y_{11} = Y_1 + Y_3 \quad , \quad y_{12} = -Y_3$$

$$y_{21} = -Y_3 \quad , \quad y_{22} = Y_2 + Y_3$$

$$\Delta_y = Y_1 Y_2 + Y_2 Y_3 + Y_3 Y_1$$

(b)

$$z_{11} = \frac{Y_2 + Y_3}{\Delta_y} \quad , \quad z_{12} = \frac{Y_3}{\Delta_y}$$

$$z_{21} = \frac{Y_3}{\Delta_y} \quad , \quad z_{22} = \frac{Y_1 + Y_3}{\Delta_y}$$

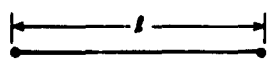

TRANSMISSION LINE

$$z_{11} = Z_0 \coth \gamma_1 \ell \quad , \quad z_{12} = \frac{Z_0}{\sinh \gamma_1 \ell}$$

$$z_{21} = \frac{Z_0}{\sinh \gamma_1 \ell} \quad , \quad z_{22} = Z_0 \coth \gamma_1 \ell$$

(c)

$$y_{11} = \frac{\coth \gamma_1 \ell}{Z_0} \quad , \quad y_{12} = \frac{-1}{Z_0 \sinh \gamma_1 \ell}$$

$$y_{21} = \frac{-1}{Z_0 \sinh \gamma_1 \ell} \quad , \quad y_{22} = \frac{\coth \gamma_1 \ell}{Z_0}$$

$\gamma_1 = \alpha_1 + j\beta_1$ = PROPAGATION CONSTANT, PER UNIT LENGTH

Z_0 = CHARACTERISTIC IMPEDANCE

B-3527-12

FIG. 2.06-1 OPEN-CIRCUIT IMPEDANCES AND SHORT-CIRCUIT ADMITTANCES OF SOME COMMON STRUCTURES

$$A = \frac{z_{11}}{z_{21}} = \frac{-y_{22}}{y_{21}} = \frac{n_{ss}}{m_{21}}$$

$$B = \frac{\Delta_z}{z_{21}} = \frac{-1}{y_{21}} = \frac{n_{sr}}{m_{21}}$$

$$C = \frac{1}{z_{21}} = \frac{-\Delta_y}{y_{21}} = \frac{n_{rr}}{m_{21}} \qquad (2.07\text{-}1)$$

$$D = \frac{z_{22}}{z_{21}} = \frac{-y_{11}}{y_{21}} = \frac{n_{rs}}{m_{21}}$$

$$z_{11} = \frac{y_{22}}{\Delta_y} = \frac{A}{C} = \frac{n_{ss}}{n_{rr}}$$

$$z_{12} = \frac{-y_{12}}{\Delta_y} = \frac{\Delta}{C} = \frac{m_{12}}{n_{rr}}$$

$$z_{21} = \frac{-y_{21}}{\Delta_y} = \frac{1}{C} = \frac{m_{21}}{n_{rr}} \qquad (2.07\text{-}2)$$

$$z_{22} = \frac{y_{11}}{\Delta_y} = \frac{D}{C} = \frac{n_{rs}}{n_{rr}}$$

$$y_{11} = \frac{z_{22}}{\Delta_z} = \frac{D}{B} = \frac{n_{rs}}{n_{sr}}$$

$$y_{12} = \frac{-z_{12}}{\Delta_z} = \frac{-\Delta}{B} = \frac{-m_{12}}{n_{sr}}$$

$$y_{21} = \frac{-z_{21}}{\Delta_z} = \frac{-1}{B} = \frac{-m_{21}}{n_{sr}} \qquad (2.07\text{-}3)$$

$$y_{22} = \frac{z_{11}}{\Delta_z} = \frac{A}{B} = \frac{n_{ss}}{n_{sr}}$$

where

$$\left.\begin{aligned} \Delta = AD - DC &= \frac{m_{21}m_{12}}{(m_{21})^2} = \frac{m_{12}}{m_{21}} \\ &= 1 \text{ (for reciprocal networks)} \end{aligned}\right\} , \qquad (2.07\text{-}4)$$

$$\Delta_z = z_{11}z_{22} - z_{12}z_{21} = \frac{n_{ss}n_{oo}}{(n_{oo})^2} = \frac{n_{ss}}{n_{oo}} \qquad (2.07\text{-}5)$$

$$\Delta_y = y_{11}y_{22} - y_{12}y_{21} = \frac{n_{oo}n_{ss}}{(n_{ss})^2} = \frac{n_{oo}}{n_{ss}} . \qquad (2.07\text{-}6)$$

If any of these various circuit parameters are expressed as a function of complex frequency p, they will consist of the ratio of two polynomials, each of which may be put in the form

$$\text{polynomial} = c(p - p_1)(p - p_2)(p - p_3) \ldots \qquad (2.07\text{-}7)$$

where c is a real constant and the p_k are the roots of the polynomial. As should be expected from the discussions in Secs. 2.02 to 2.04, the locations of the roots of these polynomials have physical significance. The quantities on the right in Eqs. (2.07-1) to (2.07-6) have been introduced to clarify this physical significance.

The symbols n_{ss}, n_{oo}, n_{os}, and n_{so} in the expressions above represent polynomials of the form in Eq. (2.07-7) whose roots are natural frequencies of vibration of the circuit under conditions indicated by the subscripts. Thus, the roots of n_{ss} are the natural frequencies of the circuit in Fig. 2.05-1 when both ports are short-circuited, while the roots of n_{oo} are natural frequencies when both ports are open-circuited. The roots of n_{os} are natural frequencies when the left port is open-circuited while the right port is short-circuited, and the inverse obtains for n_{so}. The symbols m_{12} and m_{21} represent polynomials whose roots are poles of attenuation (see Sec. 2.04) of the circuit, except for those poles of attenuation at $p = \infty$. The polynomial m_{12} has roots corresponding to the poles of attenuation for transmission to End 1 *from* End 2 in Fig. 2.05-1, while the polynomial m_{21} has roots which are poles of attenuation for

transmission to End 2 from End 1. If the network is reciprocal, $m_{12} = m_{21}$. These polynomials for a given circuit are interrelated by the expression[8]

$$n_{oo}n_{ss} = n_{so}n_{os} - m_{12}m_{21} \qquad (2.07\text{-}8)$$

and, as is discussed in Ref. 8, they can yield certain labor-saving advantages when they themselves are used as basic parameters to describe the performance of a circuit.

As is indicated in Eqs. (2.07-4) to (2.07-6), when the determinants Δ, Δ_x and Δ_y are formed as a function of p, the resulting rational function will necessarily contain cancelling polynomials. This fact can be verified by use of Eqs. (2.07-1) to (2.07-3) along with (2.07-8). Removal of the cancelling polynomials will usually cut the degree of the polynomials in these functions roughly in half. Analogous properties exist when the network contains distributed elements, although the polynomials then become of infinite degree (see Sec. 2.02) and are most conveniently represented by transcendental functions such as sinh p and cosh p. For example, for a lossless transmission line

$$n_{so} = n_{os} = Z_0 \cosh \frac{\pi p}{2\omega_0} = Z_0 \prod_{k=1}^{\infty} \left[\frac{1}{(2k-1)\omega_0}\right]^2 \{[p + j(2k-1)\omega_0][p - j(2k-1)\omega_0]\}$$

$$n_{oo} = \sinh \frac{\pi p}{2\omega_0} = \frac{\pi p}{2\omega_0} \prod_{k=1}^{\infty} \left(\frac{1}{2k\omega_0}\right)^2 [(p + j2k\omega_0)(p - j2k\omega_0)] \qquad (2.07\text{-}9)$$

$$n_{ss} = Z_0^2 \sinh \frac{\pi p}{2\omega_0}$$

$$m_{12} = m_{21} = Z_0$$

where Z_0 is the characteristic impedance of the line, and ω_0 is the radian frequency for which the line is one-quarter wavelength long. In this case, $m_{12} = m_{21}$ is a constant since all of the poles of attenuation are at infinity (see Sec. 2.04 and Ref. 8). The choice of constant multipliers for these "polynomials" is arbitrary to a certain extent in that any one multiplier may be chosen arbitrarily, but this then fixes what the other constant multipliers must be.[8]

SEC. 2.08, INCIDENT AND REFLECTED WAVES, REFLECTION COEFFICIENTS, AND ONE KIND OF TRANSMISSION COEFFICIENT

Let us suppose that it is desired to analyze the transmission across the terminals 2-2′ in Fig. 2.08-1 from the wave point of view. By definition

$$E_i + E_r = E \tag{2.08-1}$$

where E_i is the amplitude of the incident voltage wave emerging from the network, E_r is the reflected voltage wave amplitude, and E is the transmitted voltage wave amplitude (which is also the voltage that would be measured across the terminals 2-2′). If $Z_s = Z_L$, there will be no reflection* so that $E_r = 0$ and $E_i = E$. Replacing the network and generator at (a) in Fig. 2.08-1 by a Thevenin equivalent generator as shown at (b), it is readily seen that since for $Z_s = Z_L$, $E_i = E$, then

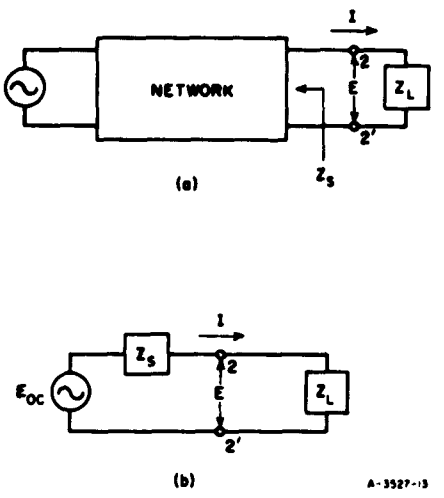

FIG. 2.08-1 CIRCUITS DISCUSSED IN SEC. 2.08 FROM THE WAVE-ANALYSIS VIEWPOINT

$$E_i = \frac{E_{oc}}{2} \tag{2.08-2}$$

where E_{oc} is the voltage which would be measured at terminals 2-2′ if they were open-circuited. Using Eqs. (2.08-1) and (2.08-2) the voltage *reflection coefficient* is defined as

$$\Gamma = \frac{E_r}{E_i} = \frac{Z_L - Z_s}{Z_L + Z_s} \tag{2.08-3}$$

An analogous treatment for current waves proceeds as follows:

$$I_i + I_r = I \tag{2.08-4}$$

---

* Note that no reflection of the voltage wave does not necessarily imply maximum power transfer. For no reflection of the voltage wave $Z_s = Z_L$, while for maximum power transfer $Z_s = Z_L^*$ where Z_L^* is the complex conjugate of Z_L.

where I_i is the incident current amplitude, I_r is the reflected current amplitude, and I is the transmitted current amplitude which is also the actual current passing through the terminals 2-2'. The incident current is

$$I_i = \frac{I_{sc}}{2} \qquad (2.08\text{-}5)$$

where I_{sc} is the current which would pass through the terminals 2-2' if they were short-circuited together. The *current reflection coefficient* is then defined as

$$\Gamma_c = \frac{I_r}{I_i} = \frac{Y_L - Y_s}{Y_L + Y_s} = -\Gamma \qquad (2.08\text{-}6)$$

where $Y_s = 1/Z_s$ and $Y_L = 1/Z_L$.

In addition, sometimes the *voltage transmission coefficient*

$$\tau = \frac{E}{E_i} = \frac{2Z_L}{Z_L + Z_s} = 1 + \Gamma \qquad (2.08\text{-}7)$$

is used. The corresponding *current transmission coefficient* is

$$\tau_c = \frac{I}{I_i} = \frac{2Y_L}{Y_L + Y_s} = 1 + \Gamma_c \quad . \qquad (2.08\text{-}8)$$

It will be noted that these transmission coefficients τ and τ_c are not the same as the transmission coefficient t discussed in Sec. 2.10.

SEC. 2.09, CALCULATION OF THE INPUT IMPEDANCE OF A TERMINATED, TWO-PORT NETWORK

The input impedance $(Z_{in})_1$ defined in Fig. 2.09-1 can be computed from Z_2 and any of the circuit parameters used to describe the performance of a two-port network. In terms of the general circuit parameters, the open-circuit impedances, and the short-circuit admittances,

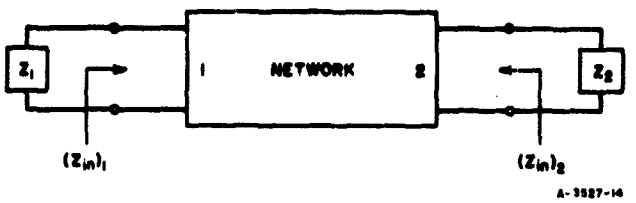

FIG. 2.09-1 DEFINITION OF INPUT IMPEDANCES COMPUTED IN SEC. 2.09

$$(Z_{in})_1 = \frac{AZ_2 + B}{CZ_2 + D} \qquad (2.09\text{-}1)$$

$$= z_{11} - \frac{z_{12}z_{21}}{z_{22} + Z_2} \qquad (2.09\text{-}2)$$

$$= \frac{y_{22} + Y_2}{y_{11}(y_{22} + Y_2) - y_{12}y_{21}} , \qquad (2.09\text{-}3)$$

respectively, where $Y_2 = 1/Z_2$. Similarly, for the impedance $(Z_{in})_2$ in Fig. 2.09-1

$$(Z_{in})_2 = \frac{DZ_1 + B}{CZ_1 + A} \qquad (2.09\text{-}4)$$

$$= z_{22} - \frac{z_{12}z_{21}}{z_{11} + Z_1} \qquad (2.09\text{-}5)$$

$$= \frac{y_{11} + Y_1}{y_{22}(y_{11} + Y_1) - y_{12}y_{21}} \qquad (2.09\text{-}6)$$

where $Y_1 = 1/Z_1$.

SEC. 2.10, CALCULATION OF VOLTAGE TRANSFER FUNCTIONS

The transfer function E_g/E_2 for the circuit in Fig. 2.10-1 can be computed if any of the sets of circuit parameters discussed in Secs. 2.05 to 2.07 are known for the network in the box. The appropriate equations are

$$\frac{E_g}{E_2} = \frac{AR_2 + B + CR_1R_2 + DR_1}{R_2} , \qquad (2.10\text{-}1)$$

$$= \frac{(z_{11} + R_1)(z_{22} + R_2) - z_{12}z_{21}}{z_{21}R_2} , \qquad (2.10\text{-}2)$$

and

$$= \frac{(y_{11} + G_1)(y_{22} + G_2) - y_{12}y_{21}}{-y_{21}G_1} . \qquad (2.10\text{-}3)$$

Transfer functions such as the E_g E_2 function presented above are commonly used but have a certain disadvantage. This disadvantage is that, depending on what the relative size of R_1 and R_2 are, complete energy transfer may correspond to any of a wide range of $|E_g/E_2|$ values. Such confusion is eliminated if the transfer function

$$\frac{(E_2)_{avail}}{E_2} = \frac{1}{2}\sqrt{\frac{R_2}{R_1}}\left(\frac{E_g}{E_2}\right) \qquad (2.10\text{-}4)$$

is used instead. The quantity

$$(E_2)_{avail} = \frac{1}{2}\sqrt{\frac{R_2}{R_1}}\,E_g \qquad (2.10\text{-}5)$$

will be referred to herein as the *available voltage*, which is the voltage across R_2 when the entire available power of the generator is absorbed by R_2. Thus, for complete energy transfer $|(E_2)_{avail}/E_2| = 1$ regardless

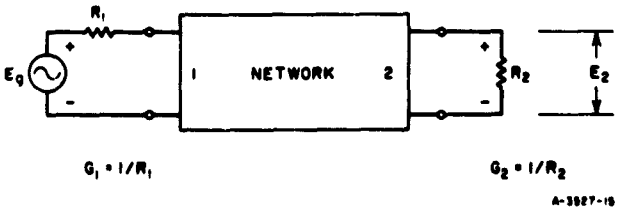

FIG. 2.10-1 A CIRCUIT DISCUSSED IN SEC. 2.10

of the relative sizes of R_2 and R_1. Note that $(E_2)_{avail}$ has the same phase as E_g.

In the literature a *transmission coefficient* t is commonly used where

$$t = \frac{1}{[(E_2)_{avail}/E_2]} = 2\sqrt{\frac{R_1}{R_2}}\left(\frac{E_2}{E_g}\right) \quad . \tag{2.10-6}$$

Note that this is not the same as the transmission coefficients τ or τ_e discussed in Sec. 2.08. The transmission coefficient t is the same, however, as the scattering coefficients $S_{12} = S_{21}$, discussed in Sec. 2.12. Also note that t is an output/input ratio of a "voltage gain" ratio, while the function in Eq. (2.10-4) is an input/output ratio or a "voltage attenuation" ratio.

SEC. 2.11. CALCULATION OF POWER TRANSFER FUNCTIONS AND "ATTENUATION"

One commonly used type of power transfer function is the *insertion loss* function

$$\frac{P_{20}}{P_2} = \left(\frac{R_2}{R_1 + R_2}\right)^2 \left|\frac{E_g}{E_2}\right|^2 \tag{2.11-1}$$

where R_1, R_2, E_g, and E_2 are defined in Fig. 2.10-1, and $|E_g\ E_2|$ can be computed by use of Eqs. (2.10-1) to (2.10-3). The quantity P_2 is the power absorbed by R_2 when the network in Fig. 2.10-1 is in place, while P_{20} is the power in R_2 when the network is removed and R_2 is connected directly to R_1 and E_g.

Insertion loss functions have the same disadvantage as the E_g/E_2 function discussed in Sec. 2.10, *i.e.*, complete power transfer may correspond to almost any value of P_{20}/P_2 depending on the relative sizes of R_1 and R_2. For this reason the power transfer function

$$\frac{P_{avail}}{P_2} = \frac{1}{4}\left(\frac{R_2}{R_1}\right)\left|\frac{E_g}{E_2}\right|^2 = \frac{1}{|t|^2} \tag{2.11-2}$$

will be used in this book instead of insertion loss. The function P_{avail}/P_2 is known as a *transducer loss ratio*, where P_2 is again the power delivered to R_2 in Fig. 2.10-1 while

$$P_{avail} = \frac{|E_g|^2}{4R_1} \tag{2.11-3}$$

is the available power of the generator composed of E_g and the internal resistance R_1. Thus, for complete power transfer $P_{avail}/P_2 = 1$ regardless of the relative size of R_1 and R_2. Note that t in Eq. (2.11-2) is the transmission coefficient defined by Eq. (2.10-6).

It will often be desirable to express P_{avail}/P_2 in db so that

$$L_A = 10 \log_{10} (P_{avail}\ P_2) \quad \text{db} \quad . \tag{2.11-4}$$

Herein, when *attenuation* is referred to, the transducer loss (*i.e.*, transducer attenuation) in db as defined in Eq. (2.11-4) will be understood, unless otherwise specified.

If we define $L_i = 10 \log_{10} P_{20}\ P_2$ as *insertion loss in db*, then the attenuation in db is

$$L_A = L_i + 10 \log_{10} \frac{(R_1 + R_2)^2}{4R_1R_2} \quad \text{db} \quad . \tag{2.11-5}$$

Note that if $R_1 = R_2$, then insertion loss and transducer attenuation are the same.

If the network in Fig. 2.11-1 contains dissipative elements which cannot be neglected, then L_A may be computed by use of Eqs. (2.11-4), (2.11-2), and any of Eqs. (2.10-1) to (2.10-3). However, if the network in the box may be regarded as lossless (*i.e.*, without any

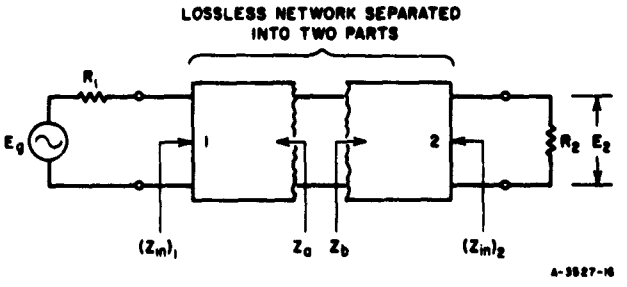

FIG. 2.11-1 A NETWORK DISCUSSED IN SEC. 2.11

dissipative elements), then some simplifications can be taken advantage of. For example, as discussed in Sec. 2.05, for a dissipationless network A and D will be purely real while B and C will be purely imaginary for frequencies $j\omega$. Because of this, the form

$$\frac{P_{avail}}{P_i} = \frac{1}{4R_1R_2}\left[(AR_2 + DR_1)^2 + \left(\frac{B + CR_1R_2}{j}\right)^2\right] \qquad (2.11\text{-}6)$$

becomes convenient for computation. This expression applies to dissipationless reciprocal networks and also to non-reciprocal dissipationless networks for the case of transmission from left to right. If we further specify that $R_1 = R_2 = R$, that the network is reciprocal (*i.e.*, $AD - BC = 1$), and that the network is symmetrical (*i.e.*, $A = D$), then Eq. (2.11-6) becomes

$$\frac{P_{avail}}{P_2} = 1 + \frac{1}{4}\left(\frac{B}{jR} - \frac{CR}{j}\right)^2 \quad . \qquad (2.11\text{-}7)$$

Furthermore, it is convenient in such cases to compute the general circuit parameters A', B', C', D' for the left half of the network only. Then by Eqs. (2.05-7) and (2.11-7), the transducer loss ratio for the over-all network is

$$\frac{P_{avail}}{P_2} = 1 + \left(\frac{A'B'}{jR} - \frac{C'D'R}{j}\right)^2 \quad . \qquad (2.11\text{-}8)$$

In the case of dissipationless networks such as that shown in Fig. 2.11-1, the power transmission is easily computed from the generator parameters and the input impedance of the dissipationless network terminated in R_2. This is because any power absorbed by $(Z_{in})_1$ must surely end up in R_2. The computations may be conveniently made in terms of the voltage reflection coefficient Γ discussed in Sec. 2.08. In these terms

$$\frac{P_{avail}}{P_2} = \frac{1}{|t|^2} = \frac{1}{1 - |\Gamma_1|^2} \qquad (2.11\text{-}9)$$

where

$$\Gamma_1 = \frac{(Z_{in})_1 - R_1}{(Z_{in})_1 + R_1} \tag{2.11-10}$$

and R_1 and $(Z_{in})_1$ are as defined in Fig. 2.11-1. The reflection coefficient at the other end is

$$\Gamma_2 = \frac{(Z_{in})_2 - R_2}{(Z_{in})_2 + R_2} \tag{2.11-11}$$

and for a dissipationless network

$$|\Gamma_1| = |\Gamma_2| \tag{2.11-12}$$

so that the *magnitude* of either reflection coefficient could be used in Eq. (2.11-9). [It should be understood in passing that the phase of Γ_1 is not necessarily the same as that of Γ_2 even though Eq. (2.11-12) holds.]

The reflection coefficient

$$\Gamma_{ab} = \frac{Z_b - Z_a}{Z_b + Z_a} \tag{2.11-13}$$

between Z_a and Z_b in Fig. 2.11-1 *cannot* be used in Eq. (2.11-9) if both Z_a and Z_b are complex. However, it can be shown that

$$|\Gamma_1| = |\Gamma_2| = \left| \frac{Z_b^* - Z_a}{Z_b + Z_a} \right| \tag{2.11-14}$$

where Z_b^* is the complex conjugate of Z_b. Thus, if $Z_a = R_a + jX_a$ and $Z_b = R_b + jX_b$, by use of Eqs. (2.11-14) and (2.11-9) we obtain

$$\frac{P_{avail}}{P_2} = \frac{(R_a + R_b)^2 + (X_a + X_b)^2}{4R_aR_b} \quad . \tag{2.11-15}$$

For cases where $Z_a = Z_b$ such as occurs at the middle of a *symmetrical* network, Eq. (2.11-15) reduces to

$$\frac{P_{avail}}{P_2} = 1 + \left(\frac{X_a}{R_a}\right)^2 \quad . \tag{2.11-16}$$

Another situation which commonly occurs in filter circuits is for the structure to be *antimetrical** about its middle. In such cases, if Z_a and Z_b in Fig. 2.11-1 are at the middle of a antimetrical network, then for all frequencies

$$Z_b = \frac{R_h^2}{Z_a} \tag{2.11-17}$$

where R_h is a real, positive constant. Defining Z_a again as $R_a + jX_a$, by Eqs. (2.11-17), (2.11-14), and (2.11-9),

$$\frac{P_{avail}}{P_2} = \frac{1}{4}\left\{\left(\frac{R_a}{R_h} + \frac{R_h}{R_a}\right)^2 + 2\left[\left(\frac{X_a}{R_h}\right)^2 - \left(\frac{X_a}{R_a}\right)^2\right] + \left(\frac{X_a}{R_a}\right)^2\left(\frac{X_a}{R_h}\right)^2\right\} \quad . \tag{2.11-18}$$

The quantity R_h is obtained most easily by evaluating

$$R_h = \sqrt{Z_a Z_b} = \text{real, positive} \tag{2.11-19}$$

at a frequency where Z_a and Z_b are both known to be real. The maximally flat and Tchebyscheff low-pass prototype filter structure whose element values are listed in Tables 4.05-1(a), (b) and 4.05-2(a), (b) are symmetrical for an odd number n of reactive elements, and they are antimetrical for an even number n of reactive elements. The step transformers discussed in Chapter 6 are additional examples of antimetrical circuits.

SEC. 2.12, SCATTERING COEFFICIENTS

In this book there will be some occasion to make use of scattering coefficients. Scattering coefficients are usually defined entirely from a wave point of view. However, for the purposes of this book it will be sufficient to simply extrapolate from previously developed concepts.

---

* This term was coined by Guillemin. See pp. 371 and 467 of Ref. 2.

The performance of any linear two-port network with terminations can be described in terms of four scattering coefficients: S_{11}, S_{12}, S_{21}, and S_{22}. With reference to the two-port network in Fig. 2.11-1, $S_{11} = \Gamma_1$ and $S_{22} = \Gamma_2$ are simply the reflection coefficients at Ends 1 and 2, respectively, as defined in Eqs. (2.11-10) and (2.11-11). The scattering coefficient S_{21} is simply the transmission coefficient, t, for transmission to End 2 from End 1 as defined in Eqs. (2.10-5) and (2.10-6). The scattering coefficient, S_{12}, is likewise the same as the transmission coefficient, t, for transmission to End 1 from End 2. Of course, if the network is reciprocal $S_{21} = S_{12}$. The relations in Sec. 2.11 involving t, Γ_1, and Γ_2, of course, apply equally well to $t = S_{12} = S_{21}$, $\Gamma_1 = S_{11}$, and $\Gamma_2 = S_{22}$, respectively.

Thus, it is seen that as far as two-port networks are concerned, the scattering coefficients are simply the reflection coefficients or transmission coefficients discussed in Secs. 2.10 and 2.11. However, scattering coefficients may be applied to networks with an arbitrary number of ports. For example, for a three-port network there are nine scattering coefficients, which may be displayed as the matrix

$$[S] = \begin{bmatrix} S_{11} & S_{12} & S_{13} \\ S_{21} & S_{22} & S_{23} \\ S_{31} & S_{32} & S_{33} \end{bmatrix} . \qquad (2.12\text{-}1)$$

For an n-port network there are n^2 coefficients. In general, for any network with resistive terminations,

$$S_{jj} = \Gamma_j = \frac{(Z_{in})_j - R_j}{(Z_{in})_j + R_j} \qquad (2.12\text{-}2)$$

is the reflection coefficient between the input impedance $(Z_{in})_j$ at Port j and the termination R_j at that port. For the other coefficients, analogously to Eqs. (2.10-5) and (2.10-6),

$$S_{jk}\Big|_{j \neq k} = \frac{E_j}{(E_j)_{avail}} \qquad (2.12\text{-}3)$$

where

$$(E_j)_{avail} = \frac{1}{2}\sqrt{\frac{R_j}{R_k}}\,(E_g)_k \quad . \tag{2.12-4}$$

The voltage E_j is the response across termination R_j at Port j due to a generator of voltage $(E_g)_k$ and internal impedance R_k at Port k. In computing the coefficients defined by Eqs. (2.12-2) to (2.12-4), all ports are assumed to always be terminated in their specified terminations R_j.

If an n-port network is reciprocal,

$$S_{jk} = S_{kj} \quad . \tag{2.12-5}$$

By Eqs. (2.11-9)and (2.11-12) for a dissipationless reciprocal two-port network

$$1 = |S_{11}|^2 + |S_{12}|^2 \quad , \tag{2.12-6}$$

$$|S_{11}| = |S_{22}| \quad , \tag{2.12-7}$$

and

$$S_{12} = S_{21} \quad . \tag{2.12-8}$$

The analogous relation for the general n-port, dissipationless, reciprocal network is

$$[I] = [S]^* [S] \tag{2.12-9}$$

where $[S]$ is the *scattering matrix* of scattering coefficients [as illustrated in Eq. (2.12-1) for the case of $n = 3$], $[S]^*$ is the same matrix with all of its complex numbers changed to their conjugates, and $[I]$ is an nth-order unit matrix. Since the network is specified to be reciprocal, Eq. (2.12-5)applies and $[S]$ is symmetrical about its principal diagonal.

For any network with resistive terminations,

$$|S_{j,k}|^2_{j \neq k} = \frac{P_j}{(P_{avail})_k} \tag{2.12-10}$$

where P_j is the power delivered to the termination R_j at Port j, and $(P_{avail})_k$ is the available power of a generator at Port k. In accord with Eq. (2.11-4) the db attenuation for transmission from Port k to Port j (with all specified terminations connected) is

$$L_A = 20 \log_{10} \left| \frac{1}{S_{jk}} \right| \quad \text{db} \quad . \qquad (2.12\text{-}11)$$

Further discussion of scattering coefficients will be found in Ref. 9.

SEC. 2.13. ANALYSIS OF LADDER CIRCUITS

Ladder circuits often occur in filter work, some examples being the low-pass prototype filters discussed in Chapter 4. The routine outlined below is particularly convenient for computing the response of such networks.

The first step in this routine is to characterize each *series* branch by its *impedance* and the *current* flowing through the branch, and each *shunt* branch by its *admittance* and the *voltage* across the branch. This characterization is illustrated in Fig. 2.13-1. Then, in general terms we define

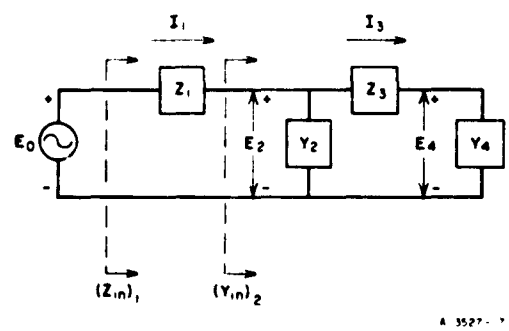

FIG. 2.13-1 A LADDER NETWORK EXAMPLE DISCUSSED IN SEC. 2.13

F_k = series impedance or shunt admittance of Branch k (2.13-1)

U_k = series-branch current or shunt-branch voltage of Branch k (2.13-2)

U_n = series-branch current or shunt-branch voltage for the last branch on the right (2.13-3)

U_0 = current or voltage associated with the driving generator on the left. (2.13-4)

In general, if Branch 1 is in shunt, U_0 should be the current of an infinite-impedance current generator; if Branch 1 is in series, U_0 should be the voltage of a zero-impedance voltage generator. Then, for all cases,

$$A_{n+1} = 1 = \frac{U_n}{U_n}$$

$$A_n = F_n A_{n+1} = \frac{U_{n-1}}{U_n}$$

$$A_{n-1} = F_{n-1} A_n + A_{n+1} = \frac{U_{n-2}}{U_n}$$

$$\cdots \qquad (2.13\text{-}5)$$

$$A_k = F_k A_{k+1} + A_{k+2} = \frac{U_{k-1}}{U_n}$$

$$\cdots$$

$$A_1 = F_1 A_2 + A_3 = \frac{U_0}{U_n} \quad .$$

Thus A_1 is the transfer function from the generator on the left to Branch n on the right. If we define

$$(F_{in})_k = \begin{array}{l} \textit{impedance} \text{ looking right through Branch } k \text{ if} \\ \text{Branch } k \text{ is in series, or } \textit{admittance} \text{ looking} \\ \text{right through Branch } k \text{ if Branch } k \text{ is in shunt,} \end{array} \qquad (2.13\text{-}6)$$

then

$$(F_{in})_k = \frac{A_k}{A_{k+1}} \quad . \qquad (2.13\text{-}7)$$

To illustrate this procedure consider the case in Fig. 2.13-1. There $n = 4$ and

$$A_5 = 1 = \frac{E_4}{E_4}$$

$$A_4 = Y_4 A_5 = \frac{I_3}{E_4}$$

$$A_3 = Z_3A_4 + A_5 = \frac{E_2}{E_4}$$

$$A_2 = Y_2A_3 + A_4 = \frac{I_1}{E_4}$$

$$A_1 = Z_1A_2 + A_3 = \frac{E_0}{E_4}$$

Thus, A_1 is the transfer function between E_0 and E_4. The impedance $(Z_{in})_1$ and admittance $(Y_{in})_2$ defined in the figure are

$$(Z_{in})_1 = \frac{A_1}{A_2}$$

$$(Y_{in})_2 = \frac{A_2}{A_3}$$

REFERENCES

1. E. A. Guillemin, *Introductory Circuit Theory* (John Wiley and Sons, New York City, 1953).
2. E. A. Guillemin, *Synthesis of Passive Networks* (John Wiley and Sons, New York City, 1957).
3. D. F. Tuttle, Jr., *Network Synthesis*, Vol. 1 (John Wiley and Sons, New York City, 1958).
4. M. E. Van Valkenburg, *Network Analysis* (Prentice-Hall, Inc., New York City, 1955).
5. E. S. Kuh and D. O. Pederson, *Principles of Circuit Synthesis* (McGraw-Hill Book Co. Inc., New York City, 1959).
6. W. W. Hansen and O. C. Lundstrom, "Experimental Determination of Impedance Functions by the Use of an Electrolytic Tank," *Proc. IRE*, **33**, pp. 528-534 (August 1945).
7. R. E. Scott, "Network Synthesis by the Use of Potential Analogs," *Proc. IRE*, **40**, pp. 970-973 (August 1952).
8. G. L. Matthaei, "Some Simplifications for Analysis of Linear Circuits," *IRE Trans. on Circuit Theory*, **CT-4**, pp. 120-124 (September 1957).
9. H. J. Carlin, "The Scattering Matrix in Network Theory," *IRE Trans. on Circuit Theory*, **CT-3**, pp. 88-97 (June 1956).

CHAPTER 3

PRINCIPLES OF THE IMAGE METHOD FOR FILTER DESIGN

SEC. 3.01, INTRODUCTION

Although the image method for filter design will not be discussed in detail in this book, it will be necessary for readers to understand the image method in order to understand some of the design techniques used in later chapters. The objective of this chapter is to supply the necessary background by discussing the physical concepts associated with the image method and by summarizing the most useful equations associated with this method. Derivations will be given for only a few equations; more complete discussions will be found in the references listed at the end of the chapter.

SEC. 3.02, PHYSICAL AND MATHEMATICAL DEFINITION OF IMAGE IMPEDANCE AND IMAGE PROPAGATION FUNCTION

The image viewpoint for the analysis of circuits is a wave viewpoint much the same as the wave viewpoint commonly used for analysis of transmission lines. In fact, for the case of a uniform transmission line the *characteristic impedance* of the line is also its *image impedance*, and if γ_t is the propagation constant per unit length then $\gamma_t l$ is the *image propagation* function for a line of length l. However, the terms *image impedance* and *image propagation function* have much more general meaning than their definition with regard to a uniform transmission line alone would suggest.

Consider the case of a two-port network which can be symmetrical, but which, for the sake of generality, will be assumed to be unsymmetrical with different impedance characteristics at End 1 than at End 2. Figure 3.02-1 shows the case of an infinite number of identical networks of this sort all connected so that at each junction either End 1s are connected together or End 2s are connected together. Since the chain of networks extends to infinity in each direction, the same impedance Z_{I1} is

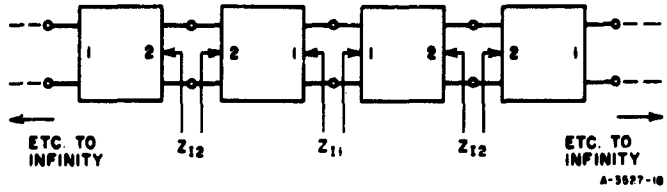

FIG. 3.02-1 INFINITE CHAIN OF IDENTICAL NETWORKS USED FOR DEFINING IMAGE IMPEDANCES AND THE IMAGE PROPAGATION FUNCTION

seen looking both left and right at a junction of the two End 1s, while at a junction of two End 2s another impedance Z_{I2} will be seen when looking either left or right. The impedances Z_{I1} and Z_{I2}, defined as indicated in Fig. 3.02-1, are the image impedances for End 1 and End 2, respectively, of the network. For an unsymmetrical network they are generally unequal.

Note that because of the way the infinite chain of networks in Fig. 3.02-1 are connected, the impedances seen looking left and right at each junction are always equal, hence there is never any reflection of a wave passing through a junction. Thus, from the wave point of view, the networks in Fig. 3.02-1 are all perfectly matched. If a wave is set to propagating towards the right, through the chain of networks, it will be attenuated as determined by the propagation function of each network, but will pass on from network to network without reflection. Note that the image impedances Z_{I1} and Z_{I2} are actually impedance of *infinite* networks, and as such they should be expected to have a mathematical form different from that of the rational impedance functions that are obtained for finite, lumped-element networks. In the cases of lumped-element filter structures, the image impedances are usually irrational functions; in the cases of microwave filter structures which involve transmission line elements, the image impedances are usually both irrational and transcendental.

An equation for the image impedance is easily derived in terms of the circuit in Fig. 3.02-2. If Z_L is made to be equal to Z_{I1} then the impedance Z_{in} seen looking in from the left of the circuit will also be equal to Z_{I1}. Now, if A, B, C, and D are the general circuit parameters for the box on the left in Fig. 3.02-2, assuming that the network is reciprocal, the

general circuit parameters A_s, B_s, C_s, and D_s for the two boxes connected as shown can be computed by use of Eq. (2.05-7). Then by Eq. (2.09-1)

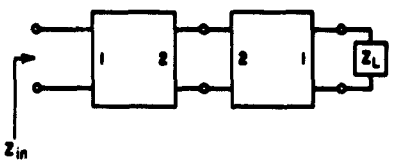

FIG. 3.02-2 CIRCUIT DISCUSSED IN SEC. 3.02

$$Z_{in} = \frac{A_s Z_L + B_s}{C_s Z_L + D_s} \quad . \qquad (3.02\text{-}1)$$

Setting $Z_{in} = Z_L = Z_{I1}$ and solving for Z_{I1} in terms of A, B, C, and D gives

$$Z_{I1} = \sqrt{\frac{AB}{CD}} \quad . \qquad (3.02\text{-}2)$$

The same procedure carried out with respect to End 2 gives

$$Z_{I2} = \sqrt{\frac{DB}{CA}} \quad . \qquad (3.02\text{-}3)$$

Figure 3.02-3 shows a network with a generator whose internal impedance is the same as the image impedance at End 1 and with a load impedance on the right equal to the image impedance at End 2. With the terminations matched to the image impedances in this manner it can be shown that

$$\frac{E_1}{E_2} = \sqrt{\frac{Z_{I1}}{Z_{I2}}}\, e^{\gamma} \qquad (3.02\text{-}4)$$

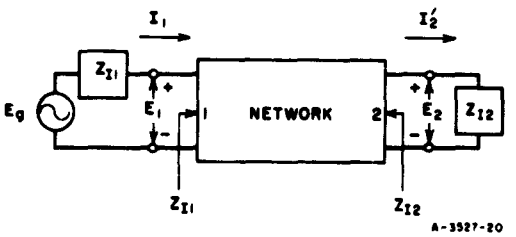

FIG. 3.02-3 NETWORK HAVING TERMINATIONS WHICH ARE MATCHED ON THE IMAGE BASIS

or

$$\frac{E_1}{E_2}\sqrt{\frac{Z_{I2}}{Z_{I1}}} = e^{\gamma} \qquad (3.02\text{-}5)$$

where

$$\gamma = \alpha + j\beta = ln\,[\sqrt{AD} + \sqrt{BC}] \qquad (3.02\text{-}6)$$

is the *image propagation function*, α is the *image attenuation* in nepers,* and β is the *image phase* in radians. Note that the $\sqrt{Z_{I2}/Z_{I1}}$ factor in Eq. (3.02-5) has the effect of making γ independent of the relative impedance levels at Ends 1 and 2, much as does the $\sqrt{R_2/R_1}$ factor in Eq. (2.10-4). An alternative form of Eq. (3.02-5) is

$$\gamma = \alpha + j\beta = ln\sqrt{\frac{E_1 I_1}{E_2 I_2'}} \qquad (3.02\text{-}7)$$

where $I_1 = E_1/Z_{I1}$ and $I_2' = E_2/Z_{I2}$ are as defined in Fig. 3.02-3.

It should be emphasized that the image propagation function defines the transmission through the circuit as indicated by Eq. (3.02-4), (3.02-5), or (3.02-7) *only if the terminations match the image impedances as in Fig. 3.02-3.* The effects of mismatch will be discussed in Sec. 3.07. For a reciprocal network the image propagation function is the same for propagation in either direction even though the network may not be symmetrical.

SEC. 3.03, RELATION BETWEEN THE IMAGE PARAMETERS AND GENERAL CIRCUIT PARAMETERS, OPEN-CIRCUIT IMPEDANCES, AND SHORT-CIRCUIT ADMITTANCES

The transmission properties of a linear two-port network can be defined in terms of its image parameters as well as in terms of the various parameters discussed in Secs. 2.05 to 2.07. Any of these other parameters can be computed from the image parameters and vice versa. These various relationships are summarized in Tables 3.03-1 and 3.03-2. For simplicity, only equations for reciprocal networks are included.

* To change nepers to decibels multiply nepers by 8.686.

Table 3.03-1

IMAGE PARAMETERS IN TERMS OF GENERAL CIRCUIT PARAMETERS, OPEN-CIRCUIT IMPEDANCES, OR SHORT-CIRCUIT ADMITTANCES

IMAGE PARAMETER	IN TERMS OF A,B,C,D	IN TERMS OF $z_{11},z_{12}=z_{21},z_{22}$	IN TERMS OF $y_{11},y_{12}=y_{21},y_{22}$	IN CONVENIENT MIXED FORM
Z_{I1}	$\sqrt{\frac{AB}{CD}}$	$\sqrt{\frac{z_{11}\,\Delta_z}{z_{22}}}$	$\sqrt{\frac{y_{22}}{y_{11}\,\Delta_y}}$	$\sqrt{\frac{z_{11}}{y_{11}}}$
Z_{I2}	$\sqrt{\frac{DB}{CA}}$	$\sqrt{\frac{z_{22}\,\Delta_z}{z_{11}}}$	$\sqrt{\frac{y_{11}}{y_{22}\,\Delta_y}}$	$\sqrt{\frac{z_{22}}{y_{22}}}$
$\gamma=\alpha+j\beta$	$\coth^{-1}\sqrt{\frac{AD}{BC}}$	$\coth^{-1}\sqrt{\frac{z_{11}z_{22}}{\Delta_z}}$	$\coth^{-1}\sqrt{\frac{y_{11}y_{22}}{\Delta_y}}$	$\coth^{-1}\sqrt{z_{11}y_{11}}$ $=\coth^{-1}\sqrt{z_{22}y_{22}}$
	$\cosh^{-1}\sqrt{AD}$	$\cosh^{-1}\left(\frac{\sqrt{z_{11}z_{22}}}{z_{21}}\right)$	$\cosh^{-1}\left(\frac{\sqrt{y_{11}y_{22}}}{y_{21}}\right)$	
	$\sinh^{-1}\sqrt{BC}$	$\sinh^{-1}\left(\frac{\sqrt{\Delta_z}}{z_{21}}\right)$	$\sinh^{-1}\left(\frac{\sqrt{\Delta_y}}{y_{21}}\right)$	
where $\Delta_z = z_{11}z_{22}-z_{12}^2$, $\Delta_y = y_{11}y_{22}-y_{12}^2$,				

Table 3.03-2

GENERAL CIRCUIT PARAMETERS, OPEN-CIRCUIT IMPEDANCES, AND SHORT-CIRCUIT ADMITTANCES IN TERMS OF IMAGE PARAMETERS

$A=\sqrt{\frac{Z_{I1}}{Z_{I2}}}\cosh\gamma$,	$B=\sqrt{Z_{I1}Z_{I2}}\sinh\gamma$
$C=\frac{\sinh\gamma}{\sqrt{Z_{I1}Z_{I2}}}$,	$D=\sqrt{\frac{Z_{I2}}{Z_{I1}}}\cosh\gamma$
$z_{11}=Z_{I1}\coth\gamma$,	$z_{12}=\frac{\sqrt{Z_{I1}Z_{I2}}}{\sinh\gamma}$
$z_{21}=z_{12}$,	$z_{22}=Z_{I2}\coth\gamma$
$y_{11}=Y_{I1}\coth\gamma$,	$y_{12}=\frac{-\sqrt{Y_{I1}Y_{I2}}}{\sinh\gamma}$
$y_{21}=y_{12}$,	$y_{22}=Y_{I2}\coth\gamma$
where $Y_{I1}=\frac{1}{Z_{I1}}$ and $Y_{I2}=\frac{1}{Z_{I2}}$.	

SEC. 3.04, IMAGE PARAMETERS FOR SOME COMMON STRUCTURES

The image parameters of the *L*-section network in Fig. 3.04-1 are given by

$$Z_{I1} = \sqrt{Z_a(Z_a + Z_c)} \qquad (3.04\text{-}1)$$

$$= \sqrt{Z_a Z_c}\sqrt{1 + \frac{Z_a}{Z_c}} \qquad (3.04\text{-}2)$$

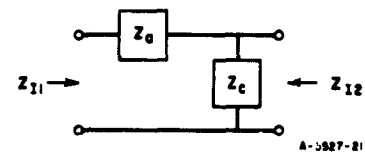

FIG. 3.04-1 AN L-SECTION NETWORK

$$Z_{I2} = \frac{Z_a Z_c}{\sqrt{Z_a(Z_a + Z_c)}} \qquad (3.04\text{-}3)$$

$$= \frac{\sqrt{Z_a Z_c}}{\sqrt{1 + \frac{Z_a}{Z_c}}} \qquad (3.04\text{-}4)$$

$$\gamma = \coth^{-1}\sqrt{1 + \frac{Z_c}{Z_a}} \qquad (3.04\text{-}5)$$

$$= \cosh^{-1}\sqrt{1 + \frac{Z_a}{Z_c}} \qquad (3.04\text{-}6)$$

$$= \sinh^{-1}\sqrt{\frac{Z_a}{Z_c}} \qquad (3.04\text{-}7)$$

Note that by Eqs. (3.04-2) and (3.04-4)

$$Z_{I1} = \frac{Z_a Z_c}{Z_{I2}} \qquad (3.04\text{-}8)$$

For the symmetrical *T*-section in Fig. 3.04-2

$$Z_{I1} = Z_{I2} = \sqrt{Z_a(Z_a + 2Z_b)} \qquad (3.04\text{-}9)$$

$$\gamma = 2 \coth^{-1} \sqrt{1 + \frac{2Z_b}{Z_a}} \quad (3.04\text{-}10)$$

$$= 2 \cosh^{-1} \left(1 + \frac{Z_a}{2Z_b}\right) \quad (3.04\text{-}11)$$

$$= 2 \sinh^{-1} \sqrt{\frac{Z_a}{2Z_b}} \quad (3.04\text{-}12)$$

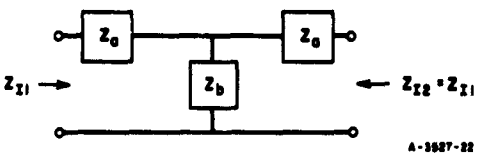

FIG. 3.04-2 A SYMMETRICAL T–SECTION NETWORK

Note that the circuit in Fig. 3.04-2 can be formed by two L-sections as in Fig. 3.04-1 put back to back so that Z_b in Fig. 3.04-2 is one-half of Z_e in Fig. 3.04-1. Then Z_{I1} will be the same for both networks and γ for the T-section is twice that for the L-section.

For the π-section in Fig. 3.04-3 the image admittances are

$$Y_{I1} = Y_{I2} = \sqrt{Y_1(Y_1 + 2Y_3)} \quad (3.04\text{-}13)$$

and

$$\gamma = 2 \coth^{-1} \sqrt{1 + \frac{2Y_3}{Y_1}} \quad (3.04\text{-}14)$$

$$= 2 \cosh^{-1} \left(1 + \frac{Y_1}{2Y_3}\right) \quad (3.04\text{-}15)$$

$$= 2 \sinh^{-1} \sqrt{\frac{Y_1}{2Y_3}} \quad (3.04\text{-}16)$$

A π-section can also be constructed from two half sections back to back, so that $Y_1 = 1/Z_e$ and $Y_3 = 1/(2Z_a)$. For Fig. 3.04-1, $Y_{I2} = 1/Z_{I2}$ will then be the same as $Y_{I2} = Y_{I1}$ in Fig. 3.04-3, while γ for Fig. 3.04-3 will again be twice that for Fig. 3.04-1.

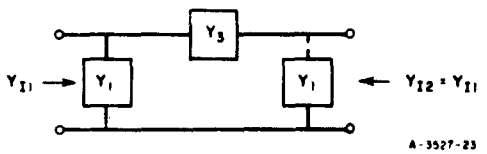

FIG. 3.04-3 A SYMMETRICAL π–SECTION NETWORK

For a uniform transmission line of length l, characteristic impedance Z_0, and propagation constant $\gamma_t = \alpha_t + j\beta_t$ per unit length,

$$Z_{I1} = Z_{I2} = Z_0 \tag{3.04-17}$$

$$\gamma = \gamma_t l = \alpha_t l + j\beta_t l \tag{3.04-18}$$

SEC. 3.05, THE SPECIAL IMAGE PROPERTIES OF DISSIPATIONLESS NETWORKS

By Table 3.03-1

$$Z_{I1} = \sqrt{\frac{z_{11}}{y_{11}}} \tag{3.05-1}$$

while

$$\gamma = \alpha + j\beta = \coth^{-1}\sqrt{z_{11}y_{11}} \quad . \tag{3.05-2}$$

For a dissipationless network, we may write for frequencies $p = j\omega$

$$z_{11} = j(X_{oc})_1 \tag{3.05-3}$$

and

$$y_{11} = \frac{1}{j(X_{sc})_1} \tag{3.05-4}$$

where $j(X_{oc})_1$ is the impedance at End 1 of the network with End 2 open-circuited, and $j(X_{sc})_1$ is the impedance at End 1 with End 2 short-circuited. Then by Eqs. (3.05-1) to (3.05-4), for dissipationless networks

$$Z_{I1} = \sqrt{-(X_{oc})_1(X_{sc})_1} \tag{3.05-5}$$

and

$$\gamma = \alpha + j\beta = \coth^{-1}\sqrt{\frac{(X_{oc})_1}{(X_{sc})_1}} \quad . \tag{3.05-6}$$

The inverse, hyperbolic cotangent function in Eq. (3.05-6) is a multivalued function, whose various possible values all differ by multiples of $j\pi$. For this reason, it is convenient to write Eq. (3.05-6) in the form

$$\gamma = \alpha + j\beta = \coth^{-1}\sqrt{\frac{(X_{oc})_1}{(X_{sc})_1}} + jn\pi \qquad (3.05\text{-}7)$$

where the inverse hyperbolic function is to be evaluated to give an imaginary part having minimum magnitude, and where the appropriate value for the integer n must be determined by examination of the circuit under consideration. Equation (3.05-7) also has the equivalent form

$$\gamma = \alpha + j\beta = \tanh^{-1}\sqrt{\frac{(X_{oc})_1}{(X_{sc})_1}} + j(2n-1)\frac{\pi}{2} \quad . \qquad (3.05\text{-}8)$$

Two distinct cases occur in the evaluation of Eq. (3.05-5) and Eq. (3.05-7) or (3.05-8) depending on whether $(X_{oc})_1$ and $(X_{sc})_1$ have the same sign or opposite signs. These two cases will be summarized separately.

Case A, Condition for a Pass Band—In this case $(X_{oc})_1$ and $(X_{sc})_1$ have opposite signs and

$$Z_{I1} = \sqrt{-(X_{oc})_1 (X_{sc})_1} = \text{real and positive.} \qquad (3.05\text{-}9)$$

It can be shown that, at the same time, the condition

$$Z_{I2} = \sqrt{-(X_{oc})_2 (X_{sc})_2} = \text{real and positive.} \qquad (3.05\text{-}10)$$

must also exist, where $(X_{oc})_2$ and $(X_{sc})_2$ are the open- and short-circuit impedances measured from End 2. Under these conditions, Eqs. (3.05-7) and (3.05-8) yield for α and β,

$$\alpha = 0 \qquad (3.05\text{-}11)$$

$$\beta = -\cot^{-1}\sqrt{\left|\frac{(X_{oc})_1}{(X_{sc})_1}\right|} \quad \text{radians}$$

$$= \left[\tan^{-1}\sqrt{\left|\frac{(X_{oc})_1}{(X_{sc})_1}\right|}\right] - \frac{\pi}{2} \quad \text{radians} \quad . \qquad (3.05\text{-}12)$$

Note that for this pass-band case, the attenuation is zero while the phase is generally non-zero and varying with frequency. In Eqs. (3.05-11) and (3.05-12) the $n\pi$ term has been omitted since the multivalued nature of these inverse trigonometric functions will be familiar to the reader (though perhaps the multivalued nature of inverse hyperbolic functions may not).

Case B, Conditions for a Stop Band—In this case $(X_{oc})_1$ and $(X_{sc})_1$ [and also $(X_{oc})_2$ and $(X_{sc})_2$] have the same sign. Then

$$Z_{I1} = \sqrt{-(X_{oc})_1(X_{sc})_1} = jX_{I1} \qquad (3.05\text{-}13)$$

and

$$Z_{I2} = \sqrt{-(X_{oc})_2(X_{sc})_2} = jX_{I2} \qquad (3.05\text{-}14)$$

are both purely imaginary. Both X_{I1} and X_{I2} must have positive slopes *vs.* frequency, in accord with Foster's reactance theorem. If $(X_{oc})_1 > (X_{sc})_1$ Eq. (3.05-7) should be used to obtain α and β:

$$\alpha = \coth^{-1}\sqrt{\frac{(X_{oc})_1}{(X_{sc})_1}} \quad \text{nepers} \qquad (3.05\text{-}15)$$

and

$$\beta = n\pi \quad \text{radians} \quad . \qquad (3.05\text{-}16)$$

If $(X_{oc})_1 < (X_{sc})_1$, Eq. (3.05-8) should be used, and it gives

$$\alpha = \tanh^{-1}\sqrt{\frac{(X_{oc})_1}{(X_{sc})_1}} \quad \text{nepers} \qquad (3.05\text{-}17)$$

and

$$\beta = (2n - 1)\frac{\pi}{2} \quad \text{radians} \quad . \qquad (3.05\text{-}18)$$

Note that for this stop-band case the image attenuation is non-zero and will vary with frequency. Meanwhile, the image phase is constant *vs.* frequency at some multiple of π, or odd multiple of $\pi/2$. However, it will be found that the image phase can make discrete jumps at points in the stop band where there are poles of attenuation for frequencies $j\omega$.

A similar analysis for dissipationless networks can be carried out using the various other expressions for the image parameters in Secs. 3.03 and 3.04. The various equations given for the image propagation constant will involve inverse hyperbolic functions of a purely real or purely imaginary argument. Due to the multivalued nature of these inverse hyperbolic functions care must be taken in evaluating them. Table 3.05-1 should prove helpful for this purpose. Note that in some cases a different equation must be used depending on whether $|u|$ or $|v|$ is greater or less than one. This is because, for example, $\cosh^{-1}w$ when taken to be a function of a real variable cannot be evaluated for $w = |u| < 1$; if however, w is a function of a complex variable the above example has a value, namely, $j(\cos^{-1}u)$. The proper value of the integer n to be used with the various equations in Table 3.05-1 must be determined by examination of the circuit at some frequency where the transmission phase is easily established. As was done in the case of Eqs. (3.05-11) and (3.05-12), the $n\pi$ terms have been omitted for forms involving inverse trigonometric functions since their multivalued nature is much more widely familiar than is that of inverse hyperbolic functions.

Table 3.05-1

EVALUATION OF SOME INVERSE HYPERBOLIC FUNCTIONS
FOR PURELY REAL OR PURELY IMAGINARY ARGUMENTS

In general, $W = U + jV$, $w = u + jv$, and n is an integer (positive, negative or zero)		
Function	**Case of $w = u$**	**Case of $w = jv$**
$W = \coth^{-1} w$	If $\lvert u\rvert > 1$, $W = \coth^{-1} u + jn\pi$	$W = 0 + j(-\cot^{-1} v)$ $= 0 + j\left[(\tan^{-1} v) - \frac{\pi}{2}\right]$
	If $\lvert u\rvert < 1$, $W = \tanh^{-1} u + j(2n-1)\frac{\pi}{2}$	
$W = \sinh^{-1} w$	$W = (-1)^{\lvert n\rvert} \sinh^{-1} u + jn\pi$	If $\lvert v\rvert \geq 1$, $W = \cosh^{-1} v + j(2n-1)\frac{\pi}{2}$ { n = odd if $v > 1$; n = even if $v < -1$
		If $\lvert v\rvert \leq 1$, $W = 0 + j \sin^{-1} v$
$W = \cosh^{-1} w$	If $\lvert u\rvert > 1$, $W = \cosh^{-1} u + jn\pi$ { n = even if $u > 1$; n = odd if $u < -1$.	$W = \sinh^{-1} v + j(2n-1)\frac{\pi}{2}$ { n = odd if $v > 0$. ; n = even if $v < 0$.
	If $\lvert u\rvert < 1$ $W = 0 + j \cos^{-1} u$	

SEC. 3.06, CONSTANT-k AND m-DERIVED FILTER SECTIONS

Constant-k and m-derived filters are classic examples of filters which are designed from the image point of view. Their properties will be briefly summarized in order to illustrate some of the image properties of dissipationless networks discussed in the preceding section, and to provide reference data. The filter sections shown are all normalized so that their image impedance is $R_0' = 1$ ohm at $\omega' = 0$ and their cutoff frequency occurs at $\omega_1' = 1$ radian/sec. However, these normalized circuits can easily be changed to other impedance and frequency scales. Each resistance, inductance, or capacitance is scaled using

$$R = \left(\frac{R_0}{R_0'}\right)R' \qquad (3.06\text{-}1)$$

$$L = \left(\frac{R_0}{R_0'}\right)\left(\frac{\omega_1'}{\omega_1}\right)L' \qquad (3.06\text{-}2)$$

or

$$C = \left(\frac{R_0'}{R_0}\right)\left(\frac{\omega_1'}{\omega_1}\right)C' \qquad (3.06\text{-}3)$$

where R', L', and C' are for the normalized circuit and R, L, and C are corresponding elements for the scaled circuit. The ratio R_0/R_0' defines the change in impedance level while ω_1/ω_1' defines the change in frequency scale.

Figure 3.06-1(a) shows a normalized constant-k filter half section. Its image impedances are

$$Z_{IT} = \sqrt{1 - (\omega')^2} \qquad (3.06\text{-}4)$$

and

$$Z_{I\pi} = \frac{1}{\sqrt{1 - (\omega')^2}} = \frac{1}{Z_{IT}} \qquad (3.06\text{-}5)$$

Its propagation function is

$$\gamma = \alpha + j\beta = 0 + j \sin^{-1}\omega' \qquad (3.06\text{-}6)$$

for the $0 \leq \omega' \leq 1$ pass band, and

$$\gamma = \alpha + j\beta = \cosh^{-1}\omega' + j\frac{\pi}{2} \qquad (3.06\text{-}7)$$

for the $1 \leq \omega' \leq \infty$ stop band, where α is in nepers and β is in radians.

Figures 3.06-1(b), (c) show sketches of the image impedance and attenuation characteristics of this structure. Note that, as discussed

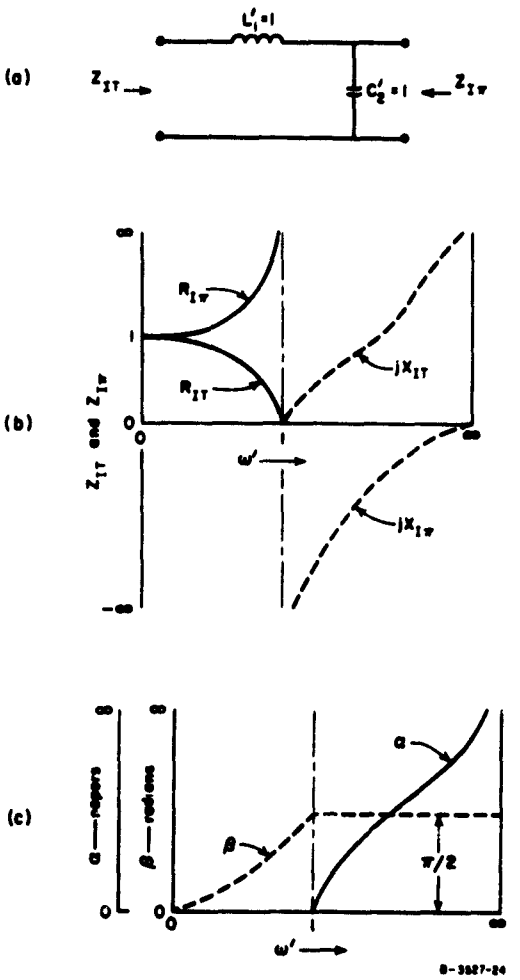

FIG. 3.06-1 THE IMAGE PROPERTIES OF NORMALIZED, CONSTANT-k HALF SECTIONS

in Sec. 3.05, Z_{IT} and $Z_{I\pi}$ are purely real in the pass band and purely imaginary in the stop band. Also note that $\alpha = 0$ in the pass band while β is constant in the stop band.

Figure 3.06-2(a) shows a "series, m-derived" half section. Its image impedances are

$$Z_{IT} = \sqrt{1 - (\omega')^2} \tag{3.06-8}$$

$$Z_{I\pi s} = \frac{1 - \left(\frac{\omega'}{\omega'_\infty}\right)^2}{\sqrt{1 - \omega'^2}} \tag{3.06-9}$$

where

$$\omega'_\infty = \frac{1}{\sqrt{1 - m^2}} \quad . \tag{3.06-10}$$

Note that Eq. (3.06-8) is identical to Eq. (3.06-4), but Eq. (3.06-9) differs from Eq. (3.06-5). The propagation function is

$$\gamma = \alpha + j\beta = 0 + j \frac{1}{2} \cos^{-1} \left[1 - \frac{2m^2}{\left(\frac{1}{\omega'}\right)^2 - (1 - m^2)} \right] \tag{3.06-11}$$

in the $0 \leq \omega' \leq 1$ pass band,

$$\gamma = \frac{1}{2} \cosh^{-1} \left[\frac{2m^2}{\left(\frac{1}{\omega'}\right)^2 - (1 - m^2)} - 1 \right] + j \frac{\pi}{2} \tag{3.06-12}$$

in the $1 = \omega' \leq \omega'_\infty$ stop band, and

$$\gamma = \frac{1}{2} \cosh^{-1} \left[1 - \frac{2m^2}{\left(\frac{1}{\omega'}\right)^2 - (1 - m^2)} \right] + j0 \tag{3.06-13}$$

in the $\omega'_\infty \leq \omega' \leq \infty$ stop band.

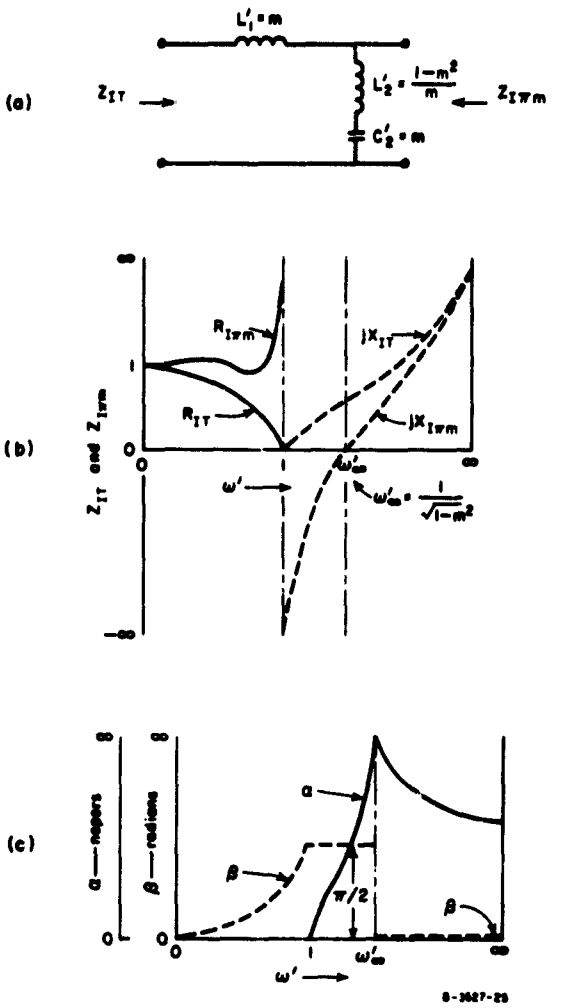

FIG. 3.06-2 NORMALIZED, SERIES, m–DERIVED HALF–SECTION CHARACTERISTICS

Figures 3.06-2(b) and (c) show sketches of the image impedance and propagation characteristics of this structure. Note that introducing a series resonance in the shunt branch in Fig. 3.06-2(a) has produced a pole of attenuation at the frequency ω'_∞ where the shunt branch short-circuits transmission. (See discussion in Sec. 2.04.) Note that $Z_{I\pi_m} = R_{I\pi_m}$ in the pass band in Fig. 3.06-2(b) is more nearly constant than is $R_{I\pi}$ in Fig. 3.06-1(b). This property of m-derived image impedances makes them helpful for improving the impedance match to resistor terminations.

The "shunt m-derived" half section in Fig. 3.06-3(a) is the dual of that in Fig. 3.06-2(a). The image impedances are

$$Z_{IT_m} = \frac{\sqrt{1-(\omega')^2}}{1-\left(\frac{\omega'}{\omega'_\infty}\right)^2} \quad , \tag{3.06-14}$$

$$Z_{I\pi} = \frac{1}{\sqrt{1-(\omega')^2}} \tag{3.06-15}$$

where again

$$\omega'_\infty = \frac{1}{\sqrt{1-m^2}} \quad , \tag{3.06-16}$$

In this case Z_{IT_m} in Eq. (3.06-14) differs from Z_{IT} in Eq. (3.06-4), but Eqs. (3.06-15) and (3.06-5) are identical. The image propagation function for this section is the same as that in Eqs. (3.06-11) to (3.06-13). Figures 3.06-3(b) and (c) show sketches of the image characteristics of this filter section. In this case, a pole of attenuation is produced at the frequency ω'_∞ where the series branch has a pole of impedance which blocks all transmission. The image impedance Z_{IT_m} is seen to be more nearly constant in the pass band than was Z_{IT} in Fig. 3.06-1(b). Thus, m-derived half sections of this type are also useful for improving the impedance match to resistor terminations.

Figure 3.06-4(a) and (b) show how constant-k and m-derived half sections may be pieced together to form a sizeable filter. In this case, three constant-k half sections are used along with two, series, m-derived,

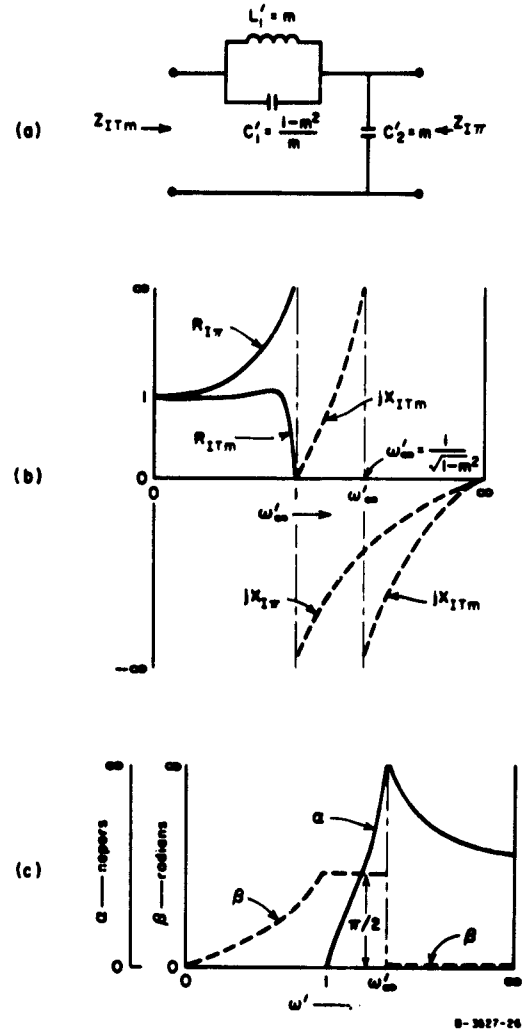

FIG. 3.06-3 NORMALIZED, SHUNT, m-DERIVED HALF-SECTION CHARACTERISTICS

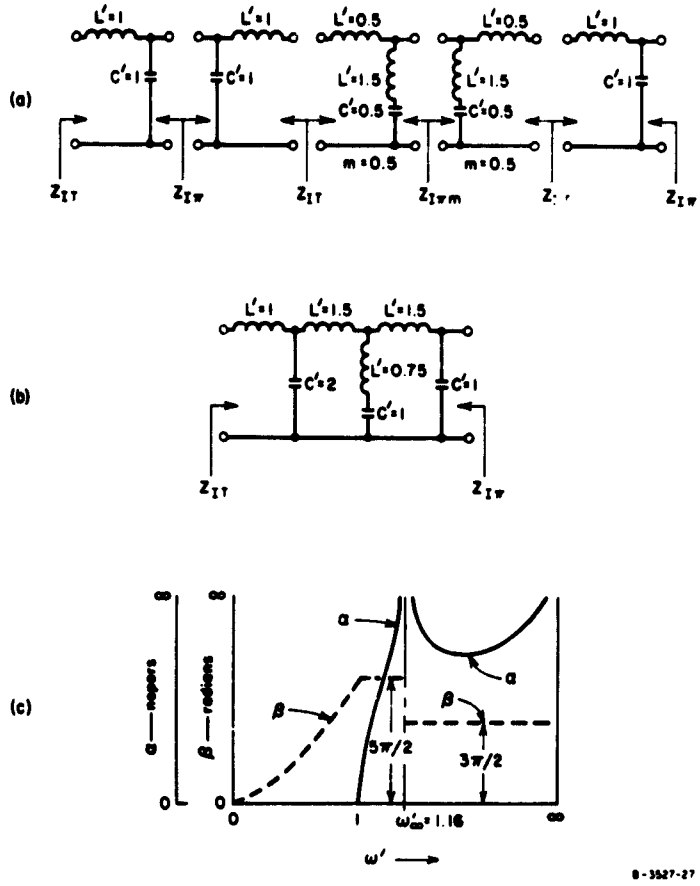

FIG. 3.06-4 A FILTER PIECED TOGETHER FROM THREE CONSTANT-k AND TWO m-DERIVED HALF SECTIONS
The resulting image propagation function is sketched at (c)

half sections. The two m-derived sections have $m = 0.5$, which introduces a pole of attenuation at $\omega'_\infty = 1.16$ and greatly increases the rate of cutoff of the filter. As indicated in Fig. 3.06-4(a) the sections are all chosen so that the image impedances match at each junction. Under these conditions when the sections are all joined together, the image attenuation and the image phase for the entire structure are simply the sum of the image attenuation and phase values for the individual sections. Likewise, with all of the sections matched to each other, the image impedances seen at the ends are the same as the image impedances of the end sections before they were connected to the interior sections.

The circuit in Fig. 3.06-4(b) would have the transmission characteristics indicated in Fig. 3.06-4(c) if it were terminated in its image impedances at both ends. However, since in practice resistor terminations are generally required, this transmission characteristic will be considerably altered (mainly in the pass band) due to the reflections at both ends of the filter. In order to reduce the magnitude of these reflections effects, it is customary with filters of this type to introduce m-derived half-sections at each end of the filter with the impedance Z_{IT_m} or $Z_{I\pi_m}$ next to the termination resistor. With $m = 0.6$, these image impedances are relatively constant in the pass band and it becomes possible to greatly reduce the reflection effects over much of the pass band. These matters will be discussed further in Secs. 3.07 and 3.08.

SEC. 3.07, THE EFFECTS OF TERMINATIONS WHICH MISMATCH THE IMAGE IMPEDANCES

The resistance terminations used on dissipationless filter structures cannot match the image impedance of the structure except at discrete frequencies in the pass band. As a result of the multiple reflections that occur, the performance of the filter may be considerably altered from that predicted by the image propagation function. This alteration is most severe in the pass band and in the stop band near cutoff. Formulas which account for the effects of such terminal reflections are summarized below.

Consider the circuit in Fig. 3.07-1 whose image impedances, Z_{I1} and Z_{I2}, may differ considerably from R_1 and R_2. The voltage attenuation ratio, E_g/E_2, may be calculated from the image parameters and the terminations using the equation

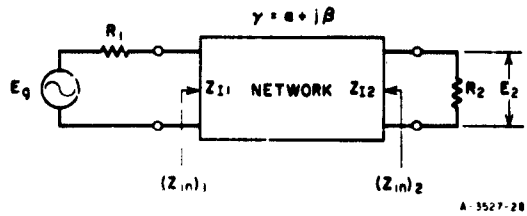

FIG. 3.07-1 NETWORK DISCUSSED IN SEC. 3.07

$$\frac{E_g}{E_2} = 2\sqrt{\frac{Z_{I1}}{Z_{I2}}}\, e^{\gamma} \left[\frac{1 - e^{-2\gamma}\Gamma_{I1}\Gamma_{I2}}{\tau_{I1}\tau_{I2}}\right] \tag{3.07-1}$$

where

$$\Gamma_{I1} = \frac{R_1 - Z_{I1}}{R_1 + Z_{I1}} \tag{3.07-2}$$

and

$$\Gamma_{I2} = \frac{R_2 - Z_{I2}}{R_2 + R_{I2}} \tag{3.07-3}$$

are the reflection coefficients at Ends 1 and 2 while

$$\tau_{I1} = \frac{2Z_{I1}}{R_1 + Z_{I1}} \tag{3.07-4}$$

and

$$\tau_{I2} = \frac{2R_2}{R_2 + Z_{I2}} \tag{3.07-5}$$

are the transmission coefficients (see Sec. 2.08). Note that these reflection and transmission coefficients are defined with respect to the image impedances rather than with respect to the actual input impedances $(Z_{in})_1$ and $(Z_{in})_2$.

The actual input impedance seen looking in End 1 with End 2 terminated in R_2 is

$$(Z_{in})_1 = Z_{I1}\left[\frac{1 + \Gamma_{I2}e^{-2\gamma}}{1 - \Gamma_{I2}e^{-2\gamma}}\right] . \qquad (3.07\text{-}6)$$

By analogy, $(Z_{in})_2$ in Fig. 3.07-1 is

$$(Z_{in})_2 = Z_{I2}\left[\frac{1 + \Gamma_{I1}e^{-2\gamma}}{1 - \Gamma_{I1}e^{-2\gamma}}\right] . \qquad (3.07\text{-}7)$$

Equations (3.07-1) to (3.07-7) apply whether the circuit has dissipation or not.

For a dissipationless network at pass band frequencies where $\gamma = 0 \pm jn\pi\big|_{n=1,2,3,\ \ldots}$ Eq. (3.07-6) shows that

$$(Z_{in})_1 = \frac{Z_{I1}}{Z_{I2}} R_2 \qquad (3.07\text{-}8)$$

while at frequencies where $\gamma = 0 \pm j(2n - 1)(\pi/2)\big|_{n=1,2,3,\ \ldots,}$

$$(Z_{in})_1 = \frac{Z_{I1}Z_{I2}}{R_2} \qquad (3.07\text{-}9)$$

where Z_{I1} and Z_{I2} will be purely real. Analogous expressions also exist for $(Z_{in})_2$.

Equation (3.07-1) is quite general, and it can be used with Eqs. (2.11-2) and (2.11-4) for computing the attenuation of a network. However, simpler expressions (about to be presented) can be used if the network is dissipationless. Such expressions become especially simple if the dissipationless network is symmetrical (*i.e.*, $Z_{I1} = Z_{I2}$) and has symmetrical terminations (*i.e.*, $R_1 = R_2$). Another case of relative simplicity is that of a dissipationless antimetrical network (see Sec. 2.11) with antimetrical terminations. Such a filter will satisfy the conditions

$$Z_{I1} = \frac{R_0^2}{Z_{I2}} \qquad (3.07\text{-}10)$$

$$R_1 = \frac{R_0^2}{R_2} \qquad (3.07\text{-}11)$$

at all frequencies, where R_0 is a positive, real constant. The constant-k half section in Fig. 3.06-1 is an example of an antimetrical network. The filter in Fig. 3.06-4 also satisfies the antimetry condition given by Eq. (3.07-10).

For dissipationless symmetrical networks with symmetrical terminations, $Z_{I1} = R_{I1}$ in the pass band and the attenuation is

$$L_A = 10 \log_{10} \left[1 + \frac{1}{4} \left(\frac{R_{I1}}{R_1} - \frac{R_1}{R_{I1}} \right)^2 \sin^2 \beta \right] \quad \text{db} \qquad (3.07\text{-}12)$$

while in the stop band $Z_{I1} = jX_{I1}$ and

$$L_A = 10 \log_{10} \left[1 + \frac{1}{4} \left(\frac{X_{I1}}{R_1} + \frac{R_1}{X_{I1}} \right)^2 \sinh^2 \alpha \right] \quad \text{db} \quad . \qquad (3.07\text{-}13)$$

Similarly for dissipationless antimetrical networks with antimetrical terminations, in the pass band

$$L_A = 10 \log_{10} \left[1 + \frac{1}{4} \left(\frac{R_{I1}}{R_1} - \frac{R_1}{R_{I1}} \right)^2 \cos^2 \beta \right] \quad \text{db} \qquad (3.07\text{-}14)$$

while in the stop band Eq. (3.07-13) applies just as for the symmetrical case. For the symmetrical case

$$\Gamma_{I1} = \Gamma_{I2} \qquad (3.07\text{-}15)$$

while for the antimetrical case

$$\Gamma_{I1} = -\Gamma_{I2} \quad . \qquad (3.07\text{-}16)$$

For the dissipationless symmetrical case the stop-band image phase is a multiple of π radians, while in the dissipationless antimetric case it is an *odd* multiple of $\pi/2$ radians.

The actual pass-band attenuation which will result from mismatched image impedances is seen by Eqs. (3.07-12) and (3.07-14) to depend strongly on the image phase, β. For given Z_{I1} and R_1 it is easily shown that the maximum possible pass-band attenuation in a dissipationless symmetrical or antimetrical network with symmetrical or antimetrical terminations, respectively, is

$$L_A = 20 \log_{10} \left(\frac{a^2 + 1}{2a} \right) \quad \text{db} \qquad (3.07\text{-}17)$$

where

$$a = \frac{Z_{I1}}{R_1} \text{ or } \frac{R_1}{Z_{I1}} \quad ,$$

with either definition giving the same answer. For symmetrical networks, the value given by Eq. (3.07-17) applies when $\beta = (2n - 1)\pi/2$ radians while $L_A = 0$ when $\beta = n\pi$ radians (where n is an integer). For antimetrical networks Eq. (3.07-17) applies when $\beta = n\pi$ radians while $L_A = 0$ when $\beta = (2n - 1)\pi/2$ radians. Figure 3.07-2 shows a plot of maximum L_A *vs.* a, and also shows the corresponding input VSWR.

SEC. 3.08, DESIGN OF MATCHING END SECTIONS TO IMPROVE THE RESPONSE OF FILTERS DESIGNED ON THE IMAGE BASIS

As mentioned in Sec. 3.06, one way in which the pass-band response of constant-k filters can be improved is to use m-derived half sections at the ends. Experience shows that a half section with m about 0.6 will cause Z_{IT_m} or $Z_{I\pi_m}$ to give the best approximation of a constant resistance in the pass band, and hence will cause the ends of the filter to give the best match to resistor terminations. As an example, Fig. 3.08-1 shows the normalized filter structure in Fig. 3.06-4(b) with matching sections added to improve the pass-band match to the one-ohm terminations shown. The matching sections also introduce poles of attenuation at $\omega'_\infty = 1.25$, which will further sharpen the cutoff characteristics of the filter.

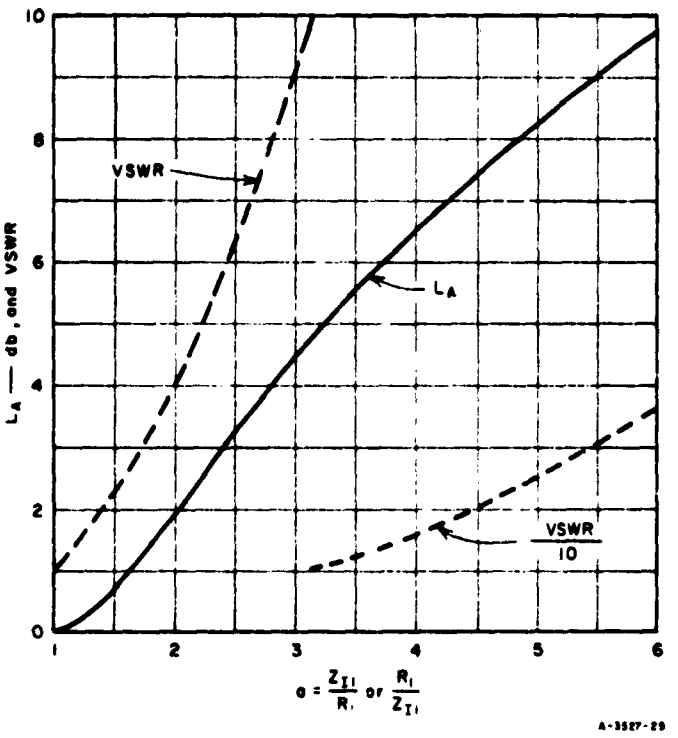

FIG. 3.07-2 MAXIMUM POSSIBLE PASS-BAND ATTENUATION AND VSWR FOR DISSIPATIONLESS SYMMETRICAL NETWORKS WITH SYMMETRICAL TERMINATIONS, OR DISSIPATIONLESS ANTIMETRICAL NETWORKS WITH ANTIMETRICAL TERMINATIONS
These values will apply if $\beta = (2n-1)(\pi/2)\big|_{n=1,2,3,\ldots,}$ for the symmetrical case or $\beta = n\pi\big|_{n=1,2,3,\ldots,}$ for the antimetrical case

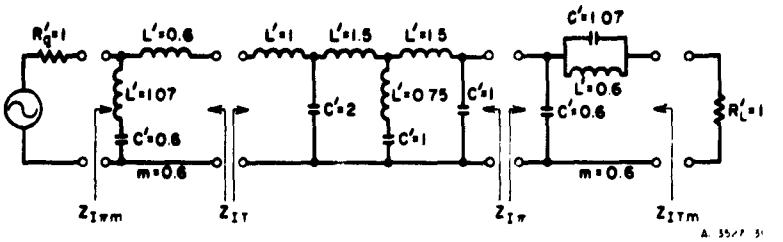

FIG. 3.08-1 THE NORMALIZED FILTER CIRCUIT IN FIG. 3.06-4(b) WITH m-DERIVED HALF SECTIONS ADDED TO IMPROVE THE PASS-BAND IMPEDANCE MATCH TO RESISTOR TERMINATIONS

In the design of microwave filter structures on the image basis, it is often desirable that the matching end sections be of the same general form as the main part of the filter. Consider the case of a wide band, band-pass filter to be constructed using filter sections as shown in Fig. 3.08-2(a). The filter sections have image characteristics as shown in Fig. 3.08-2(b), (c). Figure 3.08-3 shows the left half of a symmetrical filter formed from such sections. In this filter the interior sections of the filter are all alike, but two sections at each end are different in order to improve the pass-band match to the terminations. The design of such end sections will now be considered.

As is seen from Fig. 3.08-2(c), each section of the filter has a mid-band image phase shift of $\beta = \pi/2$. The total midband image phase shift for the end matching network in Fig. 3.08-3 at f_0 is thus $\beta = \pi$. At mid-band, then, the end matching network will operate similarly to a half-wavelength transmission line, and in Fig. 3.08-3

$$Z_{in}\Big|_{f=f_0} = R_g \quad . \tag{3.08-1}$$

Thus, if Z_I is the image impedance of the interior sections of the filter, and Z_{I_e} is the image impedance of the sections in the end matching network, then if

$$Z_I\Big|_{f=f_0} = R_g \tag{3.08-2}$$

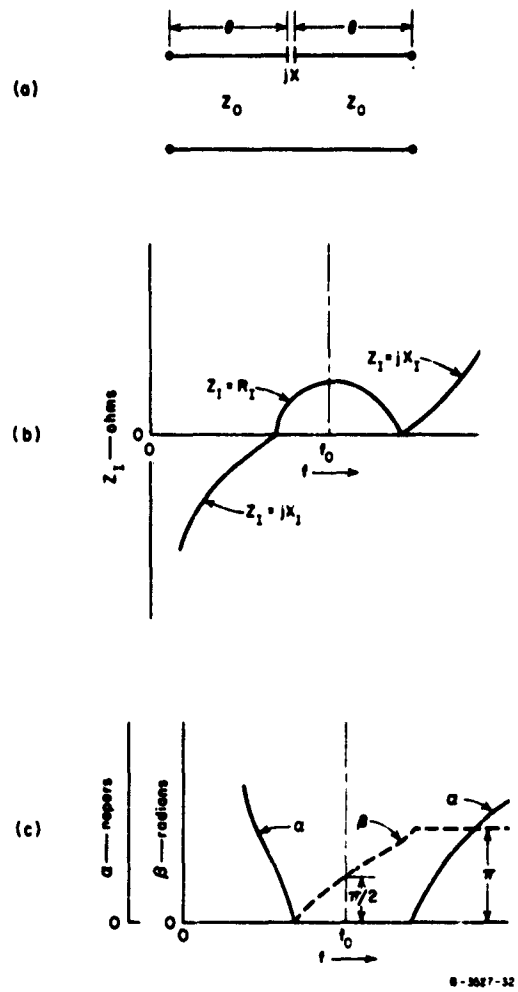

FIG. 3.08-2 A BAND-PASS FILTER SECTION USING TRANSMISSION LINES, AND ITS IMAGE CHARACTERISTICS

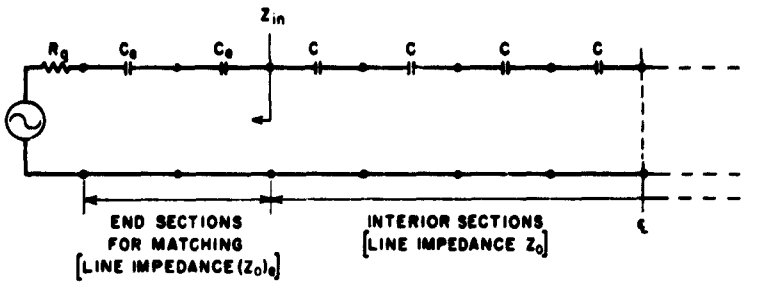

FIG. 3.08-3 ONE-HALF OF A SYMMETRICAL FILTER COMPOSED OF SECTIONS OF THE TYPE IN FIG. 3.08-2

a perfect match is assured at f_0, regardless of the size of Z_{Ie} at that frequency. At pass-band frequencies $f_{\pi/2}$ and $f_{3\pi/2}$, where the image phase shift of the end matching network is $\beta = \pi/2$ and $3\pi/2$, respectively,

$$Z_{in} = \frac{(Z_{Ie})^2}{R_g} \tag{3.08-3}$$

similarly to Eq. (3.07-9). Thus, setting $Z_{in} = Z_I$ and solving for Z_{Ie} gives

$$Z_{Ie} = \sqrt{Z_I R_g} \tag{3.08-4}$$

as the condition for a perfect impedance match when $\beta = \pi/2$ or $3\pi/2$ for the end matching network. By such procedures a perfect impedance match can be assured when the end matching network has $\pi/2$, π, or $3\pi/2$ radians image phase.

Figure 3.08-4 shows how the image impedance of the end matching network might compare with the image impedance of the interior sections for a practical design. In this case R_g is made a little less than Z_I for the interior sections at f_0, but Z_I and Z_{Ie} are both made to be equal to R_g at f_a and f_b, a little to each side of f_0, so that a perfect match will be achieved at those two frequencies. This procedure will result in a small mismatch in the vicinity of f_0, but should improve the over-all results. The end matching network is made to be more broadband than the

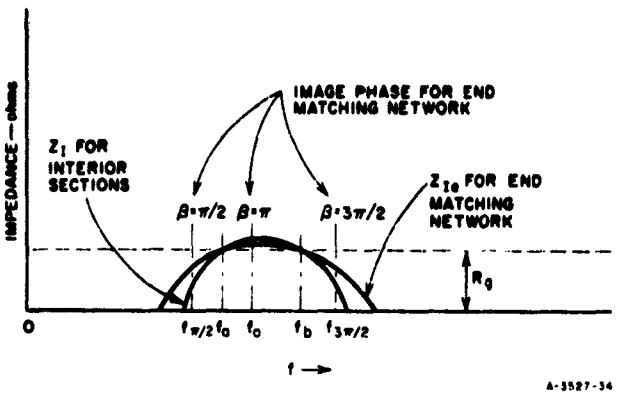

FIG. 3.08-4 RELATIVE IMAGE IMPEDANCE CHARACTERISTICS FOR THE END MATCHING NETWORK AND INTERIOR SECTIONS OF A PROPOSED FILTER OF THE FORM IN FIG. 3.08-3

interior sections of the filter so that the $\beta = \pi/2$ and $3\pi/2$ phase shift points will occur near the cutoff frequencies of the interior sections. The end matching network is designed so that Eq. (3.08-4) will be satisfied, at least approximately, at these two frequencies in order to give a good impedance match close to the cutoff frequencies of the filter. In this particular example there are only three degrees of freedom in the design of the end matching network, namely the size of C_e, the size of $(Z_0)_e$, and the length of the transmission lines in the sections of the end matching network. One degree of freedom is used in fixing the center frequency of the response, another may be used for setting $Z_{Ie} = R_g$ at frequency f_a in Fig. 3.08-4, and another may be used for satisfying Eq. (3.08-4) at $f_{\pi/2}$. Although matching conditions are not specifically forced at frequencies f_b and $f_{3\pi/2}$ in Fig. 3.08-4, they will be approximately satisfied because of the nearly symmetrical nature of the response about f_0.

The design procedure described above provides a perfect impedance match at certain frequencies and assures that the maximum mismatch throughout the pass band will not be large. In addition it should be recalled that perfect transmission will result at pass-band frequencies where the image phase of the over-all filter structure is a multiple of π radians, as well as at points where the image impedances are perfectly matched. These same principles also apply for the design of matching sections for other types of filters.

SEC. 3.09, MEASUREMENT OF IMAGE PARAMETERS

Occasionally it will be desirable to measure the image parameters of a circuit. A general method is to measure the input impedance at one end for open- and short-circuit terminations at the other end. Then

$$Z_{I1} = \sqrt{(Z_{oc})_1 (Z_{sc})_1} \tag{3.09-1}$$

$$Z_{I2} = \sqrt{(Z_{oc})_2 (Z_{sc})_2} \tag{3.09-2}$$

and for a reciprocal network

$$\gamma = \coth^{-1} \sqrt{\frac{(Z_{oc})_1}{(Z_{sc})_1}} \quad . \tag{3.09-3}$$

In these equations $(Z_{oc})_1$ and $(Z_{sc})_1$ are impedances measured at End 1 with End 2 open-circuited and short-circuited, respectively. Impedances $(Z_{oc})_2$ and $(Z_{sc})_2$ are corresponding impedances measured from End 2 with End 1 open-circuited or short-circuited.

If the network has negligible dissipation and is symmetrical, a convenient method due to Dawirs[5] can be used. Using this method the network is terminated at one port in a known resistive load R_L and its input impedance $Z_{in} = R_{in} + jX_{in}$ is measured at the other port. Then the image impedance Z_I can be computed from Z_{in} and R_L by the equation[5]

$$Z_I = R_L \sqrt{\frac{\left(\frac{R_{in}}{R_L}\right)^2 + \left(\frac{X_{in}}{R_L}\right)^2 - \left(\frac{R_{in}}{R_L}\right)}{\left(\frac{R_{in}}{R_L}\right) - 1}} \tag{3.09-4}$$

which applies for both the pass and stop bands.

Dawirs[5] has expressed this method in terms of a very useful chart which is reproduced in Fig. 3.09-1. This chart should be thought of as being superimposed on top of a Smith chart[6,7] with the zero "wavelengths toward generator" point coinciding with that of the Smith chart. Then

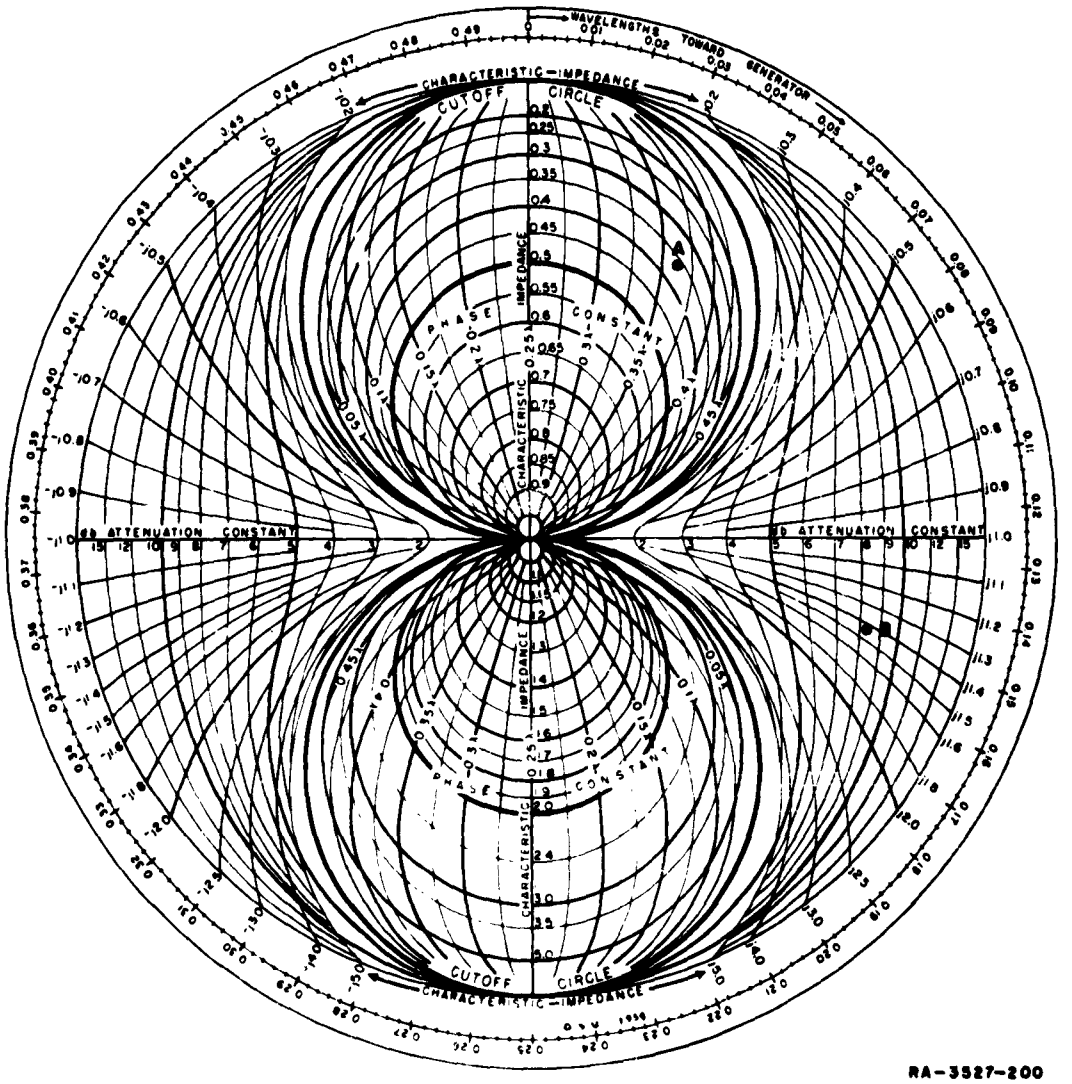

RA-3527-200

SOURCE: By courtesy of H. N. Dawirs and *Proc. IRE*.[5]

FIG. 3.09-1 DAWIRS' CHART FOR DETERMINING THE IMAGE PARAMETERS OF SYMMETRICAL, DISSIPATIONLESS NETWORKS

to obtain the image parameters, Z_{in} measured as discussed above, is normalized with respect to R_L. Next, the point Z_{in}/R_L is first plotted on a Smith chart, and then scaled to the same point on this chart by use of a scale and cursor. In the pass band the Z_{in}/R_L points will fall *within* either of the two heavy circles marked "cutoff circle," while in the stop band the Z_{in}/R_L points will fall *outside* of these circles. Further details of the use of the chart are perhaps best illustrated by examples.

Suppose that $Z_{in}/R_L = 0.20 + j\ 0.25$. Plotting this point on a Smith chart and then rescaling it to this chart gives the point shown at A in Fig. 3.09-1. The circles intersecting the vertical axis at right angles give the image impedance while the nearly vertical lines give the phase constant. Following the circle from point A around to the vertical axis gives a normalized image impedance value of $R_I/R_L = 0.35$, while the phase constant is seen to be approximately 0.37 λ. This chart uses the term "characteristic impedance" for image impedance and expresses the image phase in wavelengths for specific reference to transmission lines. However, the more general image impedance concept also applies and the corresponding image phase in radians (within some unknown multiple of π) is simply 2π times the number of wavelengths. Thus in this case $\beta = 0.37(2\pi) + n\pi$ radians.

If $Z_{in}\ R_L$ gave the point P in Fig. 3.09-1, the filter would be cut off, hence, the image impedance would be imaginary and α would be nonzero. In this case the image impedance is read by following the line to the outer edge of the chart to read $jX_I\ R_L = j\ 1.4$, while the image attenuation in db is read from the horizontal axis of the chart as being about 8.5 db. Since the network is specified to be symmetrical, the stop-band image phase will be zero or some multiple of π radians (see Sec. 3.07).

REFERENCES

1. T. E. Shea, *Transmission Networks and Wave Filters* (D. Van Nostrand Co., New York City, 1929).

2. E. A. Guillemin, *Communication Networks*, Vol. 2, Chapters 4, and 7 to 10 (John Wiley and Sons, New York City, 1935).

3. Harvard Radio Research Laboratory Staff, *Very High-Frequency Techniques*, Vol. 2, Chapters 26 and 27 by S. B. Cohn (McGraw-Hill Book Co., Inc., New York City, 1947).

4. M. E. Van Valkenburg, *Network Analysis*, Chapter 13 (Prentice-Hall, Inc., Englewood Cliffs, N.J., 1955).

5. H. N. Dawirs, "A Chart for Analyzing Transmission-Line Filters from Input Impedance Characteristics," *Proc. IRE* **43**, pp. 436-443 (April 1955).

6. P. H. Smith, "A Transmission Line Calculator," *Electronics* **12**, pp. 29-31 (January 1939).

7. E. L. Ginzton, *Microwave Measurements*, pp. 228-234 (McGraw-Hill Book Co., Inc., New York City, 1957).

CHAPTER 4

LOW-PASS PROTOTYPE FILTERS OBTAINED BY NETWORK SYNTHESIS METHODS

SEC. 4.01, INTRODUCTION

Many of the filter design methods to be discussed in later chapters of this book will make use of the lumped-element, low-pass prototype filters discussed in this chapter. Most of the low-pass, high-pass, band-pass, or band-stop microwave filters to be discussed will derive their important transmission characteristics from those of a low-pass prototype filter used in their design. Element values for such low-pass prototype filters were originally obtained by network synthesis methods of Darlington and others.[1-3] However, more recently concise equations[4-11] which are convenient for computer programming have been found for the element values of the types of prototype filters of interest in this book, and numerous filter designs have been tabulated. Some of the tables in this book were obtained from the work of Weinberg,[8,9] while others were computed at Stanford Research Institute for the purposes of this book. No discussion of formal network synthesis methods will be included in this book since these matters are discussed extensively elsewhere (see Refs. 1 to 3, for example), and since the availability of tabulated designs makes such discussion unnecessary. The main objectives of this chapter are to make clear the properties of the tabulated prototype filters, delay networks, and impedance-matching networks so that they may be used intelligently in the solution of a wide variety of microwave circuit design problems of the sorts discussed in Chapter 1.

It should be noted that the step transformers in Chapter 6 can also be used as prototypes for the design of certain types of microwave filters as is discussed in Chapter 9.

SEC. 4.02, COMPARISON OF IMAGE AND NETWORK SYNTHESIS METHODS FOR FILTER DESIGN

As was discussed in Chapter 3, the image impedance and attenuation function of a filter section are defined in terms of an infinite chain of identical filter sections connected together. Using a finite,

dissipationless filter network with resistor terminations will permit the image impedances to be matched only at discrete frequencies, and the reflection effects can cause sizeable attenuation in the pass band, as well as distortion of the stop-band edges.

In Sec. 3.08 principles were discussed for the design of end sections which reduce these reflection effects. Although such methods will definitely reduce the size of reflections in filters designed by the image method, they give no assurance as to how large the peak reflection loss values may be in the pass band. Thus, though the image method is conceptually simple, it requires a good deal of "cut and try" or "know how" if a precision design with low pass-band reflection loss and very accurately defined band edges is required.

Network synthesis methods[1,2,3] for filter design generally start out by specifying a transfer function [such as the transmission coefficient t, defined by Eq. (2.10-6)] as a function of complex frequency p. From the transfer function the input impedance to the circuit is found as a function of p. Then, by various continued-fraction or partial-fraction expansion procedures, the input impedance is expanded to give the element values of the circuit. The circuit obtained by these procedures has the same transfer function that was specified at the outset, and all guess work and "cut and try" is eliminated. Image concepts never enter such procedures, and the effects of the terminations are included in the initial specifications of the transfer function.

In general, a low-pass filter designed by the image method and an analogous filter designed for the same application by network synthesis methods will be quite similar. However, the filter designed by network synthesis methods will have somewhat different element values, to give it the specified response.

The Tchebyscheff and maximally flat transfer functions discussed in the next section are often specified for filter applications. The filters whose element values are tabulated in Sec. 4.05 will produce responses discussed in Sec. 4.03 exactly. However, in designing *microwave filters* from low-pass, lumped-element prototypes approximations will be involved. Nevertheless, the approximations will generally be very good over sizeable frequency ranges, and the use of such prototypes in determining the parameters of the microwave filter will eliminate the guess work inherent in the classical image method.

SEC. 4.03, MAXIMALLY FLAT AND TCHEBYSCHEFF FILTER ATTENUATION CHARACTERISTICS

Figure 4.03-1 shows a typical *maximally flat,** low-pass filter attenuation characteristic. The frequency ω_1', where the attenuation is L_{Ar}, is defined as the pass-band edge. This characteristic is expressed mathematically as

$$L_A(\omega') = 10 \log_{10} \left[1 + \epsilon \left(\frac{\omega'}{\omega_1'} \right)^{2n} \right] \quad \text{db} \qquad (4.03\text{-}1)$$

where

$$\epsilon = \left[\text{antilog}_{10} \frac{L_{Ar}}{10} \right] - 1 \quad . \qquad (4.03\text{-}2)$$

The response in Fig. 4.03-1 can be achieved by low-pass filter circuits such as those discussed in Secs. 4.04 and 4.05, and the parameter n in Eq. (4.03-1) corresponds to the number of reactive elements required in the circuit. This attenuation characteristic acquires its name *maximally flat* from the fact that the quantity within the square brackets in Eq. (4.03-1) has $(2n - 1)$ zero derivatives at $\omega' = 0$.

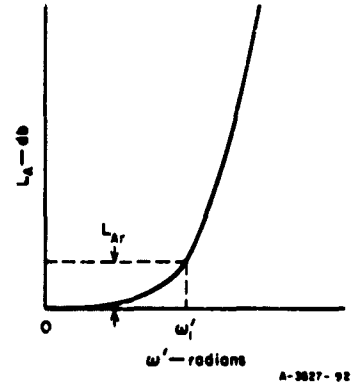

FIG. 4.03-1 A MAXIMALLY FLAT LOW-PASS ATTENUATION CHARACTERISTIC

In most cases ω_1' for maximally flat filters is defined as the 3-db band-edge point. Figure 4.03-2 shows plots of the stop-band attenuation characteristics of maximally flat filters where $L_{Ar} = 3$ db, for $n = 1$ to 15. Note that for convenience in plotting the data $|\omega'/\omega_1'| - 1$ was used for the abscissa. The magnitude sign is used on ω'/ω_1' because the low-pass to band-pass or band-stop mappings to be discussed in later chapters can yield negative values of ω'/ω_1' for which the attenuation is interpreted to be the same as for positive values of ω'/ω_1'.

Another commonly used attenuation characteristic is the *Tchebyscheff* or "equal-ripple" characteristic shown in Fig. 4.03-3. In this case L_{Ar}

* This characteristic is also known as a *Butterworth* filter characteristic.

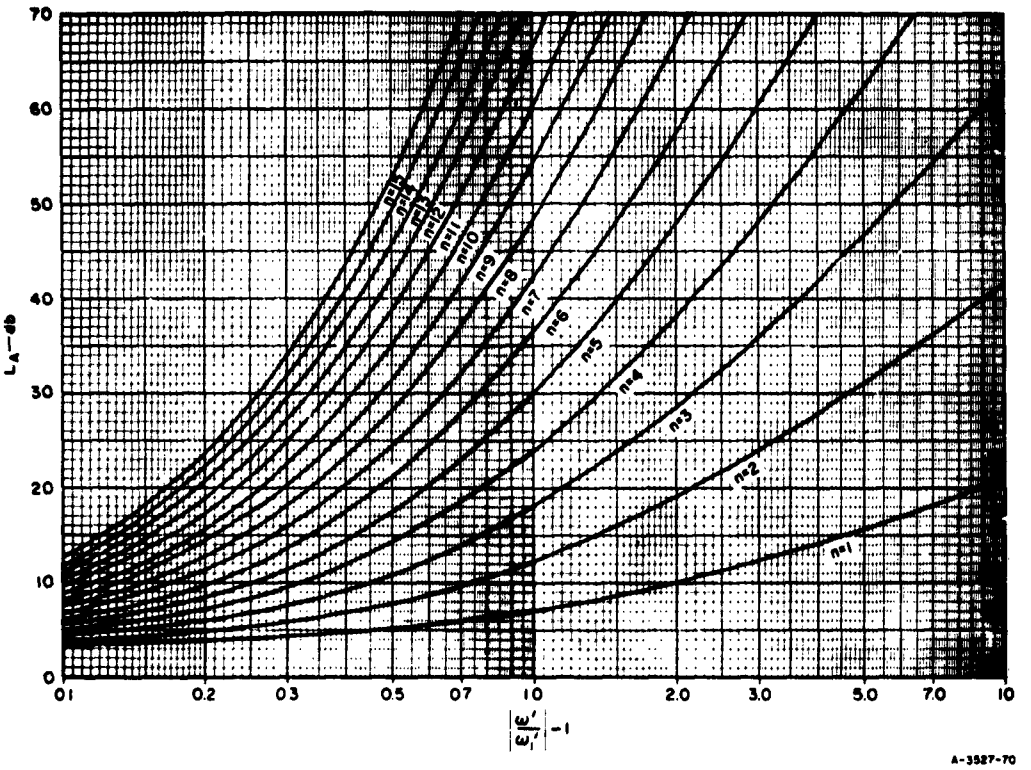

FIG. 4.03-2 ATTENUATION CHARACTERISTICS OF MAXIMALLY FLAT FILTERS
The Frequency ω_1' is the 3-db Band-Edge Point

is again the maximum db attenuation in the pass band, while ω_1' is the equal-ripple band edge. Attenuation characteristics of the form in Fig. 4.03-3 may be specified mathematically as

$$L_A(\omega') = 10 \log_{10} \left\{ 1 + \epsilon \cos^2 \left[n \cos^{-1} \left(\frac{\omega'}{\omega_1'} \right) \right] \right\}_{\omega' \leq \omega_1'} \qquad (4.03\text{-}3)$$

and

$$L_A(\omega') = 10 \log_{10} \left\{ 1 + \epsilon \cosh^2 \left[n \cosh^{-1} \left(\frac{\omega'}{\omega_1'} \right) \right] \right\}_{\omega' \geq \omega_1'} \qquad (4.03\text{-}4)$$

where

$$\epsilon = \left[\text{antilog}_{10}\left(\frac{L_{Ar}}{10}\right)\right] - 1 \quad . \tag{4.03-5}$$

This type of characteristic can also be achieved by the filter structures described in Secs. 4.04 and 4.05, and the parameter n in Eqs. (4.03-3) and (4.03-4) is again the number of reactive elements in the circuit. If n is even there will be $n/2$ frequencies where $L_A = 0$ for a low-pass Tchebyscheff response, while if n is odd there will be $(n + 1)/2$ such frequencies. Figures 4.03-4 to 4.03-10 show the stop-band attenuation characteristics of Tchebyscheff filters having L_{Ar} = 0.01, 0.10, 0.20, 0.50, 1.00, 2.00, and 3.00 db pass-band ripple. Again, $|\omega'/\omega_1'| - 1$ is used as the abscissa.

It is interesting to compare the maximally flat attenuation characteristics in Fig. 4.03-2 with the Tchebyscheff characteristics in Figs. 4.03-4 to 4.03-10. It will be seen that for a given pass-band attenuation tolerance, L_{Ar}, and number of reactive elements, n, that a Tchebyscheff filter will give a much sharper rate of cutoff. For example, the maximally flat characteristics in Fig. 4.03-2 and the Tchebyscheff characteristics in Fig. 4.03-10 both have L_{Ar} = 3 db. For the n = 15 maximally flat case, 70 db attenuation is reached at ω' = 1.7 ω_1'; for the n = 15 Tchebyscheff case, 70 db attenuation is reached at ω' = 1.18 ω_1'. Because of their sharp cutoff, Tchebyscheff characteristics are often preferred over other possible characteristics; however, if the reactive elements of a filter have appreciable dissipation loss the shape of the pass-band response of any type of filter will be altered as compared with the lossless case, and the effects will be particularly large in a Tchebyscheff filter. These matters will be discussed in Sec. 4.13. Maximally flat filters have often been reputed to have less delay distortion than Tchebyscheff

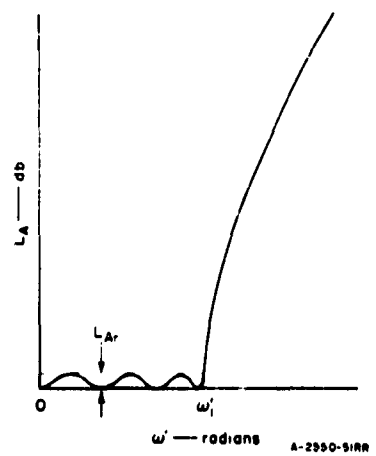

FIG. 4.03-3 A TCHEBYSCHEFF LOW-PASS CHARACTERISTIC

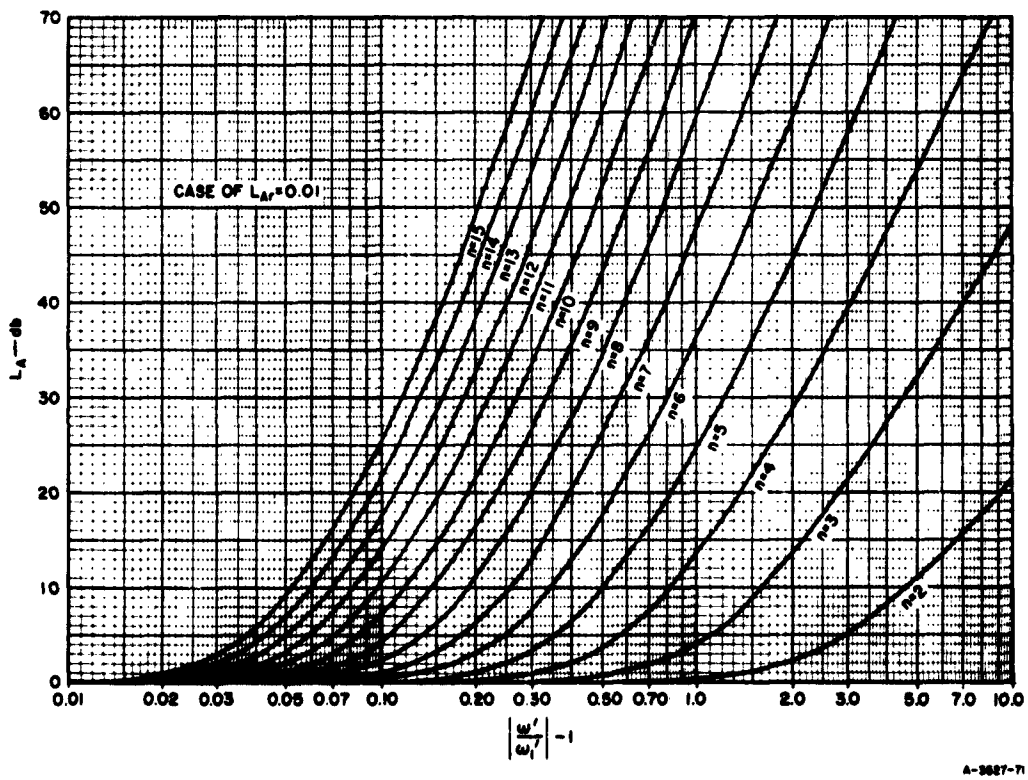

FIG. 4.03-4 0.01-db-RIPPLE TCHEBYSCHEFF FILTER CHARACTERISTICS

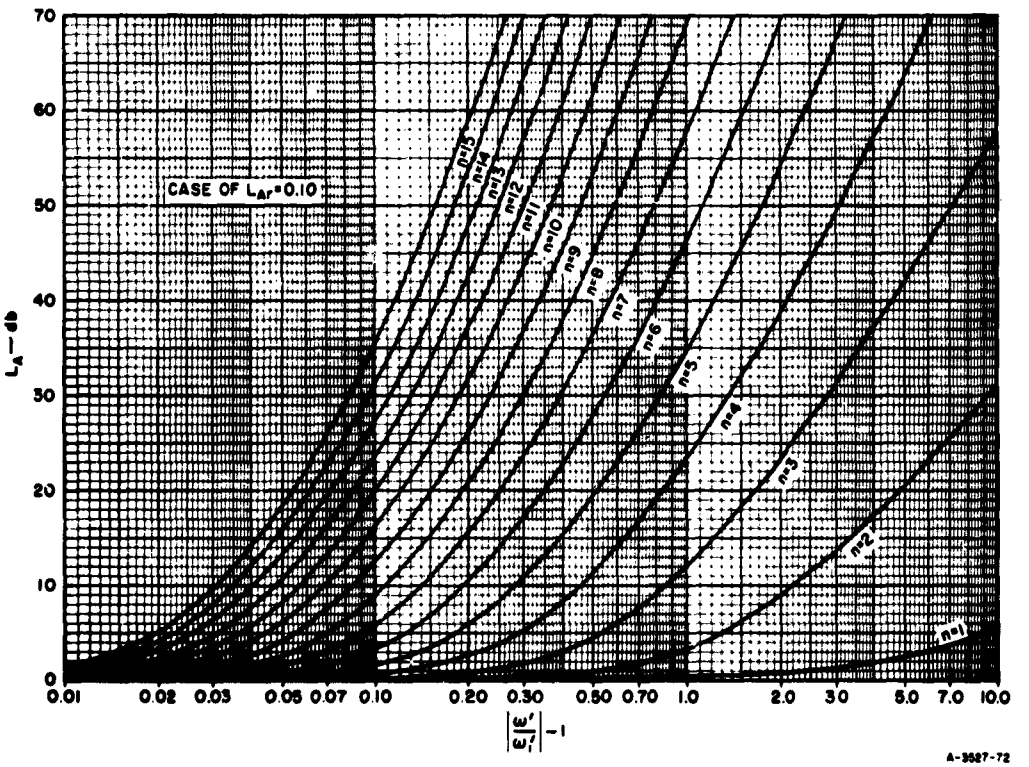

FIG. 4.03-5 0.10-db-RIPPLE TCHEBYSCHFFF FILTER CHARACTERISTICS

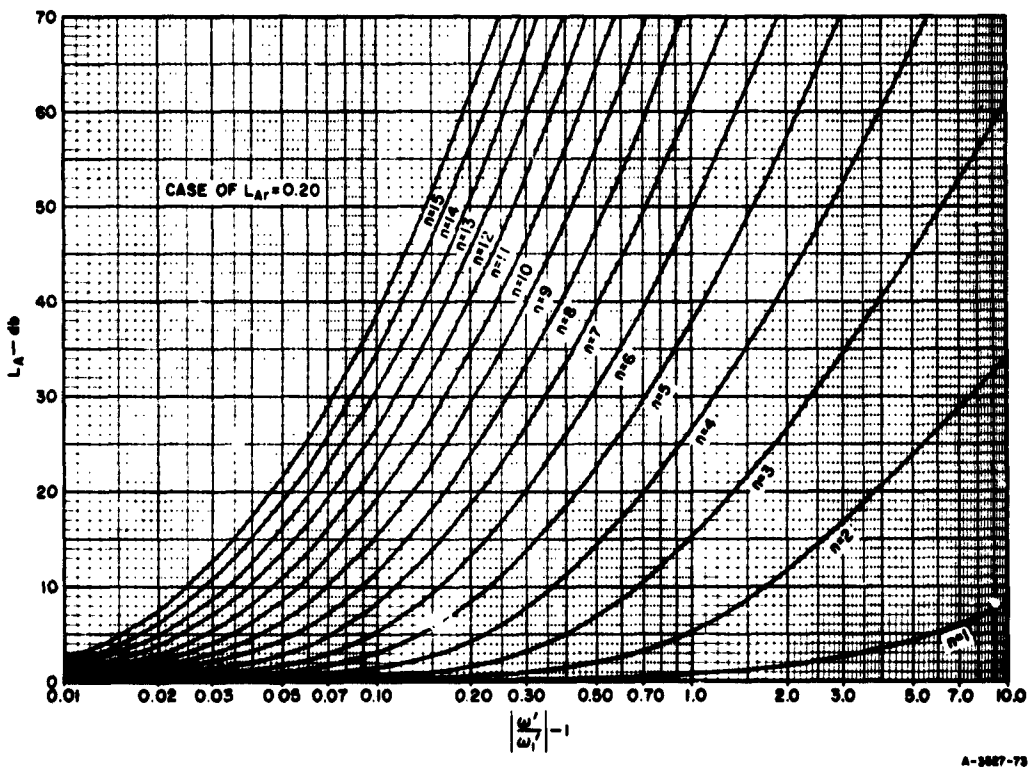

FIG. 4.03-6 0.20-db-RIPPLE TCHEBYSCHEFF FILTER CHARACTERISTICS

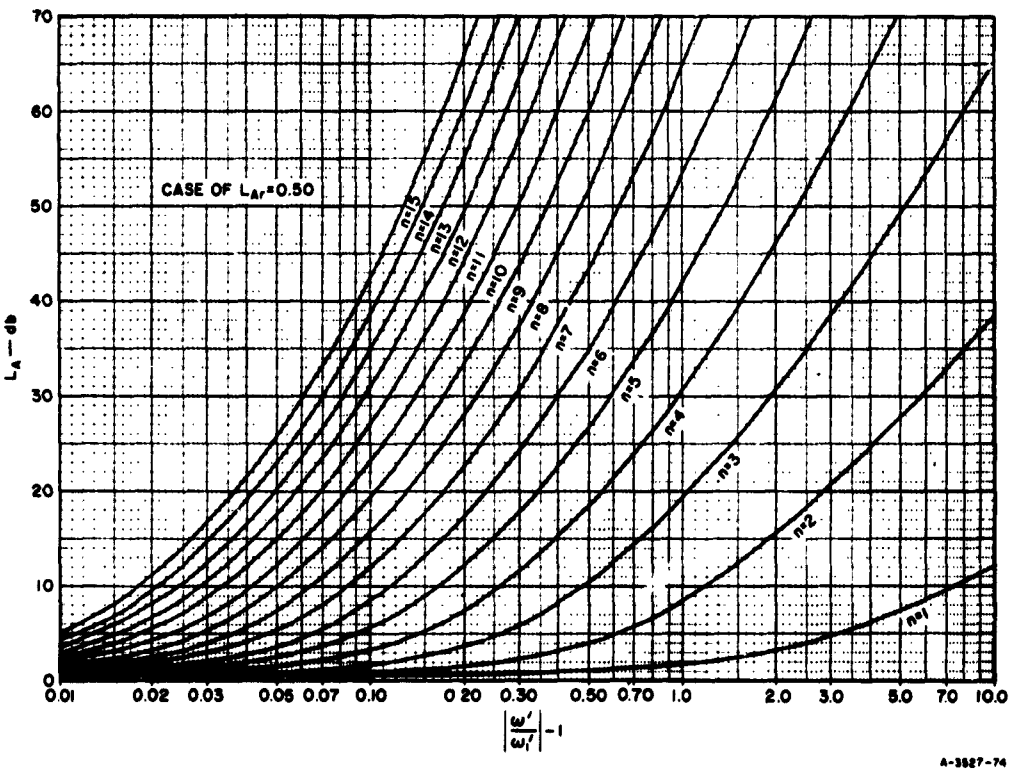

FIG. 4.03-7 0.50-db-RIPPLE TCHEBYSCHEFF FILTER CHARACTERISTICS

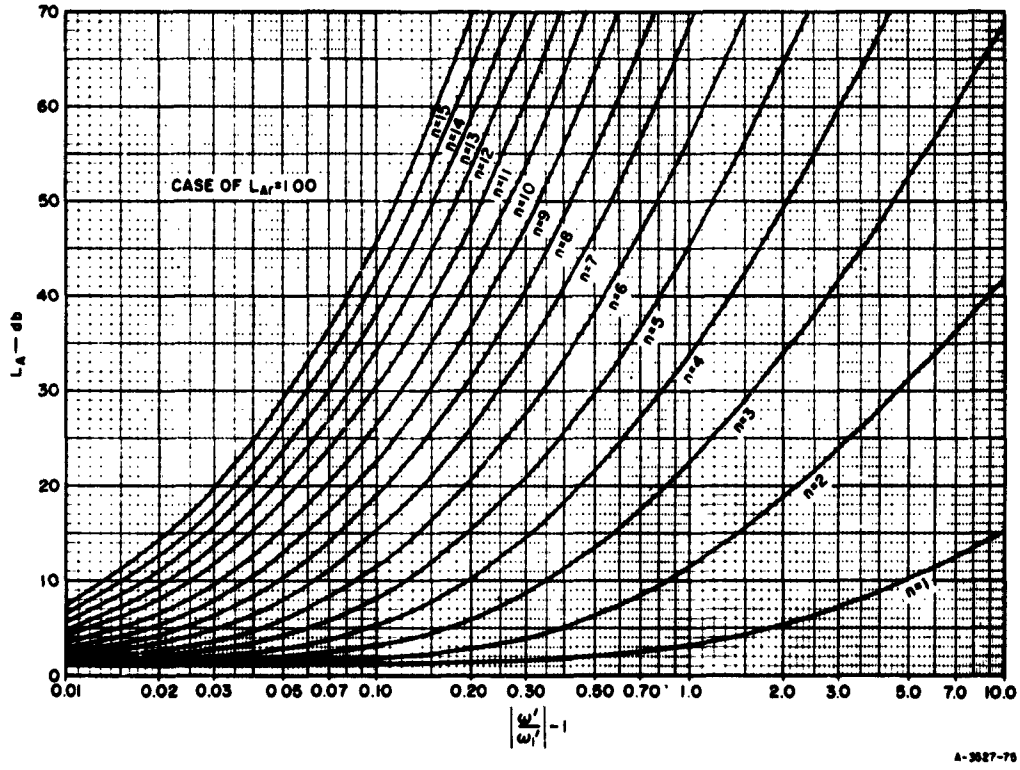

FIG. 4.03-8 1.00-db-RIPPLE TCHEBYSCHEFF FILTER CHARACTERISTICS

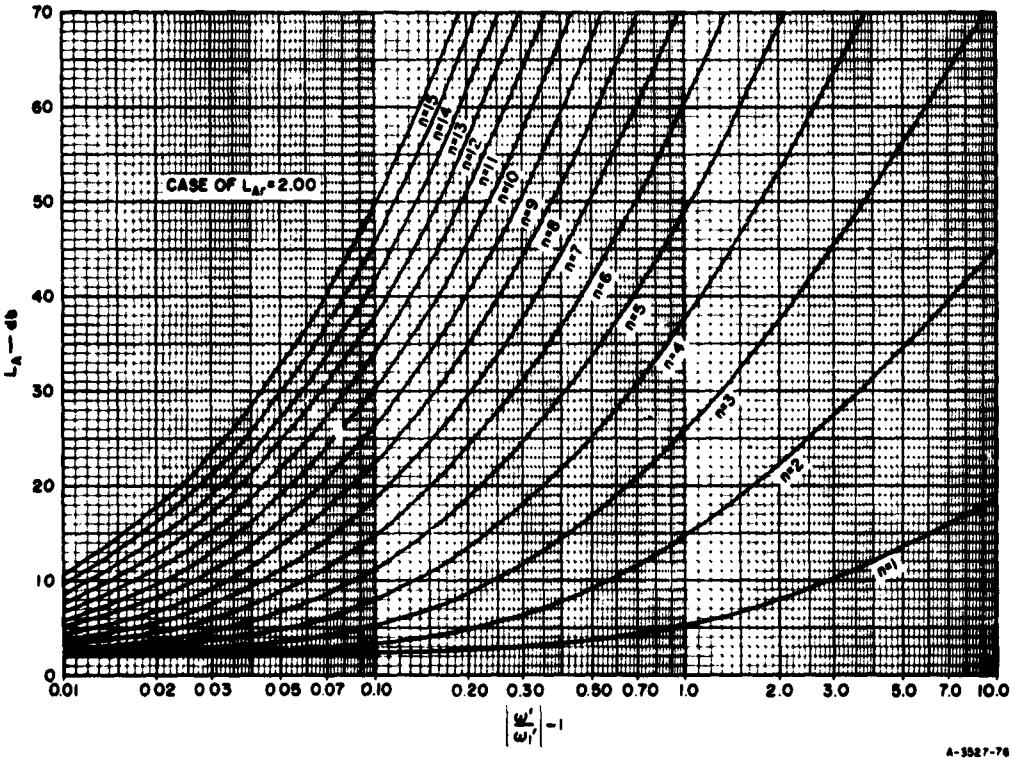

FIG. 4.03-9 2.00-db-RIPPLE TCHEBYSCHEFF FILTER CHARACTERISTICS

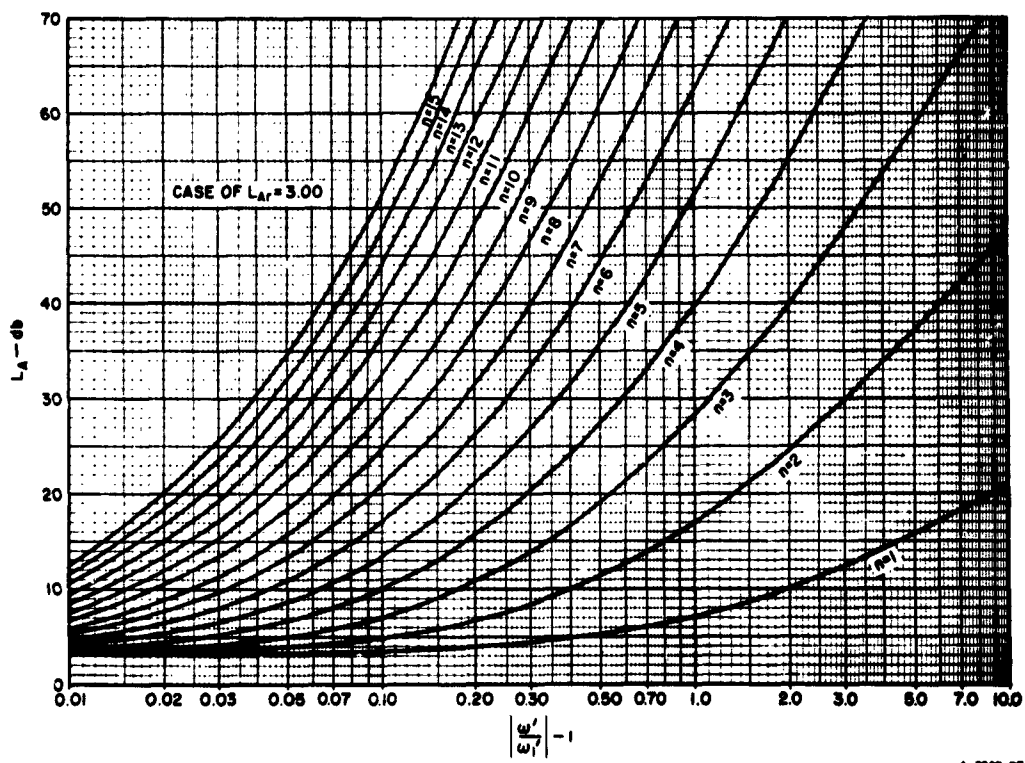

FIG. 4.03-10 3.00-db-RIPPLE TCHEBYSCHEFF FILTER CHARACTERISTICS

filters; however, as discussed in Sec. 4.08, this may not be true, depending on the size of L_{Ar}.

The maximally flat and Tchebyscheff characteristics in Figs. 4.03-1 and 4.03-3 are not the only possible characteristics of this type. For example, the Tchebyscheff characteristics of the impedance-matching-network prototypes to be discussed in Secs. 4.09 and 4.10 will be similar in shape, but L_A will not touch zero at the bottom of the ripples. Sometimes Tchebyscheff filters are designed to have both an equal-ripple characteristic in the pass band, and an "equal-ripple" approximation of a specified attenuation level in the stop band. Although such filters are used at low frequencies, they are very difficult to design precisely for use at microwave frequencies. One possible exception is the type of microwave filter discussed in Sec. 7.03.

SEC. 4.04, DEFINITION OF CIRCUIT PARAMETERS FOR LOW-PASS PROTOTYPE FILTERS

The element values $g_0, g_1, g_2, \cdots, g_n, g_{n+1}$ of the low-pass prototype filters discussed in this chapter are defined as shown in Fig. 4.04-1.

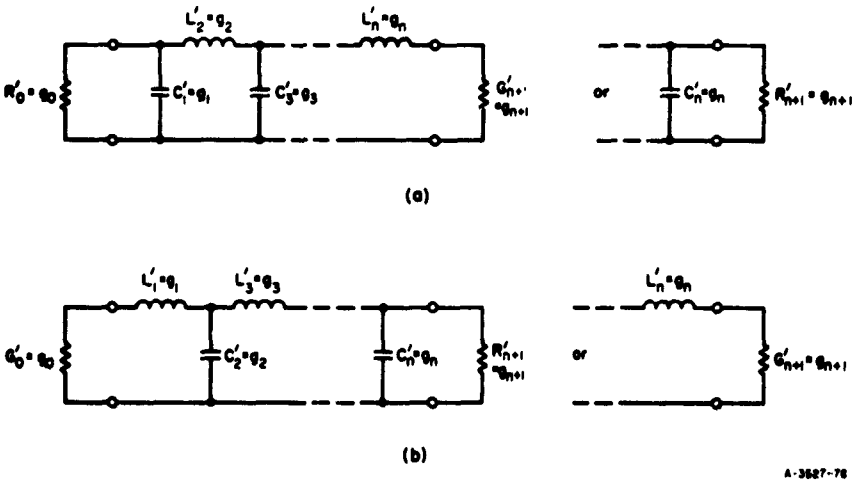

FIG. 4.04-1 DEFINITION OF PROTOTYPE FILTER PARAMETERS $g_0, g_1, g_2, \cdots, g_n, g_{n+1}$
A prototype circuit is shown at (a) and its dual is shown at (b). Either form will give the same response.

One possible form of a prototype filter is shown at (a) while its dual is shown at (b). Either form may be used, since both give identical responses. Since the networks are reciprocal, either the resistor on the left or the one on the right may be defined as the generator internal impedance. It should be noted that in Fig. 4.04-1 the following conventions are observed:

$$g_k\big|_{k=1 \text{ to } n} = \begin{cases} \text{the inductance of a series coil,} \\ \text{or the capacitance of a shunt capacitor} \end{cases}$$

$$g_0 = \begin{cases} \text{the generator resistance } R_0' \text{ if } g_1 = C_1' \text{, but is} \\ \text{defined as the generator conductance } G_0' \text{ if } g_1 = L_1' \end{cases} \tag{4.04-1}$$

$$g_{n+1} = \begin{cases} \text{the load resistance } R_{n+1}' \text{ if } g_n = C_n' \text{, but is} \\ \text{defined as the load conductance } G_{n+1}' \text{ if } g_n = L_n' \end{cases} .$$

The reason for using these conventions is that they lead to equations of identical form whether a given circuit or its dual is used. Besides the circuit element values, g_k, an additional prototype parameter, ω_1', will also be used. The parameter ω_1' is the radian frequency of the pass-band edge, which is defined in Figs. 4.03-1 and 4.03-3 for maximally flat and Tchebyscheff filters of the sort discussed here. Its definition in the case of maximally flat time-delay filters is discussed in Sec. 4.07.

The element values of the prototype filters discussed in this chapter are all normalized to make $g_0 = 1$ and $\omega_1' = 1$. These prototypes are easily changed to other impedance levels and frequency scales by the following transformations applied to the circuit elements. For resistances or conductances,

$$R = \left(\frac{R_0}{R_0'}\right)R' \quad \text{or} \quad G = \left(\frac{G_0}{G_0'}\right)G' \quad . \tag{4.04-2}$$

For inductances,

$$L = \left(\frac{R_0}{R_0'}\right)\left(\frac{\omega_1'}{\omega_1}\right)L' = \left(\frac{G_0'}{G_0}\right)\left(\frac{\omega_1'}{\omega_1}\right)L' \quad . \tag{4.04-3}$$

And, for capacitances,

$$C = \left(\frac{R_0'}{R_0}\right)\left(\frac{\omega_1'}{\omega_1}\right) C' = \left(\frac{G_0}{G_0'}\right)\left(\frac{\omega_1'}{\omega_1}\right) C' \quad . \qquad (4.04\text{-}4)$$

In these equations the primed quantities are for the normalized prototype and the unprimed quantities are for the corresponding scaled circuit. As indicated from the preceding discussion, for the prototypes in this chapter, $g_0 = R_0' = 1$ or $g_0 = G_0' = 1$.

As an example of how this scaling is accomplished, suppose that we have a low-pass prototype with $R_0' = 1.000$ ohm, $C_1' = 0.8430$ farad, $L_2' = 0.6220$ henry, and $G_3' = 1.3554$ mho. These element values are for a Tchebyscheff filter with 0.10-db ripple and an equal-ripple band edge of $\omega_1' = 1$ radian. [See the case of 0.10-db ripple and $n = 2$ in Table 4.05-2(a).] Assuming that it is desired to scale this prototype so that $R_0 = 50$ ohms and so that the equal-ripple band edge occurs at $f_1 = 1000$ Mc, then $(R_0/R_0') = 50$, and $(\omega_1'/\omega_1) = 1/(2\pi 10^9) = 0.159 \times 10^{-9}$. Next, by Eqs. (4.04-2) to (4.04-4), $R_0 = 50$ ohm, $C_1 = (1/50)\ (0.159 \times 10^{-9})\ (0.8430) = 2.68 \times 10^{-12}$ farad, $L_2 = 50\ (0.159 \times 10^{-9})\ (0.6220) = 4.94 \times 10^{-10}$ henry, and $G_3 = (1/50)\ (1.3554) = 0.0271$ mho.

SEC. 4.05, DOUBLY TERMINATED, MAXIMALLY FLAT AND TCHEBYSCHEFF PROTOTYPE FILTERS

For maximally flat filters having resistor terminations at both ends, a response of the form of that in Fig. 4.03-1 with $L_{Ar} = 3$ db, $g_0 = 1$, and $\omega_1' = 1$, the element values may be computed as follows:[5]

$$\begin{aligned} g_0 &= 1 \\ g_k &= 2 \sin\left[\frac{(2k-1)\pi}{2n}\right], \quad k = 1, 2, \ldots, n \qquad (4.05\text{-}1) \\ g_{n+1} &= 1 \quad . \end{aligned}$$

Table 4.05-1(a) gives element values for such filters having $n = 1$ to 10 reactive elements, while Table 4.05-1(b) presents corresponding filters with $n = 11$ to 15 reactive elements.

Table 4.05-1(a)

ELEMENT VALUES FOR FILTERS WITH MAXIMALLY FLAT ATTENUATION HAVING
$g_0 = 1$, $\omega_1' = 1$, and $n = 1$ to 10
The responses are of the form in Fig. 4.03-1 with $L_{Ar} = 3$ db

VALUE OF n	g_1	g_2	g_3	g_4	g_5	g_6	g_7	g_8	g_9	g_{10}	g_{11}
1	2.000	1.000									
2	1.414	1.414	1.000								
3	1.000	2.000	1.000	1.000							
4	0.7654	1.848	1.848	0.7654	1.000						
5	0.6180	1.618	2.000	1.618	0.6180	1.000					
6	0.5176	1.414	1.932	1.932	1.414	0.5176	1.000				
7	0.4450	1.247	1.802	2.000	1.802	1.247	0.4450	1.000			
8	0.3902	1.111	1.663	1.962	1.962	1.663	1.111	0.3902	1.000		
9	0.3473	1.000	1.532	1.879	2.000	1.879	1.532	1.000	0.3473	1.000	
10	0.3129	0.9080	1.414	1.782	1.975	1.975	1.782	1.414	0.9080	0.3129	1.000

Table 4.05-1(b)

ELEMENT VALUES FOR FILTERS WITH MAXIMALLY FLAT ATTENUATION HAVING
$g_0 = 1$, $\omega_1' = 1$, and $n = 11$ to 15
The responses are of the form in Fig. 4.03-1 with $L_{Ar} = 3$ db

VALUE OF n	g_1	g_2	g_3	g_4	g_5	g_6	g_7	g_8
11	0.2846	0.8308	1.3097	1.6825	1.9189	2.0000	1.9189	1.6825
12	0.2610	0.7653	1.2175	1.5867	1.8477	1.9828	1.9828	1.8477
13	0.2410	0.7092	1.1361	1.4970	1.7709	1.9418	2.0000	1.9418
14	0.2239	0.6605	1.0640	1.4142	1.6934	1.8877	1.9874	1.9874
15	0.2090	0.6180	1.0000	1.3382	1.6180	1.8270	1.9563	2.0000

	g_9	g_{10}	g_{11}	g_{12}	g_{13}	g_{14}	g_{15}	g_{16}
11	1.3097	0.8308	0.2846	1.0000				
12	1.5867	1.2175	0.7653	0.2610	1.0000			
13	1.7709	1.4970	1.1361	0.7092	0.2410	1.0000		
14	1.8877	1.6934	1.4142	1.0640	0.6605	0.2239	1.0000	
15	1.9563	1.8270	1.6180	1.3382	1.0000	0.6180	0.2090	1.0000

For Tchebyscheff filters having resistor terminations at both ends, with responses of the form shown in Fig. 4.03-3 having L_{Ar} db pass-band ripple, $g_0 = 1$, and $\omega_1' = 1$, the element values may be computed as follows:[4,5] first compute

$$\beta = \ln\left(\coth\frac{L_{Ar}}{17.37}\right)$$

$$\gamma = \sinh\left(\frac{\beta}{2n}\right)$$

$$a_k = \sin\left[\frac{(2k-1)\pi}{2n}\right], \quad k = 1, 2, \ldots, n$$

$$b_k = \gamma^2 + \sin^2\left(\frac{k\pi}{n}\right), \quad k = 1, 2, \ldots, n \qquad (4.05\text{-}2)$$

then compute

$$g_1 = \frac{2a_1}{\gamma}$$

$$g_k = \frac{4a_{k-1}a_k}{b_{k-1}g_{k-1}}, \qquad k = 2, 3, \ldots, n$$

$$g_{n+1} = 1 \text{ for } n \text{ odd}$$

$$= \coth^2\left(\frac{\beta}{4}\right) \text{ for } n \text{ even} \quad .$$

Table 4.05-2(a) gives element values for such filters for various L_{Ar} and $n = 1$ to 10 reactive elements. Table 4.05-2(b) gives corresponding data for filters having $n = 11$ to 15 reactive elements.

It will be noted that all of the filter prototypes discussed in this section are symmetrical if n is odd. If n is even, they have the property of antimetry mentioned in Secs. 2.11 and 3.07. Under this condition one half of the network is the reciprocal of the other half of the network with respect to a positive real constant R_k, where R_k may be defined as

$$R_k = \sqrt{R_0' R_{n+1}'} \qquad (4.05\text{-}3)$$

Table 4.05-2(a)

ELEMENT VALUES FOR TCHEBYSCHEFF FILTERS HAVING $g_0 = 1$, $\omega_1' = 1$, AND RESPONSES OF THE FORM IN FIG. 4.03-3 WITH VARIOUS db RIPPLE

Cases of $n = 1$ to 10

VALUE OF n	g_1	g_2	g_3	g_4	g_5	g_6	g_7	g_8	g_9	g_{10}	g_{11}
0.01 db ripple											
1	0.0960	1.0000									
2	0.4488	0.4077	1.1007								
3	0.6291	0.9702	0.6291	1.0000							
4	0.7128	1.2003	1.3212	0.6476	1.1007						
5	0.7563	1.3049	1.5773	1.3049	0.7563	1.0000					
6	0.7813	1.3600	1.6896	1.5350	1.4970	0.7098	1.1007				
7	0.7969	1.3924	1.7481	1.6331	1.7481	1.3924	0.7969	1.0000			
8	0.8072	1.4130	1.7824	1.6833	1.8529	1.6193	1.5554	0.7333	1.1007		
9	0.8144	1.4270	1.8043	1.7125	1.9057	1.7125	1.8043	1.4270	0.8144	1.0000	
10	0.8196	1.4369	1.8192	1.7311	1.9362	1.7590	1.9055	1.6527	1.5817	0.7446	1.1007
0.1 db ripple											
1	0.3052	1.0000									
2	0.8430	0.6220	1.3554								
3	1.0315	1.1474	1.0315	1.0000							
4	1.1088	1.3061	1.7703	0.8180	1.3554						
5	1.1468	1.3712	1.9750	1.3712	1.1468	1.0000					
6	1.1681	1.4039	2.0562	1.5170	1.9029	0.8618	1.3554				
7	1.1811	1.4228	2.0966	1.5733	2.0966	1.4288	1.1811	1.0000			
8	1.1897	1.4346	2.1199	1.6010	2.1699	1.5640	1.9444	0.8778	1.3554		
9	1.1956	1.4425	2.1345	1.6167	2.2053	1.6167	2.1345	1.4425	1.1956	1.0000	
10	1.1999	1.4481	2.1444	1.6265	2.2253	1.6418	2.2046	1.5821	1.9628	0.8853	1.3554
0.2 db ripple											
1	0.4342	1.0000									
2	1.0378	0.6745	1.5386								
3	1.2275	1.1525	1.2275	1.0000							
4	1.3028	1.2844	1.9761	0.8468	1.5386						
5	1.3394	1.3370	2.1660	1.3370	1.3394	1.0000					
6	1.3598	1.3632	2.2394	1.4555	2.0974	0.8838	1.5386				
7	1.3722	1.3781	2.2756	1.5001	2.2756	1.3781	1.3722	1.0000			
8	1.3804	1.3875	2.2963	1.5217	2.3413	1.4925	2.1349	0.8972	1.5386		
9	1.3860	1.3938	2.3093	1.5340	2.3728	1.5340	2.3093	1.3938	1.3860	1.0000	
10	1.3901	1.3983	2.3181	1.5417	2.3904	1.5536	2.3720	1.5066	2.1514	0.9034	1.5386
0.5 db ripple											
1	0.6986	1.0000									
2	1.4029	0.7071	1.9841								
3	1.5963	1.0967	1.5963	1.0000							
4	1.6703	1.1926	2.3661	0.8419	1.9841						
5	1.7058	1.2296	2.5408	1.2296	1.7058	1.0000					
6	1.7254	1.2479	2.6064	1.3137	2.4758	0.8696	1.9841				
7	1.7372	1.2583	2.6381	1.3444	2.6381	1.2583	1.7372	1.0000			
8	1.7451	1.2647	2.6564	1.3590	2.6964	1.3389	2.5093	0.8796	1.9841		
9	1.7504	1.2690	2.6678	1.3673	2.7239	1.3673	2.6678	1.2690	1.7504	1.0000	
10	1.7543	1.2721	2.6754	1.3725	2.7392	1.3806	2.7231	1.3485	2.5239	0.8842	1.9841

Table 4.05-2(a) *Concluded*

VALUE OF n	g_1	g_2	g_3	g_4	g_5	g_6	g_7	g_8	g_9	g_{10}	g_{11}
1.0 db ripple											
1	1.0177	1.0000									
2	1.8219	0.6850	2.6599								
3	2.0236	0.9941	2.0236	1.0000							
4	2.0991	1.0644	2.8311	0.7892	2.6599						
5	2.1349	1.0911	3.0009	1.0911	2.1349	1.0000					
6	2.1546	1.1041	3.0634	1.1518	2.9367	0.8101	2.6599				
7	2.1664	1.1116	3.0934	1.1736	3.0934	1.1116	2.1664	1.0000			
8	2.1744	1.1161	3.1107	1.1839	3.1488	1.1696	2.9685	0.8175	2.6599		
9	2.1797	1.1192	3.1215	1.1897	3.1747	1.1897	3.1215	1.1192	2.1797	1.0000	
10	2.1836	1.1213	3.1286	1.1933	3.1890	1.1990	3.1738	1.1763	2.9824	0.8210	2.6599
2.0 db ripple											
1	1.5296	1.0000									
2	2.4881	0.6075	4.0957								
3	2.7107	0.8327	2.7107	1.0000							
4	2.7925	0.8806	3.6063	0.6819	4.0957						
5	2.8310	0.8985	3.7827	0.8985	2.8310	1.0000					
6	2.8521	0.9071	3.8467	0.9393	3.7151	0.6964	4.0957				
7	2.8655	0.9119	3.8780	0.9535	3.8780	0.9119	2.8655	1.0000			
8	2.8733	0.9151	3.8948	0.9605	3.9335	0.9510	3.7477	0.7016	4.0957		
9	2.8790	0.9171	3.9056	0.9643	3.9598	0.9643	3.9056	0.9171	2.8790	1.0000	
10	2.8831	0.9186	3.9128	0.9667	3.9743	0.9704	3.9589	0.9554	3.7619	0.7040	4.0957
3.0 db ripple											
1	1.9953	1.0000									
2	3.1013	0.5339	5.8095								
3	3.3487	0.7117	3.3487	1.0000							
4	3.4389	0.7483	4.3471	0.5920	5.8095						
5	3.4817	0.7618	4.5381	0.7618	3.4817	1.0000					
6	3.5045	0.7685	4.6061	0.7929	4.4641	0.6033	5.8095				
7	3.5182	0.7723	4.6386	0.8039	4.6386	0.7723	3.5182	1.0000			
8	3.5277	0.7745	4.6575	0.8089	4.6990	0.8018	4.4990	0.6073	5.8095		
9	3.5340	0.7760	4.6692	0.8118	4.7272	0.8118	4.6692	0.7760	3.5340	1.0000	
10	3.5384	0.7771	4.6768	0.8136	4.7425	0.8164	4.7260	0.8051	4.5142	0.6091	5.8095

Table 4.05-2(b)

ELEMENT VALUES FOR TCHEBYSCHEFF FILTERS HAVING $g_0 = 1$, $\omega_1' = 1$, AND RESPONSES OF THE FORM IN FIG. 4.03-3 WITH VARIOUS db RIPPLE.

Cases of $n = 11$ to 15

VALUE OF n	g_1	g_2	g_3	g_4	g_5	g_6	g_7	g_8	g_9	g_{10}	g_{11}	g_{12}	g_{13}	g_{14}	g_{15}	g_{16}
0.01 db ripple																
11	0.8234	1.4442	1.8298	1.7437	1.9554	1.7856	1.9554	1.7437	1.8298	1.4442	0.8234	1.0000				
12	0.8264	1.4497	1.8377	1.7527	1.9684	1.8022	1.9837	1.7883	1.9293	1.6695	1.5957	0.7508	1.1007			
13	0.8287	1.4540	1.8437	1.7594	1.9777	1.8134	2.0014	1.8134	1.9777	1.7594	1.8437	1.4540	0.8287	1.0000		
14	0.8305	1.4573	1.8483	1.7644	1.9845	1.8214	2.0132	1.8290	2.0048	1.8029	1.9422	1.6792	1.6041	0.7545	1.1007	
15	0.8320	1.4600	1.8520	1.7684	1.9897	1.8272	2.0216	1.8394	2.0216	1.8272	1.9897	1.7684	1.8520	1.4600	0.8320	1.0000
0.10 db ripple																
11	1.2031	1.4523	2.1515	1.6332	2.2378	1.6559	2.2378	1.6332	2.1515	1.4523	1.2031	1.0000				
12	1.2055	1.4554	2.1566	1.6379	2.2462	1.6646	2.2562	1.6372	2.2200	1.5912	1.9726	0.8894	1.3554			
13	1.2074	1.4578	2.1605	1.6414	2.2521	1.6704	2.2675	1.6704	2.2521	1.6414	2.1605	1.4578	1.2074	1.0000		
14	1.2089	1.4596	2.1636	1.6441	2.2564	1.6745	2.2751	1.6786	2.2696	1.6648	2.2283	1.5963	1.9784	0.8919	1.3554	
15	1.2101	1.4612	2.1660	1.6461	2.2598	1.6776	2.2804	1.6839	2.2804	1.6776	2.2598	1.6461	2.1660	1.4612	1.2101	1.0000
0.20 db ripple																
11	1.3931	1.4015	2.3243	1.5469	2.4014	1.5646	2.4014	1.5469	2.3243	1.4015	1.3931	1.0000				
12	1.3954	1.4040	2.3289	1.5505	2.4088	1.5713	2.4176	1.5656	2.3856	1.5136	2.1601	0.9069	1.5386			
13	1.3972	1.4059	2.3323	1.5532	2.4140	1.5758	2.4276	1.5758	2.4140	1.5532	2.3323	1.4059	1.3972	1.0000		
14	1.3986	1.4073	2.3350	1.5553	2.4178	1.5790	2.4342	1.5821	2.4294	1.5714	2.3929	1.5176	2.1653	0.9089	1.5386	
15	1.3997	1.4085	2.3371	1.5569	2.4207	1.5813	2.4388	1.5862	2.4388	1.5813	2.4207	1.5569	2.3371	1.4085	1.3997	1.0000
0.50 db ripple																
11	1.7572	1.2743	2.6809	1.3759	2.7488	1.3879	2.7488	1.3759	2.6809	1.2743	1.7572	1.0000				
12	1.7594	1.2760	2.6848	1.3784	2.7551	1.3925	2.7628	1.3886	2.7349	1.3532	2.5317	0.8867	1.9841			
13	1.7610	1.2772	2.6878	1.3802	2.7596	1.3955	2.7714	1.3955	2.7596	1.3802	2.6878	1.2772	1.7610	1.0000		
14	1.7624	1.2783	2.6902	1.3816	2.7629	1.3976	2.7771	1.3997	2.7730	1.3925	2.7412	1.3558	2.5362	0.8882	1.9841	
15	1.7635	1.2791	2.6920	1.3826	2.7654	1.3991	2.7811	1.4024	2.7811	1.3991	2.7654	1.3826	2.6920	1.2791	1.7635	1.0000
1.00 db ripple																
11	2.1865	1.1229	3.1338	1.1957	3.1980	1.2041	3.1980	1.1957	3.1338	1.1229	2.1865	1.0000				
12	2.1887	1.1241	3.1375	1.1974	3.2039	1.2073	3.2112	1.2045	3.1849	1.1796	2.9898	0.8228	2.6599			
13	2.1904	1.1250	3.1403	1.1987	3.2081	1.2094	3.2192	1.2094	3.2081	1.1987	3.1403	1.1250	2.1904	1.0000		
14	2.1917	1.1257	3.1425	1.1996	3.2112	1.2108	3.2245	1.2123	3.2207	1.2073	3.1908	1.1815	2.9944	0.8239	2.6599	
15	2.1928	1.1263	3.1442	1.2004	3.2135	1.2119	3.2282	1.2142	3.2282	1.2119	3.2135	1.2004	3.1442	1.1263	2.1928	1.0000
2.00 db ripple																
11	2.8863	0.9195	3.9181	0.9682	3.9834	0.9737	3.9834	0.9682	3.9181	0.9195	2.8863	1.0000				
12	2.8886	0.9203	3.9219	0.9693	3.9894	0.9758	3.9967	0.9740	3.9701	0.9575	3.7695	0.7052	4.0957			
13	2.8904	0.9209	3.9247	0.9701	3.9936	0.9771	4.0048	0.9771	3.9936	0.9701	3.9247	0.9209	2.8904	1.0000		
14	2.8919	0.9214	3.9269	0.9707	3.9967	0.9781	4.0101	0.9791	4.0062	0.9758	3.9761	0.9587	3.7739	0.7060	4.0957	
15	2.8930	0.9218	3.9287	0.9712	3.9990	0.9788	4.0139	0.9803	4.0139	0.9788	3.9990	0.9712	3.9287	0.9218	2.8930	1.0000
3.00 db ripple																
11	3.5420	0.7778	4.6825	0.8147	4.7523	0.8189	4.7523	0.8147	4.6825	0.7778	3.5420	1.0000				
12	3.5445	0.7784	4.6865	0.8155	4.7587	0.8204	4.7664	0.8191	4.7381	0.8067	4.5224	0.6101	5.8095			
13	3.5465	0.7789	4.6896	0.8162	4.7631	0.8214	4.7751	0.8214	4.7631	0.8162	4.6896	0.7789	3.5465	1.0000		
14	3.5480	0.7792	4.6919	0.8166	4.7664	0.8222	4.7808	0.8229	4.7766	0.8204	4.7444	0.8076	4.5272	0.6107	5.8095	
15	3.5493	0.7795	4.6938	0.8170	4.7689	0.8227	4.7847	0.8238	4.7847	0.8227	4.7689	0.8170	4.6938	0.7795	3.5493	1.0000

and where R'_0 and R'_{n+1} are the resistances of the terminations at the ends of the filter. If Z'_k is the impedance of one branch of the filter ladder network, then

$$Z'_{n+1-k} = \frac{R_k^2}{Z'_k} \qquad (4.05\text{-}4)$$

where Z'_{n+1-k} is the dual branch at the other end of the filter. By Eq. (4.05-4) it will be seen that the inductive reactances at one end of the filter are related to the capacitive susceptances at the other end by

$$\omega C'_{n+1-k} = \frac{\omega L'_k}{R_k^2} \quad . \qquad (4.05\text{-}5)$$

Also,

$$\omega L'_{n+1-k} = R_k^2 \omega C'_k \qquad (4.05\text{-}6)$$

so that it is possible to obtain the element values of the second half of the filter from those of the first half if the filter is antimetrical, (as well as when the filter is symmetrical).

It will be found that the symmetry and antimetry properties discussed above will occur in maximally flat and Tchebyscheff filters of the form in Fig. 4.04-1 having terminations at both ends, provided that the filter is designed so that $L_A = 0$ at one or more frequencies in the pass band as shown in Figs. 4.03-1 and 4.03-3. The maximally flat and Tchebyscheff filters discussed in Secs. 4.06, 4.09, and 4.10 do not have this property. The maximally flat time-delay filters in Sec. 4.07 are not symmetrical or antimetrical, even though $L_A = 0$ at $\omega' = 0$.

In some rare cases designs with n greater than 15 may be desired. In such cases good approximate designs can be obtained by augmenting an $n = 14$ or $n = 15$ design by repeating the two middle elements of the filter. Thus, suppose that an $n = 18$ design is desired. An $n = 14$ design can be augmented to $n = 18$ by breaking the circuit immediately following the g_7 element, repeating elements g_6 and g_7 twice, and then continuing on with element g_8 and the rest of the elements. Thus, letting primed g's indicate element values for the $n = 18$ filter, and unprimed g's indicate element values from the $n = 14$ design, the $n = 18$ design would have the element values

$$g_0' = g_0 \ , \quad g_1' = g_1 \ , \quad g_2' = g_2, \cdots, g_6' = g_6 \ ,$$

$$g_7' = g_7 \ , \quad g_8' = g_6 \ , \quad g_9' = g_7 \ , \quad g_{10}' = g_6 \ , \quad g_{11}' = g_7$$

$$g_{12}' = g_8 \ , \quad g_{13}' = g_9, \cdots, \quad g_{18}' = g_{14} \ , \quad g_{19}' = g_{15} \ .$$

This is, of course, an approximate procedure, but it is based on the fact that for a given Tchebyscheff ripple the element values in a design change very little as n is varied, once n is around 10 or more. This is readily seen by comparing the element values for different values of n, down the columns at the left in Table 4.05-2(b).

SEC. 4.06, SINGLY TERMINATED MAXIMALLY FLAT AND TCHEBYSCHEFF FILTERS

All of the prototype filters discussed in Sec. 4.05 have resistor terminations at both ends. However, in some cases it is desirable to use filters with a resistor termination at one end only. Figure 4.06-1 shows an example of such a filter with a resistor termination on the left and a zero internal impedance voltage generator on the right to drive the circuit. In this case the attenuation L_A defined by Eq. (2.11-4) does not apply, since a zero internal impedance voltage generator has infinite available power. The power absorbed by the circuit is

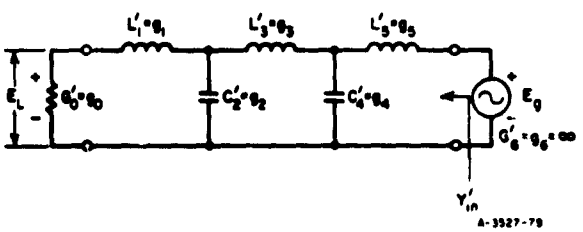

FIG. 4.06-1 AN $n = 5$ REACTIVE ELEMENT SINGLY TERMINATED FILTER DRIVEN BY A ZERO-IMPEDANCE VOLTAGE GENERATOR

$$P = |E_g|^2 \ \mathrm{Re}\ Y_{in}' \qquad (4.06\text{-}1)$$

where Y_{in}' and E_g are defined in the Fig. 4.06-1. Since all of the power must be absorbed in G_0',

$$|E_g|^2 \ \mathrm{Re}\ Y_{in}' = |E_L|^2 G_0' \qquad (4.06\text{-}2)$$

and

$$\left|\frac{E_g}{E_L}\right| = \sqrt{\frac{G_0'}{\mathrm{Re}\ Y_{in}'}} \ . \qquad (4.06\text{-}3)$$

Thus in this case it is convenient to use the *voltage attenuation* function

$$L_g = 20 \log_{10} \left| \frac{E_g}{E_L} \right| = 10 \log_{10} \frac{G_0'}{\text{Re } Y_{in}'} \quad \text{db} \quad . \quad (4.06\text{-}4)$$

Figure 4.06-2 shows the dual case to that in Fig. 4.06-1. In this latter case the circuit is driven by an *infinite-impedance current generator* and it is convenient to use the *current attenuation* function defined as

$$L_I = 20 \log_{10} \left| \frac{I_g}{I_L} \right| = 10 \log_{10} \frac{R_0'}{\text{Re } Z_{in}'} \quad \text{db} \quad (4.06\text{-}5)$$

where I_g, I_L, R_0', and Z_{in}' are as defined in Fig. 4.06-2. If L_A and L_{Ar} in Sec. 4.03 are replaced by analogous quantities L_g and L_{gr}, or L_I and L_{Ir}, all of the equations and charts in Sec. 4.03 apply to the singly terminated maximally flat or Tchebyscheff filters of this section as well as to the doubly terminated filters in Sec. 4.05.

Equation (4.06-1) shows that for a given generator voltage, E_g, the power transmission through the filter is controlled entirely by Re Y_{in}'. Thus, if the filter in Fig. 4.06-1 is to have a maximally flat or Tchebyscheff transmission characteristic, Re Y_{in}' must also have such a characteristic. Figure 4.06-3 shows the approximate shape of Re Y_{in}' and Im Y_{in}' for the circuit in Fig. 4.06-1 if designed to give a Tchebyscheff transmission characteristic. The curves in Fig. 4.06-3 also apply to the circuit in Fig. 4.06-2 if Y_{in}' is replaced by Z_{in}'. As will be discussed in Chapter 16, this property of Re Y_{in}' or Re Z_{in}' for singly loaded filters makes them quite useful in the design of diplexers and multiplexers. Prototypes of this sort will also be useful for the design of filters to be driven by energy sources that look approximately like a zero-impedance voltage generator or an infinite-impedance current generator. A typical example is a pentode tube which, from its plate circuit may resemble a current generator with a capacitor in parallel. In such cases a broadband response can be obtained if the shunt capacitance is used as the first element of a singly terminated filter.

Orchard[5] gives formulas for singly terminated maximally flat filters normalized so that $g_0 = 1$, and $\omega_1' = 1$ at the band-edge point where $L_I = L_{Ir}$ or $L_g = L_{gr}$ is 3 db. They may be written as follows:

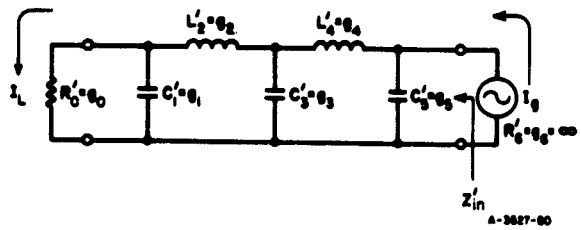

FIG. 4.06-2 THE DUAL CIRCUIT TO THAT IN FIG. 4.06-1
In this case the generator is an infinite-impedance current generator.

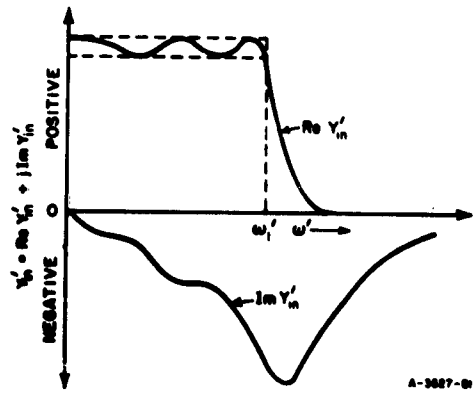

FIG. 4.06-3 THE APPROXIMATE FORM OF THE INPUT ADMITTANCE Y'_{in} IN FIG. 4.06-1 FOR AN $n = 5$ REACTIVE-ELEMENT, SINGLY TERMINATED TCHEBYSCHEFF FILTER

$$a_k = \sin \frac{\pi}{2} \frac{(2k-1)}{n}, \quad k = 1, 2, \ldots, n$$

$$c_k = \cos^2 \left(\frac{\pi k}{2n}\right), \quad k = 1, 2, \ldots, n$$

with the element values

$$g_1 = a_1 \tag{4.06-6}$$

$$g_k = \frac{a_k a_{k-1}}{c_{k-1} g_{k-1}}, \quad k = 2, 3, \ldots, n$$

$$g_{n+1} = \infty$$

$$[\text{check: } g_n = n g_1]$$

where the g_k defined above are to be interpreted as in Fig. 4.04-1(a) and (b). Table 4.06-1 gives element values for such filters for the cases of $n = 1$ to $n = 10$.

Table 4.06-1

ELEMENT VALUES FOR SINGLY TERMINATED MAXIMALLY FLAT FILTERS HAVING $g_0 = 1$, $g_{n+1} = \infty$, AND $\omega_1' = 1$

VALUE OF n	g_1	g_2	g_3	g_4	g_5	g_6	g_7	g_8	g_9	g_{10}	g_{11}
1	1.0000	∞									
2	0.7071	1.4142	∞								
3	0.5000	1.3333	1.5000	∞							
4	0.3827	1.0824	1.5772	1.5307	∞						
5	0.3090	0.8944	1.3820	1.6944	1.5451	∞					
6	0.2588	0.7579	1.2016	1.5529	1.7593	1.5529	∞				
7	0.2225	0.6560	1.0550	1.3972	1.6588	1.7988	1.5576	∞			
8	0.1951	0.5776	0.9370	1.2588	1.5283	1.7287	1.8246	1.5607	∞		
9	0.1736	0.5155	0.8414	1.1408	1.4037	1.6202	1.7772	1.8424	1.5628	∞	
10	0.1564	0.4654	0.7626	1.0406	1.2921	1.5100	1.6869	1.8121	1.8552	1.5643	∞

Note: Data by courtesy of L. Weinberg and the Journal of the Franklin Institute[9]

For singly loaded Tchebyscheff filters having $g_0 = 1$, $\omega_1' = 1$, and L_{Ar} or L_{gr} db pass-band ripple, Orchard's equations[5] give

$$\beta = \ln \left[\coth \frac{(L_{Ar} \text{ or } L_{gr})}{17.37} \right]$$

$$\gamma = \sinh\left(\frac{\beta}{2n}\right)$$

$$a_k = \sin\frac{\pi(2k-1)}{2n}, \quad k = 1, 2, \ldots, n$$

$$d_k = \left(\gamma^2 + \sin^2\frac{\pi k}{2n}\right)\cos^2\frac{\pi k}{2n}, \quad k = 1, 2, \ldots, n-1$$

(4.06-7)

with element values

$$g_1 = \frac{a_1}{\gamma}$$

$$g_k = \frac{a_k a_{k-1}}{d_{k-1} g_{k-1}}, \quad k = 1, 2, \ldots, n$$

$$g_{n+1} = \infty .$$

Table 4.06-2 presents element values for singly terminated filters for various amounts of Tchebyscheff ripple.

SEC. 4.07, MAXIMALLY FLAT TIME-DELAY PROTOTYPE FILTERS

The voltage attenuation ratio $(E_2)_{avail}/E_2$ (see Sec. 2.10) for a normalized, maximally flat, time-delay filter may be defined as[10,9]

$$\frac{(E_2)_{avail}}{E_2} = cp' y_n(1/p') \qquad (4.07\text{-}1)$$

where $p' = \sigma' + j\omega'$ is the normalized complex-frequency variable, c is a real, positive constant, and

$$y_n(1/p') = \sum_{k=0}^{n} \frac{(n+k)!}{(n-k)!\,k!\,(2p')^k} \qquad (4.07\text{-}2)$$

Table 4.06-2

ELEMENT VALUES FOR SINGLY TERMINATED TCHEBYSCHEFF FILTERS HAVING $g_0 = 1$, $g_{n+1} = \infty$, AND $\omega_1' = 1$

VALUE OF n	g_1	g_2	g_3	g_4	g_5	g_6	g_7	g_8	g_9	g_{10}	g_{11}
0.10 db ripple											
1	0.1526	∞									
2	0.4215	0.7159	∞								
3	0.5158	1.0864	1.0895	∞							
4	0.5544	1.1994	1.4576	1.2453	∞						
5	0.5734	1.2490	1.5562	1.5924	1.3759	∞					
6	0.5841	1.2752	1.5999	1.6749	1.7236	1.4035	∞				
7	0.5906	1.2908	1.6236	1.7107	1.7987	1.7395	1.4745	∞			
8	0.5949	1.3008	1.6380	1.7302	1.8302	1.8070	1.8163	1.4660	∞		
9	0.5978	1.3076	1.6476	1.7423	1.8473	1.8343	1.8814	1.7991	1.5182	∞	
10	0.6000	1.3124	1.6542	1.7503	1.8579	1.8489	1.9068	1.8600	1.8585	1.4964	∞
0.20 db ripple											
1	0.2176	∞									
2	0.5189	0.8176	∞								
3	0.6137	1.1888	1.1900	∞							
4	0.6514	1.2935	1.5615	1.2898	∞						
5	0.6697	1.3382	1.6541	1.6320	1.4356	∞					
6	0.6799	1.3615	1.6937	1.7083	1.7870	1.4182	∞				
7	0.6861	1.3752	1.7149	1.7401	1.8590	1.7505	1.5161	∞			
8	0.6902	1.3840	1.7276	1.7571	1.8880	1.8144	1.8623	1.4676	∞		
9	0.6930	1.3899	1.7360	1.7675	1.9034	1.8393	1.9257	1.7974	1.5512	∞	
10	0.6950	1.3941	1.7418	1.7744	1.9127	1.8523	1.9500	1.8560	1.8962	1.4914	∞
0.50 db ripple											
1	0.3493	∞									
2	0.7014	0.9403	∞								
3	0.7981	1.3001	1.3465	∞							
4	0.8352	1.3916	1.7279	1.3138	∞						
5	0.8529	1.4291	1.8142	1.6426	1.5388	∞					
6	0.8627	1.4483	1.8494	1.7101	1.9018	1.4042	∞				
7	0.8685	1.4596	1.8675	1.7371	1.9712	1.7254	1.5982	∞			
8	0.8725	1.4666	1.8750	1.7508	1.9980	1.7838	1.9571	1.4379	∞		
9	0.8752	1.4714	1.8856	1.7591	2.0116	1.8055	2.0203	1.7571	1.6238	∞	
10	0.8771	1.4748	1.8905	1.7645	2.0197	1.8165	2.0432	1.8119	1.9816	1.4539	∞
1.00 db ripple											
1	0.5088	∞									
2	0.9110	0.9957	∞								
3	1.0118	1.3332	1.5088	∞							
4	1.0495	1.4126	1.9093	1.2817	∞						
5	1.0674	1.4441	1.9938	1.5908	1.6652	∞					
6	1.0773	1.4601	2.0270	1.6507	2.0491	1.3457	∞				
7	1.0832	1.4694	2.0437	1.6736	2.1192	1.6489	1.7118	∞			
8	1.0872	1.4751	2.0537	1.6850	2.1453	1.7021	2.0922	1.3691	∞		
9	1.0899	1.4790	2.0601	1.6918	2.1583	1.7213	2.1574	1.6707	1.7317	∞	
10	1.0918	1.4817	2.0645	1.6961	2.1658	1.7306	2.1803	1.7215	2.1111	1.3801	∞
2.00 db ripple											
1	0.7648	∞									
2	1.2441	0.9766	∞								
3	1.3553	1.2740	1.7717	∞							
4	1.3962	1.3389	2.2169	1.1727	∞						
5	1.4155	1.3640	2.3049	1.4468	1.9004	∞					
6	1.4261	1.3765	2.3383	1.4974	2.3304	1.2137	∞				
7	1.4328	1.3836	2.3551	1.5159	2.4063	1.4836	1.9379	∞			
8	1.4366	1.3881	2.3645	1.5251	2.4332	1.5298	2.3646	1.2284	∞		
9	1.4395	1.3911	2.3707	1.5304	2.4463	1.5495	2.4386	1.4959	1.9553	∞	
10	1.4416	1.3932	2.3748	1.5337	2.4538	1.5536	2.4607	1.5419	2.3794	1.2353	∞
3.00 db ripple											
1	0.9976	∞									
2	1.5506	0.9109	∞								
3	1.6744	1.1739	2.0302	∞							
4	1.7195	1.2292	2.5272	1.0578	∞						
5	1.7409	1.2501	2.6227	1.3015	2.1491	∞					
6	1.7522	1.2606	2.6578	1.3455	2.6309	1.0876	∞				
7	1.7591	1.2666	2.6750	1.3614	2.7141	1.3282	2.1827	∞			
8	1.7638	1.2701	2.6852	1.3690	2.7436	1.3687	2.6618	1.0982	∞		
9	1.7670	1.2726	2.6916	1.3733	2.7577	1.3827	2.7414	1.3380	2.1970	∞	
10	1.7692	1.2744	2.6958	1.3761	2.7655	1.3893	2.7683	1.3774	2.6753	1.1032	∞

NOTE: Most of the data in this table were obtained by courtesy of L. Weinberg and the Journal of the Franklin Institute.

is a Bessel polynomial function of $1/p'$. Equations (4.07-1) and (4.07-2) reduce to a simple polynomial of the form

$$\frac{(E_2)_{avail}}{E_2} = P_n(p') = (p')^n a_n + (p')^{n-1} a_{n-1} + \ldots + p' a_1 + a_0 \quad . \tag{4.07-3}$$

Let

$$\phi' = \arg \left. \frac{(E_2)_{avail}}{E_2} \right|_{p'=j\omega'} = \tan^{-1} \frac{\text{Im } P_n(j\omega)}{\text{Re } P_n(j\omega)} \quad \text{radians} \quad . \tag{4.07-4}$$

Then, as was discussed in Sec. 1.05, the time delay (*i.e.*, group delay) is

$$t'_d = \frac{d\phi'}{d\omega'} \quad \text{secs} \tag{4.07-5}$$

where ω' is in radians per second. The transfer function, defined by Eqs. (4.07-1) and (4.07-2) has the property that its group delay, t'_d, has the maximum possible number of zero derivatives with respect to ω' at $\omega' = 0$, which is why it is said to have maximally flat time delay. The time delay, t'_d, may be expressed as[10,9]

$$t'_d = t'_{d0} \left(1 - \frac{1}{\left(\frac{\omega'}{\omega'_1}\right)^2 \left\{ \frac{\pi\omega'_1}{2\omega'} \left[J^2_{-n-\frac{1}{2}} \left(\frac{\omega'}{\omega'_1}\right) + J^2_{n+\frac{1}{2}} \left(\frac{\omega'}{\omega'_1}\right) \right] \right\}} \right) \tag{4.07-6}$$

where $J_{-n-\frac{1}{2}}(\omega'/\omega'_1)$ and $J_{n+\frac{1}{2}}(\omega'/\omega'_1)$ are Bessel functions of ω'/ω'_1, and

$$t'_{d0} = \frac{1}{\omega'_1} \tag{4.07-7}$$

is the group delay as $\omega' \to 0$. The magnitude of $(E_2)_{avail}/E_2$ is

$$\left|\frac{(E_2)_{avail}}{E_2}\right| = c\left(\frac{\omega'}{\omega_1'}\right)^{n+1}\left\{\frac{m\omega_1'}{2\omega'}\left[J^2_{-n-\frac{1}{2}}\left(\frac{\omega'}{\omega_1'}\right) + J^2_{n+\frac{1}{2}}\left(\frac{\omega'}{\omega_1'}\right)\right]\right\}^{\frac{1}{2}} \tag{4.07-8}$$

and for increasing n the attenuation approaches the Gaussian form[11,10,9]

$$L_A = \frac{10\left(\frac{\omega'}{\omega_1'}\right)^2}{(2n-1)\ ln\ 10} \quad db \quad . \tag{4.07-9}$$

For $n \geq 3$ the 3 db bandwidth is nearly

$$\left(\frac{\omega'}{\omega_1'}\right)_{3\ db} = \sqrt{(2n-1)\ ln\ 2} \quad . \tag{4.07-10}$$

Weinberg[9] has prepared tables of element values for normalized maximally flat time-delay filters, and the element values in Table 4.07-1 are from his work. These element values are normalized so that $t'_{d0} = 1/\omega_1' = 1$ second, and $g_0 = 1$. In order to obtain a different time delay, t_{d0}, the frequency scale must be changed by the factor

$$\frac{\omega_1}{\omega_1'} = \frac{t'_{d0}}{t_{d0}} \tag{4.07-11}$$

using the scaling procedure discussed in Sec. 4.04. Weinberg also presents some computed data showing time delay and attenuation in the

Table 4.07-1

ELEMENT VALUES FOR MAXIMALLY FLAT TIME DELAY FILTERS
HAVING $g_0 = 1$ and $\omega_1' = 1/t'_{d0} = 1$

VALUE OF n	g_1	g_2	g_3	g_4	g_5	g_6	g_7	g_8	g_9	g_{10}	g_{11}	g_{12}
1	2.0000	1.0000										
2	1.5774	0.4226	1.0000									
3	1.2550	0.5528	0.1922	1.0000								
4	1.0598	0.5116	0.3181	0.1104	1.0000							
5	0.9303	0.4577	0.3312	0.2090	0.0718	1.0000						
6	0.8377	0.4116	0.3158	0.2364	0.1480	0.0505	1.0000					
7	0.7677	0.3744	0.2944	0.2378	0.1778	0.1104	0.0375	1.0000				
8	0.7125	0.3446	0.2735	0.2297	0.1867	0.1387	0.0855	0.0289	1.0000			
9	0.6678	0.3203	0.2547	0.2184	0.1859	0.1506	0.1111	0.0682	0.0230	1.0000		
10	0.6305	0.3002	0.2384	0.2066	0.1808	0.1539	0.1240	0.0911	0.0557	0.0187	1.0000	
11	0.5989	0.2834	0.2243	0.1954	0.1739	0.1528	0.1296	0.1039	0.0761	0.0465	0.0154	1.0000

Note: Data by courtesy of L. Weinberg and the Journal of the Franklin Institute.[9]

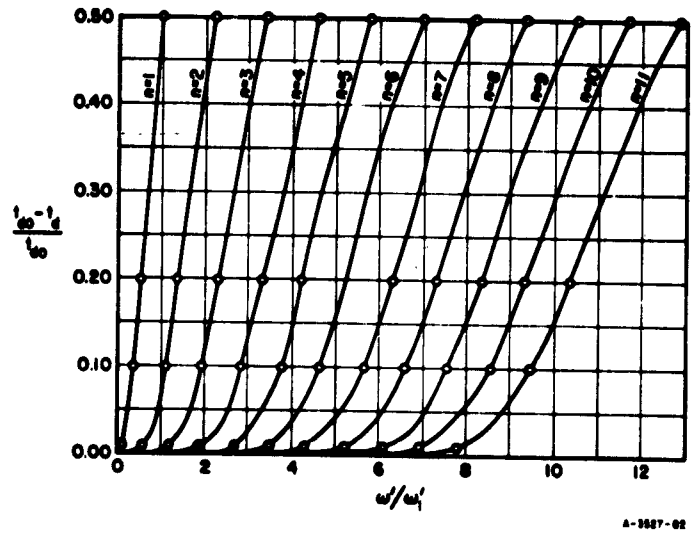

NOTE: Plotted from data prepared by L. Weinberg and published in the *Journal of the Franklin Institute.*[9]

FIG. 4.07-1 TIME-DELAY CHARACTERISTICS OF MAXIMALLY FLAT TIME-DELAY FILTERS

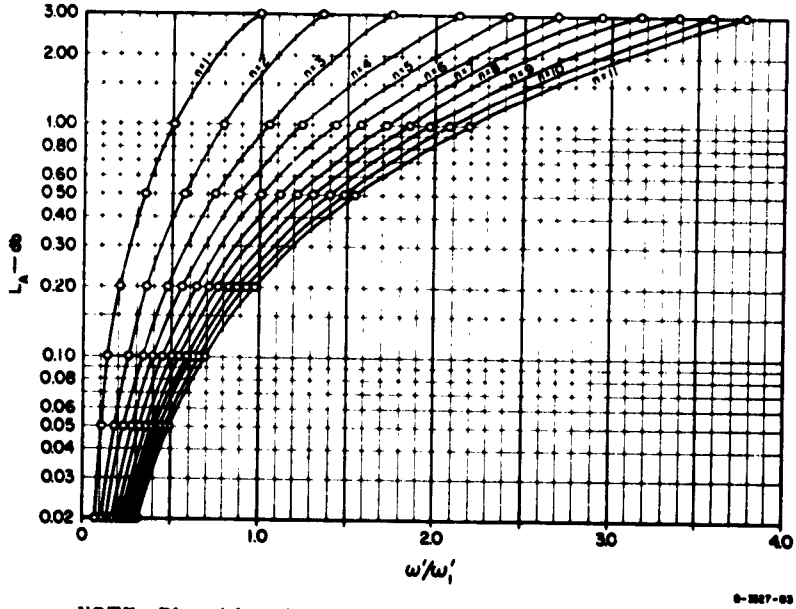

NOTE: Plotted from data prepared by L. Weinberg and published in the *Journal of the Franklin Institute.*[9]

FIG. 4.07-2 PASS-BAND ATTENUATION CHARACTERISTICS OF MAXIMALLY FLAT TIME-DELAY FILTERS

vicinity of the pass band for filters with $n = 1$ to 11. His data have been plotted in Figs. 4.07-1 and 4.07-2, and curves have been drawn in to aid in interpolating between data points. Although the time-delay characteristics are very constant in the pass-band region, these filters will be seen to have low-pass filter attenuation characteristics which are generally inferior to those of ordinary maximally flat attenuation or Tchebyscheff filters having the same number of reactive elements.

SEC. 4.08, COMPARISON OF THE TIME-DELAY CHARACTERISTICS OF VARIOUS PROTOTYPE FILTERS

If the terminations of a prototype filter are equal or are not too greatly different, the group time delay as $\omega' \to 0$ can be computed from the relation*

$$t'_{d0} = \left.\frac{d\phi}{d\omega'}\right|_{\omega' \to 0} = \frac{1}{2}\sum_{k=1}^{n} g_k \quad \text{seconds} \qquad (4.08\text{-}1)$$

where $g_1, g_2, \ldots, g_n$ are the prototype element values as defined in Fig. 4.04-1. Also in Table 4.13-1 and Fig. 4.13-2 a coefficient C_n is tabulated for maximally flat and Tchebyscheff prototype filters where

$$t'_{d0} = C_n \quad \text{seconds} \qquad (4.08\text{-}2)$$

which is exact.

If the frequency scale of a low-pass prototype is altered so that ω'_1 becomes ω_1, then the time scale is altered so that as $\omega \to 0$ the delay is

$$t_{d0} = t'_{d0}\frac{\omega'_1}{\omega_1} \quad \text{seconds} \quad . \qquad (4.08\text{-}3)$$

If a band-pass filter is designed from a low-pass prototype, then the *midband* time delay is (at least for narrow-band cases)†

---

* This equation is due to S. B. Cohn and can be derived by use of Eqs. (4.13-9) and (4.13-11) to follow.

† This is the approximate delay for a lumped-element band-pass filter consisting of a ladder of series and shunt resonators. If transmission line circuits are used there may be additional time delay due to the physical length of the filter.

$$t_{d0} = \frac{2\omega_1'}{\omega_2 - \omega_1} t_{d0}' \qquad (4.08\text{-}4)$$

where ω_1 and ω_2 are the pass-band edges of the band-pass response corresponding to ω_1' for the low-pass response.

In order to determine the time delay at other frequencies it is necessary to work from the transfer functions. For all of the prototype filters discussed in this chapter the voltage attenuation ratio $(E_2)_{avail}/E_2$ defined in Sec. 2.10 can be represented by a polynomial $P_n(p')$ so that

$$\frac{(E_2)_{avail}}{E_2} = P_n(p')$$

where $p' = \sigma' + j\omega'$ is the complex frequency variable. In the case of prototype filters with maximally flat attenuation, n reactive elements, $\omega_1' = 1$, and $L_{Ar} = 3$ db (see Fig. 4.03-1), $P_n(p')$ is for n even

$$P_n(p') = c \prod_{m=1}^{n/2} \left\{ (p')^2 + \left[2 \cos \frac{\pi(2m-1)}{2n} \right] p' + 1 \right\} \qquad (4.08\text{-}5)$$

and for n odd

$$P_n(p') = c(p+1) \prod_{m=1}^{(n-1)/2} \left[(p')^2 + \left(2 \cos \frac{\pi m}{n} \right) p' + 1 \right] \qquad (4.08\text{-}6)$$

where c is a real constant.

For Tchebyscheff prototype filters having n reactive elements, $\omega_1' = 1$, and L_{Ar} db ripple (see Fig. 4.03-3), $P_n(p')$ is for n even

$$P_n(p', x) = c \prod_{m=1}^{n/2} \left\{ (p')^2 + \left[2x \cos \frac{\pi(2m-1)}{2n} \right] p' + x^2 + \sin^2 \frac{\pi(2m-1)}{2n} \right\} \qquad (4.08\text{-}7)$$

and for n odd with $n \geq 3$

$$P_n(p',x) = c(p' + x) \prod_{m=1}^{(n-1)/2} \left[(p')^2 + \left(2x \cos \frac{\pi m}{n}\right) p' + x^2 + \sin^2 \frac{\pi m}{n}\right] \tag{4.08-8}$$

where

$$x = \sinh \left[\frac{1}{n} \sinh^{-1} \sqrt{\frac{1}{\left(\text{antilog}_{10} \frac{L_{Ar}}{10}\right) - 1}}\right] \tag{4.08-9}$$

and c is again a real constant. The constants c in Eqs. (4.08-5) to (4.08-9) are to be evaluated so as to fix the minimum attenuation of the response. For example, for the Tchebyscheff response in Fig. 4.03-3, c would be evaluated so as to make, $L_A = 20 \log_{10} (E_2)_{avail}/E_2 = 0$ at the bottom of the pass-band ripples. However, for the Tchebyscheff response in the impedance-matching filter response to be presented in Fig. 4.09-2 a different value of c would be required since L_A never goes to zero in this latter case. Both cases would, however, have identical phase shift and time delay characteristics.

The phase shift and group time delay for filters with maximally flat or Tchebyscheff attenuation characteristics can be computed by use of Eqs. (4.08-5) to (4.08-9) above and Eqs. (4.07-4) and (4.07-5). Cohn[12] has computed the phase and time delay characteristics for various prototype filters with $n = 5$ reactive elements in order to compare their relative merit in situations where time-delay characteristics are important. His results are shown in Fig. 4.08-1 to 4.08-3.

Figure 4.08-1 shows the phase characteristics of Tchebyscheff filters having 0.01-db and 0.5-db ripple with $\omega_1' = 1$, and a maximally flat attenuation filter with its 3-db point at $\omega_1' = 1$. The 3-db points of the Tchebyscheff filters are also indicated. Note that the 0.5-db ripple filter has considerably more curvature in its phase characteristic than either the 0.01-db ripple or maximally flat attenuation filters. It will be found that in general the larger the ripple of a Tchebyscheff filter the larger the curvature of the phase characteristic will be in the vicinity of ω_1'. As a result, the larger the ripple, the more the delay distortion will be near cutoff.

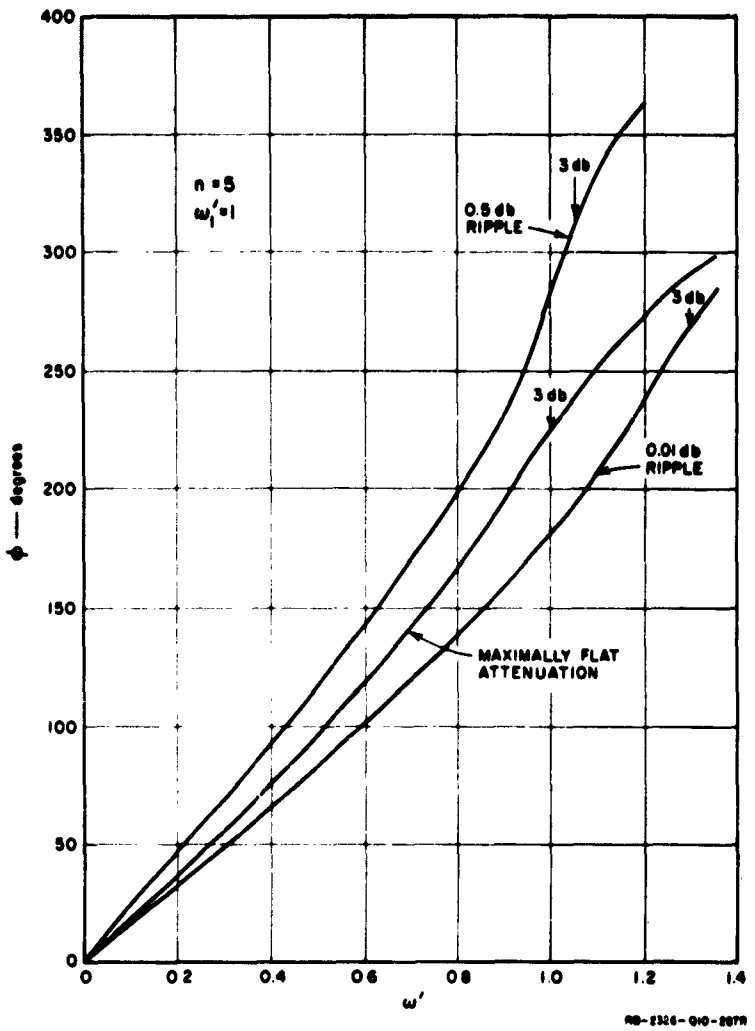

SOURCE: Final Report, Contract DA 36-039 SC-74862, Stanford Research Institute, reprinted in *The Microwave Journal* (see Ref. 13 by S. B. Cohn).

FIG. 4.08-1 PHASE-SHIFT CHARACTERISTICS OF FILTERS WITH MAXIMALLY FLAT OR TCHEBYSCHEFF ATTENUATION RESPONSES AND n = 5

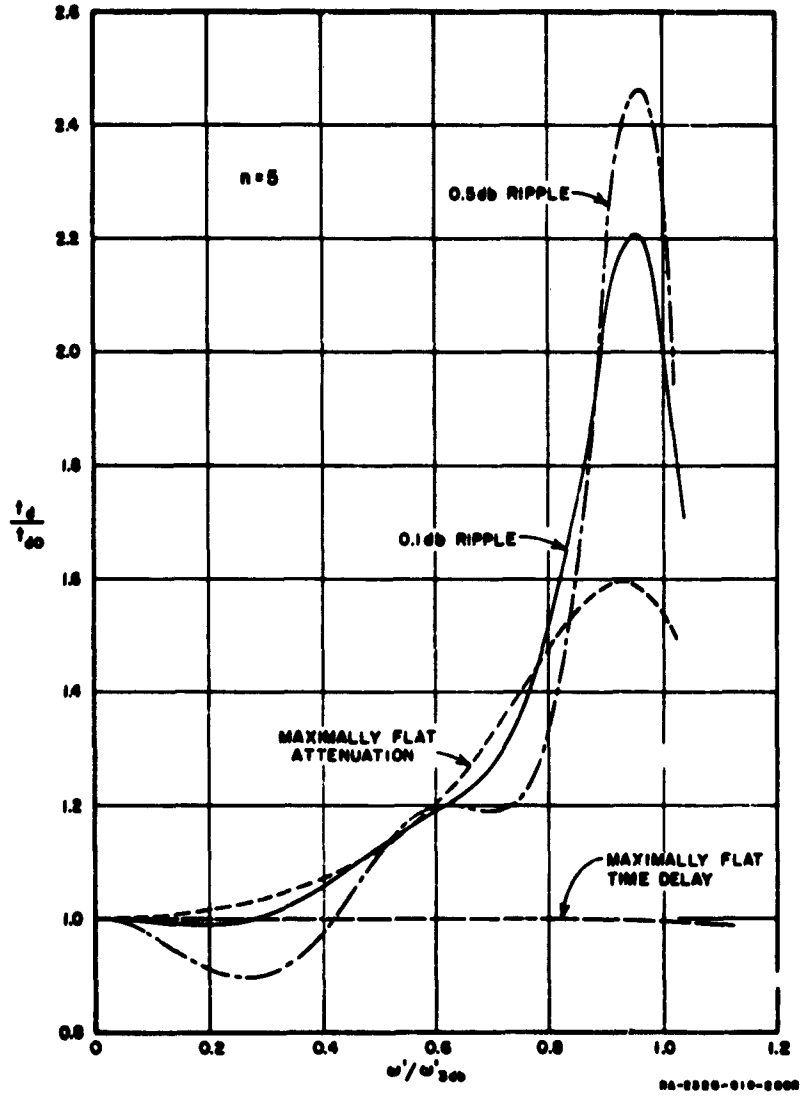

SOURCE: Final Report, Contract DA 36-039 SC-74862, Stanford Research Institute, reprinted in *The Microwave Journal* (see Ref. 13 by S. B. Cohn).

FIG. 4.08-2 NORMALIZED TIME DELAY vs. ω'/ω'_{3db} FOR VARIOUS PROTOTYPE FILTERS

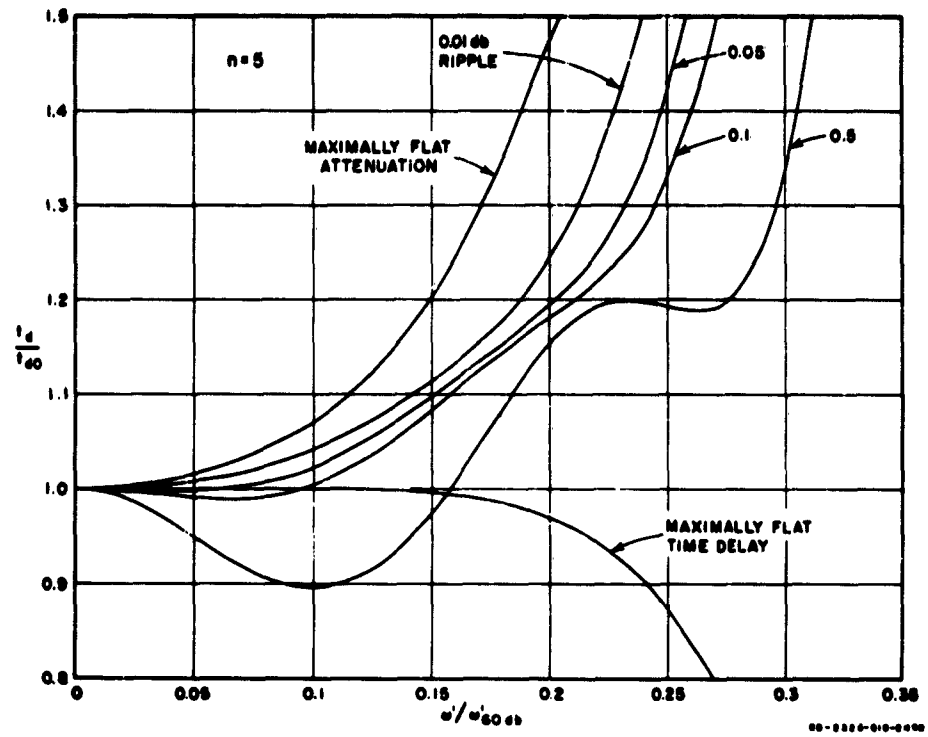

SOURCE: Final Report, Contract DA 36-039 SC-74862, Stanford Research Institute, reprinted in *The Microwave Journal* (see Ref. 13 by S. B. Cohn).

FIG. 4.08-3 NORMALIZED TIME DELAY vs. ω'/ω'_{60db} FOR VARIOUS PROTOTYPE FILTERS

Figure 4.08-2 shows the time delay characteristics of 0.1- and 0.5-db ripple Tchebyscheff filters, of a maximally flat attenuation filter, along with that of a maximally flat time delay filter. The scale of t_d is normalized to the time delay t_{d0}, obtained as $\omega' \to 0$, and the frequency scale is normalized to the frequency $\omega'_{3\,db}$ where L_A = 3 db for each case. Note that the time-delay characteristic of the 0.5-db ripple filter is quite erratic, but that delay characteristics for the 0.1-db ripple filter are superior to those of the maximally flat attenuation filter. The 0.1-db-ripple curve is constant within ±1 percent for $\omega'/\omega'_{3\,db} \leq 0.31$ while the maximally flat filter is within this tolerance only for $\omega'/\omega'_{3\,db} \leq 0.16$. The maximally flat time-delay filter is seen to have by far the most constant time delay of all. However, the equal-ripple band for the 0.1-db-ripple filter extends to

0.88 $\omega'/\omega'_{3\ db}$ while the maximally flat time delay filter has about 2.2 db attenuation at that frequency. (See Fig. 4.07-2.) Thus, it is seen that maximally flat time-delay filters achieve a more constant time delay at the cost of a less constant attenuation characteristic.

In some cases a band of low loss and low distortion is desired up to a certain frequency and then a specified high attenuation is desired at an adjacent higher frequency. Figure 4.08-3 shows the time-delay characteristics of various prototype filters with the frequency scale normalized to the 60-db attenuation frequency $\omega'_{60\ db}$ for each filter. For a ±1 percent tolerance on t_d, a 0.1-db-ripple filter is found to be usable to 0.106 $\omega'_{60\ db}$ while a maximally flat attenuation filter is within this tolerance only to 0.040 $\omega'_{60\ db}$. For a ±10 percent tolerance on t_d a 0.5-db-ripple filter is usable to 0.184 $\omega'_{60\ db}$ while the maximally flat attenuation filter is usable only to 0.116 $\omega'_{60\ db}$. The maximally flat time-delay filter again has by far the broadest usable band for a given time-delay tolerance; however, its reflection loss will again be an important consideration. For example, for $\omega' = 0.1\ \omega'_{60\ db}$ its attenuation is 1.25 db and its attenuation is 3 db for $\omega' = 0.15\ \omega'_{60\ db}$. In contrast the 0.1-db-ripple prototype filter has 0.1 db attenuation or less out to $\omega' = 0.294\ \omega'_{60\ db}$.

The choice between these various types of filters will depend on the application under consideration. In most cases where time delay is of interest in microwave filters, the filters used will probably be band-pass filters of narrow or moderate bandwidth. Such filters can be designed from prototype filters or step transformers by methods discussed in Chapters 8, 9, and 10.* For cases where the spectrum of a signal being transmitted is appreciable as compared with the bandwidth of the filter, variations in either time delay or pass-band attenuation within the signal spectrum will cause signal distortion.[13] However, for example, a maximally flat time-delay filter which has very little delay distortion and a monotonically increasing attenuation will tend to round a pulse out without overshoot or ringing, while a filter with a sharp cutoff (such as a Tchebyscheff filter) will tend to cause ringing.[13] The transient response requirements for the given application will be dominant considerations when choosing a filter type for such cases where the signal spectrum and filter pass band are of similar bandwidth.

---

* As is discussed in Sec. 1.05, most microwave filters will have extra time delay over that of their prototypes because of the electrical length of their physical structures.

In other situations the signal spectrum may be narrow compared with the bandwidth of the filter so that the spectral components of a given signal see essentially constant attenuation and delay for any common filter response, and distortion of the signal shape may thus be negligible. In such cases a choice of filter response types may depend on considerations of allowable time delay tolerance over the range of possible frequencies, allowable variation of attenuation in the carrier operating band, and required rate of cutoff. For example, if time-delay constancy was of major importance and it didn't matter whether signals with different carrier frequencies suffered different amounts of attenuation, a maximally flat time-delay filter would be the best choice.

SEC. 4.09, PROTOTYPE, TCHEBYSCHEFF IMPEDANCE-MATCHING NETWORKS GIVING MINIMUM REFLECTION

In this section the low-pass impedance matching of loads representable as a resistance and inductance in series, and of loads representable as a resistor and capacitance in parallel will be discussed. A load of the former type with a matching network of the sort to be treated is shown in Fig. 4.09-1. In general, the elements g_0, and g_1 in the circuits in Fig. 4.04-1(a), (b) may be regarded as loads, and the remainder of the reactive elements regarded as impedance-matching networks. For convenience it will be assumed that the impedance level of the load to be matched has been normalized so that the resistor or conductance is equal to one, and that the frequency scale has been normalized so that the edge of the desired band of good impedance match is $\omega_1' = 1$.

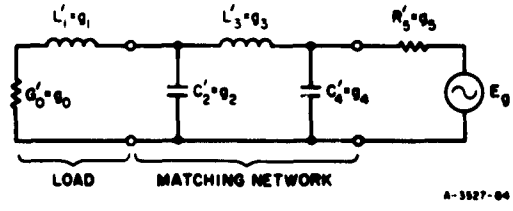

FIG. 4.09-1 A LOAD WITH A LOW-PASS IMPEDANCE-MATCHING NETWORK (Case of n = 4)

As was discussed in Sec. 1.03, if an impedance having a reactive part is to be matched over a band of frequencies, an optimum impedance-matching network must necessarily have a filter-like characteristic. Any degree of impedance match in frequency regions other than that for which a good match is required will detract from the performance possible in the band where

good match is required. Thus, the sharper the cutoff of a properly designed matching network, the better its performance can be.

Another important property of impedance-matching networks is that if the load has a reactive part, perfect power transmission to the load is possible only at discrete frequencies, and not over a band of frequencies. Furthermore, it will usually be found that the over-all transmission can be improved if at least a small amount of power is reflected at all frequencies. This is illustrated in Fig. 4.09-2, where it will be assumed that the designer's objective is to keep $(L_A)_{max}$ as small as possible from $\omega' = 0$ to $\omega' = \omega_1'$, where the db attenuation L_A refers to the attenuation of the power received by the load with respect to the available power of the generator (see Sec. 2.11). If $(L_A)_{min}$ is made very small so as to give very efficient transmission at the bottoms of the pass-band ripples, the excessively good transmission at these points must be compensated for by excessively poor transmission at the crests of the ripples, and as a result, $(L_A)_{max}$ will increase. On the

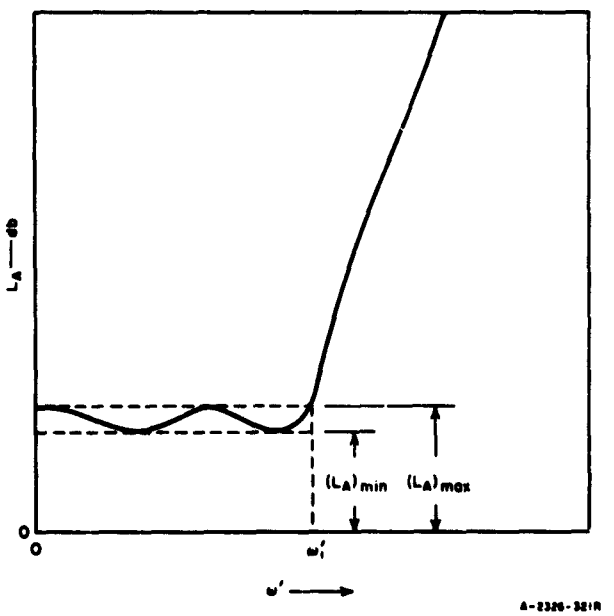

FIG. 4.09-2 DEFINITION OF $(L_A)_{max}$ AND $(L_A)_{min}$ FOR TCHEBYSCHEFF IMPEDANCE MATCHING NETWORKS DISCUSSED HEREIN

other hand if $(L_A)_{min}$ is specified to be nearly equal to $(L_A)_{max}$, the small pass-band ripple will result in a reduced rate of cutoff for the filter; as indicated above, this reduced rate of cutoff will degrade the performance and also cause $(L_A)_{max}$ to increase. Thus, it is seen that for a given load, a given number of impedance-matching elements, and a given impedance-matching bandwidth, there is some definite value of Tchebyscheff pass-band ripple $(L_A)_{max} - (L_A)_{min}$ that goes with a minimum value of $(L_A)_{max}$. The prototype impedance-matching networks discussed in this section are optimum in this sense, *i.e.*, they do minimize $(L_A)_{max}$ for a load and impedance-matching network of the form in Fig. 4.09-1 or its generalization in terms of Figs. 4.04-1(a), (b).

It is convenient to characterize the loads under consideration by their *decrement*, which is defined as

$$\delta = \frac{1}{g_0 g_1 \omega_1'} \qquad (4.09\text{-}1)$$

$$= \frac{1}{G_0' L_1' \omega_1'} \quad \text{or} \quad \frac{1}{R_0' C_1' \omega_1'} \quad ,$$

where the various quantities in this equation are as indicated in Figs. 4.09-1, 4.09-2, and 4.04-1(a), (b). Note that δ is the reciprocal of the Q of the load evaluated at the edge of the impedance-matching band and *that δ evaluated for the un-normalized load is the same as that for the normalized load.* Figure 4.09-3 shows the minimum value of $(L_A)_{max}$ *vs* δ for circuits having $n = 1$ to $n = 4$ reactive elements (also for case of $n = \infty$). Since one of the reactive elements in each case is part of the load, the $n = 1$ case involves no L or C impedance-matching elements, the optimum result being determined only by optimum choice of driving-generator internal impedance. Note that for a given value of δ, $(L_A)_{max}$ is decreased by using more complex matching networks (*i.e.*, larger values of n). However, a point of diminishing returns is rapidly reached so that it is usually not worthwhile to go beyond $n = 3$ or 4. Note that $n = \infty$ is not greatly better than $n = 4$.

Figure 4.09-4 shows the db Tchebyscheff ripple *vs* δ for minimum $(L_A)_{max}$. Once again, going to larger values of n will give better results, since when n is increased, the size of the ripple is reduced for a given δ. For $n = \infty$ the ripple goes to zero.

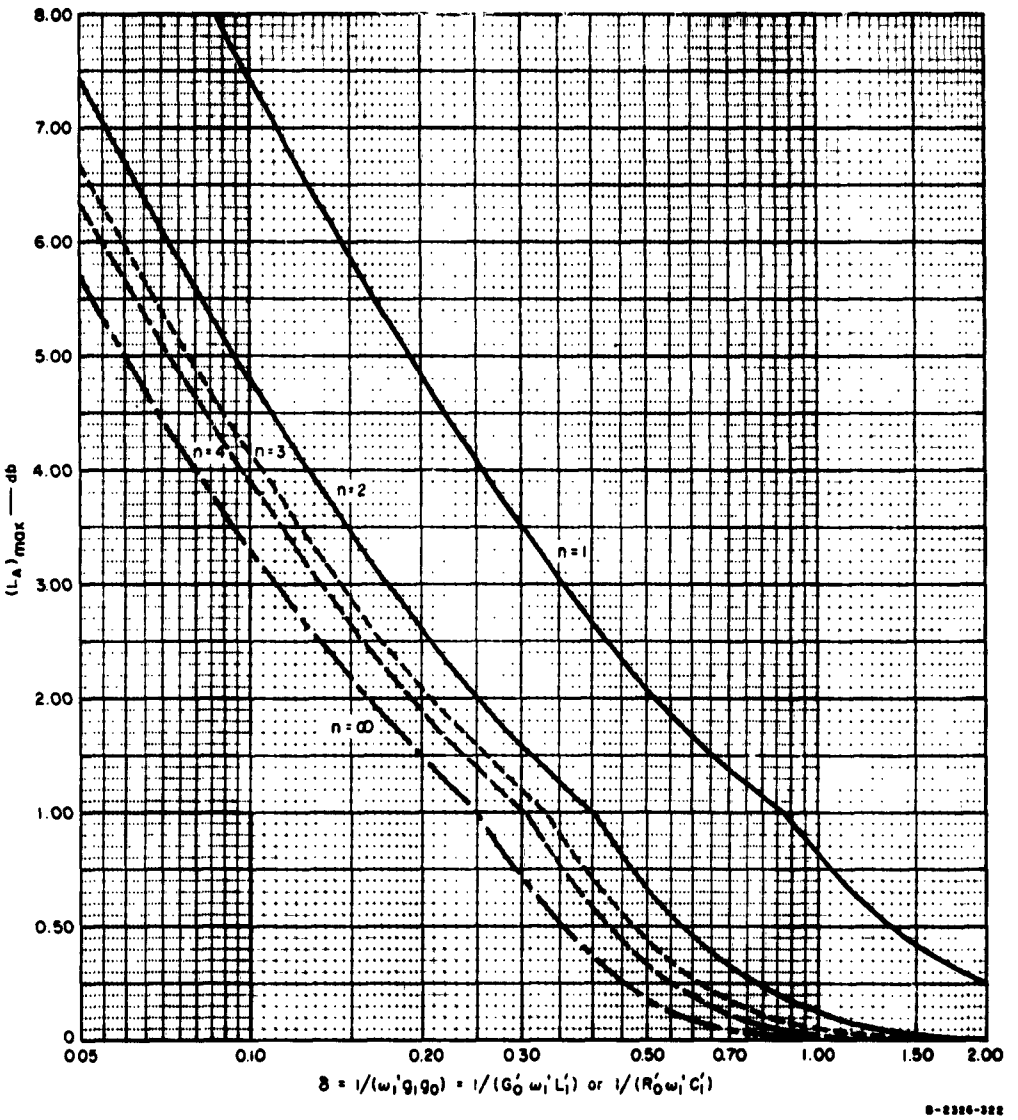

FIG. 4.09-3 $(L_A)_{max}$ vs. δ FOR THE IMPEDANCE-MATCHING NETWORKS WHOSE ELEMENT VALUES ARE GIVEN IN FIGS. 4.09-5 TO -8

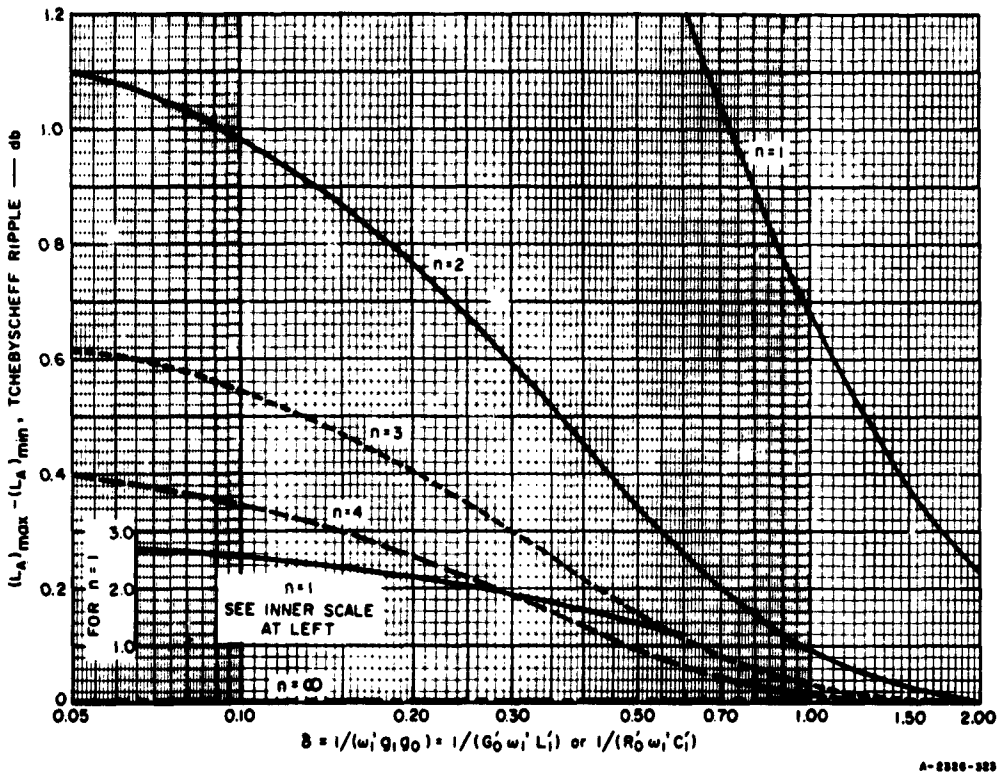

FIG. 4.09-4 TCHEBYSCHEFF RIPPLE IN db vs. δ FOR THE IMPEDANCE-MATCHING NETWORKS WHOSE ELEMENT VALUES ARE GIVEN IN FIGS. 4.09-5 TO 4.09-8

Figures 4.09-5 to 4.09-8 show charts of element values *vs* δ for optimum Tchebyscheff matching networks. Their use is probably best illustrated by an example. Suppose that an impedance match is desired to a load which can be represented approximately by a 50-ohm resistor ($G_0 = 0.020$ mho) in series with an inductance $L_1 = 3.98 \times 10^{-8}$ henry, and that good impedance match is to extend up to $f_1 = 1$ Gc so that $\omega_1 = 2\pi f_1 = 6.28 \times 10^9$. Then the decrement is $\delta = 1/(G_0 \omega_1 L_1) = 1/(0.020 \times 6.28 \times 10^9 \times 3.98 \times 10^{-8}) = 0.20$. After consulting Figs. 4.09-3 and 4.09-4 for $\delta = 0.20$ let us suppose that $n = 4$ is chosen which calls for $(L_A)_{max} = 1.9$ db and a ripple of about 0.25 db. Then by Fig. 4.09-8 (which is for $n = 4$) we obtain for $g_0 = 1$, $\omega_1' = 1$, and $\delta = 0.20$: $g_1/10 = 0.50$, $g_2 = 0.445$, $g_3/10 = 0.54$, $g_4 = 0.205$, and $g_5/10 = 0.39$. This corresponds to the circuit in Fig. 4.09-1 with $g_0 = G_0' = 1$, $g_1 = 5.00 = L_1'$, $g_2 = 0.445 = C_2'$, $g_3 = 5.40 = L_3'$, $g_4 = 0.205 = C_4'$, and $g_5 = 3.90 = R_5'$. Un-normalizing this by use of Eqs. (4.04-2) to (4.04-4) with $(G_0, G_0') = 0.020/1$ and $\omega_1'/\omega_1 = 1/(6.28 \times 10^9) = 1.59 \times 10^{-10}$ gives: $G_0 = 0.020$ mho, $L_1 = 3.98 \times 10^{-8}$ henry, $C_2 = 1.415 \times 10^{-12}$ farad, $L_3 = 4.29 \times 10^{-8}$ henry, $C_4 = 6.52 \times 10^{-13}$ farad, and $R_5 = 195$ ohms. Note that G_0 and L_1 are the original elements given for the load. The physical realization of microwave structures for such an application can be accomplished using techniques discussed in Chapter 7.

It is interesting to note how much the impedance-matching network design discussed above actually improves the power transfer to the load. If the R-L load treated above were driven directly by a generator with a 50-ohm internal impedance, the loss would approach 0 db as $f \to 0$, but it would be 8.6 db at $f_1 = 1$ Gc. By Figs. 4.09-3 to 4.09-5, the optimum $n = 1$ design for this case would call for the generator internal impedance to be about 256 ohms, which would give about 2.6 db loss as $f \to 0$ and 5.9 db loss at 1 Gc (a reduction of 2.7 db from the preceding case). Thus, the $n = 4$ design with only 1.9 db maximum loss and about 0.25 db variation across the operating band is seen to represent a major improvement in performance. Going to larger values of n would give still greater improvement, but even with $n = \infty$, $(L_A)_{max}$ would still be about 1.46 db.

In most microwave cases band-pass rather than low-pass impedance matching networks are desired. The design of such networks is discussed in Chapter 11 working from the prototypes in this section. One special feature of band-pass impedance-matching networks is that they are easily designed to permit any desired value of generator internal resistance,

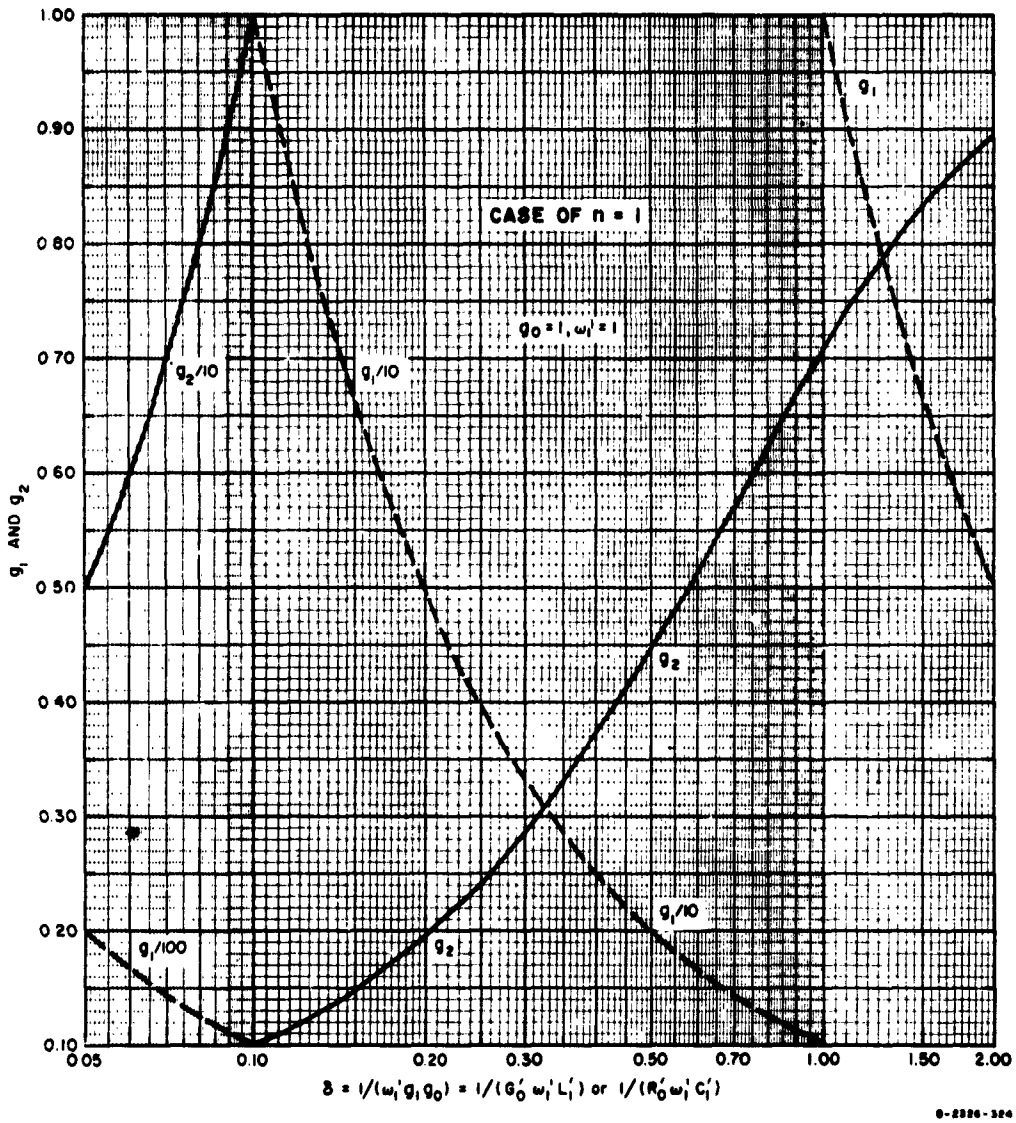

FIG. 4.09-5 ELEMENT VALUES vs. δ FOR TCHEBYSCHEFF IMPEDANCE-MATCHING NETWORKS THAT MINIMIZE $(L_A)_{max}$

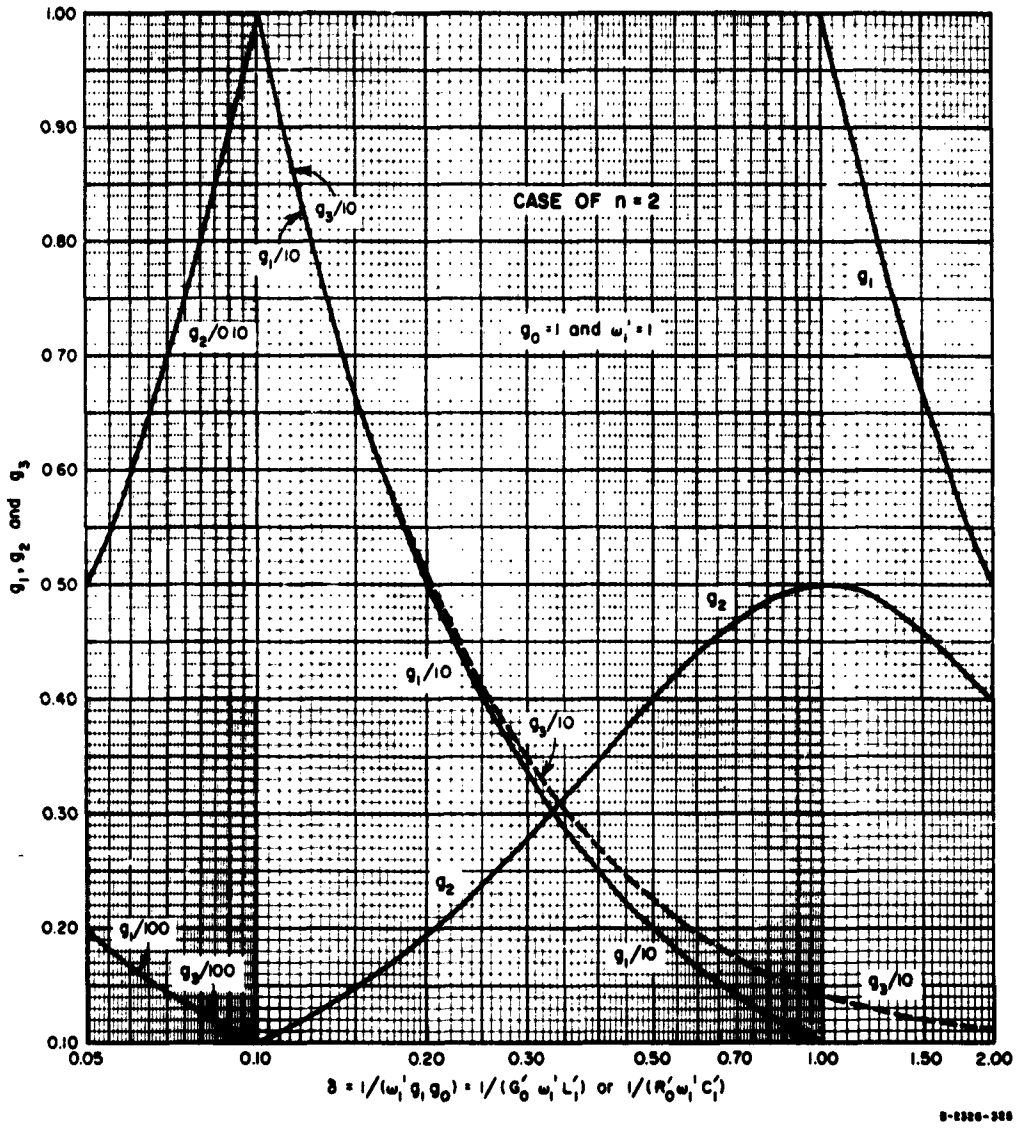

FIG. 4.09-6 ELEMENT VALUES vs. δ FOR TCHEBYSCHEFF IMPEDANCE-MATCHING NETWORKS THAT MINIMIZE $(L_A)_{max}$

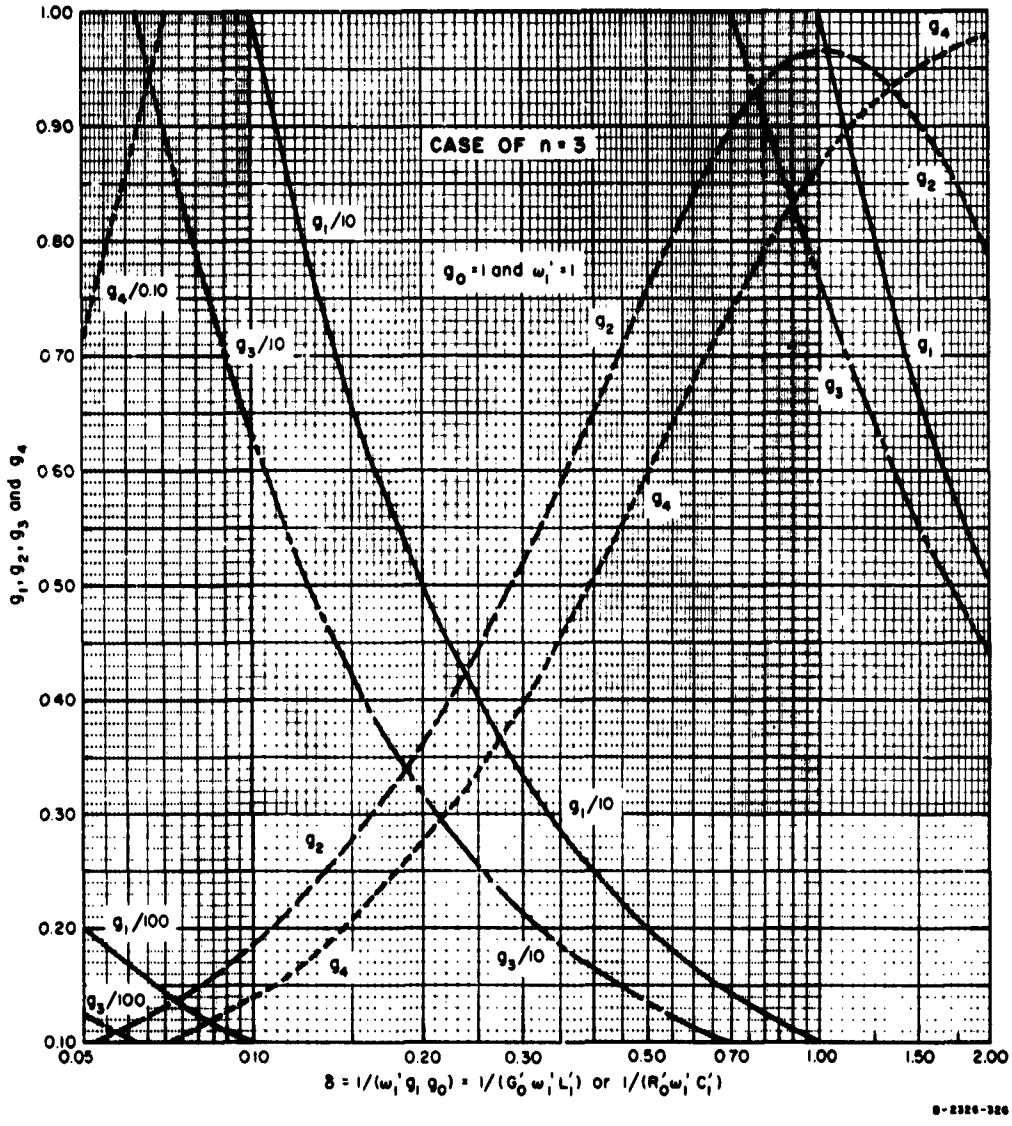

FIG. 4.09-7 ELEMENT VALUES vs. δ FOR TCHEBYSCHEFF IMPEDANCE-MATCHING NETWORKS THAT MINIMIZE $(L_A)_{max}$

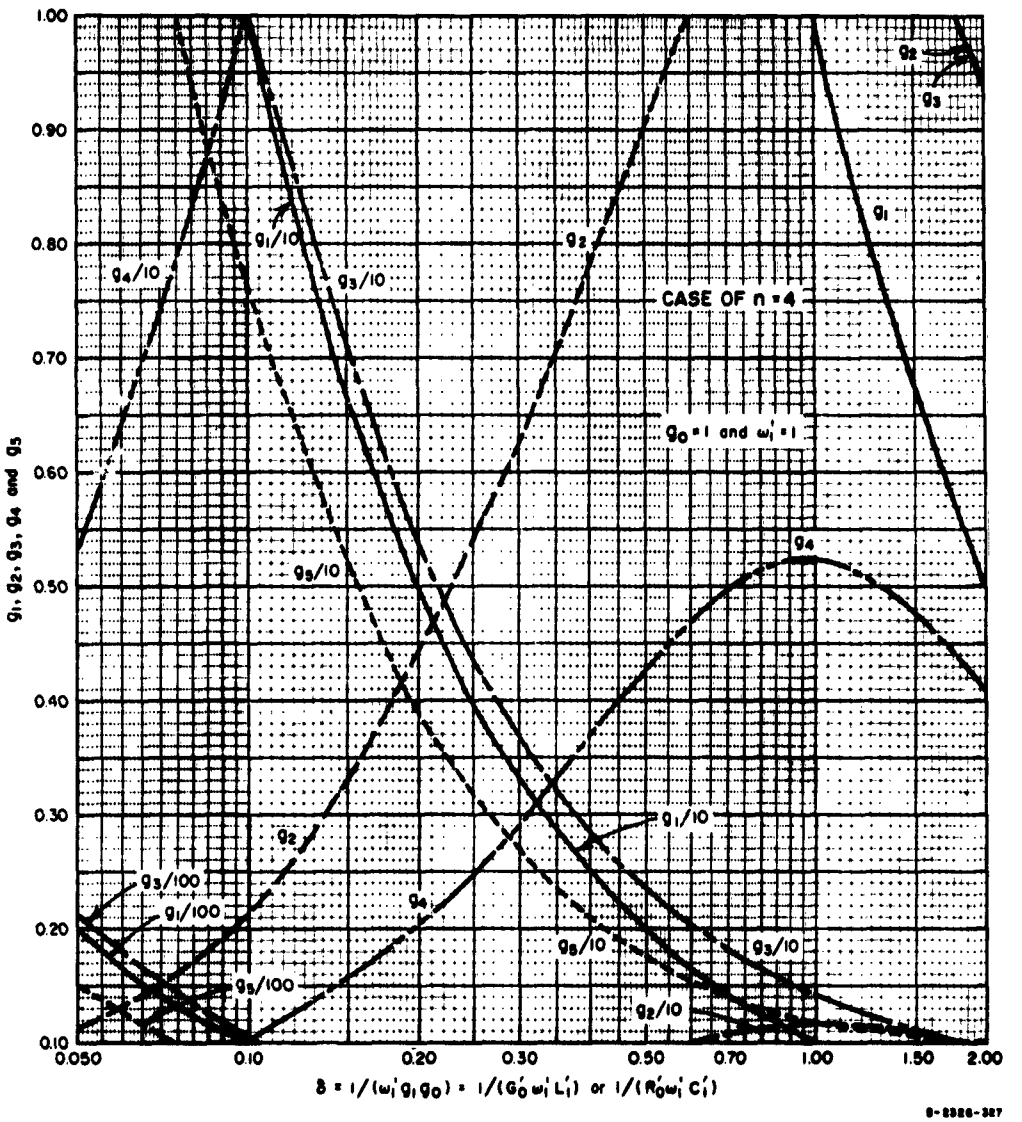

FIG. 4.09-8 ELEMENT VALUES vs. δ FOR TCHEBYSCHEFF IMPEDANCE-MATCHING NETWORKS THAT MINIMIZE $(L_A)_{max}$

whereas low-pass matching networks must have a specified generator internal resistance for optimum design.

The attenuation characteristics of the impedance-matching networks discussed in this section and in Sec. 4.10 may be computed by

$$L_A' = L_A + (L_A)_{min} \quad \text{db} \tag{4.09-2}$$

where L_A' is the attenuation of the impedance-matching network and L_A is obtained by Eqs. (4.03-3) to (4.03-5), or by Figs. 4.03-4 to 4.03-10 for the appropriate db Tchebyscheff ripple $L_{Ar} = (L_A)_{max} - (L_A)_{min}$.

In the next section the calculation of prototype impedance-matching networks so as to give a specified Tchebyscheff ripple [at the cost of a larger $(L_A)_{max}$] will be discussed. The method by which Figs. 4.09-3 to 4.09-8 were prepared will also be outlined.

SEC. 4.10. COMPUTATION OF PROTOTYPE IMPEDANCE-MATCHING NETWORKS FOR SPECIFIED RIPPLE OR MINIMUM REFLECTION

The networks discussed in the preceding section were specified so that $(L_A)_{max}$ was to be as small as possible. Under that condition, it was necessary to accept whatever pass-band Tchebyscheff ripple the charts might call for in the case of any given design. Alternatively, we may specify the pass-band Tchebyscheff ripple and accept whatever value of $(L_A)_{max}$ may result. Since in some cases keeping the pass-band attenuation constant may be the major consideration, computation of prototype matching-network element values for a specified Tchebyscheff ripple will be briefly outlined.

Prototype circuits for specified decrement $\delta = 1/(g_0 g_1 \omega_1')$ and db ripple may be obtained as follows. First compute[14]

$$H = \text{antilog}_{10} \frac{(\text{db Tchebyscheff ripple})}{10} \tag{4.10-1}$$

and

$$d = \sinh\left[\frac{\sinh^{-1}\sqrt{\frac{1}{H-1}}}{n}\right] \tag{4.10-2}$$

where n is the number of reactive elements in the prototype. Next compute

$$e = d - 2\delta \sin\left(\frac{\pi}{2n}\right) \tag{4.10-3}$$

and the maximum, pass-band reflection coefficient value

$$|\Gamma|_{max} = \frac{\cosh\ (n \sinh^{-1} e)}{\cosh\ (n \sinh^{-1} d)} \quad . \tag{4.10-4}$$

Then the $(L_A)_{max}$ value which must be accepted is

$$(L_A)_{max} = 10 \log_{10} \frac{1}{1 - |\Gamma|^2_{max}} \quad . \tag{4.10-5}$$

Figure 4.10-1 shows a plot of $(L_A)_{max}$ *vs* δ for various values of n and various amounts of Tchebyscheff ripple amplitude $[(L_A)_{max} - (L_A)_{min}]$. Suppose that $\delta = 0.10$ and 0.10-db ripple is desired with $n = 2$. This chart shows that $(L_A)_{max}$ will then be 5.9 db. By Figs. 4.09-3 and 4.09-4 it is seen that for the same δ, when $(L_A)_{max}$ is minimized, $(L_A)_{max} = 4.8$ db while the ripple is 0.98 db. Thus, the price for reducing the ripple from 0.98 db to 0.10 db is an increase in $(L_A)_{max}$ of about 1.1 db.

Green's work[6,7] appears to provide the easiest means for determining the element values. Using his equations altered to the notation of this chapter, we obtain

$$D = \frac{d}{\delta \sin\left(\frac{\pi}{2n}\right)} - 1 = \frac{g_0 g_1}{g_{n+1} g_n} \tag{4.10-6}$$

where the g_j's are as defined in Fig. 4.04-1. The element values are then computed by use of the equations

$$g_1 = \frac{1}{\delta \omega_1' g_0} \tag{4.10-7}$$

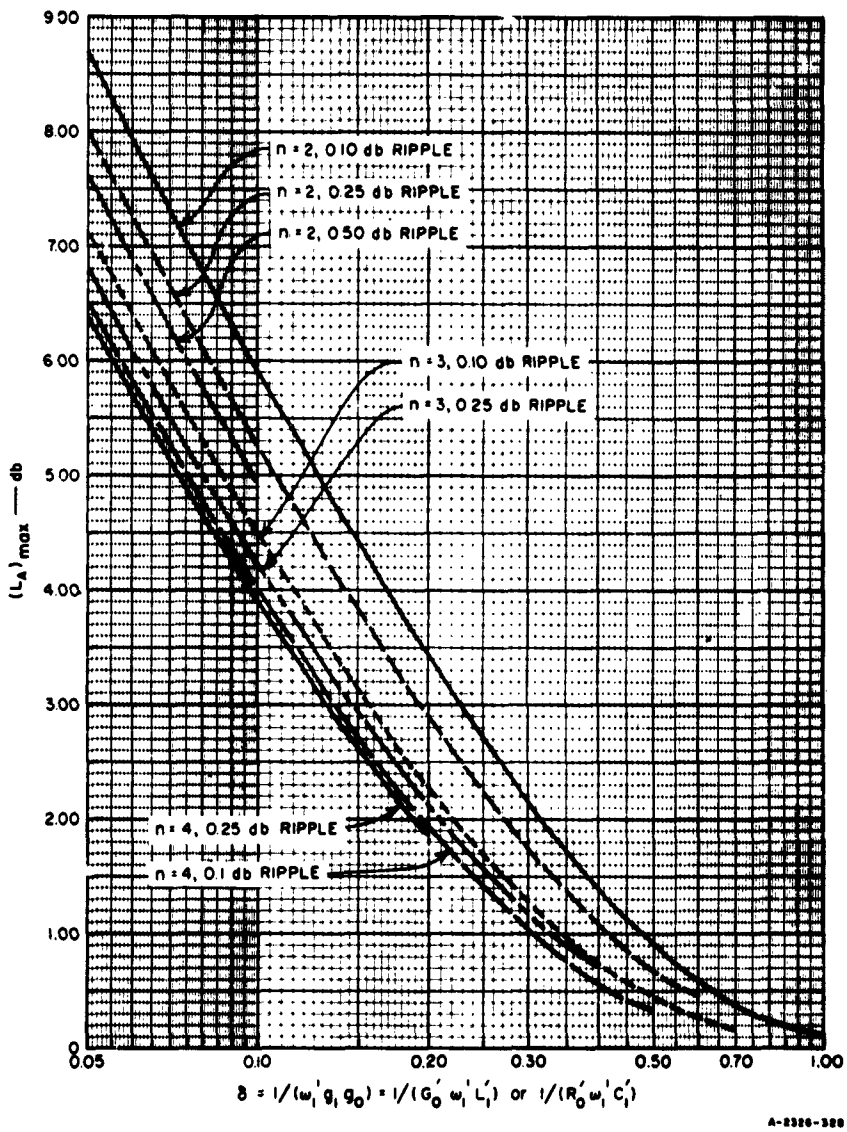

FIG. 4.10-1 $(L_A)_{max}$ vs. δ FOR IMPEDANCE-MATCHING NETWORKS HAVING A SPECIFIED TCHEBYSCHEFF RIPPLE

$$g_j\big|_{j=2\ \text{to}\ n} = \frac{1}{g_{j-1}(k_{j-1,j})^2(\omega_1')^2} \tag{4.10-8}$$

$$g_{n+1} = \frac{1}{D\delta g_n \omega_1'} \tag{4.10-9}$$

where the $k_{j-1,j}$ are coupling coefficients to be evaluated as shown below.

Green's equations for the $k_{j-1,j}$ are[6,7]

$n = 2$

$$k_{12} = \sqrt{\frac{1 + (1 + D^2)\delta^2}{2}} \tag{4.10-10}$$

$n = 3$

$$k_{12} = \sqrt{\frac{3}{8}\left[1 + \left(1 + \frac{D^2}{3}\right)\delta^2\right]} \tag{4.10-11}$$

$$k_{23} = \sqrt{\frac{3}{8}\left[1 + \left(\frac{1}{3} + D^2\right)\delta^2\right]} \tag{4.10-12}$$

$n = 4$

$$k_{12} = \sqrt{\frac{1}{2\sqrt{2}}\left[1 + \left(1 + \frac{8D^2}{\alpha^4}\right)\delta^2\right]} \tag{4.10-13}$$

$$k_{23} = \sqrt{\frac{2}{\alpha^2}\left[1 + \frac{2}{\alpha^2}(1 + D^2)\delta^2\right]} \tag{4.10-14}$$

$$k_{34} = \sqrt{\frac{1}{2\sqrt{2}}\left[1 + \left(\frac{8}{\alpha^4} + D^2\right)\delta^2\right]} \tag{4.10-15}$$

where

$$\alpha^2 = 2(2 + \sqrt{2}) \approx 6.83 \quad .$$

Also, *for n arbitrary,*

$$k_{r,r+1} = \sqrt{\frac{\sin^2 r\theta \cos^2 r\theta + (\cos^2 r\theta + D^2 \sin^2 r\theta)(\sin^2 \theta)\delta^2}{\sin (2r-1)\theta \sin (2r+1)\theta}} \tag{4.10-16}$$

where

$$\theta = 2\pi/n \quad .$$

It is usually convenient to normalize the prototype design so that $g_0 = 1$ and $\omega_1' = 1$, as has been done with the tabulated designs in this chapter.

The element values for the prototype matching networks discussed in Sec. 4.09 and plotted in Figs. 4.09-5 to 4.09-8 could have been obtained using Green's charts[7] of coupling coefficients and D values along with Eqs. (4.10-7) to (4.10-9).* However, in order to ensure high accuracy, to add the $n = 1$ case, and to cover a somewhat wider range of decrements than was treated by Green, the computations for the charts in Sec. 4.09 were carried out from the beginning. The procedure used was that described below.

Fano[14] has shown that, for low-pass networks of the type under consideration, $(L_A)_{max}$ will be as small as possible if

$$\frac{\tanh na}{\cosh a} = \frac{\tanh nb}{\cosh b} \tag{4.10-17}$$

where

$$a = \sinh^{-1} d \tag{4.10-18}$$

$$a = \sinh^{-1} e \tag{4.10-19}$$

and d and e are as indicated in Eqs. (4.10-2) and (4.10-3). By Eqs. (4.10-18), (4.10-19), and (4.10-3),

$$b = \sinh^{-1}\left[\sinh a - 2\delta \sin \frac{\pi}{2n}\right] \quad . \tag{4.10-20}$$

* Barton (see Ref. 15) has independently also computed charts equivalent to the coupling-coefficient charts of Green. Barton, however, includes the maximally flat case in addition.

A computer program was set up to find values of a and b that satisfy Eq. (4.10-17) under the constraint given by Eq. (4.10-20). From these a and b values for various δ, values for d and e were obtained by $d = \sinh a$ and $e = \sinh b$. When values of d and e had been obtained for various δ, the element values for the networks were computed using Eqs. (4.10-6) to (4.10-15).

The data for the charts in Fig. 4.09-3 were obtained by using the values of a and b *vs* δ obtained above, and then computing $(L_A)_{max}$ by use of Eqs. (4.10-18), (4.10-19), (4.10-4), and (4.10-5). The data in Fig. 4.09-4 were obtained by solving Eqs. (4.10-18), (4.10-19), (4.10-1) and (4.10-2) for the db ripple as a function of a and b.

Lossless impedance matching networks for some more general forms of loads are discussed in Refs. 14, 16, 17, and 18. However, much work remains to be done on the practical, microwave realization of the more complicated forms of matching networks called for in such cases. At the present time the prototype networks in Sec. 4.09 and this section appear to have the widest range of usefulness in the design of low-pass, high-pass, and band-pass microwave impedance matching networks in the forms discussed in Chapters 7, and 11.

SEC. 4.11, PROTOTYPES FOR NEGATIVE-RESISTANCE AMPLIFIERS

As was discussed in Sec. 1.04, if a dissipationless filter with resistor terminations has one termination replaced by a negative resistance of the same magnitude, the circuit can become a negative-resistance amplifier. It was noted that, if $\Gamma_1(p)$ is the reflection coefficient between a positive resistance R_0 and the filter, when R_0 is replaced by $R_C'' = -R_0$, the reflection coefficient at that end of the filter becomes

$$\Gamma_1''(p) = \frac{1}{\Gamma_1(p)} \tag{4.11-1}$$

where $p = \sigma + j\omega$ is the complex frequency variable. Then, referring to Figs. 1.04-1 and 1.04-2, the gain of the amplifier as measured at a circulator will be

$$\frac{P_r}{P_{avail}} = |\Gamma_1''(p)|^2_{p=j\omega} = |\Gamma_3''(p)|^2_{p=j\omega} \tag{4.11-2}$$

where P_r is the power reflected into the circulator by the negative-resistance amplifier. If L_A is the attenuation (*i.e.*, transducer loss) in db (as defined in Sec. 2.11) for the dissipationless filter with positive terminations, then the transducer gain when R_0 is replaced by $R_0'' = -R_0$ will be

$$\frac{P_r}{P_{avail}} = \frac{1}{1 - |t|^2} \tag{4.11-3}$$

where

$$|t|^2 = \frac{1}{\text{antilog}_{10} \frac{L_A}{10}} \quad . \tag{4.11-4}$$

and t is the transmission coefficient (for positive terminations) discussed in Secs. 2.10 and 2.11. Figure 4.11-1 shows a graph of L_A in db

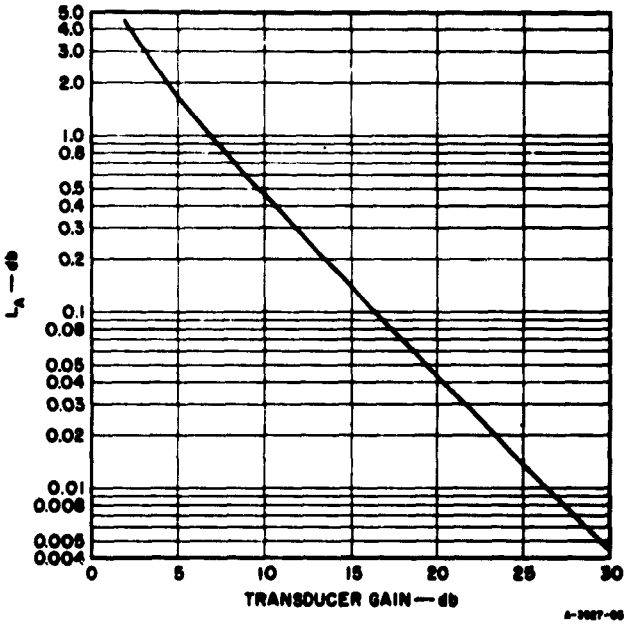

FIG. 4.11-1 ATTENUATION OF A PASSIVE FILTER vs. TRANSDUCER GAIN OF THE CORRESPONDING NEGATIVE-RESISTANCE AMPLIFIER USING A CIRCULATOR

for a filter with positive resistance terminations vs the db transducer gain of the corresponding negative-resistance amplifier with a circulator, as determined using the above relations.

The prototype impedance-matching filters discussed in Secs. 4.09 and 4.10 can also be used as prototypes for negative-resistance amplifiers. With regard to their use, some consideration must be given to the matter of stability. Let us define $\Gamma_1(p)$ as the reflection coefficient between any of the filters in Fig. 4.04-1 and the termination $g_0 = R_0$ or G_0 at the left and $\Gamma_n(p)$ as the reflection coefficient at the other end. It can be shown that the poles of a reflection coefficient function are the frequencies of natural vibration of the circuit (see Secs. 2.02 to 2.04), hence, they must lie in the left half of the complex-frequency plane if the circuit is passive. However, the zeros of $\Gamma_1(p)$, or of $\Gamma_n(p)$, can lie in either the left or right half of the p-plane. Since $\Gamma_1''(p) = 1/\Gamma_1(p)$, the *zeros* of $\Gamma_1(p)$ for the passive filter become the *poles* of $\Gamma_1''(p)$ for the negative-resistance amplifier. Thus, in choosing a filter as a prototype for a negative-resistance amplifier, it is important that $\Gamma_1(p)$ have its zeros in the left half plane since if they are not, when these zeros become poles of $\Gamma_1''(p)$ for the negative-resistance amplifier they will cause exponentially increasing oscillations (*i.e.*, until some non-linearity in the circuit limits the amplitude).

The mathematical data given in Secs. 4.09 and 4.10 for filter prototypes of the various forms in Fig. 4.04-1 are such that the reflection coefficient $\Gamma_1(p)$ involving the termination g_0 on the left will have all of its zeros in the left half of the p-plane, while the reflection coefficient $\Gamma_n(p)$ involving the termination g_{n+1} on the right will have all of its zeros in the right half plane.* For this reason it is seen that the termination g_0 at the left must be the one which is replaced by its negative, *never* the termination g_{n+1} at the right.

Let us suppose that a prototype is desired to give 15 db peak gain with 2 db Tchebyscheff ripple. Then by Fig. 4.11-1, $(L_A)_{min} = 0.138$ db, $(L_A)_{max} = 0.22$ db, and the ripple of the passive filter is $0.220 - 0.138 = 0.082$ db. The parameter d in Sec. 4.10 is then computed by use of Eqs. (4.10-1) and (4.10-2).

---

* An exception to this occurs when $e = 0$ in Eq. (4.10-3) which leads to $(L_A)_{min} = 0$ in Fig. 4.09-2. Then the zeros of $\Gamma_1(p)$ and $\Gamma_n(p)$ are all on the $p = j\omega$ axis of the p-plane.

Next the parameter δ is obtained as follows: compute

$$|t|_x^2 = \frac{1}{\text{antilog}_{10} \frac{(L_A)_{max}}{10}} \tag{4.11-5}$$

$$|\Gamma|_{max} = \sqrt{1 - |t|_x^2} \tag{4.11-6}$$

$$e = \sinh \left\{ \frac{\cosh^{-1} \left[|\Gamma|_{max} \cosh \left(n \sinh^{-1} d \right) \right]}{n} \right\} \tag{4.11-7}$$

and then

$$\delta = \frac{d - e}{2 \sin \frac{\pi}{2n}} \quad . \tag{4.11-8}$$

[Equations (4.11-5) to (4.11-8) were obtained using Eqs. (4.10-3) to (4.10-5).] Having values for d and δ (and having chosen a value for n) the element values may be computed as indicated by Eqs. (4.10-6) to (4.10-16). In some cases the designs whose element values are plotted in Figs. 4.09-5 to 4.09-8 will be satisfactory and computations will be unnecessary.

In some cases (such as for the low-pass prototype for the band-pass negative-resistance amplifier example discussed in Sec. 11.10) the decrement δ of the prototype may be fixed, and the choice of low-pass prototype may hinge around the question: What maximum gain value can be achieved for the given δ with acceptable value of pass-band gain ripple? This question can readily be answered by use of Eqs. (4.10-1) to (4.10-5). First, an estimate is made of the db pass-band ripple for the filter with positive terminations which will result in an acceptable amount of pass-band ripple in $|\Gamma_1''(j\omega'')|^2$ *vs* ω' when the positive termination g_0 is replaced by a negative termination $-g_0$. Then, having specified δ and the db ripple of the passive filter response by Eqs. (4.10-1) to (4.10-5) the parameters H, d, e, $(L_A)_{max}$, and $(L_A)_{min} = (L_A)_{max}$ − (db ripple) for the filter with g_0 positive can be determined. Knowing $(L_A)_{max}$ and $(L_A)_{min}$ for the passive filter (*i.e.*, for g_0 positive), the pass-band maximum and minimum gain with g_0 replaced by $-g_0$ and with a circulator attached

at the other end, can be obtained from Fig. 4.11-1. If the response is not as desired, more desirable characteristics may be achieved by starting with a different value of pass-band ripple for the filter with positive terminations. Having arrived at a trade-off between peak gain and size of pass-band gain ripple, which is acceptable for the application at hand, the element values for the prototype are computed using the equations in Sec. 4.10 from n, δ, d, and whatever convenient ω_1' value is specified. Note that the larger the number of elements n, the flatter the response can be for a given gain. But as n gets large the improvement in performance per unit increase in n is small. Thus, *if δ for the load, and the peak gain are both specified,* it may not be possible to make the gain ripples as small as may be desired even if the number n of reactive elements is infinite.

SEC. 4.12, CONVERSION OF FILTER PROTOTYPES TO USE IMPEDANCE- OR ADMITTANCE-INVERTERS AND ONLY ONE KIND OF REACTIVE ELEMENT

In deriving design equations for certain types of band-pass and band-stop filters it is desirable to convert the prototypes in Fig. 4.04-1 which use both inductances and capacitances to equivalent forms which use only inductances or only capacitances. This can be done with the aid of the idealized inverters which are symbolized in Fig. 4.12-1.

An idealized *impedance inverter* operates like a quarter-wavelength line of characteristic impedance K at all frequencies. Therefore, if it is terminated in an impedance Z_b on one end, the impedance Z_a seen looking in at the other end is

$$Z_a = \frac{K^2}{Z_b} \quad . \tag{4.12-1}$$

An idealized *admittance inverter* as defined herein is the admittance representation of the same thing, *i.e.*, it operates like a quarter-wavelength line of characteristic admittance J at all frequencies. Thus, if an admittance Y_b is attached at one end, the admittance Y_a seen looking in the other end is

$$Y_a = \frac{J^2}{Y_b} \quad . \tag{4.12-2}$$

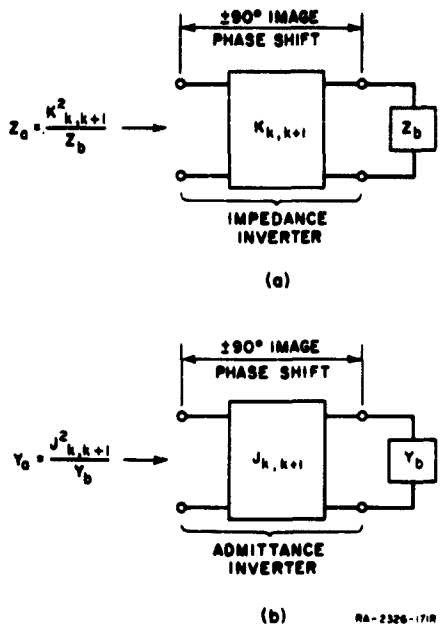

SOURCE: Final Report, Contract DA 36-039 SC-74862, Stanford Research Institute, reprinted in *IRE Trans., PGMTT* (see Ref. 1 of Chapter 10, by G. L. Matthaei).

FIG. 4.12-1 DEFINITION OF IMPEDANCE INVERTERS AND ADMITTANCE INVERTERS

As indicated in Fig. 4.12-1, an inverter may have an image phase shift of either ±90 degrees or an odd multiple thereof.

Because of the inverting action indicated by Eqs. (4.12-1) and (4.12-2) a series inductance with an inverter on each side looks like a shunt capacitance from its exterior terminals. Likewise, a shunt capacitance with an inverter on both sides looks like a series inductance from its external terminals. Making use of this property, the prototype circuits in Fig. 4.04-1 can be converted to either of the equivalent forms in Fig. 4.12-2 which have identical transmission characteristics to those prototypes in Fig. 4.04-1. As can be seen from Eqs. (4.12-1) and (4.12-2), inverters have the ability to shift impedance or admittance levels depending on the choice of the K or J parameters. For this reason in Fig. 4.12-2(a) the sizes of R_A, R_B, and the inductances L_{ak} may be chosen arbitrarily and the response will be identical to that of the original prototype as in Fig. 4.04-1 provided that the inverter parameters $K_{k,k+1}$ are specified as indicated by the equations in Fig. 4.12-2(a). The same holds for the circuit in Fig. 4.12-2(b) only on the dual basis. Note that the g_k values referred to in the equations in Fig. 4.12-2 are the prototype element values as defined in Fig. 4.04-1.

A way that the equations for the $K_{k,k+1}$ and $J_{k,k+1}$ can be derived will now be briefly considered. A fundamental way of looking at the relation between the prototype circuits in Figs. 4.04-1(a), (b) and the corresponding circuit in, say, Fig. 4.12-2(a) makes use of the concept of duality. A given circuit as seen through an impedance inverter looks like the dual of that given circuit. Thus, the impedances seen from

inductor L_{a1} in Fig. 4.12-2(a) are the same as those seen from inductance L_1' in Fig. 4.04-1(b), except for an impedance scale factor. The impedances seen from inductor L_{a2} in Fig. 4.12-2(a) are identical to those seen from inductance L_2' in Fig. 4.04-1(a), except for a possible impedance scale change. In this manner the impedances in any point of the circuit in Fig. 4.12-2(a) may be quantitatively related to the corresponding impedances in the circuits in Fig. 4.04-1(a), (b).

Figure 4.12-3(a) shows a portion of a low-pass prototype circuit that has been open-circuited just beyond the capacitor C_{k+1}. The dual circuit is shown at (b), where it should be noted that the open circuit

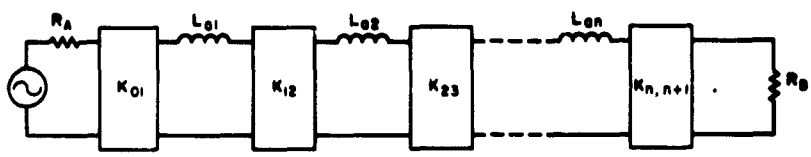

$$K_{01} = \sqrt{\frac{R_A L_{a1}}{g_0 g_1}} \quad , \quad K_{k,k+1}\Big|_{k=1 \text{ to } n-1} = \sqrt{\frac{L_{ak} L_{a(k+1)}}{g_k g_{k+1}}} \quad , \quad K_{n,n+1} = \sqrt{\frac{L_{an} R_B}{g_n g_{n+1}}}$$

(a) MODIFIED PROTOTYPE USING IMPEDANCE INVERTERS

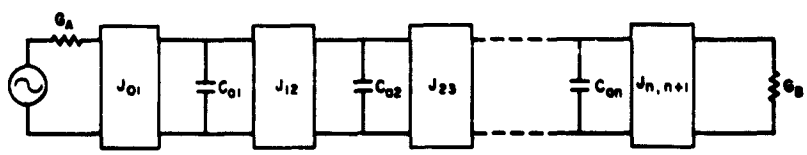

$$J_{01} = \sqrt{\frac{G_A C_{a1}}{g_0 g_1}} \quad , \quad J_{k,k+1}\Big|_{k=1 \text{ to } n-1} = \sqrt{\frac{C_{ak} C_{a(k+1)}}{g_k g_{k+1}}} \quad , \quad J_{n,n+1} = \sqrt{\frac{C_{an} G_B}{g_n g_{n+1}}}$$

(b) MODIFIED PROTOTYPE USING ADMITTANCE INVERTERS

RB-2326-77-1729

SOURCE: Final Report, Contract DA 36-039 SC-74862, Stanford Research Institute, reprinted in *IRE Trans., PGMTT* (see Ref. 1 of Chapter 10, by G. L. Matthaei).

FIG. 4.12-2 LOW-PASS PROTOTYPES MODIFIED TO INCLUDE IMPEDANCE INVERTERS OR ADMITTANCE INVERTERS The $g_0, g_1, \ldots, g_{n+1}$ are obtained from the original prototype as in Fig. 4.04-1, while the $R_A, L_{a1}, \ldots, L_{an}$, and R_B or the $G_A, C_{a1}, \ldots, C_{an}$ and G_B may be chosen as desired.

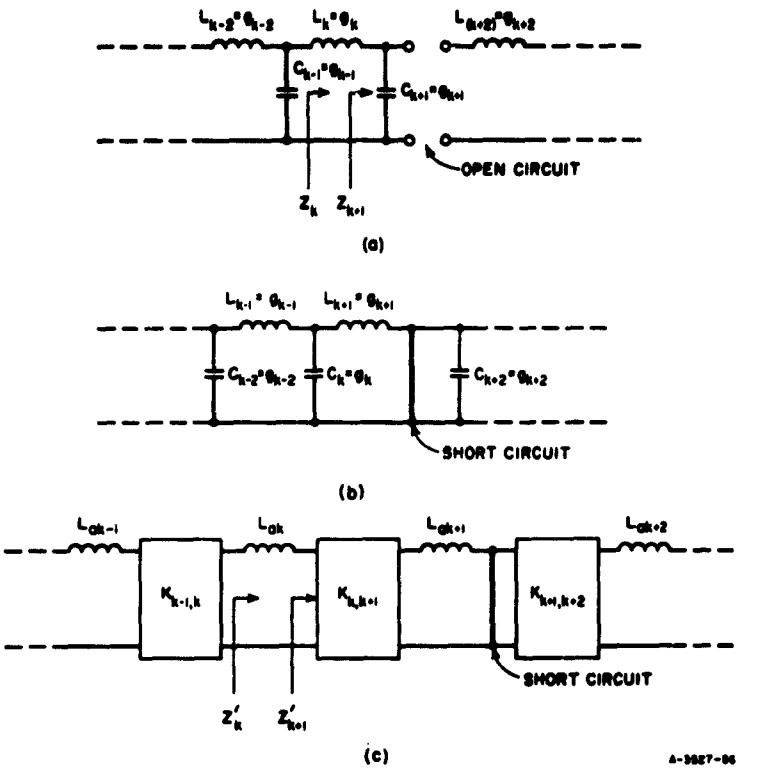

FIG. 4.12-3 SOME CIRCUITS DISCUSSED IN SEC. 4.12
A ladder circuit is shown at (a), and its dual is shown at (b). The analogous K-inverter form of these two circuits is shown at (c).

shown at (a) becomes a short circuit in the dual case. The corresponding circuit using all series inductors and K inverters is shown at (c). The circuits in Fig. 4.12-3 will be convenient for deriving the formula for $K_{k,k+1}$ in terms of L_{ak}, L_{ak+1}, and the prototype element values g_k and g_{k+1}. The open- and short-circuits are introduced merely to simplify the equations.

Referring to Fig. 4.12-3, in the circuit at (a),

$$Z_k = j\omega L_k + \frac{1}{j\omega C_{k+1}} \qquad (4.12\text{-}3)$$

Meanwhile in the circuit at (c)

$$Z'_k = j\omega L_{ak} + \frac{K^2_{k,k+1}}{j\omega L_{ak+1}} \quad . \qquad (4.12\text{-}4)$$

Now Z_k' must be identical to Z_k except for an impedance scale change of L_{ak}/L_k. Therefore

$$Z_k' = \frac{L_{ak}}{L_k} Z_k = j\omega L_{ak} + \frac{L_{ak}}{L_k} \frac{1}{j\omega C_{k+1}} \quad . \qquad (4.12\text{-}5)$$

Equating the second terms in Eqs. (4.12-4) and (4.12-5) gives, after some rearrangement,

$$K_{k,k+1} = \sqrt{\frac{L_{ak} L_{ak+1}}{L_k C_{k+1}}} \quad . \qquad (4.12\text{-}6)$$

Since $L_k = g_k$ and $C_{k+1} = g_{k+1}$, Eq. (4.12-6) is equivalent to the equation for $K_{k,k+1}$ given in Fig. 4.12-2(a). It is easily seen that by moving the positions of the open- and short-circuit points correspondingly, the same procedure would apply for calculation of the K's for all the inverters except those at the ends. Hence, Eq. (4.12-6) applies for $k = 1, 2, \ldots, n-1$.

Next consider Fig. 4.12-4. At (a) is shown the last two elements of a prototype circuit and at (b) is shown a corresponding form with a K inverter. In the circuit at (a)

$$Z_n = j\omega L_n + \frac{1}{G_{n+1}} \qquad (4.12\text{-}7)$$

while at (b)

$$Z_n' = j\omega L_{an} + \frac{K_{n,n+1}^2}{R_B} \quad . \qquad (4.12\text{-}8)$$

Since Z_n' must equal Z_n within a scale factor L_{an}/L_n,

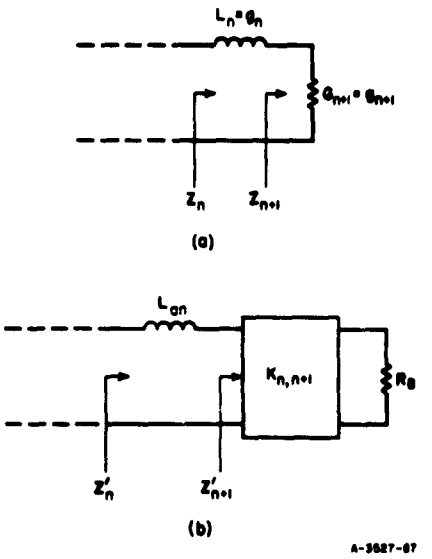

FIG. 4.12-4 ADDITIONAL CIRCUITS DISCUSSED IN SEC. 4.12
The end portion of a prototype circuit is shown at (a) while at (b) is shown the corresponding end portion of a circuit with K-inverters.

$$Z'_n = \frac{L_{an}}{L_n} Z_n = j\omega L_{an} + \frac{L_{an}}{L_n} \frac{1}{G_{n+1}} \quad . \qquad (4.12\text{-}9)$$

Equating the second terms of Eqs. (4.12-8) and (4.12-9) leads to the result

$$K_{n,n+1} = \sqrt{\frac{L_{an} R_B}{L_n G_{n+1}}} \quad . \qquad (4.12\text{-}10)$$

Substituting g_n and g_{n+1} for L_n and G_{n+1}, respectively, gives the equation for $K_{n,n+1}$ shown in Fig. 4.12-2.

The derivation of the equations for the $J_{k,k+1}$ parameters in Fig. 4.12-2(b) may be carried out in like manner on the admittance (*i.e.*, dual) basis.

SEC. 4.13, EFFECTS OF DISSIPATIVE ELEMENTS IN PROTOTYPES FOR LOW-PASS, BAND-PASS, OR HIGH-PASS FILTERS

Any practical microwave filter will have elements with finite Q's, and in many practical situations it is important to be able to estimate the effect of these finite element Q's on pass-band attenuation. When a filter has been designed from a low-pass prototype filter it is convenient to relate the microwave filter element Q's to dissipative elements in the prototype filter and then determine the effects of the dissipative elements on the prototype filter response. Then the increase in pass-band attenuation of the prototype filter due to the dissipative elements will be the same as the increase in pass-band attenuation (at the corresponding frequency) of the microwave filter due to the finite element Q's.

The element Q's referred to below are those of the elements of a low-pass filter at its cutoff frequency ω_1 and are defined as

$$Q_k = \frac{\omega_1 L_k}{R_k} \quad \text{or} \quad \frac{\omega_1 C_k}{G_k} \qquad (4.13\text{-}1)$$

where R_k is the parasitic resistance of the inductance L_k, and G_k is the parasitic conductance of the capacitance C_k.* In the case of a band-pass

* Here, the unprimed L_k, R_k, C_k, G_k, and ω_1 values are meant to apply to any low-pass filter, whether it is a normalized prototype or not. Later in this section primes will be introduced to aid in distinguishing between the low-pass prototype parameters and those of the corresponding band-pass or high-pass filter.

filter which is designed from a low-pass prototype, if $(Q_{BP})_k$ is the mid-band unloaded Q of the kth resonator of the band-pass filter, then the corresponding Q of the kth reactive element of the prototype is

$$Q_k = w(Q_{BP})_k \quad . \tag{4.13-2}$$

In this equation w is the fractional bandwidth of the band-pass filter as measured to its pass-band edges which correspond to the ω_1' pass-band edge of the low-pass prototype (see Chapter 8). The unloaded Q of the resonators can be estimated by use of the data in Chapter 5, or it can be determined by measurements as in Sec. 11.02.

In the case of a high-pass filter designed from a low-pass prototype, the element Q's of the prototype should be made to be the same as the Q's of the corresponding elements of the high-pass filter at its cutoff frequency.

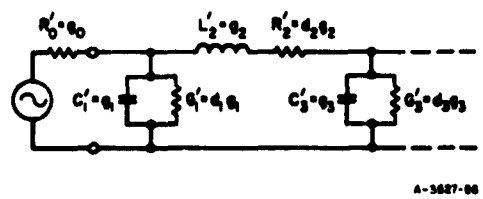

FIG. 4.13-1 LOW-PASS PROTOTYPE FILTER WITH DISSIPATIVE ELEMENTS ADDED

Figure 4.13-1 shows a portion of a low-pass prototype filter with parasitic loss elements introduced. Note that the parasitic loss element to go with reactive element g_k is designated as $d_k g_k$, where d_k will be referred to herein as a *dissipation factor*. Using this notation Eq. (4.13-1) becomes $Q_k = \omega_1' g_k/(d_k g_k) = \omega_1'/d_k$ where ω_1' is the cutoff frequency of the low-pass prototype. Thus,

$$d_k = \frac{\omega_1'}{Q_k} \quad . \tag{4.13-3}$$

Then for a series branch of a prototype filter

$$Z_k = j\omega' L_k' + R_k' = (j\omega' + d_k) g_k \tag{4.13-4}$$

and for a shunt branch

$$Y_k = j\omega' C_k' + G_k' = (j\omega' + d_k) g_k \tag{4.13-5}$$

A special case of considerable practical interest is that where the Q's of all the elements are the same so that $d_k = d$ for $k = 1$ to n. Then, as can be seen from Eqs. (4.13-4) and (4.13-5), the effects of dissipation can be accounted for by simply replacing the frequency variable $j\omega'$ for the lossless circuit by $(j\omega' + d)$ to include the losses. For example, this substitution can be made directly in the transfer functions in Eqs. (4.07-1), (4.08-5) to (4.08-8) in order to compute the transfer characteristics with parasitic dissipation included. At DC the function $(j\omega' + d)$ becomes simply d, so that if

$$\frac{(E_2)_{avail}}{E_2} = P_n(p')\big|_{p'=j\omega'} = a_n(j\omega')^n + \ldots + a_1\, j\omega' + a_0 \quad (4.13\text{-}6)$$

for a dissipationless prototype, the DC loss for a prototype with uniform dissipation d is for $\omega' = 0$

$$\left.\frac{(E_2)_{avail}}{E_2}\right|_{\omega'=0} = P_n(d) = a_n d^n + \ldots + a_1 d + a_0 \quad (4.13\text{-}7)$$

where $(E_2)_{avail}/E_2$ is as defined in Sec. 2.10. Usually d is small so that only the last two terms of Eq. (4.13-7) are significant. Then it is easily shown that

$$(\Delta L_A)_0 = 20 \log_{10} [C_n d + 1] \text{ db} \quad (4.13\text{-}8)$$

$$\approx 8.686\, C_n d$$

where $(\Delta L_A)_0$ is the db *increase* in attenuation at $\omega' = 0$ when d is finite, over the attenuation when $d = 0$ (*i.e.*, when there is no dissipation loss).* The coefficient $C_n = a_1/a_0$ where a_1 and a_0 are from polynomial $P_n(j\omega')$ in Eq. (4.13-6).

In the case of low-pass prototypes for band-pass filters, $(\Delta L_A)_0$ is also the increase in the *midband* loss of the corresponding band-pass filter as a result of finite resonator Q's. For high-pass filters designed

* For example, a dissipationless, 0.5-db ripple Tchebyscheff filter with $n = 4$ would have $L_A = 0.5$ db for $\omega' = 0$. If uniform dissipation is introduced the attenuation for $\omega' = 0$ will become $L_A = 0.5 + (\Delta L_A)_0$ db.

from low-pass prototypes, $(\Delta L_A)_0$ relates to the attenuation as $\omega \to \infty$. Equation (4.13-8) applies both for prototypes such as those in Sec. 4.05 which for the case of no dissipation loss have points where L_A is zero, and also for the impedance-matching network prototypes in Secs. 4.09 and 4.10 which even for the case of no dissipation have non-zero L_A at all frequencies.

Table 4.13-1 is a tabulation of the coefficients C_n for prototype filters having maximally flat attenuation with their 3-db point at $\omega_1' = 1$. Figure 4.13-2 shows the C_n coefficients for Tchebyscheff filters plotted *vs* db pass-band ripple. In this case the equal-ripple band edge is $\omega_1' = 1$. Note that above about 0.3 db-ripple, the curves fall for n even and rise for n odd. This phenomenon is related to the fact that a Tchebyscheff prototype filter with n even has a ripple maximum at $\omega' = 0$, while a corresponding filter with n odd has a ripple minimum at that frequency. There is apparently a tendency for the effects of dissipation to be most pronounced at ripple minima.

Table 4.13-1

MAXIMALLY FLAT ATTENUATION FILTER COEFFICIENTS C_n FOR USE IN EQ. (4.13-8)

These coefficients are for filters with their 3-db point at $\omega_1' = 1$ and are equal to the group time delay in seconds as ω' approaches zero [see Eq. (4.08-2)]

n	C_n	n	C_n
1	1.00	9	5.76
2	1.41	10	6.39
3	2.00	11	7.03
4	2.61	12	7.66
5	3.24	13	8.30
6	3.86	14	8.93
7	4.49	15	9.57
8	5.13		

Bode[19] gives an equation for ΔL_A, the increase in attenuation due to uniform dissipation, as a function of the attenuation phase slope and the dissipation factor, d. Bode's equation may be expressed in the form

$$\Delta L_A = 8.686\, d\, \frac{d\varphi}{d\omega'} \quad \text{db} \tag{4.13-9}$$

where

$$\varphi = \arg \frac{(E_2)_{avail}}{E_2} \tag{4.13-10}$$

and in this case ΔL_A is the increase in attenuation at, ω', the frequency, at which $d\varphi/d\omega'$ is evaluated.* Thus, this equation provides a convenient

* It can be seen from Eqs. (4.13-8) and (4.13-9) that the C_n coefficients in Table 4.13-1 and Fig. 4.13-2 are equal to the group time delay in seconds as ω' approaches zero.

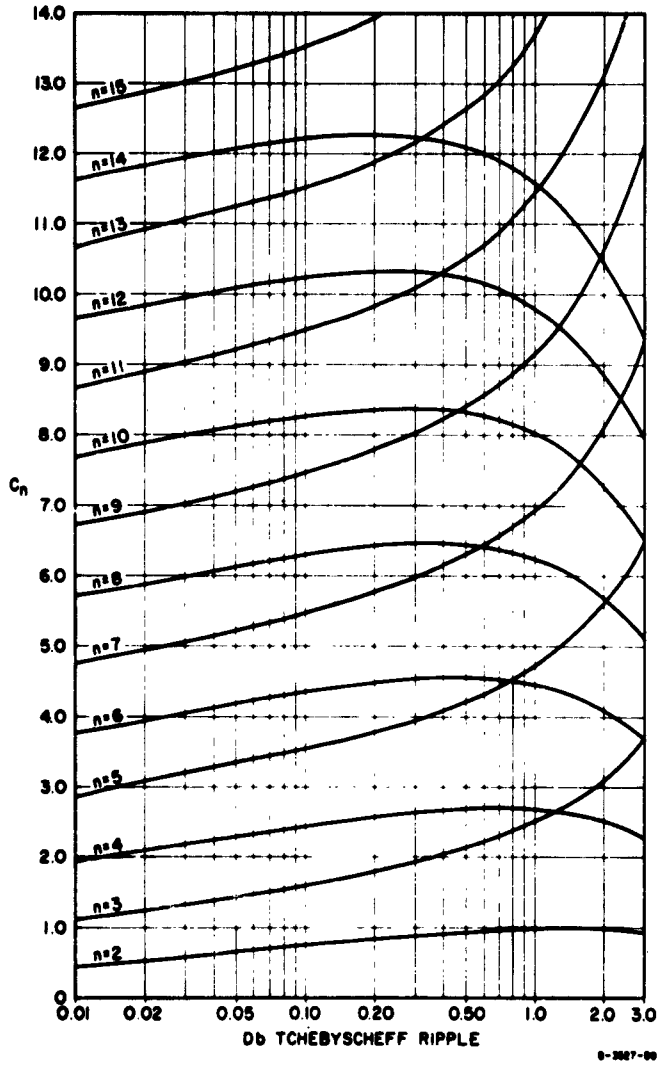

FIG. 4.13-2 PROTOTYPE TCHEBYSCHEFF FILTER COEFFICIENTS C_n vs. db TCHEBYSCHEFF RIPPLE, FOR PROTOTYPES WITH n REACTIVE ELEMENTS AND $\omega_1' = 1$
These coefficients are for use in Eq. (4.13-8). They are also the group time delay in seconds as ω' approaches zero (see Eq. 4.08-2).

means for estimating the effects of uniform dissipation at any frequency. Bode's discussion[19] indicates that for cases where all the inductances have a given Q, Q_L, and all of the capacitances have another Q, Q_c, good results can be obtained by computing d as $2\omega_1'/(Q_L + Q_c)$.

Cohn[20] has presented another formula which is convenient for estimating the effects of dissipation loss of low-pass prototypes for $\omega' = 0$. His formula may be expressed in the form

$$(\Delta L_A)_0 = 4.343 \sum_{k=1}^{n} d_k g_k \quad \text{db} \qquad (4.13\text{-}11)$$

where the d_k are given by Eq. (4.13-3), and the prototype element values g_k are specifically assumed to have been normalized so that $g_0 = 1$ (as has been done for all of the prototypes discussed in this chapter). Note that this formula does not require that the dissipation be uniform. Equation (4.13-11) was derived by assuming that the load and source resistances are both one ohm, and that the effect of each R_k' or G_k' in Fig. 4.13-1 at $\omega' = 0$ is to act as voltage or current divider with respect to one ohm.[20] As a result, Eq. (4.13-11) can lead to appreciable error if the load and source resistances are sizeably different, though it generally gives very good results if the terminations are equal or at least not very greatly different.*

Table 4.13-2 compares the accuracy of Eqs. (4.13-8), (4.13-9), and (4.13-11) for various Tchebyscheff filters having uniform dissipation. Cases 1 to 3, which are for filters with $n = 4$ reactive elements, have

Table 4.13-2

COMPARISON OF ACCURACY OF EQS. (4.13-8), (4.13-9), AND (4.13-11) FOR COMPUTING $(\Delta L_A)_0$ FOR VARIOUS TCHEBYSCHEFF FILTERS HAVING UNIFORM DISSIPATION

CASE	n	db RIPPLE	Q	$(\Delta L_A)_0$ ACTUAL VALUE	$(\Delta L_A)_0$ BY EQ. (4.13-8)	$(\Delta L_A)_0$ BY EQ. (4.13-9)	$(\Delta L_A)_0$ BY EQ. (4.13-11)
1	4	0.5	100	0.236	0.232	--	0.264
2	4	2.0	100	0.223	0.214	--	0.346
3	4	2.0	10	2.39	1.95	--	3.46
4	5	0.5	100	0.364	0.357	0.35	0.365
5	5	0.5	10	3.55	3.05	3.5	3.65

* Equation (4.13-11) can be made to be more accurate for the case of unequal terminations by multiplying its right-hand side by $4R_0R_{n+1}/(R_0 + R_{n+1})^2$ where R_0 and R_{n+1} are the resistances of the terminations. This can be seen from the alternate point of view in Sec. 6.14.

unequal terminations; hence, Eq. (4.13-11) has relatively low accuracy if the pass-band ripples are large. Equation (4.13-8) gives reduced accuracy if the value of Q is very low. This happens as a result of using only the last two terms in Eq. (4.13-7). The actual value of $(\Delta L_A)_0$ was computed by using as many terms in Eq. (4.13-7) as was required in order to obtain high accuracy. The values computed using Eq. (4.13-9) were obtained by computing phase slope from Fig. 4.08-1. Note that the results are quite good. The $Q = 10$ values included in Table 4.13-2 are of practical interest since in the case of low-pass prototypes of band-pass filters the element Q's for the low-pass prototype can become quite low if the fractional bandwidth w of the band-pass filter is small [see Eq. (4.13-2)].

The above discussion treats the effects of parasitic dissipation at $\omega' = 0$, and the important question arises as to what the loss will be elsewhere in the pass band. Equation (4.13-9) provides convenient means for obtaining an approximate answer to this question. Since it says that ΔL_A at any frequency is proportional to the attenuation phase slope (*i.e.*, the group time delay) at that frequency, we can estimate ΔL_A across the pass band by examining the phase slope across that band. As seen from the examples in Fig. 4.08-1, the phase slope in typical cases is greatest near the cutoff frequency. In Fig. 4.08-1 the slope near cutoff is 2.66, 1.73, and 1.49 times the slope at $\omega' = 0$ for the cases of 0.5-db ripple, 0.01-db ripple, and maximally flat responses, respectively. Thus ΔL_A near cutoff will be greater than $(\Delta L_A)_0$ at $\omega' = 0$ by about these factors. These results are typical and are useful in obtaining an estimate of what to expect in practical situations.

SEC. 4.14, APPROXIMATE CALCULATION OF PROTOTYPE STOP-BAND ATTENUATION

Cohn[20] has derived a convenient formula for computing the attenuation of low-pass filters at frequencies well into their stop bands. This formula is derived using the assumption that the reactances of the series inductances are very large compared to the reactances of the shunt capacitors. When this condition holds, the voltage at one node of the filter may be computed with good accuracy from that at the preceding node using a simple voltage divider computation.[20] Cohn further simplifies his formula by use of the assumption that $(\omega^2 L_k C_{k+1} - 1) \approx \omega^2 L_k C_{k+1}$.

Cohn's formula, when put in the notation of the low-pass prototype filters in this chapter, is

$$L_A = 20 \log_{10} [(\omega')^n (g_1 g_2 g_3 \cdots g_n)] - 10 \log_{10} \left(\frac{4}{g_0 g_{n+1}}\right) \quad \text{db} \qquad (4.14\text{-}1)$$

where g_0, g_1, $\cdots$, g_{n+1} are the prototype element values defined in Fig. 4.04-1(a), (b) and ω' is the prototype radian frequency variable. For this formula to have high accuracy, ω' should be a number of times as large as ω_1', the filter cutoff frequency.

As an example, consider a Tchebyscheff filter with $n = 4$ reactive elements and 0.2 db ripple. By Table 4.05-2(a), $g_0 = 1$, $g_1 = 1.3028$, $g_2 = 1.2844$, $g_3 = 1.9761$, $g_4 = 0.8468$, $g_5 = 1.5386$, and the cutoff frequency is $\omega_1' = 1$. By Eq. (4.14-1), to slide-rule accuracy

$$L_A = 20 \log_{10} [(\omega')^4 (4.29)] - 10 \log_{10} 6.15 \quad . \qquad (4.14\text{-}2)$$

Evaluating Eq. (4.14-2) for $\omega' = 3$ gives $L_A = 43.1$ db. By Fig. 4.03-6 we find that the actual attenuation is 42 db. Repeating the calculation for $\omega' = 2$ gives $L_A = 28.8$ db as compared to 26.5 db by Fig. 4.03-6. Thus it appears that even for values of ω'/ω_1' as small as 2, Eq. (4.14-1) gives fairly good results. The error was +2.3 db for $\omega' = 2$ and +1.1 db for $\omega' = 3$.

Equation (4.14-1) neglects the effects of dissipation in the circuit. This is valid as long as the dissipative elements in the prototype can be assumed to be arranged as are those in Fig. 4.13-1. This arrangement of dissipative elements is usually appropriate for prototypes for low-pass, band-pass, and high-pass filters. However, in the case of prototypes for band-stop filters, the different arrangement of dissipative elements discussed in Sec. 4.15 should be assumed. For that case Eq. (4.14-1) will be quite inaccurate in some parts of the stop band.

SEC. 4.15, PROTOTYPE REPRESENTATION OF DISSIPATION LOSS IN BAND-STOP FILTERS

In the case of band-stop filters, the effects of parasitic dissipation in the filter elements are usually more serious in the stop band

than in the pass band. The stop band usually has one or more frequencies where, if the filter had no dissipation loss, the attenuation would be infinite. However, dissipation loss in the resonators will prevent the attenuation from going to infinity and in some cases may reduce the maximum stop-band attenuation to an unacceptably low value. If a band-stop filter is designed from a low-pass prototype, it is quite easy to compute the effects of finite resonator Q's on the maximum stop-band attenuation.

The solid lines in Fig. 4.15-1 shows a Tchebyscheff low-pass prototype response along with the response of a band-stop filter designed from

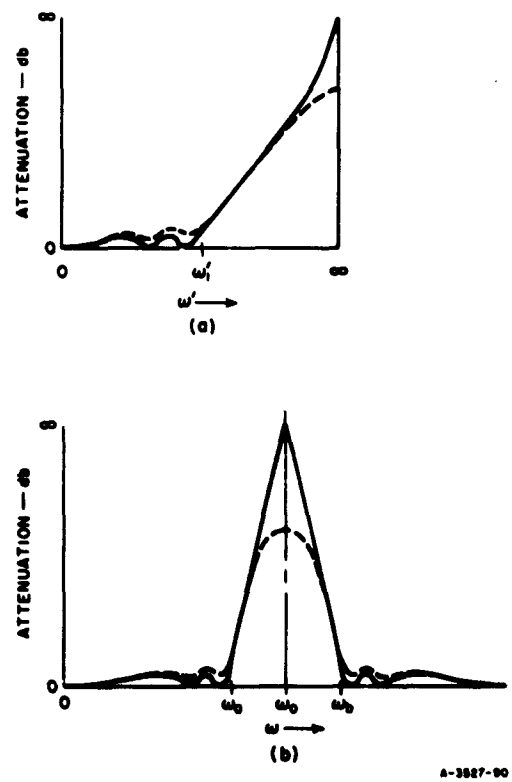

FIG. 4.15-1 A LOW-PASS PROTOTYPE RESPONSE IS SHOWN AT (a), AND THE CORRESPONDING BAND-STOP FILTER RESPONSE IS SHOWN AT (b)
The dashed lines show the effects of dissipation loss.

this prototype, both for the case of no incidental dissipation. For a typical band-stop filter the resonators are resonant at the center of the stop band (instead of at the center of the pass band as is the case for a typical band-pass filter), and as a result the loss effects are most severe at the center of the stop band. The dashed line in Fig. 4.15-1(b) shows how dissipation loss in the resonators will round off the attenuation characteristic of a band-stop filter. The dashed line in Fig. 4.15-1(a) shows the corresponding effect in a low-pass prototype filter.

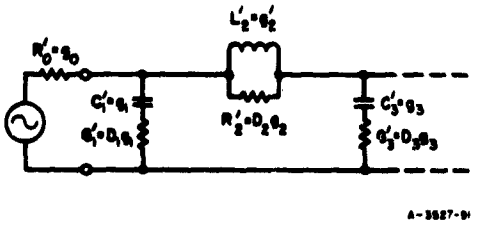

FIG. 4.15-2 LOW-PASS PROTOTYPE FILTER WITH DISSIPATIVE ELEMENTS ADDED AS REQUIRED FOR COMPUTING PEAK STOP-BAND ATTENUATION OF CORRESPONDING BAND-STOP FILTERS

It is easily seen that in order for resistor elements to affect the attenuation of a prototype filter as shown by the dashed line in Fig. 4.15-1, they should be introduced into the prototype circuit as shown in Fig. 4.15-2. Note that in this case as $\omega' \to \omega_1'$ the reactive elements have negligible influence and the circuit operates in the same way as a ladder network of resistors. In Fig. 4.15-2 the Q of the kth reactive element is given by*

$$Q_k = \frac{R_k'}{\omega_1' L_k'} \quad \text{or} \quad \frac{G_k'}{\omega_1' C_k'} \tag{4.15-1}$$

$$= \frac{D_k}{\omega_1'} \tag{4.15-2}$$

where ω_1' is the cutoff frequency in Fig. 4.15-1(a). The unloaded Q, $(Q_{BSF})_k$, of the kth resonator of the band-stop filter is related to Q_k of the prototype (at frequency ω_1') by

$$Q_k = w(Q_{BSF})_k \tag{4.15-3}$$

* Note that these unusual definitions of Q result from the manner in which the dissipative elements are introduced in each branch of the filter.

where

$$w = \frac{\omega_b - \omega_a}{\omega_0} \tag{4.15-4}$$

and ω_a, ω_b, and ω_0 are as defined in Fig. 4.15-1(b). By Eq. (4.15-2),

$$D_k = \omega_1' Q_k \tag{4.15-5}$$

and as shown in Fig. 4.15-2,

$$R_k' \text{ or } G_k' = D_k g_k \big|_{k=1,2,\ldots,n} \tag{4.15-6}$$

where the g_k are the prototype filter elements as defined in Fig. 4.04-1.

As previously mentioned, when $\omega' \to \infty$ the reactive elements in Fig. 4.15-2 may be neglected, and the attenuation can be computed from the remaining network of resistors. In typical cases, resistances of the series branches will be very large compared to the resistances of the shunt branches, and Cohn's method for computing the stop-band attenuation of low-pass filters[20] can be adapted to cover this case also. The resulting equation is

$$(L_A)_\infty = 20 \log_{10} [(D_1 D_2 \cdots D_n)(g_1 g_2 \cdots g_n)] - 10 \log_{10} \left(\frac{4}{g_0 g_{n+1}} \right) \text{ db} \tag{4.15-7}$$

which is analogous to Eq. (4.14-1) for the reactive attenuation of a low-pass filter.

As an example, let us suppose that a band-stop filter is desired with a fractional stop-band width of $w = 0.02$ (referred to the 3 db points), and that maximally flat pass bands are desired. Let us assume further that the resonator Q's at the mid-stop-band frequency are 700 and that the maximum stop-band attenuation is to be computed. By Eq. (4.15-3) $Q_1 = Q_2 = 0.02\ (700) = 14$. By Table 4.05-1(a) the elements values of the desired $n = 2$ low-pass prototype are $g_0 = 1$, $g_1 = 1.414$, $g_2 = 1.414$, and $g_3 = 1$. Also, ω_1' which in this case is the 3-db band-edge

frequency, is equal to unity. By Eq. (4.15-5), $D_1 = D_2 = 14$, and, to slide-rule accuracy, Eq. (4.15-7) gives $(L_A)_\infty = 45.8$ db. In comparison, using the method of Sec. 2.13 to compute the attenuation from the ladder of resistors gives $(L_A)_\infty = 46.7$ db.

As is suggested by the dashed lines in Fig. 4.15-1, the effects of dissipation in the pass band are for this case most severe at the pass-band edge, and they decrease to zero as the frequency moves away from the pass-band edge (within the pass band). The increase in loss due to dissipation at the band-edge frequency can be estimated by use of the formula*

$$(\Delta L_A)\big|_{\omega_1'} \approx 8.686 \sum_{k=1}^{n} \frac{\omega_1' g_k}{Q_k} \quad . \tag{4.15-8}$$

This formula represents only an estimate, but should be reasonably accurate for cases such as when an $n = 5$, 0.1-db ripple prototype is used. For cases where very large Tchebyscheff ripples are used this equation will underestimate the loss; when very small ripples are used it will overestimate the loss. For 0.1-db ripple, if n were reduced to 2 or 1, Eq. (4.15-8) would tend to overestimate the band-edge loss. For typical practical cases, Eq. (4.15-8) should never have an error as great as a factor of 2.

Equation (4.15-8) was obtained from Eq. (4.13-11) by the use of two approximations. The first is that for the arrangement of dissipative elements shown in Fig. 4.13-1, the added loss ΔL_A due to dissipation at the band edge ω_1' is roughly twice the value $(\Delta L_A)_0$ of the loss due to dissipation when $\omega' = 0$. This was shown by examples in Sec. 4.13 to be a reasonably good approximation for typical low-pass prototype filters, though it could be markedly larger if very large pass-band ripples are used. The second approximation assumes that a filter with dissipative elements as shown in Fig. 4.15-2 can be approximated at the frequency ω_1' by the corresponding circuit in Fig. 4.13-1. The reactive element values g_k are assumed to have been unchanged, and also the Q's of the individual reactive element are assumed to be unchanged; however, *the manner in which the dissipation is introduced has been changed.* This approximation is valid to the extent that

---

* This formula is based on Eq. (4.13-11) which assumes that the prototype element values have been normalized so that $g_0 = 1$.

$$\frac{\omega_1' g_k}{Q_k} + j g_k \omega_1' \approx \frac{Q_k \omega_1' g_k}{Q_k^2 + 1} + j \frac{\omega_1' g_k}{1 + \left(\frac{1}{Q_k}\right)^2} \qquad (4.15\text{-}9)$$

represents a good approximation. It is readily seen that this is a good approximation even for Q's as low as 10. Thus to summarize the basis for Eq. (4.15-8)—the equation as it stands gives a rough estimate of the attenuation due to dissipation at band edge for the situation where the dissipative elements are introduced as shown in Fig. 4.13-1. We justify the use of this same equation for the case of dissipative elements arranged as in Fig. 4.15-2 on the basis of the approximation in Eq. (4.15-9). It shows that as long as the reactive elements are the same, and the element Q's are the same, and around 10 or higher, it doesn't make much difference which way the dissipative elements are connected as far as their effect on transmission loss is concerned.

REFERENCES

1. S. Darlington, "Synthesis of Reactance 4-Poles Which Produce Prescribed Insertion Loss Characteristics," *Jour. Math. and Phys.*, Vol. 18, pp. 257-353 (September 1939).

2. E. A. Guillemin, *Synthesis of Passive Networks* (John Wiley and Sons, Inc., New York, 1957).

3. M. E. Van Valkenburg, *Introduction to Modern Network Synthesis* (John Wiley and Sons, New York, 1960).

4. V. Belevitch, "Tchebyscheff Filters and Amplifier Networks," *Wireless Engineer*, Vol. 29, pp. 106-110 (April 1952).

5. H. J. Orchard, "Formula for Ladder Filters," *Wireless Engineer*, Vol. 30, pp. 3-5 (January 1953).

6. E. Green, "Synthesis of Ladder Networks to Give Butterworth or Chebyshev Response in the Pass Band," *Proc. IEE* (London) Part IV, Monograph No. 88 (1954).

7. E. Green, *Amplitude-Frequency Characteristics of Ladder Networks*, pp. 62-78, Marconi's Wireless Telegraph Co., Ltd., Chelmsford, Essex, England (1954).

8. L. Weinberg, "Network Design by Use of Modern Synthesis Techniques and Tables," *Proc. of Nat. Elec. Conf.*, Vol. 12 (1956).

9. L. Weinberg, "Additional Tables for Design of Optimum Ladder Networks," Parts I and II, *Journal of the Franklin Institute*, Vol. 264, pp. 7-23 and 127-138 (July and August 1957).

10. L. Storch, "Synthesis of Constant-Time-Delay Ladder Networks Using Bessel Polynomials," *Proc. IRE* **42**, pp. 1666-1675 (November 1954).

11. W. E. Thomson, "Networks with Maximally Flat Delay," *Wireless Engineer*, Vol. 29, pp. 255-263 (October 1952).

12. S. B. Cohn, "Phase-Shift and Time-Delay Response of Microwave Narrow-Band Filters," *The Microwave Journal*, Vol. 3, pp. 47-51 (October 1960).

13. M. J. Di Toro, "Phase and Amplitude Distortion in Linear Networks," *Proc. IRE* **36**, pp. 24-36 (January 1948).

14. R. M. Fano, "Theoretical Limitations on the Broadband Matching of Arbitrary Impedances," *J. Franklin Inst.*, Vol. 249, pp. 57-83 and 139-154 (January and February 1950).

15. B. F. Barton, "Design of Efficient Coupling Networks," Technical Report 44, Contract DA 36-039-SC-63203, Electronic Defense Group, University of Michigan, Ann Arbor, Michigan (March 1955).

16. H. J. Carlin, "Gain-Bandwidth Limitations on Equalizers and Matching Networks," *Proc. IRE* **42**, pp. 1676-1685 (November 1954).

17. G. L. Matthaei, "Synthesis of Tchebyscheff Impedance-Matching Networks, Filters, and Interstages," *IRE Trans. PGCT* **3**, pp. 162-172 (September 1956).

18. H. J. Carlin, "Synthesis Techniques for Gain-Bandwidth Optimization in Passive Transducers," *Proc. IRE* **48**, pp. 1705-1714 (October 1960).

19. H. W. Bode, *Network Analysis and Feedback Amplifier Design* pp. 216-222 (D. Van Nostrand Co., Inc., New York, 1945).

20. S. B. Cohn, "Dissipation Loss in Multiple-Coupled-Resonator Filters," *Proc. IRE* **47**, pp. 1342-1348 (August 1959).

CHAPTER 5

PROPERTIES OF SOME COMMON MICROWAVE FILTER ELEMENTS

SEC. 5.01, INTRODUCTION

Previous chapters have summarized a number of important concepts necessary for the design of microwave filters and have outlined various procedures for later use in designing filters from the image viewpoint and from the insertion-loss viewpoint. In order to construct filters that will have measured characteristics as predicted by these theories, it is necessary to relate the design parameters to the dimensions and properties of the structures used in such filters. Much information of this type is available in the literature. The present chapter will attempt to summarize information for coaxial lines, strip lines, and waveguides that is most often needed in filter design. No pretense of completeness is made, since a complete compilation of such data would fill several volumes. It is hoped that the references included will direct the interested reader to sources of more detailed information on particular subjects.

SEC. 5.02, GENERAL PROPERTIES OF TRANSMISSION LINES

Transmission lines composed of two conductors operating in the transverse electromagnetic (TEM) mode are very useful as elements of microwave filters. Lossless lines of this type have a characteristic or image impedance Z_0, which is independent of frequency f, and waves on these lines are propagated at a velocity, v, equal to the velocity of light in the dielectric filling the line. Defining R, L, G, and C as the resistance, inductance, conductance and capacitance per unit length for such a line, it is found that Z_0 and the propagation constant γ_t are given by

$$Z_0 = \frac{1}{Y_0} = \sqrt{\frac{R + j\omega L}{G + j\omega C}} = \sqrt{\frac{Z}{Y}} \text{ ohms} \qquad (5.02\text{-}1)$$

$$\gamma_t = \alpha_t + j\beta_t = \sqrt{(R + j\omega L)(G + j\omega C)} = \sqrt{ZY} \qquad (5.02\text{-}2)$$

where $\omega = 2\pi f$. When the line is lossless, α_t is zero and

$$\beta_t = \omega \sqrt{LC} \quad \text{radians/unit length} \qquad (5.02\text{-}3)$$

$$v = \frac{\omega}{\beta_t} = \frac{1}{\sqrt{LC}} \quad \text{distance/second} \qquad (5.02\text{-}4)$$

$$Z_0 = \sqrt{\frac{L}{C}} = \frac{1}{vC} = vL \text{ ohms} \quad . \qquad (5.02\text{-}5)$$

In practice a line will have some finite amount of attenuation

$$\alpha_t = \alpha_c + \alpha_d \qquad (5.02\text{-}6)$$

where α_c is the attenuation due to conductor loss and α_d the attenuation due to loss in the dielectric. For small attenuations *

$$\alpha_c = \frac{R}{2Z_0} = \frac{\beta_t}{2Q_c} \quad \text{nepers} \qquad (5.02\text{-}7)$$

$$\alpha_d = \frac{G}{2Y_0} = \frac{\beta_t}{2Q_d} = \frac{\beta_t}{2 \tan \delta} \quad \text{nepers} \qquad (5.02\text{-}8)$$

where $Q_c = \omega L/R$, $Q_d = \omega C/G$, and $\tan \delta$ is the loss tangent of the dielectric material filling the line. The total Q of the transmission line used as a resonator is given by

$$\frac{1}{Q} = \frac{1}{Q_c} + \frac{1}{Q_d} \quad . \qquad (5.02\text{-}9)$$

These definitions are in agreement with those given in terms of the resonator reactance and susceptance slope parameters in Sec. 5.08. For a slightly lossy line the characteristic impedance and propagation constant become

* To convert nepers to decibels, multiply by 8.686.

$$\beta_t = \omega\sqrt{LC}\left[1 - \frac{1}{4Q_cQ_d} + \frac{1}{8Q_d^2} + \frac{1}{8Q_c^2}\right] \qquad (5.02\text{-}10),$$

$$Z_0 = \sqrt{\frac{L}{C}}\left[1 + \frac{j}{2}\left(\frac{1}{Q_d} - \frac{1}{Q_c}\right)\right] \quad . \qquad (5.02\text{-}11)$$

The TEM modes can also propagate on structures containing more than two conductors. Examples of such structures with two conductors contained within an outer shield are described in Sec. 5.05. Two principal modes can exist on such two-conductor structures: an even mode in which the currents in the two conductors flow in the same direction, and an odd mode in which the currents on the conductors flow in opposite directions. The velocity of propagation of each of these modes in the lossless case is equal to the velocity of light in the dielectric medium surrounding the conductors. However, the characteristic impedance of the even mode is different from that of the odd mode.

SEC. 5.03, SPECIAL PROPERTIES OF COAXIAL LINES

The characteristic impedance Z_0 of a coaxial line of outer diameter b and inner diameter d, filled with a dielectric material of relative dielectric constant ϵ_r, is

$$Z_0 = \frac{60}{\sqrt{\epsilon_r}} ln\,\frac{b}{d} \quad \text{ohms} \quad . \qquad (5.03\text{-}1)$$

This expression is plotted in Fig. 5.03-1. The attenuation α_c of a copper coaxial line due to ohmic losses in the copper is

$$\alpha_c = 1.898 \times 10^{-4}\sqrt{\epsilon_r}\sqrt{f_{Gc}}\left(\frac{1 + b/d}{b\ ln\ b/d}\right) \quad \text{db/unit length} \quad (5.03\text{-}2)$$

where f_{Gc} is measured in gigacycles. (Here the copper is assumed to be very smooth and corrosion-free.) The attenuation is a minimum for b/d of 3.6 corresponding to $\sqrt{\epsilon_r}\,Z_0$ of 77 ohms.

The attenuation α_d of the coaxial line (or any other TEM line) due to losses in the dielectric is

$$\alpha_d = \frac{27.3\sqrt{\epsilon_r}\tan\delta}{\lambda} \quad \text{db/unit length} \qquad (5.03\text{-}3)$$

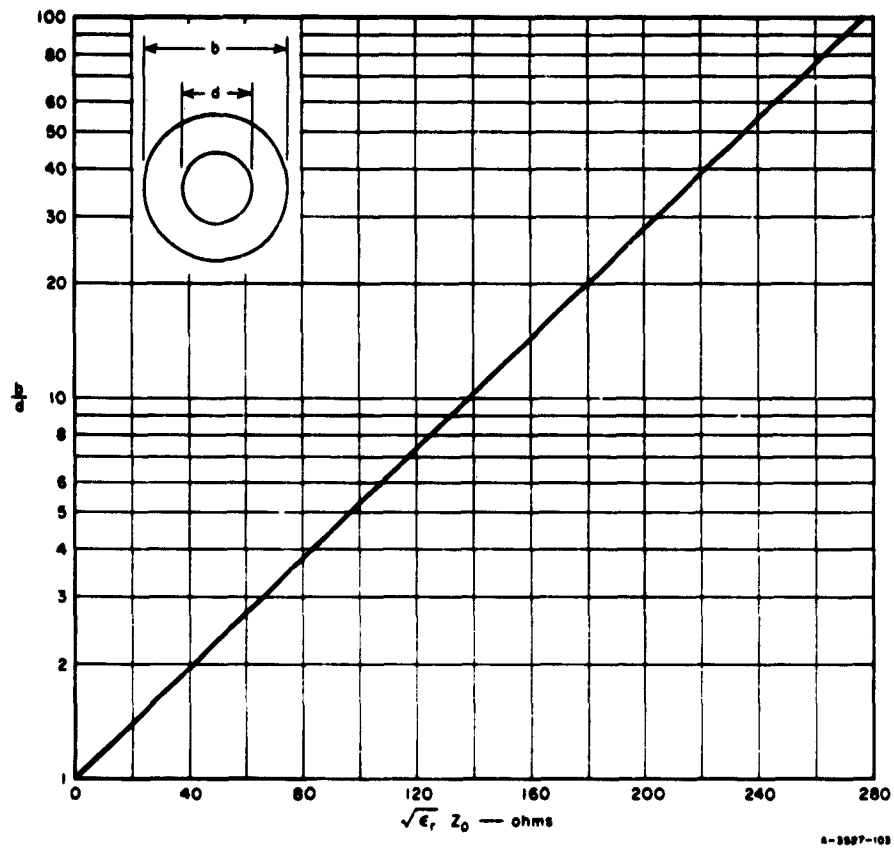

FIG. 5.03-1 COAXIAL-LINE CHARACTERISTIC IMPEDANCE

where tan δ is the loss tangent of the dielectric, and λ is the free-space wavelength. The total attenuation α_t is the sum of α_c and α_d. The attenuation of a coaxial line due to ohmic losses in the copper is shown in Fig. 5.03-2.

The Q of a dielectric-filled coaxial line may be expressed as

$$\frac{1}{Q} = \frac{1}{Q_c} + \frac{1}{Q_d} \qquad (5.03\text{-}4)$$

where $Q_c = \pi\sqrt{\epsilon_r}/\lambda\alpha_c$ depends only on the conductor loss and Q_d depends only on the dielectric loss. The Q_c of a dielectric-filled coaxial line is independent of ϵ_r and is given by the expression

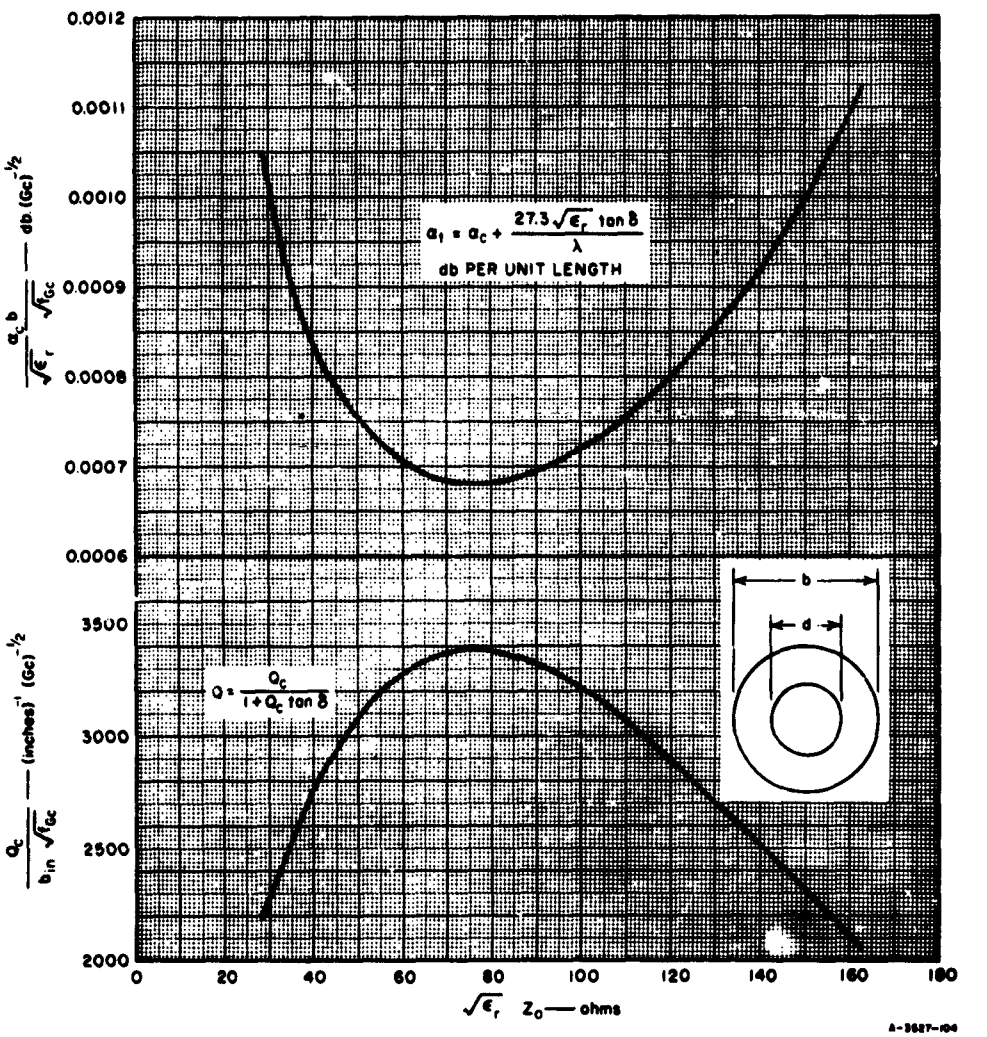

FIG. 5.03-2 COAXIAL-LINE ATTENUATION AND Q

$$Q_c = 1.215 \times 10^4 \sqrt{f_{Ge}} \frac{b \ln b/d}{[1 + b/d]} \qquad (5.03\text{-}5)$$

where b and d are measured in inches. The value of Q_d for the coaxial line or any TEM line is

$$Q_d = \frac{1}{\tan \delta} \quad . \qquad (5.03\text{-}6)$$

The values of Q_c for a copper coaxial line are plotted in Fig. 5.03-2.

Breakdown will occur in an air-filled coaxial line at atmospheric pressure when the maximum electric field E_a reaches a value of approximately 2.9×10^4 volts per cm. The average power P that can be transmitted on a matched coaxial line under these conditions is

$$P = \frac{E_a^2}{480} b^2 \frac{\ln b/d}{(b/d)^2} \quad \text{watts} \quad . \qquad (5.03\text{-}7)$$

When the outer diameter b is fixed, the maximum power can be transmitted when b/d is 1.65, corresponding to Z_0 of 30 ohms.

The first higher-order TE mode in a coaxial line will propagate when the average circumference of the line is approximately equal to the wavelength in the medium filling the line. The approximate cutoff frequency, f_c (in gigacycles), of this mode is

$$(f_c)_{Ge} = \frac{7.51}{\sqrt{\epsilon_r}} (b + d) \qquad (5.03\text{-}8)$$

where b and d are measured in inches.

SEC. 5.04, SPECIAL PROPERTIES OF STRIP LINES

The characteristic impedance of strip line can be calculated by conformal mapping techniques; however, the resulting formulas are rather complex. Figure 5.04-1 shows the characteristic impedance, Z_0, of a common type of strip line with a rectangular center conductor,[1,2] for various values of $t/b \leq 0.25$, and $0.1 \leq w/b \leq 4.0$. The values shown are exact for $t/b = 0$ and are accurate to within about 1 percent for other

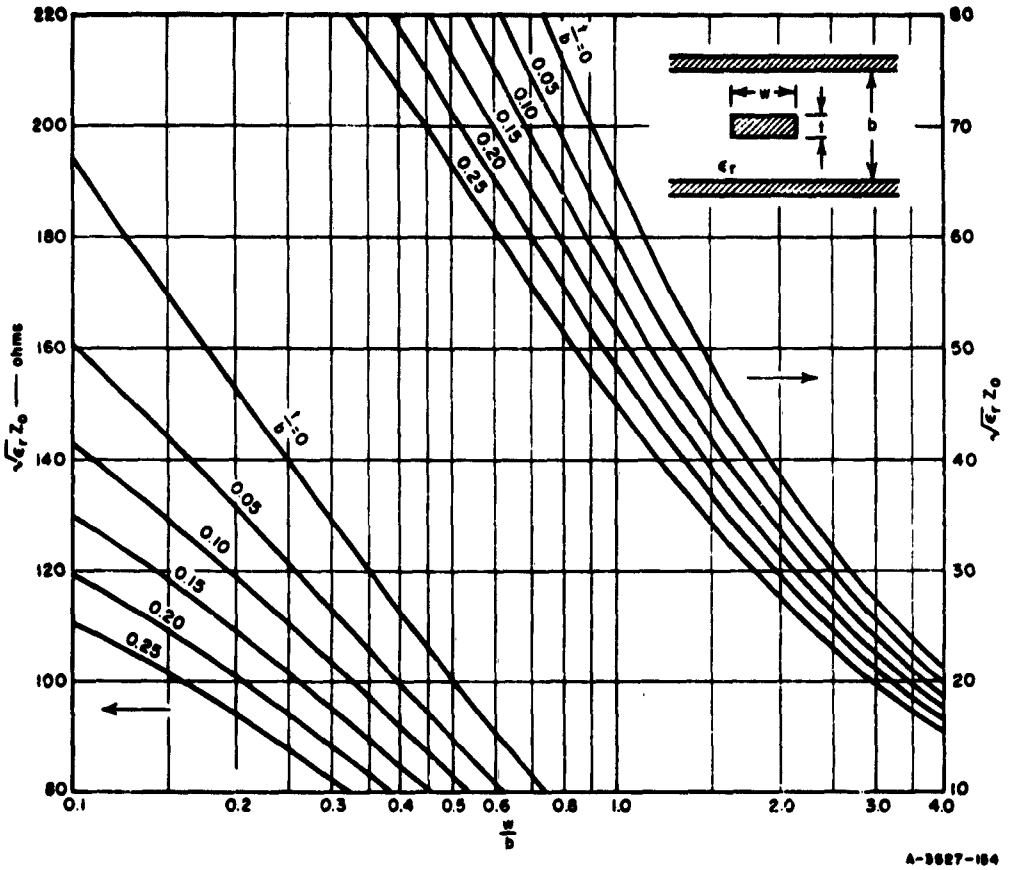

SOURCE: Final Report, Contract DA 36-039 SC-63232, SRI; reprinted in *IRE Trans., PGMTT* (see Ref. 2, by S. B. Cohn).

FIG. 5.04-1 GRAPH OF Z_0 vs. w/b FOR VARIOUS VALUES OF t/b

values of t/b. Figure 5.04-2 shows exact values of Z_0 for all values of t/b, and $w/b \leq 1.6$.[3]

The theoretical attenuation α_c due to ohmic losses in a copper strip line filled with a dielectric of relative dielectric constant ϵ_r, is shown in Fig. 5.04-3. The attenuation α_d due to the dielectric loss is given by Eq. (5.03-3). As in the case of the coaxial line, the total attenuation α_t is the sum of α_c and α_d.

The Q of a dielectric-filled strip line is given by Eq. (5.03-4). The Q_c of a dielectric-filled line is shown plotted in Fig. 5.04-4.[12] As in the case of the coaxial line, Q_d is the reciprocal of tan δ.

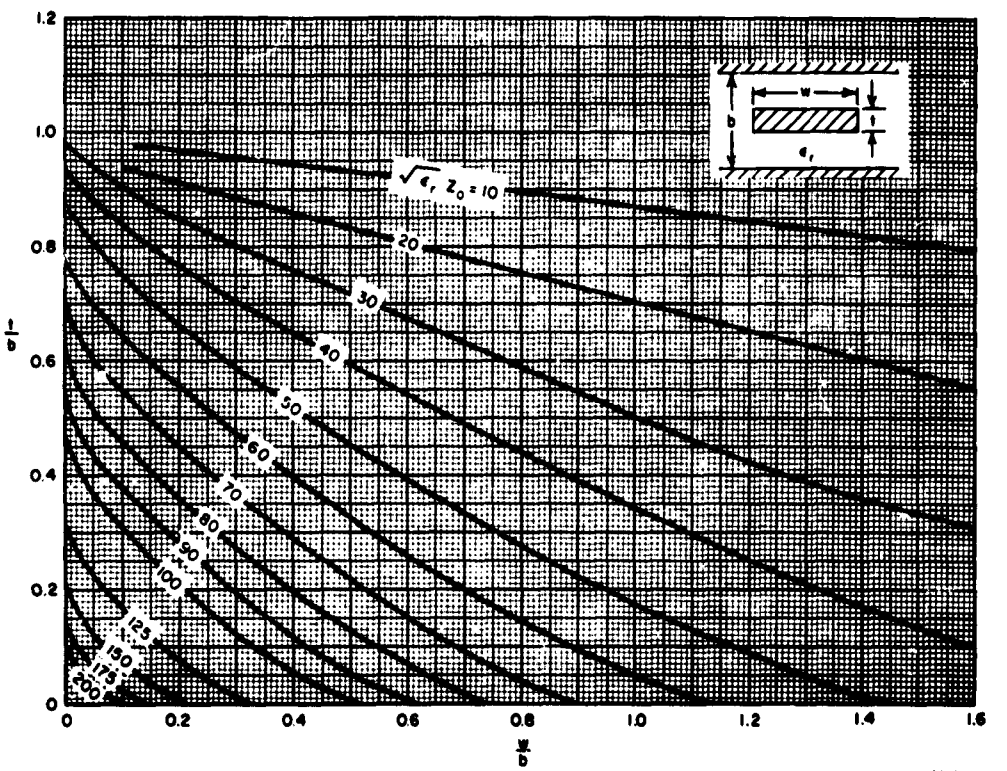

SOURCE: *IRE Trans. PGMTT* (see Ref. 3, by R. H. T. Bates).

FIG. 5.04-2 GRAPH OF Z_0 vs. w/b FOR VARIOUS VALUES OF t/b

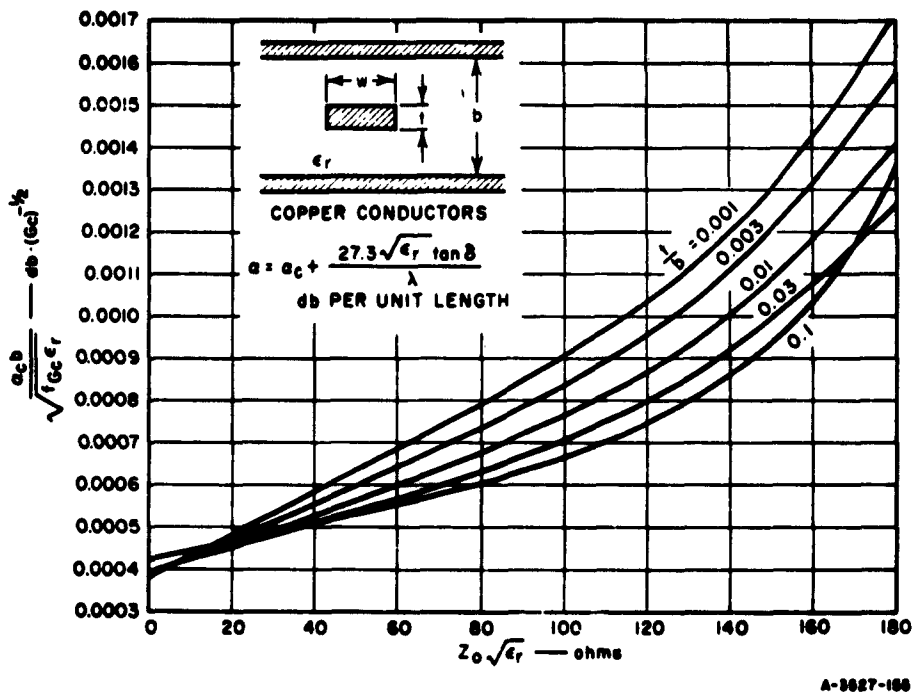

SOURCE: Final Report, Contract DA 36-039 SC-63232, SRI; reprinted in *IRE Trans., PGMTT* (see Ref. 2, by S. B. Cohn).

FIG. 5.04-3 THEORETICAL ATTENUATION OF COPPER-SHIELDED STRIP LINE IN A DIELECTRIC MEDIUM ϵ_r

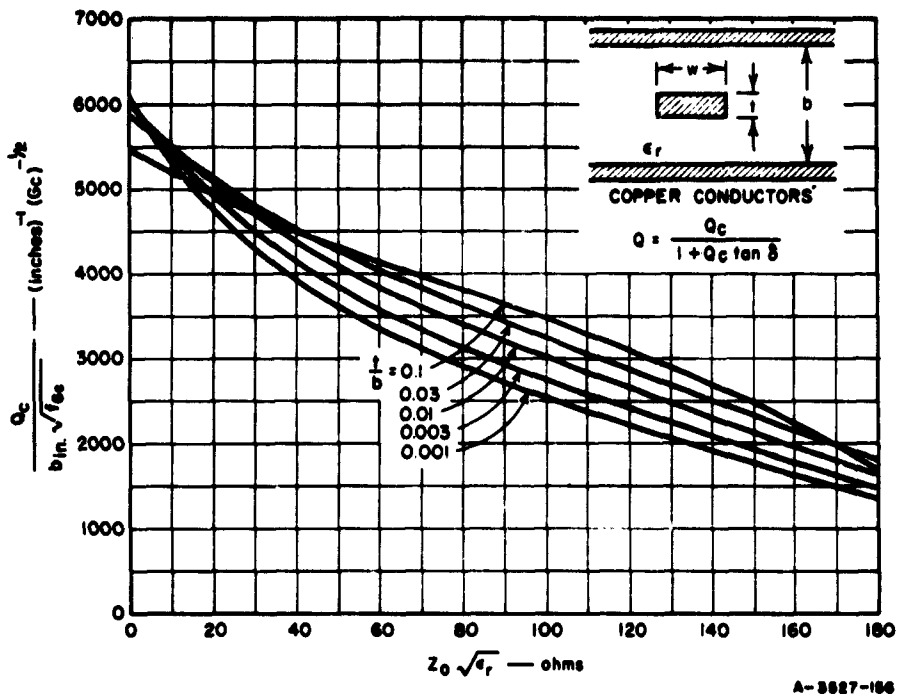

SOURCE: Final Report, Contract DA 36-039 SC-63232, SRI; reprinted in *IRE Trans., PGMTT* (see Ref. 2, by S. B. Cohn).

FIG. 5.04-4 THEORETICAL Q OF COPPER-SHIELDED STRIP LINE IN A DIELECTRIC MEDIUM ϵ_r

The average power, P (measured in kw), that can be transmitted along a matched strip line having an inner conductor with rounded corners is plotted in Fig. 5.04-5. In this figure the ground plane spacing b is measured in inches, and the breakdown strength of air is taken as 2.9×10^4 volts/cm. An approximate value of Z_0 can be obtained from Figs. 5.04-1 and 5.04-2.

The first higher-order mode that can exist in a strip line, in which the two ground planes have the same potential, has zero electric-field strength on the longitudinal plane containing the center line of the strip, and the electric field is oriented perpendicular to the strip and ground plane. The free-space cutoff wavelength, λ_c of this mode is

$$\lambda_c = \sqrt{\epsilon_r}\left[\frac{2w}{b} + \frac{4d}{b}\right]b$$

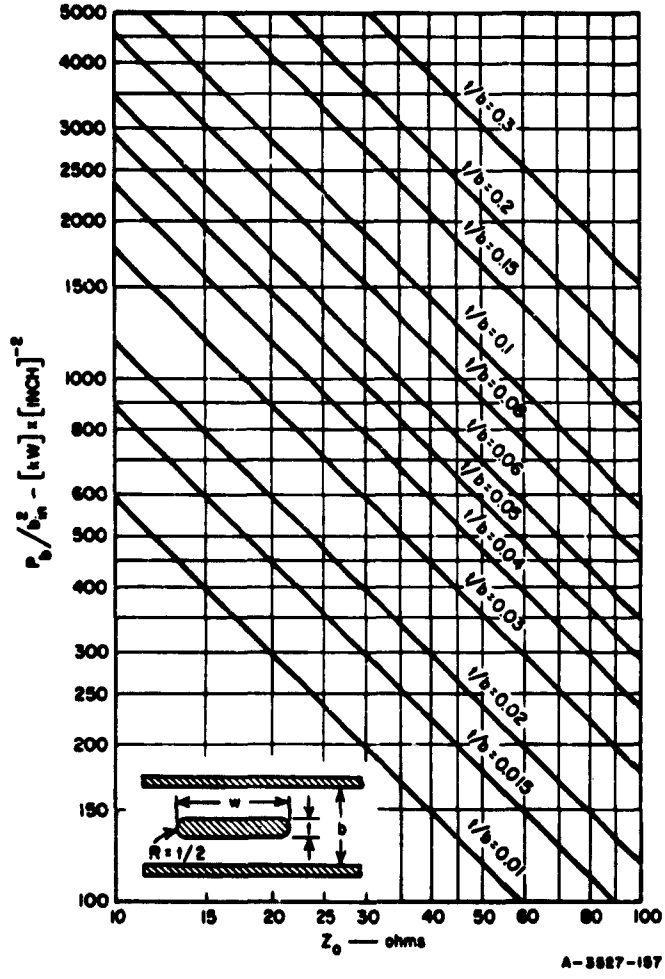

FIG. 5.04-5 THEORETICAL BREAKDOWN POWER OF AIR-DIELECTRIC ROUNDED-STRIP TRANSMISSION LINE

where d is a function of the cross section of the strip line. If $t/b \approx 0$ and $w/b \geq 0.35$, then $4d/b$ is a function of b/λ_c alone and is given in Table 5.04-1.

Table 5.04-1

THE QUANTITY $4d/b$ *vs.* b/λ_c FOR $w/b \geq 0.35$ AND $t/b \approx 0$

b/λ_c	$4d/b$
0.00	0.882
0.20	0.917
0.30	0.968
0.35	1.016
0.40	1.070
0.45	1.180
0.50	1.586

SEC. 5.05, PARALLEL-COUPLED LINES AND ARRAYS OF LINES BETWEEN GROUND PLANES

A number of strip-line components utilize the natural coupling existing between parallel conductors. Examples of such components are directional couplers, filters, baluns, and delay lines such as interdigital lines. A number of examples of parallel-coupled lines are shown in Fig. 5.05-1. The (a), (b), and (c) configurations shown are primarily useful in applications where weak coupling between the lines is desired. The (d), (e), (f), and (g) configurations are useful where strong coupling between the lines is desired.

The characteristics of these coupled lines can be specified in terms of Z_{oe} and Z_{oo}, their even and odd impedances, respectively. Z_{oe} is defined as the characteristic impedance of one line to ground when equal currents are flowing in the two lines. Z_{oo} is defined as the characteristic impedance of one line to ground when equal and opposite currents are flowing in the two lines. Figure 5.05-2 illustrates the electric field configuration over the cross section of the lines shown in Fig. 5.05-1(a) when they are excited in the even and odd modes.

Thin Strip Lines--The exact even-mode characteristic impedance of the infinitesimally thin strip configuration of Fig. 5.05-1(a) is[4]

$$Z_{oe} = \frac{30\pi}{\sqrt{\epsilon_r}} \cdot \frac{K(k_e')}{K(k_e)} \quad \text{ohms} \tag{5.05-1}$$

where

$$k_e = \tanh\left(\frac{\pi}{2} \cdot \frac{w}{b}\right) \cdot \tanh\left(\frac{\pi}{2} \cdot \frac{w+s}{2}\right) \tag{5.05-2}$$

$$k_e' = \sqrt{1 - k_e^2} \tag{5.05-3}$$

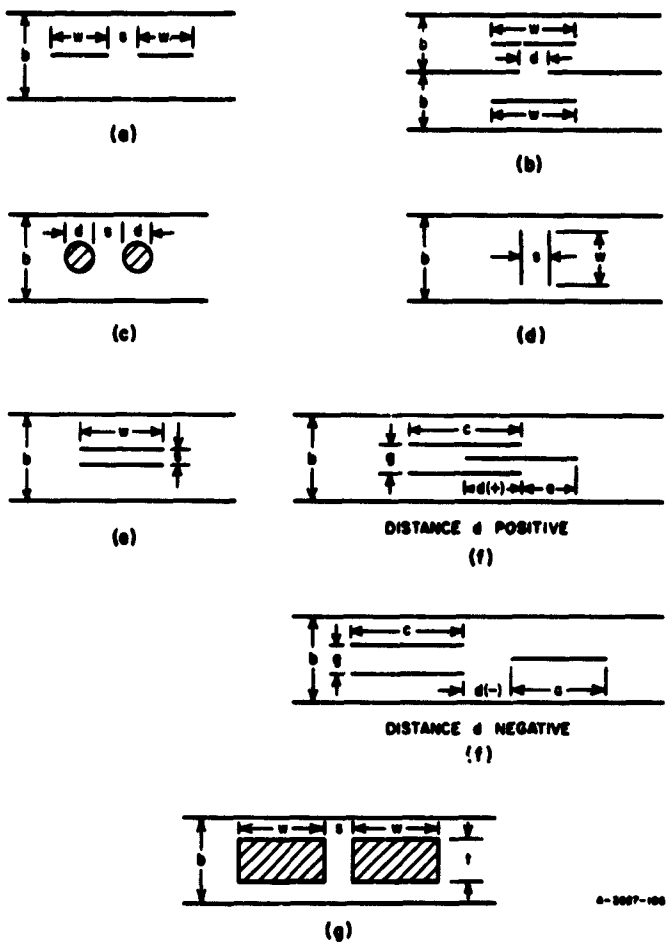

FIG. 5.05-1 CROSS SECTIONS OF VARIOUS COUPLED-TRANSMISSION-LINE CONFIGURATIONS

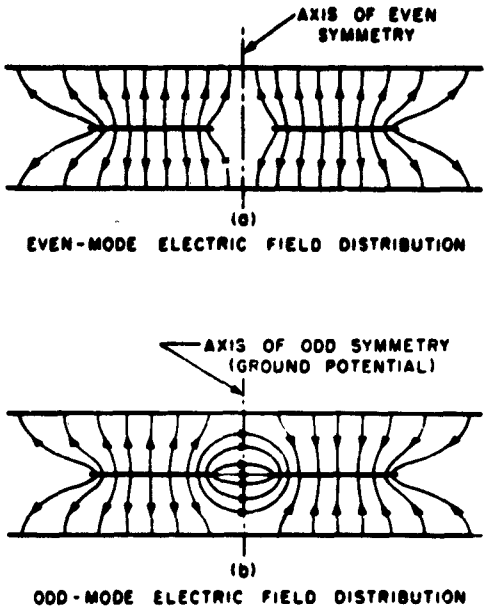

SOURCE: Final Report, Contract DA 36-039 SC-63232, SRI; reprinted in *IRE Trans., PGMTT* (see Ref. 4, by S. B. Cohn).

FIG. 5.05-2 FIELD DISTRIBUTIONS OF THE EVEN AND ODD MODES IN COUPLED STRIP LINE

and ϵ_r is the relative dielectric constant of the medium of propagation. The exact odd-mode impedance in the same case is[1]

$$Z_{oo} = \frac{30\pi}{\sqrt{\epsilon_r}} \cdot \frac{K(k_o')}{K(k_o)} \text{ ohms} \qquad (5.05\text{-}4)$$

where

$$k_o = \tanh\left(\frac{\pi}{2} \cdot \frac{w}{b}\right) \cdot \coth\ \frac{\pi}{2} \cdot \left(\frac{w+s}{b}\right) \qquad (5.05\text{-}5)$$

$$k_o' = \sqrt{1 - k_o^2} \qquad (5.05\text{-}6)$$

and K is the complete elliptic integral of the first kind. Convenient tables of $K(k')/K(k)$ have been compiled by Oberhettinger and Magnus.[5] Nomographs giving the even- and odd-mode characteristic impedances are presented in Figs. 5.05-3(a) and (b).

Thin Lines Coupled Through a Slot—The thin-strip configuration shown in Fig. 5.05-1(b) with a thin wall separating the two lines has a value of $Z_{oo} = Z_0$, which is the characteristic impedance of an uncoupled line as given in Sec. 5.04. The even-mode characteristic impedance Z_{ee} is given approximately by

$$\frac{1}{Z_{ee}} = \frac{1}{2}\left[\frac{1}{Z_{oo}} + \frac{1}{Z}\right] \tag{5.05-7}$$

where

$$Z = \frac{30\pi}{\sqrt{\epsilon_r}} \frac{K(k')}{K(k)} \tag{5.05-8}$$

$$k = \sqrt{\frac{\cosh \frac{\pi w}{b} - 1}{\cosh \frac{\pi w}{b} + \cosh \frac{\pi d}{b}}} \tag{5.05-9}$$

and

$$k' = \sqrt{1 - k^2} \quad . \tag{5.05-10}$$

Round Wires—The even- and odd-mode characteristic impedances of round lines placed midway between ground planes as shown in Fig. 5.05-1(c) are given approximately by

$$Z_{ee} - Z_{oo} = \frac{120}{\sqrt{\epsilon_r}} \ln \coth \frac{\pi s}{2b} \tag{5.05-11}$$

$$Z_{ee} + Z_{oo} = \frac{120}{\sqrt{\epsilon_r}} \ln \frac{4b}{\pi d} \quad . \tag{5.05.12}$$

These should give good results, at least when $d/b < 0.25$ and $s/b > 3\ d/b$.

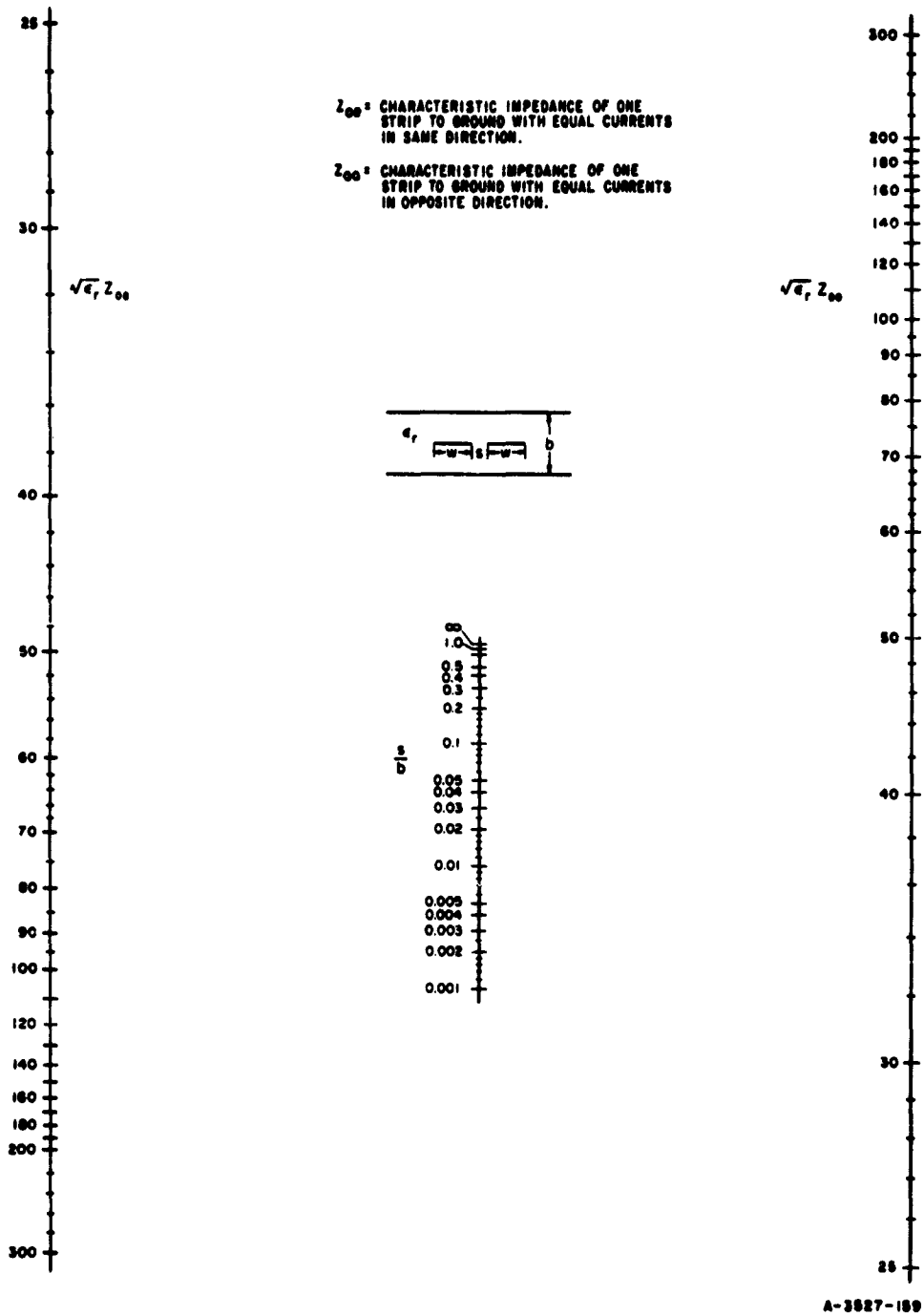

SOURCE: Final Report, Contract DA 36-039 SC-63232, SRI; reprinted in *IRE Trans., PGMTT* (see Ref. 4, by S. B. Cohn).

FIG. 5.05-3(a) NOMOGRAM GIVING s/b AS A FUNCTION OF Z_{oo} AND Z_{oo} IN COUPLED STRIP LINE

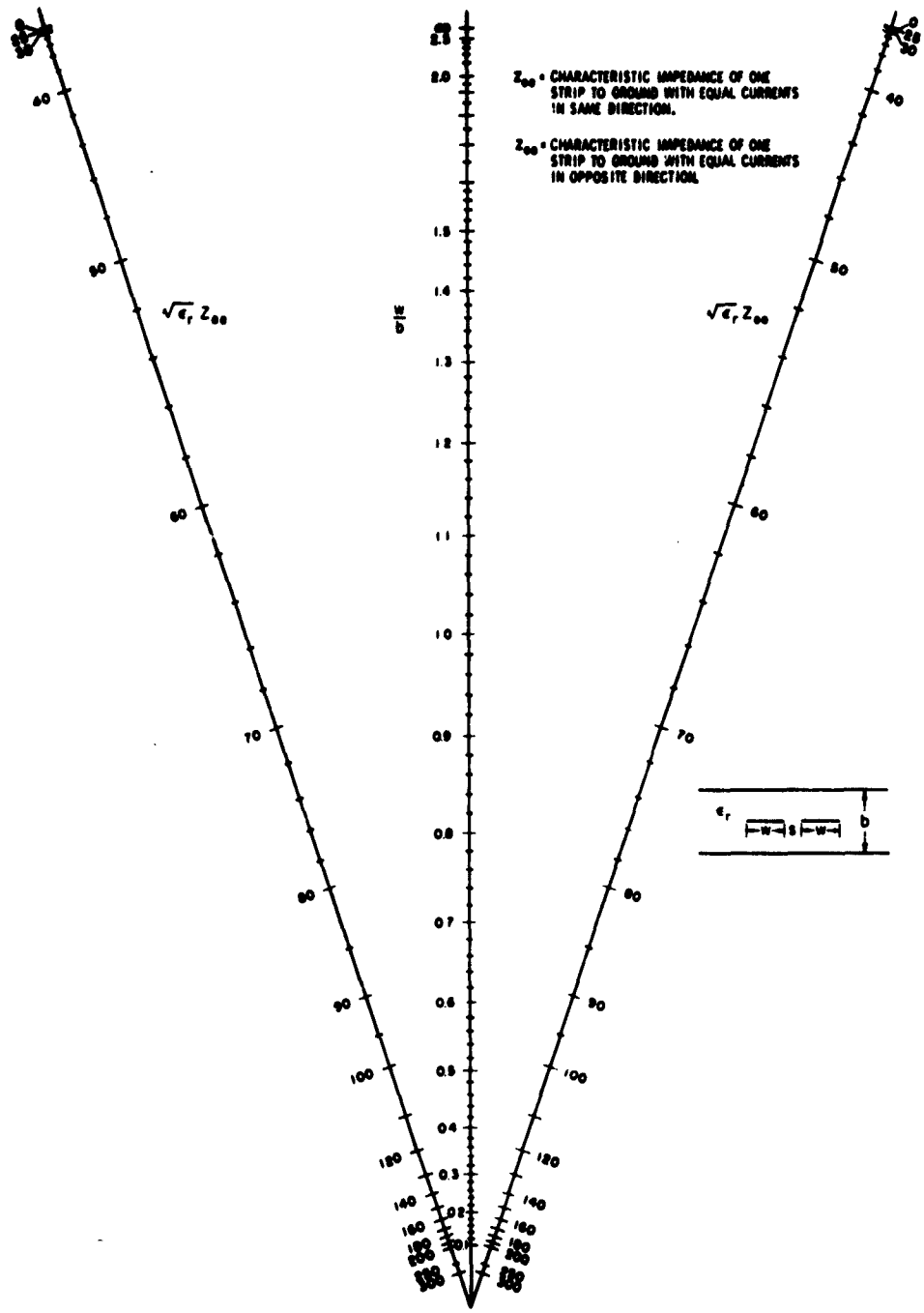

SOURCE: Final Report, Contract DA 36-039 SC-63232, SRI; reprinted in *IRE Trans., PGMTT* (see Ref. 4, by S. B. Cohn).

FIG. 5.05-3(b) NOMOGRAM GIVING w/b AS A FUNCTION OF Z_{oo} AND Z_{oo} IN COUPLED STRIP LINE

Thin Lines Vertical to the Ground Planes—The even- and odd-mode characteristic impedances of the thin coupled lines shown in Fig. 5.05-1(d) are given approximately by the formulas[6]

$$Z_{oe} = \frac{188.3}{\sqrt{\epsilon_r}} \frac{K(k)}{K(k')} \tag{5.05-13}$$

$$Z_{oo} = \frac{296.1}{\sqrt{\epsilon_r}} \frac{1}{\frac{b}{s}\cos^{-1} k + \ln \frac{1}{k}} \quad . \tag{5.05-14}$$

In these formulas k' is a parameter equal to $\sqrt{1 - k^2}$, and K is the complete elliptic integral of the first kind. The ratio w/b is given by

$$\frac{w}{b} = \frac{2}{\pi}\left\{\tan^{-1}\left[\frac{k'}{k}\sqrt{\frac{1 - \frac{k}{k'}\frac{s}{b}}{1 + \frac{k'}{k}\frac{s}{b}}}\right] - \frac{s}{b}\tanh^{-1}\sqrt{\frac{1 - \frac{k}{k'}\frac{s}{b}}{1 + \frac{k'}{k}\frac{s}{b}}}\right\} . \tag{5.05-15}$$

The inverse cosine and tangent functions are evaluated in radians between 0 and $\pi/2$. To find the dimensions of the lines for particular values of Z_{oe} and Z_{oo}, one first determines the value of the k from Eq. (5.05-13) and the tables of $K(k)/K(k')$ *vs.* k in Ref. 5. Then b/s is determined from Eq. (5.05-14) and finally w/b is determined from Eq. (5.05-15). Equations (5.05-13) through (5.05-15) are accurate for all values of w/b and s/b, as long as w/s is greater than about 1.0.

Thin Lines Superimposed—The formulas for the even- and odd-mode characteristic impedances of the coupled lines shown in Fig. 5.05-1(e) reduce to fairly simple expressions when $(w/b)/(1 - s/b) \geq 0.35$.[6] It is found that

$$Z_{oe} = \frac{188.3/\sqrt{\epsilon_r}}{\frac{w/b}{1 - s/b} + \frac{C'_{fe}}{\epsilon}} \tag{5.05-16}$$

$$Z_{oo} = \frac{188.3/\sqrt{\epsilon_r}}{\frac{w/b}{1 - s/b} + \frac{w}{s} + \frac{C'_{fo}}{\epsilon}} \quad . \tag{5.05-17}$$

The capacitance C'_{f_e} is the capacitance per unit length that must be added at each edge of each strip to the parallel plate capacitance, so that the total capacitance to ground for the even mode will be correct. C'_{f_o} is the corresponding quantity for the odd mode and ϵ_r is the relative dielectric constant. The even- and odd-mode fringing capacitances are plotted in Fig. 5.05-4.

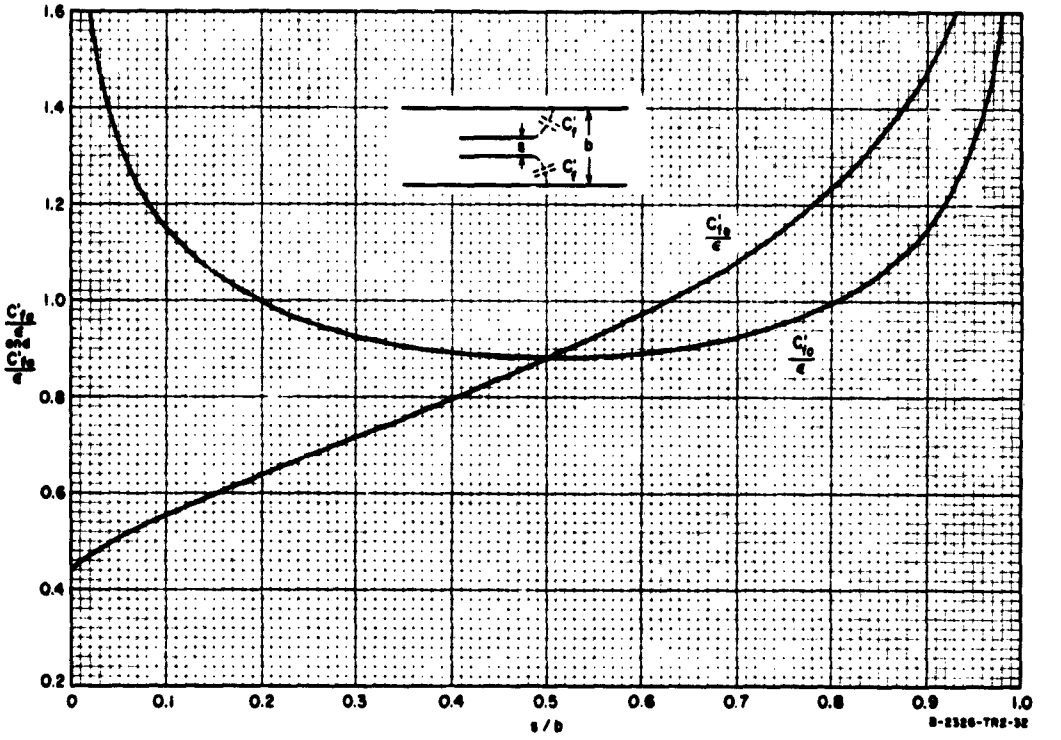

SOURCE: Final Report, Contract DA-36-039 SC-74862, SRI; reprinted in *IRE Trans., PGMTT* (see Ref. 5, by S. B. Cohn).

FIG. 5.05-4 EVEN- AND ODD-MODE FRINGING CAPACITANCES FOR BROADSIDE-COUPLED VERY THIN STRIPS PARALLEL TO THE GROUND PLANES

The even- and odd-mode characteristic impedances of the coupled lines shown in Figs. 5.05-1(a), (d), and (e) are modified slightly when the strips have a finite thickness. Correction terms that account for the effects of finite thickness have been derived by Cohn.[7]

Interleaved Thin Lines—The configuration of coupled strip lines illustrated in Fig. 5.05-1(f), in which the two lines of width c are always operated at the same potential, is particularly useful when it is desired to obtain tight coupling with thin strips that are supported by a homogeneous dielectric, of relative dielectric constant ϵ_r, that completely fills the region between the ground planes.[32] The dimensions of the strips for particular values of Z_{oe} and Z_{oo} can be determined with the aid of Figs. 5.05-5 through 5.05-8. For this purpose one needs the definitions that

$$\sqrt{\epsilon_r}\, Z_{oe} = \frac{376.6\epsilon}{C_{oe}} \qquad (5.05\text{-}18)$$

$$\sqrt{\epsilon_r}\, Z_{oo} = \frac{376.6\epsilon}{C_{oo}} \qquad (5.05\text{-}19)$$

where C_{oe} and C_{oo} are the total capacities to ground per unit length of the strips of width c or the strip of width a, when the lines are excited in the even and odd modes, respectively. The absolute dielectric constant ϵ is equal to 0.225 ϵ_r pf per inch. Using the values of Z_{oe} and Z_{oo} which are assumed to be known, one then computes $\Delta C/\epsilon$ from

$$\frac{\Delta C}{\epsilon} = \frac{188.3}{\sqrt{\epsilon_r}}\left[\frac{1}{Z_{oo}} - \frac{1}{Z_{oe}}\right] = \frac{1}{2}\left[\frac{C_{oo}}{\epsilon} - \frac{C_{oe}}{\epsilon}\right] \qquad (5.05\text{-}20)$$

Values of b and g are then selected and d/g is determined from Fig. 5.05-5. Next, values of $C'_{c\infty}/\epsilon$ and C'_{ce}/ϵ are read from Figs. 5.05-6 and 5.05-7. These quantities, together with the value of C_{oe}/ϵ from Eq. (5.05-18), are then substituted in Eq. (5.05-21) to give c/b:

$$c/b = \frac{1 - g/b}{2}\left[\frac{1}{2}C_{oe}/\epsilon - C'_{c\infty}/\epsilon - C'_{ce}/\epsilon\right] \quad . \qquad (5.05\text{-}21)$$

Finally, C'_{oe}/ϵ is found from Fig. 5.05-8 and substituted in Eq. (5.05-22) to give a/b:

$$\frac{a}{b} = \frac{1}{2}\left[\frac{1}{2}C_{oe}/\epsilon - C'_{oe}/\epsilon - 0.441\right] \quad . \qquad (5.05\text{-}22a)$$

Thus all the physical dimensions are determined.

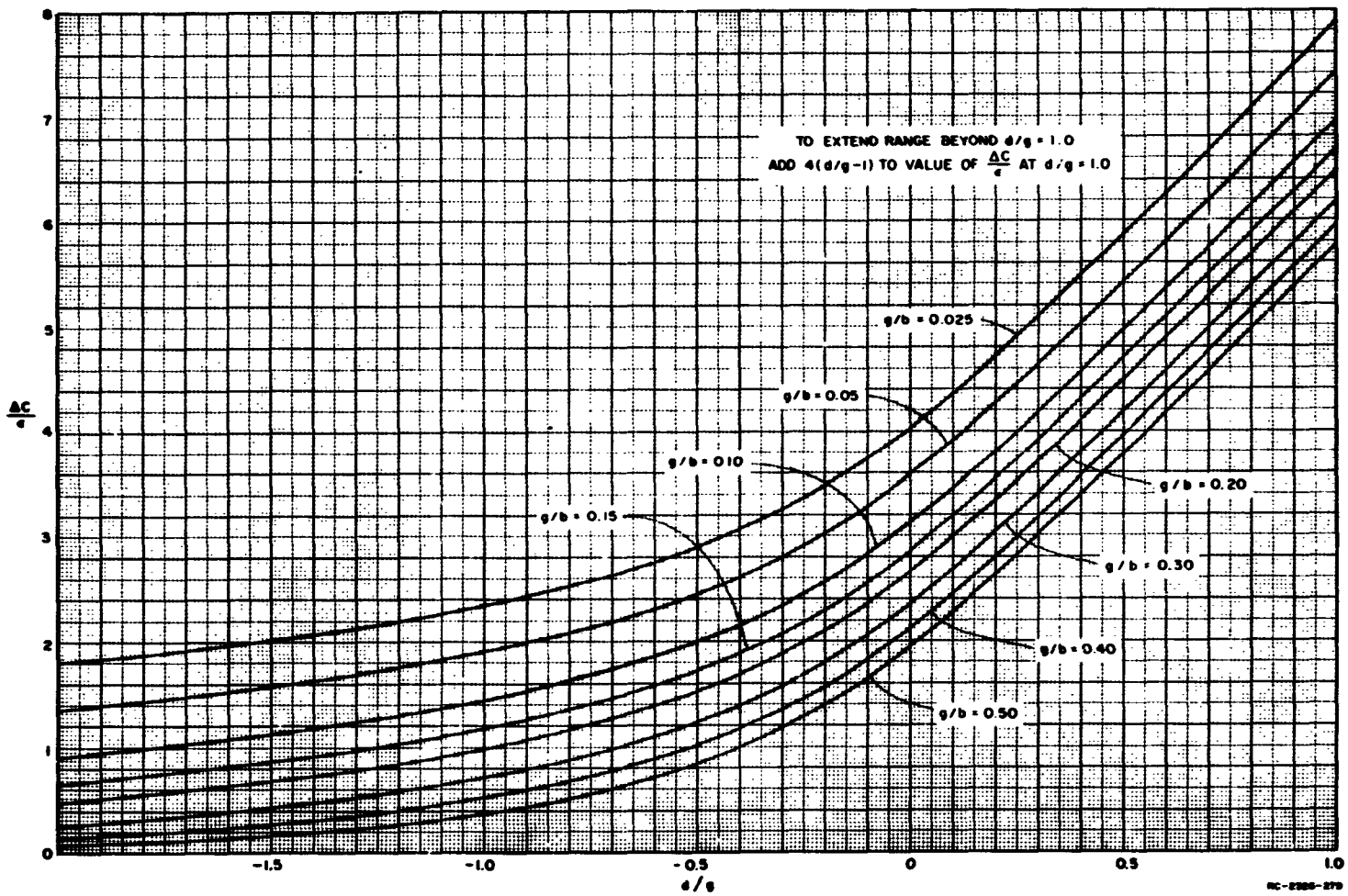

SOURCE: Final Report, Contract DA 36-039 SC-74862, SRI; reprinted in *IRE Trans., PGMTT* (see Ref. 32, by W. J. Getsinger).

FIG. 5.05-5 INTER-STRIP CAPACITANCE FOR CONFIGURATION IN FIG. 5.05-1(f)

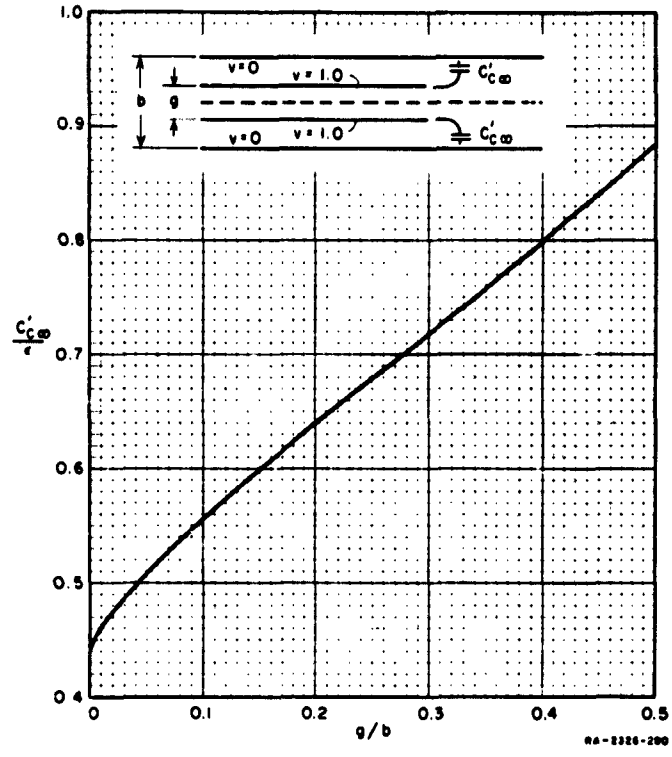

SOURCE: Final Report, Contract DA 36-039 SC-74862, SRI; reprinted in *IRE Trans., PGMTT* (see Ref. 32, by W. J. Getsinger).

FIG. 5.05-6 FRINGING CAPACITANCE OF OFFSET THIN STRIP IN FIG. 5.05-1(f)

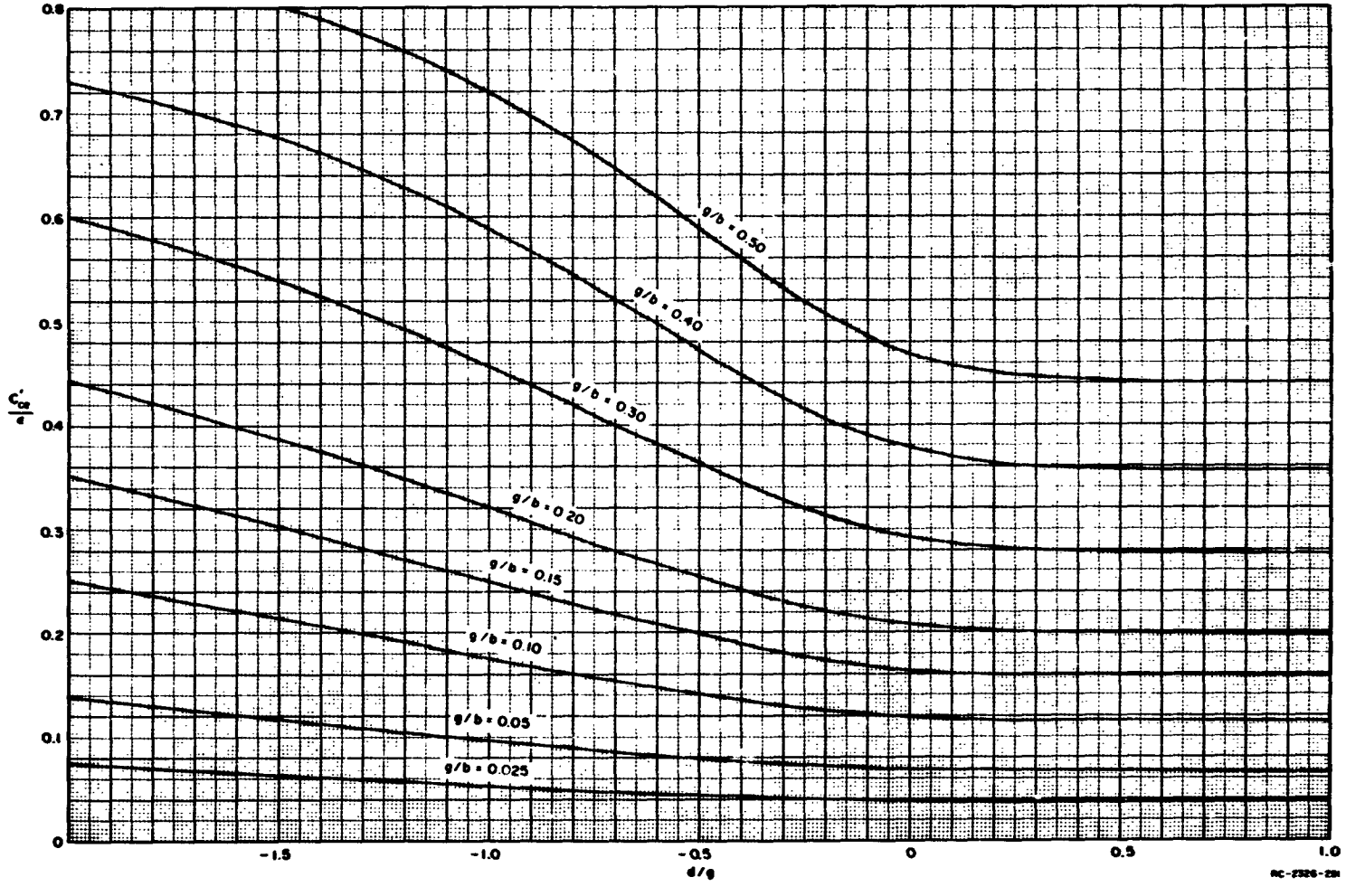

SOURCE: Final Report, Contract DA 36-039 SC-74862, SRI; reprinted in *IRE Trans., PGMTT* (see Ref. 32, by W. J. Getsinger).

FIG. 5.05-7 EVEN MODE, RIGHT-EDGE, FRINGING CAPACITANCE TO GROUND FOR EACH OF THE DOUBLE STRIPS OF WIDTH c IN FIG. 5.05-1(f)

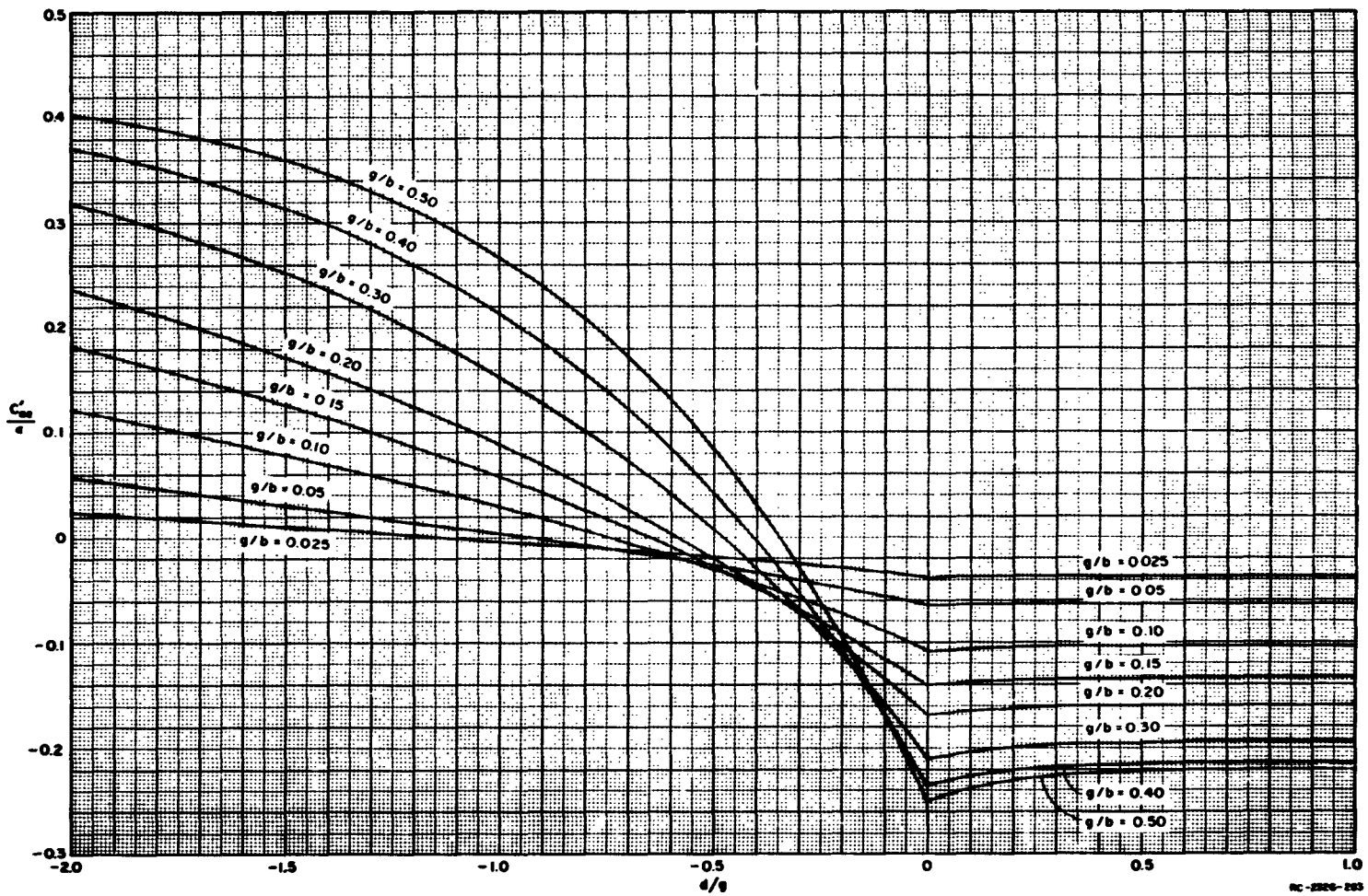

SOURCE: Final Report, Contract DA 36-039 SC-74862, SRI; reprinted in *IRE Trans., PGMTT* (see Ref. 32, by W. J. Getsinger).

FIG. 5.05-8 EVEN MODE, LEFT-EDGE, FRINGING CAPACITANCE TO GROUND FOR THE SINGLE STRIP OF WIDTH a OR a + d IN FIG. 5.05-1(f)

These formulas are exact in the limit of a and $c >> b$ so that fringing fields at opposite edges of the strips do not interact. They are accurate to within 1.24 percent when $a/b \geq 0.35$ and $[(c/b)/(1 - g/b)] \geq 0.35$. If these conditions are not satisfied, it is possible to make approximate corrections based on increasing the parallel plate capacitance to compensate for the loss of fringing capacitance due to interaction of the fringing fields. If an initial value a_1/b is found to be less than 0.35, a new value, a_2/b, can be used where

$$\frac{a_2}{b} = \frac{0.07 + a_1/b}{1.20} \qquad (5.05\text{-}22b)$$

provided $0.1 < a_2/b < 0.35$. A similar formula for correcting an initial value c_1/b gives a new value c_2/b, as

$$\frac{c_2}{b} = \frac{[0.07(1 - g/b) + c_1/b]}{1.20} , \qquad (5.05\text{-}22c)$$

provided g/b is fairly small and $0.1 < (c_2/b)/(1 - g/b)$.

When the strip of width a is inserted so far between the strips of width c that $d/g > 1.0$ the even-mode values C'_{ee}/ϵ and C'_{ce}/ϵ, do not change from their values at $d/g = 1.0$. However the value of $\Delta C/\epsilon$ does change and it can be found simply by adding $4(d/g - 1)$ to the value of $\Delta C/\epsilon$ at $d/g = 1.0$. For spacing between the strips of width c greater than $g/b = 0.5$, or for a separation $d/g < -2.0$, some of the configurations shown in Fig. 5.05-1(a), (b), or (c) are probably more suitable.

Thick Rectangular Bars—The thick rectangular bar configuration of coupled transmission lines, illustrated in Fig. 5.05-1(g) can also be conveniently used where tight coupling between lines is desired.[33] The dimensions of the strips for particular values of Z_{oe} and Z_{oo} can be determined with the aid of Figs. 5.05-9 and 5.05-10(a), (b). A convenient procedure for using the curves is as follows. First one determines $\Delta C/\epsilon$ from Eq. (5.05-20), using the specified values of Z_{oe} and Z_{oo}. Next a convenient value of t/b is selected and the value of s/b is determined from Fig. 5.05-9. The value of w/b is then determined from the equation

$$\frac{w}{b} = \frac{1}{2}\left(1 - \frac{t}{b}\right)\left[\frac{C_{oe}}{2\epsilon} - \frac{C'_{fe}}{\epsilon} - \frac{C'_f}{\epsilon}\right] . \qquad (5.05\text{-}23)$$

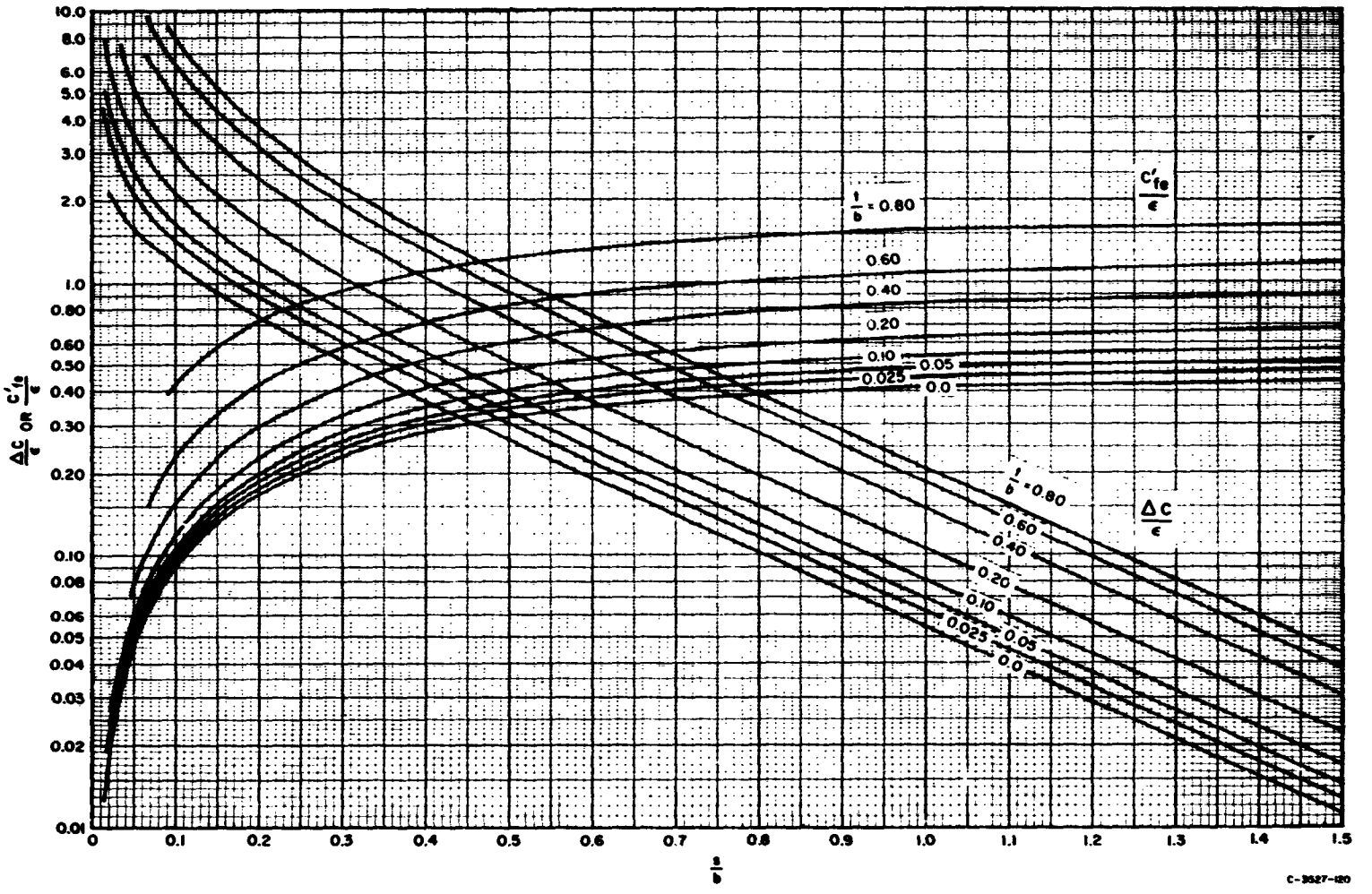

SOURCE: Quarterly Report 2, Contract DA 36-039 SC-87398, SRI; reprinted in *IRE Trans., PGMTT* (see Ref. 33, by W. J. Getsinger).

FIG. 5.05-9 NORMALIZED EVEN-MODE FRINGING CAPACITANCE C'_{fe}/ϵ AND INTERBAR CAPACITANCE $\Delta C/\epsilon$ FOR COUPLED RECTANGULAR BARS

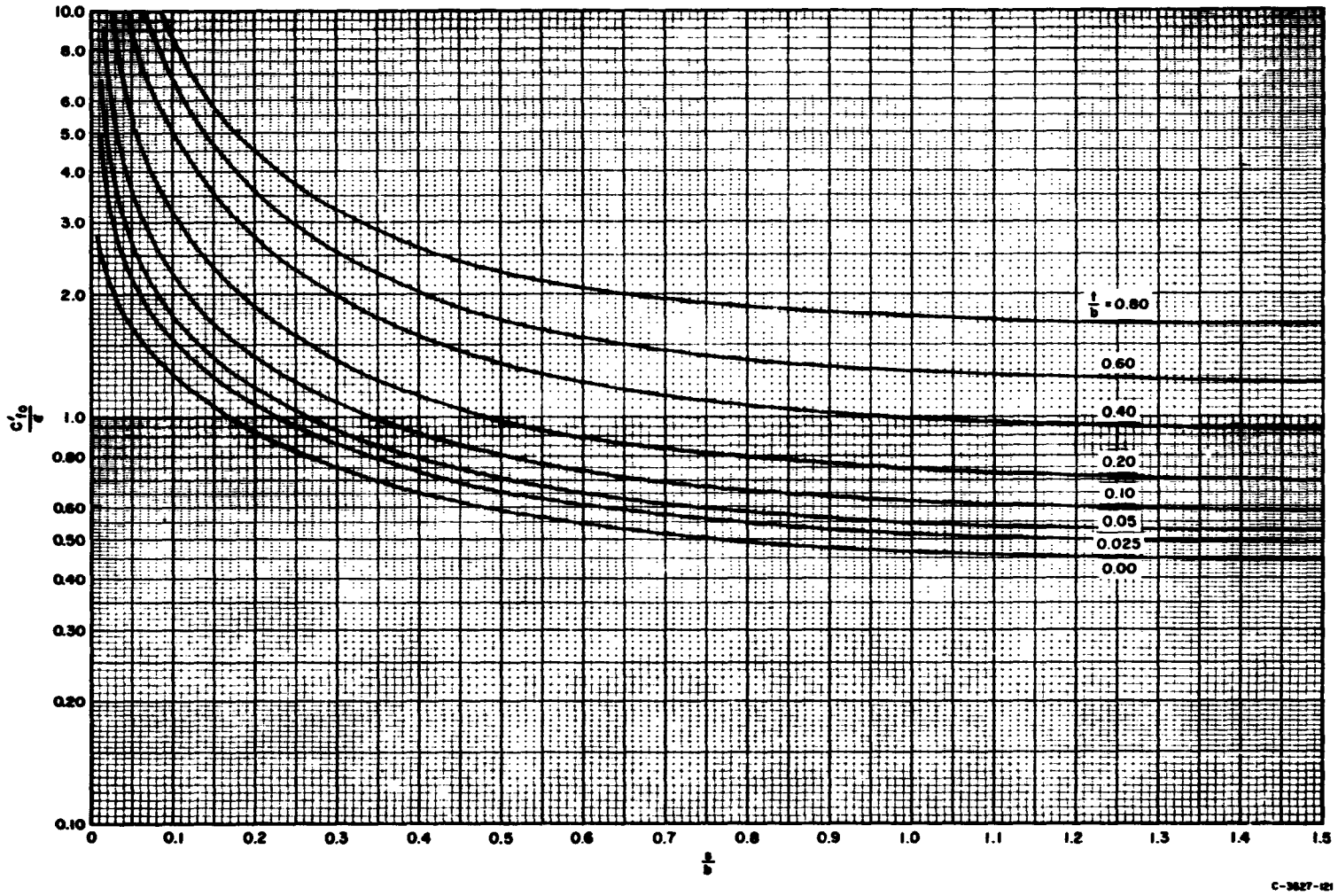

SOURCE: Quarterly Report 2, Contract DA 36-039 SC-87398, SRI; reprinted in *IRE Trans., PGMTT* (see Ref. 33, by W. J. Getsinger).

FIG. 5.05-10(a) NORMALIZED ODD-MODE FRINGING CAPACITANCE FOR RECTANGULAR BARS

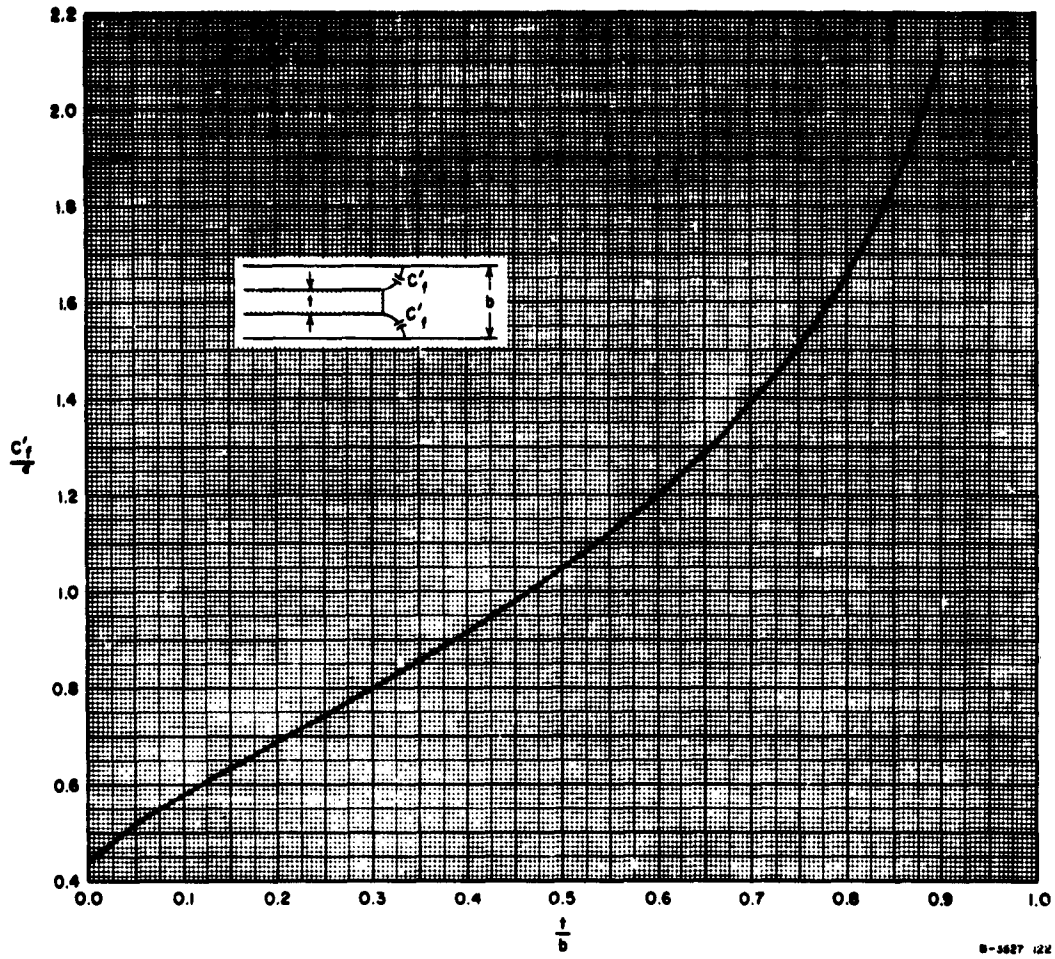

SOURCE: Quarterly Report 2, Contract DA 36-039 SC-87398, SRI; reprinted in *IRE Trans., PGMTT* (see Ref. 33, by W. J. Getsinger).

FIG. 5.05-10(b) NORMALIZED FRINGING CAPACITANCE FOR AN ISOLATED RECTANGULAR BAR

The value of C_{oe} to use is determined from the specified value of Z_{oe} using Eq. (5.05-18). The fringing capacitance C'_{fe} for the even mode can be read from Fig. 5.05-9, and C'_f can be determined from Fig. 5.05-10(b). The curves in Fig. 5.05-10(a) allow one to determine C'_{fo} directly.

The various fringing and parallel-plate capacitances used in the above discussion are illustrated in Fig. 5.05-11. Note that the odd-mode fringing capacitances C'_{fo} correspond to the fringing capacitances between the inner edges of the bars and a metallic wall halfway between the bars. It is seen that the total odd mode capacitance of a bar is

$$\frac{C_{oo}}{\epsilon} = 2\left[\frac{C_p}{\epsilon} + \frac{C'_{fo}}{\epsilon} + \frac{C'_f}{\epsilon}\right] \qquad (5.05\text{-}24)$$

and the total even mode capacitance of a bar is

$$\frac{C_{oe}}{\epsilon} = 2\left[\frac{C_p}{\epsilon} + \frac{C'_{fe}}{\epsilon} + \frac{C'_f}{\epsilon}\right] . \qquad (5.05\text{-}25)$$

The normalized per-unit-length parallel plate capacitance $C_p/\epsilon = 2w/(b - t)$, and $\epsilon = 0.225\epsilon_r$ pf per inch.

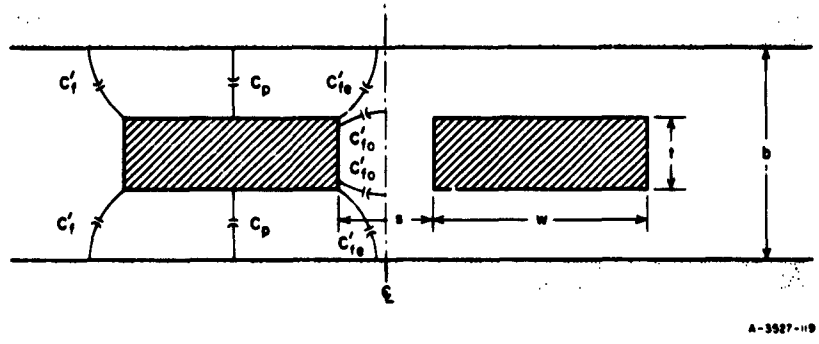

SOURCE: Quarterly Report 2, Contract DA 36-039 SC-87398, SRI; reprinted in *IRE Trans., PGMTT* (see Ref. 33, by W. J. Getsinger).

FIG. 5.05-11 COUPLED RECTANGULAR BARS CENTERED BETWEEN PARALLEL PLATES ILLUSTRATING THE VARIOUS FRINGING AND PARALLEL PLATE CAPACITIES

The even- and odd-mode fringing capacitances C'_{fe}/ϵ and C'_{fo}/ϵ were derived by conformal mapping techniques and are exact in limits of $[w/b/(1 - t/b)] \to \infty$. It is believed that when $[w/b/(1 - t/b)] > 0.35$ the interaction between the fringing fields is small enough so that the values of C_{oo}/ϵ and C_{oe}/ϵ determined from Eqs. (5.05-24) and (5.05-25) are reduced by a maximum of 1.24 percent of their true values.

In situations where an initial value, w/b is found from Eq. (5.05-23) to be less than $0.35\ [1 - (t/b)]$ so that the fringing fields interact, a new value of w'/b can be used where

$$\frac{w'}{b} = \frac{\left\{0.07\left[1 - \frac{t}{b}\right] + \frac{w}{b}\right\}}{1.20} \qquad (5.05\text{-}26)$$

provided $0.1 < (w'/b)/[1 - (t/b)] < 0.35$.

Unsymmetrical Parallel-Coupled Lines—Figure 5.05-12 shows an unsymmetrical pair of parallel-coupled lines and various line capacitances. Note that C_a is the capacitance per unit length between Line a and ground, C_{ab} is the capacitance per unit length between Line a and Line b, while C_b is the capacitance per unit length between Line b and ground. When C_a is not equal to C_b, the two lines will have different odd- and even-mode admittances as is indicated by Eqs. (1) in Table 5.05-1. In terms of odd- and even-mode capacitances, for Line a

$$C^a_{oo} = C_a + 2C_{ab}\,, \qquad C^a_{oe} = C_a \qquad (5.05\text{-}27)$$

while for Line b

$$C^b_{oo} = C_b + 2C_{ab}\,, \qquad C^b_{oe} = C_b\,. \qquad (5.05\text{-}28)$$

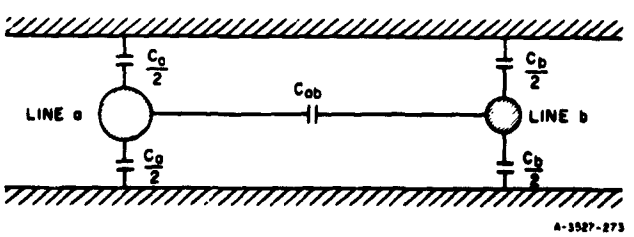

FIG. 5.05-12 AN UNSYMMETRICAL PAIR OF PARALLEL-COUPLED LINES C_a, C_{ab}, and C_b are line capacitances per unit length.

For symmetrical parallel-coupled lines the odd-mode impedances are simply the reciprocals of the odd-mode admittances, and analogously for the even-mode impedances and admittances. However, as can be demonstrated from Eqs. (2) in Table 5.05-1, this is not the case for unsymmetrical parallel-coupled lines. For unsymmetrical lines, the odd- and even-mode impedances are not simply the reciprocals of the odd- and even-mode

Table 5.05-1

RELATIONS BETWEEN LINE ADMITTANCES, IMPEDANCES, AND CAPACITANCES PER UNIT LENGTH OF UNSYMMETRICAL PARALLEL-COUPLED LINES

v = velocity of light in media of propagation

= $1.18 \times 10^{10}/\sqrt{\epsilon_r}$ inches/sec.

η_0 = intrinsic impedance of free space = 376.7 ohms

ϵ = dielectric constant = $0.225\,\epsilon_r$ $\mu\mu f$/inch

$$\left.\begin{aligned} Y^a_{oe} &= vC_a\,, & Y^a_{oo} &= v(C_a + 2C_{ab}) \\ Y^b_{oe} &= vC_b\,, & Y^b_{oo} &= v(C_b + 2C_{ab}) \end{aligned}\right\} \quad (1)$$

$$\left.\begin{aligned} Z^a_{oe} &= \frac{C_b + 2C_{ab}}{vF}\,, & Z^a_{oo} &= \frac{C_b}{vF} \\ Z^b_{oe} &= \frac{C_a + 2C_{ab}}{vF}\,, & Z^b_{oo} &= \frac{C_a}{vF} \end{aligned}\right\} \quad (2)$$

where $F = C_aC_b + C_aC_{ab} + C_bC_{ab}$

$$\left.\begin{aligned} \frac{C_a}{\epsilon} &= \frac{\eta_0 Y^a_{oe}}{\sqrt{\epsilon_r}}\,, & \frac{C_{ab}}{\epsilon} &= \frac{\eta_0}{\sqrt{\epsilon_r}}\left(\frac{Y^a_{oo} - Y^a_{oe}}{2}\right) \\ \frac{C_b}{\epsilon} &= \frac{\eta_0 Y^b_{oe}}{\sqrt{\epsilon_r}}\,, & \frac{C_{ab}}{\epsilon} &= \frac{\eta_0}{\sqrt{\epsilon_r}}\left(\frac{Y^b_{oo} - Y^b_{oe}}{2}\right) \end{aligned}\right\} \quad (3)$$

$$\left.\begin{aligned} \frac{C_a}{\epsilon} &= \frac{\eta_0 2Z^b_{oo}}{\sqrt{\epsilon_r}H}\,, & \frac{C_{ab}}{\epsilon} &= \frac{\eta_0}{\sqrt{\epsilon_r}}\left(\frac{Z^b_{oo} - Z^b_{oe}}{H}\right) \\ \frac{C_b}{\epsilon} &= \frac{\eta_0 2Z^a_{oo}}{\sqrt{\epsilon_r}H}\,, & \frac{C_{ab}}{\epsilon} &= \frac{\eta_0}{\sqrt{\epsilon_r}}\left(\frac{Z^a_{oo} - Z^a_{oe}}{H}\right) \end{aligned}\right\} \quad (4)$$

where $H = Z^a_{oe}\,Z^b_{oo} + Z^b_{oe}\,Z^a_{oo}$.

admittances. The reason for this lies in the fact that when the odd- and even-mode *admittances* are computed the basic definition of these admittances assumes that the lines are being driven with *voltages of identical magnitude* with equal or opposite phase, while the *currents* in the lines may be of different magnitudes. When the odd- and even-mode *impedances* are computed, the basic definition of these impedances assumes that the lines are being driven by *currents of identical magnitude* with equal or opposite phases, while magnitudes of the *voltages* on the two lines may be different. These two different sets of boundary conditions can be seen to lead to different voltage-current ratios if the lines are unsymmetrical.

Some unsymmetrical parallel-coupled lines which are quite easy to design are shown in Fig. 5.05-13. Both bars have the same height, and both are assumed to be wide enough so that the interactions between the

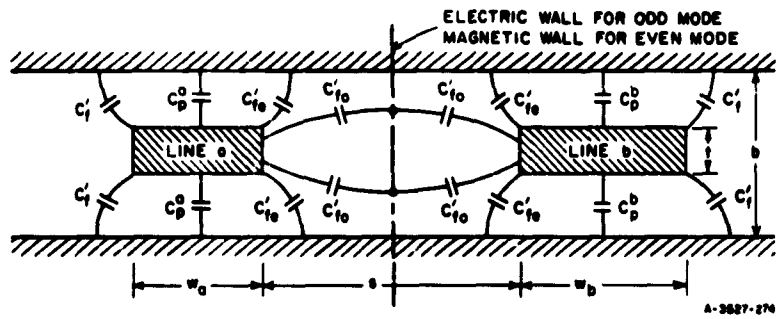

FIG. 5.05-13 CROSS-SECTION OF UNSYMMETRICAL, RECTANGULAR-BAR PARALLEL-COUPLED LINES

fringing fields at the right and left sides of each bar are negligible, or at least small enough to be corrected for by use of Eq. (5.05-26). On this basis the fringing fields are the same for both bars, and their different capacitances C_a and C_b to ground are due entirely to different parallel-plate capacitances C_p^a and C_p^b. For the structure shown

$$\begin{aligned} C_a &= 2(C_p^a + C_f' + C_{fo}') \\ C_{ab} &= (C_{fo}' - C_{fo}') \\ C_b &= 2(C_p^b + C_f' + C_{fo}') \end{aligned} \qquad (5.05\text{-}29)$$

To design a pair of lines such as those in Fig. 5.05-13 so as to have specified odd- and even-mode admittances or impedances, first use Eqs. (3) or (4) in Table 5.05-1 to compute C_a/ϵ, C_{ab}/ϵ, and C_b/ϵ. Select a convenient value for t/b, and noting that

$$\frac{\Delta C}{\epsilon} = \frac{C_{ab}}{\epsilon} \quad , \tag{5.05-30}$$

use Fig. 5.05-9 to determine s/b, and also C'_{fe}/ϵ. Using t/b and Fig. 5.05-10(b) determine C'_f/ϵ, and then compute

$$\frac{w_a}{b} = \frac{1}{2}\left(1 - \frac{t}{b}\right)\left[\frac{1}{2}\left(\frac{C_a}{\epsilon}\right) - \frac{C'_{fe}}{\epsilon} - \frac{C'_f}{\epsilon}\right] \tag{5.05-31}$$

$$\frac{w_b}{b} = \frac{1}{2}\left(1 - \frac{t}{b}\right)\left[\frac{1}{2}\left(\frac{C_b}{\epsilon}\right) - \frac{C'_{fe}}{\epsilon} - \frac{C'_f}{\epsilon}\right] \quad . \tag{5.05-32}$$

Knowing the ground-plane spacing b, the required bar widths w_a and w_b are then determined. This procedure also works for the thin-strip case where $t/b = 0$. If either w_a/b or w_b/b is less than $0.35[1 - t/b]$, Eq. (5.05-26) should be applied to obtain corrected values.

Arrays of Parallel-Coupled Lines--Figure 5.05-14 shows an array of parallel-coupled lines such as is used in the interdigital-line filters discussed in Chapt. 10. In the structure shown, all of the bars have the same t/b ratio and the other dimensions of the bars are easily obtained

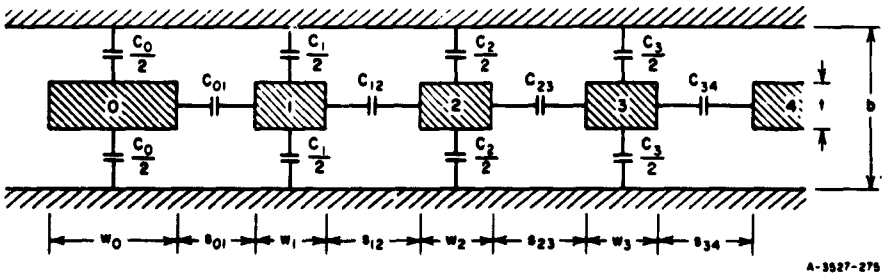

SOURCE: Quarterly Progress Report 4, Contract DA 36-039 SC-87398, SRI; reprinted in the *IRE Trans. PGMTT* (see Ref. 3 of Chapter 10, by G. L. Matthaei)

FIG. 5.05-14 CROSS SECTION OF AN ARRAY OF PARALLEL-COUPLED LINES BETWEEN GROUND PLANES

by generalizing the procedure described for designing the unsymmetrical parallel-coupled lines in Fig. 5.05-13. In the structure in Fig. 5.05-14 the electrical properties of the structure are characterized in terms of the self-capacitances C_k per unit length of each bar with respect to ground, and the mutual capacitances $C_{k,k+1}$ per unit length between adjacent bars k and $k+1$. This representation is not necessarily always highly accurate because there can conceivably be a significant amount of fringing capacitance in some cases between a given line element, and, for example, the line element beyond the nearest neighbor. However, at least for geometries such as that shown, experience has shown this representation to have satisfactory accuracy for applications such as interdigital filter design.

For design of the parallel-coupled array structures discussed in this book, equations will be given for the normalized self and mutual capacitances C_k/ϵ and $C_{k,k+1}/\epsilon$ per unit length for all the lines in the structure. Then the cross-sectional dimensions of the bars and spacings between them are determined as follows. First, choose values for t and b. Then, since

$$\frac{(\Delta C)_{k,k+1}}{\epsilon} = \frac{C_{k,k+1}}{\epsilon} \qquad (5.05\text{-}33)$$

Fig. 5.05-9 can be used to determine $s_{k,k+1}$ b. In this manner, the spacings $s_{k,k+1}$ between all the bars are obtained. Also, using Fig. 5.05-9, the normalized fringing capacitances $(C'_{fe})_{k,k+1}/\epsilon$ associated with the gaps $s_{k,k+1}$ between bars are obtained. Then the normalized width of the kth bar is

$$\frac{w_k}{b} = \frac{1}{2}\left(1 - \frac{t}{b}\right)\left[\frac{1}{2}\left(\frac{C_k}{\epsilon}\right) - \frac{(C'_{fe})_{k-1,k}}{\epsilon} - \frac{(C'_{fe})_{k,k+1}}{\epsilon}\right] . \qquad (5.05\text{-}34)$$

In the case of the bar at the end of the array (the bar at the far left in Fig 5.05-14), C'_{fe}/ϵ for the edge of the bar which has no neighbor must be replaced by C'_f/ϵ which is determined from Fig. 5.05-10(b). Thus, for example, for Bar 0 in Fig. 5.05-14,

$$\frac{w_0}{b} = \frac{1}{2}\left(1 - \frac{t}{b}\right)\left[\frac{1}{2}\left(\frac{C_0}{\epsilon}\right) - \frac{C'_f}{\epsilon} - \frac{(C'_{fe})_{01}}{\epsilon}\right] . \qquad (5.05\text{-}35)$$

If $w_k/b < 0.35[1 - t/b]$ for any of the bars, the width correction given in Eq. (5.05-26) should be applied to those bars where this condition exists.

SEC. 5.06, SPECIAL PROPERTIES OF WAVEGUIDES

A waveguide consisting of a single hollow conductor that can propagate electromagnetic energy above a certain cutoff frequency, f_c, is also a very useful element in microwave filters. A waveguide can propagate an infinite number of modes, which can be characterized as being either TE (transverse electric) or TM (transverse magnetic). The TE modes have a magnetic field but no electric field in the direction of propagation, while TM modes have an electric field but no magnetic field in the direction of propagation. Usually a waveguide is operated so that it propagates energy in a single mode, and under this condition it can be described as a transmission line with a propagation constant γ_t and a characteristic impedance Z_0. The propagation constant for a waveguide is uniquely defined. The characteristic impedance of a waveguide can be considered to be the wave impedance of the guide, Z_w (*i.e.*, the ratio of the transverse electric to the transverse magnetic field in the guide), multiplied by a constant. The value of the constant depends on what definition of characteristic impedance is employed (*i.e.*, voltage-current, voltage-power, or current-power). Thus it is seen that the characteristic impedance of a waveguide is not a unique quantity, as it is in the case of a TEM transmission line. However, this lack of uniqueness turns out to be unimportant in waveguide filter calculations because one can always normalize all waveguide equivalent circuit elements to the characteristic impedance of the guide.

In a lossless waveguide filled with dielectric of relative dielectric constant ϵ_r, the guide wavelength λ_g, free-space wavelength λ, wavelength in the dielectric λ_1, and cutoff wavelength λ_c, are related as

$$\frac{1}{\lambda_1^2} = \frac{\epsilon_r}{\lambda^2} = \frac{1}{\lambda_g^2} + \frac{1}{\lambda_c^2} \quad . \tag{5.06-1}$$

The characteristic impedance that we shall assume for convenience to equal the wave impedance is

$$Z_0 = \frac{1}{Y_0} = \begin{cases} \frac{377}{\sqrt{\epsilon_r}} \lambda_g/\lambda_1 & \text{TE modes} \\ \frac{377}{\sqrt{\epsilon_r}} \lambda_1/\lambda_g & \text{TM modes} \end{cases} \quad . \tag{5.06-2}$$

The propagation phase constant β_t is

$$\beta_t = \frac{2\pi}{\lambda_g} \text{ radians/unit length} \quad . \tag{5.06-3}$$

The most common form of waveguide for use in microwave filters is a rectangular waveguide of width a and height b operating in a TE_{10} mode. TE_{m0} modes have cutoff wavelengths

$$\lambda_c = \frac{2a}{m} \quad . \tag{5.06-4}$$

The index m equals the number of half-waves of variation of the electric field across the width, a, of the guide. The cutoff frequency f_c (measured in gigacycles) is related to the cutoff wavelength in inches as

$$f_c = \frac{11.8}{\lambda_c} \sqrt{\epsilon_r} \quad . \tag{5.06-5}$$

The dominant mode, that is, the one with the lowest cutoff frequency, is the TE_{10} mode.

The dominant mode in circular waveguide of diameter D is the TE_{11} mode. The cutoff wavelength of the TE_{11} mode is $1.706D$.

The attenuation of these modes due to losses in the copper conductors are for TE_{m0} modes in rectangular guide

$$\alpha_c\,(TE_{m0}) = \frac{1.90 \times 10^{-4} \sqrt{\epsilon_r} \sqrt{f}}{b} \frac{\left[1 + \frac{2b}{a}\left(\frac{f_c}{f}\right)^2\right]}{\sqrt{1 - \left(\frac{f_c}{f}\right)^2}} \text{ db/unit length} \tag{5.06-6}$$

and for the TE_{11} mode in circular guide

$$\alpha_{c(TE_{11})} = \frac{3.80 \times 10^{-4} \sqrt{\epsilon_r} \sqrt{f} \left[\left(\frac{f_c}{f} \right)^2 + 0.420 \right]}{D \sqrt{1 - \left(\frac{f_c}{f} \right)^2}} \quad \text{db/unit length} \qquad (5.06\text{-}7)$$

where f is measured in gigacycles. These values of attenuation are plotted in Fig. 5.06-1.

The attenuation caused by losses in the dielectric in any waveguide mode is

$$\alpha_d = \frac{27.3 \tan \delta}{\lambda_1} \left(\frac{\lambda_g}{\lambda_1} \right) \quad \text{db/unit length} \qquad (5.06\text{-}8)$$

where $\tan \delta$ is the loss tangent of the dielectric. The unloaded Q, of a waveguide* is

$$\frac{1}{Q} = \frac{1}{Q_d} + \frac{1}{Q_c} \qquad (5.06\text{-}9)$$

where Q_d depends only on losses in the dielectric and is given by

$$Q_d = \frac{1}{\tan \delta} \qquad (5.06\text{-}10)$$

and Q_c depends only on the ohmic losses in the waveguide walls and is given by

$$Q_c = \frac{\pi \lambda_g}{\lambda_1^2 \alpha_c} \quad . \qquad (5.06\text{-}11)$$

* Additional discussion relevant to the use of waveguides as resonators will be found in Sec. 5.08.

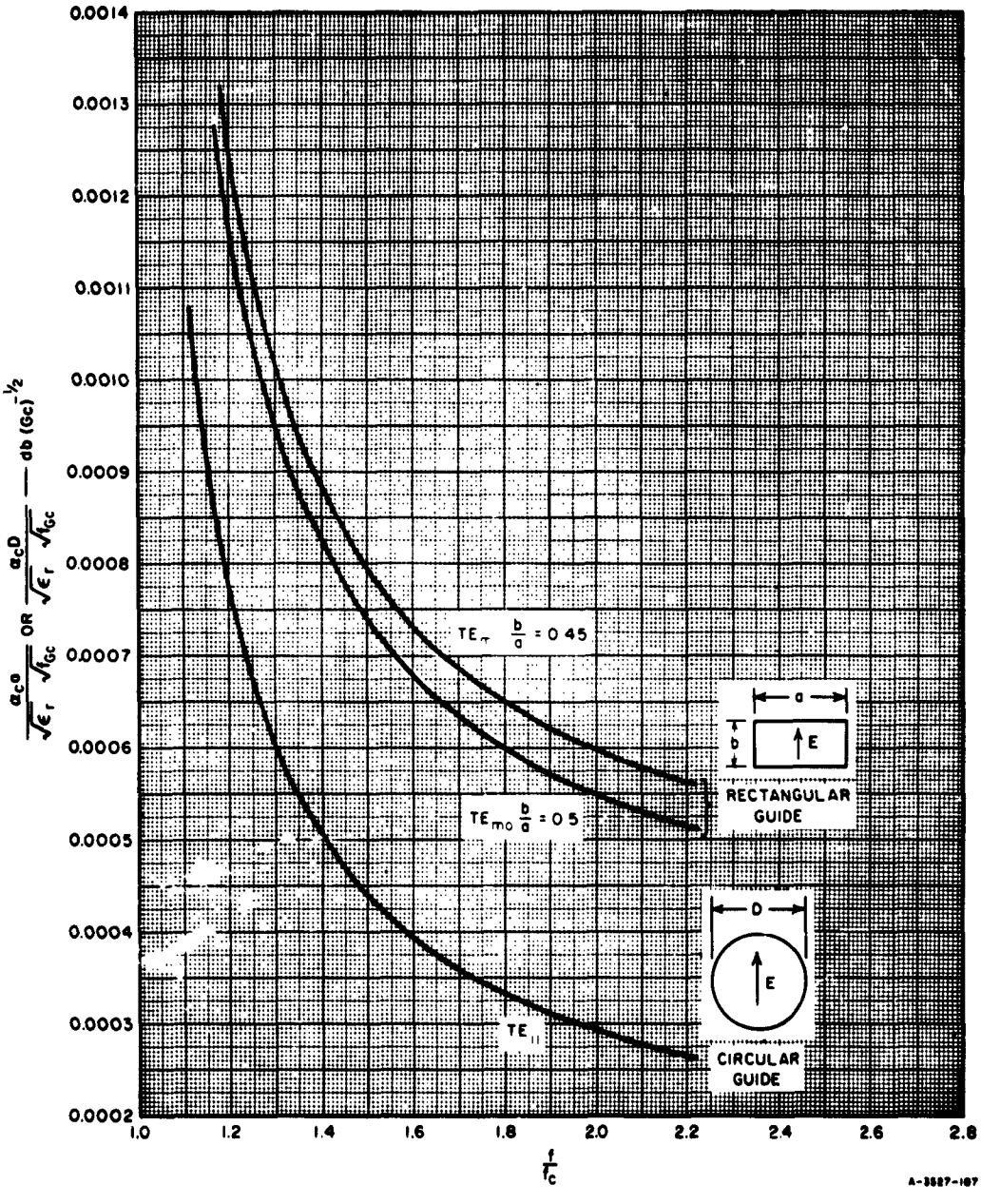

FIG. 5.06-1 WAVEGUIDE ATTENUATION DATA

For rectangular copper waveguides operating in the TE_{n0} mode, we have

$$Q_c(TE_{n0}) = \frac{1.212 \times 10^4 \, b \sqrt{f}}{1 + \frac{2b}{a}\left(\frac{f_c}{f}\right)^2} \qquad (5.06\text{-}12)$$

where a and b are measured in inches, and f in gigacycles. For a circular waveguide operating in the TE_{11} mode, we have

$$Q_c(TE_{11}) = \frac{0.606 \times 10^4 \, D \sqrt{f}}{0.420 + \left(\frac{f_c}{f}\right)^2} \qquad (5.06\text{-}13)$$

where D is measured in inches and f in gigacycles. These expressions for Q_c are plotted in Fig. 5.06-2.

The power-handling capacity P_{max} of air-filled guides, at atmospheric pressure, assuming a breakdown strength of 29 kv/cm, for the TE_{n0} mode in rectangular guide is

$$P_{max}(TE_{n0}) = 3.6 \, ab \, \frac{\lambda}{\lambda_g} \quad \text{megawatts} \quad , \qquad (5.06\text{-}14)$$

and for the TE_{11} mode in circular guide

$$P_{max}(TE_{11}) = 2.7 \, D^2 \, \frac{\lambda}{\lambda_g} \quad \text{megawatts} \qquad (5.06\text{-}15)$$

where P_{max} is average power in megawatts and the dimensions are in inches.

In a rectangular waveguide operating in the TE_{10} mode, with an aspect ratio b/a of 0.5 or 0.45, the next higher-order mode is the TE_{20} with cutoff wavelength $\lambda_c = a$. Next come the TE_{11} or TM_{11} modes each of which has the same cutoff wavelength, $\lambda_c = 2ab/\sqrt{a^2 + b^2}$. In the circular waveguide, the next higher-order mode is the TM_{01} mode, which has $\lambda_c = 1.305 \, D$.

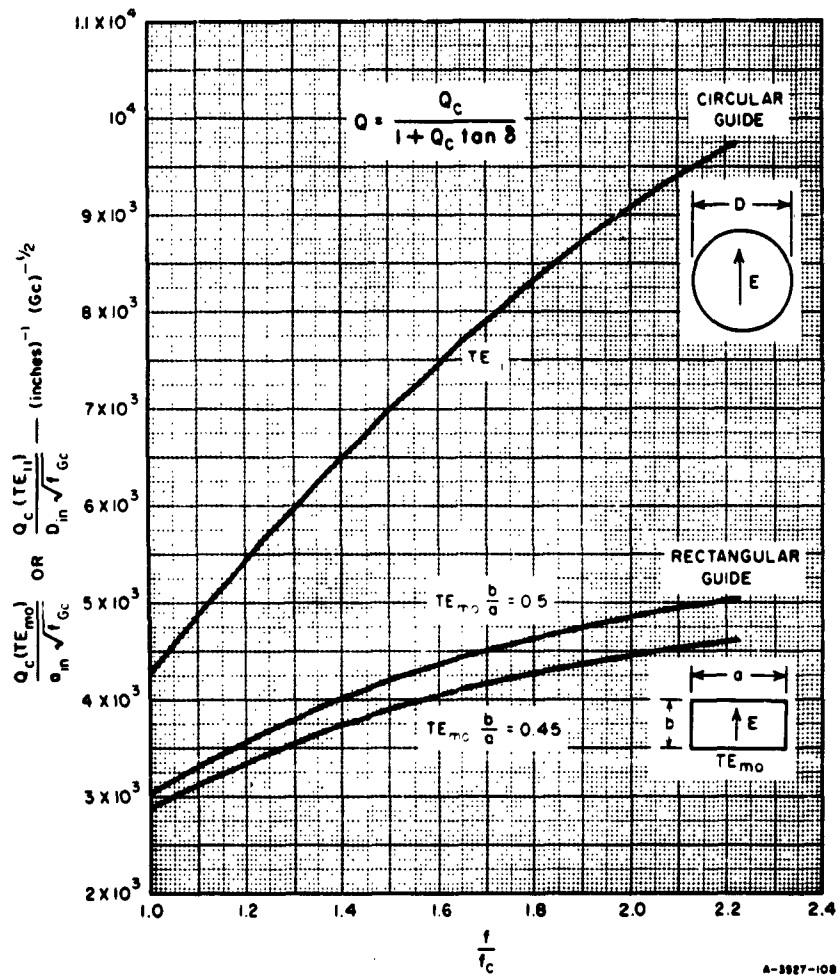

FIG. 5.06-2 WAVEGUIDE Q DATA

SEC. 5.07. COMMON TRANSMISSION LINE DISCONTINUITIES

This section presents formulas and curves for some of the common discontinuities in transmission lines. Other more complete results are to be found in the literature.[8, 9, 10, 11, 12, 13]

Changes in Diameter of Coaxial Lines—When a change is made in the diameter of either the inner or outer conductor of a coaxial line, or in both conductors simultaneously, the equivalent circuits can be represented as shown in Fig. 5.07-1.[10, 11] The equivalent shunt capacity, C_d, for each of these cases is given in Fig. 5.07-2. These equivalent circuits apply when the operating frequency is appreciably below the cutoff frequency of the next higher-order propagating mode.

Changes in Width of Center Conductor of a Strip Line—The change in width of the center conductor of a strip line introduces an inductive reactance in series with the line.[12] In most situations this reactance is small and can be neglected. The approximate equivalent circuit for this situation is shown in Fig. 5.07-3.

Compensated Right-Angle Corner in Strip Line—A low-VSWR right-angle corner can be made in strip line if the outside edge of the strip is beveled. Figure 5.07-4 shows the dimensions of some matched right-angle corners for a plate-spacing-to-wavelength ratio, b/λ, of 0.0845. These data were obtained for a center strip conductor having negligible thickness; however, the data should apply with acceptable accuracy for strips of moderate thickness.

Fringing Capacitance for Semi-Infinite Plate Centered Between Parallel Ground Planes—The exact fringing capacitance, C'_f, from one corner of a semi-infinite plate centered between parallel ground planes is

$$C'_f = \frac{\epsilon}{\pi}\left\{\frac{2}{1-\frac{t}{b}}\ln\left(\frac{1}{1-\frac{t}{b}}+1\right)-\left(\frac{1}{1-\frac{t}{b}}-1\right)\ln\left[\frac{\cdot}{\left(1-\frac{t}{d}\right)^2}-1\right]\right\} \quad \mu\mu f/\text{inch}$$

where $\epsilon = 0.225\,\epsilon_r$ micromicrofarads per inch and ϵ_r is the relative dielectric constant of the material between the semi-infinite plate and the ground planes. Fringing capacitance, C'_f, is plotted in Fig. 5.07-5.

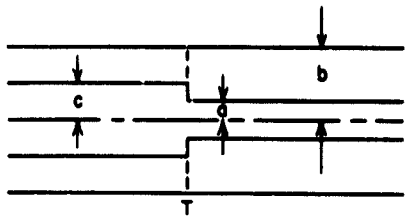

LONGITUDINAL SECTION

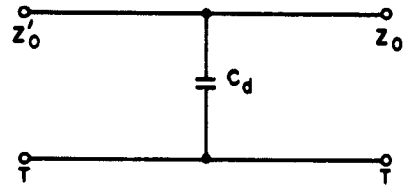

EQUIVALENT CIRCUIT

$$\frac{Z_0'}{Z_0} = \frac{\ln \frac{b}{c}}{\ln \frac{b}{a}} \qquad C_d = 2\pi b C_{d1}'$$

(a) STEP IN INNER CONDUCTOR

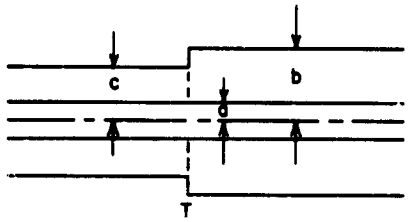

LONGITUDINAL SECTION

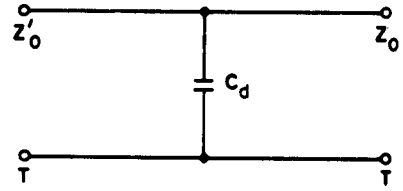

EQUIVALENT CIRCUIT

$$\frac{Z_0'}{Z_0} = \frac{\ln \frac{c}{a}}{\ln \frac{b}{a}} \qquad C_d = 2\pi a C_{d2}'$$

(b) STEP IN OUTER CONDUCTOR

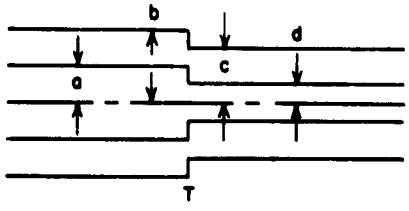

LONGITUDINAL SECTION

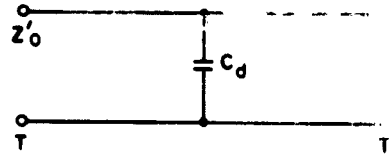

EQUIVALENT CIRCUIT

$$\frac{Z_0'}{Z_0} = \frac{\ln \frac{b}{a}}{\ln \frac{c}{d}} \qquad C_d = 2\pi c C_{d1}' + 2\pi a C_{d2}'$$

(c) STEP IN INNER AND OUTER CONDUCTORS

A-3527-139

FIG. 5.07-1 COAXIAL-LINE DISCONTINUITIES

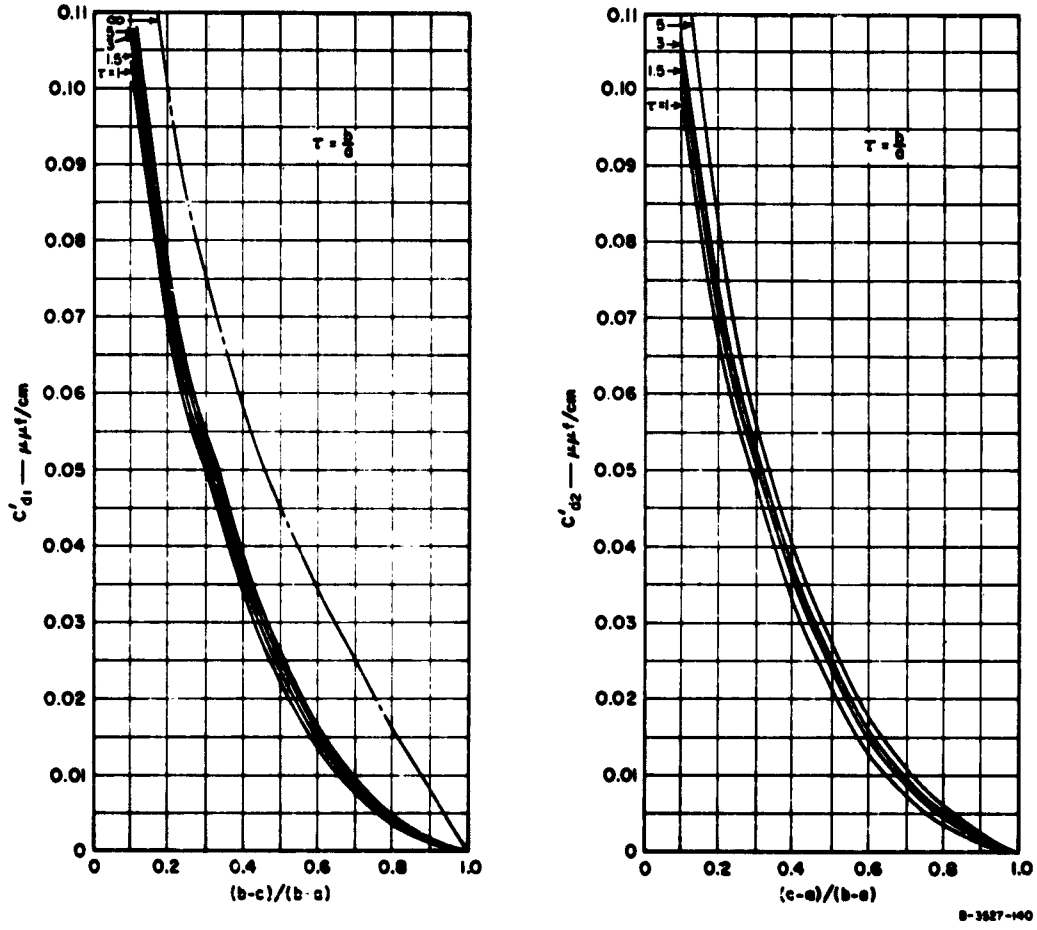

SOURCE: *Proc. IRE* (see Ref. 10 and 11 by J. R. Whinnery and H. W. Jamieson).

FIG. 5.07-2 COAXIAL-LINE-STEP FRINGING CAPACITIES

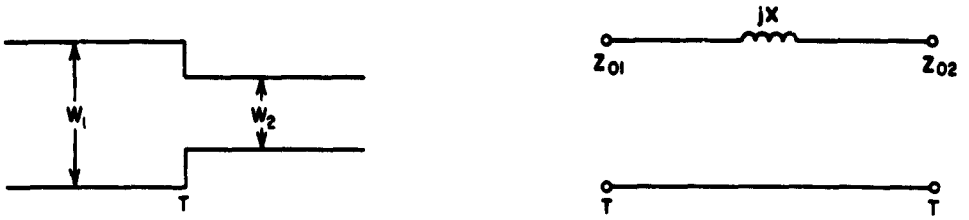

TOP VIEW

EQUIVALENT CIRCUIT

$$X = \frac{60\pi b}{\lambda} \ln \csc\left[\frac{\pi}{2}\frac{Z_{02}}{Z_{01}}\right]$$

SOURCE: *IRE Trans., PGMTT* (see Ref. 12, by A. A. Oliner).

FIG. 5.07-3 STRIP-LINE STEP EQUIVALENT CIRCUIT

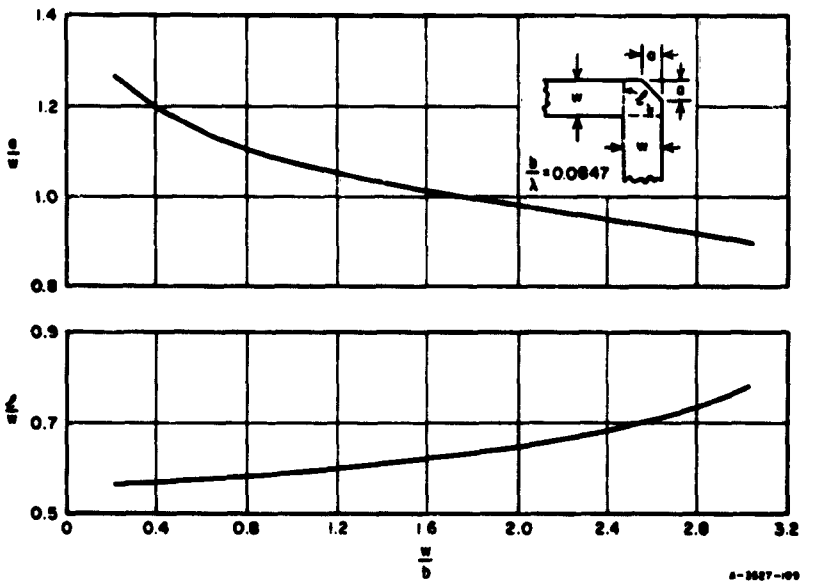

FIG. 5.07-4 MATCHED STRIP-LINE CORNER
The parameter ℓ is the effective length around the corner.

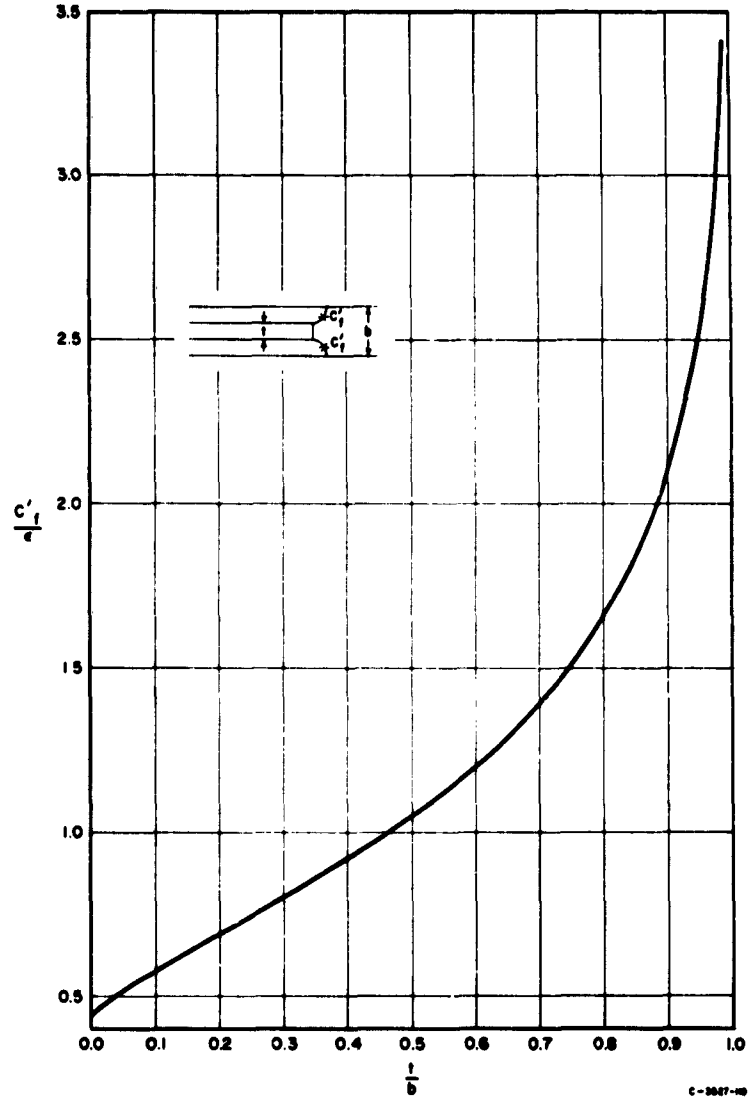

SOURCE: Final Report Contract DA 36-039 SC-63232, SRI; reprinted in *IRE Trans., PGMTT* (see Ref. 2, by S. B. Cohn).

FIG. 5.07-5 EXACT FRINGING CAPACITANCE FOR A SEMI-INFINITE PLATE CENTERED BETWEEN PARALLEL GROUND PLANES

Strip-Line T-Junctions—A symmetrical strip-line *T*-junction of the type illustrated in Fig. 5.07-6(a) can be represented by the equivalent circuit shown in Fig. 5.07-6(b). A short-circuit placed in turn in each of the three arms, at distances equal to multiples of one-half wavelength from the corresponding reference planes labeled P_1 and P_2, will block transmission between the other two arms of the junction.

Measured values obtained for the equivalent circuit parameters of sixteen different strip-line *T*-junctions are shown in Figs. 5.07-7, 5.07-8, and 5.07-9. The thickness, t, of the strips used in these measurements was 0.020 inch, while the ground-plane spacing was 0.500 inch. The widths of the strips having 35, 50, 75, and 100 ohms characteristic impedance were 1.050, 0.663, 0.405, and 0.210 inches, respectively. Measurements carried out in the frequency band extending from 2 to 5 Gc, corresponding to values of b/λ varying from 0.085 to 0.212. It was found that the reference plane positions were almost independent of frequency for all sixteen *T*-junctions, and therefore only the values corresponding to b/λ of 0.127 are shown in Fig. 5.07-7. It is seen from an inspection of Fig. 5.07-8 that A, the equivalent transformer turns ratio squared, is sensitive to frequency and has a value approximately equal to unity for b/λ very small, and decreases considerably for larger values of b/λ. The values of the discontinuity susceptance, B_d, vary considerably from one junction to another, and in some instances are quite frequency-sensitive. It is believed that B_d is essentially capacitive in nature. Thus positive values of B_d correspond to an excess of capacitance at the junction, while negative values correspond to a deficiency.

Although the data presented in Figs. 5.07-7, 5.07-8, and 5.07-9 are for *T*-junctions with air-filled cross section and with the ratio $t/b = 0.040$, these data may be applied to other cross sections. For instance, it is expected that these data should hold for any strip-thickness ratio, t/b, up to at least 0.125 if the same characteristic impedances are maintained.

In the case of a dielectric-filled section, $\epsilon_r > 1$, the data are expected to apply with good accuracy if one divides the characteristic impedances Z_{01} and Z_{02} by $\sqrt{\epsilon_r}$ and multiples b/λ and B_d/Y_0 by $\sqrt{\epsilon_r}$.

Change in Height of a Rectangular Waveguide[8]—The equivalent circuit of the junction of two waveguides of different height but the same width, which are both operating in the TE_{10} mode can be represented as shown in

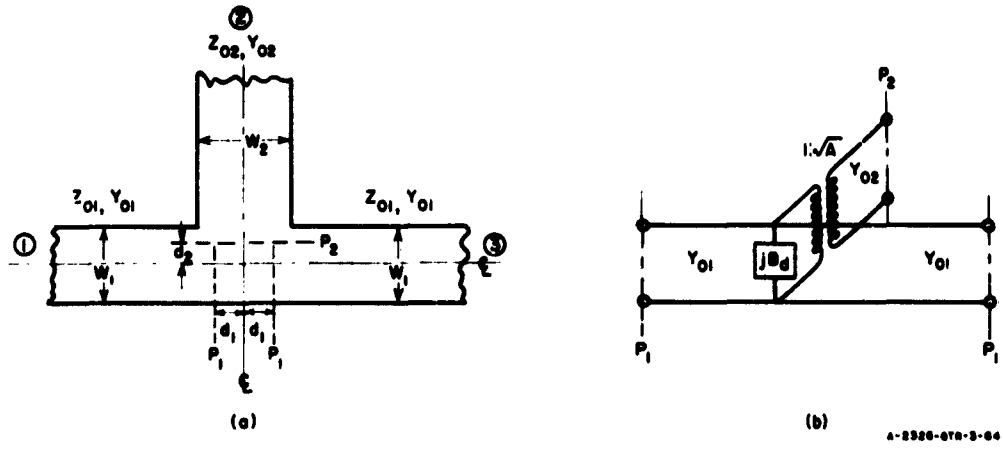

FIG. 5.07-6 EQUIVALENT CIRCUIT OF A STRIP-LINE T-JUNCTION

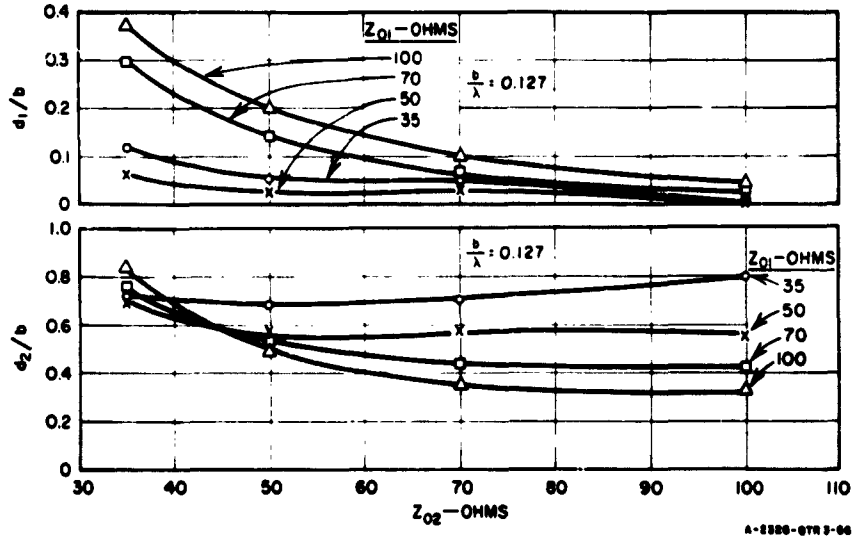

FIG. 5.07-7 REFERENCE-PLANE LOCATIONS vs. Z_{02}

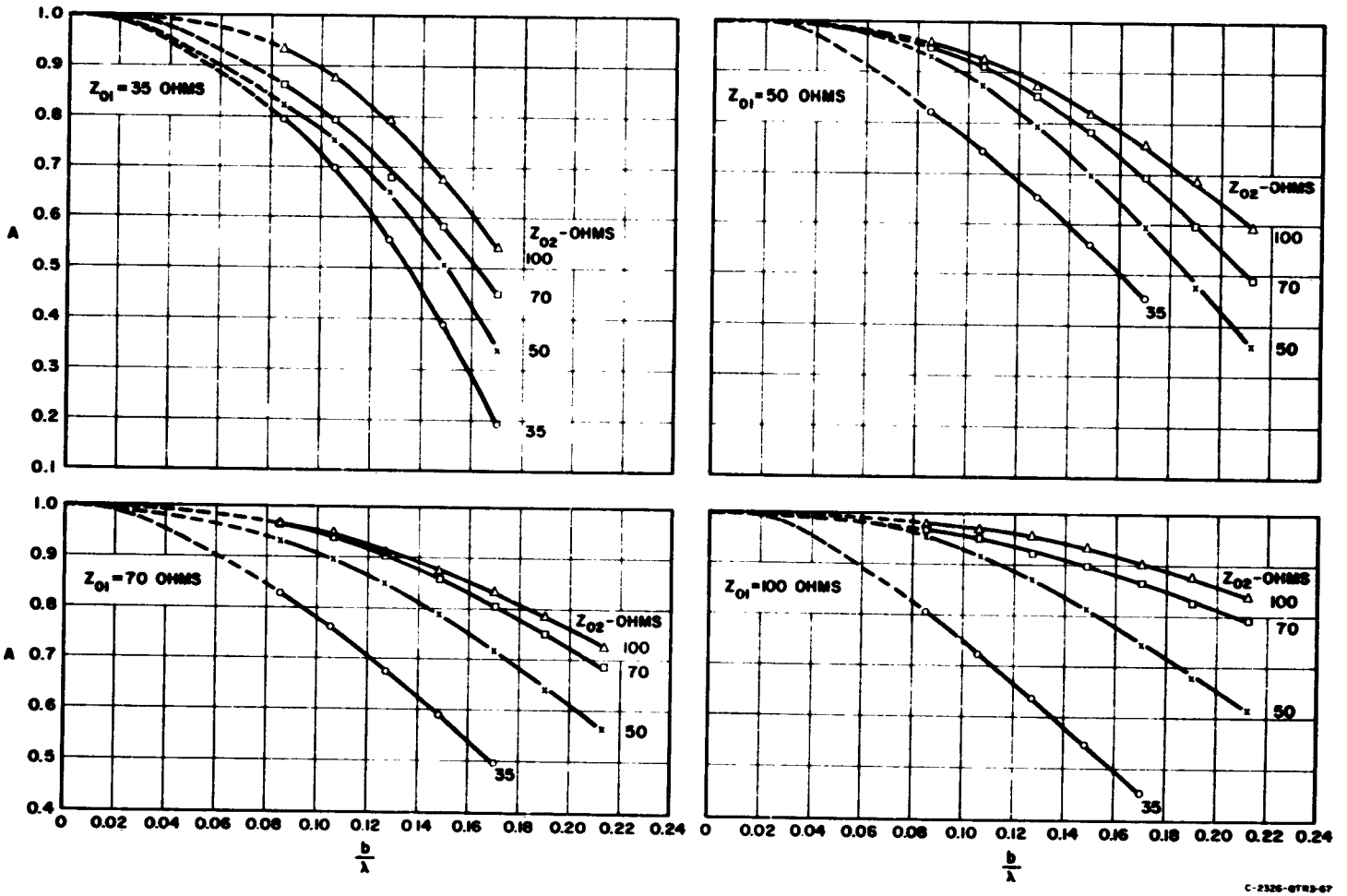

FIG. 5.07-8 MEASURED TRANSFORMER-TURNS RATIO SQUARED FOR SIXTEEN STRIP-LINE T-JUNCTIONS

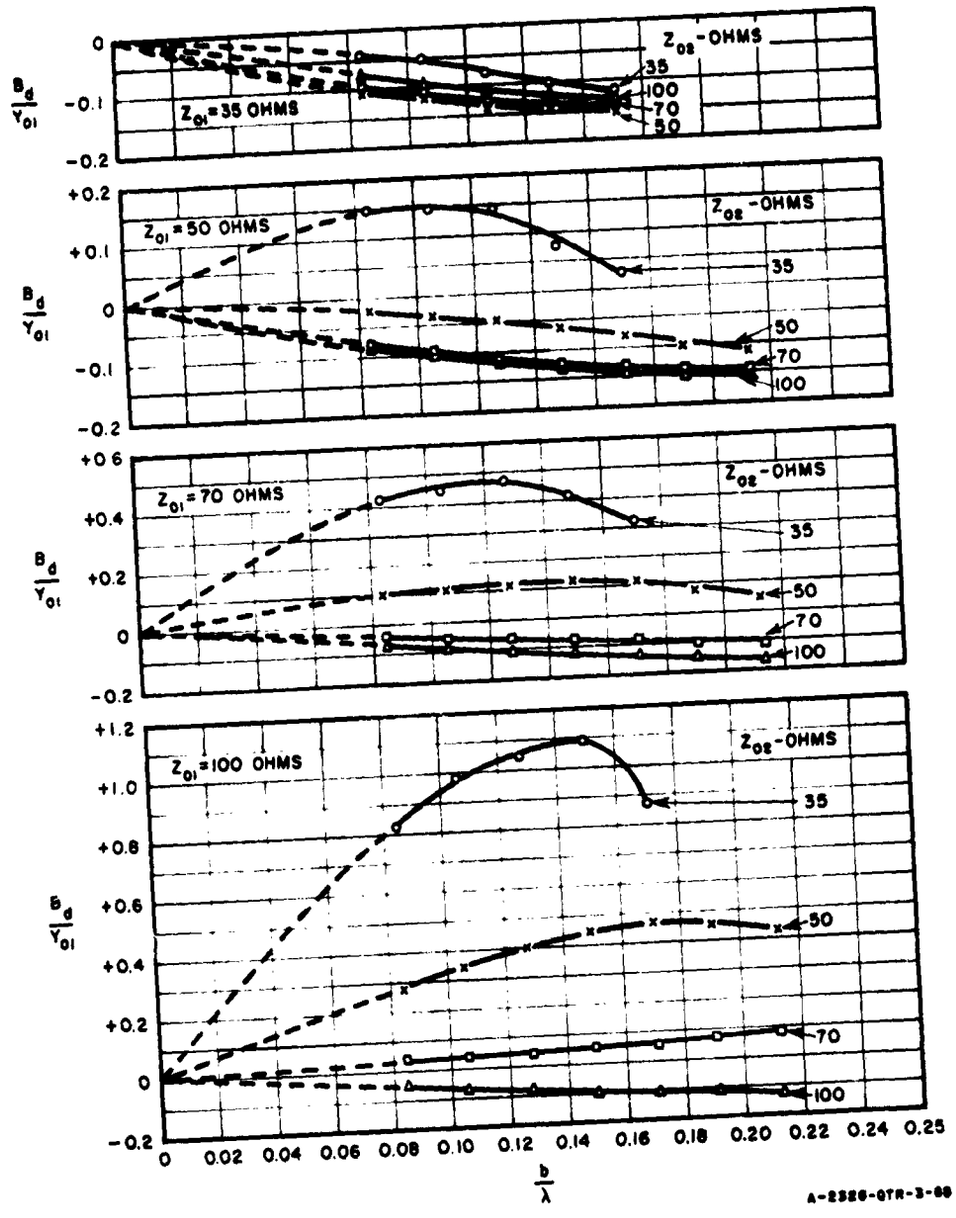

FIG. 5.07-9 MEASURED DISCONTINUITY SUSCEPTANCE OF SIXTEEN STRIP-LINE T-JUNCTIONS

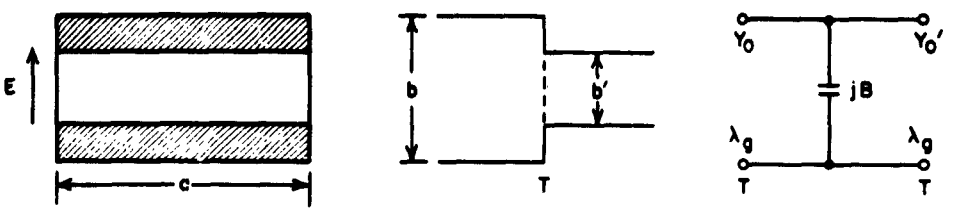

CROSS SECTIONAL VIEW | SIDE VIEW | EQUIVALENT CIRCUIT

$$\frac{Y_0}{Y_0'} = \frac{b'}{b}$$

(a) SYMMETRIC JUNCTION

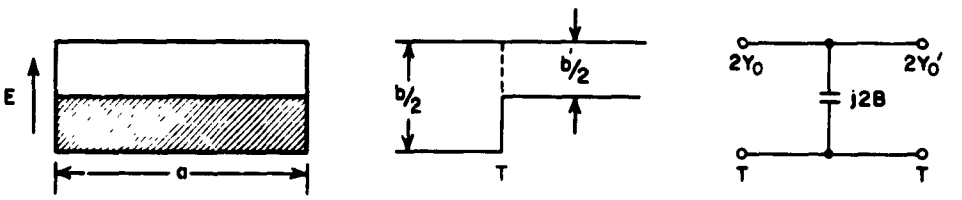

CROSS SECTIONAL VIEW | SIDE VIEW | EQUIVALENT CIRCUIT

$$\frac{Y_0}{Y_0'} = \frac{b'}{b}$$

(b) ASYMMETRIC JUNCTION

A-3827-161

SOURCE: *Waveguide Handbook* (see Ref. 8, edited by N. Marcuvitz).

FIG. 5.07-10 EQUIVALENT CIRCUIT FOR CHANGE IN HEIGHT OF RECTANGULAR WAVEGUIDE

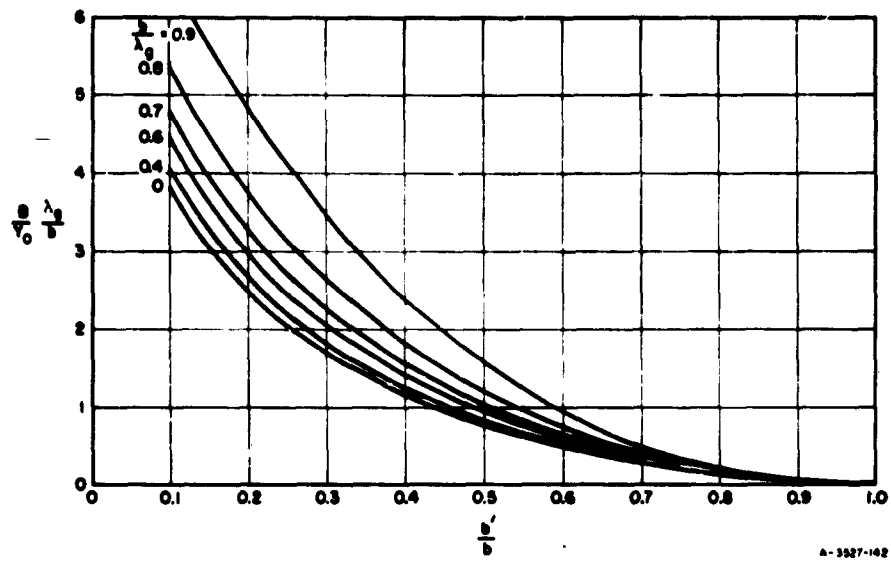

SOURCE: *Waveguide Handbook* (see Ref. 8, edited by N. Marcuvitz).

FIG. 5.07-11 SHUNT SUSCEPTANCE FOR CHANGE IN HEIGHT OF RECTANGULAR GUIDE

Fig. 5.07-10. The normalized susceptance $B\lambda_g/Y_0 b$ is plotted in Fig. 5.07-11 for various values of b/λ_g, and is accurate to about 1 percent for $b/\lambda_g \leq 1$.

SEC. 5.08, TRANSMISSION LINES AS RESONATORS

In many microwave filter designs, a length of transmission line terminated in either an open-circuit or a short-circuit is often used as a resonator. Figure 5.08-1 illustrates four resonators of this type, together with their lumped-constant equivalent circuits. It is to be noted that the resonators in Fig. 5.08-1(a) and 5.08-1(b) each have lengths which are multiples of one-half guide wavelength, and that the lumped-constant equivalent circuit of the transmission line which is short-circuited at one end is the dual of the equivalent circuit of the transmission line with an open-circuit termination. Similarly, the resonators in Fig. 5.08-1(c) and 5.08-1(d) have lengths which are odd multiples of one-quarter guide wavelength, and their lumped constant equivalent circuits are also duals of one another. The quantities α_g, λ_{g0} and λ_0 are the attenuation of the transmission line in nepers per unit length, the guide wavelength at the resonant frequency, and the plane-wave wavelength at the resonant frequency, respectively, in the dielectric medium filling the resonator.

The equivalence between the lumped constant circuits and the microwave circuits shown was established in the following fashion. The values of the resistance, R, and conductance, G, in the lumped-constant equivalent circuits were determined as the values of these quantities for the various lines at the resonance angular frequency, ω_0. The reactive elements in the lumped-constant equivalent circuits were determined by equating the slope parameters (defined below) of the lumped-element circuits to those of the transmission-line circuits which exhibited the same type of resonance. The general definition of the *reactance slope parameter* $\mathscr{x}$, which applies to circuits that exhibit a series type of resonance, is

$$\mathscr{x} = \frac{\omega_0}{2} \left.\frac{dX}{d\omega}\right|_{\omega_0} \quad \text{ohms} \qquad (5.08\text{-}1)$$

where X is the reactance portion of the input impedance to the circuit. The *susceptance slope parameter* $\mathscr{b}$, which applies to circuits that exhibit a parallel type of resonance, is

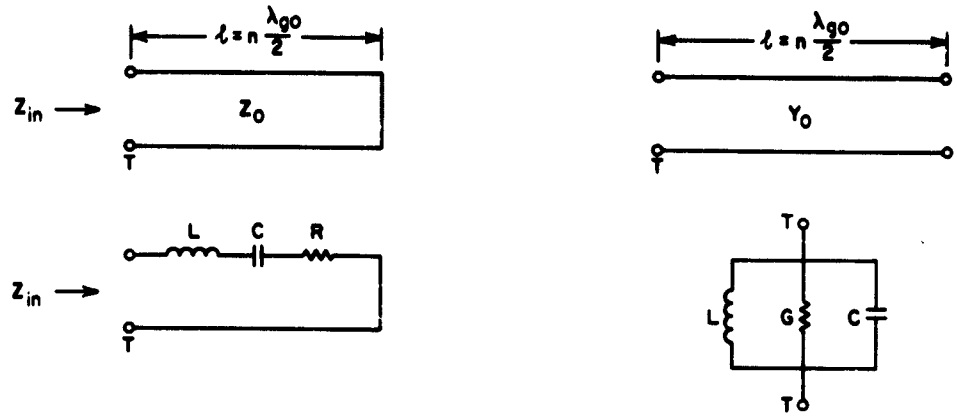

$$R = Z_0\alpha_t\ell = \frac{n}{2}Z_0\alpha_t\lambda_{g0}$$

$$x = \omega_0 L = \frac{1}{\omega_0 C} = \frac{n\pi Z_0}{2}\left(\frac{\lambda_{g0}}{\lambda_0}\right)^2$$

$$Z_{in} = R + jx\left(\frac{\omega}{\omega_0} - \frac{\omega_0}{\omega}\right)$$

$$Q = \frac{x}{R} = \frac{\pi\lambda_{g0}}{\alpha_t\lambda_0^2}$$

$$n = 1, 2, 3, \ldots$$

(a)

$$G = Y_0\alpha_t\ell = \frac{n}{2}Y_0\alpha_t\lambda_{g0}$$

$$b = \omega_0 C = \frac{1}{\omega_0 L} = \frac{n\pi Y_0}{2}\left(\frac{\lambda_{g0}}{\lambda_0}\right)^2$$

$$Y_{in} = G + jb\left(\frac{\omega}{\omega_0} - \frac{\omega_0}{\omega}\right)$$

$$Q = \frac{b}{G} = \frac{\pi\lambda_{g0}}{\alpha_t\lambda_0^2}$$

$$n = 1, 2, 3, \ldots$$

(b)

A-3827-152

FIG. 5.08-1 SOME TRANSMISSION LINE RESONATORS

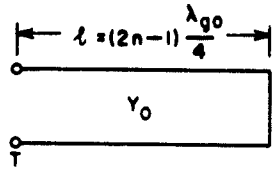

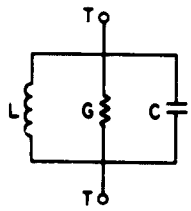

$$G = Y_0 \alpha_t \ell = \frac{(2n-1)}{4} Y_0 \alpha_t \lambda_{g0}$$

$$b = \omega_0 C = \frac{1}{\omega_0 L} = \frac{(2n-1)}{4} \pi Y_0 \left(\frac{\lambda_{g0}}{\lambda_0}\right)^2$$

$$Y_{in} = G + jb\left(\frac{\omega}{\omega_0} - \frac{\omega_0}{\omega}\right)$$

$$Q = \frac{b}{G} = \frac{\pi \lambda_{g0}}{\alpha_t \lambda_0^2}$$

$$n = 1, 2, 3, \ldots$$

(c)

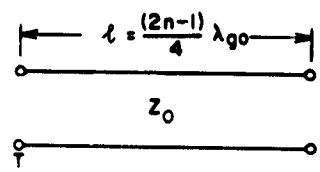

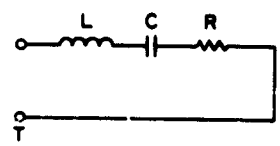

$$R = Z_0 \alpha_t \ell = \frac{(2n-1)}{4} Z_0 \alpha_t \lambda_{g0}$$

$$x = \omega_0 L = \frac{1}{\omega_0 C} = \frac{(2n-1)}{4} \pi Z_0 \left(\frac{\lambda_{g0}}{\lambda_0}\right)^2$$

$$Z_{in} = R + jx\left(\frac{\omega}{\omega_0} - \frac{\omega_0}{\omega}\right)$$

$$Q = \frac{x}{R} = \frac{\pi \lambda_{g0}}{\alpha_t \lambda_0^2}$$

$$n = 1, 2, 3, \ldots$$

(d)

A-3827-153

FIG. 5.08-1 Concluded

$$b = \frac{\omega_0}{2} \left.\frac{dB}{d\omega_0}\right|_{\omega_0} \quad \text{mhos} \qquad (5.08\text{-}2)$$

where B is the susceptance component of the input admittance of the circuit.

The above general definitions for slope parameters provide a convenient means for relating the resonance properties of any circuit to a simple lumped equivalent circuit such as those in Fig. 5.08-1. The reactance slope parameter x given by Eq. (5.08-1) is seen to be equal to $\omega_0 L = 1/(\omega_0 C)$ for the equivalent, series, lumped-element circuit, while the susceptance slope parameter b is equal to $\omega_0 C = 1/(\omega_0 L)$ for the equivalent, parallel, lumped-element circuit. Considerable use will be made of these parameters in later chapters dealing with band-pass and band-stop microwave filters.

It should be noted in Fig. 5.08-1 that the use of reactance or susceptance slope parameters also leads to convenient expressions for Q, and for the input impedance or admittance of the circuit in the vicinity of resonance. For narrow-band microwave applications, the approximate equivalence

$$\left(\frac{\omega}{\omega_0} - \frac{\omega_0}{\omega}\right) \approx 2\left(\frac{\omega - \omega_0}{\omega_0}\right) \qquad (5.08\text{-}3)$$

is often convenient for use in the expressions for input impedance or admittance.

SEC. 5.09, COUPLED-STRIP-TRANSMISSION-LINE FILTER SECTIONS

The natural electromagnetic coupling that exists between parallel transmission lines can be used to advantage in the design of filters and directional couplers.[14, 15, 16, 17, 18, 19, 20] In this section, formulas are given for filter sections constructed of parallel-coupled lines of the types illustrated in Fig. 5.05-1. Several cases involving unsymmetrical parallel-coupled lines as in Figs. 5.05-12 and 5.05-13 are also considered.

The ten coupling arrangements that can be obtained from a pair of symmetrical, coupled transmission lines by placing open- or short-circuits on various terminal pairs, or by connecting ends of the lines together,

are illustrated in Fig. 5.09-1. In this figure, schematic diagrams of single sections of each type are shown, together with their image parameters and either their open-circuit impedances or their short-circuit admittances. In addition, equivalent open-wire transmission-line circuits for eight of the coupled transmission line sections are shown beneath the corresponding schematic diagram.

In the schematic diagrams of the coupled-transmission-line sections in Fig. 5.09-1, the input and output ports are designated by small open circles. The image impedance seen looking into each of these ports is also indicated near each port. Open-circuited ports of the coupled lines are shown with no connection, while short-circuited ports are designated with the standard grounding symbol. In the equivalent transmission-line circuits shown beside the schematic diagrams, a two-wire line representation is used. In each case, the characteristic impedance or admittance of the lengths of transmission line is shown, together with the electrical length, θ. The equivalence between the parallel-coupled line sections and the non-parallel-coupled line sections shown is exact.

Figure 5.09-2 shows the same parallel-coupled sections as appear in Figs. 5.09-1(b), (c), (d), but for cases where the strip transmission lines have unsymmetrical cross sections.* The line capacitances C_a, C_{ab}, and C_b per unit length are as defined in Fig. 5.05-12. It is interesting to note that in the case of Fig. 5.09-2(a) the line capacitances per unit length for the left and right shunt stub in the equivalent open-wire representation are the same as the corresponding capacitances per unit length between Line a and ground, and Line b and ground, respectively. Meanwhile, the capacitance per unit length for the connecting line in the open-wire circuit is the same as the capacitance per unit length *between* Lines a and b of the parallel-coupled representation. In Fig. 5.09-2(b) the dual situation holds, where L_a and L_b are the self-inductances per unit length of Lines a and b in the parallel-coupled representation, while L_{ab} is the mutual inductance per unit length between the parallel-coupled lines. Since the line capacitances are more convenient to deal with, the line impedances of the equivalent open-wire circuit are also given in terms of C_a, C_{ab}, and C_b, for all three cases in Fig. 5.09-2. The quantity v indicated in Fig. 5.09-2 is the velocity of light in the medium of propagation.

* The results in Fig. 5.09-2 and also those in Figs. 5.09-3 and 5.09-4 were obtained by extension of the results in Refs. 19 and 20.

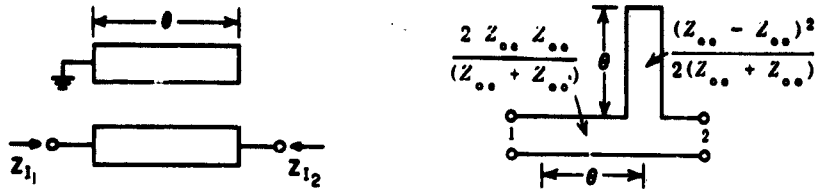

SCHEMATIC AND EQUIVALENT CIRCUIT

$$z_{11} - z_{12} = j \frac{2 Z_{oe} Z_{oo}}{Z_{oe} + Z_{oo}} \tan \frac{\theta}{2}$$

$$z_{12} = -j \frac{2 Z_{oe} Z_{oo}}{Z_{oe} + Z_{oo}} \csc \theta$$

$$z_{22} - z_{11} = j \frac{(Z_{oe} - Z_{oo})^2}{2(Z_{oe} + Z_{oo})} \tan \theta$$

TWO-PORT CIRCUIT PARAMETERS

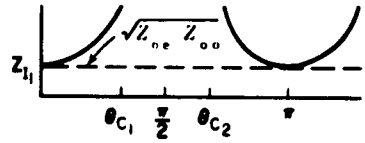

$$\cos \theta_{c_1} = -\cos \theta_{c_2} = \left[\frac{\frac{Z_{oe}}{Z_{oo}} - 1}{\frac{Z_{oe}}{Z_{oo}} + 1} \right]$$

$$\cosh (\alpha + j\beta) = \frac{[(Z_{oe} + Z_{oo})^2 \cos^2 \theta - (Z_{oe} - Z_{oo})^2]^{1/2}}{2\sqrt{Z_{oe} Z_{oo}}}$$

$$Z_{I_2} = \frac{Z_{oe} Z_{oo}}{Z_{I_1}} \quad , \quad Z_{I_1} = \frac{2 Z_{oe} Z_{oo} \cos \theta}{[-(Z_{oe} - Z_{oo})^2 + (Z_{oe} + Z_{oo})^2 \cos^2 \theta]^{1/2}}$$

IMAGE PARAMETERS

(a) LOW PASS

A-3527-A162

SOURCE: Adapted from figures in Final Report, Contract DA 36-039 SC-64625, SRI; which were reprinted in *IRE Trans. PGMTT* (see Ref. 19 by E. M. T. Jones and J. T. Bolljahn).

FIG. 5.09-1 SOME PARALLEL-COUPLED TRANSMISSION-LINE FILTER SECTIONS

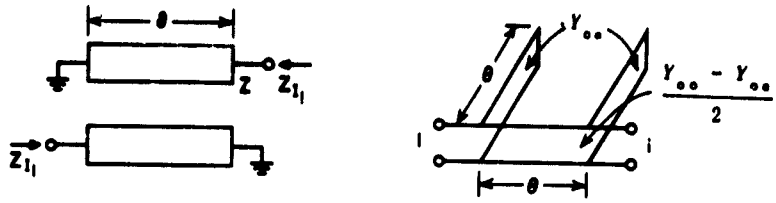

SCHEMATIC AND EQUIVALENT CIRCUIT

$$y_{11} = -j \frac{(Y_{oo} + Y_{oo})}{2} \cot \theta$$

$$y_{12} = -j \frac{(Y_{oo} - Y_{oo})}{2} \csc \theta$$

TWO-PORT CIRCUIT PARAMETERS

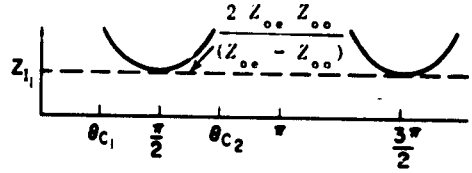

$$\cosh (\alpha + j\beta) = \left[\frac{\frac{Z_{oe}}{Z_{oo}} + 1}{\frac{Z_{oe}}{Z_{oo}} - 1} \right] \cos \theta$$

$$\cos \theta_{c_1} = -\cos \theta_{c_2} = \left[\frac{\frac{Z_{oe}}{Z_{oo}} - 1}{\frac{Z_{oe}}{Z_{oo}} + 1} \right]$$

$$Z_{I_1} = \frac{2 Z_{oe} Z_{oo} \sin \theta}{[(Z_{oe} - Z_{oo})^2 - (Z_{oe} + Z_{oo})^2 \cos^2 \theta]^{1/2}}$$

IMAGE PARAMETERS

(b) BAND PASS

A-3527-8162

FIG. 5.09-1 Continued

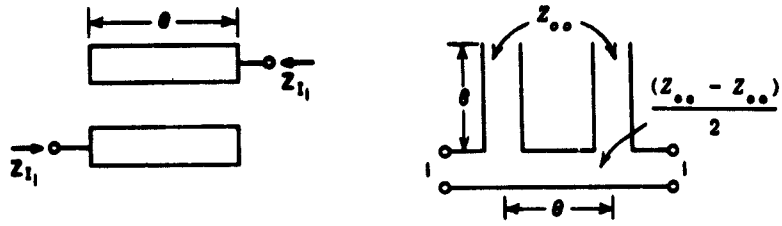

SCHEMATIC AND EQUIVALENT CIRCUIT

$$z_{11} = -j \frac{(Z_{oe} + Z_{oo})}{2} \cot \theta$$

$$z_{12} = -j \frac{(Z_{oe} - Z_{oo})}{2} \csc \theta$$

TWO-PORT CIRCUIT PARAMETERS

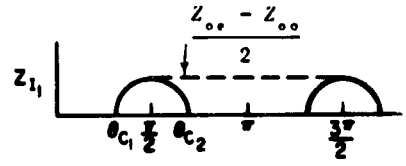

$$\cos \theta_{c_1} = -\cos \theta_{c_2} = \left[\frac{\frac{Z_{oe}}{Z_{oo}} - 1}{\frac{Z_{oe}}{Z_{oo}} + 1}\right]$$

$$Z_{I_1} = \frac{[(Z_{oe} - Z_{oo})^2 - (Z_{oe} + Z_{oo})^2 \cos^2 \theta]^{1/2}}{2 \sin \theta}$$

$$\cosh (\alpha + j\beta) = \left[\frac{\frac{Z_{oe}}{Z_{oo}} + 1}{\frac{Z_{oe}}{Z_{oo}} - 1}\right] \cos \theta$$

IMAGE PARAMETERS

(c) BAND PASS

A-3527-C162

FIG. 5.09-1 Continued

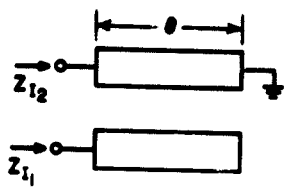

SCHEMATIC

$$z_{11} = -j\,(Z_{oe} + Z_{oo})\,\frac{\cot\theta}{2} + j\,\frac{(Z_{oe} - Z_{oo})^2}{Z_{oe} + Z_{oo}}\,\csc 2\theta$$

$$z_{12} = j\,(Z_{oe} - Z_{oo})\,\frac{\tan\theta}{2}$$

$$z_{22} = j\,(Z_{oe} + Z_{oo})\,\frac{\tan\theta}{2}$$

TWO-PORT CIRCUIT PARAMETERS

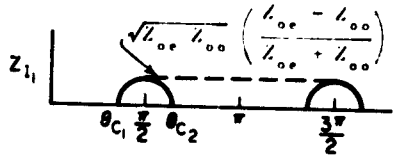

$$\cos\theta_{c_1} = -\cos\theta_{c_2} = \left[\frac{\frac{Z_{oe}}{Z_{oo}} - 1}{\frac{Z_{oe}}{Z_{oo}} + 1}\right]$$

$$Z_{I_1} = \frac{\sqrt{Z_{oe}\,Z_{oo}}\,[(Z_{oe} - Z_{oo})^2 - (Z_{oe} + Z_{oo})^2\cos^2\theta]^{1/2}}{\sin\theta\,(Z_{oe} + Z_{oo})}$$

$$Z_{I_2} = \frac{Z_{oe}\,Z_{oo}}{Z_{I_1}}$$

$$\cosh(\alpha + j\beta) = \frac{1}{\sin\theta}\left[1 - \left(\frac{Z_{oe} + Z_{oo}}{Z_{oe} - Z_{oo}}\right)^2\cos^2\theta\right]^{1/2}$$

IMAGE PARAMETERS

(d) BAND PASS

A-3527-0162

FIG. 5.09-1 Continued

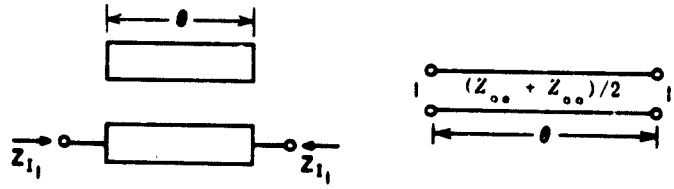

SCHEMATIC AND EQUIVALENT CIRCUIT

$$z_{11} - z_{12} = j \frac{(Z_{oe} + Z_{oo})}{2} \tan \frac{\theta}{2} \qquad z_{12} = -j \frac{(Z_{oe} + Z_{oo})}{2} \csc \theta$$

TWO-PORT CIRCUIT PARAMETERS

$$Z_{I_1} = \frac{Z_{oe} + Z_{oo}}{2} \qquad \theta = \theta$$

IMAGE PARAMETERS

(e) ALL PASS

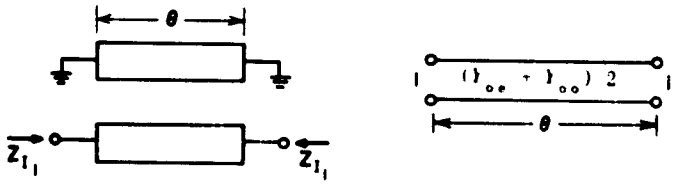

SCHEMATIC AND EQUIVALENT CIRCUIT

$$y_{11} - y_{12} = j \frac{(Y_{oe} + Y_{oo})}{2} \tan \frac{\theta}{2} \qquad y_{12} = -j \frac{(Y_{oe} + Y_{oo})}{2} \csc \theta$$

TWO-PORT CIRCUIT PARAMETERS

$$Z_{I_1} = \frac{2 Z_{oe} Z_{oo}}{Z_{oe} + Z_{oo}} \qquad \theta = \theta$$

IMAGE PARAMETERS

(f) ALL PASS

A-3527-E162

FIG. 5.09-1 Continued

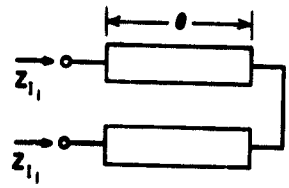

SCHEMATIC

$$z_{11} - z_{12} = j\sqrt{Z_{oe} Z_{oo}} \tan\left[\frac{Z_{oe} Z_{oo}}{Z_{oe} \cot\theta - Z_{oo} \tan\theta}\right]$$

$$z_{12} = -j\sqrt{Z_{oe} Z_{oo}} \csc\left[\frac{2 Z_{oe} Z_{oo}}{Z_{oe} \cot\theta - Z_{oo} \tan\theta}\right]$$

TWO-PORT CIRCUIT PARAMETERS

$$\cos\beta = \frac{\frac{Z_{oe}}{Z_{oo}} - \tan^2\theta}{\frac{Z_{oe}}{Z_{oo}} + \tan^2\theta}, \quad \tan\beta = \frac{2 Z_{oe} Z_{oo}}{(Z_{oe} \cot\theta - Z_{oo} \tan\theta)} \quad Z_{I_1} = \sqrt{Z_{oe} Z_{oo}}$$

IMAGE PARAMETERS

(g) ALL PASS

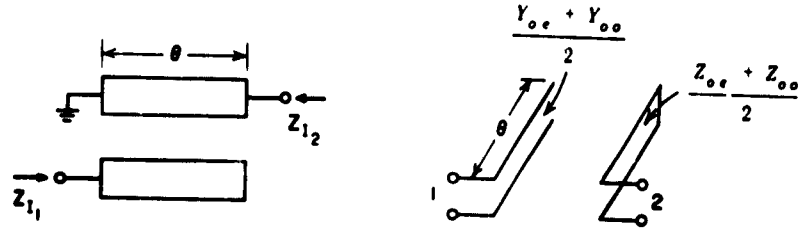

SCHEMATIC AND EQUIVALENT CIRCUIT

$$y_{11} = j\frac{(Y_{oo} + Y_{oe})}{2}\tan\theta \qquad z_{22} = j\frac{(Z_{oe} + Z_{oo})}{2}\tan\theta \qquad z_{12} = y_{12} = 0$$

TWO-PORT CIRCUIT PARAMETERS

$$Z_{I_1} = -j\frac{2 Z_{oo} Z_{oe}}{Z_{oo} + Z_{oe}}\cot\theta \qquad Z_{I_2} = \frac{Z_{oe} Z_{oo}}{Z_{I_1}} \qquad \alpha = \alpha$$

IMAGE PARAMETERS

(h) ALL STOP

A-3527-F162

FIG. 5.09-1 Continued

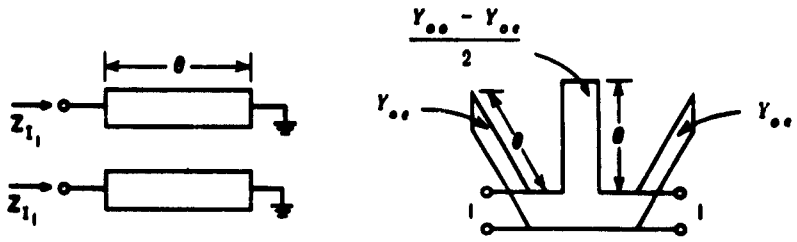

SCHEMATIC AND EQUIVALENT CIRCUIT

$$y_{11} - y_{12} = -j\, Y_{oo} \cot \theta \qquad y_{12} = -j\, \frac{(Y_{oo} - Y_{oe})}{2} \cot \theta$$

TWO-PORT CIRCUIT PARAMETERS

$$\cosh \alpha = \frac{Z_{oo} + Z_{oe}}{Z_{oo} - Z_{oe}} \qquad Z_{I_1} = j\sqrt{Z_{oo}\, Z_{oe}} \tan \theta$$

IMAGE PARAMETERS

(i) ALL STOP

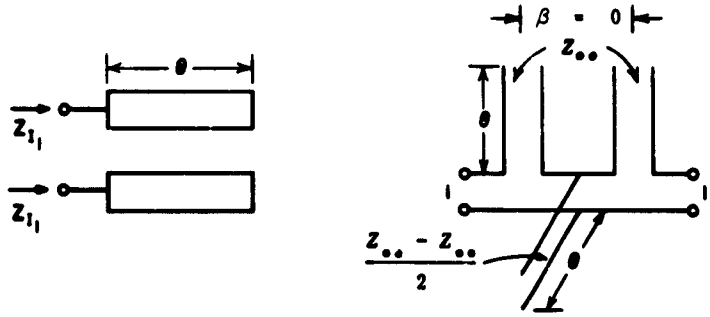

SCHEMATIC AND EQUIVALENT CIRCUIT

$$z_{11} - z_{12} = -j\, Z_{oo} \cot \theta \qquad z_{12} = -j\, \frac{(Z_{oo} - Z_{oe})}{2} \cot \theta$$

TWO-PORT CIRCUIT PARAMETERS

$$Z_{I_1} = -j\sqrt{Z_{oo}\, Z_{oe}} \cot \theta \qquad \cosh \alpha = \frac{Z_{oo} + Z_{oe}}{Z_{oo} - Z_{oe}}$$

IMAGE PARAMETERS

(j) ALL STOP

A-3527-6162

FIG. 5.09-1 Concluded

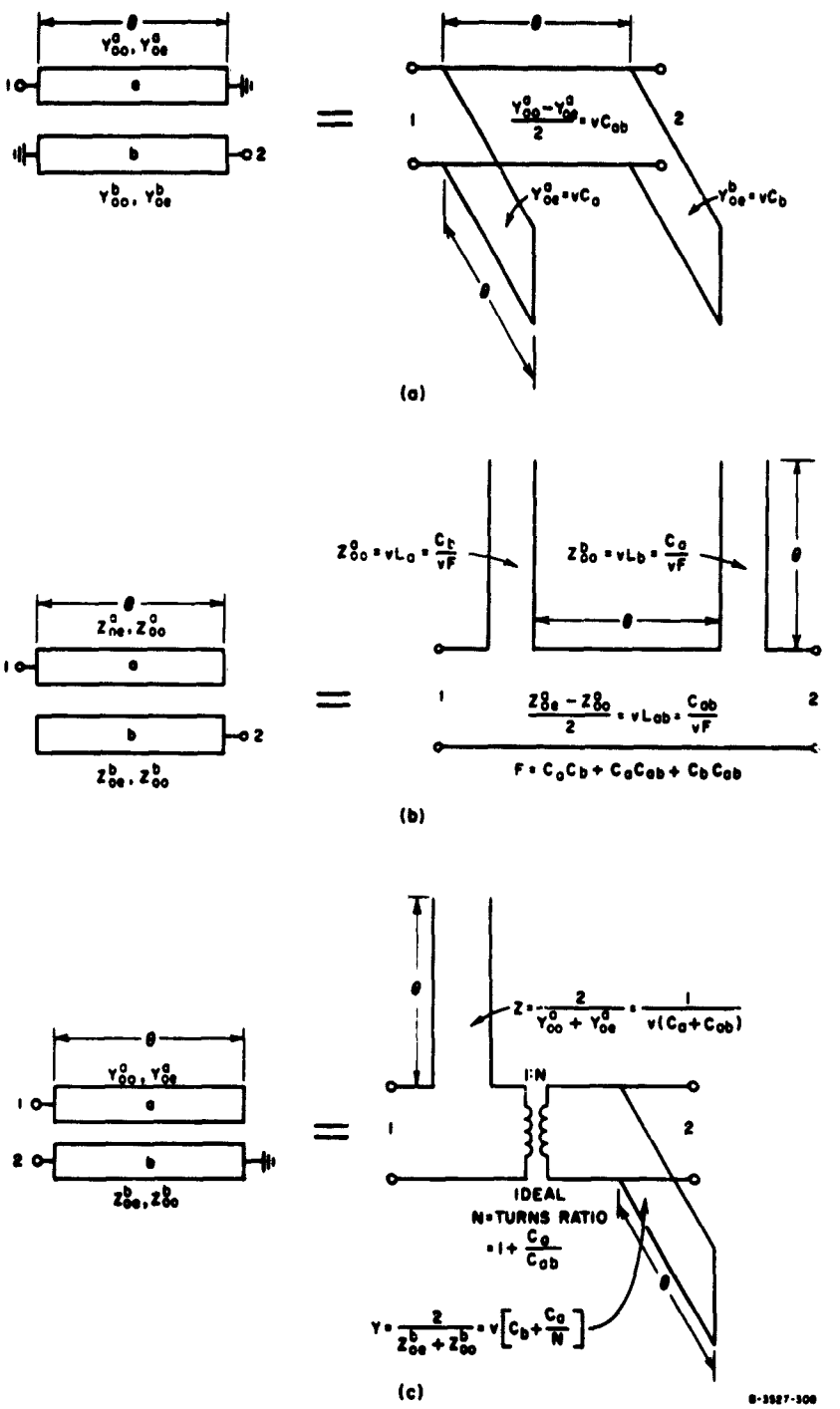

FIG. 5.09-2 SOME USEFUL UNSYMMETRICAL PARALLEL-COUPLED STRIP-LINE SECTIONS AND THEIR EQUIVALENT OPEN-WIRE LINE SECTIONS
Parameters C_a, C_{ab}, and C_b are line capacitances per unit length as defined in Fig. 5.05-12. v = velocity of propagation. All lines are of the same length.

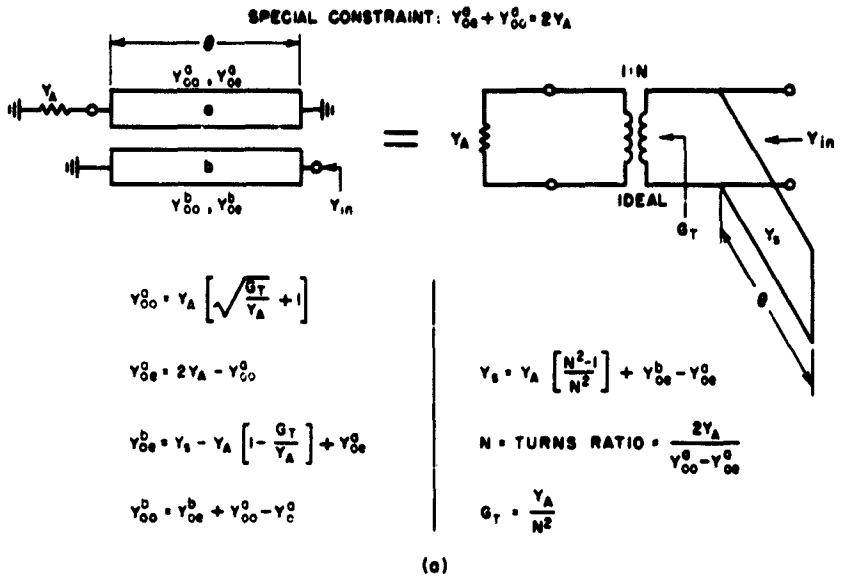

FIG. 5.09-3 SOME PARALLEL-COUPLED STRIP-LINE AND OPEN-WIRE-LINE EQUIVALENCES WHICH APPLY UNDER SPECIAL CONSTRAINTS

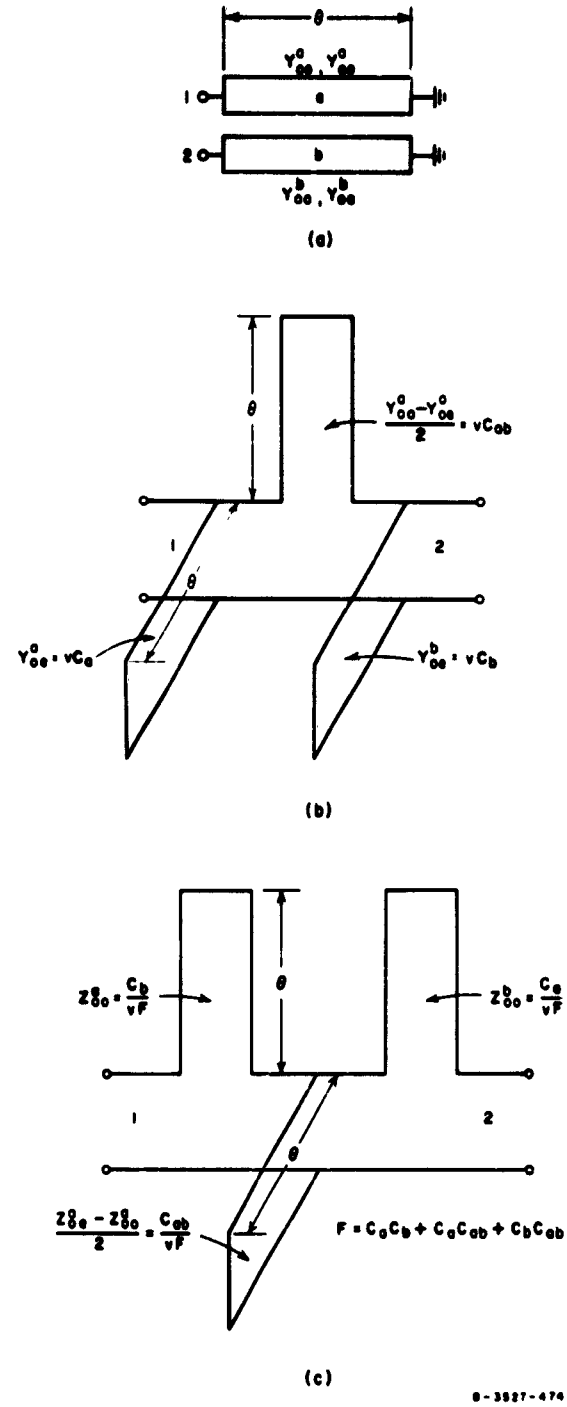

FIG. 5.09-4 A PARALLEL-COUPLED SECTION AND TWO OPEN-WIRE-LINE CIRCUITS WHICH ARE EXACTLY EQUIVALENT
The C_a, C_{ab}, and C_b are as indicated in Fig. 5.05-12.

In the cases of the circuits in Figs. 5.09-2(a), and (b), if the parallel-coupled sections are properly terminated, their equivalent open-wire line circuit simplifies in a very interesting and useful way. This is illustrated in Fig. 5.09-3(a) and (b). Note that when the indicated constraints are applied, the equivalent open-wire circuit reduces to simply an ideal transformer and a single stub. In spite of the constraint equations which are enforced in these circuits, there are still sufficient degrees of freedom so that for specified Y_s and G_T or Z_s and R_T, a wide range of Y_A or Z_A, respectively, can be accommodated. For this reason these two structures will prove quite useful for use with certain types of band-pass filters for the purpose of effectively realizing a series- or shunt-stub resonator, along with obtaining an impedance transformation which will accommodate some desired terminating impedance. In a somewhat more complex way, the circuit in Fig. 5.09-2(c) will also prove useful for similar purposes.

Figure 5.09-4 shows the parallel-coupled section in Fig. 5.09-1(i) generalized to cover the case where the two strip lines may be of different widths. At (a) is shown the structure under consideration, while at (b) and (c) are shown two open-wire line structures which are identically equivalent electrically to the strip-line structure at (a). As previously indicated, parallel-coupled structures of this sort are all-stop structures as they stand, but when properly used with lumped capacitances, they become the basis for the comb-line form of filter discussed in Sec. 8.13.

SEC. 5.10, IRIS-COUPLED WAVEGUIDE JUNCTIONS

Bethe[21, 22, 23, 24] has developed a general perturbation technique for calculating the scattering of power by small irises connecting one transmission line with another. The theory is applicable even though the two transmission lines have different cross sections and operate in different modes; however, it applies rigorously only to infinitesimally thin irises whose dimensions are small in terms of the operating wavelength. These irises should be located far from any corners, in a transmission-line wall whose radius of curvature is large in terms of wavelength. In practice it is found that the theory holds reasonably well even when the irises are located relatively close to sharp corners in transmission-line walls of fairly small radii of curvature. For irises of finite thickness, it is found that Bethe's theory is still applicable except that the

transmission through the iris is reduced.[25] In many instances it is possible to use Cohn's frequency correction[25] where the iris dimensions are not negligibly small with respect to a wavelength.

Bethe's original derivations[21, 22, 23] appeared in a series of MIT Radiation Laboratory Reports, copies of which are quite difficult to obtain. Recently Collin[26] has derived some of Bethe's results using a different approach, and these results are readily available. Marcuvitz[27] recast much of Bethe's work and derived many equivalent circuits for iris-coupled transmission lines, many of which are presented in the *Waveguide Handbook*.[8] A paper by Oliner[28] contains some additional circuits for iris-coupled lines.

Bethe's calculation of the scattering of power by small irises actually consists of two distinct steps. The first step is the computation of the electric dipole moment, $\bar{p}$, and the magnetic dipole moment, $\bar{m}$, induced in the iris by the exciting fields. The next step is the calculation of the fields radiated by the electric and magnetic dipole moments.

Figure 5.10-1 illustrates two parallel-plane transmission lines connected by a small iris. The electric field, E_{on}, in the bottom line will couple through the iris in the manner shown in Fig. 5.10-1(a). To a first-order approximation, the distorted field within the iris can be considered to arise from two electric dipole moments, each of strength $\bar{p}$, induced in the iris by the exciting electric field E_{on} as shown in Fig. 5.10-1(b). The electric dipole moment in the upper line is parallel to E_{on}, while the electric dipole moment in the lower line is oppositely directed.

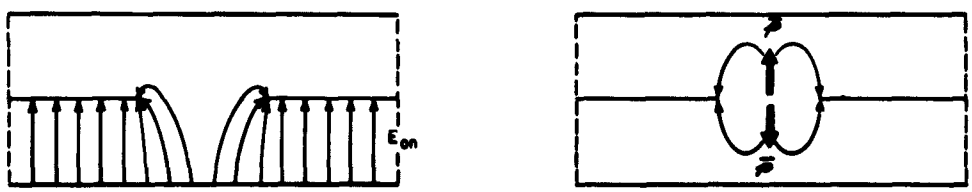

FIG. 5.10-1 ELECTRIC DIPOLE MOMENTS INDUCED IN AN IRIS BY AN ELECTRIC FIELD NORMAL TO THE PLANE OF THE IRIS

Figure 5.10-2 illustrates the magnetic field coupling through an iris connecting two parallel-plane transmission lines. Again the distorted magnetic field within the iris can be considered to arise from two magnetic dipole moments each of strength $\bar{m}$, induced in the iris by the exciting tangential magnetic field, H_{ot}. The magnetic dipole moment in the upper line is directed anti-parallel to H_{ot}, while that in the lower line is oppositely directed and parallel to H_{ot}.

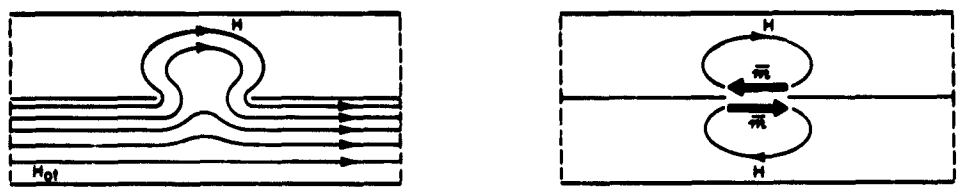

(a) (b) A-3627-112

FIG. 5.10-2 MAGNETIC DIPOLE MOMENTS INDUCED IN AN IRIS BY A MAGNETIC FIELD TANGENTIAL TO THE PLANE OF THE IRIS

The strength of the electric dipole moment, $\bar{p}$, is proportional to the product of the electric polarizability P of the iris and the exciting field, E_{on}. Its value in mks units is

$$\bar{p} = \epsilon_0 P E_{on} \bar{n} \qquad (5.10\text{-}1)$$

where $\epsilon_0 = 8.854 \times 10^{-12}$ farads meter, and $\bar{n}$ is a unit vector directed away from the iris on the side opposite from the exciting field.

The strength of the magnetic dipole moment is proportional to the product of the magnetic polarizability, M, of the iris and exciting tangential magnetic field H_{ot}. For the usual type of iris that has axes of symmetry, the magnetic dipole moment is, in mks units,

$$-\bar{m} = M_1 H_{ou} \bar{u} + M_2 H_{ov} \bar{v} \quad . \qquad (5.10\text{-}2)$$

In this expression the unit vectors $\bar{u}$ and $\bar{v}$ lie in the plane of the iris along the axes of symmetry, M_1 and M_2 are the magnetic polarizabilities,

and H_{eu} and H_{ev} the exciting magnetic fields along the $\bar{u}$ and $\bar{v}$ axes, respectively.

The electric dipole moment, $\bar{p}$, set up in an iris by an exciting electric field, will radiate power into a given mode in the secondary waveguide only when the electric field of the mode to be excited has a component parallel to the dipole moment, $\bar{p}$. Similarly the magnetic dipole moment $\bar{m}$ set up in the aperture by an exciting magnetic field will radiate power into a given mode in the secondary waveguide only when the magnetic field of the mode to be excited has a component parallel to the magnetic dipole moment $\bar{m}$.

In order to be able to apply Bethe's theory, it is necessary to know the electric polarizability P and the magnetic polarizabilities M_1 and M_2 of the iris. Theoretical values of the polarizabilities can only be obtained for irises of simple shapes. For example, a *circular iris* of diameter d has a value of $M_1 = M_2 = d^3/6$ and $P = d^3/12$. A long, narrow iris of length l and width w has $P = M_2 = (\pi/16)\ lw^2$, if the exciting magnetic field is parallel to the narrow dimension of the slit (the $\bar{v}$ direction in this case), and the exciting electric field is perpendicular to the plane of the slit. The polarizabilities of elliptical irises have also been computed. In addition, the polarizabilities of irises of other shapes that are too difficult to calculate have been measured by Cohn[29, 30] in an electrolytic tank. The measured values of the polarizability of a number of irises are shown in Figs. 5.10-3 and 5.10-4(a),(b), together with the theoretical values for elliptical irises. Circular irises are the easiest to machine, but sometimes elongated irises are required in order to obtain adequate coupling between rectangular waveguides.

For many applications the equivalent-circuit representation of iris-coupled transmission lines is more convenient than the scattering representation. Figures 5.10-5 to 5.10-12 contain the equivalent-circuit representations of several two- and three-port waveguide junctions coupled by infinitesimally thin irises. Most of the information in the figures is self-explanatory. It is to be noted that in each case the reference planes for the equivalent circuits are at the center of gravity of the iris. The symbol K used in some circuits stands for an impedance inverter as defined in Sec. 4.12. Also included in each figure is the power transmission coefficient through the iris, expressed as the square of the magnitude of the scattering coefficient. (Sec. 2.12).

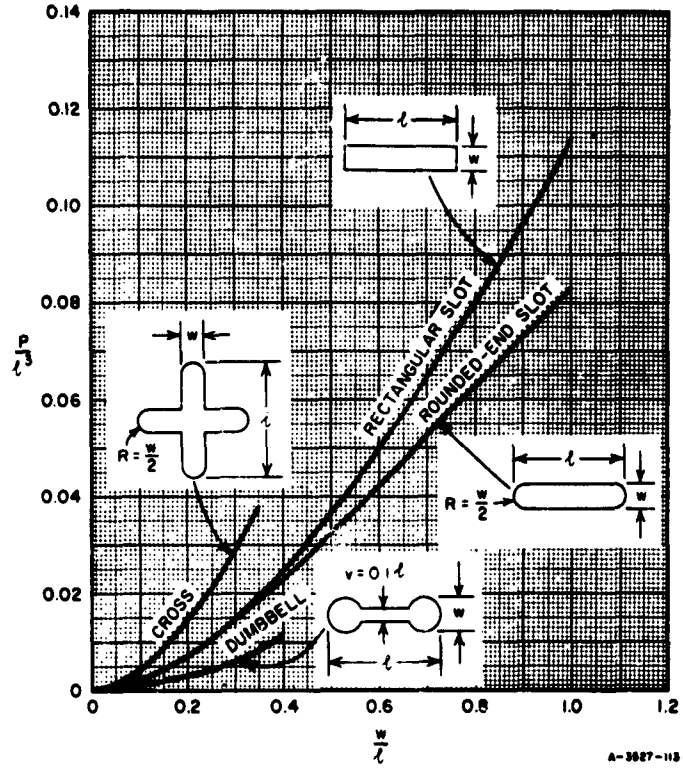

SOURCE: *Proc. IRE* (see Ref. 30, by S. B. Cohn).

FIG. 5.10-3 MEASURED ELECTRIC POLARIZABILITIES OF RECTANGULAR, ROUNDED, CROSS- AND DUMBBELL-SHAPED SLOTS

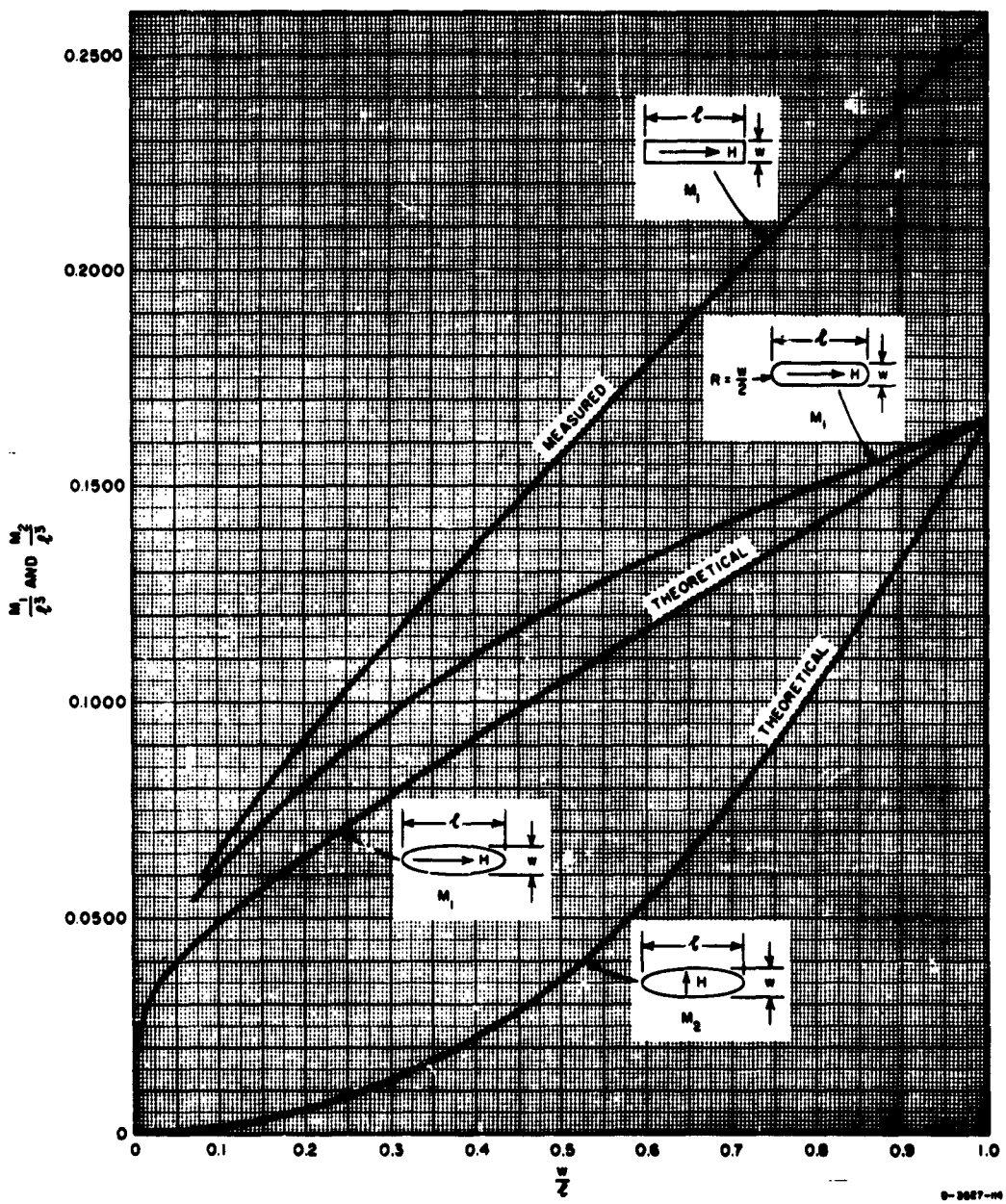

SOURCE: *Proc. IRE* (see Ref. 29, by S. B. Cohn).

FIG. 5.10-4(a) MAGNETIC POLARIZABILITIES OF RECTANGULAR, ROUNDED-END, AND ELLIPTICAL SLOTS

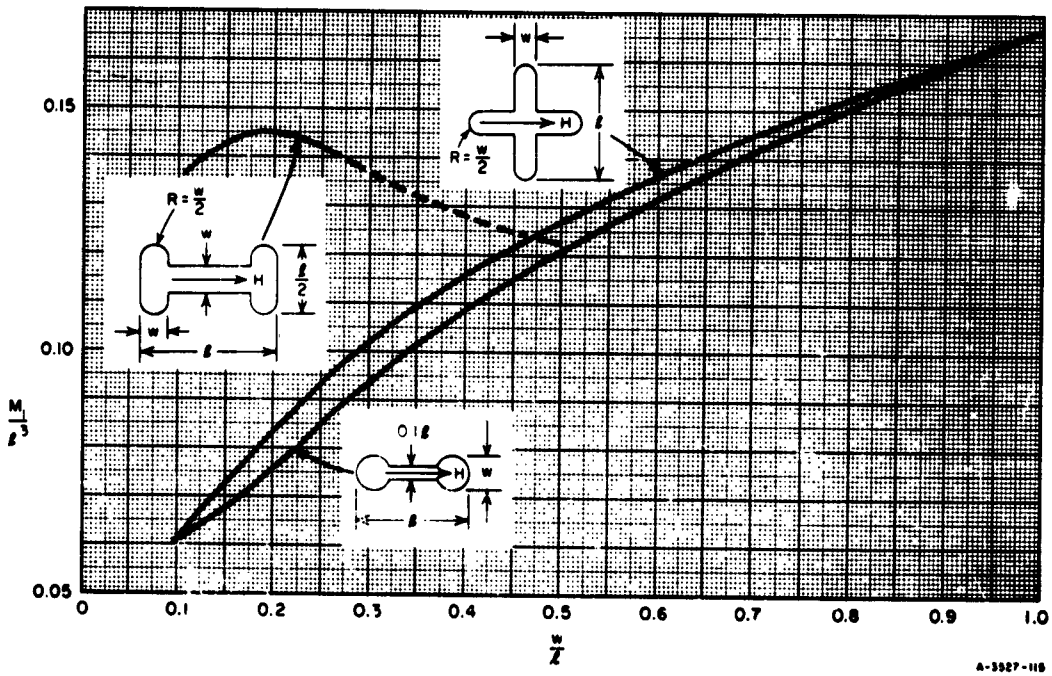

SOURCE: Proc. *IRE* (see Ref. 29, by S. B. Cohn).

FIG. 5.10-4(b) MAGNETIC POLARIZABILITIES OF H-, CROSS-, AND DUMBBELL-SHAPED APERTURES

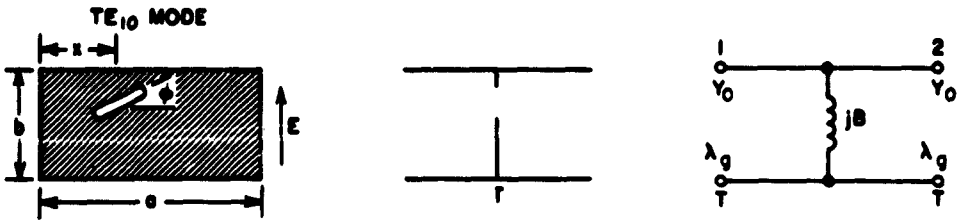

$$\frac{B}{Y_0} = -\frac{ab\lambda_g}{4\pi M \sin^2 \frac{\pi x}{a}} \qquad M = M_1 \cos^2 \phi + M_2 \sin^2 \phi \qquad \lambda_g = \frac{\lambda}{\sqrt{1 - \left(\frac{\lambda}{2a}\right)^2}}$$

$$|S_{12}|^2 = \frac{4Y_0^2}{|B|^2} = \frac{64\pi^2 M^2 \sin^4 \frac{\pi x}{a}}{a^2 b^2 \lambda_g^2}$$

A-3527-144

Adapted from the *Waveguide Handbook* (see Ref. 8 edited by N. Marcuvitz)

FIG. 5.10-5 IRIS CONNECTING RECTANGULAR WAVEGUIDES OF THE SAME CROSS SECTION

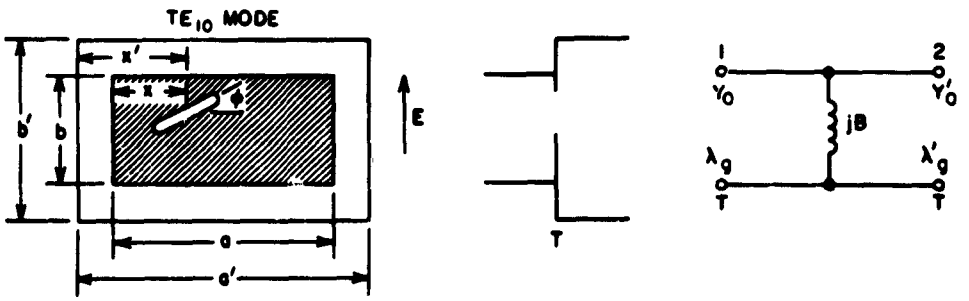

$$|S_{12}|^2 = \frac{4Y_0^2}{|B|^2} \cdot \frac{Y_0'}{Y_0} \sqrt{\frac{64\pi^2 M^2 \sin^2 \frac{\pi x'}{a} \sin^2 \frac{\pi x}{a}}{aa'bb'\lambda_g \lambda_g'}}$$

$$\lambda_g = \frac{\lambda}{\sqrt{1 - \left(\frac{\lambda}{2a}\right)^2}} \qquad M = M_1 \cos^2 \phi + M_2 \sin^2 \phi \qquad \lambda_g' = \frac{\lambda}{\sqrt{1 - \left(\frac{\lambda}{2a'}\right)^2}}$$

$$\frac{Y_0'}{Y_0} = \frac{\lambda_g ab}{\lambda_g' a' b'} \frac{\sin^2 \frac{\pi x'}{a'}}{\sin^2 \frac{\pi x}{a}} \qquad \frac{B}{Y_0} = -\frac{ab\lambda_g}{4\pi M \sin^2 \frac{\pi x}{a}}$$

A-3527-145

Adapted from the *Waveguide Handbook* (see Ref. 8 edited by N. Marcuvitz)

FIG. 5.10-6 IRIS CONNECTING RECTANGULAR WAVEGUIDES OF DIFFERENT CROSS SECTIONS

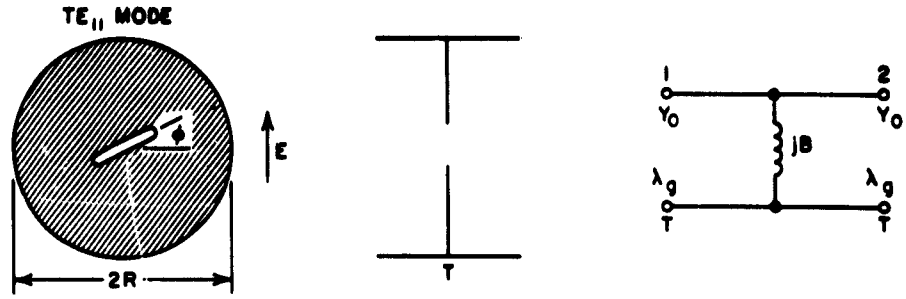

CROSS SECTIONAL VIEW SIDE VIEW EQUIVALENT CIRCUIT

$$|S_{12}|^2 = \frac{4Y_0^2}{|B|^2} = \frac{64\pi^2M^2}{9R^4\lambda_g^2}$$

$$\lambda_g = \frac{\lambda}{\sqrt{1-\left(\frac{\lambda}{3.41R}\right)^2}}$$

$$M = M_1\cos^2\phi + M_2\sin^2\phi$$

$$\frac{B}{Y_0} = -\frac{0.955(\pi R^2)\lambda_g}{4\pi M}$$

Adapted from the *Waveguide Handbook* (see Ref. 8 edited by N. Marcuvitz) A-3827-146

FIG. 5.10-7 IRIS CONNECTING CIRCULAR WAVEGUIDES OF THE SAME RADIUS

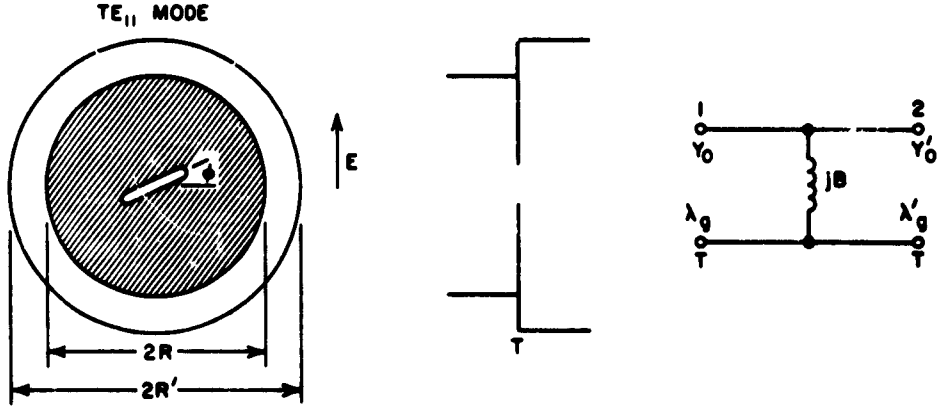

CROSS SECTIONAL VIEW SIDE VIEW EQUIVALENT CIRCUIT

$$\lambda_g' = \frac{\lambda}{\sqrt{1-\left(\frac{\lambda}{3.41R'}\right)^2}}$$

$$\frac{Y_0'}{Y_0} = \frac{R^2\lambda_g}{R'^2\lambda_g'}$$

$$\frac{B}{Y_0} = -\frac{0.955(\pi R^2)\lambda_g}{4\pi M}$$

$$\lambda_g = \frac{\lambda}{\sqrt{1-\left(\frac{\lambda}{3.41R}\right)^2}}$$

$$|S_{12}|^2 = \frac{4Y_0^2}{|B|^2}\cdot\frac{Y_0'}{Y_0} = \frac{64\pi^2M^2}{9R^2R'^2\lambda_g\lambda_g'}$$

$$M = M_1\cos^2\phi + M_2\sin^2\phi$$

A-3827-145

Adapted from the *Waveguide Handbook* (see Ref. 8 edited by N. Marcuvitz)

FIG. 5.10-8 IRIS CONNECTING CIRCULAR WAVEGUIDES OF DIFFERENT RADII

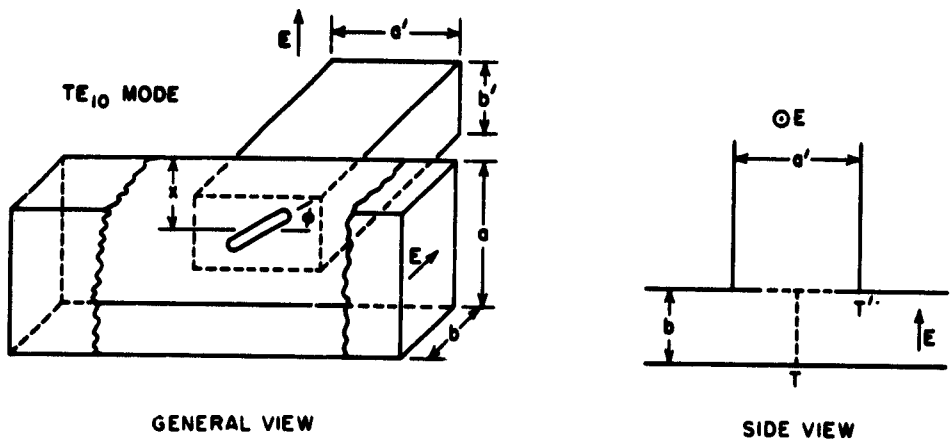

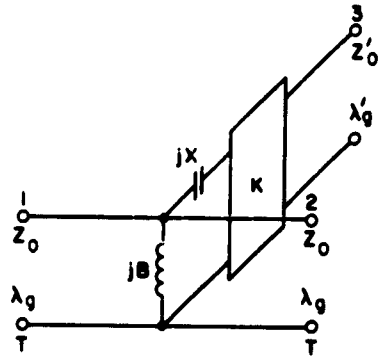

$$|S_{13}|^2 = |S_{23}|^2 = \frac{K^2}{Z_0^2} \cdot \frac{Z_0}{Z_0'} \cdot \frac{Z_0^2}{|X|^2} = \frac{4\pi^2 \lambda_g M^2}{\lambda_g' a' b' a^3 b} \cos^2 \frac{\pi x}{a}$$

$$\frac{X}{Z_0} = -\frac{a^3 b}{\pi \lambda_g M \cos^2 \frac{\pi x}{a}} \qquad \frac{B}{Y_0} = -\frac{4\pi \lambda_g P}{a \lambda^2 b} \sin^2 \frac{\pi x}{a} \qquad \frac{K}{Z_0} = \frac{2a}{\lambda_g \cos \frac{\pi x}{a}}$$

$$\frac{Z_0'}{Z_0} = \frac{\lambda_g' a' b'}{\lambda_g a b} \qquad \lambda_g = \frac{\lambda}{\sqrt{1 - \left(\frac{\lambda}{2a}\right)^2}} \qquad \lambda_g' = \frac{\lambda}{\sqrt{1 - \left(\frac{\lambda}{2a'}\right)^2}}$$

$$M = M_1 \cos^2 \phi + M_2 \sin^2 \phi$$

A-3827-147

FIG. 5.10-9 IRIS-COUPLED SHUNT T-JUNCTION IN RECTANGULAR GUIDE E-PLANE

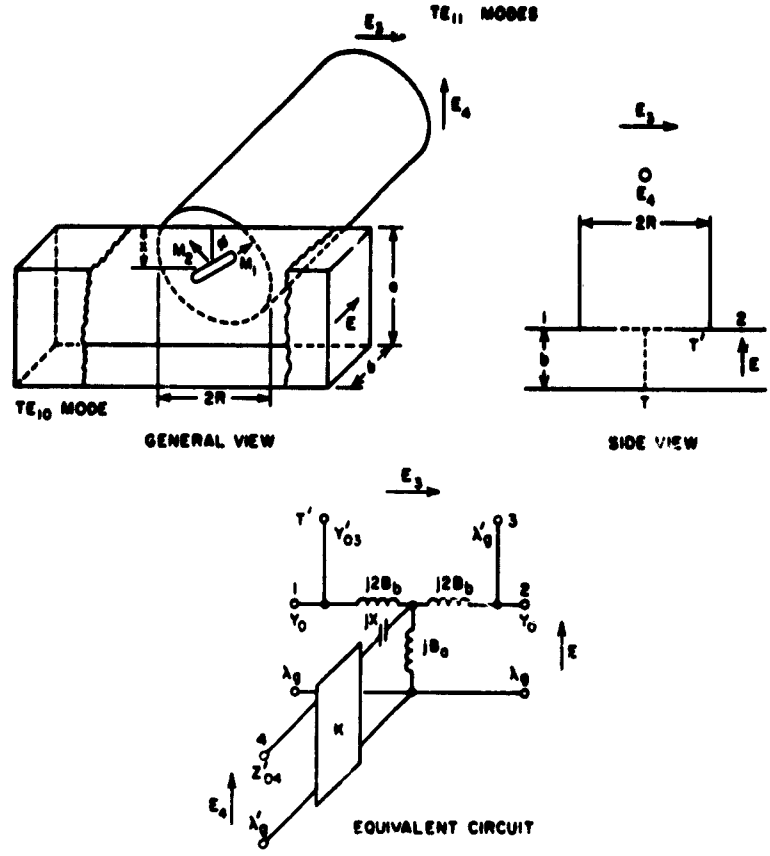

$$|S_{14}|^2 = |S_{24}|^2 = \frac{K^2}{Z_0^2} \cdot \frac{Z_0}{Z'_{04}} \cdot \frac{Z_0^2}{|X|^2} = \frac{4\pi^2 M'^2 \lambda_g \cos^2 \frac{\pi x}{a}}{3R^2 a^3 b \lambda'_g} \qquad \frac{K}{Z_0} = \frac{2a}{\lambda_g \cos \frac{\pi x}{a}}$$

$$|S_{13}|^2 = |S_{23}|^2 = \frac{Y'_{03}}{Y_0} \cdot \frac{Y_0^2}{|B_b|^2} = \frac{16\pi^2 M^2 \sin^2 \frac{\pi x}{a}}{3R^2 ab \lambda_g \lambda'_g} \qquad \frac{B_b}{Y_0} = -\frac{\lambda_g ab}{4\pi M \sin^2 \frac{\pi x}{a}}$$

$$\lambda'_g = \frac{\lambda}{\sqrt{1 - \left(\frac{\lambda}{3.41R}\right)^2}} \qquad \frac{B_a}{Y_0} = -\frac{4\pi \lambda_g P}{a\lambda^2 b} \sin^2 \frac{\pi x}{a} \qquad \lambda_g = \frac{\lambda}{\sqrt{1 - \left(\frac{\lambda}{2a}\right)^2}}$$

$$\frac{Y'_{03}}{Y_0} = \frac{ab\lambda_g}{3R^2 \lambda'_g \sin^2 \frac{\pi x}{a}} \qquad \frac{Z'_{04}}{Z_0} = \frac{3R^2 \lambda'_g}{ab\lambda_g} \qquad \frac{X}{Z_0} = -\frac{a^3 b}{\pi \lambda_g M' \cos^2 \frac{\pi x}{a}}$$

$$M' = M_1 \sin^2 \phi + M_2 \cos^2 \phi \qquad M = M_1 \cos^2 \phi + M_2 \sin^2 \phi$$

Adapted from the *Waveguide Handbook* (see Ref. 8 edited by N. Marcuvitz)

0-3627-140

FIG. 5.10-10 IRIS-COUPLED T-JUNCTION OF RECTANGULAR AND CIRCULAR GUIDES

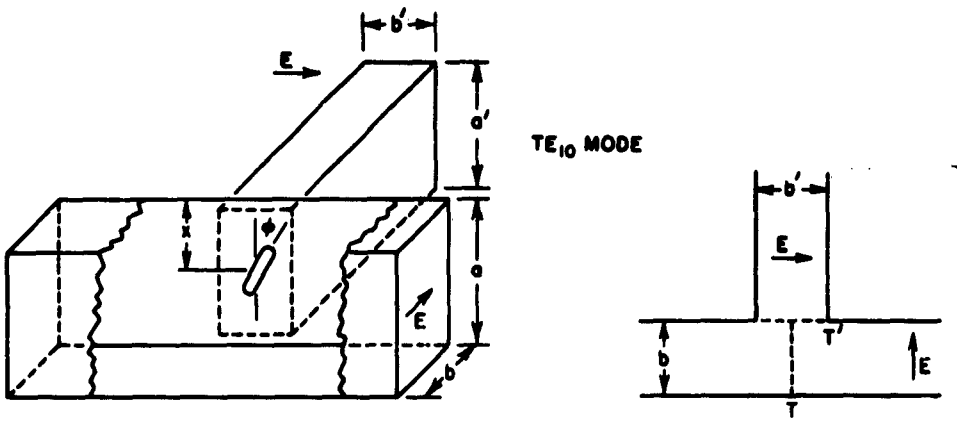

GENERAL VIEW

SIDE VIEW

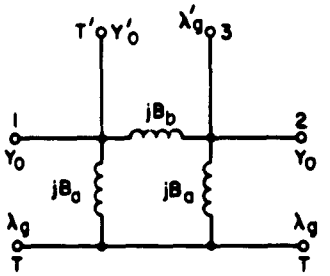

EQUIVALENT CIRCUIT

$$|S_{13}|^2 = |S_{23}|^2 = \frac{Y_0'}{Y_0} \cdot \frac{Y_0^2}{|B_b|^2} = \frac{16\pi^2 M^2 \sin^2 \frac{\pi x}{a}}{aa'bb'\lambda_g\lambda_g'}$$

$$\frac{B_b}{Y_0} = -\frac{\lambda_g ab}{4\pi M \sin^2 \frac{\pi x}{a}} \qquad \frac{B_a}{Y_0} = -\frac{2\pi\lambda_g P}{ab\lambda^2} \sin^2 \frac{\pi x}{a} + \frac{\pi M'\lambda_g}{2a^3 b} \cos^2 \frac{\pi x}{a}$$

$$\frac{Y_0'}{Y_0} = \frac{ab\lambda_g}{a'b'\lambda_g' \sin^2 \frac{\pi x}{a}} \qquad \lambda_g = \frac{\lambda}{\sqrt{1 - \left(\frac{\lambda}{2a}\right)^2}} \qquad \lambda_g' = \frac{\lambda}{\sqrt{1 - \left(\frac{\lambda}{2a'}\right)^2}}$$

$$M = M_1 \cos^2 \phi + M_2 \sin^2 \phi \qquad M' = M_1 \sin^2 \phi + M_2 \cos^2 \phi$$

A-3827-149

Adapted from the *Waveguide Handbook* (see Ref. 8 edited by N. Marcuvitz)

FIG. 5.10-11 IRIS-COUPLED SERIES T-JUNCTION IN RECTANGULAR GUIDE, E-PLANE

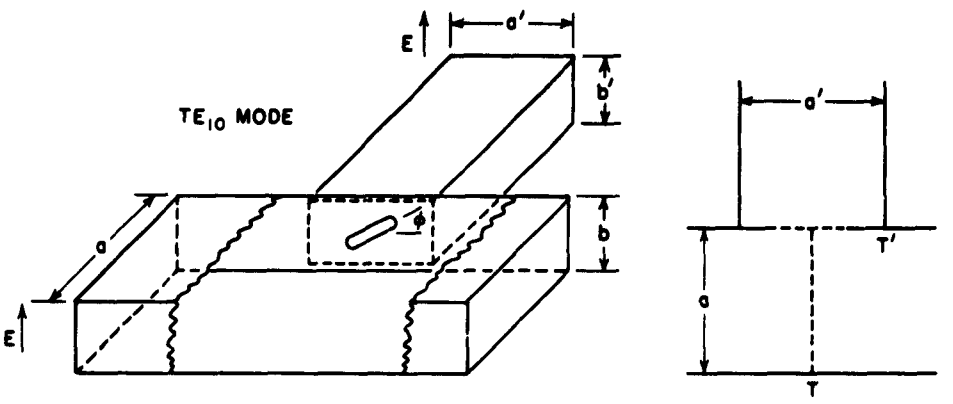

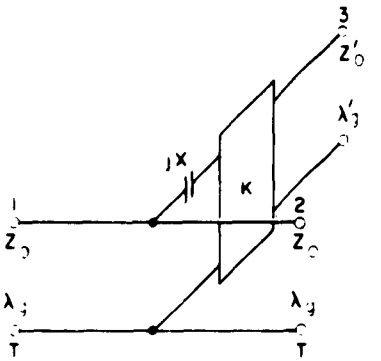

$$S_{13}{}^2 = S_{23}{}^2 = \frac{K^2}{Z_0^2} \cdot \frac{Z_0}{Z_0'} \cdot \frac{Z_0^2}{|X|^2} = \frac{4\pi^2 \lambda_g M^2}{\lambda_g' a' b' a^3 b}$$

$$\frac{X}{Z_0} = -\frac{a^3 b}{\pi \lambda_g M} \qquad M = M_1 \cos^2 \phi + M_2 \sin^2 \phi \qquad \frac{Z_0'}{Z_0} = \frac{\lambda_g' a' b'}{\lambda_g a b}$$

$$\lambda_g = \frac{\lambda}{\sqrt{1 - \left(\frac{\lambda}{2a}\right)^2}} \qquad \frac{K}{Z_0} = \frac{2a}{\lambda_g} \qquad \lambda_g' = \frac{\lambda}{\sqrt{1 - \left(\frac{\lambda}{2a'}\right)^2}}$$

A-3527-150

Adapted from the *Waveguide Handbook* (see Ref. 8 edited by N. Marcuvitz)

FIG. 5.10-12 IRIS-COUPLED SHUNT T-JUNCTION IN RECTANGULAR GUIDE, H-PLANE

When the irises are not small with respect to free-space wavelength, it is found that the equivalent circuits of Figs. 5.10-5 to 5.10-12 apply with good accuracy if the static magnetic polarizability M_1 given in Fig. 5.10-4 is replaced by the magnetic polarizability M_1'. The expression for M_1' is

$$M_1' = \frac{M_1}{1 - \left(\frac{\lambda_c}{\lambda}\right)^2} \qquad (5.10\text{-}3)$$

where λ_c is the free-space wavelength at the cutoff frequency for the lowest-order mode in a waveguide having the same cross section as the iris, and λ is the free-space wavelength at the frequency of operation. For long, thin irises of length l, λ_c is approximately equal to $2l$.

The finite thickness, t, of an iris reduces the transmission through it. It is found that the total attenuation α of a thick iris is predicted with reasonable approximation as the sum of the attenuation α_0 of a thin iris and the attenuation α_1 of a length of transmission line having a length equal to the iris thickness. Thus,

$$\alpha_0 = 10 \log_{10} \frac{1}{|S_{21}|^2} \quad \text{db} \qquad (5.10\text{-}4)$$

and

$$\alpha_1 = \frac{54.6tA}{\lambda_c}\sqrt{1 - \left(\frac{\lambda_c}{\lambda}\right)^2} \quad \text{db} \qquad (5.10\text{-}5)$$

where A is an empirically determined constant approximately equal to one for a round hole.[25] For an elongated slot of length l in a wall t thick, A is about 3 if $t < 0.02\ l$, but A decreases in size as t becomes larger.[25]

The information in Eqs. (5.10-3), (5.10-4), and (5.10-5) can be combined to yield an equivalent polarizability M_1', for a thick iris whose cross-sectional dimensions are not small in terms of a wavelength. The expression is

$$M'_{1t} = \frac{M_1}{1 - \left(\frac{\lambda_c}{\lambda}\right)^2} \, 10^{-\left[\frac{2.73 t A}{\lambda_c}\sqrt{1-\left(\frac{\lambda_c}{\lambda}\right)^2}\right]} . \qquad (5.10\text{-}6)$$

SEC. 5.11, RESONANT FREQUENCIES AND UNLOADED Q OF WAVEGUIDE RESONATORS

Two important characteristics of a waveguide resonator that are useful in the design of waveguide filters are the resonant frequency of the resonator and its unloaded Q, Q_u. This section presents curves and formulas yielding these quantities for completely closed cavities of the rectangular and cylindrical varieties. When a small coupling iris is cut in a cavity its resonant frequency and Q_u will be nearly the same as those of the unperturbed cavity.

Rectangular Waveguide Resonators—Rectangular resonators are probably used more often in waveguide filters than any other type. An example of such a resonator is illustrated in Fig. 5.11-1(a). The modes that can exist in this resonator are conveniently divided into two sets, the transverse electric TE-modes and the transverse-magnetic TM-modes. The TE-modes have no electric field components, E, along the z axis and the TM-modes have no magnetic field components, H, along the z axis. The two types of modes are further specified in terms of the integers l, m, and n. These are defined as

l = number of half-period variations of E and H along x
m = number of half-period variations of E and H along y
n = number of half-period variations of E and H along z.

For a given set of integers a mode is completely specified, and the modes are designated as either $TE_{l,m,n}$ or $TM_{l,m,n}$.

The resonant frequencies are given by the equation

$$f^2AB = 34.82 \left\{\frac{B}{A} l^2 + \frac{A}{B} m^2 + \frac{AB}{L^2} n^2\right\} \qquad (5.11\text{-}1)$$

where A, B, and L are measured in inches, and f is expressed in gigacycles. Figure 5.11(a) also contains a mode chart in which f^2A^2 is plotted as a function of A^2/L^2 for all of the TE- and TM-modes having

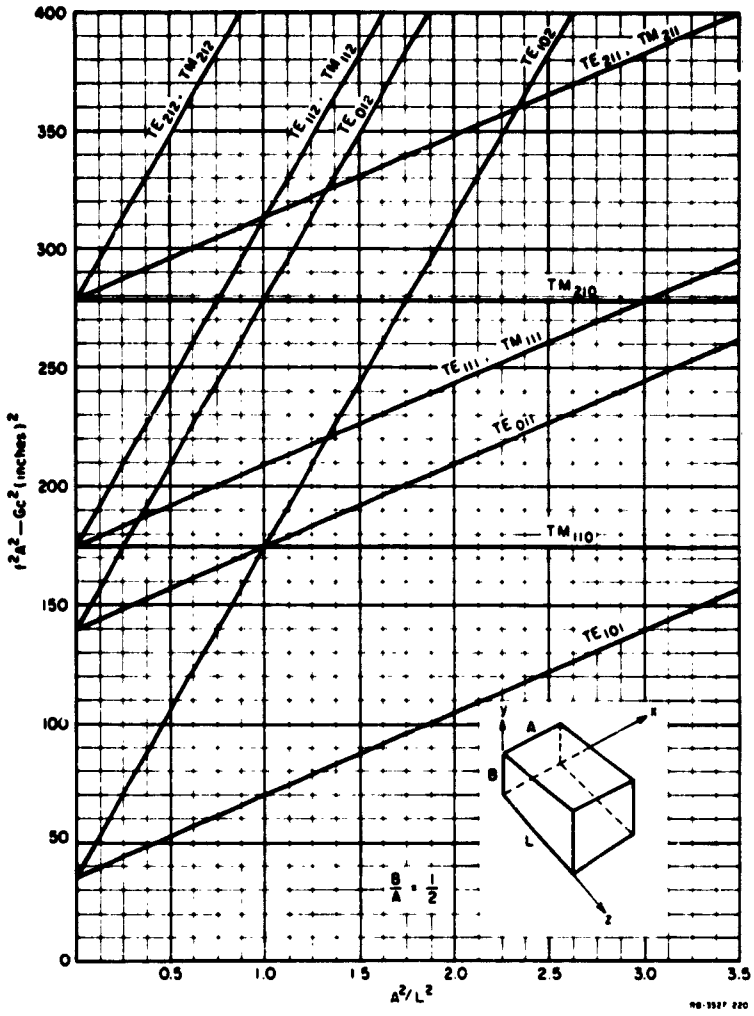

FIG. 5.11-1(a) MODE CHART FOR RECTANGULAR WAVEGUIDE RESONATOR WITH B/A = 1/2
The dimensions A, B, and L are measured in inches and frequency f is measured in gigacycles

l, m, $n \leq 2$ in a cavity in which $B/A = 1/2$. In this figure, all dimensions are in inches, and frequency is measured in gigacycles.

The unloaded Q of a cavity is most conveniently tabulated in the dimensionless form $Q_u\delta/\lambda$ where δ is the skin depth and λ is the free space wavelength. Table 5.11-1 presents values of δ/λ for various metals having polished, corrosion-free surfaces.

Table 5.11-1

VALUES OF δ/λ FOR VARIOUS METALS
The Values Given Are For Polished, Corrosion-Free Surfaces.
The Frequency f_{Ge} Is In Gigacycles.

Silver,	$\delta/\lambda = 6.76 \times 10^{-6}\sqrt{f_{Ge}}$
Copper,	$\delta/\lambda = 6.95 \times 10^{-6}\sqrt{f_{Ge}}$
Aluminum,	$\delta/\lambda = 8.70 \times 10^{-6}\sqrt{f_{Ge}}$
Brass,	$\delta/\lambda = 13.4 \times 10^{-6}\sqrt{f_{Ge}}$

For TE-modes we find that $Q_u(\delta/\lambda)$ is given by:[31]

$$Q_u \frac{\delta}{\lambda} = \frac{ABL}{4} \times \frac{(p^2 + q^2)\ (p^2 + q^2 + r^2)^{3/2}}{AL[p^2r^2 + (p^2 + q^2)^2] + BL[q^2r^2 + (p^2 + q^2)^2] + ABr^2(p^2 + q^2)}, \tag{5.11-2}$$

for (l and m) > 0;

$$Q_u \frac{\delta}{\lambda} = \frac{ABL}{2} \cdot \frac{(q^2 + r^2)^{3/2}}{q^2L(B + 2A) + r^2B(L + 2A)}, \quad \text{for } l = 0; \tag{5.11-3}$$

and

$$Q_u \frac{\delta}{\lambda} = \frac{ABL}{2} \cdot \frac{(p^2 + r^2)^{3/2}}{p^2L(A + 2B) + r^2A(L + 2B)}, \quad \text{for } m = 0 \tag{5.11-4}$$

where $p = 1/A$, $q = m/B$, $r = n/L$. Figure 5.11-1(b) shows a chart of $Q_u(\delta/\lambda)$ *versus* A/L for various aspect ratios $k = A/B$ for the TE_{101} mode.

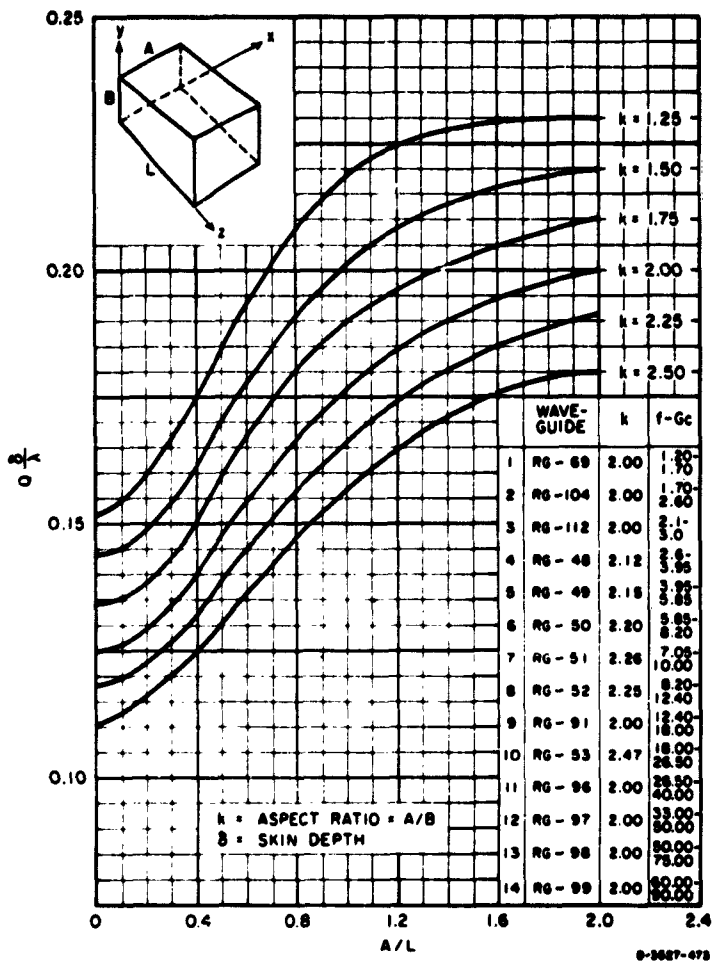

SOURCE: U. S. Army Signal Research and Development Laboratory, Ft. Monmouth, N.J.

FIG. 5.11-1(b) CHART FOR ESTIMATING THE UNLOADED Q OF TE_{101}-MODE RECTANGULAR WAVEGUIDE RESONATORS

For the TM-modes we find that Q_u is given by:[31]

$$Q_u \frac{\delta}{\lambda} = \frac{ABL}{4} \cdot \frac{(p^2 + q^2)\ (p^2 + q^2 + r^2)^{1/2}}{p^2B(A + L) + q^2A(B + L)}, \quad \text{for } n > 0 \ ; \qquad (5.11\text{-}5)$$

and

$$Q_u \frac{\delta}{\lambda} = \frac{ABL}{2} \cdot \frac{(p^2 + q^2)^{3/2}}{p^2B(A + 2L) + q^2A(B + 2L)}, \quad \text{for } n = 0 \ . \qquad (5.11\text{-}6)$$

Right-Circular-Cylinder Resonators—Cylindrical resonators of the type illustrated in Fig. 5.11-2 also have normal modes that can be characterized as TE-modes when there are no electric field components, E, along the z axis, and as TM-modes when there are no magnetic field components, H, along the z axis. The individual TE- and TM-modes are further identified by means of the three integers l, m, and n, which are defined as follows:

l = number of full-period variations of E_r with respect to θ

m = number of half-period variations of E_θ with respect to r

n = number of half-period variations of E_r with respect to z

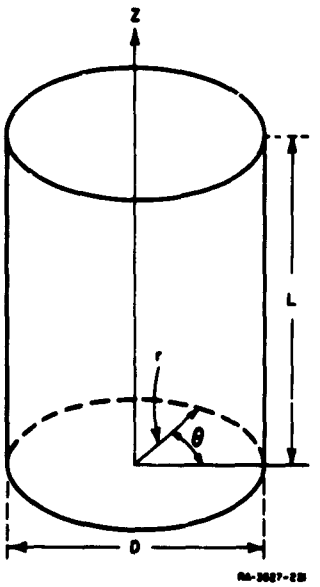

SOURCE: *Technique of Microwave Measurements*, see Ref. 31 by C. G. Montgomery

FIG. 5.11-2 RIGHT-CIRCULAR-CYLINDER RESONATOR

where E_r and E_θ are the field components in the r and θ directions. As in the case of the rectangular cavity modes the right circular cylinder modes are also designated as $TE_{l,m,n}$ or $TM_{l,m,n}$. The resonant frequencies of these modes are given by the expression[31]

$$f^2D^2 = 139.3\left\{\left(\frac{x_{l,m}}{\pi}\right)^2 + \left(\frac{nD}{2L}\right)^2\right\} . \qquad (5.11\text{-}7)$$

In this expression f is measured in gigacycles, the dimensions D and L are measured in inches. The quantities $x_{l,s}$ are

$$\begin{aligned} x_{l,s} &= \text{mth root of } J_l'(x) = 0 \text{ for the TE-modes} \\ x_{l,s} &= \text{mth root of } J_l(x) = 0 \text{ for the TM-modes} \end{aligned} \quad . \tag{5.11-8}$$

Values of a few of these roots are given in Table 5.11-2.

Table 5.11-2

ROOTS OF $J_l(x)$ AND $J_l'(x)$

TE-mode	x_{ln}	TM-mode	x_{ln}
11*n*	1.841	01*n*	2.405
21*n*	3.054	11*n*	3.832
01*n*	3.832	21*n*	5.136
31*n*	4.201	02*n*	5.520
41*n*	5.318	31*n*	6.380
12*n*	5.332	12*n*	7.016
51*n*	6.415	41*n*	7.588
22*n*	6.706	22*n*	8.417
02*n*	7.016	03*n*	8.654
61*n*	7.501	51*n*	8.772
32*n*	8.016	32*n*	9.761
13*n*	8.536	61*n*	9.936
71*n*	8.578	13*n*	10.174
42*n*	9.283		
81*n*	9.648		
23*n*	9.970		
03*n*	10.174		

Source: *Technique of Microwave Measurements*, see Ref. 31, by C. G. Montgomery.

Figure 5.11-3 is a mode chart in which f^2D^2 is plotted as a function of D^2/L^2, for several of the lower-order TE- and TM-modes. In this figure all dimensions are in inches and frequency is measured in gigacycles.

Values of Q_u for right-circular-cylinder copper resonators are plotted for TE-modes in Figs. 5.11-4 and 5.11-5, and for TM-modes in Fig. 5.11-6.

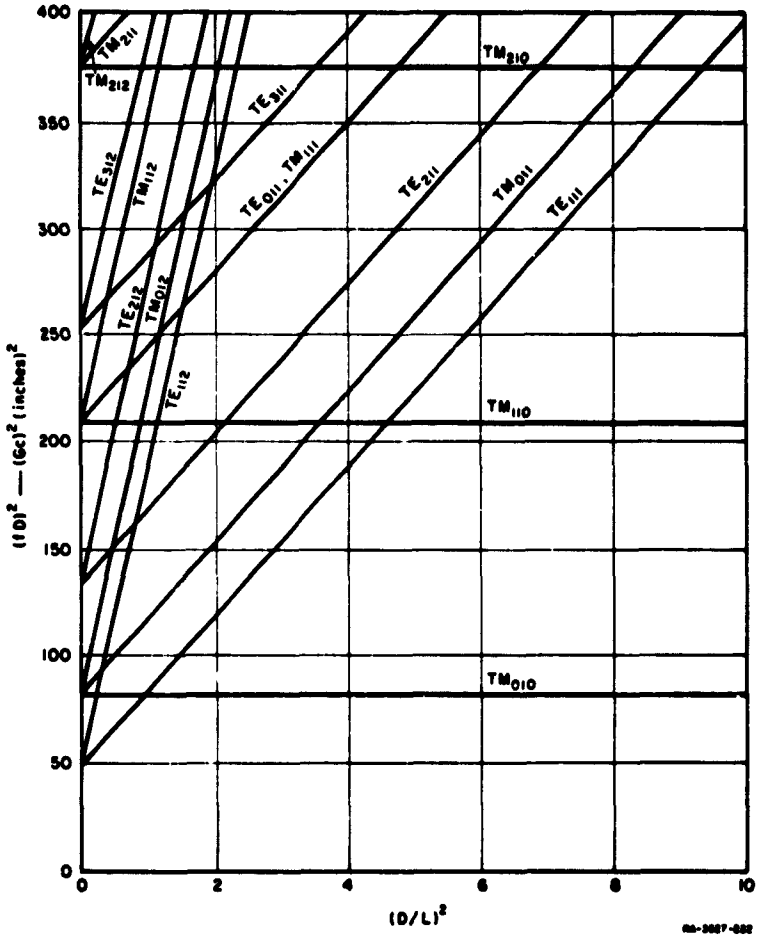

SOURCE: *Technique of Microwave Measurements*, see Ref. 31 by C. G. Montgomery

FIG. 5.11-3 MODE CHART FOR RIGHT-CIRCULAR-CYLINDER RESONATOR
The diameter D and length L are measured in inches and the frequency f is measured in gigacycles

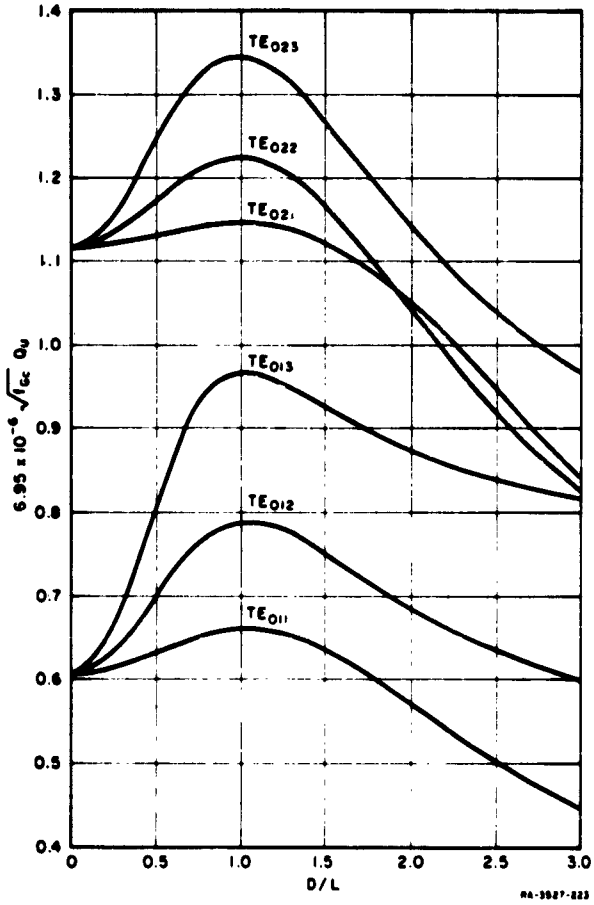

SOURCE: *Technique of Microwave Measurements*, see Ref. 31 by C. G. Montgomery

FIG. 5.11-4 THEORETICAL UNLOADED Q OF SEVERAL TE_0-MODES IN A RIGHT-CIRCULAR-CYLINDER COPPER RESONATOR
Frequency is measured in gigacycles

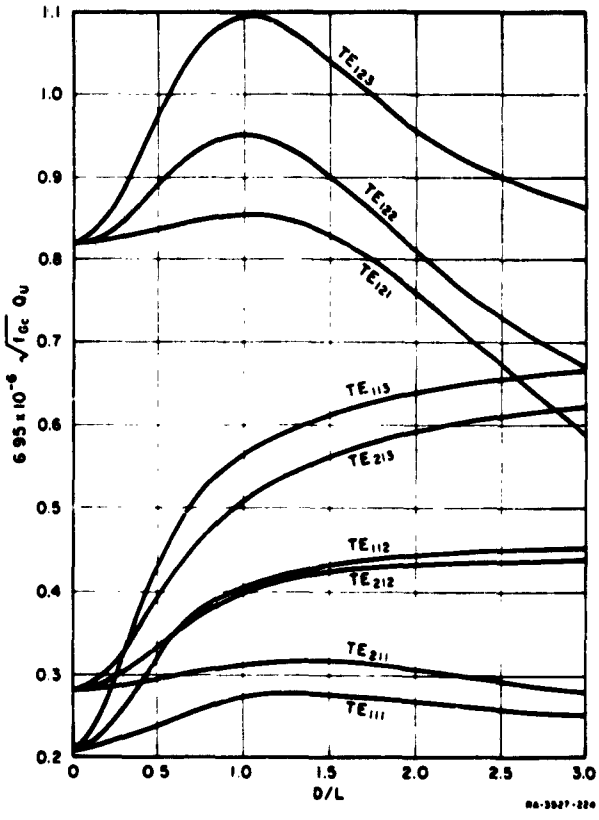

SOURCE: *Technique of Microwave Measurements*, see Ref. 31 by C. G. Montgomery

FIG. 5.11-5 THEORETICAL UNLOADED Q OF SEVERAL TE-MODES IN A RIGHT-CIRCULAR-CYLINDER COPPER RESONATOR
Frequency is measured in gigacycles

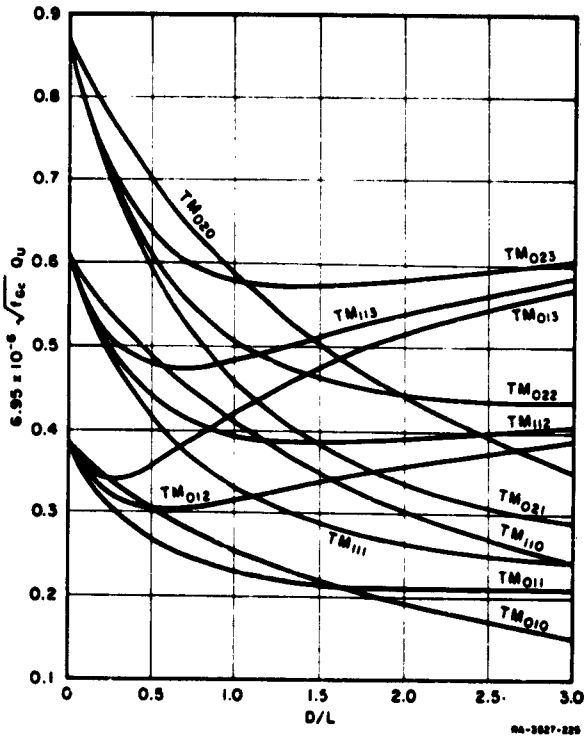

SOURCE: *Technique of Microwave Measurements*, see Ref. 31 by C. G. Montgomery

FIG. 5.11-6 THEORETICAL UNLOADED Q OF SEVERAL TM-MODES IN A RIGHT-CIRCULAR-CYLINDER RESONATOR
Frequency is measured in gigacycles

REFERENCES

1. S. B. Cohn, "Characteristic Impedance of the Shielded-Strip Transmission Line," *IRE Trans., PGMTT*-2, pp. 52-72 (July 1954).

2. S. B. Cohn, "Problems in Strip Transmission Lines," *IRE Trans., PGMTT*-3, 2, pp. 119-126 (March 1955).

3. R. H. T. Bates, "The Characteristic Impedance of Shielded Slab Line," *IRE Trans., PGMTT*-4, pp. 28-33 (January 1956).

4. S. B. Cohn, "Shielded Coupled-Strip Transmission Lines," *IRE Trans., PGMTT*-3, pp. 29-38 (October 1955).

5. F. Oberhettinger and W. Magnus, *Anwendung der Elliptischen Functionen in Physick and Technik*, (Springer-Verlag, Berlin, 1949).

6. S. B. Cohn, "Characteristic Impedances of Broadside-Coupled Strip Transmission Lines," *IRE* Trans., PGMTT-8, 6, pp. 633-637 (November 1960).

7. S. B. Cohn, "Thickness Corrections for Capacitive Obstacles and Strip Conductors," *IRE Trans., PGMTT*-8, 6, pp. 638-644 (November 1960).

8. N. Marcuvitz, *Waveguide Handbook*, MIT Radiation Laboratory Series, Vol. 10 (McGraw Hill Book Co., Inc., New York City, 1951).

9. T. Moreno, *Microwave Transmission Design Data* (Dover Publications Inc., New York City, 1958).

10. J. R. Whinnery and H. W. Jamieson, "Equivalent Circuits for Discontinuities in Transmission Lines," *Proc. IRE* 32, 2, pp. 98-114 (February 1944).

11. J. R. Whinnery, H. W. Jamieson and T. E. Robbins, "Coaxial-Line Discontinuities," *Proc. IRE* 32, 11, pp. 695-709 (November 1944).

12. A. A. Oliner, "Equivalent Circuits for Discontinuities in Balanced Strip Transmission Line," *IRE Trans., PGMTT*-3, 2, pp. 134-143 (March 1955).

13. H. M. Altschuler and A. A. Oliner, "Discontinuities in the Center Conductor of Symmetric Strip Transmission Line," *IRE Trans., PGMTT*-8, 3, pp. 328-339 (May 1960).

14. A. Alford, "Coupled Networks in Radio-Frequency Circuits," *Proc. IRE* 29, pp. 55-70 (February 1941).

15. J. J. Karakash and D. E. Mode, "A Coupled Coaxial Transmission-Line Band-Pass Filter," *Proc. IRE* 38, pp. 48-52 (January 1950).

16. W. L. Firestone, "Analysis of Transmission Line Directional Couplers," *Proc. IRE* 42, pp. 1529-1538 (October 1954).

17. B. M. Oliver, "Directional Electromagnetic Couplers," *Proc. IRE*, Vol. 42, pp. 1686-1692 (November 1954).

18. R. C. Knechtli, "Further Analysis of Transmission-Line Directional Couplers," *Proc. IRE* 43, pp. 867-869 (July 1955).

19. E. M. T. Jones and J. T. Bolljahn, "Coupled-Strip-Transmission-Line Filters and Directional Couplers," *IRE Trans., PGMTT*-4, 2, pp. 75-81 (April 1956).

20. H. Ozaki and J. Ishii, "Synthesis of a Class of Strip-Line Filters," *IRE Trans., PGCT*-5, pp. 104-109 (June 1958).

21. H. A. Bethe, "Lumped Constants for Small Irises," Report 43-22, M.I.T. Radiation Laboratory, Cambridge, Massachusetts (March 1943).

22. H. A. Bethe, "Theory of Side Windows in Waveguides," Report 43-27, M.I.T. Radiation Laboratory, Cambridge, Massachusetts (April 1943).

23. H. A. Bethe, "Formal Theory of Waveguides of Arbitrary Cross Section," Report 43-26, M.I.T. Radiation Laboratory, Cambridge, Massachusetts (March 1943).

24. H. A. Bethe, "Theory of Diffraction by Small Holes," *Phys. Rev.* Vol. 66, pp. 163-182 (1944).

25. S. B. Cohn, "Microwave Coupling by Large Apertures," *Proc. IRE* 40, pp. 696-699 (June 1952).

26. R. E. Collin, *Field Theory of Guided Waves*, Sec. 7.3 (McGraw Hill Book Co., Inc., New York City, 1960).

27. N. Marcuvitz, "Waveguide Circuit Theory: Coupling of Waveguides by Small Apertures," Report No. R-157-47, Microwave Research Institute, Polytechnic Institute of Brooklyn (1947) PIB-106.

28. A. A. Oliner, "Equivalent Circuits for Small Symmetrical Longitudinal Apertures and Obstacles," *IRE Trans., PGMTT*-8 1, pp. 72-80 (January 1960).

29. S. B. Cohn, "Determination of Aperture Parameters by Electrolytic Tank Measurements," *Proc. IRE* 39, pp. 1416-1421 (November 1951).

30. S. B. Cohn, "The Electric Polarizability of Apertures of Arbitrary Shape," *Proc. IRE* 40, pp. 1069-1071 (September 1952).

31. C. G. Montgomery, *Technique of Microwave Measurements*, Secs. 5.4 and 5.5 (McGraw-Hill Book Co., New York City, N.Y., 1947).

32. W. J. Getsinger, "A Coupled Strip-Line Configuration Using Printed-Circuit Construction that Allows Very Close Coupling," *IRE Trans., PGMTT*-9, pp. 535-544 (November 1961).

33. W. J. Getsinger, "Coupled Rectangular Bars Between Parallel Plates," *IRE Trans., PGMTT*-10, pp. 65-72 (January 1962).

CHAPTER 6

STEPPED-IMPEDANCE TRANSFORMERS AND FILTER PROTOTYPES

SEC. 6.01, INTRODUCTION

The objective of this chapter is to present design equations and numerical data for the design of quarter-wave transformers, with two applications in mind: the first application is as an impedance-matching device or, literally, transformer; the second is as a prototype circuit, which shall serve as the basis for the design of various band-pass and low-pass filters.

This chapter is organized into fifteen sections, with the following purpose and content:

- Section 6.01 is introductory. It also discusses applications, and gives a number of definitions.
- Sections 6.02 and 6.03 deal with the performance characteristics of quarter-wave transformers and half-wave filters. In these parts the designer will find what *can* be done, not how to do it.
- Sections 6.04 to 6.10 tell *how* to design quarter-wave transformers and half-wave filters. If simple, general design formulas were available, and solvable by nothing more complicated than a slide-rule, these sections would be much shorter.
- Section 6.04 gives exact formulas and tables of complete designs for Tchebyscheff and maximally flat transformers of up to four sections.
- Section 6.05 gives tables of designs for maximally flat (but not Tchebyscheff) transformers of up to eight sections.
- Section 6.06 gives a first-order theory for Tchebyscheff and maximally flat transformers of up to eight sections, with explicit formulas and numerical tables. It also gives a general first-order formula, and refers to existing numerical tables published elsewhere which are suitable for up to 39 sections, and for relatively wide (but not narrow) bandwidths.
- Section 6.07 presents a modified first-order theory, accurate for larger transformer ratios than can be designed by the (unmodified) first-order theory of Sec. 6.06.

- Section 6.08 deals with the discontinuity effects of non-ideal junctions, and first-order corrections to compensate for them.
- Sections 6.09 and 6.10 apply primarily to prototypes for filters, since they are concerned with large impedance steps. They become exact only in the limit as the output-to-input impedance ratio, R, tends to infinity. Simple formulas are given for any number of sections, and numerical tables on lumped-constant filters are referred to.

Note: Sections 6.09 and 6.10 complement Secs. 6.06 and 6.07, which give exact results only in the limit as R tends to zero. It is pointed out that the dividing line between "small R" and "large R" is in the order of $[2/(\text{quarter-wave transformer bandwidth})]^{2n}$, where n is the number of sections. This determines whether the first-order theory of Secs. 6.06 and 6.07, or the formulas of Secs. 6.09 and 6.10 are to be used. An example (Example 3 of Sec. 6.09) where R is in this borderline region, is solved by both the "small R" and the "large R" approximations, and both methods give tolerably good results for most purposes.

- Sections 6.11 and 6.12 deal with "inhomogeneous" transformers, which are not uniformly dispersive, since the cutoff wavelength changes at each step.
- Section 6.13 describes a particular transformer whose performance and over-all length are similar to those of a single-section quarter-wave transformer, but which requires only matching sections whose characteristic impedances are equal to the input and output impedances.
- Section 6.14 considers dissipation losses. It gives a general formula for the midband dissipation loss.
- Section 6.15 relates group delay to dissipation loss in the pass band, and presents numerical data in a set of universal curves.

Quarter-wave transformers have numerous applications besides being impedance transformers; an understanding of their behavior gives insight into many other physical situations not obviously connected with impedance transformations. The design equations and numerical tables have, moreover, been developed to the point where they can be used conveniently for the synthesis of circuits, many of which were previously difficult to design.

Circuits that can be designed using quarter-wave transformers as a prototype include: impedance transformers[1-6] (as in this chapter); reactance-coupled filters[7-9] (Chapt. 9); short-line low-pass filters (Sec. 7.06); branch-guide directional couplers[10] (Chapt. 13); as well as optical multi-layer filters and transformers,[11,12] and acoustical transformers.[13,14]

The attenuation functions considered here are all for maximally flat or Tchebyscheff response in the pass band. It is of interest to note that occasionally other response shapes may be desirable. Thus TEM-mode coupled-transmission-line directional couplers are analytically equivalent to quarter-wave transformers (Chapt. 13), but require functions with maximally flat or equal-ripple characteristics in the *stop* band. Other attenuation functions may be convenient for other applications, but will not be considered here.

As in the design of all microwave circuits, one must distinguish between the ideal circuits analyzed, and the actual circuits that have prompted the analysis and which are the desired end product. To bring this out explicitly, we shall start with a list of definitions:[15]

Homogeneous transformer—a transformer in which the ratios of internal wavelengths and characteristic impedances at different positions along the direction of propagation are independent of frequency.

Inhomogeneous transformer—a transformer in which the ratios of internal wavelengths and characteristic impedances at different positions along the direction of propagation may change with frequency.

Quarter-wave transformer—a cascade of sections of lossless, uniform* transmission lines or media, each section being one-quarter (internal) wavelength long at a common frequency.

* A uniform transmission line, medium, etc., is here defined as one in which the physical and electrical characteristics do not change with distance along the direction of propagation. This is a generalization of the IRE definition of *uniform waveguide* (see Ref. 16).

Note: Homogeneous and inhomogeneous quarter-wave transformers are now defined by a combination of the above definitions. For instance, an *inhomogeneous quarter-wave transformer* is a quarter-wave transformer in which the ratios of internal wavelengths and characteristic impedances taken between different sections, may change with frequency.

Ideal junction—the connection between two impedances or transmission lines, when the electrical effects of the connecting wires, or the junction discontinuities, can be neglected. (The junction effects may later be represented by equivalent reactances and transformers, or by positive and negative line lengths, etc.)

Ideal quarter-wave transformer—a quarter-wave transformer in which all of the junctions (of guides or media having different characteristic impedances) may be treated as ideal junctions.

Half-wave filter—a cascade of sections of lossless uniform transmission lines or media, each section being one-half (internal) wavelength long at a common frequency.

Synchronous tuning condition—a filter consisting of a series of discontinuities spaced along a transmission line is synchronously tuned if, at some fixed frequency in the pass band, the reflections from any pair of *successive* discontinuities are phased to give the maximum cancellation. (A quarter-wave transformer is a synchronously tuned circuit if its impedances form a monotone sequence. A half-wave filter is a synchronously tuned circuit if its impedances alternately increase and decrease at each step along its length.)

Synchronous frequency—the "fixed frequency" referred to in the previous definition will be called the *synchronous frequency*. (In the case of quarter-wave transformers, all sections are one-quarter wavelength long at the synchronous frequency; in the case of half-wave filters, all sections are one-half wavelength long at the synchronous frequency. Short-line, low-pass filters may also be derived from half-wave filters, with the synchronous frequency being thought of as zero frequency.)

The realization of transmission-line discontinuities by impedance steps is equivalent to their realization by means of ideal impedance inverters (Sec. 4.12). The main difference is that while impedance steps can be physically realized over a wide band of frequencies (at least for small steps), ideal impedance inverters can be approximated over only limited bandwidths. As far as using either circuit as a mathematical model, or prototype circuit, is concerned, they give equivalent results, as can be seen from Fig. 6.01-1.

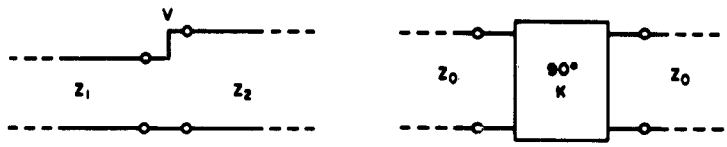

IMPEDANCE STEP	IMPEDANCE INVERTER
LINE CHARACTERISTIC IMPEDANCES = Z_1, Z_2	LINE CHARACTERISTIC IMPEDANCES = Z_0
IMPEDANCE RATIO OR JUNCTION VSWR: $V = Z_2/Z_1$ OR Z_1/Z_2, WHICHEVER >1	IMPEDANCE OF INVERTER = K
ELECTRICAL LENGTH = 0 AT ALL FREQUENCIES	ELECTRICAL LENGTH = 90° AT ALL FREQUENCIES

FOR SAME COUPLING:

$$\text{JUNCTION VSWR, } V = \left(\frac{K}{Z_0}\right)^{\pm 2} > 1$$

A-3527-291

SOURCE: Quarterly Progress Report 4, Contract DA 36-039 SC-87398, SRI; reprinted in *IRE Trans. PGMTT* (See Ref. 36 by L. Young)

FIG. 6.01-1 CONNECTION BETWEEN IMPEDANCE STEP AND IMPEDANCE INVERTER

SEC. 6.02, THE PERFORMANCE OF HOMOGENEOUS QUARTER-WAVE TRANSFORMERS

This section summarizes the relationships between the pass-band and stop-band attenuation, the fractional bandwidth, w_q, and the number of sections or resonators, n. Although the expressions obtained hold exactly only for ideal quarter-wave transformers, they hold relatively accurately for real physical quarter-wave transformers and for certain filters, either without modification or after simple corrections have been applied to account for junction effects, etc.

A quarter-wave transformer is depicted in Fig. 6.02-1. Define the quarter-wave transformer fractional bandwidth, w_q, by

$$w_q = 2\left(\frac{\lambda_{g1} - \lambda_{g2}}{\lambda_{g1} + \lambda_{g2}}\right) \qquad (6.02\text{-}1)$$

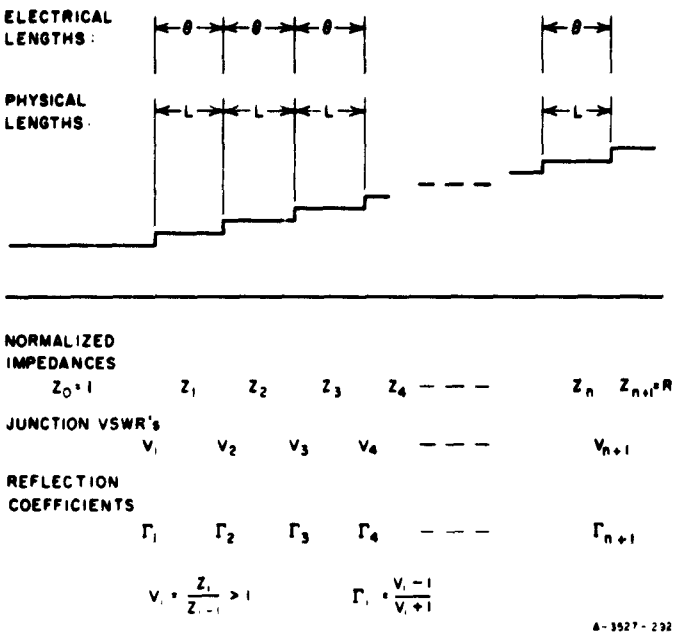

SOURCE: Quarterly Progress Report 4, Contract DA 36-039 SC-87398, SRI; reprinted in *IRE Trans. PGMTT* (See Ref. 36 by L. Young)

FIG. 6.02-1 QUARTER-WAVE TRANSFORMER NOTATION

where λ_{g1} and λ_{g2} are the longest and shortest guide wavelengths, respectively, in the pass band of the quarter-wave transformer. The length, L, of each section (Fig. 6.02-1) is nominally one-quarter wavelength at center frequency and is given by

$$L = \frac{\lambda_{g1}\lambda_{g2}}{2(\lambda_{g1} + \lambda_{g2})} = \frac{\lambda_{g0}}{4} \qquad (6.02\text{-}2)$$

where the center frequency is defined as that frequency at which the guide wavelength λ_g is equal to λ_{g0}.

When the transmission line is non-dispersive, the free-space wavelength λ may be used in Eqs. (6.02-1) and (6.02-2), which then become

$$w_q = 2\left(\frac{\lambda_1 - \lambda_2}{\lambda_1 + \lambda_2}\right) = 2\left(\frac{f_2 - f_1}{f_2 + f_1}\right) \qquad (6.02\text{-}3)$$

and

$$L = \frac{\lambda_1\lambda_2}{2(\lambda_1 + \lambda_2)} = \frac{\lambda_0}{4} \qquad (6.02\text{-}4)$$

where f stands for frequency.

The transducer loss ratio (Sec. 2.11) is defined as the ratio of P_{avail}, the available generator power, to P_L, the power actually delivered to the load. The "excess loss," $\mathcal{E}$, is herein defined by

$$\mathcal{E} = \frac{P_{avail}}{P_L} - 1 \qquad (6.02\text{-}5)$$

For the maximally flat quarter-wave transformer of n sections and over-all impedance ratio R (Fig. 6.02-1) $\mathcal{E}$ is given by

$$\mathcal{E} = \frac{(R-1)^2}{4R}\cos^{2n}\theta = \mathcal{E}_0\cos^{2n}\theta \qquad (6.02\text{-}6)$$

where

$$\theta = \frac{\pi}{2}\frac{\lambda_{g0}}{\lambda_g} \qquad (6.02\text{-}7)$$

λ_{g0} being the guide wavelength at band center, when $\theta = \pi/2$; and where

$$\mathcal{E}_0 = \frac{(R-1)^2}{4R} \qquad (6.02\text{-}8)$$

is the greatest excess loss possible. (It occurs when θ is an integral multiple of π, since the sections then are an integral number of half-wavelengths long.)

The 3-db fractional bandwidth of the maximally flat quarter-wave transformer is given by

$$w_{q,3db} = \frac{4}{\pi}\sin^{-1}\left[\frac{4R}{(R-1)^2}\right]^{1/2n} \qquad (6.02\text{-}9)$$

The fractional bandwidth of the maximally flat quarter-wave transformer between the points of x-db attenuation is given by

$$w_{q,xdb} = \frac{4}{\pi}\sin^{-1}\left\{\frac{4R\,[\text{antilog}\,(x/10) - 1]}{(R-1)^2}\right\}^{1/2n} \qquad (6.02\text{-}10)$$

For the Tchebyscheff transformer of fractional bandwidth w_q,

$$\left.\begin{aligned} \mathcal{E} &= \frac{(R-1)^2}{4R}\,\frac{T_n^2(\cos\theta/\mu_0)}{T_n^2(1/\mu_0)} \\ &= \mathcal{E}_r T_n^2(\cos\theta/\mu_0) \end{aligned}\right\} \qquad (6.02\text{-}11)$$

where

$$\mu_0 = \sin\left(\frac{\pi w_q}{4}\right) , \qquad (6.02\text{-}12)$$

T_n is a Tchebyscheff polynomial (of the first kind) of order n, and where the quantity

$$\mathcal{E}_r = \frac{(R-1)^2}{4R}\,\frac{1}{T_n^2(1/\mu_0)} = \frac{\mathcal{E}_a}{T_n^2(1/\mu_0)} \qquad (6.02\text{-}13)$$

is the maximum excess loss in the pass band. [Compare also Eq. (6.02-18), below.] The shape of these response curves for maximally flat and Tchebyscheff quarter-wave transformers is shown in Fig. 6.02-2. Notice that the peak transducer loss ratio for any quarter-wave transformer is

$$\frac{P_{avail}}{P_L} = \mathcal{E}_a + 1 = \frac{(R+1)^2}{4R} \qquad (6.02\text{-}14)$$

and is determined solely by the output-to-input impedance ratio, R.

For the maximally flat transformer, the 3-db fractional bandwidth, $w_{q,3db}$, is plotted against log R for $n = 2$ to $n = 15$ in Fig. 6.02-3. The attenuation given by Eq. (6.02-6) can also be determined from the corresponding lumped-constant, low-pass, prototype filter (Sec. 4.03). If ω' is the frequency variable of the maximally flat, lumped-constant, low-pass prototype, and ω_1' is its band edge, then

$$\frac{\omega'}{\omega_1'} = \frac{\cos\theta}{\mu_0} \qquad (6.02\text{-}15)$$

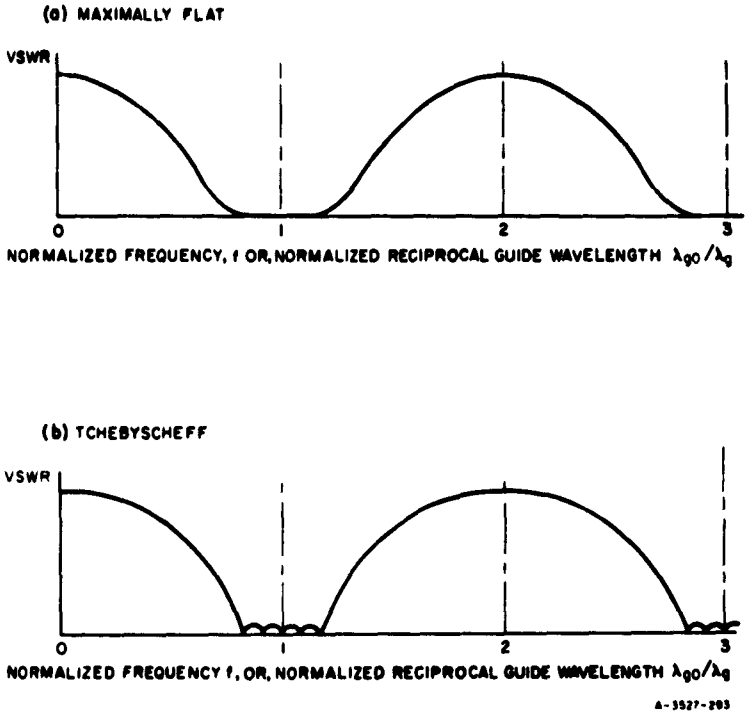

SOURCE: Quarterly Progress Report 4, Contract DA 36-039 SC-87398, SRI; reprinted in *IRE Trans. PGMTT* (See Ref. 36 by L. Young)

FIG. 6.02-2 QUARTER-WAVE TRANSFORMER CHARACTERISTICS

where μ_0 is defined by Eq. (6.02-12), and w_q (which occurs in the definition of μ_0) is the fractional bandwidth of the maximally flat quarter-wave transformer between points of the same attenuation as the attenuation of the maximally flat low-pass filter at $\omega' = \omega_1'$. This enables one to turn the graph of attenuation versus ω'/ω_1' in Fig. 4.03-2 into a graph of attenuation versus $\cos\theta$ of the quarter-wave transformer, using Eq. (6.02-15).

For the Tchebyscheff transformer,

$$\frac{\mathcal{E}_e}{\mathcal{E}_r} = T_n^2(1/\mu_0) = M(n, w_q) \qquad (6.02\text{-}16)$$

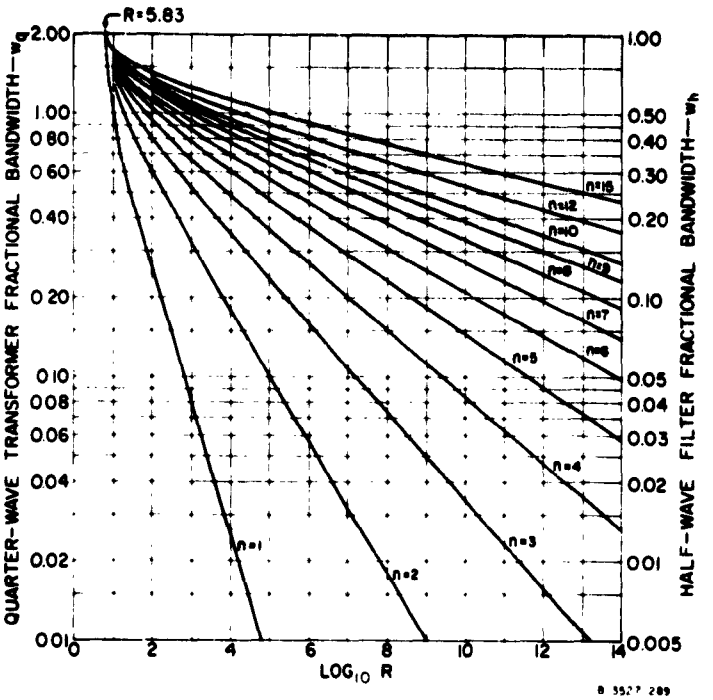

SOURCE: Quarterly Progress Report 4, Contract DA 36-039 SC-87398, SRI; reprinted in *IRE Trans. PGMTT* (See Ref. 36 by L. Young)

FIG. 6.02-3 3-db BANDWIDTHS OF MAXIMALLY FLAT TRANSFORMERS

where M is thus defined as a function of the number of sections, n, and the bandwidth, w_q. It shows how much the pass-band tolerance increases when it is desired to improve the peak rejection. The function M in Eq. (6.02-16) is given in Table 6.02-1 for all fractional bandwidths, w_q, in steps of 10 percent, for $n = 2$ to $n = 15$. The smallest fractional bandwidth in Table 6.02-1 is $w_q = 0.1$. For small bandwidths,

$$\frac{\mathcal{E}_a}{\mathcal{E}_r} = T_n^2(1/\mu_0) = M(n, w_q) \approx \frac{1}{4}\left(\frac{8}{\pi w_q}\right)^{2n}, \quad (w_q \text{ small}) . \tag{6.02-17}$$

Table 6.02-1

$$M(n, w_q) \qquad T_n^2 \left[\frac{1}{\sin (\pi w_q / 4)} \right]$$

n \ w_q	0.1	0.2	0.3	0.4	0.5	0.6	0.7	0.8	0.9	1.0
2	0.1049 * 6	0.6517 * 4	0.1274 * 4	0.3978 * 3	0.1601 * 3	0.7575 * 2	0.4001 * 2	0.2293 * 2	0.1400 * 2	0.9000 * 1
3	0.6795 * 8	0.1052 * 7	0.9094 * 5	0.1584 * 5	0.4036 * 4	0.1306 * 4	0.4972 * 3	0.2130 * 3	0.9966 * 2	0.5000 * 2
4	0.4402 *11	0.1699 * 9	0.6491 * 7	0.6313 * 6	0.1020 * 6	0.2265 * 5	0.6246 * 4	0.2013 * 4	0.7291 * 3	0.2890 * 3
5	0.2851 *14	0.2742 *11	0.4634 * 9	0.2517 * 8	0.2578 * 7	0.3930 * 6	0.7852 * 5	0.1906 * 5	0.5353 * 4	0.1682 * 4
6	0.1847 *17	0.4427 *13	0.3308 *11	0.1003 *10	0.6516 * 8	0.6819 * 7	0.9872 * 6	0.1806 * 6	0.3933 * 5	0.9801 * 4
7	0.1196 *20	0.7148 *15	0.2361 *13	0.3999 *11	0.1646 *10	0.1183 * 9	0.1241 * 8	0.1710 * 7	0.2890 * 6	0.5712 * 5
8	0.7751 *22	0.1154 *18	0.1685 *15	0.1594 *13	0.4162 *11	0.2052 *10	0.1560 * 9	0.1620 * 8	0.2123 * 7	0.3329 * 6
9	0.5021 *25	0.1863 *20	0.1203 *17	0.6355 *14	0.1052 *13	0.3561 *11	0.1961 *10	0.1535 * 9	0.1560 * 8	0.1940 * 7
10	0.3252 *28	0.3008 *22	0.8590 *18	0.2533 *16	0.2658 *14	0.6178 *12	0.2466 *11	0.1454 *10	0.1146 * 9	0.1131 * 8
11	0.2107 *31	0.4856 *24	0.1132 *20	0.1010 *18	0.6720 *15	0.1072 *14	0.3100 *12	0.1377 *11	0.8422 * 9	0.6592 * 8
12	0.1365 *34	0.7840 *26	0.4377 *22	0.4026 *19	0.1698 *17	0.1860 *15	0.3898 *13	0.1304 *12	0.6188 *10	0.3842 * 9
13	0.8842 *36	0.1266 *29	0.3124 *24	0.1605 *21	0.4292 *18	0.3227 *16	0.4901 *14	0.1235 *13	0.4547 *11	0.2239 *10
14	0.5728 *39	0.2044 *31	0.2230 *26	0.6397 *22	0.1084 *20	0.5598 *17	0.6161 *15	0.1170 *14	0.3340 *12	0.1305 *11
15	0.3710 *42	0.3299 *33	0.1592 *28	0.2550 *24	0.2742 *21	0.9712 *18	0.7746 *16	0.1108 *15	0.2454 *13	0.7607 *11

Table 6.02-1 (concluded)

n \ w_q	1.1	1.2	1.3	1.4	1.5	1.6	1.7	1.8	1.9	2.0
2	0.6046 * 1	0.4226 * 1	0.3066 * 1	0.2308 * 1	0.1804 * 1	0.1467 * 1	0.1243 * 1	0.1103 * 1	0.1024 * 1	1.0
3	0.2654 * 2	0.1479 * 2	0.8611 * 1	0.5234 * 1	0.3331 * 1	0.2236 * 1	0.1601 * 1	0.1241 * 1	0.1056 * 1	1.0
4	0.1230 * 3	0.5553 * 2	0.2634 * 2	0.1308 * 2	0.6802 * 1	0.3739 * 1	0.2213 * 1	0.1454 * 1	0.1102 * 1	1.0
5	0.5771 * 3	0.2125 * 3	0.8288 * 2	0.3398 * 2	0.1459 * 2	0.6610 * 1	0.3219 * 1	0.1762 * 1	0.1162 * 1	1.0
6	0.2713 * 4	0.8170 * 3	0.2631 * 3	0.8965 * 2	0.3206 * 2	0.1206 * 2	0.4853 * 1	0.2197 * 1	0.1239 * 1	1.0
7	0.1276 * 5	0.3145 * 4	0.8380 * 3	0.2379 * 3	0.7120 * 2	0.2239 * 2	0.7490 * 1	0.2802 * 1	0.1334 * 1	1.0
8	0.6006 * 5	0.1211 * 5	0.2671 * 4	0.6327 * 3	0.1588 * 3	0.4197 * 2	0.1174 * 2	0.3639 * 1	0.1450 * 1	1.0
9	0.2826 * 6	0.4666 * 5	0.8515 * 4	0.1684 * 4	0.3552 * 3	0.7907 * 2	0.1858 * 2	0.4790 * 1	0.1590 * 1	1.0
10	0.1329 * 7	0.1797 * 6	0.2715 * 5	0.4483 * 4	0.7950 * 3	0.1493 * 3	0.2959 * 2	0.6371 * 1	0.1756 * 1	1.0
11	0.6257 * 7	0.6923 * 6	0.8656 * 5	0.1194 * 5	0.1780 * 4	0.2825 * 3	0.4730 * 2	0.8542 * 1	0.1954 * 1	1.0
12	0.2944 * 8	0.2667 * 7	0.2760 * 6	0.3179 * 5	0.3986 * 4	0.5347 * 3	0.7581 * 2	0.1152 * 2	0.2187 * 1	1.0
13	0.1385 * 9	0.1027 * 8	0.8800 * 6	0.8465 * 5	0.8928 * 4	0.1012 * 4	0.1216 * 3	0.1560 * 2	0.2463 * 1	1.0
14	0.6518 * 9	0.3956 * 8	0.2806 * 7	0.2254 * 6	0.1999 * 5	0.1918 * 4	0.1954 * 3	0.2120 * 2	0.2787 * 1	1.0
15	0.3067 *10	0.1524 * 9	0.8947 * 7	0.6003 * 6	0.4478 * 5	0.3632 * 4	0.3142 * 3	0.2888 * 2	0.3167 * 1	1.0

*4 means "multiply by 10^4," and so on.

SOURCE: Quarterly Progress Report 4, Contract DA 36-039 SC-87398, SRI; reprinted in *IRE Trans. PGMTT* (see Ref. 36 by L. Young)

Equation (6.02-17) is accurate to better than about 1 percent for w_q less than 0.1.

The attenuation given by Eq. (6.02-11) for the Tchebyscheff quarter-wave transformer can also be determined from the graphs in Figs. 4.03-4 to 4.03-10 for the corresponding lumped-constant, low-pass, prototype filter [as already explained for the maximally flat case in connection with Eq. (6.02-15)] by using the same Eq. (6.02-15) except that now ω_1' is the Tchebyscheff (equal-ripple) band edge of the low-pass filter.

In the design of transformers as such, one is interested only in the pass-band performance for small R (usually less than 100), and this is expressed in terms of maximum VSWR rather than maximum attenuation. Tables 6.02-2 through 6.02-5 give directly the maximum VSWR inside the pass band for transformers with output-to-input impedance ratios, R, of less than 100, and fractional bandwidths, w_q, up to 120 percent, for transformers of n = 1, 2, 3, and 4 sections.[4] For all other cases, the maximum VSWR may be worked out from Table 6.02-1, using the relation

$$\mathcal{E}_r = \frac{(V_r - 1)^2}{4V_r} \qquad (6.02\text{-}18)$$

where V_r is the ripple VSWR (maximum VSWR in the pass band), together with Eqs. (6.02-8) and (6.02-16).

Example 1—Determine the minimum number of sections for a transformer of impedance ratio R = 100 to have a VSWR of less than 1.15 over a 100-percent bandwidth (w_q = 1.0).

From Eq. (6.02-18), for V_r = 1.15,

$$\mathcal{E}_r = 0.00489 \qquad (6.02\text{-}19)$$

and from Eq. (6.02-8), for R = 100,

$$\mathcal{E}_e = 24.5 \quad . \qquad (6.02\text{-}20)$$

Table 6.02-2

MAXIMUM VSWR FOR SINGLE-SECTION QUARTER-WAVE TRANSFORMERS

IMPEDANCE RATIO, R	BANDWIDTH, w_q					
	0.2	0.4	0.6	0.8	1.0	1.2
1.25	1.03	1.07	1.11	1.14	1.17	1.20
1.50	1.06	1.13	1.20	1.27	1.33	1.39
1.75	1.09	1.19	1.30	1.39	1.49	1.57
2.00	1.12	1.24	1.38	1.51	1.64	1.76
2.50	1.16	1.34	1.53	1.73	1.93	2.12
3.00	1.20	1.43	1.68	1.95	2.21	2.47
4.00	1.26	1.58	1.95	2.35	2.76	3.15
5.00	1.32	1.73	2.21	2.74	3.30	3.83
6.00	1.37	1.86	2.45	3.12	3.82	4.50
8.00	1.47	2.11	2.92	3.86	4.86	5.84
10.00	1.55	2.35	3.37	4.58	5.88	7.16
12.50	1.65	2.63	3.92	5.47	7.15	8.81
15.00	1.75	2.90	4.47	6.36	8.41	10.46
17.50	1.84	3.17	5.01	7.25	9.67	12.10
20.00	1.92	3.43	5.54	8.11	10.93	13.74
25.00	2.08	3.95	6.60	9.86	13.44	17.02
30.00	2.24	4.45	7.65	11.60	15.95	20.30
40.00	2.54	5.45	9.73	15.07	20.96	26.85
50.00	2.82	6.43	11.81	18.54	25.97	33.40
60.00	3 10	7.40	13.88	22.00	30.98	39.95
80 00	3.63	9.34	18.02	28.92	40.98	53.04
100.00	4.16	11.27	22.15	35.83	50.98	66.13

Table 6.02-3

MAXIMUM VSWR FOR TWO-SECTION QUARTER-WAVE TRANSFORMERS

IMPEDANCE RATIO, R	BANDWIDTH, w_q					
	0.2	0.4	0.6	0.8	1.0	1.2
1.25	1.00	1.01	1.03	1.05	1.08	1.11
1.50	1.01	1.02	1.05	1.09	1.15	1.22
1.75	1.01	1.03	1.07	1.13	1.21	1.32
2.00	1.01	1.04	1.08	1.16	1.27	1.41
2.50	1.01	1.05	1.12	1.22	1.37	1.58
3.00	1.01	1.06	1.14	1.27	1.47	1.74
4.00	1.02	1.08	1.19	1.37	1.64	2.04
5.00	1.02	1.09	1.23	1.45	1.80	2.33
6.00	1.03	1.11	1.26	1.53	1.95	2.60
8.00	1.03	1.13	1.33	1.67	2.23	3.13
10.00	1.04	1.15	1.38	1.80	2.50	3.64
12.50	1.04	1.18	1.45	1.95	2.82	4.27
15.00	1.05	1.20	1.51	2.09	3.13	4.89
17.50	1.05	1.22	1.57	2.23	3.44	5.50
20.00	1.05	1.24	1.62	2.36	3.74	6.11
25.00	1.06	1.27	1.72	2.62	4.33	7.32
30.00	1.07	1.30	1.82	2.87	4.91	8.52
40.00	1.08	1.36	2.00	3.36	6.06	10.91
50.00	1.09	1.41	2.17	3.83	7.20	13.29
60.00	1.10	1.46	2.34	4.30	8.33	15.66
80.00	1.12	1.55	2.65	5.21	10.57	20.41
100.00	1.13	1.63	2.96	6.11	12.81	25.15

SOURCE: *IRE Trans. PGMTT* (see Ref. 4 by L. Young)

Table 6.02-4

MAXIMUM VSWR FOR THREE-SECTION QUARTER-WAVE TRANSFORMERS

IMPEDANCE RATIO, R	BANDWIDTH, w_q					
	0.2	0.4	0.6	0.8	1.0	1.2
1.25	1.00	1.00	1.01	1.02	1.03	1.06
1.50	1.00	1.00	1.01	1.03	1.06	1.11
1.75	1.00	1.00	1.02	1.04	1.08	1.16
2.00	1.00	1.01	1.02	1.05	1.11	1.20
2.50	1.00	1.01	1.03	1.07	1.14	1.28
3.00	1.00	1.01	1.03	1.08	1.18	1.35
4.00	1.00	1.01	1.04	1.11	1.24	1.47
5.00	1.00	1.01	1.05	1.13	1.29	1.59
6.00	1.00	1.02	1.06	1.15	1.33	1.69
8.00	1.00	1.02	1.07	1.18	1.42	1.88
10.00	1.00	1.02	1.08	1.21	1.49	2.06
12.50	1.00	1.03	1.09	1.25	1.58	2.28
15.00	1.00	1.03	1.11	1.28	1.66	2.48
17.50	1.00	1.03	1.12	1.31	1.73	2.68
20.00	1.00	1.03	1.12	1.34	1.81	2.87
25.00	1.00	1.04	1.14	1.39	1.95	3.25
30.00	1.01	1.04	1.16	1.43	2.08	3.62
40.00	1.01	1.05	1.19	1.52	2.33	4.34
50.00	1.01	1.06	1.21	1.60	2.57	5.05
60.00	1.01	1.06	1.23	1.68	2.80	5.75
80.00	1.01	1.07	1.28	1.82	3.25	7.13
100.00	1.01	1.08	1.31	1.95	3.69	8.51

SOURCE: *IRE Trans. PGMTT* (see Ref. 4 by L. Young)

Table 6.02-5

MAXIMUM VSWR FOR FOUR-SECTION QUARTER-WAVE TRANSFORMERS

IMPEDANCE RATIO, R	BANDWIDTH, w_q					
	0.2	0.4	0.6	0.8	1.0	1.2
1.25	1.00	1.00	1.00	1.00	1.01	1.03
1.50	1.00	1.00	1.00	1.01	1.02	1.06
1.75	1.00	1.00	1.00	1.01	1.03	1.08
2.00	1.00	1.00	1.00	1.02	1.04	1.10
2.50	1.00	1.00	1.01	1.02	1.06	1.14
3.00	1.00	1.00	1.01	1.03	1.07	1.17
4.00	1.00	1.00	1.01	1.03	1.09	1.22
5.00	1.00	1.00	1.01	1.04	1.11	1.27
6.00	1.00	1.00	1.01	1.05	1.13	1.31
8.00	1.00	1.00	1.02	1.06	1.16	1.39
10.00	1.00	1.00	1.02	1.07	1.18	1.46
12.50	1.00	1.00	1.02	1.08	1.21	1.54
15.00	1.00	1.00	1.02	1.08	1.24	1.62
17.50	1.00	1.00	1.03	1.09	1.26	1.69
20.00	1.00	1.01	1.03	1.10	1.28	1.76
25.00	1.00	1.01	1.03	1.11	1.33	1.88
30.00	1.00	1.01	1.04	1.13	1.36	2.01
40.00	1.00	1.01	1.04	1.15	1.43	2.24
50.00	1.00	1.01	1.05	1.17	1.50	2.46
60.00	1.00	1.01	1.05	1.18	1.56	2.67
80.00	1.00	1.01	1.06	1.22	1.67	3.08
100.00	1.00	1.01	1.07	1.25	1.78	3.48

SOURCE: *IRE Trans. PGMTT* (see Ref. 4 by L. Young)

Hence, Eq. (6.02-16) gives

$$M(n,w_q) = T_n^2(1/\mu_0) = \frac{\mathcal{P}_a}{\mathcal{P}_r} = 0.501 \times 10^4 \qquad (6.02\text{-}21)$$

From Table 6.02-1, in the column $w_q = 1.0$, it is seen that this value of $M(n,w_q)$ falls between $n = 5$ and $n = 6$. Therefore, the transformer must have at least six sections. (See also Example 1 of Sec. 6.07)

SEC. 6.03, THE PERFORMANCE OF HOMOGENEOUS HALF-WAVE FILTERS

The half-wave filter was defined in Sec. 6.01. It is shown in Fig. 6.03-1. Its fractional bandwidth w_h is defined [compare Eq. (6.02-1)] by

$$w_h = 2\left(\frac{\lambda_{g1} - \lambda_{g2}}{\lambda_{g1} + \lambda_{g2}}\right) \qquad (6.03\text{-}1)$$

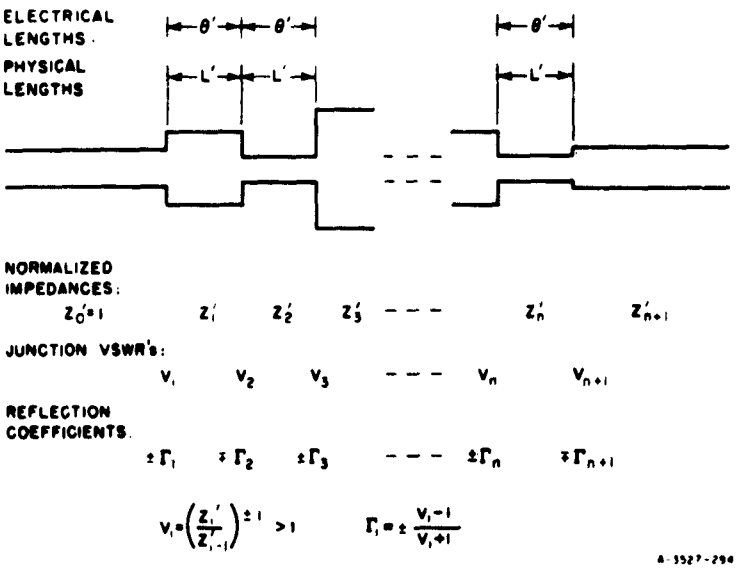

SOURCE: Quarterly Progress Report 4, Contract DA 36-039 SC-87398, SRI; reprinted in *IRE Trans. PGMTT* (See Ref. 36 by L. Young)

FIG. 6.03-1 HALF-WAVE FILTER NOTATION

and the length L' of each section [compare Eq. (6.02-2)] is

$$L' = \frac{\lambda_{g1}\lambda_{g2}}{\lambda_{g1} + \lambda_{g2}} = \frac{\lambda_{g0}}{2} \qquad (6.03.2)$$

where λ_{g1} and λ_{g2} are the longest and shortest wavelengths, respectively, in the pass band *of the half-wave filter*. This can be simplified for non-dispersive lines by dropping the suffix "g," as in Eqs. (6.02-3) and (6.02-4). A half-wave filter *with the same junction VSWRs* V_i (Figs. 6.02-1 and 6.03-1) as a quarter-wave transformer of bandwidth w_q has a bandwidth

$$w_h = \frac{w_q}{2} \qquad (6.03-3)$$

since its sections are twice as long and therefore twice as frequency-sensitive. The performance of a half-wave filter generally can be determined directly from the performance of the quarter-wave transformer with the same number of sections, n, and junction VSWRs V_i, by a linear scaling of the frequency axis by a scale-factor of 2. Compare Figs. 6.03-2 and 6.02-2. The quarter-wave transformer with the same n and V_i as the half-wave filter is herein called its *prototype* circuit.

In the case of the half-wave filter, R is the maximum VSWR, which is no longer the output-to-input impedance ratio, as for the quarter-wave transformer, but may generally be defined as the product of the junction VSWRs:

$$R = V_1 V_2 \cdots V_{n+1} \qquad (6.03-4)$$

This definition applies to both the quarter-wave transformer and the half-wave filter, as well as to filters whose prototype circuits they are. (In the latter case, the V_i are the individual discontinuity VSWRs as in Chapter 9.)

The equations corresponding to Eqs. (6.02-6) through (6.02-18) will now be restated, wherever they differ, for the half-wave filter.

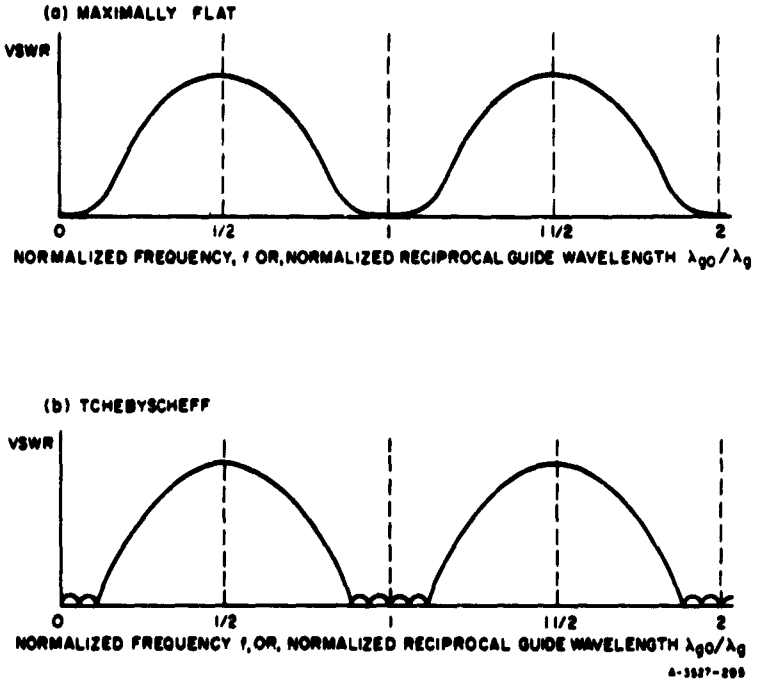

SOURCE: Quarterly Progress Report 4, Contract DA 36-039 SC-87398, SRI; reprinted in *IRE Trans. PGMTT* (See Ref. 36 by L. Young)

FIG. 6.03-2 HALF-WAVE FILTER CHARACTERISTICS

For the maximally flat half-wave filter of n sections,

$$\mathcal{E} = \frac{(R-1)^2}{4R} \sin^{2n}\theta' = \mathcal{E}_c \sin^{2n}\theta' \qquad (6.03\text{-}5)$$

where

$$\theta' = \pi \frac{\lambda_{g0}}{\lambda_g} = 2\theta \qquad (6.03\text{-}6)$$

instead of Eq. (6.02-7), so that $\theta' = \pi$ (instead of $\theta = \pi/2$) at band center. The 3-db bandwidth of the maximally flat half-wave filter is

$$w_{h,3db} = \frac{w_{g,3db}}{2} \qquad (6.03\text{-}7)$$

and the bandwidth between the points of x-db attenuation is

$$w_{h,x\,db} = \frac{w_{q,x\,db}}{2} \tag{6.03-8}$$

which can be obtained from Eqs. (6.02-9) and (6.02-10).

For the Tchebyscheff half-wave filter,

$$\left.\begin{aligned} \mathcal{E} &= \frac{(R-1)^2}{4R}\,\frac{T_n^2(\sin\theta'/\mu_0)}{T_n^2(1/\mu_0)} \\ &= \mathcal{E}_r T_n^2(\sin\theta'/\mu_0) \end{aligned}\right\} \tag{6.03-9}$$

where

$$\mu_0 = \sin\left(\frac{\pi w_q}{4}\right) = \sin\left(\frac{\pi w_h}{2}\right) . \tag{6.03-10}$$

The quantities $\mathcal{E}_a$, $\mathcal{E}_r$, and the maximum transducer loss ratio are still given by Eqs. (6.02-8), (6.02-13), and (6.02-14). For maximally flat half-wave filters, the graph of Fig. 6.02-3 can again be used, but with the right-hand scale.

The lumped-constant, low-pass, prototype filter graphs in Figs. 4.03-2 and 4.03-4 to 4.03-10 may again be used for both the maximally flat and Tchebyscheff half-wave filters by substituting

$$\frac{\omega'}{\omega_1'} = \frac{\sin\theta'}{\mu_0} \tag{6.03-11}$$

for Eq. (6.02-15), where μ_0 is given by Eq. (6.03-10).

Equation (6.02-16) and Table 6.02-1 still apply, using Eq. (6.03-3) to convert between w_q and w_h.

Example 1—Find R for a half-wave filter of six sections having a Tchebyscheff fractional bandwidth of 60 percent with a pass-band ripple of 1 db.

Here, $w_h = 0.6$, or $w_q = 1.2$. From Eq. (6.02-13),

$$\text{antilog } (0.1) - 1 = \frac{(R-1)^2}{4R} \frac{1}{T_6^2(1/\mu_0)} \qquad (6.03\text{-}12)$$

and from Table 6.02-1 for $w_q = 1.2$,

$$1.259 - 1 = \frac{(R-1)^2}{4R} \frac{1}{817} .$$

Hence, $R = 850$.

SEC. 6.04, EXACT TCHEBYSCHEFF AND MAXIMALLY FLAT SOLUTIONS FOR UP TO FOUR SECTIONS

Enough exact solutions will be presented to permit the solution of all intermediate cases by interpolation for Tchebyscheff and maximally flat transformers and filters having up to four sections.

The solutions were obtained from Collin's formulas.[2] With the notation of Fig. 6.02-1, they can be reduced to the expressions given below. The equations are first given for maximally flat transformers and then for Tchebyscheff transformers.

For maximally flat transformers with $n = 2$, 3, and 4:

$\underline{n = 2}$

$$V_1 = R^{1/4}$$
$$V_2 = R^{1/2} \qquad (6.04\text{-}1)$$

$\underline{n = 3}$

$$V_1^2 + 2R^{1/2}V_1 - \frac{2R^{1/2}}{V_1} - \frac{R}{V_1^2} = 0$$
$$V_2 = R^{1/2}/V_1 \qquad (6.04\text{-}2)$$

$\underline{n = 4}$

$$V_1 = A_1 R^{1/8}$$
$$V_2 = R^{1/4}$$
$$V_3 = R^{1/4}/A_1^2 \qquad (6.04\text{-}3)$$

where

$$\left(\frac{1}{A_1^2} - A_1^2\right) = 2\left(\frac{R^{1/4} - 1}{R^{1/4} + 1}\right) . \qquad \text{(6.04-3) (contd.)}$$

For Tchebyscheff Transformers with $n = 2$, 3, and 4:

$\underline{n = 2}$

$$V_1^2 = \sqrt{C^2 + R} + C$$

$$V_2 = R/V_1^2$$

where

$$C = \frac{(R - 1)\mu_0^2}{2(2 - \mu_0^2)}$$

and μ_0 is given by Eq. (6.01-12). (6.04-4)

$\underline{n = 3}$

$$V_1^2 + 2\sqrt{R}\, V_1 - \frac{2\sqrt{R}}{V_1} - \frac{R}{V_1^2} = \frac{3\mu_0^2(R - 1)}{4 - 3\mu_0^2}$$

$$V_2 = R^{1/2}/V_1 \qquad (6.04-5)$$

$\underline{n = 4}$

$$V_1 = \left\{R\left[B + \left(B^2 + \frac{A^2}{R}\right)^{1/2}\right]\right\}^{1/2}$$

$$V_2 = \frac{1}{A}$$

$$V_3 = \frac{A^2 R}{V_1^2} \qquad (6.04-6)$$

where

$$A^2 = \frac{1 - 1/R}{2t_1t_2} + \left[\frac{(1 - 1/R)^2}{4t_1^2t_2^2} + \frac{1}{R}\right]^{1/2}$$

$$B = \frac{1}{2}\left(\frac{A}{A + 1}\right)^2 \left[(t_1 + t_2)\left(A^2 - \frac{1}{A^2R}\right) - 2A + \frac{2}{AR}\right]$$

and

$$t_1 = \frac{2\sqrt{2}}{(\sqrt{2} + 1)\mu_0^2} - 1$$

$$t_2 = \frac{2\sqrt{2}}{(\sqrt{2} - 1)\mu_0^2} - 1$$

(6.04-6) (contd.)

A difference between typical quarter-wave transformers, and half-wave filters suitable for use as prototypes for microwave filters, is that, for the former, R is relatively small (usually less than 100) and only the pass-band performance is of interest; for the latter, R is relatively large, and the performance in both pass band and stop band is important. Two sets of tables are presented for n = 2, 3, and 4. The first set (Tables 6.04-1 to 6.04-4) cover R from 1 to 100. Since these tables are most likely to be used in the design of transformers, the impedances Z_1 and Z_2 (Fig. 6.02-1) are tabulated; the remaining impedances are obtained from the symmetry relation, which can be written (for any n)

$$Z_iZ_{n+1-i} = R \qquad (6.04\text{-}7)$$

(where the Z_i are normalized so that $Z_0 = 1$), or

$$V_i = V_{n+2-i} \qquad (6.04\text{-}8)$$

$$\Gamma_i = \pm\Gamma_{n+2-i} \ . \qquad (6.04\text{-}9)$$

Table 6.04-1

Z_1 FOR TWO-SECTION QUARTER-WAVE TRANSFORMERS*

(For $w_q = 2.0$, $Z_1 = Z_2 = \sqrt{R}$)

IMPEDANCE RATIO, R	BANDWIDTH, $\frac{\Delta f}{f_0}$									
	0.0	0.2	0.4	0.6	0.8	1.0	1.2	1.4	1.6	1.8
1.00	1.00000	1.00000	1.00000	1.00000	1.00000	1.00000	1.00000	1.000	1.000	1.000
1.25	1.05737	1.05810	1.06034	1.06418	1.06979	1.07725	1.08650	1.096	1.107	1.115
1.50	1.10668	1.10808	1.11236	1.11973	1.13051	1.14495	1.16292	1.183	1.203	1.218
1.75	1.15016	1.15218	1.15837	1.16904	1.18469	1.20572	1.23199	1.261	1.291	1.314
2.00	1.18921	1.19181	1.19979	1.21360	1.23388	1.26122	1.29545	1.334	1.373	1.402
2.50	1.25743	1.26113	1.27247	1.29215	1.32117	1.36043	1.40979	1.466	1.522	1.564
3.00	1.31607	1.32079	1.33526	1.36042	1.39764	1.44816	1.51179	1.584	1.656	1.711
4.00	1.41421	1.42080	1.44105	1.47640	1.52892	1.60049	1.69074	1.793	1.894	1.971
5.00	1.49535	1.50366	1.52925	1.57405	1.64084	1.73205	1.84701	1.977	2.105	2.200
6.00	1.56508	1.57501	1.60563	1.65937	1.73970	1.84951	1.98768	2.143	2.295	2.407
8.00	1.68179	1.69473	1.73475	1.80527	1.91107	2.05579	2.23693	2.439	2.633	2.775
10.00	1.77828	1.79402	1.84281	1.92906	2.05879	2.23607	2.45663	2.700	2.931	3.100
12.50	1.88030	1.89934	1.95846	2.06334	2.22139	2.43686	2.70282	2.994	3.266	3.463
15.00	1.96799	1.99014	2.05909	2.18171	2.36672	2.61818	2.92611	3.259	3.568	3.791
17.50	2.04531	2.07045	2.14880	2.28850	2.49938	2.78500	3.13212	3.505	3.847	4.093
20.00	2.11474	2.14275	2.23019	2.38640	2.62224	2.94048	3.32447	3.733	4.107	4.374
25.00	2.23607	2.26955	2.37439	2.56229	2.84580	3.22539	3.67741	4.152	4.583	4.888
30.00	2.34035	2.37903	2.50046	2.71863	3.04734	3.48399	3.99798	4.533	5.013	5.353
40.00	2.51487	2.56334	2.71614	2.99167	3.40499	3.94578	4.57017	5.210	5.779	6.179
50.00	2.65915	2.71681	2.89921	3.22888	3.72073	4.35536	5.07697	5.808	6.454	6.907
60.00	2.78316	2.84956	3.06024	3.44157	4.00711	4.72769	5.53691	6.350	7.065	7.565
80.00	2.99070	3.07359	3.33788	3.81681	4.51833	5.39296	6.35680	7.314	8.150	8.733
100.00	3.16228	3.26067	3.57565	4.14625	4.97177	5.98279	7.08181	8.164	9.107	9.763

* Z_2 is given by

$$Z_2 = R/Z_1$$

SOURCE: *IRE Trans. PGMTT* (see Ref. 4 by I. Young)

Table 6.04-2

Z_1 FOR THREE-SECTION QUARTER-WAVE TRANSFORMERS*

(For $w_q = 2.0$, $Z_1 = Z_2 = Z_3 = \sqrt{R}$)

IMPEDANCE RATIO, R	BANDWIDTH, w_q									
	0.0	0.2	0.4	0.6	0.8	1.0	1.2	1.4	1.6	1.8
1.00	1.00000	1.00000	1.00000	1.00000	1.00000	1.00000	1.00000	1.000	1.000	1.000
1.25	1.02829	1.02883	1.03051	1.03356	1.03839	1.04567	1.05636	1.071	1.091	1.109
1.50	1.05202	1.05303	1.05616	1.06186	1.07092	1.08465	1.10495	1.134	1.170	1.207
1.75	1.07255	1.07396	1.07839	1.08644	1.09933	1.11892	1.14805	1.189	1.243	1.298
2.00	1.09068	1.09247	1.09808	1.10830	1.12466	1.14966	1.18702	1.240	1.310	1.382
2.50	1.12177	1.12422	1.13192	1.14600	1.16862	1.20344	1.25594	1.332	1.434	1.535
3.00	1.14793	1.15096	1.16050	1.17799	1.20621	1.24988	1.31621	1.413	1.543	1.673
4.00	1.19071	1.19474	1.20746	1.23087	1.26891	1.32837	1.41972	1.556	1.736	1.917
5.00	1.22524	1.23013	1.24557	1.27412	1.32078	1.39428	1.50824	1.679	1.907	2.133
6.00	1.25439	1.26003	1.27790	1.31105	1.36551	1.45187	1.58676	1.790	2.060	2.329
8.00	1.30219	1.30916	1.33128	1.37253	1.44091	1.55057	1.72383	1.985	2.333	2.677
10.00	1.34089	1.34900	1.37482	1.42320	1.50397	1.63471	1.84304	2.159	2.577	2.984
12.50	1.38110	1.39048	1.42039	1.47674	1.57157	1.72651	1.97543	2.354	2.849	3.329
15.00	1.41512	1.42564	1.45924	1.52282	1.63055	1.80797	2.09480	2.532	3.098	3.640
17.50	1.44475	1.45630	1.49328	1.56355	1.68331	1.88193	2.20457	2.698	3.325	3.924
20.00	1.47108	1.48359	1.52371	1.60023	1.73135	1.95013	2.30687	2.848	3.541	4.191
25.00	1.51650	1.53075	1.57661	1.66464	1.81693	2.07364	2.49446	3.129	3.934	4.678
30.00	1.55498	1.57080	1.62184	1.72040	1.89229	2.18447	2.66499	3.384	4.288	5.124
40.00	1.61832	1.63691	1.69719	1.81471	2.02249	2.38028	2.97034	3.845	4.920	5.909
50.00	1.66978	1.69080	1.75924	1.89378	2.13434	2.55256	3.24219	4.249	5.480	6.600
60.00	1.71340	1.73661	1.81246	1.96266	2.23376	2.70860	3.49018	4.616	5.987	7.226
80.00	1.78522	1.81232	1.90144	2.08004	2.40750	2.98700	3.93524	5.286	6.896	8.338
100.00	1.84359	1.87411	1.97500	2.17928	2.55856	3.23420	4.33178	5.870	7.700	9.318

* Z_2 and Z_3 are given by

$$Z_2 = \sqrt{R}$$

$$Z_3 = R/Z_1$$

SOURCE: *IRE Trans. PGMTT* (see Ref. 4 by L. Young)

Table 6.04-3

Z_1 FOR FOUR-SECTION QUARTER-WAVE TRANSFORMERS*

(For $w_q = 2.0$, $Z_1 = Z_2 = Z_3 = Z_4 = \sqrt{R}$)

IMPEDANCE RATIO, R	BANDWIDTH, w_q									
	0.0	0.2	0.4	0.6	0.8	1.0	1.2	1.4	1.6	1.8
1.00	1.00000	1.00000	1.00000	1.00000	1.00000	1.00000	1.00000	1.000	1.000	1.000
1.25	1.01405	1.01440	1.01553	1.01761	1.02106	1.02662	1.03560	1.050	1.073	1.102
1.50	1.02570	1.02635	1.02842	1.03227	1.03866	1.04898	1.06576	1.903	1.137	1.193
1.75	1.03568	1.03659	1.03949	1.04488	1.05385	1.06838	1.09214	1.131	1.194	1.277
2.00	1.04441	1.04558	1.04921	1.05598	1.06726	1.08559	1.11571	1.165	1.247	1.354
2.50	1.05933	1.06088	1.06577	1.07494	1.09026	1.11531	1.15681	1.226	1.342	1.495
3.00	1.07176	1.07364	1.07963	1.09086	1.10967	1.14059	1.19218	1.280	1.426	1.622
4.00	1.09190	1.09435	1.10216	1.11685	1.14159	1.18259	1.25182	1.371	1.574	1.847
5.00	1.10801	1.11093	1.12026	1.13784	1.16759	1.21721	1.30184	1.450	1.703	2.045
6.00	1.12153	1.12486	1.13549	1.15559	1.18974	1.24702	1.34555	1.520	1.820	2.225
8.00	1.14356	1.14758	1.16043	1.18482	1.22654	1.29722	1.42054	1.642	2.028	2.545
10.00	1.16129	1.16588	1.18060	1.20863	1.25683	1.33920	1.48458	1.749	2.213	2.828
12.50	1.17961	1.18483	1.20156	1.23353	1.28883	1.38421	1.55461	1.869	2.420	3.146
15.00	1.19506	1.20082	1.21931	1.25475	1.31638	1.42350	1.61690	1.977	2.609	3.433
17.50	1.20847	1.21471	1.23478	1.27335	1.34074	1.45869	1.67357	2.077	2.784	3.699
20.00	1.22035	1.22703	1.24854	1.28998	1.36269	1.49074	1.72593	2.170	2.948	3.946
25.00	1.24078	1.24824	1.27232	1.31891	1.40125	1.54791	1.82099	2.342	3.249	4.399
30.00	1.25803	1.26618	1.29251	1.34367	1.43467	1.59831	1.90654	2.498	3.524	4.809
40.00	1.28632	1.29564	1.32587	1.38498	1.49127	1.68552	2.05820	2.780	4.015	5.538
50.00	1.30920	1.31953	1.35308	1.41905	1.53879	1.76055	2.19214	3.031	4.451	6.182
60.00	1.32853	1.33974	1.37624	1.44833	1.58022	1.82732	2.31378	3.261	4.848	6.765
80.00	1.36025	1.37297	1.41455	1.49736	1.65091	1.94412	2.53156	3.674	5.556	7.801
100.00	1.38591	1.39992	1.44587	1.53798	1.71073	2.04579	2.72559	4.043	6.183	8.715

* See Footnote, Table 6.04-4

SOURCE: *IRE Trans. PGMTT* (see Ref. 4 by L. Young)

Table 6.04-4

Z_2 FOR FOUR-SECTION QUARTER-WAVE TRANSFORMERS *

(For $w_q = 2.0$, $Z_1 = Z_2 = Z_3 = Z_4 = \sqrt{R}$)

IMPEDANCE RATIO, R	BANDWIDTH, w_q									
	0.0	0.2	0.4	0.6	0.8	1.0	1.2	1.4	1.6	1.8
1.00	1.00000	1.00000	1.00000	1.00000	1.00000	1.00000	1.00000	1.000	1.000	1.000
1.25	1.07223	1.07260	1.07371	1.07559	1.07830	1.08195	1.08683	1.093	1.102	1.112
1.50	1.13512	1.13584	1.13799	1.14162	1.14685	1.15394	1.16342	1.176	1.193	1.214
1.75	1.19120	1.19224	1.19537	1.20065	1.20827	1.21861	1.23248	1.251	1.277	1.307
2.00	1.24206	1.24340	1.24745	1.25431	1.26420	1.27764	1.29572	1.320	1.354	1.393
2.50	1.33204	1.33396	1.33974	1.34954	1.36370	1.38300	1.40907	1 445	1.494	1.551
3.00	1.41051	1.41296	1.42036	1.43290	1.45105	1.47583	1.50943	1.556	1.620	1.694
4.00	1.54417	1.54760	1.55795	1.57553	1.60102	1.63596	1.68360	1.750	1.842	1.947
5.00	1.65686	1.66118	1.67423	1.69642	1.72864	1.77292	1.83358	1.918	2.037	2.170
6.00	1.75529	1.76043	1.77600	1.80248	1.84098	1.89401	1.96694	2.069	2.212	2.371
8.00	1.92323	1.92990	1.95009	1.98446	2.03453	2.10376	2.19954	2.335	2.524	2.730
10.00	2.06509	2.07315	2.09756	2.13915	2.19984	2.28397	2.40096	2.568	2.798	3.046
12.50	2.21803	2.22770	2.25698	2.30691	2.37988	2.48134	2.62317	2.826	3.105	3.399
15.00	2.35186	2.36303	2.39686	2.45455	2.53898	2.65667	2.82190	3.059	3.383	3.719
17.50	2.47169	2.48426	2.52237	2.58739	2.68264	2.81570	3.00321	3.273	3.639	4.014
20.00	2.58072	2.59463	2.63681	2.70880	2.81433	2.96208	3.17095	3.472	3.878	4.288
25.00	2.77447	2.79089	2.84069	2.92575	3.05065	3.22609	3.47548	3.836	4.315	4.789
30.00	2.94423	2.96299	3.01989	3.11712	3.26008	3.46148	3.74905	4.165	4.711	5.243
40.00	3.23492	3.25798	3.32792	3.44754	3.62377	3.87328	4.23198	4.750	5.415	6.049
50.00	3.48136	3.50835	3.59021	3.73029	3.93704	4.23091	4.65555	5.266	6.038	6.759
60.00	3.69752	3.72816	3.82111	3.98025	4.21547	4.55096	5.03760	5.734	6.601	7.401
80.00	4.06810	4.10544	4.21877	4.41293	4.70063	5.11329	5.71502	6.568	7.603	8.543
100.00	4.38263	4.42610	4.55802	4.78420	5.12003	5.60394	6.31175	7.304	8.487	9.548

* Z_1 is given in Table 6.04-3, Z_3 and Z_4 are given by

$$Z_3 = R/Z_2$$

$$Z_4 = R/Z_1$$

SOURCE: *IRE Trans. PGMTT* (see Ref. 4 by L. Young)

The characteristic impedances, Z_i, are obtained from the junction VSWRs, V_i, using Fig. 6.02-1 for the quarter-wave transformer and Fig. 6.03-1 for the half-wave filter. It is convenient to normalize with respect to Z_0, and as a result, the values of Z_1, Z_2, ... given in the tables are for $Z_0 = 1$. The tables giving the Z_i all refer to quarter-wave transformers. To obtain the Z_i' of half-wave filters, obtain the V_i from Fig. 6.02-1, and use these V_i to obtain the Z_i' from Fig. 6.03-1. This gives the half-wave filter with the same attenuation characteristics as the quarter-wave transformer, but having a bandwidth $w_h = \frac{1}{2}w_q$. (Compare Figs. 6.02-2 and 6.03-2.)

The solutions of Eqs. (6.04-1) to (6.04-6) for larger values of R are presented in the second set of tables (Tables 6.04-5 to 6.04-8). They give the values of V_2 and V_3 for $n = 2$, 3, and 4. The remaining values of V are obtained from Eq. (6.04-8) and

$$V_1 V_2 \ldots V_{n+1} = R \qquad (6.04\text{-}10)$$

which, for even n, reduces to

$$(V_1 V_2 \ldots V_{n/2})^2 V_{(n/2)+1} = R \qquad (6.04\text{-}11)$$

and for odd n, reduces to

$$(V_1 V_2 \ldots V_{(n+1)/2})^2 = R \quad . \qquad (6.04\text{-}12)$$

Equations (6.04-7) to (6.04-12) hold for all values of n.

Tables 6.04-5 to 6.04-8 give the step VSWRs for R from 10 to ∞ in multiples of 10. Note that for Tchebyscheff transformers V_2, V_3, ..., V_n and $V_1/(R)^{\frac{1}{2}} = V_{n+1}/(R)^{\frac{1}{2}}$ tend toward finite limits as R tends toward infinity, as can be seen from Eqs. 6.04-1 to 6.04-6 for n up to 4, by letting R tend toward infinity. (For limiting values as R tends toward infinity and $n > 4$, see Sec. 6.10.) The tables give fractional bandwidths, w_q, from 0 to 2.00 in steps of 0.20. [The greatest possible bandwidth is $w_q = 2.00$, by definition, as can be seen from Eq. (6.02-1).]

Table 6.04-5

V_2 FOR TWO-SECTION QUARTER-WAVE TRANSFORMERS

m_q \ Log R	0	1	2	3	4	5	6	7	8	9	10	∞
0	1.0	3.1622	10.0000	31.6227	100.0000	316.2278	•	•	•	•	•	∞
0.2	1.0	3.1070	9.4056	26.0349	55.6931	76.0577	80.2075	80.6742	80.7215	80.7263	80.7267	80.7267
0.4	1.0	2.9446	7.8214	15.2942	19.2101	19.8657	19.9363	19.9434	19.9441	19.9442	19.9443	19.9443
0.6	1.0	2.6872	5.8168	8.1357	8.6395	8.6971	8.7030	8.7036	8.7037	8.7037	8.7037	8.7037
0.8	1.0	2.3592	4.0455	4.6882	4.7783	4.7878	4.7887	4.7888	4.7889	4.7889	4.7889	4.7889
1.0	1.0	2.0000	2.7937	2.9763	2.9976	2.9997	3.0000	3.0000	3.0000	3.0000	3.0000	3.0000
1.2	1.0	1.6569	1.9939	2.0491	2.0550	2.0556	2.0557	2.0557	2.0557	2.0557	2.0557	2.0557
1.4	1.0	1.3708	1.5000	1.5172	1.5190	1.5192	1.5192	1.5192	1.5192	1.5192	1.5192	1.5192
1.6	1.0	1.1635	1.2055	1.2105	1.2110	1.2111	1.2111	1.2111	1.2111	1.2111	1.2111	1.2111
1.8	1.0	1.0405	1.0491	1.0500	1.0501	1.0502	1.0502	1.0502	1.0502	1.0502	1.0502	1.0502
2.0	1.0	1.0000	1.0000	1.0000	1.0000	1.0000	1.0000	1.0000	1.0000	1.0000	1.0000	1.0000

SOURCE: Quarterly Progress Report 4, Contract DA 36-039 SC-87398, SRI; reprinted in *IRE Trans. PGMTT* (see Ref. 36 by L. Young)

Table 6.04-6

V_2 FOR THREE-SECTION QUARTER-WAVE TRANSFORMERS

m_q \ Log R	0	1	2	3	4	5	6	7	8	9	10	∞
0	1.0	2.358	5.424	12.14	26.66	57.99	125.50	270.94	584.31	•	•	∞
0.2	1.0	2.344	5.337	11.68	24.46	47.69	79.82	101.7501	106.0067	107.3998	107.4618	107.4679
0.4	1.0	2.300	5.064	10.30	18.10	24.4154	26.1709	26.3912	26.4138	26.4161	26.4163	26.4164
0.6	1.0	2.222	4.5885	8.1000	10.6644	11.3276	11.4081	11.4163	11.4171	11.4172	11.4173	11.4173
0.8	1.0	2.103	3.9083	5.5671	6.1014	6.1728	6.1802	6.1809	6.1810	6.1810	6.1810	6.1810
1.0	1.0	1.9344	3.0919	3.6649	3.7630	3.7736	3.7747	3.7748	3.7748	3.7748	3.7748	3.7748
1.2	1.0	1.7158	2.3085	2.4686	2.4884	2.4904	2.4906	2.4907	2.4907	2.4907	2.4907	2.4907
1.4	1.0	1.4647	1.7022	1.7428	1.7472	1.7477	1.7477	1.7477	1.7477	1.7477	1.7477	1.7477
1.6	1.0	1.2269	1.2995	1.3089	1.3099	1.3100	1.3101	1.3101	1.3101	1.3101	1.3101	1.3101
1.8	1.0	1.0596	1.0731	1.0746	1.0747	1.0748	1.0748	1.0748	1.0748	1.0748	1.0748	1.0748
2.0	1.0	1.0000	1.0000	1.0000	1.0000	1.0000	1.0000	1.0000	1.0000	1.0000	1.0000	1.0000

SOURCE: Quarterly Progress Report 4, Contract DA 36-039 SC-87398, SRI; reprinted in *IRE Trans. PGMTT* (see Ref. 36 by L. Young)

Table 6.04-7

V_2 FOR FOUR-SECTION QUARTER-WAVE TRANSFORMERS

w_q \ Log R	0	1	2	3	4	5	6	7	8	9	10	∞
0	1.0	1.7782	3.1622	5.6234	10.0000	17.7827	31.6227	56.2341	100.0000	177.8279	316.2277	∞
0.2	1.0	1.7781	3.1616	5.6200	9.9808	17.6752	31.0220	52.9321	82.9105	106.5498	113.2186	114.1604
0.4	1.0	1.7766	3.1524	5.5677	9.6904	16.1089	23.4997	27.3837	28.0996	28.1787	28.1367	28.1877
0.6	1.0	1.7698	3.1107	5.3364	8.4944	11.2447	12.1344	12.2543	12.2667	12.2680	12.2681	12.2682
0.8	1.0	1.7503	2.9928	4.7320	6.1880	6.6331	6.6915	6.6975	6.6981	6.6982	6.6982	6.6982
1.0	1.0	1.7054	2.7392	3.7126	4.0665	4.1171	4.1225	4.1230	4.1230	4.1231	4.1231	4.1231
1.2	1.0	1.6172	2.3157	2.6617	2.7224	2.7290	2.7297	2.7298	2.7298	2.7298	2.7298	2.7298
1.4	1.0	1.4676	1.8065	1.8903	1.9004	1.9014	1.9016	1.9016	1.9016	1.9016	1.9016	1.9016
1.6	1.0	1.2645	1.3725	1.3886	1.3904	1.3905	1.3906	1.3906	1.3906	1.3906	1.3906	1.3906
1.8	1.0	1.0768	1.0956	1.0978	1.9080	1.0980	1.0980	1.0980	1.0980	1.0980	1.0980	1.0980
2.0	1.0	1.0000	1.0000	1.0000	1.0000	1.0000	1.0000	1.0000	1.0000	1.0000	1.0000	1.0000

SOURCE: Quarterly Progress Report 4, Contract DA 36-039 SC-87398, SRI; reprinted in *IRE Trans. PGMTT* (see Ref. 36 by L. Young)

Table 6.04-8

V_3 FOR FOUR-SECTION QUARTER-WAVE TRANSFORMERS

w_q \ Log R	0	1	2	3	4	5	6	7	8	9	10	∞
0	1.0	2.3448	5.2063	10.7833	21.1024	39.7366	73.0562	132.4190	238.0478	425.9232	760.0403	∞
0.2	1.0	2.3266	5.1045	10.3536	19.5265	34.4781	56.7950	85.7685	114.9996	132.4555	136.7239	137.7307
0.4	1.0	2.2728	4.8133	9.1941	15.6771	23.5245	30.2006	33.0054	33.4806	33.5323	33.5375	33.5382
0.6	1.0	2.1853	4.3689	7.6018	11.1871	13.5788	14.2420	14.3279	14.3367	14.3376	14.3377	14.3378
0.8	1.0	2.0664	3.8146	5.8599	7.2224	7.5865	7.6326	7.6374	7.6379	7.6380	7.6380	7.6380
1.0	1.0	1.9169	3.1842	4.1904	4.5121	4.5564	4.5610	4.5615	4.5615	4.5615	4.5615	4.5615
1.2	1.0	1.7347	2.5101	2.8558	2.9136	2.9199	2.9205	2.9206	2.9206	2.9206	2.9206	2.9206
1.4	1.0	1.5163	1.8739	1.9587	1.9688	1.9699	1.9700	1.9700	1.9700	1.9700	1.9700	1.9700
1.6	1.0	1.2767	1.3880	1.4045	1.4062	1.4064	1.4064	1.4064	1.4064	1.4064	1.4064	1.4064
1.8	1.0	1.0777	1.0967	1.0989	1.0991	1.0992	1.0992	1.0992	1.0992	1.0992	1.0992	1.0992
2.0	1.0	1.0000	1.0000	1.0000	1.0000	1.0000	1.0000	1.0000	1.0000	1.0000	1.0000	1.0000

SOURCE: Quarterly Progress Report 4, Contract DA 36-039 SC 87398, SRI; reprinted in *IRE Trans. PGMTT* (see Ref. 36 by L. Young)

When interpolating, it is generally sufficient to use only the two nearest values of V or Z. In that case, a linear interpolation on a log V or log Z against log R scale is preferable. Such interpolations, using only first differences, are most accurate for small R and for large R, and are least accurate in the neighborhood

$$R \sim \left(\frac{2}{w_q}\right)^{2(n-1)} \qquad (6.04\text{-}13)$$

In this region, second- or higher-order differences may be used (or a graphical interpolation may be more convenient) to achieve greater accuracy.

Example 1—Design a quarter-wave transformer for $R = 2.5$, to have a VSWR less than 1.02 over a 20-percent bandwidth.

Here, $R = 2.5$ and $w_q = 0.2$. From Table 6.02-2, it can be seen that one section is not enough, but Table 6.02-3 indicates that two sections will do. From Table 6.04-1, we obtain $Z_1 = 1.261$, and from Eq. (6.04-7), $Z_2 = 1.982$.

Example 2—Find the step VSWRs V_1, V_2, V_3, and V_4 for a three-section quarter-wave transformer of 80-percent bandwidth and $R = 200$. Also, find the maximum pass-band VSWR.

Here, $n = 3$ and $w_q = 0.8$. For $R = 100$, from Table 6.04-6,

$$V_2 = 3.9083 ,$$

$$\therefore \log V_2 = 0.5920 .$$

For $R = 1000$,

$$V_2 = 5.5671 ,$$

$$\therefore \log V_2 = 0.7456 .$$

Now, for $R = 200$,

$$\log R = 2.301 \quad .$$

Interpolating linearly,

$$\log V_2 = 0.5920 + 0.301(0.7456 - 0.5920)$$

$$= 0.6382$$

$$\therefore \quad V_2 = 4.347 = V_3 \text{ also} \quad .$$

From Eq. (6.04-10) or (6.04-12),

$$(V_1 V_2)^2 = R$$

$$\therefore \quad V_1 = V_4 = 2.086 \quad .$$

The maximum pass-band VSWR, V_r, is found from Eqs. (6.02-8), (6.02-13), and Table 6.02-1, which give $\mathcal{E}_r = 0.23$, and then Eq. (6.02-18) determines the maximum pass-band VSWR, $V_r = 2.5$.

SEC. 6.05, EXACT MAXIMALLY FLAT SOLUTIONS FOR UP TO EIGHT SECTIONS

Enough exact solutions will be presented to permit the solution of all intermediate cases by interpolation, for maximally flat transformers with up to eight sections.

The solutions were obtained by Riblet's method.[3] This is a tedious procedure to carry out numerically; it requires high accuracy, especially for large values of R. In the limit as R becomes very large, approximate formulas adapted from the direct-coupled cavity filter point of view in Chapter 8 become quite accurate, and become exact in the limit, as R tends to infinity. This will be summarized in Sec. 6.09. For our present purposes, it is sufficient to point out that, for maximally flat transformers, the ratios

$$\left.\begin{aligned} A_1 &= A_{n+1} = V_1/R^{1/2n} \\ A_i &= V_i/R^{1/n}, \quad i \neq 1 \text{ or } n+1 \end{aligned}\right\} \qquad (6.05\text{-}1)$$

tend to finite limits as R tends to infinity (see Sec. 6.10).

Table 6.05-1 gives the impedances Z_1 to Z_4 (Fig. 6.02-1) of maximally flat quarter-wave transformers of 5, 6, 7, and 8 sections for values of R up to 100. The impedances of maximally flat transformers of 2, 3, and 4 sections were already given in tables 6.04-1 to 6.04-4 (case of $w_q = 0$). The remaining impedances not given in these tables are determined from Eq. (6.04-7).

Table 6.05-2 gives the A_i defined in Eq. (6.05-1) for maximally flat transformers of from 3 to 8 sections for values of R from 1 to ∞ in multiples of 10. The A_i change relatively little over the infinite range of R, thus permitting very accurate interpolation. The V_i are then obtained from Eqs. (6.05-1), (6.04-8), and (6.04-10). The case $n = 2$ is not tabulated, since the formulas in Eq. (6.04-1) are so simple.

SEC. 6.06, APPROXIMATE DESIGN WHEN R IS SMALL

First-Order Theory—Exact numerical Tchebyscheff solutions for $n > 4$, corresponding to the maximally flat solutions up to $n = 8$ in Sec. 6.05 have not yet been computed. When the output-to-input impedance ratio, R, approaches unity, the reflection coefficients of the impedance steps approach zero, and a first-order theory is adequate. The first-order theory assumes that each discontinuity (impedance step) sets up a reflected wave of small amplitude, and that these reflected waves pass through the other small discontinuities without setting up further second-order reflections. This theory holds for "small R" as defined by

$$R < \left(\frac{2}{w_q}\right)^{n/2} \qquad (6.06\text{-}1)$$

and can be useful even when R approaches $(2/w_q)^n$, particularly for large bandwidths. [Compare with Eqs. (6.07-2) and (6.09-1).]

Table 6.05-1

IMPEDANCES OF MAXIMALLY FLAT TRANSFORMERS

R	n = 5		n = 6			n = 7			n = 8			
	Z_1	Z_2	Z_1	Z_2	Z_3	Z_1	Z_2		Z_1	Z_2	Z_3	Z_4
1.5	1.01277	1.07904	1.00636	1.04540	1.14960	1.00318	1.02570	1.09628	1.00158	1.01438	1.06041	1.15872
2.0	1.02201	1.13908	1.01096	1.07904	1.26929	1.00547	1.04448	1.17039	1.00273	1.02481	1.10571	1.28658
2.5	1.02931	1.18816	1.01458	1.10608	1.37082	1.00727	1.05944	1.23157	1.00363	1.03307	1.14243	1.39558
3.0	1.03539	1.23002	1.01759	1.12884	1.45995	1.00878	1.07195	1.28415	1.00438	1.03997	1.17355	1.49162
3.5	1.04061	1.26672	1.02018	1.14861	1.53996	1.01007	1.08275	1.33055	1.00503	1.04590	1.20071	1.57813
4.0	1.04521	1.29954	1.02246	1.16613	1.61292	1.01121	1.09229	1.37227	1.00560	1.05114	1.22490	1.65722
4.5	1.04932	1.32931	1.02450	1.18191	1.68026	1.01223	1.10085	1.41030	1.00611	1.05583	1.24678	1.73039
5.0	1.05305	1.35663	1.02635	1.19631	1.74297	1.01315	1.10863	1.44534	1.00658	1.06009	1.26681	1.79870
6.0	1.05962	1.40549	1.02961	1.22186	1.85731	1.01479	1.12240	1.50837	1.00740	1.06762	1.30252	1.92356
7.0	1.06530	1.44845	1.03243	1.24413	1.96010	1.01620	1.13436	1.56414	1.00812	1.07414	1.33381	2.03617
8.0	1.07032	1.48696	1.03493	1.26395	2.05396	1.01746	1.14496	1.61440	1.00875	1.07992	1.36177	2.13926
9.0	1.07482	1.52196	1.03717	1.28186	2.14066	1.01859	1.15451	1.66032	1.00932	1.08513	1.38714	2.23474
10.0	1.07892	1.55413	1.03921	1.29822	2.22148	1.01962	1.16322	1.70270	1.00984	1.08987	1.41041	2.32393
15.0	1.09531	1.68600	1.04740	1.36450	2.56378	1.02375	1.19830	1.87818	1.01194	1.10895	1.50543	2.70350
20.0	1.10760	1.78804	1.05356	1.41497	2.84017	1.02688	1.22484	2.01581	1.01354	1.12335	1.57860	3.01198
25.0	1.11753	1.87251	1.05855	1.45628	3.07621	1.02942	1.24645	2.13089	1.01484	1.13507	1.63889	3.27666
30.0	1.12592	1.94524	1.06277	1.49152	3.28448	1.03158	1.26482	2.23080	1.01594	1.14502	1.69087	3.51111
35.0	1.13322	2.00950	1.06646	1.52243	3.47223	1.03347	1.28087	2.31965	1.01692	1.15371	1.73661	3.72308
40.0	1.13969	2.06729	1.06973	1.55006	3.64407	1.03515	1.29518	2.40004	1.01778	1.16146	1.77770	3.91762
45.0	1.14552	2.12000	1.07268	1.57510	3.80311	1.03667	1.30812	2.47372	1.01857	1.16845	1.81513	4.09813
50.0	1.15084	2.16856	1.07538	1.59807	3.95162	1.03805	1.31996	2.54192	1.01928	1.17485	1.84958	4.26701
60.0	1.16027	2.25588	1.08017	1.63911	4.22331	1.04052	1.34106	2.66530	1.02056	1.18624	1.91145	4.57684
70.0	1.16847	2.33312	1.08434	1.67513	4.46845	1.04268	1.35951	2.77519	1.02168	1.19620	1.96609	4.85724
80.0	1.17575	2.40267	1.08805	1.70736	4.69297	1.00460	1.37597	2.87473	1.02269	1.20507	2.01523	5.11474
90.0	1.18230	2.46613	1.09139	1.73661	4.90095	1.04634	1.39087	2.96605	1.02359	1.21310	2.06003	5.35379
100.0	1.18828	2.52464	1.09444	1.76343	5.09522	1.04793	1.40450	3.05064	1.02442	1.22043	2.10129	5.57761

SOURCE: Quarterly Progress Report 4, Contract DA 36-039 SC-87398, SRI; reprinted in *IRE Trans. PGMTT* (see Ref. 36 by I. Young)

Table 6.05-2

A_i OF MAXIMALLY FLAT TRANSFORMERS

$$\left(\begin{array}{l} A_1 = A_{n+1} = V_1/R^{1/2n} \\ A_i = V_i/R^{1/n}, \text{ when } i \neq 1, n+1 \end{array}\right)$$

Log R	$n = 3$	$n = 4$*	$n = 5$		$n = 6$			$n = 7$			$n = 8$			
	A_1	A_1	A_1	A_2	A_1	A_2	A_3	A_1	A_2	A_3	A_1	A_2	A_3	A_4
0	1.0000	1.0000	1.0000	1.0000	1.0000	1.0000	1.0000	1.0000	1.0000	1.0000	1.0000	1.0000	1.0000	1.0000
1	0.9135	0.8708	0.8570	0.9088	0.8577	0.8510	1.1658	0.8649	0.8210	1.0534	0.8744	0.8093	0.9704	1.2355
2	0.8557	0.7793	0.7497	0.8458	0.7456	0.7478	1.3411	0.7541	0.6941	1.1250	0.7682	0.6699	0.9682	1.4926
3	0.8239	0.7221	0.6755	0.8084	0.6619	0.6837	1.5107	0.6664	0.6110	1.2147	0.6803	0.5736	0.9966	1.7432
4	0.8080	0.6883	0.6263	0.7873	0.6013	0.6451	1.6629	0.5987	0.5578	1.3131	0.6000	0.5084	1.0468	1.9665
5	0.8004	0.6689	0.5943	0.7753	0.5582	0.6217	1.7911	0.5473	0.5238	1.4103	0.5519	0.4645	1.1088	2.1524
6	0.7968	0.6579	0.5738	0.7684	0.5281	0.6073	1.8934	0.5087	0.5016	1.4992	0.5069	0.4348	1.1745	2.2997
7	0.7951	0.6516	0.5607	0.7643	0.5071	0.5983	1.9717	0.4801	0.4871	1.5760	0.4717	0.4144	1.2384	2.4125
8	0.7943	0.6481	0.5523	0.7618	0.4926	0.5924	2.0296	0.4590	0.4773	1.6394	0.4444	0.4003	1.2969	2.4976
9	--	0.6461	0.5471	0.7603	0.4827	0.5886	2.0716	0.4436	0.4707	1.6900	0.4234	0.3904	1.3481	2.5610
10	--	0.6450	0.5437	0.7594	0.4758	0.5861	2.1013	0.4324	0.4661	1.7293	0.4074	0.3834	1.3914	2.6078
11	--	--	0.5416	0.7588	0.4712	0.5845	2.1222	0.4242	0.4630	1.7593	0.3952	0.3784	1.4270	2.6423
12	--	--	0.5403	0.7584	0.4680	0.5833	2.1366	0.4183	0.4607	1.7817	0.3860	0.3747	1.4557	2.6681
∞	0.7937	0.6436	0.5380	0.7579	0.4612	0.5810	2.1684	0.4031	0.4553	1.8433	0.3578	0.3646	1.5538	2.7430

* For $n = 4$, $A_2 = 1.0000$

SOURCE: Quarterly Progress Report 4, Contract DA 36-039 SC-87398, SRI; reprinted in *IRE Trans. PGMTT* (see Ref. 36 by L. Young)

Denote the reflection coefficients of an n = section transformer or filter by

$$\Gamma_i \quad , \text{ where } i = 1, 2, \ldots, n + 1$$

to give a Tchebyscheff response of bandwidth, w_q. Let

$$c = \cos\left(\frac{\pi w_q}{4}\right) \tag{6.06-2}$$

The quantity c is related to μ_0 of Eq. (6.02-12) by

$$c^2 + \mu_0^2 = 1 \quad . \tag{6.06-3}$$

Then, for n-section Tchebyscheff transformers, the following ratio formulas relate the reflection coefficients up to $n = 8$.

For $n = 2$,

$$\Gamma_1:\Gamma_2 = 1:2c^2 \quad . \tag{6.06-4}$$

For $n = 3$,

$$\Gamma_1:\Gamma_2 = 1:3c^2 \quad . \tag{6.06-5}$$

For $n = 4$,

$$\Gamma_1:\Gamma_2:\Gamma_3 = 1:4c^2:2c^2(2 + c^2) \quad . \tag{6.06-6}$$

For $n = 5$,

$$\Gamma_1:\Gamma_2:\Gamma_3 = 1:5c^2:5c^2(1 + c^2) \quad . \tag{6.06-7}$$

For $n = 6$,

$$\Gamma_1:\Gamma_2:\Gamma_3:\Gamma_4 = 1:6c^2:3c^2(2 + 3c^2):2c^2(3 + 6c^2 + c^4) \quad . \tag{6.06-8}$$

For $n = 7$,

$$\Gamma_1:\Gamma_2:\Gamma_3:\Gamma_4 = 1:7c^2:7c^2(1 + 2c^2):7c^2(1 + 3c^2 + c^4) \quad . \tag{6.06-9}$$

For $n = 8$,

$$\Gamma_1:\Gamma_2:\Gamma_3:\Gamma_4:\Gamma_5 = 1:8c^2:4c^2(2 + 5c^2):8c^2(1 + 4c^2 + 2c^4): 2c^2(4 + 18c^2 + 12c^4 + c^6) \quad . \tag{6.06-10}$$

Table 6.06-1 tabulates the Γ_i/Γ_1 for all fractional bandwidths in steps of 20 percent in w_q, for transformers of up to eight sections. The Γs are obtained from the appropriate one of the above equations, or from Table 6.06-1, together with Eq. (6.04-9) and the specified value of R (see Example 1 of Sec. 6.06). When $w_q = 0$ (maximally flat case), the Γs reduce to the binomial coefficients. (A general formula for any n will be given below.)

Range of Validity of First-Order Theory—For a transformer of given bandwidth, as R increases from unity on up, the Γ_i all increase at the same rate according to the first-order theory, keeping the ratios Γ_i/Γ_1 constant. Eventually one of the Γ_i would exceed unity, resulting in a physically impossible situation, and showing that the first-order theory has been pushed too far. To extend the range of validity of the first-order theory, it has been found advantageous to substitute $\log V_i$ for Γ_i. This substitution,[17] which appears to be due to W. W. Hansen,[1] might be expected to work better, since, first, $\log V_i$ will do just as well as Γ_i when the Γ_i are small compared to unity, as then

$$\left.\begin{aligned} \log V_i &= \log \frac{1+\Gamma_i}{1-\Gamma_i} \\ &= \text{constant} \times \Gamma_i \end{aligned}\right\} \qquad (6.06\text{-}11)$$

and, second, $\log V_i$ can increase indefinitely with increasing $\log R$ and still be physically realizable.

The first-order theory generally gives good results in the pass band when $\log V_i$ is substituted for Γ_i, provided that R is "small" as defined by Eq. (6.06-1). (Compare end of Sec. 6.10.)

Example 1—Design a six-section quarter-wave transformer of 40-percent bandwidth for an impedance ratio of $R = 10$. [This transformer will have a VSWR less than 1.005 in the pass band, from Eqs. (6.02-8) and (6.02-18) and Table 6.02-1.]

Here $(2/w_q)^{n/2} = 125$, which is appreciably greater than $R = 10$. Therefore, we can proceed by the first-order theory. From Table 6.06-1,

Table 6.06-1

TABLE OF Γ_i Γ_1

BANDWIDTH, ω_T	$n = 2$	$n = 3$	$n = 4$		$n = 5$		$n = 6$			$n = 7$			$n = 8$			
	$i = 2$	$i = 2$	$i = 2$	$i = 3$	$i = 2$	$i = 3$	$i = 2$	$i = 3$	$i = 4$	$i = 2$	$i = 3$	$i = 4$	$i = 2$	$i = 3$	$i = 4$	$i = 5$
0.0	2.0000	3.0000	4.0000	6.0000	5.0000	10.0000	6.0000	15.0000	20.0000	7.0000	21.0000	35.0000	8.0000	28.0000	56.0000	70.0000
0.2	1.9511	2.9266	3.9021	5.8054	4.8776	9.6359	5.8532	14.4181	19.1298	6.8287	20.1519	33.3120	7.8042	26.8373	53.1111	66.1559
0.4	1.8090	2.7135	3.6180	5.2543	4.5225	8.6132	5.4270	12.7903	16.7247	6.3316	17.7855	28.6925	7.2361	23.5988	45.2566	55.7879
0.6	1.5878	2.3817	3.1756	4.4361	3.9695	7.1208	4.7634	10.4357	13.3273	5.5572	14.3810	22.2954	6.3511	18.9564	34.5254	41.8439
0.8	1.3090	1.9635	2.6180	3.4748	3.2725	5.4144	3.9271	7.7825	9.6284	4.5816	10.5789	15.5402	5.2361	13.8037	23.4303	27.7539
1.0	1.0000	1.5000	2.0000	2.5000	2.5000	3.7500	3.0000	5.2500	6.2500	3.5000	7.0000	9.6250	4.0000	9.0000	14.0000	16.1250
1.2	0.6910	1.0365	1.3820	1.6207	1.7275	2.3243	2.0729	3.1472	3.5878	2.4184	4.0895	5.2138	2.7639	5.1512	7.2434	8.0793
1.4	0.4122	0.6183	0.8244	0.9094	1.0305	1.2429	1.2366	1.6190	1.7639	1.4428	2.0375	2.3961	1.6489	2.4985	3.1483	3.3919
1.6	0.1910	0.2865	0.3820	0.4002	0.4775	0.5231	0.5730	0.6550	0.6841	0.6684	0.7961	0.8660	0.7639	0.9463	1.0697	1.1133
1.8	0.0489	0.0734	0.0979	0.0991	0.1224	0.1254	0.1468	0.1522	0.1540	0.1713	0.1797	0.1840	0.1958	0.2078	0.2152	0.2177
2.0	0	0	0	0	0	0	0	0	0	0	0	0	0	0	0	0

SOURCE: Quarterly Progress Report 4, Contract DA 36-039 SC-87398, SRI; reprinted in *IRE Trans. PGMTT* (see Ref. 36 by L. Young)

$$\log V_1 : \log V_2 : \log V_3 : \log V_4 = 1 : 5.4270 : 12.7903 : 16.7247$$

$$\therefore \quad \frac{\log V_1}{\log R} = \frac{\log V_1}{\sum_{i=1}^{7} \log V_i} = \frac{1}{55.1593} = 0.01813 \quad .$$

Since $\log R = \log 10 = 1$,

$$\therefore V_1 = V_7 = \text{antilog } (0.01813) = 1.0426$$

$$V_2 = V_6 = \text{antilog } (5.4270 \times 0.01813) = 1.254$$

$$V_3 = V_5 = \text{antilog } (12.7903 \times 0.01813) = 1.705$$

and

$$V_4 = \text{antilog } (16.7247 \times 0.01813) = 2.010 \quad .$$

Hence

$$Z_1 = V_1 = 1.0426$$

$$Z_2 = V_2 Z_1 = 1.308$$

$$Z_3 = V_3 Z_2 = 2.228$$

$$Z_4 = V_4 Z_3 = 4.485$$

$$Z_5 = V_5 Z_4 = 7.65$$

$$Z_6 = V_6 Z_5 = 9.60$$

$$R = Z_7 = V_7 Z_6 = 10.00$$

Relation to Dolph-Tchebyscheff Antenna Arrays—When R is small, numerical solutions of certain cases up to $n = 39$ may be obtained through the use of existing antenna tables. The first-order Tchebyscheff transformer problem is mathematically the same as Dolph's solution[18] of the linear array, and the correspondences shown in Table 6.06-2 may be set up.

Table 6.06-2

TRANSFORMER-ARRAY CORRESPONDENCES

TCHEBYSCHEFF TRANSFORMER	DOLPH-TCHEBYSCHEFF ARRAY
First-order theory	Optical diffraction theory
Synchronous tuning	Uniform phase (or linear phase taper)
Frequency	Angle in space
Transformer length	Array length
Pass band	Side-lobe region
Stop band	Main lobe
Reflection coefficient	Radiation field
Number of steps $(n + 1)$	Number of elements
$M(n, w_q)$	Side-lobe ratio
$10 \log_{10} M$	Side-lobe level in db
$\log V_i$	Element currents, I_i

SOURCE: Quarterly Progress Report 4, Contract DA 36-039 SC-87398, SRI; reprinted in *IRE Trans. PGMTT* (see Ref. 36 by L. Young)

The calulation of transformers from tables or graphs of array solutions is best illustrated by an example.

Example 2—Design a transformer of impedance ratio $R = 5$ to have a maximum VSWR, V_r, of less than 1.02 over a 140-percent bandwidth $(w_q = 1.4)$.

It is first necessary to determine the minimum number of sections. This is easily done as in Example 1 of Sec. 6.02, using Table 6.02-1, and is determined to be $n = 11$.

Applying the test of Eq. (6.06-1)

$$\left(\frac{2}{w_q}\right)^{n/2} = 50$$

whereas R is only 5, and so we may expect the first-order theory to furnish an accurate design.

The most extensive tables of array solutions are contained in Ref. 19. (Some additional tables are given in Ref. 20.) We first work out M from Eqs. (6.02-8), (6.02-18), and (6.02-16), and find $M = 8000$. Hence the side-lobe level is

$$10 \log_{10} M = 39.0 \text{ db} \quad .$$

From Table II in Ref. 19, the currents of an $n + 1 = 12$ element array of side-lobe level 39 db are respectively proportional to 3.249, 6.894, 12.21, 18.00, 22.96, 25.82, 25.82, 22.96, 18.00, 12.21, 6.894, and 3.249. Their sum is 178.266. Since the currents are to be proportional to log V_i, and since $R = 5$, log $R = 0.69897$, we multiply these currents by 0.69897/178.266 = 0.003921 to obtain the log V_i. Taking antilogarithms yields the V_i and, finally, multiplying yields the Z_i (as in Example 1). Thus Z_0 through R are respectively found to be 1.0, 1.0298, 1.09585, 1.2236, 1.4395, 1.7709, 2.2360, 2.8233, 3.4735, 4.0861, 4.5626, 4.8552, and 5.0000. The response of this transformer is plotted in Fig. 6.06-1, and is found to satisfy the specifications almost perfectly.

In antenna theory, one is usually not interested in side-lobe ratios in excess of 40 db; this is as far as the antenna tables take us. Only fairly large bandwidths can be calculated with this 40-db limit. For

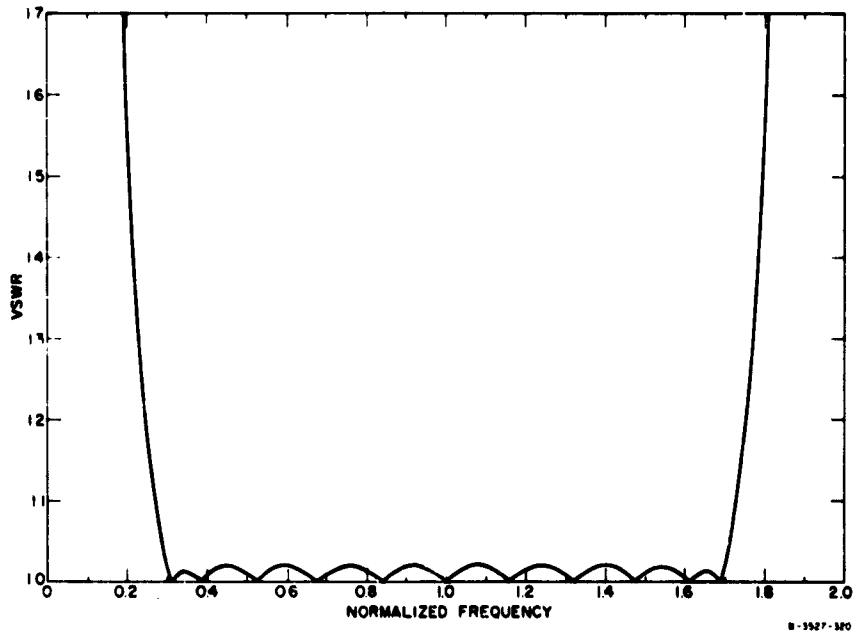

SOURCE: Quarterly Progress Report 4, Contract DA 36-039 SC-87398, SRI; reprinted in *IRE Trans. PGMTT* (See Ref. 36 by L. Young)

FIG. 6.06-1 ANALYZED PERFORMANCE OF TRANSFORMER DESIGNED IN EXAMPLE 2 OF SEC. 6.06

example, Table 6.02-1 shows that for $n = 2$ this limits us to $w_q > 0.18$; for $n = 4$, to $w_q > 0.67$; for $n = 8$, to $w_q > 1.21$; and for $n = 12$, to $w_q > 1.52$. A general formula for all cases has been given by G. J. Van der Maas,[21] which becomes, when adapted to the transformer,

$$\frac{\Gamma_i}{\Gamma_1} = \frac{n}{n+1-i} \sum_{r=0}^{i-2} \binom{n+1-i}{r+1} \binom{i-2}{r} c^{2(r+1)} \tag{6.06-12}$$

for $2 \leq i \leq (n/2) + 1$, where c is given by Eq. (6.06-2), and $\binom{a}{b}$ are the binomial coefficients

$$\binom{a}{b} = \frac{a!}{b!(a-b)!} \tag{6.06-13}$$

SEC. 6.07, APPROXIMATE DESIGN FOR UP TO MODERATELY LARGE R

Modified First-Order Theory—In Sec. 6.06 a first-order theory was presented which held for "small" values of R as defined by Eq. (6.06-1). In Sec. 6.09, there will be presented formulas that hold for "large" values of R as defined by Eq. (6.09-1). This leaves an intermediate region without explicit formulas. Since exact numerical solutions for maximally flat transformers of up to eight sections have been tabulated (Tables 6.05-1 and 6.05-2), these might be used in conjunction with either the "small R" or the "large R" theories to extend the one upward or the other downward in R, and so obtain more accurate solutions for Tchebyscheff transformers with R in this intermediate region. This idea is applied here to the first-order ("small R") theory only, as will be explained. It extends the range of the first-order theory from the upper limit given by Eq. (6.06-1) up to "moderately large" values of R as defined by

$$R < \left(\frac{2}{w_q}\right)^n \tag{6.07-1}$$

and gives acceptable results even up to the square of this limit,

$$R < \left(\frac{2}{w_q}\right)^{2n} \quad . \tag{6.07-2}$$

[Compare with Eqs. (6.06-1) and (6.09-1).] Of course, when R is less than specified by Eq. (6.06-1), there is no need to go beyond the simpler first-order theory of Sec. 6.06.

The first step in the proposed modification of the first-order theory is to form ratios of the Γ_i, which will be denoted by γ_i, with the property that

$$\left(\frac{\Gamma_i}{\sum_{i=1}^{n+1}\Gamma_i}\right)_{\substack{\text{Tchebyscheff}\\ \text{transformer}}} = \gamma_i \left(\frac{\Gamma_i}{\sum_{i=1}^{n+1}\Gamma_i}\right)_{\substack{\text{maximally flat}\\ \text{transformer}}} \tag{6.07-3a}$$

The γ_i are functions of n (the same n for both transformers) and w_q (the bandwidth of the desired Tchebyscheff transformer). The substitution of $\log V_i$ for Γ_i will again be used, and therefore $\sum_{i=1}^{n+1}\Gamma_i$ is replaced by $\log R$, according to Eq. (6.04-10). If now we choose R to be the same for both the Tchebyscheff transformer and the corresponding maximally flat transformer, then Eq. (6.07-3) reduces to

$$(\log V_i)_{\substack{\text{Tchebyscheff}\\ \text{transformer}}} = \gamma_i (\log V_i)_{\substack{\text{maximally flat}\\ \text{transformer}}} \tag{6.07-3b}$$

The modification to the first-order theory now consists in using the *exact* $\log V_i$ of the maximally flat transformer where these are known (Tables 6.05-1 and 6.05-2). The γ_i could be obtained from Eq. (6.07-3) and Table 6.06-1, but are tabulated for greater convenience in Table 6.07-1. The numbers in the first row of this table are, by definition, all unity. The application of this table is illustrated by an example given below.

Range of Validity of the Modified First-Order Theory—The analyzed performance of a first-order design, modified as explained above and to be illustrated in Example 1, agrees well with the predicted performance, provided that R satisfies Eq. (6.07-1) or at least Eq. (6.07-2). (In this regard, compare the end of Sec. 6.10.)

As a rough but useful guide, the first-order modification of the exact maximally flat design generally gives good results when the pass-band maximum VSWR is less than or equal to $(1 + w_q^2)$, where w_q is the equal-ripple quarter-wave transformer bandwidth [Eq. (6.02-1)]. By definition, it becomes exact when $w_q = 0$.

Example 1—In Example 1 of Sec. 6.02, it was shown that a quarter-wave transformer of impedance ratio $R = 100$, fractional bandwidth $w_q = 1.00$, and maximum pass-band VSWR of less than 1.15 must have at least six sections ($n = 6$). Calculate the normalized line impedances, Z_i, of this quarter-wave transformer. Predict the maximum pass-band VSWR, V_p. Then, also find the bandwidth, w_h, and normalized line impedances, Z_i', of the corresponding half-wave filter.

First, check that R is small enough for the transformer to be solved by a first-order theory. Using Eq. (6.06-1),

$$\left(\frac{2}{w_q}\right)^{n/2} = 2^3 = 8 \quad . \tag{6.07-4}$$

Therefore the unmodified first-order theory would not be expected to give good results, since $R = 100$ is considerably greater than 8. Using Eqs. (6.07-1) and (6.07-2),

$$\left.\begin{aligned} \left(\frac{2}{w_q}\right)^{n} &= 64 \\ \left(\frac{2}{w_q}\right)^{2n} &= 2048 \quad . \end{aligned}\right\} \tag{6.07-5}$$

Table 6.07-1

TABLE OF γ_i

BAND-WIDTH, w_q	$n = 2$		$n = 3$		$n = 4$			$n = 5$		
	$i = 1$	$i = 2$	$i = 1$	$i = 2$	$i = 1$	$i = 2$	$i = 3$	$i = 1$	$i = 2$	$i = 3$
0	1.00000	1.00000	1.00000	1.00000	1.00000	1.00000	1.00000	1.00000	1.00000	1.00000
0.2	1.01237	0.98762	1.01869	0.99376	1.02501	0.99992	0.99176	1.03135	1.00611	0.99380
0.4	1.05014	0.94985	1.07715	0.97428	1.10418	0.99873	0.96695	1.13188	1.02379	0.97491
0.6	1.11488	0.88511	1.18283	0.93905	1.25124	0.99336	0.92510	1.32337	1.05062	0.94234
0.8	1.20882	0.79117	1.34975	0.88341	1.49381	0.97770	0.86512	1.65171	1.08104	0.89430
1.0	1.33333	0.66666	1.60000	0.80000	1.88235	0.94117	0.78431	2.20689	1.10344	0.82758
1.2	1.48643	0.51356	1.96415	0.67861	2.50599	0.86581	0.67690	3.16718	1.09426	0.73614
1.4	1.65823	0.34176	2.47172	0.50942	3.51015	0.72344	0.53202	4.88788	1.00739	0.60751
1.6	1.82565	0.17434	3.10921	0.29692	5.05657	0.48290	0.33727	7.99760	0.76377	0.41835
1.8	1.95226	0.04773	3.72647	0.09117	6.97198	0.17063	0.11515	12.82256	0.31389	0.16079
2.0	2.0	0	4.0	0	8.0	0	0	16.0	0	0

Table 6.07-1 (*concluded*)

BAND-WIDTH, w_q	$n = 6$				$n = 7$				$n = 8$				
	$i = 1$	$i = 2$	$i = 3$	$i = 4$	$i = 1$	$i = 2$	$i = 3$	$i = 4$	$i = 1$	$i = 2$	$i = 3$	$i = 4$	$i = 5$
0	1.00000	1.00000	1.00000	1.00000	1.00000	1.00000	1.00000	1.00000	1.00000	1.00000	1.00000	1.00000	1.00000
0.2	1.03774	1.01235	0.99748	0.99258	1.04417	1.01861	1.00200	0.99381	1.05063	1.02492	1.00701	0.99643	0.99294
0.4	1.16027	1.04946	0.98935	0.97026	1.18937	1.07581	1.00731	0.97503	1.21921	1.10279	1.02757	0.98531	0.97167
0.6	1.39965	1.11118	0.97375	0.93268	1.48033	1.17521	1.01374	0.94298	1.56565	1.24295	1.05997	0.96526	0.93590
0.8	1.82608	1.19520	0.94743	0.87911	2.01888	1.32138	1.01702	0.89639	2.23202	1.46088	1.10036	0.93387	0.88496
1.0	2.58585	1.29292	0.90505	0.80808	3.02958	1.51479	1.00986	0.83313	3.54939	1.77469	1.14087	0.88734	0.81762
1.2	3.99301	1.37951	0.83778	0.71630	5.03077	1.73806	0.97968	0.74941	6.33721	2.18942	1.16586	0.81969	0.73143
1.4	6.75454	1.39211	0.72904	0.59571	9.30719	1.91834	0.90301	0.63717	12.81069	2.64044	1.14312	0.72021	0.62075
1.6	12.45111	1.18908	0.54369	0.42589	19.21633	1.83488	0.72848	0.47546	29.51655	2.81846	0.99755	0.56381	0.46943
1.8	23.25581	0.56899	0.23596	0.17906	41.69381	1.02030	0.35677	0.21919	74.08908	1.81333	0.54984	0.28471	0.23041
2.0	32.0	0	0	0	64.0	0	0	0	128.0	0	0	0	0

SOURCE: Quarterly Progress Report 4, Contract DA 36-039 SC-87398, SRI; reprinted in *IRE Trans. PGMTT* (see Ref. 36 by L. Young)

Therefore the modified first-order theory should work quite well, although we may expect noticeable but not excessive deviation from the desired performance since $R = 100$ is slightly greater than $(2/w_q)^n = 64$.

From Table 6.05-1 and Fig. 6.02-1, or from Table 6.05-2 and Eq. (6.05-1), it can be seen that a maximally flat transformer of six sections with $R = 100$ has

$$\left.\begin{aligned} V_1 &= V_7 = 1.094 \quad \therefore \log V_1 = 0.0391 \\ V_2 &= V_6 = 1.610 \quad \therefore \log V_2 = 0.2068 \\ V_3 &= V_5 = 2.892 \quad \therefore \log V_3 = 0.4612 \\ V_4 &= 3.851 \quad \therefore \log V_4 = 0.5856 \end{aligned}\right\} \quad (6.07\text{-}6)$$

The log VSWRs of the required 100-percent bandwidth transformer are now obtained, according to Eq. (6.07-3b), multiplying the log Vs in Eq. (6.07-6) by the appropriate values of γ in Table 6.06-2:

$$\left.\begin{aligned} \log V_1 &= 0.0391 \times 2.586 = 0.1011 \\ \log V_2 &= 0.2068 \times 1.293 = 0.2679 \\ \log V_3 &= 0.4612 \times 0.905 = 0.4170 \\ \log V_4 &= 0.5856 \times 0.808 = 0.4733 \end{aligned}\right\} \quad (6.07\text{-}7)$$

$$\left.\begin{aligned} \therefore V_1 &= V_7 = 1.262 \\ V_2 &= V_6 = 1.853 \\ V_3 &= V_5 = 2.612 \\ V_4 &= 2.974 \end{aligned}\right\} \quad (6.07\ 8)$$

Now this product $V_1V_2 \ldots V_7$ equals 105.4, instead of 100. It is therefore necessary to scale the V_i slightly downward, so that their product reduces to exactly 100. The preferred procedure is to reduce V_1 and V_7 by a factor of $(100/105.4)^{1/12}$ while reducing $V_2, \ldots, V_6$ by a factor of $(100/105.4)^{1/6}$. [In general, if R' and R are respectively

the trial and desired impedance ratios, then for an n-section transformer, the scaling factor is $(R/R')^{1/n}$ for $V_2, V_3, \ldots V_n$, and $(R/R')^{1/2n}$ for V_1 and V_{n+1}.] It can be shown [see Example 2 of Sec. 6.09 and Eq. (6.09-2)] that this type of scaling, where V_1 and V_{n+1} are scaled by the square root of the scaling factor for $V_2, \ldots, V_n$, has as its principal effect a slight increase in bandwidth while leaving the pass-band ripple almost unaffected. Since the approximate designs generally fall slightly short in bandwidth, while coming very close to, or even improving on, the specified pass-band ripple, this method of scaling is preferable. Subtracting 0.0038 from $\log V_1$ and 0.0076 from the remaining $\log V_i$ in Eq. (6.07-7) gives the new V_i

$$\left.\begin{aligned} V_1 &= V_7 = 1.251 \\ V_2 &= V_6 = 1.821 \\ V_3 &= V_5 = 2.566 \\ V_4 &= 2.922 \end{aligned}\right\} \qquad (6.07\text{-}9)$$

and for the corresponding normalized line impedances of the quarter-wave transformer (Fig. 6.02-1),

$$\left.\begin{aligned} Z_0 &= 1.0 \\ Z_1 &= V_1 = 1.251 \\ Z_2 &= Z_1 V_2 = 2.280 \\ Z_3 &= Z_2 V_3 = 5.850 \\ Z_4 &= Z_3 V_4 = 17.10 \\ Z_5 &= Z_4 V_5 = 43.91 \\ Z_6 &= Z_5 V_6 = 79.94 \\ R &= Z_6 V_7 = 100.00 \end{aligned}\right\} \qquad (6.07\text{-}10)$$

We note in passing that the product of the VSWRs before reduction was 105.4 instead of the specified 100. If the discrepancy between these two numbers exceeds about 5 to 10 percent, the predicted performance will usually not be realized very closely. This provides an additional internal check on the accuracy of the design.

The maximum transducer attenuation and VSWR in the pass band predicted from Eq. (6.02-16) and Table 6.02-1 are

$$\left.\begin{aligned} \mathcal{E}_r &= 0.0025 \text{ , or } 0.011 \text{ db} \quad . \\ \text{Therefore by Eq. (6.02-18) ,} & \\ V_r &= 1.106 \quad . \end{aligned}\right\} \qquad (6.07\text{-}11)$$

The computed plot of V against normalized frequency, f, of this transformer (or against λ_{g0}/λ_g if the transformer is dispersive) is shown in Fig. 6.07-1. The bandwidth is 95 percent (compared to 100 percent predicted) for a maximum pass-band VSWR of 1.11.

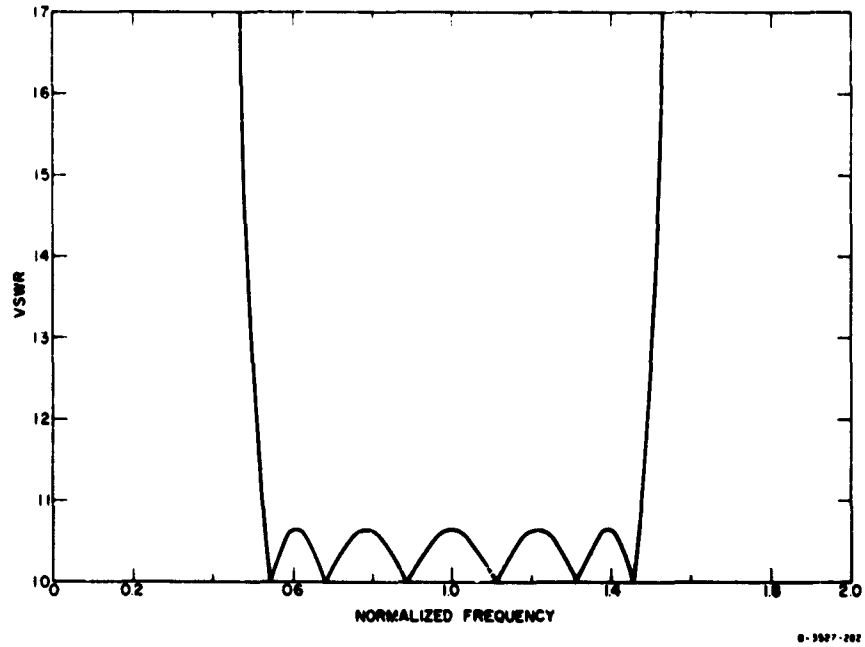

SOURCE: Quarterly Progress Report 4, Contract DA 36-039 SC-87398, SRI; reprinted in *IRE Trans. PGMTT* (See Ref. 36 by L. Young)

FIG. 6.07-1 ANALYZED PERFORMANCE OF TRANSFORMER DESIGNED IN EXAMPLE 1 OF SEC. 6.07

(Notice that the response has equal ripple heights with a maximum VSWR of 1.065 over an 86-percent bandwidth.)

The bandwidth w_h of the half-wave filter for a maximum VSWR of 1.11 will be just half the corresponding bandwidth of the quarter-wave transformer, namely, 47.5 percent (instead of the desired 50 percent). The normalized line impedances of the half-wave filter are (see Fig. 6.03-1):

$$\left.\begin{aligned}
Z_0' &= 1.0 \quad \text{(input)} \\
Z_1' &= V_1 = 1.251 \\
Z_2' &= Z_1'/V_2 = 0.6865 \\
Z_3' &= Z_2' V_3 = 1.764 \\
Z_4' &= Z_3'/V_4 = 0.604 \\
Z_5' &= Z_4' V_5 = 1.550 \\
Z_6' &= Z_5'/V_6 = 0.850 \\
Z_7' &= Z_6' V_7 = 1.065 \quad \text{(output)} \quad .
\end{aligned}\right\} \qquad (6.07\text{-}12)$$

It should be noticed that the output impedance, Z_7', of the half-wave filter is also the VSWR of the filter or transformer at center frequency[9] (Fig. 6.07-1).

In this example it was not necessary to interpolate from the tables for the V_i or Z_i. When R is not given exactly in the tables, the interpolation procedure explained at the end of Sec. 6.04 should be followed.

SEC 6.08, CORRECTION FOR SMALL-STEP DISCONTINUITY CAPACITANCES

A discontinuity in waveguide or coaxial-line cross-section cannot be represented by a change of impedance only--*i.e.*, practical junctions are non-ideal (see Sec. 6.01). The equivalent circuit for a small change in inner or outer diameter of a coaxial line can be represented by an ideal junction shunted by a capacitance,[22] and the same representation is possible for an E-plane step in rectangular

waveguide.[23] This shunt capacitance has only a second-order effect on the magnitude of the junction VSWR, since it contributes a smaller component in quadrature with the (already small) reflection coefficient of the step. Its main effect is to move the reference planes with real Γ out of the plane of the junction. Since the spacing between adjacent and facing reference planes should be one-quarter wavelength at center frequency, the physical junctions should be moved the necessary amount to accomplish this. Formulas have been given by Cohn.[1] The procedure outlined here is equivalent to Cohn's formulas, but is in pictorial form, showing the displaced reference planes, and should make the numerical working of a problem a little easier. The necessary formulas are summarized in Fig. 6.08-1 which shows the new reference plane positions. The low-impedance end is shown on the left, the high-impedance end on the right. There are two reference planes with real Γ associated with each junction, one seen from the low-impedance side, and one seen from the high-impedance side (Fig. 6.08-1). When the two "terminal-pairs" of a junction are situated in the appropriate reference planes, it is equivalent to an ideal junction. The following results can be shown to hold generally when the step discontinuity can be represented by a shunt capacitance:

(1) The two reference planes associated with any junction are both in the higher impedance line (to the right of the junction in Fig. 6.08-1).

(2) The two reference planes associated with any junction are always in the order shown in Fig. 6.08-1--*i.e.*, the reference plane seen from the higher impedance line is nearer to the junction.

(3) As the step vanishes, both reference planes fall into the plane of the junction.

(4) The reference plane seen from the higher impedance line (the one nearer to the junction) is always within one-eighth of a wavelength of the junction. (The other reference plane is not so restricted.)

The spacing between junctions is then determined as shown in Fig. 6.08-1. It is seen that the 90-degree lengths overlap, and that the separation between junctions will therefore generally be *less* than one-quarter wavelength, although this does not necessarily always hold (*e.g.*, if $x_1 > X_2$).

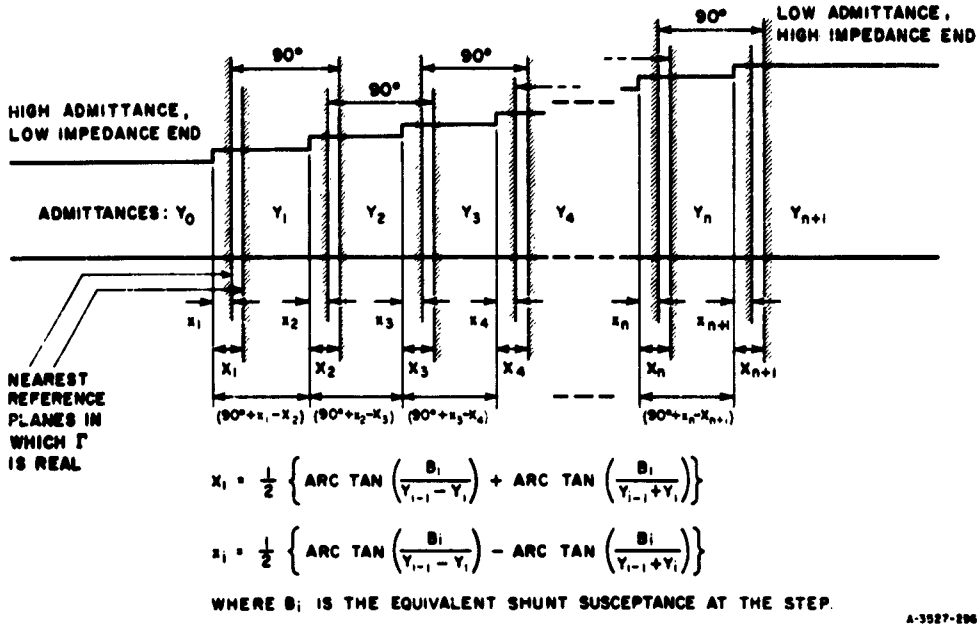

FIG. 6.08-1 LENGTH CORRECTIONS FOR DISCONTINUITY CAPACITANCES

Example 1—Design a transformer from 6.5- by 1.3-inch rectangular waveguide to 6.5- by 3.25-inch rectangular waveguide to have a VSWR less than 1.03 from at least 1180 to 1430 megacycles.

Here $R = 2.5$

$$\lambda_{g1} = 15.66 \text{ inches}, \quad \lambda_{g2} = 10.68 \text{ inches} .$$

From Eq. (6.02-2),

$$\lambda_{g0} = 12.68 \text{ inches}, \text{ and } \frac{\lambda_{g0}}{4} = 3.17 \text{ inches} ,$$

while Eq. (6.02-1) gives $w_q = 0.38$. From Tables 6.02-3 and 6.02-4, it can be seen that at least three sections are needed. We shall select $w_q = 0.50$, which still meets the specification that the pass-band VSWR be less than 1.03 (see Table 6.02-4). From Table 6.04-2, the b dimensions of such a transformer are

b_0 = 1.300 inches

b_1 = 1.479 inches

b_2 = 2.057 inches

b_3 = 2.857 inches

b_4 = 3.250 inches .

Make all the steps symmetrical (as in Fig. 6.08-2), since in this case the length corrections would be appreciable if the steps were unsymmetrical.

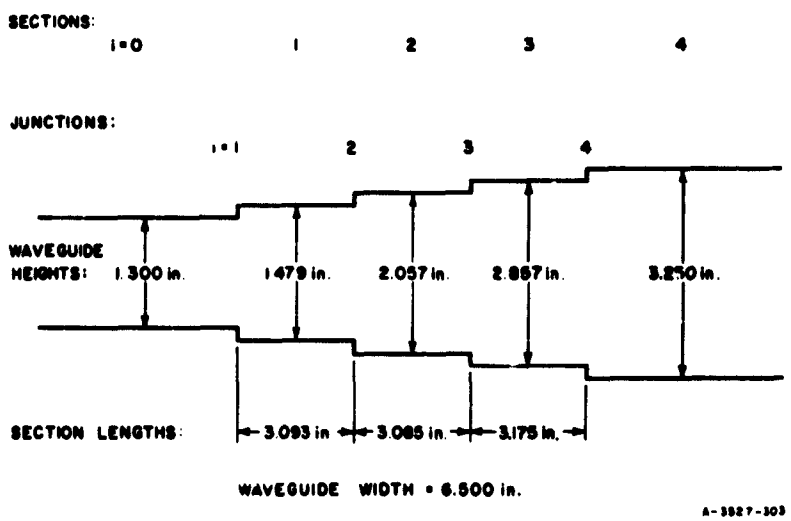

FIG. 6.08-2 SOLUTION TO EXAMPLE 1 OF SEC. 6.08 ILLUSTRATING LENGTH CORRECTIONS FOR DISCONTINUITY CAPACITANCES

Now make up a table as follows:

QUANTITY	SECTION OR JUNCTION NO. (see Fig. 6.08-2)			
	1	2	3	4
b_i/λ_g	0.117	0.162	0.225	0.256
$b_{i-1}/b_i = Y_i/Y_{i-1}$	0.88	0.72	0.72	0.88
$\left(\frac{B_i}{Y_i}\frac{\lambda_g}{b_i}\right)$ (from Figs. 5.07-10 and -11)	0.06	0.26	0.26	0.06
B_i/Y_i	0.007	0.0421	0.0585	0.0154
B_i/Y_{i-1}	0.0062	0.0303	0.0421	0.0135
$\frac{B_i/Y_{i-1}}{1 - Y_i/Y_{i-1}}$	0.052	0.108	0.150	0.113
$\frac{B_i/Y_{i-1}}{1 + Y_i/Y_{i-1}}$	0.0033	0.0176	0.0245	0.0072
X_i electrical degrees (from Fig. 6.08-1)	1.59	3.60	5.00	3.45
x_i electrical degrees (from Fig. 6.08-1)	1.40	2.59	3.60	3.03
$(X_{i+1} - x_i)$ electrical degrees	2.20	2.41	−0.15	
$\frac{\lambda_{g0}}{360}(X_{i+1} - x_i)$ inches	0.077	0.085	−0.005	

The last line subtracted from 3.17 inches gives the section lengths. The first two sections are somewhat shorter than one-quarter wavelength, while the third section is slightly longer. The final dimensions are shown in Fig. 6.08-2.

SEC. 6.09, APPROXIMATE DESIGN WHEN R IS LARGE

Theory—Riblet's procedure,[3] while mathematically elegant and although it holds for all values of R, is computationally very tedious, and the accuracy required for large R can lead to difficulties

even with a large digital computer. Collin's formulas[2] are more convenient (Sec. 6.04) but do not go beyond $n = 4$ (Tables 6.04-1 to 6.04-8). Riblet's procedure has been used to tabulate maximally flat transformers up to $n = 8$ (Tables 6.06-1 and 6.06-2). General solutions applicable only to "small R" have been given in Secs. 6.06 and 6.07, and are tabulated in Tables 6.06-1 and 6.07-1. In this part, convenient formulas will be given which become exact only when R is "large," as defined by

$$R \gg \left(\frac{2}{w_q}\right)^n \quad . \tag{6.09-1}$$

These solutions are suitable for most practical *filter* applications (but not for practical *transformer* applications). [Compare with Eqs. (6.06-1) and (6.07-2).]

For "large R" (or small w_q), stepped impedance transformers and filters may be designed from low-pass, lumped-constant, prototype filters (Chapter 4) whose elements are denoted by g_i ($i = 0, 1, \ldots, n+1$).* The transformer or filter step VSWRs are obtained from

$$\left.\begin{aligned} V_1 &= V_{n+1} = \frac{4}{\pi}\frac{g_0 g_1 \omega_1'}{w_q} \\ V_i &= \frac{16}{\pi^2}\frac{\omega_1'^2}{w_q^2} g_{i-1} g_i \text{ , when } 2 \le i \le n \\ &(V_i \text{ large, } w_q \text{ small}) \end{aligned}\right\} \tag{6.09-2}$$

where ω_1' is the radian cutoff frequency of the low-pass prototype and w_q is the quarter-wave transformer fractional bandwidth [given by Eq. (6.02-1) for Tchebyscheff transformers and Eqs. (6.02-9) or (6.02-10) for maximally flat transformers]. Again, the half-wave filter bandwidth, w_h, is equal to one-half w_q [Eq. (6.03-3)].

*Note: Here it is assumed that in the prototypes defined in Fig. 4.04-1, the circuit is symmetric or antimetric (see Sec. 4.05).

The V_i and Γ_i are symmetrical about the center in the sense of Eqs. (6.04-8) and (6.04-9), when the prototype is symmetrical or antimetrical as was assumed.

With Tables 4.05-1, 4.05-2, 4.06-1, 4.06-2, and 4.07-1, it is easy to use Eq. (6.09-1). One should, however, always verify that the approximations are valid, and this is explained next. Procedures to be used in borderline cases, and the accuracy to be expected, will be illustrated by examples.

Range of Validity—The criteria given in Eqs. (6.06-1) and (6.07-1) are reversed. The validity of the design formulas given in this part depends on R being large enough. It is found that the analyzed performance agrees well with the predicted performance (after adjusting R, if necessary, as in Examples 2 and 3 of this section) provided that Eq. (6.09-1) is satisfied; R should exceed $(2/w_q)^n$ by preferably a factor of about 10 or 100 or more. (Compare end of Sec. 6.10.) The ranges of validity for "small R" and "large R" overlap in the region between Eqs. (6.07-2) and (6.09-1), where both procedures hold only indifferently well. (See Example 3 of this section.)

For the maximally flat transformer, Eq. (6.09-1) still applies fairly well, when $w_{q,3db}$ is substituted for w_q.

As a rough but useful guide, the formulas of this section generally result in the predicted performance in the pass band when the pass-band maximum VSWR exceeds about $(1 + w_q^2)$. This rule must be considered indeterminate for the maximally flat case ($w_q = 0$), when the following rough generalization may be substituted: The formulas given in this section for maximally flat transformers or filters generally result in the predicted performance when the maximally flat quarter-wave transformer 3-db fractional bandwidth, $w_{q,3db}$, is less than about 0.40.* The half-wave filter fractional bandwidth, $w_{h,3db}$, must, of course, be less than half of this, or 0.20.

After the filter has been designed, a good way to check on whether it is likely to perform as predicted is to multiply all the VSWRs, $V_1V_2 \ldots V_{n+1}$, and to compare this product with R derived from the performance specifications using Table 6.02-1 and Eq. (6.02-13). If they

*Larger 3-db fractional bandwidths can be designed accurately for small n, for example up to about $w_{q,3db} = 0.60$ for $n = 2$.

agree within a factor of about 2, then after scaling each V so that their VSWR product finally equals R, good agreement with the desired performance may be expected.

Three examples will be worked out, illustrating a narrow-band and a wide-band design, and one case where Eq. (6.09-1) is no longer satisfied.

Example 1—Design a half-wave filter of 10-percent fractional bandwidth with a VSWR ripple of 1.10, and with at least 30-db attenuation 10 percent from center frequency.

Here $w_h = 0.1$, $\therefore w_q = 0.2$. A VSWR of 1.10 corresponds to an insertion loss of 0.01 db. From Eqs. (6.03-12) and (6.03-10), or (6.02-17) and (6.02-12),

$$\mu_0 = \sin \frac{\pi w_h}{2} = \sin 9^\circ = 0.1564 \quad .$$

At 10 percent from center frequency, by Eq. (6.03-11),

$$\frac{\omega'}{\omega_1'} = \frac{\sin \theta'}{\mu_0} = \frac{\sin 172^\circ}{0.1564} = 1.975 \quad .$$

From Fig. 4.03-4, a 5-section filter would give only 24.5 db at a frequency 10 percent from band center, but a six-section filter will give 35.5 db. Therefore, we must choose $n = 6$ to give at least 30-db attenuation 10 percent from center frequency.

The output-to-input impedance ratio of a six-section quarter-wave transformer of 20-percent fractional bandwidth and 0.01-db ripple is given by Table 6.02-1 and Eq. (6.02-13) and yields (with $\varepsilon_r = 0.0023$ corresponding to 0.01-db ripple)

$$R = 4.08 \times 10^{10} \quad . \qquad (6.09\text{-}3)$$

Thus R exceeds $(2/w_q)^n$ by a factor of 4×10^4, which by Eq. (6.09-1) is ample, so that we can proceed with the design.

From Table 4.05-2(a), for $n = 6$ and 0.01-db ripple (corresponding to a maximum VSWR of 1.10), and from Eq. (6.09-2)

$$\left.\begin{aligned} V_1 &= V_7 = 4.98 \\ V_2 &= V_6 = 43.0 \\ V_3 &= V_5 = 92.8 \\ V_4 &= 105.0 \end{aligned}\right\} \quad (6.09\text{-}4)$$

This yielded the response curve shown in Fig. 6.09-1, which is very close to the design specification in both the pass and stop bands. The half-wave filter line impedances are

$$\left.\begin{aligned} Z_0' &= 1.0 \quad \text{(input)} \\ Z_1' &= V_1 = 4.98 \\ Z_2' &= Z_1'/V_2 = 0.1158 \\ Z_3' &= Z_2' V_3 = 10.74 \\ Z_4' &= Z_3'/V_4 = 0.1023 \\ Z_5' &= Z_4' V_5 = 9.50 \\ Z_6' &= Z_5'/V_6 = 0.221 \\ Z_7' &= Z_6' V_7 = 1.10 \quad \text{(output)} \end{aligned}\right\} \quad (6.09\text{-}5)$$

Note that $Z_7' = 1.10$ is also the VSWR at center frequency (Fig. 6.09-1).

The corresponding quarter-wave transformer has a fractional bandwidth of 20 percent; its line impedances are

$$\left.\begin{aligned} Z_0 &= 1.0 \quad \text{(input)} \\ Z_1 &= V_1 = 4.98 \\ Z_2 &= Z_1 V_2 = 2.14 \times 10^2 \\ Z_3 &= Z_2 V_3 = 1.987 \times 10^4 \\ Z_4 &= Z_3 V_4 = 2.084 \times 10^6 \\ Z_5 &= Z_4 V_5 = 1.9315 \times 10^9 \\ Z_6 &= Z_5 V_6 = 8.30 \times 10^9 \\ R = Z_7 &= Z_6 V_7 = 4.135 \times 10^{10} \quad \text{(output)} \end{aligned}\right\} \quad (6.09\text{-}6)$$

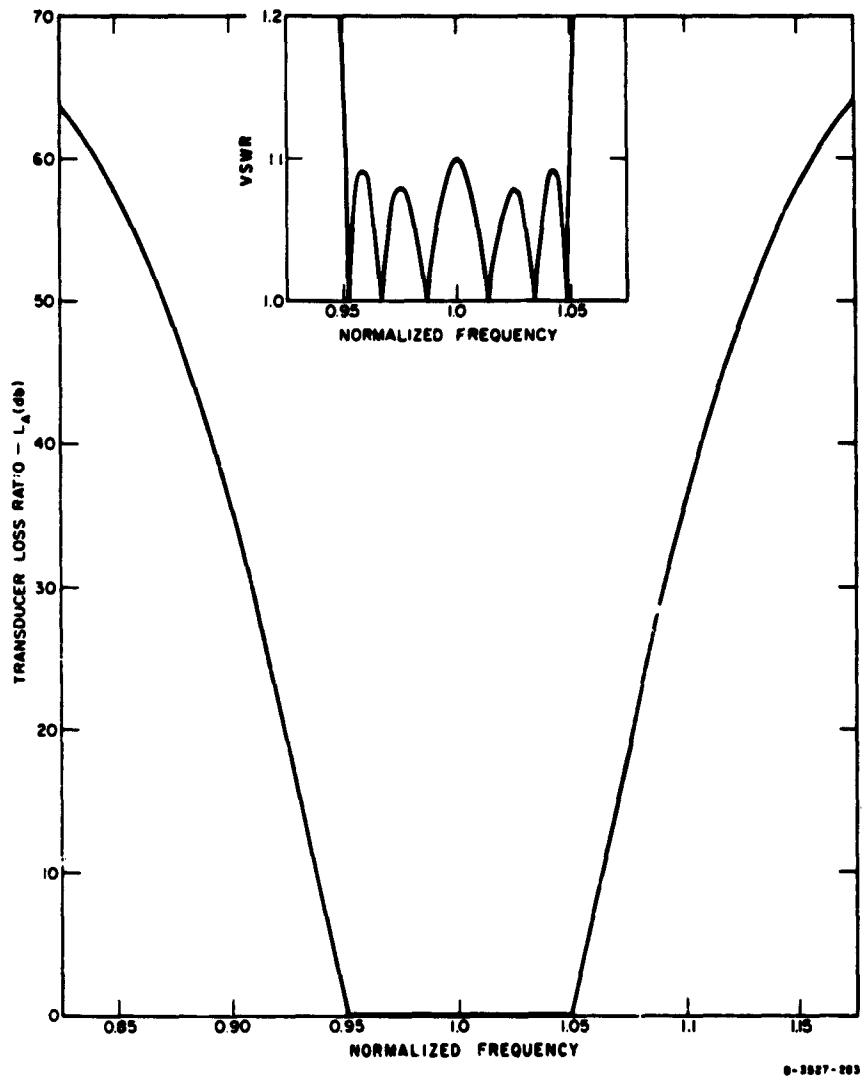

SOURCE: Quarterly Progress Report 4, Contract DA 36-039 SC-87398, SRI; reprinted in *IRE Trans. PGMTT* (See Ref. 36 by L. Young)

FIG. 6.09-1 ANALYZED PERFORMANCE OF HALF-WAVE FILTER DESIGNED IN EXAMPLE 1 OF SEC. 6.09

which is within about 1½ percent of R in Eq. (6.09-3). Therefore we would expect an accurate design, which is confirmed by Fig. 6.09-1. The attenuation of 35.5 db at $f = 1.1$ is also exactly as predicted.

Example 2—It is required to design a half-wave filter of 60-percent bandwidth with a 2-db pass-band ripple. The rejection 10 percent beyond the band edges shall be at least 20 db.

Here $w_h = 0.6$, $\therefore w_q = 1.2$. As in the previous example, it is determined that at least six sections will be required, and that the rejection 10 percent beyond the band edges should then be 22.4 db.

From Eq. (6.02-13) and Table 6.02-1 it can be seen that, for an exact design, R would be 1915; whereas $(2/w_q)^n$ is 22. Thus R exceeds $(2/w_q)^n$ by a factor of less than 100, and therefore, by Eq. (6.09-1), we would expect only a fairly accurate design with a noticeable deviation from the specified performance. The step VSWRs are found by Eq. (6.09-2) to be

$$\left.\begin{aligned} V_1 &= V_7 = 3.028 \\ V_2 &= V_6 = 2.91 \\ V_3 &= V_5 = 3.93 \\ V_4 &= 4.06 \end{aligned}\right\} \qquad (6.09\text{-}7)$$

Their product is 4875, whereas from Eq. (6.02-13) and Table 6.02-1, R should be 1915. The V_i must therefore be reduced. As in Example 1 of Sec. 6.07, we shall scale the V_i so as to slightly increase the bandwidth, without affecting the pass-band ripple. Since from Eq. (6.09-2) V_1 and V_{n+1} are inversely proportional to w_q, whereas the other $(n - 1)$ junction VSWRs, namely V_2, V_3, ... V_n, are inversely proportional to the square of w_q, reduce V_1 and V_7 by a factor of

$$\left(\frac{1915}{4875}\right)^{1/2n} = \left(\frac{1915}{4875}\right)^{1/12} = 0.9251 \quad ,$$

and V_2 through V_6 by a factor of

$$\left(\frac{1915}{4875}\right)^{1/n} = \left(\frac{1915}{4875}\right)^{1/6} = 0.8559 \quad .$$

(Compare Example 1 of Sec. 6.07.) This reduces R from 4875 to 1915. Hence,

$$\left.\begin{aligned} V_1 &= V_7 = 2.803 \\ V_2 &= V_6 = 2.486 \\ V_3 &= V_5 = 3.360 \\ V_4 &= 3.470 \quad . \end{aligned}\right\} \qquad (6.09\text{-}8)$$

The half-wave filter line impedances are now

$$\left.\begin{aligned} Z_0' &= 1.0 \quad \text{(input)} \\ Z_1' &= 2.803 \\ Z_2' &= 1.128 \\ Z_3' &= 3.788 \\ Z_4' &= 1.092 \\ Z_5' &= 3.667 \\ Z_6' &= 1.475 \\ Z_7' &= 4.135 \quad \text{(output)} \quad . \end{aligned}\right\} \qquad (6.09\text{-}9)$$

Since the reduction of R, from 4875 to 1915, is a relatively large one, we may expect some measurable discrepancy between the predicted and the analyzed performance. The analyzed performances of the designs given by Eqs. (6.09-7) and (6.09-8), before and after correction for R, are shown in Fig. 6.09-2. For most practical purposes, the agreement after correction for R is quite acceptable. The bandwidth for 2-db insertion loss is 58 percent instead of 60 percent; the rejection is exactly as specified.

Discussion—The half-wave filter of Example 1 required large impedance steps, the largest being $V_4 = 105$. It would therefore be impractical to build it as a stepped-impedance filter; it serves, instead as a prototype for a reactance-coupled cavity filter (Sec. 9.04).

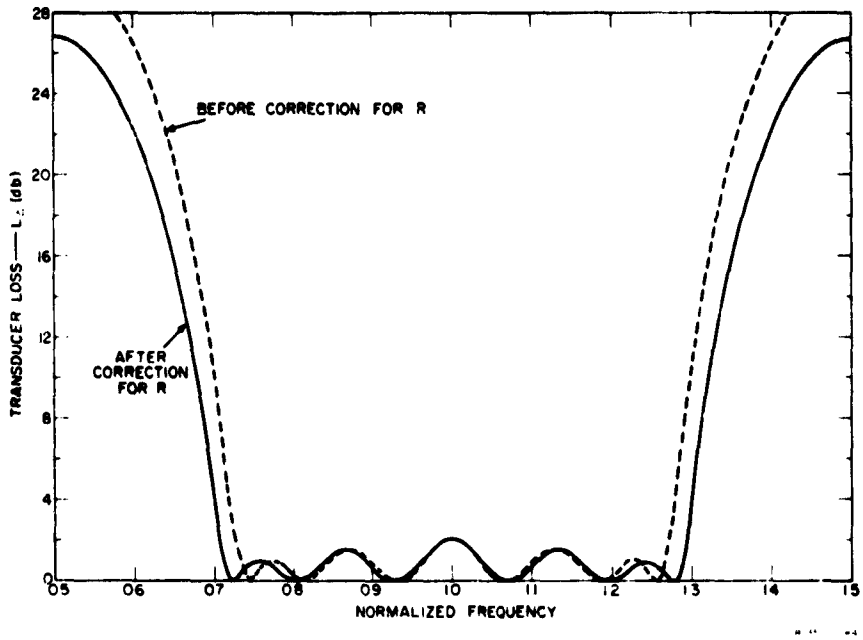

SOURCE: Quarterly Progress Report 4, Contract DA 36-039 SC-87398, SRI; reprinted in *IRE Trans. PGMTT* (See Ref. 36 by L. Young)

FIG. 6.09-2 ANALYZED PERFORMANCE OF TWO HALF-WAVE FILTERS DESIGNED IN EXAMPLE 2 OF SEC. 6.09

This is typical of narrow-band filters. The filter given in the second example, like many wide-band filters, may be built directly from Eq. (6.09-9) since the largest impedance step is $V_4 = 3.47$ and it could be constructed after making a correction for junction discontinuity capacitances (see Sec. 6.08). Such a filter would also be a low-pass filter (see Fig. 6.03-2). It would have identical pass bands at all harmonic frequencies, and it would attain its peak attenuation at one-half the center frequency (as well as at 1.5, 2.5, etc., times the center frequency, as shown in Fig. 6.03-2). The peak attenuation can be calculated from Eqs. (6.02-8) and (6.09-3). In Example 1 of Sec. 6.09 the peak attenuation is 100 db, but the impedance steps are too large to realize in practice. In Example 2 of Sec. 6.09 the impedance steps could be realized, but the peak attenuation is only 27 db. Half-wave filters are therefore more useful as prototypes for

other filter-types which are easier to realize physically. If shunt inductances or series capacitances were used (in place of the impedance steps) to realize the V_i and to form a direct-coupled-cavity filter, then the attenuation below the pass band is increased and reaches infinity at zero frequency; the attenuation above the pass band is reduced, as compared with the symmetrical response of the half-wave filters (Figs. 6.09-1 and 6.09-2). The derivation of such filters from the quarter-wave transformer or half-wave filter prototypes will be presented in Chapter 9.

Example 3—This example illustrates a case when neither the first-order theory (Sec. 6.06) nor the method of this part are accurate, but both may give usable designs. These are compared to the exact design.

It is required to design the best quarter-wave transformer of four sections, with output-to-input impedance ratio $R = 31.6$, to cover a fractional bandwidth of 120 percent.

Here $n = 4$ and $w_q = 1.2$. From Eq. (6.02-13) and Table 6.02-1, the maximum VSWR in the pass band is 2.04. Proceeding as in the previous example, and after reducing the product $V_1V_2 \ldots V_5$ to 31.6 (this required a relatively large reduction factor of 4), yields Design A shown in Table 6.09-1. Its computed VSWR is plotted in Fig. 6.09-3 (continuous line, Case A).

Since R exceeds $(2/w_q)^n$ by a factor of only 4 [see Eq. 6.09-1)], the first-order procedure of Sec. 6.07 may be more appropriate. This is also indicated by Eq. (6.07-2), which is satisfied, although Eq. (6.07-1) is not. Proceeding as in Example 1 of Sec. 6.07 yields Design B, shown in Table 6.09-1 and plotted in Fig. 6.09-3 (dash-dot line, Case B).

Table 6.09-1

THE THREE DESIGNS OF EXAMPLE 3

A—"Large R" Approximation.
B—"Small R" Approximation.
C—Exact Design.

	DESIGN		
	A	B	C
$V_1 = V_5$	1.656	1.780	1.936
$V_2 = V_4$	2.028	2.091	1.988
V_3	2.800	2.289	2.140

SOURCE: Quarterly Progress Report 4, Contract DA 36-039 SC-87398, SRI; reprinted in *IRE Trans. PGMTT* (see Ref. 36 by L. Young)

In this example, the exact design can also be obtained from Tables 6.04-3 and 6.04-4, by linear interpolation of log V against log R. This gives Design C shown in Table 6.09-1 and plotted in Fig. 6.09-3 (broken line, Case C).

Designs A and B both give less fractional bandwidth than the 120 percent asked for, and smaller VSWR peaks than the 2.04 allowed.

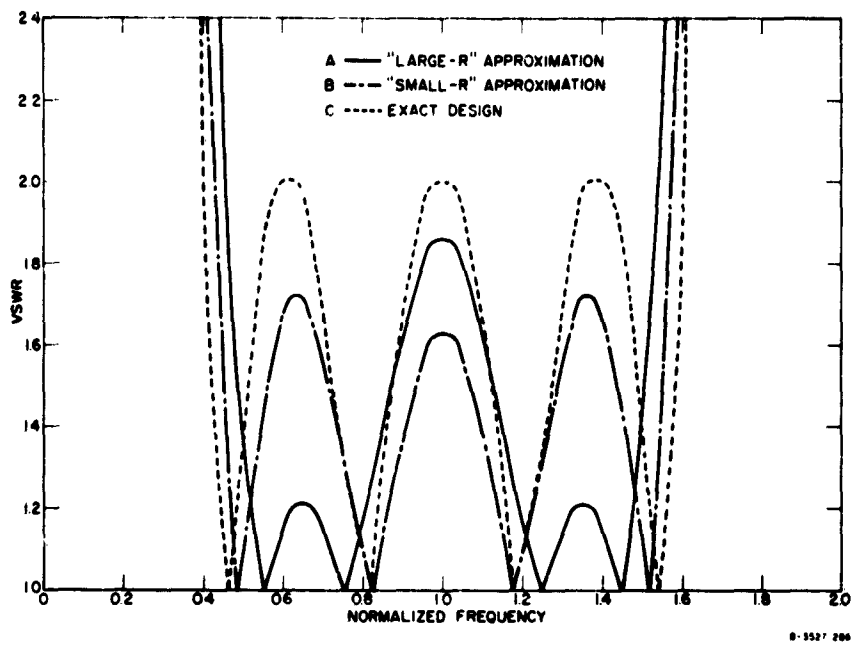

SOURCE: Quarterly Progress Report 4, Contract DA 36-039 SC-87398, SRI; reprinted in *IRE Trans. PGMTT* (See Ref. 36 by L. Young)

FIG. 6.09-3 ANALYZED PERFORMANCE OF THREE QUARTER-WAVE TRANSFORMERS DESIGNED IN EXAMPLE 3 OF SEC. 6.09

The fractional bandwidth (between $V = 2.04$ points) of Design A is 110 percent, and of Design B is 115 percent, and only the exact equal-ripple design, Design C, achieves exactly 120 percent. It is rather astonishing that two approximate designs, one based on the premise $R = 1$, and one on $R \to \infty$, should agree so well.

SEC. 6.10, ASYMPTOTIC BEHAVIOR AS R TENDS TO INFINITY

Formulas for direct-coupled cavity filters with reactive discontinuities are given in Chapter 8. These formulas become exact only in the limit as the bandwidth tends to zero. This is not the only restriction. The formulas in Secs. 8.05 and 8.06 for transmission-line filters, like the formulas in Eq. (6.09-2), hold only when Eq. (6.09-1) or its equivalent is satisfied. [Define the V_i as the VSWRs of the reactive discontinuities at center frequency; R is still given by Eq. (6.04-10); for w_q in Eq. (6.09-1), use twice the filter fractional

bandwidth in reciprocal guide wavelength.] The variation of the V_i with bandwidth is correctly given by Eq. (6.09-2) for small bandwidths. These formulas can be adapted for design of both quarter-wave transformers and half-wave filters, as in Eq. (6.09-2), and hold even better in this case than when the discontinuities are reactive. [This might be expected since the line lengths between discontinuities for half-wave filters become exactly one-half wavelength at band-center, whereas they are only approximately 180 electrical degrees long in direct-coupled cavity filters (see Fig. 8.06-1)].

Using Eq. (6.09-2) and the formulas of Eqs. (4.05-1) and (4.05-2) for the prototype element values g_i ($i = 0, 1, 2, \ldots, n, n+1$), one can readily deduce some interesting and useful results for the V_i as R tends to infinity. One thus obtains, for the junction VSWRs of Tchebyscheff transformers and filters,

$$\left.\begin{aligned} \lim_{R\to\infty} V_i &= \left(\frac{8}{\pi w_q}\right)^2 \frac{\sin\left(\frac{2i-3}{2n}\pi\right)\sin\left(\frac{2i-1}{2n}\pi\right)}{\sin^2\left(\frac{i-1}{n}\pi\right)} \\ &= \left(\frac{4}{\pi w_h}\right)^2 \frac{\sin\left(\frac{2i-3}{2n}\pi\right)\sin\left(\frac{2i-1}{2n}\pi\right)}{\sin^2\left(\frac{i-1}{n}\pi\right)} \\ &= \left(\frac{4}{\pi w_h}\right)^2 \left[1 - \left(\frac{\sin\frac{\pi}{2n}}{\sin\left(\frac{i-1}{n}\pi\right)}\right)^2\right] \\ &\quad (i = 2, 3, \ldots, n) \quad . \end{aligned}\right\} \qquad (6.10\text{-}1)$$

The quantity

$$w_h^2 \lim_{R\to\infty} (V_i) = \left(\frac{w_q}{2}\right)^2 \lim_{R\to\infty} (V_i) \qquad (6.10\text{-}2)$$

is tabulated in Table 6.10-1 for $i = 2, 3, \ldots, n$ and for $n = 2, 3, \ldots, 14$.

Table 6.10-1

TABLE OF $\left(\frac{w_q}{2}\right)^2 \lim_{R\to\infty} (V_i)$ FOR SMALL w_q

$[V_i = V_{n+2-i}]$

n	$i = 2$	$i = 3$	$i = 4$	$i = 5$	$i = 6$	$i = 7$	$i = 8$
2	0.81056						
3	1.08075						
4	1.14631	1.38372					
5	1.17306	1.44999					
6	1.18675	1.47634	1.51254				
7	1.19474	1.48981	1.53668				
8	1.19981	1.49773	1.54885	1.55943			
9	1.20325	1.50282	1.55596	1.57073			
10	1.20568	1.50631	1.56052	1.57727	1.58146		
11	1.20747	1.50880	1.56365	1.58145	1.58762		
12	1.20882	1.51066	1.56589	1.58431	1.59153	1.59351	
13	1.20987	1.51207	1.56757	1.58636	1.59419	1.59723	
14	1.21070	1.51318	1.56886	1.58789	1.59610	1.59975	1.60081

SOURCE: Quarterly Progress Report 4, Contract DA 36-039 SC-87398, SRI; reprinted in *IRE Trans. PGMTT* (see Ref. 36 by L. Young)

We notice that for Tchebyscheff transformers and filters, the $V_i (i \neq 1, n+1)$ tend to finite limits, and thus $V_1 = V_{n+1}$ tend to a constant times $R^{1/2}$. We also see that

$$w_h^2 V_i < \frac{16}{\pi^2} = 1.62115 \quad (i = 2, 3, \ldots, n) \qquad (6.10\text{-}3)$$

for all n, and tends to $16/\pi^2$ only in the limit $i \to n/2 \to \infty$.

For maximally flat transformers, the V_i all tend to infinity with R, but the quantities

$$\left.\begin{aligned} A_1 = A_{n+1} &= \frac{V_1}{R^{1/2n}} \\ A_i &= \frac{V_i}{R^{1/n}} \quad (i = 2, 3, \ldots, n) \end{aligned}\right\} \qquad (6.10\text{-}4)$$

tend toward finite limits given by

$$\left.\begin{aligned} \lim_{R\to\infty} A_1 &= 2^{(n-1)/n} \sin\left(\frac{\pi}{2n}\right) \\ \lim_{R\to\infty} A_i &= 2^{2(n-1)/n} \sin\left(\frac{2i-1}{2n}\pi\right)\sin\left(\frac{2i-3}{2n}\pi\right) \\ &\qquad (i \neq 1,\ n+1) \end{aligned}\right\} \quad (6.10\text{-}5)$$

from which we see that

$$\left.\begin{aligned} V_1 &= V_{n+1} < \left(\frac{4^{n-1}}{R}\right)^{1/2n} \\ V_i &< \left(\frac{4^{n-1}}{R}\right)^{1/n} \quad (i \neq 1,\ n+1) \end{aligned}\right\} \quad (6.10\text{-}6)$$

for all n. They tend toward the values on the right hand side only in the limit $i \to n/2 \to \infty$.

To show how a typical V_i approaches its asymptotic value, the exact solution for V_2 when $n = 4$ is plotted in Fig. 6.10-1 for all fractional bandwidths w_q in steps of 0.20. It is seen that each curve consists of two almost linear regions with a sharp knee joining them. In the sloping region above the origin ("small R"), the approximations of Sec. 6.06 or 6.07 apply; in the horizontal region ("large R"), the approximations of Sec. 6.09 apply. These two sets of approximations probably hold as well as they do because the knee region is so small.

The exact asymptotic values of $w_h^2 V_i = (w_q/2)^2 V_i$ are plotted against w_q in Fig. 6.10-2. If Eq. (6.10-1) were exact instead of approximate, then all of the curves would be horizontal straight lines. As it is, Eq. (6.10-1) gives the correct value only on the $w_q = 0$ axis. As the bandwidth increases, $w_h^2 V_i$ departs from the value at $w = 0$ slowly at first, then reaches a minimum, and finally all curves pass through unity at $w_q = 2$ ($w_h = 1$). The values of $(w_q/2)^2 V_i$ at $w_q = 0$ up to $n = 8$ are also shown in Fig. 6.10-2. (They can be obtained more accurately from Table 6.10-1.) They all lie below the value $16/\pi^2 = 1.62115$, and

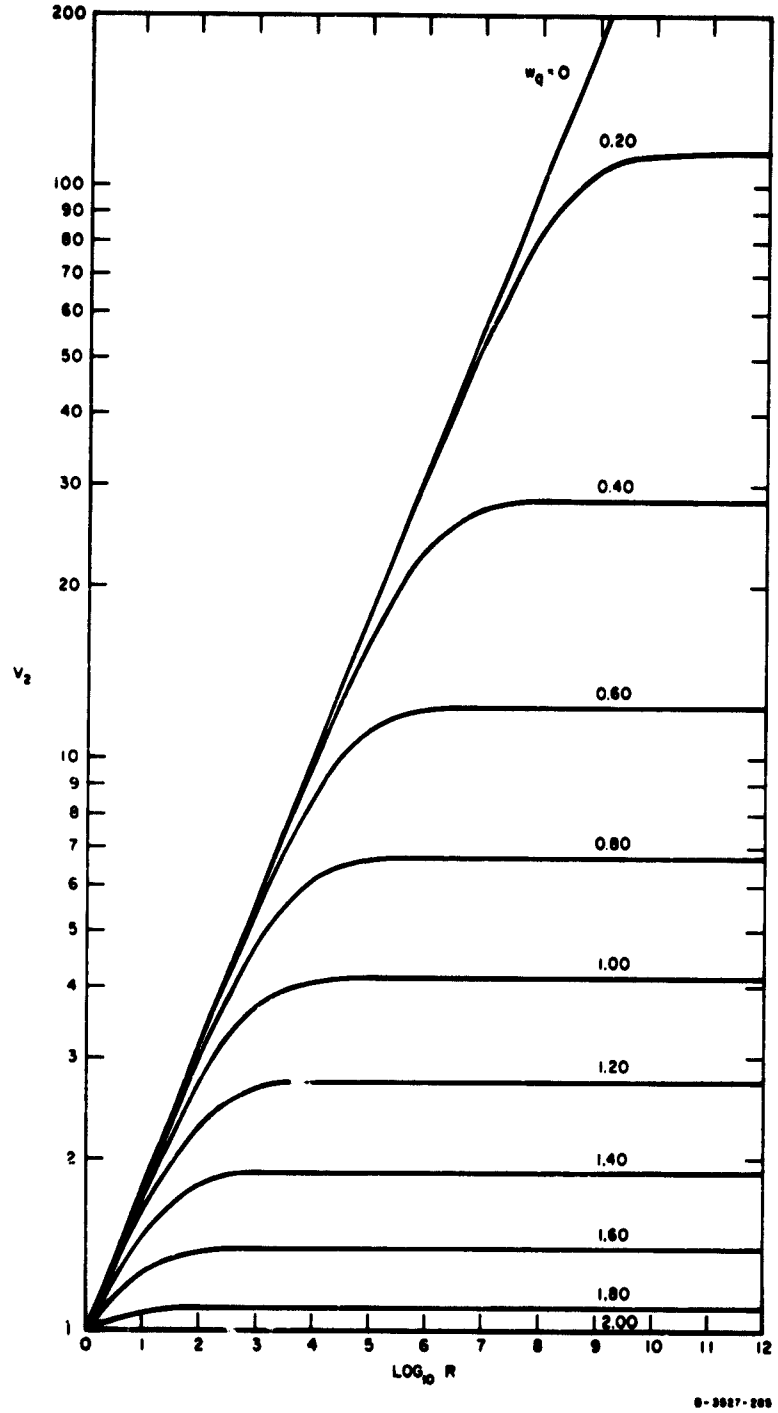

SOURCE: Quarterly Progress Report 4, Contract DA 36-039 SC-87398, SRI; reprinted in *IRE Trans. PGMTT* (See Ref. 36 by L. Young)

FIG. 6.10-1 V_2 VERSUS log R OF FOUR-SECTION TRANSFORMER FOR ALL FRACTIONAL BANDWIDTHS IN STEPS OF 0.20

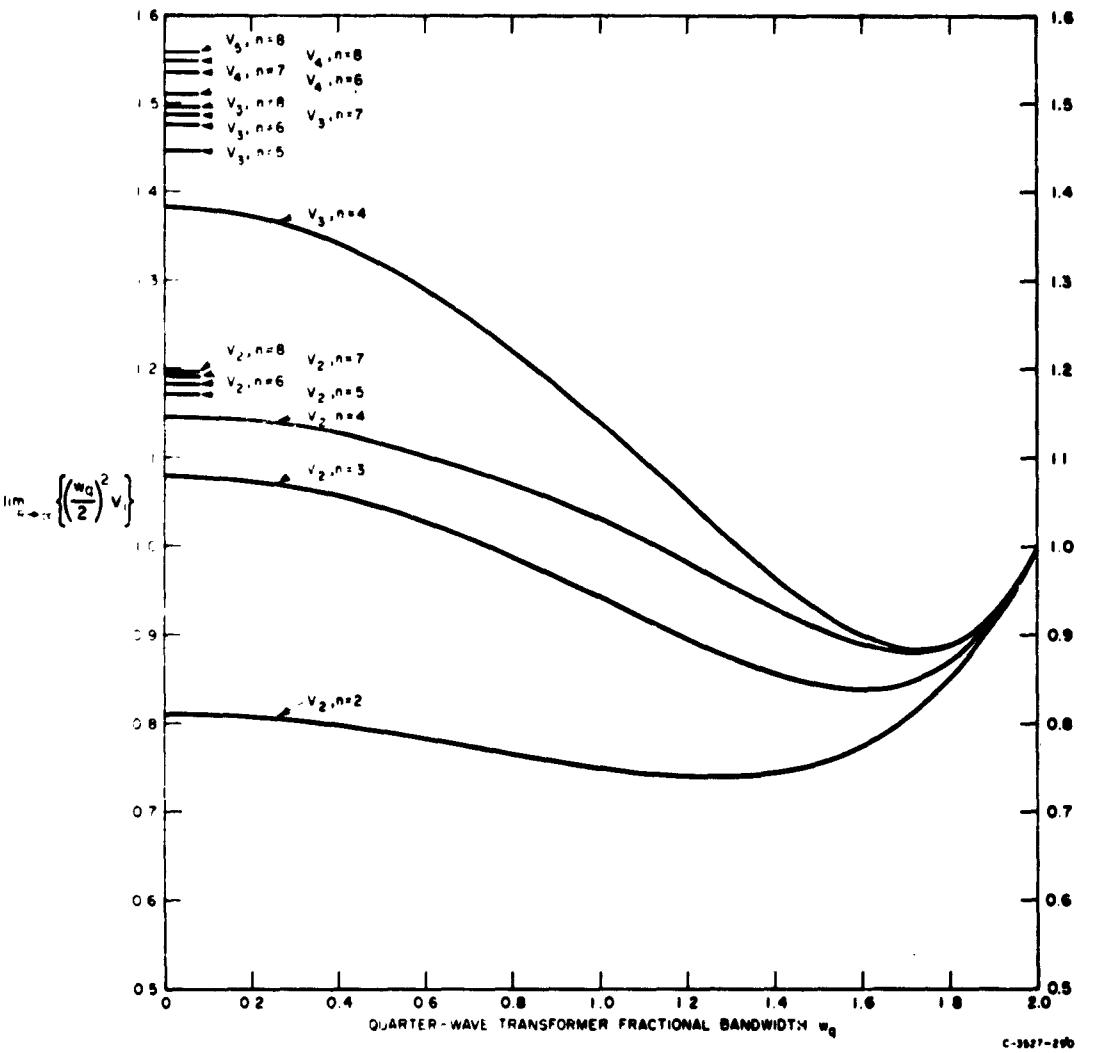

SOURCE: Quarterly Progress Report 4, Contract DA 36-039 SC-87398, SRI; reprinted in *IRE Trans. PGMTT* (see Ref. 36 by L. Young)

FIG. 6.10-2 $\lim_{R\to\infty} (w_q/2)^2 V_i$ PLOTTED AGAINST FRACTIONAL BANDWIDTH FOR TRANSFORMERS HAVING UP TO FOUR SECTIONS, AND SHOWN FOR SMALL w_q UP TO EIGHT SECTIONS

may be expected to exhibit the same sort of general behavior as do the curves up to $n = 4$, for which the exact solutions were obtained from Eqs. (6.04-4) to (6.04-6).

The asymptotic values of the V_i for $i = 2, 3, \ldots, n$, and for a given fractional bandwidth, are seen to be fairly independent of n, on examination of Eq. (6.10-1), Table 6.10-1, or Fig. 6.10-2. It follows that the same is true of $V_1/\sqrt{R} = V_{n+1}/\sqrt{R}$. Thus, as R increases indefinitely, so do V_1 and V_{n+1}; on the other hand for "small R," V_1^2 and V_{n+1}^2 are less than the other V_i (*not* squared) for small and moderately wide fractional bandwidths (up to about 100-percent bandwidths, by Table 6.06-1). If we assume that in the knee region (Fig. 6.10-1) $V_1^2 = V_{n+1}^2$ are of the order of the other V_i, then in the knee region R is of the order of $(V_i)^n$, for any $i \neq 1, n+1$. From Eq. (6.09-2), R is therefore inversely proportional to (const. $\times w_q)^{2n}$, and from the previous remarks this constant of proportionality is reasonably independent of n. Using Fig. 6.10-1 for example, the constant is very close to the value ½. This leads to the magnitude formulas of Eqs. (6.06-1), (6.07-1), (6.07-2), and (6.09-1), which have been confirmed by numerous sample solutions.

SEC. 6.11, INHOMOGENEOUS WAVEGUIDE QUARTER-WAVE TRANSFORMERS OF ONE SECTION

Inhomogeneous transformers were defined in Sec. 6.01. They come about, for instance, when rectangular waveguides having different 'a' dimensions are cascaded; or when rectangular waveguides are combined with ridged, circular, or other types of waveguide; or when the materials of an optical multi-layer are not uniformly dispersive.

At first, only ideal waveguide transformers will be considered. The junction effects in non-ideal transformers can be compensated by adjusting the lengths as in Sec. 6.08, except that the step discontinuity effects cannot usually be represented by a shunt capacitance alone. Only very limited information on waveguide junctions (other than E-plane steps) is available,[23] and for large steps the designer may have to make individual measurements on each junction.

The notation for an inhomogeneous quarter-wave transformer of one section is shown in Fig. 6.11-1.

To obtain zero reflection at center frequency (where the section length is one-quarter guide-wavelength) a sufficient condition is that

$$Z_1 = (Z_0 Z_2)^{1/2} \qquad (6.11\text{-}1)$$

where Z_0, Z_1, and Z_2 are the characteristic impedances of the input waveguide, the transformer section, and the output waveguide, respectively (Fig. 6.11-1). For a *homogeneous* transformer Eq. (6.11-1) determines the design completely, since the three cutoff wavelengths are the same ($\lambda_{c0} = \lambda_{c1} = \lambda_{c2}$); in the case of rectangular waveguide, the three wide dimensions are then equal ($a_0 = a_1 = a_2$) . However, even when a homogeneous transformer is possible, that is, when $\lambda_{c0} = \lambda_{c2}$, we may prefer to make λ_{c1} different, and thus choose to make the transformer inhomogeneous. This gives an extra degree of freedom, which, it turns out, can always be used to: (1), lower the VSWR near center frequency, and simultaneously (2), shorten the transformer.

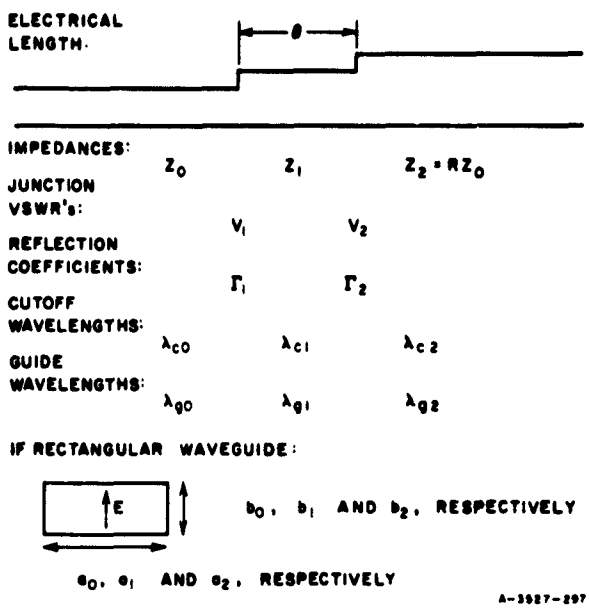

FIG. 6.11-1 INHOMOGENEOUS QUARTER-WAVE TRANSFORMER OF ONE SECTION

When λ_{c0} and λ_{c2} are not equal, an inhomogeneous transformer results of necessity. For a match at center frequency, Eq. (6.11-1) still holds, but there are an infinity of possible cutoff wavelengths, λ_{c1} (equal to $2a_1$ for rectangular waveguide). This general case will now be considered. (If a homogeneous transformer is required, then λ_{c0} can be set equal to λ_{c2} at any stage.)

It can be shown[5] that the excess loss [see Eq. (6.02-5)] is given by

$$\mathcal{E} = \frac{1}{T_1^2 T_2^2}\left[(\Gamma_2 - \Gamma_1)^2 + 4\Gamma_1\Gamma_2 \cos^2\theta\right] \quad . \qquad (6.11\text{-}2)$$

For no attenuation at center frequency ($\theta = \pi/2$), it is only necessary that $\Gamma_1 = \Gamma_2$, which is equivalent to Eq. (6.11-1). Minimizing the frequency variation of $\mathcal{E}$ at center frequency, leads for both TE and TM modes to:

$$\lambda_{g1}^2 = \frac{1}{2}\left[\frac{\lambda_{g0}^2 + \lambda_{g2}^2}{1 + \left(\frac{\pi}{4}\right)^2 \frac{(Z_2 - Z_0)^2}{Z_2 Z_0}}\right] \qquad (6.11\text{-}3)$$

Note that

$$(\lambda_{g1\ opt.})^2 < \frac{1}{2}(\lambda_{g0}^2 + \lambda_{g2}^2) \qquad (6.11\text{-}4)$$

and that further, if $\lambda_{c0} = \lambda_{c2}$,

$$\lambda_{c1\ opt.} > \lambda_{c0} = \lambda_{c2} \quad . \qquad (6.11\text{-}5)$$

Therefore, one can always improve upon a homogeneous transformer ($\lambda_{c1} = \lambda_{c0} = \lambda_{c2}$). The computed VSWR against normalized wavelength of three transformers matching from $a_0 = 0.900$ in., $b_0 = 0.050$ in., to $a_2 = 0.900$ in., $b_0 = 0.400$ in. waveguide, at a center frequency of 7211 megacycles ($\lambda_0 = 1.638$ in.) is shown in Fig. 6.11-2 for transformer guide widths of $a_1 = 0.900$ in. (homogeneous), $a_1 = 0.990$ in., and $a_1 = 1.90$ in. (optimum). Beyond this value the performance deteriorates again. The performance changes very slowly around the optimum value.

It is seen that for the best inhomogeneous transformer ($a_1 = 1.90$ in.), the VSWR *vs.* frequency slope is slightly better than 45 percent of that for the homogeneous transformer. Moreover a_1 is so uncritical that it

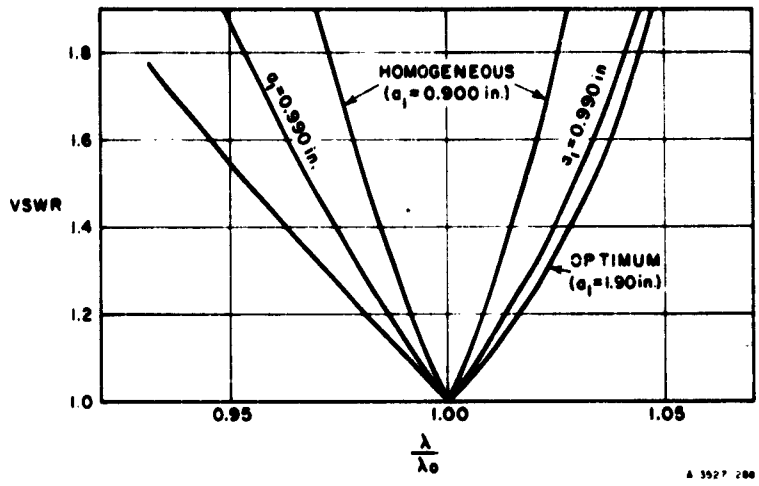

SOURCE: *IRE Trans. PGMTT* (See Ref. 5 by L. Young)

FIG. 6.11-2 VSWR AGAINST WAVELENGTH OF THREE QUARTER-WAVE TRANSFORMERS OF ONE SECTION, ALL FROM 0.900-INCH BY 0.050-INCH WAVEGUIDE TO 0.900-INCH BY 0.400-INCH WAVEGUIDE. CENTER FREQUENCY = 7211 Mc

may be reduced from 1.90 in. to 1.06 in. and the improvement remains better than 50 percent. This is very useful in practice, since a_1 cannot be made much greater than a_0 or a_2 without introducing higher-order modes or severe junction discontinuities.

The example selected above for numerical and experimental investigation has a higher transformer impedance ratio (R = 8), and operates considerably closer to cutoff (λ_0/λ_c = 0.91), than is common. In such a situation the greatest improvement can be obtained from optimizing a_1. In most cases (low R and low dispersion) the improvement obtained in making the transformer section less dispersive than that of a homogeneous transformer will only be slight. This technique, then, is most useful only for highly dispersive, high-impedance-ratio transformers.

Table 6.11-1 connects (λ/λ_c) with (λ_g/λ), and is useful in the solution of inhomogeneous transformer problems.

To compensate for the junction effects, we note that a non-ideal junction can always be represented by an ideal junction, but the non-ideal junction's reference planes (in which the junction reflection coefficient

Table 6.11-1

RELATIONS BETWEEN λ_g, λ_c, AND λ

$\left(\frac{\lambda}{\lambda_c}\right)$	$\left(\frac{\lambda_g}{\lambda}\right)$	$\left(\frac{\lambda_g}{\lambda}\right)^2$	$\left(\frac{\lambda_g}{\lambda_c}\right)$	$\left(\frac{\lambda_c}{\lambda_g}\right)$
0.50	1.1547	1.3333	0.5773	1.7320
0.51	1.1625	1.3515	0.5929	1.6866
0.52	1.1707	1.3706	0.6087	1.6426
0.53	1.1792	1.3906	0.6250	1.5999
0.54	1.1881	1.4116	0.6415	1.5586
0.55	1.1973	1.4336	0.6585	1.5184
0.56	1.2070	1.4568	0.6759	1.4794
0.57	1.2170	1.4812	0.6937	1.4414
0.58	1.2275	1.5069	0.7119	1.4045
0.59	1.2385	1.5339	0.7307	1.3684
0.60	1.2500	1.5625	0.7500	1.3333
0.61	1.2619	1.5926	0.7698	1.2990
0.62	1.2745	1.6244	0.7902	1.2654
0.63	1.2876	1.6580	0.8112	1.2326
0.64	1.3014	1.6937	0.8329	1.2005
0.65	1.3159	1.7316	0.8553	1.1691
0.66	1.3310	1.7717	0.8785	1.1382
0.67	1.3470	1.8145	0.9025	1.1080
0.68	1.3638	1.8601	0.9274	1.0782
0.69	1.3815	1.9087	0.9532	1.0489
0.70	1.4002	1.9607	0.9801	1.0202
0.71	1.4200	2.0165	1.0082	0.9918
0.72	1.4409	2.0764	1.0375	0.9638
0.73	1.4631	2.1408	1.0681	0.9362
0.74	1.4867	2.2104	1.1001	0.9089
0.75	1.5118	2.2857	1.1338	0.8819
0.76	1.5386	2.3674	1.1693	0.8551
0.77	1.5672	2.4563	1.2068	0.8286
0.78	1.5980	2.5536	1.2464	0.8022
0.79	1.6310	2.6602	1.2885	0.7760
0.80	1.6666	2.7777	1.3333	0.7500
0.81	1.7052	2.9078	1.3812	0.7239
0.82	1.7471	3.0525	1.4326	0.6980
0.83	1.7928	3.2144	1.4880	0.6720
0.84	1.8430	3.3967	1.5481	0.6459
0.85	1.8983	3.6036	1.6135	0.6197
0.86	1.9596	3.8402	1.6853	0.5933
0.87	2.0281	4.1135	1.7645	0.5667
0.88	2.1053	4.4326	1.8527	0.5397
0.89	2.1931	4.8100	1.9519	0.5123
0.90	2.2941	5.2631	2.0647	0.4843
0.91	2.4119	5.8173	2.1948	0.4556
0.92	2.5515	6.5104	2.3474	0.4259
0.93	2.7206	7.4019	2.5302	0.3952
0.94	2.9310	8.5910	2.7551	0.3629
0.95	3.2025	10.2564	3.0424	0.3286
0.96	3.5714	12.7551	3.4285	0.2916
0.97	4.1134	16.9204	3.9900	0.2506
0.98	5.0251	25.2525	4.9246	0.2030
0.99	7.0888	50.2512	7.0179	0.1424
1.00	∞	∞	∞	0

Γ is real) are no longer in the plane of the junction. This can be compensated for E-plane steps, as explained in Sec. 6.08. In compound junctions involving both E-plane and H-plane steps, if the junction discontinuities of these steps are small enough, they may be treated separately of each other using the junction data in Marcuvitz;[23] the two corrections are then superimposed. In most cases, fortunately, these two corrections tend to oppose each other; the shunt inductance effect of the H-plane step partly cancels the shunt capacitance effect of the E-plane step. When for a rectangular waveguide operating in the TE_{10} mode, both the width a and height b are to be increased together (or decreased together), the condition for resonance of the two reactive discontinuities coincides with the condition for equal characteristic impedances,

$$\left(\frac{b}{a}\frac{\lambda_g}{\lambda}\right)_{\text{Waveguide 1}} = \left(\frac{b}{a}\frac{\lambda_g}{\lambda}\right)_{\text{Waveguide 2}} \qquad (6.11\text{-}6)$$

according to Ref. 24, p. 170; when an increase in the 'a' dimension is accompanied by a decrease in the 'b' dimension (or vice versa), then an empirical equation showing when the reactive discontinuities resonate and so cancel is given in Ref. 25, but it is not known how accurate this empirical data is.

In addition to the phase perturbation introduced by the non-ideal junction, there may also be a noticeable effect on the magnitude of the reflection coefficient. (In the case of E-plane steps alone, the latter is usually negligible; see Sec. 6.08.) The increase in the magnitude of the reflection coefficient for H-plane steps in rectangular waveguide can be derived from the curves in Marcuvitz[23] (pp. 296-304). The junction VSWR is then greater than the impedance ratio of the two guides. For instance, in the example already quoted, the output-to-input impedance ratio, R, is equal to 8 with ideal junctions. However, because of the additional reflection due to junction susceptances, this goes up to an effective R of 9.6 (confirmed experimentally[5]).

As a general rule, for rectangular waveguides the change in the 'a' dimension of an H-plane step should be kept below about 10-20 percent if the junction effects are to be treated as first-order corrections to the ideal transformer theory. This is mainly to keep the reference plane

from moving too far out of the junction plane (see Marcuvitz,[23] Fig. 5.24-2, p. 299, and Fig. 5.24-5, p. 303). Symmetrical junctions are to be preferred to asymmetrical junctions. Larger H-plane steps are permissible as the guide nears cutoff (smaller 'a' dimension).

SEC. 6.12, INHOMOGENEOUS WAVEGUIDE QUARTER-WAVE TRANSFORMERS OF TWO OR MORE SECTIONS

The condition that an ideal inhomogeneous transformer of two sections (Fig. 6.12-1) be *maximally flat* can be written for both TE and TM modes:

$$\left(\frac{Z_2}{Z_1}\right)^2 = R \tag{6.12-1}$$

$$\lambda_{g2}^2 - \lambda_{g1}^2 = \frac{1}{2}(\lambda_{g3}^2 - \lambda_{g0}^2) \tag{6.12-2}$$

$$\left(\frac{Z_1}{Z_0}\right)^2 = \frac{\lambda_{g1}^2 + \lambda_{g2}^2 R^{1/2}}{\lambda_{g1}^2 + \lambda_{g2}^2 R^{-1/2}} \tag{6.12-3}$$

with the notation of Fig. 6.12-1. Equations (6.12-1) to (6.12-3) are only three conditions for the four parameters λ_{g1}, λ_{g2}, Z_1, Z_2; or in rectangular waveguide, for a_1, a_2, b_1, b_2. Thus there are an infinity of maximally flat transformers of two sections (just as there was an infinity of matching transformers of one section), and some have flatter responses than others. An example is shown in Fig. 6.12-2, in which ideal junctions are assumed. The transformation in this case is between two rectangular waveguides, namely $a_0 = 8$ in., $b_0 = 2$ in., to be transformed to $a_3 = 5$ in., $b_3 = 3$ in., at a center frequency of 1300 megacycles. The various values of a_1 taken are shown in Fig. 6.12-2. There is probably an optimum (or "flattest maximally flat") transformer, but this has not been found. Instead, it is suggested that a_1 and a_2 be chosen to minimize junction discontinuities and keep the transformer as nearly ideal as possible.

Equation (6.12-3) is plotted in Fig. 6.12-3, with $(\lambda_{g2}/\lambda_{g1})^2$ running from 0.5 to 2.5, for $R = 1, 2, \ldots, 9, 10$.

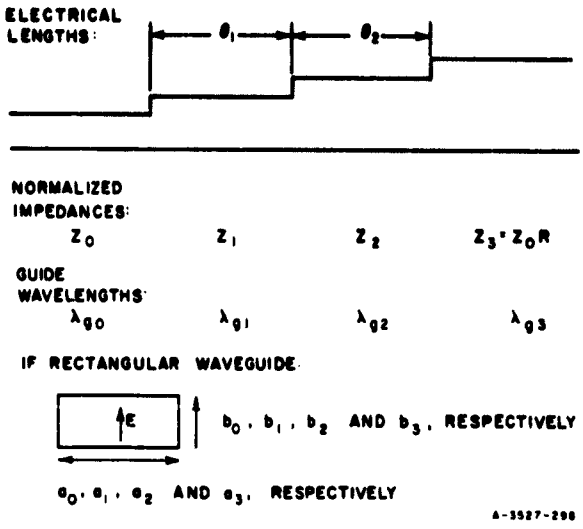

FIG. 6.12-1 INHOMOGENEOUS QUARTER-WAVE TRANSFORMER OF TWO SECTIONS

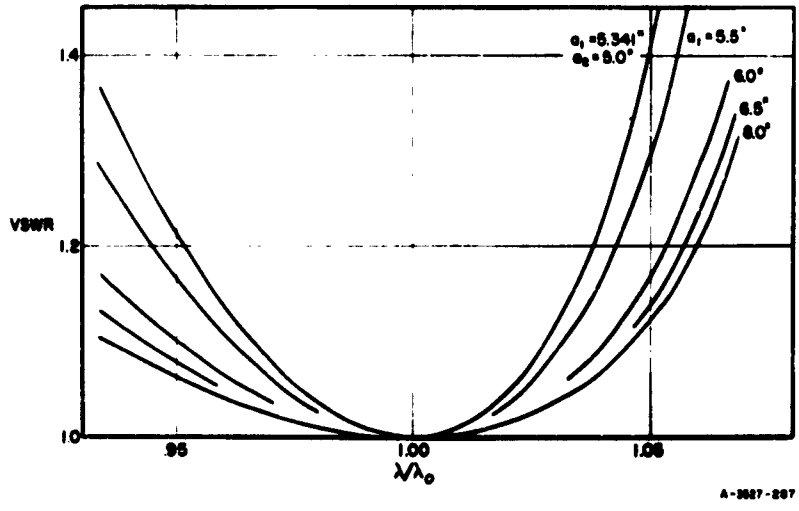

SOURCE: *IRE Trans. PGMTT* (see Ref. 6 by L. Young)

FIG. 6.12-2 VSWR AGAINST WAVELENGTH OF SEVERAL TWO-SECTION MAXIMALLY FLAT TRANSFORMERS, ALL FROM 8-INCH BY 2-INCH WAVEGUIDE TO 5-INCH BY 3-INCH WAVEGUIDE. CENTER FREQUENCY = 1300 Mc

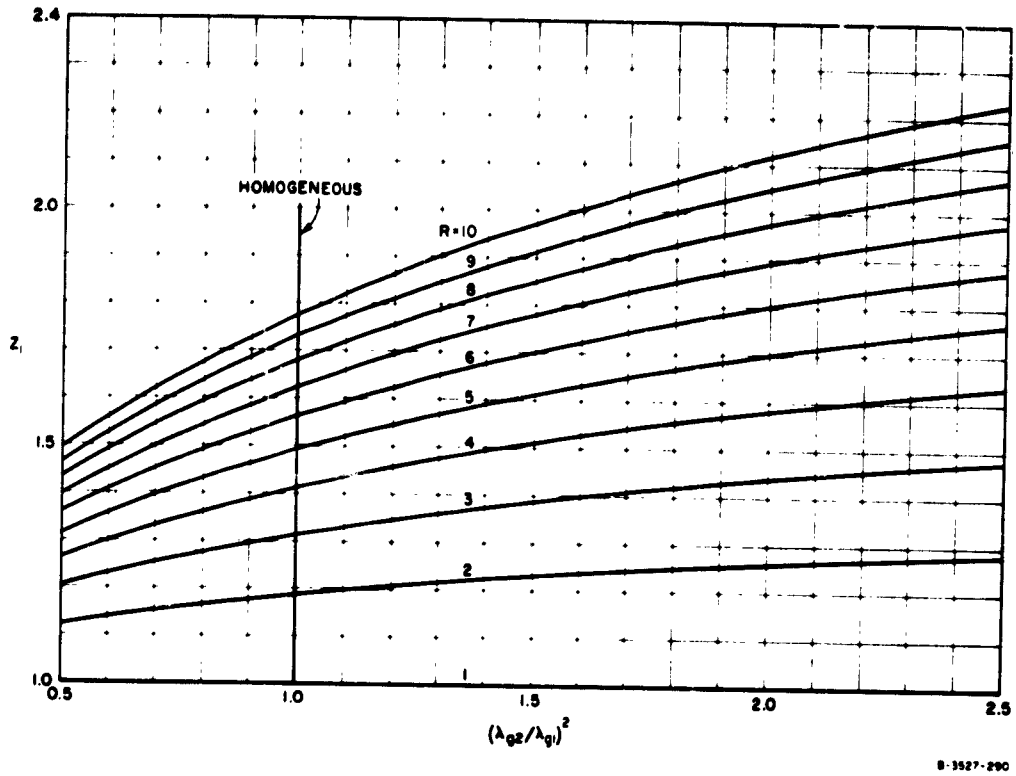

SOURCE: The Microwave Journal (see Ref. 15 by L. Young)

FIG. 6.12-3 DEPENDENCE OF Z_1 ON $(\lambda_{g2}/\lambda_{g1})^2$ TO OBTAIN A MAXIMALLY FLAT TRANSFORMER, FOR TEN VALUES OF R

In most practical applications the transformer should have minimum reflection over a finite frequency band, rather than have maximally flat frequency response. No exact method has yet been found to *broad-band* inhomogeneous transformers, but an approximate design procedure has worked out very well. This consists of first designing for maximally flat response, and then applying the inhomogeneous transformer theory as a multiplicative "correction" to the impedance ratios.[6]

Example 1—Design a transformer from 0.900- by 0.400-inch (WR-90, or RG-52/U or RG-67/U) to 0.750- by 0.400-inch waveguide to have a VSWR of better than 1.10 over a 13-percent frequency band. Here, λ_0 = 1.390 inches.

The reciprocal-guide-wavelength fractional bandwidth is approximately $(d\lambda_g/\lambda_g)/(d\lambda/\lambda) = (\lambda_g/\lambda)^2$ times the frequency fractional bandwidth of 0.13. The arithmetic mean of $(\lambda_g/\lambda)^2$ for the $a = 0.900$-inch and the $a = 0.750$-inch waveguides is $(2.47 + 7.04)/2 = 4.75$, so that the $(1/\lambda_g)$ bandwidth is approximately $4.75 \times 13 = 62$ percent. The characteristic impedance is proportional to $(b/a)(\lambda_g/\lambda)$, as in Eq. (6.11-6), and the output-to-input impedance ratio, R, is 2.027. A homogeneous transformer of $R = 2.027$, to have a VSWR of less than 1.10 over a 62-percent bandwidth, must have at least two sections, according to Table 6.02-3. Therefore choose $n = 2$.

Since the transformer is inhomogeneous, first design the maximally flat transformer. The choice of one waveguide 'a' dimension is arbitrary, so long as none of the steps exceeds about 10-20 percent. Selecting $a_1 = 0.850$ inch, Eq. (6.12-2) yields $a_2 = 0.771$ inch and then Eqs. (6.12-1) and (6.12-3), or Fig. 6.12-3, yield $b_1 = 0.429$ inch, $b_2 = 0.417$ inch. (Note that none of the H-plane steps exceed 10 percent.) The computed performance of this maximally flat transformer, assuming ideal waveguide junctions, is shown by the broken line in Fig. 6.12-4.

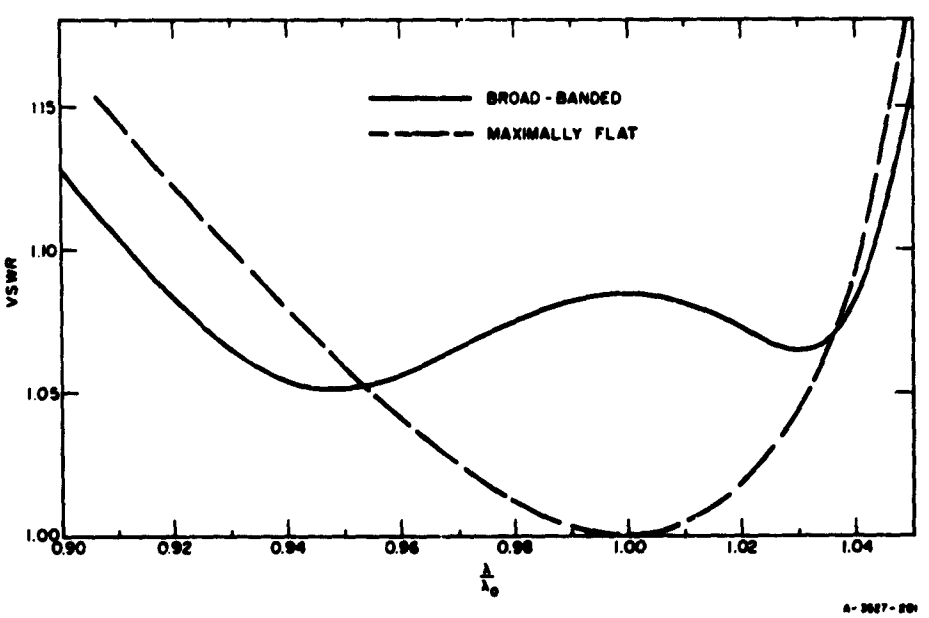

SOURCE: *IRE Trans. PGMTT* (see Ref. 6 by L. Young)

FIG. 6.12-4 VSWR AGAINST WAVELENGTH OF BROADBANDED AND MAXIMALLY FLAT TRANSFORMERS

To broadband this transformer (minimize its reflection over the specified 13 percent frequency band), we note from Table 6.04-1 that, for a two-section homogeneous transformer of $R = 2.027$ to be modified from maximally flat to 62 percent bandwidth, Z_1 increases about 2 percent, and Z_2 is reduced about 2 percent. Applying exactly the same "corrections" to b_1 and b_2 then yields $b_1 = 0.437$ inch and $b_2 = 0.409$ inch. The 'a' dimensions are not affected. The computed performance of this transformer is shown in Fig. 6.12-4 (solid line), and agrees very well with the predicted performance.

In the computations, the effects of having junctions that are non-ideal have not been allowed for. Before such a transformer is built, these effects should be estimated and first-order length corrections should be applied as indicated in Secs. 6.11 and 6.08.

Transformers having $R = 1$—It is sometimes required to change the 'a' dimension keeping the input and output impedances the same ($R = 1$). It may also sometimes be convenient to effect an inhomogeneous transformer by combining a homogeneous transformer (which accounts for all or most of the impedance change) with such an inhomogeneous transformer (which accounts for little or none of the impedance change but all of the change in the 'a' dimension). Such inhomogeneous transformers are sketched in Fig. 6.12-5. We set $R = 1$ in Eqs. (6.12-1) and (6.12-2) and obtain

$$Z_0 = Z_1 = Z_2 = Z_3 \quad . \tag{6.12-4}$$

The reflection coefficients at each junction are zero at center frequency, and we may add the requirement that the rates of change of the three reflection coefficients with frequency be in the ratio 1:2:1. This then leads to

$$\left.\begin{aligned} \lambda_{g1}^2 &= \frac{3\lambda_{g0}^2 + \lambda_{g3}^2}{4} \\ \lambda_{g2}^2 &= \frac{\lambda_{g0}^2 + 3\lambda_{g3}^2}{4} \end{aligned}\right\} \quad . \tag{6.12-5}$$

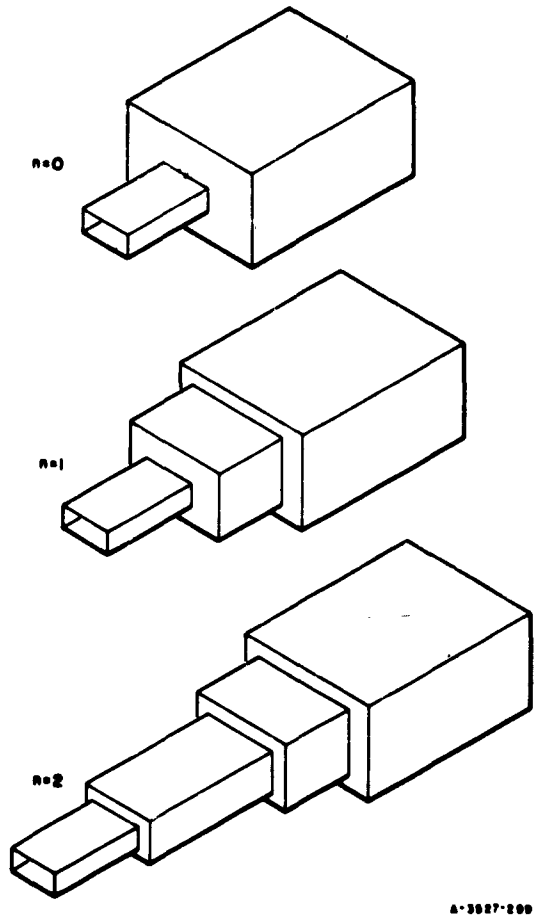

FIG. 6.12-5 INHOMOGENEOUS TRANSFORMERS WITH R = 1

Equations (6.12-2), (6.12-4), and (6.12-5) then determine all the waveguide dimensions.

Example 2—Find the 'a' dimensions of an ideal two-section quarter-wave transformer in rectangular waveguide from a_{in} = 1.372 inches to a_{out} = 1.09 inches to have R = 1 and to conform with Eqs. (6.12-2), (6.12-4), and (6.12-5). Here, λ_0 = 1.918 inches.

The solution is readily found to be a_1 = 1.226 inches and a_2 = 1.117 inches. In order for the impedances to be the same at center frequency, as required by Eq. (6.12-4), the 'b' dimensions have to be in

the ratio $b_0:b_1:b_2:b_3 = 1:0.777:0.582:0.526$, since $Z \propto (b/a)\ (\lambda_g/\lambda)$. The performance of this transformer is shown in Fig. 6.12-6.

The performances of two other transformers are also shown in Fig. 6.12-6, both with the same input and output waveguide dimensions as in Example 2, given above, and both therefore also with $R = 1$. The optimum one-section transformer has $Z_2 = Z_1 = Z_0$, from Eq. (6.11-3), but requires $\lambda_{g1}^2 = (\lambda_{g0}^2 + \lambda_{g2}^2)/2$, where suffix 2 now refers to the output. This yields $a_1 = 1.157$ inches. The third, and only V-shaped, characteristic in Fig. 6.12-6 results when the two waveguides are joined without benefit of intermediate transformer sections. The match at center frequency is ensured by the 'b' dimensions which are again chosen so that $R = 1$ at center frequency.

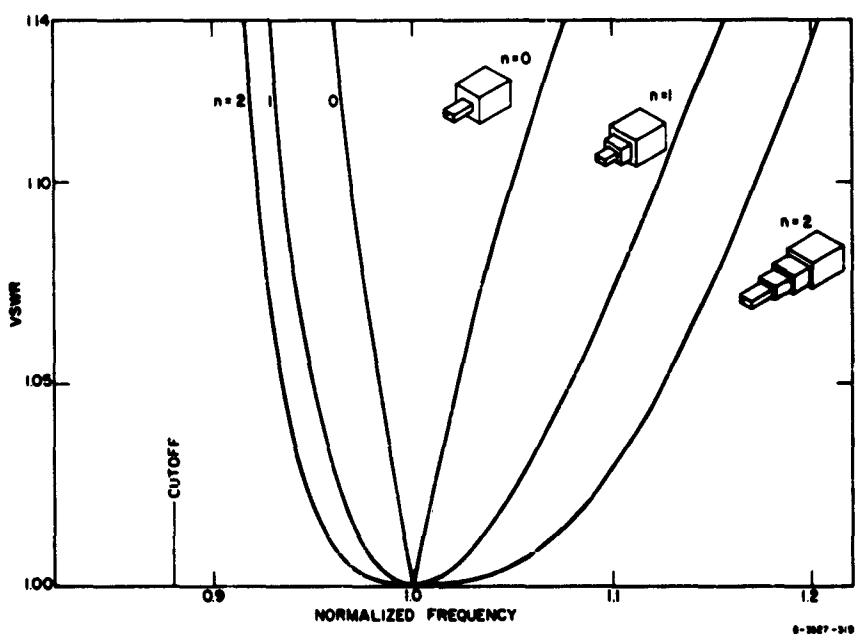

FIG. 6.12-6 PERFORMANCE OF THREE INHOMOGENEOUS TRANSFORMERS ALL WITH R = 1, HAVING NO INTERMEDIATE SECTION (n = 0), ONE SECTION (n = 1), AND TWO SECTIONS (n = 2), RESPECTIVELY

Transformers with more than two sections—No design equations have been discovered for $n > 2$. If a two-section transformer, as in Example 1 of Sec. 6.12, does not give adequate performance, there are two ways open to the designer: When the cutoff wavelengths λ_c of the input and output waveguides are only slightly different, the transformer may be designed as if it were homogeneous. In this case the λ_c of the intermediate sections may be assigned arbitrary values intermediate to the input and output values of λ_c; the impedances are selected from the tables for homogeneous transformers for a fractional bandwidth based o. the guide wavelength, Eq. (6.02-1), of that waveguide which is nearest to being cutoff. Even though the most dispersive guide is thus selected for the homogeneous prototype, the frequency bandwidth of the inhomogeneous transformer will still come out less, and when the spread in λ_c is appreciable, considerably less. Thus, this method applies only to transformers that are nearly homogeneous in the first place.

The second method is to design the transformer in two parts: one an inhomogeneous transformer of two sections with $R = 1$, as in Example 2 of this section; the other a homogeneous transformer with the required R, preferably built in the least dispersive waveguide.

Example 3—Design a quarter-wave transformer in rectangular waveguide from $a_{in} = 1.372$ inches to $a_{out} = 1.09$ inches, when $R = 4$. Here, $\lambda_0 = 1.918$ inches.

Selecting a three-section homogeneous transformer of prototype bandwidth $w_q = 0.30$ and $R = 4$, in $a = 1.372$-inch waveguide, followed by the two-section inhomogeneous transformer of Example 2 of this section, gives

$$
\begin{aligned}
a_0 &= 1.372 \text{ inches}, & Z_0 &= 1.0, \\
a_1 &= 1.372 \text{ inches}, & Z_1 &= 1.19992, \\
a_2 &= 1.372 \text{ inches}, & Z_2 &= 2.0, \\
a_3 &= 1.372 \text{ inches}, & Z_3 &= 3.33354, \\
a_4 &= 1.276 \text{ inches}, & Z_4 &= 4.0, \\
a_5 &= 1.117 \text{ inches}, & Z_5 &= 4.0, \\
a_6 &= 1.090 \text{ inches}, & Z_6 &= 4.0 .
\end{aligned}
$$

The 'b' dimensions may again be obtained from $Z \propto (b/a)\ (\lambda_g/\lambda)$, as in Example 2 of this section. The performance of this five-section transformer is shown in Fig. 6.12-7. Its VSWR is less than 1.05 over a 20-percent frequency band, although it comes within 6 percent of cutoff at one end.

Where a low VSWR over a relatively wide pass band is important, and where there is room for four or five sections, the method of Example 3 of this section is generally the best.

SEC. 6.13, A NONSYNCHRONOUS TRANSFORMER

All of the quarter-wave transformers considered so far have been synchronously tuned (see Sec. 6.01); the impedance ratio at any junction has been less than the output-to-input impedance ratio, R. It is possible to obtain the same or better electrical performance with an ideal

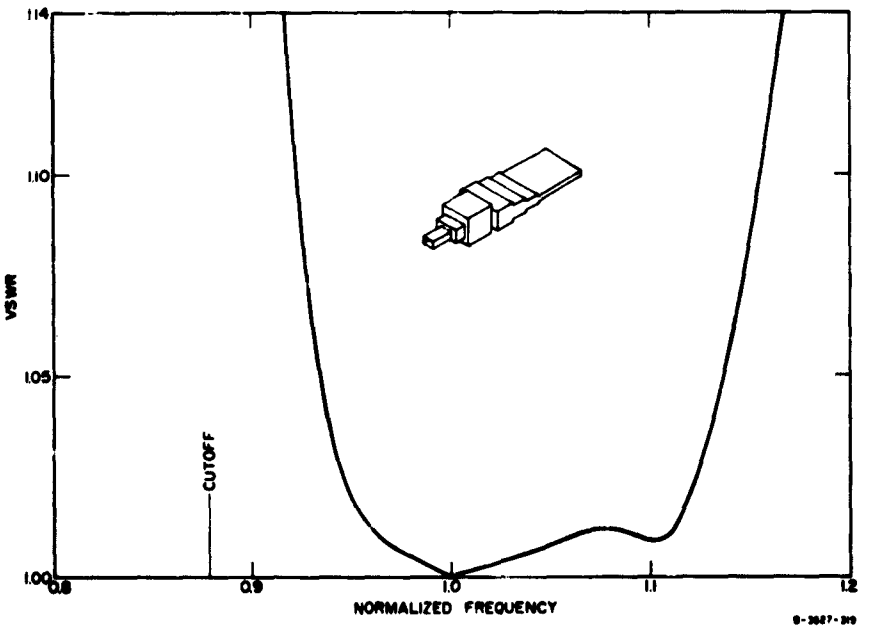

FIG. 6.12-7 PERFORMANCE OF A FIVE-SECTION INHOMOGENEOUS TRANSFORMER

nonsynchronous transformer of shorter length; however, the impedance ratios at the junctions generally exceed R by a large factor, and for more than two sections such "supermatched" transformers appear to be impractical. There is one case of a nonsynchronous transformer that is sometimes useful. It consists of two sections, whose respective impedances are equal to the output and input impedances, as shown in Fig. 6.13-1. The whole transformer is less than one-sixth wavelength long, and its performance is about the same as that of a single-section quarter-wave transformer. It can be shown[26] that the length of each section for a perfect match has to be equal to

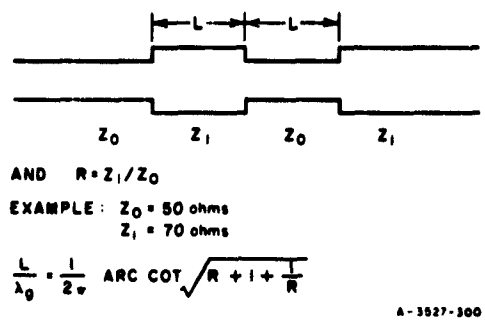

FIG. 6.13-1 A NONSYNCHRONOUS TRANSFORMER

$$L = \frac{1}{2\pi} \text{ arc cot } \left(R + 1 + \frac{1}{R}\right)^{1/2} \quad \text{wavelengths} \qquad (6.13\text{-}1)$$

which is always less than 30 electrical degrees, and becomes 30 degrees only in the limit as R approaches unity. It can be shown further that, for small R, the slope of the VSWR *vs.* frequency characteristic is greater than that for the corresponding quarter-wave transformer by a factor of $2/\sqrt{3}$ (about 15 percent greater); but then the new transformer is only two-thirds the over-all length ($\lambda_g/6$ compared to $\lambda_g/4$).

The main application of this transformer is in cases where it is difficult to come by, or manufacture, a line of arbitrary impedance. Thus if it is desired to match a 50-ohm cable to a 70-ohm cable, it is not necessary to look for a 59.1-ohm cable; instead, the matching sections can be one piece of 50-ohm and one piece of 70-ohm cable. Similarly, if it is desired to match one medium to another, as in an optical multilayer antireflection coating, this could be accomplished without looking for additional dielectric materials.

SEC. 6.14, INTERNAL DISSIPATION LOSSES

In Sec. 4.13 a formula was derived for the center-frequency increase in attenuation $(\Delta L_A)_0$ due to dissipation losses. Equation (4.13-11) applies to lumped-constant filters which are reflectionless at band center, and also includes those transmission-line filters which can be derived from the low-pass lumped-constant filters of Chapter 4 (see, for example, Sec. 6.09). If, however, the filter has not been derived from a lumped-constant prototype, then it is either impossible or inconvenient to use Eq. (4.13-11). What is required is a formula giving the dissipation loss in terms of the transmission-line filter parameters, such as the V_i instead of the g_i.

Define S_i as the VSWR at center frequency seen inside the ith filter cavity, or transformer section, when the output line is matched (Fig. 6.14-1). Here the numbering is such that $i = 1$ refers to the section or transmission-line cavity nearest the generator. Let

$$|\rho_i| = \frac{S_i - 1}{S_i + 1} \tag{6.14-1}$$

be the amplitude of the reflection coefficient in the ith cavity, corresponding to the VSWR S_i. Let[12,27]

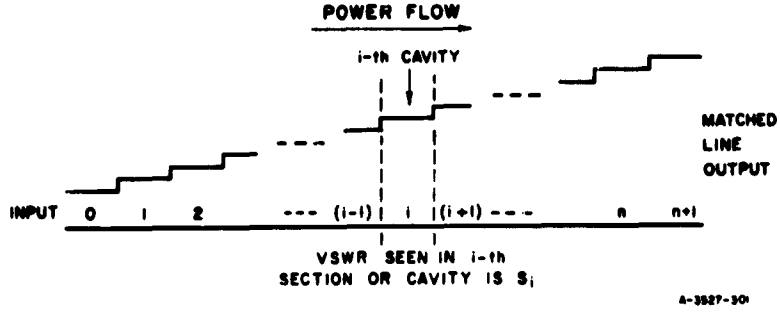

FIG. 6.14-1 VSWR INSIDE A FILTER OR TRANSFORMER

$$U_i = \frac{\text{Gross Power Flow}}{\text{Net Power Flow}}$$

$$= \frac{1 + |\rho_i|^2}{1 - |\rho_i|^2} \qquad (6.14\text{-}2)$$

$$= \frac{S_i^2 + 1}{2S_i} \quad .$$

The attenuation of transmission lines or dielectric media is usually denoted by α, but it is measured in various units for various purposes. Let

$$\left.\begin{aligned} \alpha_d &= \text{attenuation measured in decibels per unit length} \\ \alpha_n &= \text{attenuation measured in nepers per unit length} \\ \alpha_0 &= \text{absorption coefficient (used in optics}^{12}\text{)} \quad . \end{aligned}\right\} (6.14\text{-}3)$$

The absorption coefficient, α_0, is defined as the fraction of the incident power absorbed per unit length. Thus, if P_{inc} is the incident power (or irradiance) in the z-direction, then

$$\alpha_0 = -\frac{1}{P_{inc}} \cdot \frac{dP_{inc}}{dz} \quad . \qquad (6.14.4)$$

These three attenuation constants, α_d, α_n, and α_0, are related as follows:

$$\begin{aligned} \alpha_n &= \alpha_0/2 \text{ nepers} \\ \alpha_d &= (10 \log_{10} e)\alpha_0 = 4.343\alpha_0 \text{ decibels} \qquad (6.14\text{-}5) \\ &= (20 \log_{10} e)\alpha_n = 8.686\alpha_n \text{ decibels} \quad . \end{aligned}$$

Denote the length of the ith cavity or section by l_i. If each l_i is equal to an integral number of quarter-wavelengths, with impedance maxima and minima at the ends, as is the case with synchronously tuned,

stepped-impedance filters and transformers at center frequency, then the dissipation loss (if small) is given by[12]

$$\left.\begin{aligned}(\Delta L_A)_0 &= (1-|\rho_0|^2)\sum_{i=1}^{n}\alpha_{di}l_iU_i \quad \text{decibels}\\ &= (1-|\rho_0|^2)\sum_{i=1}^{n}\alpha_{ni}l_iU_i \quad \text{nepers}\\ &= (1-|\rho_0|^2)\sum_{i=1}^{n}\alpha_{0i}l_iU_i\\ &\quad \text{as a fraction of the incident power}\end{aligned}\right\} \quad (6.14\text{-}6)$$

where $|\rho_0|$ is again the reflection coefficient amplitude at the input.

To calculate the dissipation loss from Eq. (6.14-6), the gross-to-net power flow ratio, U_i, has to be determined from Eq. (6.14-2). For half-wave filters this is particularly simple, since

$$S_i = \left(\frac{Z_i'}{Z_{n+1}'}\right)^{\pm 1} > 1 \quad (6.14\text{-}7)$$

where Z_i' is the impedance of the line forming the ith cavity and Z_{n+1}' is the output impedance of the half-wave filter. The half-wave filter impedances, Z_i', can be worked out as in Example 1 of Sec. 6.07, or Examples 1 and 2 of Sec. 6.09, or from Fig. 6.03-1. Since the filter or transformer is synchronously tuned,

$$\left.\begin{aligned}S_n &= V_{n+1}\\ S_{n-1} &= \left(\frac{V_n}{S_n}\right)^{\pm 1} > 1\end{aligned}\right\} \quad (6.14\text{-}8)$$

$$
\left.
\begin{aligned}
S_i &= \left(\frac{V_{i+1}}{S_{i+1}}\right)^{\pm 1} > 1 \\
&\cdots\cdots \\
S_1 &= \left(\frac{V_2}{S_2}\right)^{\pm 1} > 1 \\
\text{Input VSWR} &= S_0 = \left(\frac{V_1}{S_1}\right)^{\pm 1} > 1 \quad .
\end{aligned}
\right\} \qquad (6.14\text{-}8)\ \text{(contd.)}
$$

The internal VSWR, S_i, for synchronous filters, can also be written in the form

$$
S_i = \left(\frac{V_{i+1}V_{i+3}V_{i+5}\cdots}{V_{i+2}V_{i+4}\cdots\cdots}\right)^{\pm 1} > 1 \quad . \qquad (6.14\text{-}9)
$$

The highest suffix of any V in this equation is $n + 1$.

Narrow-Band Filters—For narrow-band filters of large R (filters with large stop-band attenuation), Eq. (6.09-2) combined with the formulas[7] for the g_i (Sec. 4.03) shows that the V_i increase toward the center (compare Table 6.10-1 or Fig. 6.10-2). Therefore, the positive exponent must be taken in Eq. (6.14-9) and hence throughout Eq. (6.14-8). Then

$$
V_i = S_i S_{i-1} \quad (i = 1, 2, \ldots, n+1) \quad . \qquad (6.14\text{-}10)
$$

Since the output is matched ($S_{n+1} = 1$), and from Eq. (6.04-10), the maximum possible VSWR (in the stop band) is

$$
R = S_0(S_1 S_2 \ldots S_n)^2 \quad . \qquad (6.14\text{-}11)
$$

With the restriction of constant R, it can be shown[12] that when all the $\alpha_i l_i$ products are equal, Eq. (6.14-6) gives minimum dissipation loss

when all the S_i are made equal. The internal V_i are then all equal to each other, and equal to the square of $V_1 = V_{n+1}$. Such a filter (called a "periodic filter") gives minimum band-center dissipation loss for a given R (*i.e.*, for a given maximum stop-band attenuation). (In optical terms, it gives maximum "contrast".) General formulas including filters of this type have been given by Mielenz[28] and by Abelès.[29]

Since the attenuation, α_n, and the unloaded Q, Q_u, are related by[30]

$$\alpha_n = \frac{1}{Q_u}\frac{\pi}{\lambda_g}\left(\frac{\lambda_g}{\lambda}\right)^2 , \qquad (6.14\text{-}12)$$

therefore $(\Delta L_A)_0$ can be expressed in terms of Q_u,

$$\left.\begin{aligned}(\Delta L_A)_0 &= (1-|\rho_0|^2)\,\pi \sum_{i=1}^{n}\frac{1}{Q_{ui}}\frac{l_i}{\lambda_{gi}}\left(\frac{\lambda_{gi}}{\lambda}\right)^2 U_i \qquad \text{nepers}\\ &= 27.28\,(1-|\rho_0|^2) \sum_{i=1}^{n}\frac{1}{Q_{ui}}\frac{l_i}{\lambda_{gi}}\left(\frac{\lambda_{gi}}{\lambda}\right)^2 U_i \qquad \text{decibels}\end{aligned}\right\} \qquad (6.14\text{-}13)$$

To relate this to Eq. (4.13-11), we must assume narrow-band filters with large R. As in Chapter 4 and Ref. 31, it is convenient to normalize the low-pass filter prototype elements to $g_0 = 1$. In Eq. (4.13-2) and in Ref. 31, w is the frequency fractional bandwidth, related to w_q or w_h (Secs. 6.02 and 6.03) of dispersive waveguide filters by[32]

$$w = w_q\left(\frac{\lambda}{\lambda_g}\right)^2 \quad \text{or} \quad w_h\left(\frac{\lambda}{\lambda_g}\right)^2 \qquad (6.14\text{-}14)$$

whichever is appropriate. This can be shown to lead, for small w and large R, to

$$(\Delta L_A)_0 = (1 - |\rho_0|^2)\,\frac{\omega_1'}{2w}\sum_{i=1}^{n}\frac{g_i}{Q_{ui}} \quad \text{nepers}$$

$$= (1 - |\rho_0|^2)\,\frac{\omega_1'}{2w}\,(10\log_{10}e)\sum_{i=1}^{n}\frac{g_i}{Q_{ui}} \quad \text{decibels} \qquad (6.14\text{-}15)$$

It differs from Eq. (4.13-11) and Ref. 31 for the low-pass lumped-constant filter by an additional factor

$$(1 - |\rho_0|^2) = 1/\text{antilog}\,[|(L_A)_0|/10] \quad . \qquad (6.14\text{-}16)$$

If this factor is added to Eq. (4.13-11) or Eq. (1) in Ref. 31, they also become more accurate. [For instance, multiplying the last column in Table 4.13-2 by the factor in Eq. (6.14-16), approximates the exact values in the first column for $(L_A)_0$ more closely, reducing the error by an order of magnitude in every case.]

Equation (6.14-6) is the most accurate available formula for the dissipation loss at center frequency of a quarter-wave or half-wave filter, and can be applied to any such filter directly; Eq. (6.14-15) is the most accurate available formula for band-pass filters derived from the low-pass lumped-constant filter prototype of Chapter 4. Equation (6.14-6) or (6.14-15) determines the dissipation loss at the center of the pass band. The dissipation loss generally stays fairly constant over most of the pass band, rising to sharp peaks just outside both edges, as indicated in Fig. 6.14-2(a). When the total attenuation (reflection loss plus dissipation loss) is plotted against frequency, the appearance of the response curve in a typical case is as shown in Fig. 6.14-2(b); the two "dimples" are due to the two dissipation peaks shown in Fig. 6.14-2(a).

The two peaks of dissipation loss near the two band-edges may be attributed to a build-up in the internal fields and currents. Thus we would expect the power-handling capacity of the filter to be approximately

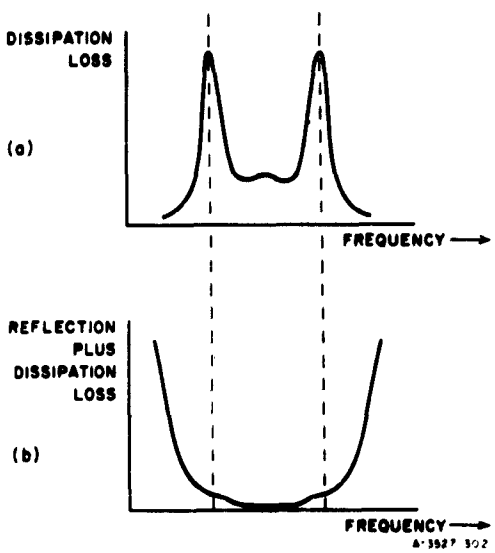

SOURCE: Jour. Opt. Soc. Am. (see Ref. 12 by L. Young)

FIG. 6.14-2 ATTENUATION CHARACTERISTICS OF FILTERS

inversely proportional to the dissipation loss, as the frequency changes. An increase in stored energy for a matched filter is in turn associated with a reduced group velocity,[32] or increased group delay. Thus we would expect the group delay through the filter to be approximately proportional to the dissipation loss, as the frequency changes. This has already been pointed out in Sec. 4.13. These questions are taken up further in Sec. 6.15.

Example 1—The parameters of a half-wave filter are: $Z_0' = 1$, $Z_1' = 245.5$, $Z_2' = 0.002425$, $Z_3' = 455.8$, $Z_4' = 0.0045$, $Z_5' = 1.106$ (corresponding to a 0.01-db pass-band ripple for a lossless filter of bandwidth $w_h = 0.00185$). Calculate the center-frequency dissipation loss if this filter is constructed in waveguide having an attenuation of 4.05 db/100 ft. Wavelength = $\lambda_0 = 1.437$ inches; waveguide width = $a = 1.015$ inches.

The guide wavelength is

$$\lambda_{g0} = 2.034 \text{ inches}$$

and

$$(\lambda_{g0}/\lambda_0)^2 = 2.00 \quad .$$

The internal VSWRs are by Eq. (6.14-7),

$$S_1 = (Z_1'/Z_5') = 222.0$$
$$S_2 = (Z_5'/Z_2') = 455.8$$
$$S_3 = (Z_3'/Z_5') = 412.5$$

$$S_4 = (Z_5'/Z_4') = 245.5$$
$$S_5 = 1.0 \quad \text{(by definition)} \quad .$$

Summing these gives

$$\sum_{i=1}^{4} U_i = \frac{1}{2} \sum_{i=1}^{4} S_i = 667.9 \quad .$$

Since the center-frequency input VSWR is equal to $Z_5' = 1.106$, therefore

$$|\rho_0|^2 = 0.0025 \quad .$$

Hence from the first of Eqs. (6.14-6),

$$(\Delta L_A)_0 = 0.9975 \times \frac{4.05}{100 \times 12} \times 1.017 \times 667.9 \text{ decibels}$$

$$= 2.29 \text{ db} \quad .$$

SEC. 6.15, GROUP DELAY

The slope of the phase-versus-frequency curve of a matched filter is a measure of the group delay through the filter. This has already been discussed in Sec. 4.08, and results for some typical low-pass filter prototypes with $n = 5$ elements are given in Figs. 4.08-1 and 4.08-2. In this section, group delay, dissipation loss, and power-handling capacity will be examined in terms of stepped-impedance filters, such as the quarter-wave transformer prototype.

It can be shown[33] that the group delay at center frequency f_0 through a homogeneous matched quarter-wave transformer is given by

$$f_0(t_d)_0 = \frac{1}{4}\left(\frac{\lambda_{g0}}{\lambda_0}\right) \sum_{i=1}^{n} U_i \qquad (6.15\text{-}1)$$

where t_d is the phase slope $d\phi/d\omega$ and may be interpreted as the group delay in the pass band. (The phase slope $t_d = d\phi/d\omega$ will, as usual,

be referred to as the group delay also outside the pass band, although its physical meaning is not clear when the attenuation varies rapidly with frequency.)

The group delay of a half-wave filter is just twice that of its quarter-wave transformer prototype; in general, the group delay of any matched stepped-impedance filter at center frequency is given by[33]

$$f_0(t_d)_0 = \sum_{i=1}^{n} \left(\frac{\lambda_{gi}}{\lambda}\right)_0^2 \left(\frac{l_i}{\lambda_{gi}}\right)_0 U_i \quad . \qquad (6.15\text{-}2)$$

Combining Eq. (6.15-2) with Eq. (6.14-6) when $\rho_0 = 0$ (filter matched at center frequency), and when the attenuation constants α and guide wavelengths λ_g are the same in each section, yields

$$\Delta L_A = \alpha\lambda_g(\lambda/\lambda_g)^2 f_0 t_d \qquad (6.15\text{-}3)$$

where α may be measured in units of nepers per unit length (α_n), or in units of decibels per unit length (α_d), ΔL_A being measured accordingly in nepers or decibels.

Equation (6.15-3) can also be written

$$\Delta L_A = \frac{\pi}{Q_u} f_0 t_d \qquad \text{nepers} \quad . \qquad (6.15\text{-}4)$$

These equations have been proved for center frequency only. It can be argued from the connection between group velocity and stored energy[33] that the relations (6.15-3) and (6.15-4) between dissipation loss and group delay should hold fairly well over the entire pass band. For this reason the suffix 0 has been left out of Eqs. (6.15-3) and (6.15-4). This conclusion can also be reached through Eqs. (4.13-2), (4.13-3) and (4.13-9) in Chapter 4.

Example 1—Calculate the time delay $(t_d)_0$ at the center frequency of the filter in Example 1 of Sec. 6.14 from its center-frequency dissipation loss, $(\Delta L_A)_0$.

From Eq. (6.15-3),

$$f_0(t_d)_0 = \left(\frac{\lambda_g}{\lambda}\right)^2 \frac{(\Delta L_A)_0}{\alpha\lambda_g} \text{ cycles at center frequency}$$

$$= 2.00 \times \frac{2.29}{\left(\frac{4.05 \times 2.034}{100 \times 12}\right)} \text{cycles at center frequency}$$

$$= 668 \text{ cycles at center frequency} .$$

Since $\lambda_0 = 1.437$ inches, which corresponds to $f_0 = 8220$ Mc. therefore

$$(t_d)_0 = \frac{668}{8220} \text{ microseconds}$$

$$= 81.25 \text{ nanoseconds} .$$

Universal Curves of Group Delay—Curves will be presented in Figs. 6.15-1 through 6.15-10 which apply to stepped-impedance transformers and filters of large R and small bandwidth (up to about $w_q = 0.4$). They were computed for specific cases (generally $R = 10^{2n}$ and $w_q = 0.20$), but are plotted in a normalized fashion and then apply generally for large R, small w. The response is plotted not directly against frequency, but against

$$x = \pm\sigma\left(\frac{f - f_0}{f_0}\right) \qquad (6.15\text{-}5)$$

with σ given by

$$\sigma = pR^{1/2n} \qquad (6.15\text{-}6)$$

where p is the length of each section measured in quarter-wavelengths. (Thus $p = 1$ for a quarter-wave transformer, and $p = 2$ for a half-wave

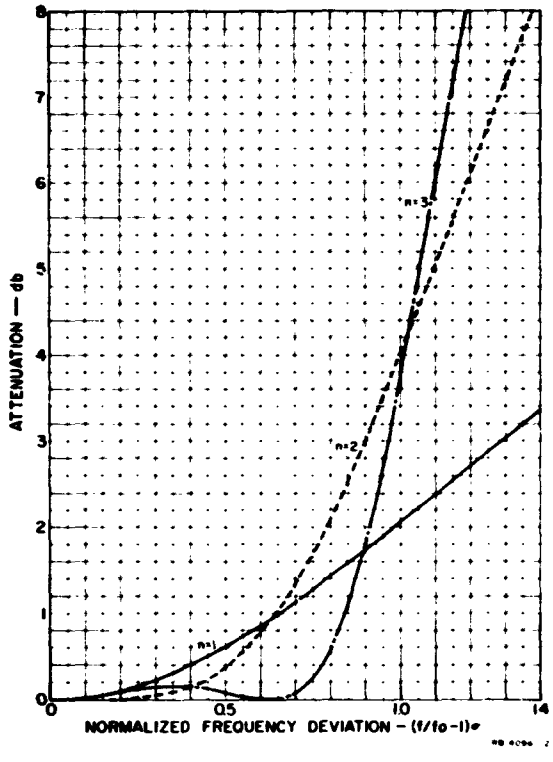

SOURCE: Quarterly Progress Report 1, Contract AF 30(602)-2734, SRI (see Ref. 33 by L. Young)

FIG. 6.15-1 ATTENUATION CHARACTERISTICS OF PERIODIC FILTERS OF n = 1, 2, AND 3 SECTIONS

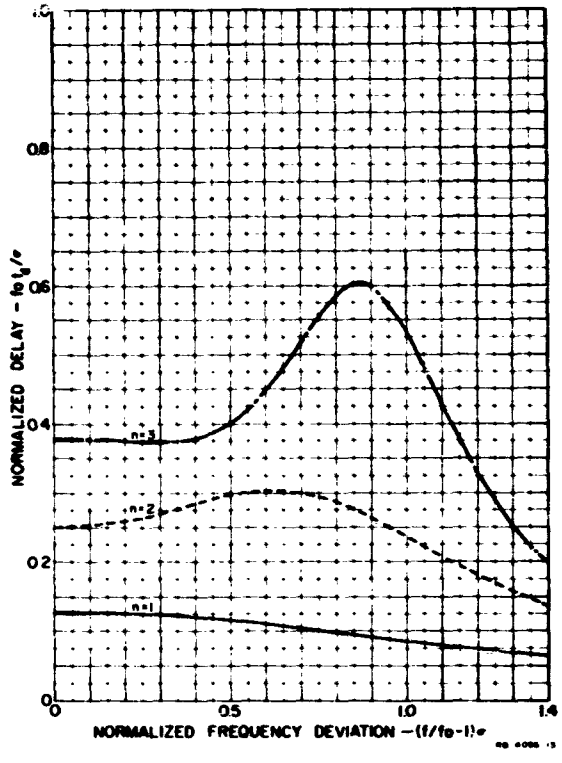

SOURCE: Quarterly Progress Report 1, Contract AF 30(602)-2734, SRI (see Ref. 33 by L. Young)

FIG. 6.15-2 GROUP DELAY OF PERIODIC FILTERS OF n = 1, 2, AND 3 SECTIONS

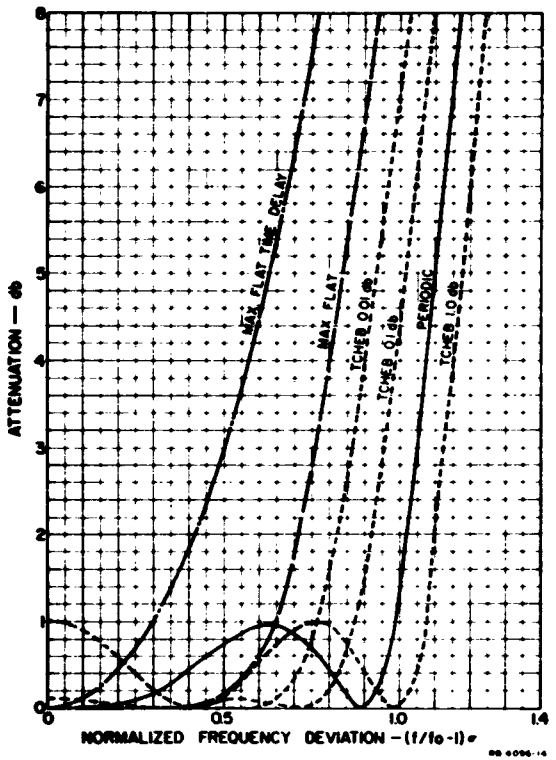

SOURCE: Quarterly Progress Report 1, Contract AF 30(602)-2734, SRI (see Ref. 33 by L. Young)

FIG. 6.15-3 ATTENUATION CHARACTERISTICS OF SIX FILTERS OF n = 4 SECTIONS

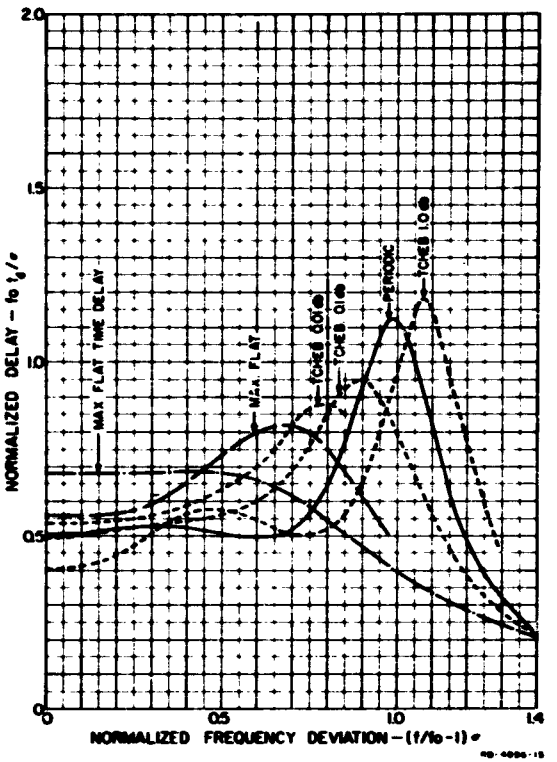

SOURCE: Quarterly Progress Report 1, Contract AF 30(602)-2734, SRI (see Ref. 33 by L. Young)

FIG. 6.15-4 TIME DELAY CHARACTERISTICS OF SIX FILTERS OF n = 4 SECTIONS

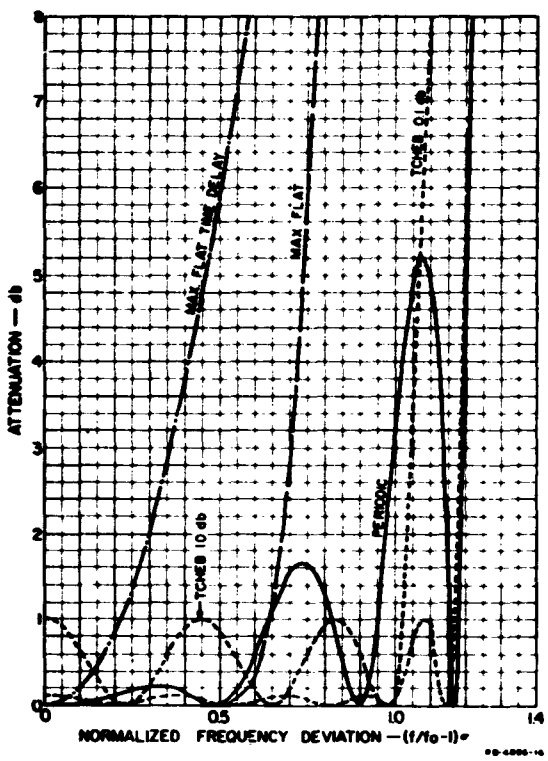

SOURCE: Quarterly Progress Report 1, Contract AF 30(602)-2734, SRI (see Ref. 33 by L. Young)

FIG. 6.15-5 ATTENUATION CHARACTERISTICS OF FIVE FILTERS OF n = 8 SECTIONS

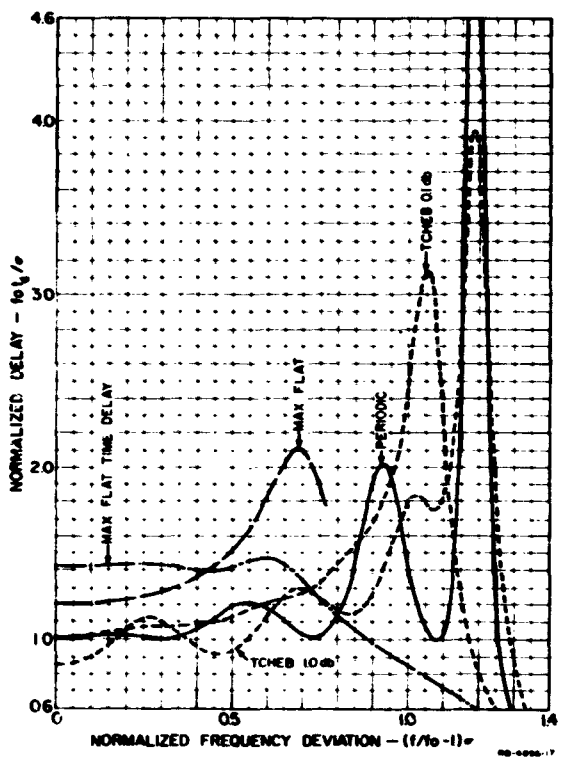

SOURCE: Quarterly Progress Report 1, Contract AF 30(602)-2734, SRI (see Ref. 33 by L. Young)

FIG. 6.15-6 TIME DELAY CHARACTERISTICS OF FIVE FILTERS OF n = 8 SECTIONS

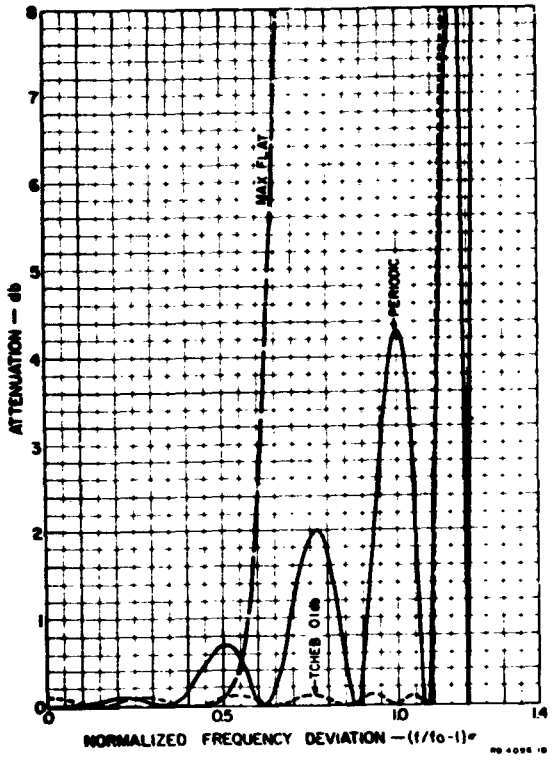

SOURCE: Quarterly Progress Report 1, Contract AF 30(602)-2734, SRI (see Ref. 33 by L. Young)

FIG. 6.15-7 ATTENUATION CHARACTERISTICS OF THREE FILTERS OF n = 12 SECTIONS

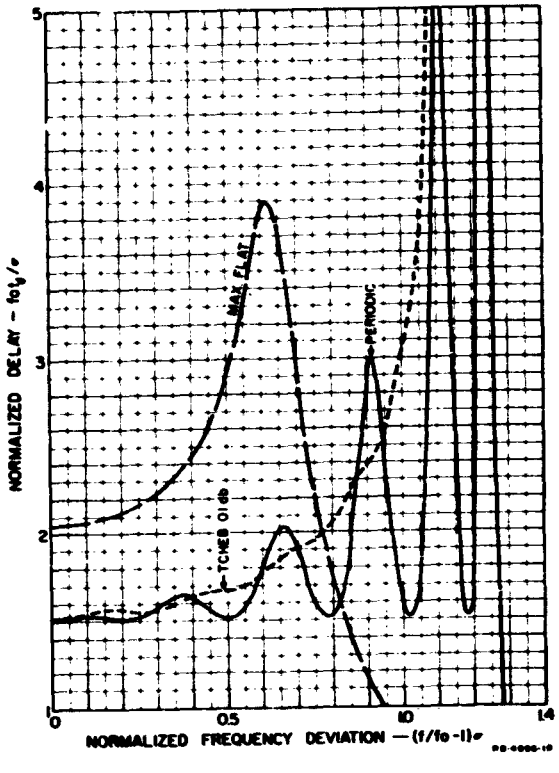

SOURCE: Quarterly Progress Report 1, Contract AF 30(602)-2734, SRI (see Ref. 33 by L. Young)

FIG. 6.15-8 GROUP DELAY CHARACTERISTICS OF THREE FILTERS OF n = 12 SECTIONS

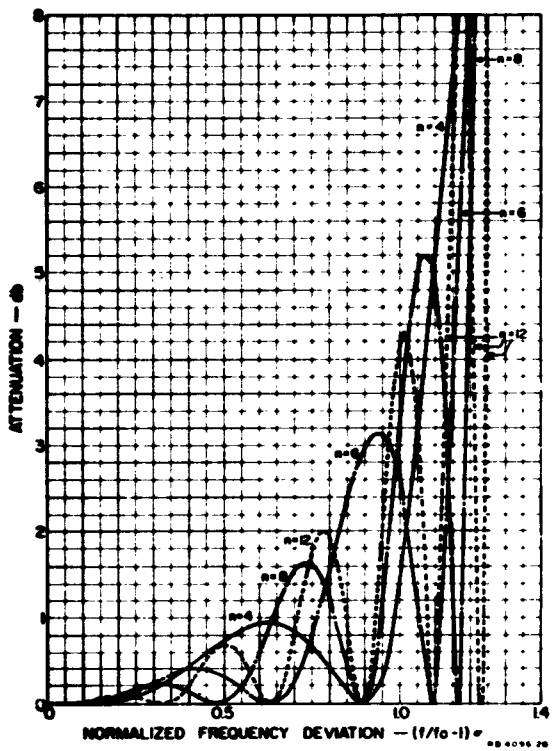

SOURCE: Quarterly Progress Report 1, Contract AF 30(602)-2734, SRI (see Ref. 33 by L. Young)

FIG. 6.15-9 ATTENUATION CHARACTERISTICS OF FOUR PERIODIC FILTERS WITH UP TO n = 12 SECTIONS

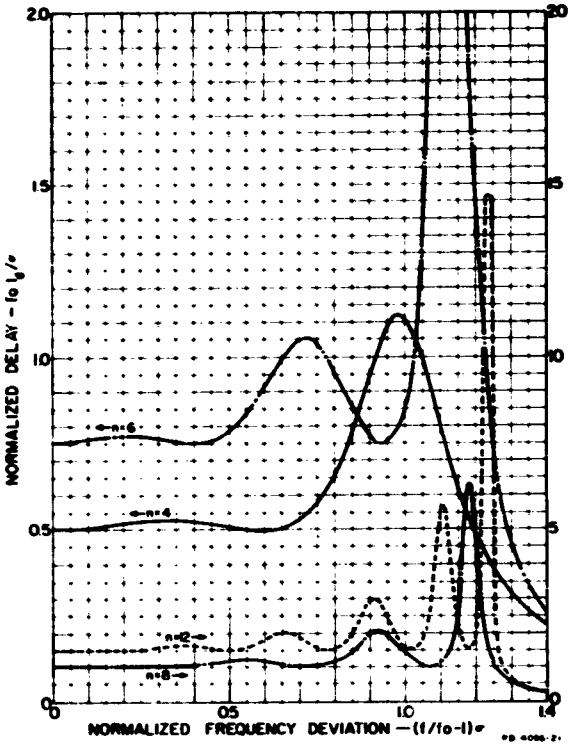

SOURCE: Quarterly Progress Report 1, Contract AF 30(602)-2734, SRI (see Ref. 33 by L. Young)

FIG. 6.15-10 GROUP DELAY CHARACTERISTICS OF FOUR PERIODIC FILTERS WITH UP TO n = 12 SECTIONS

filter.) For maximally flat filters, Eq. (6.15-6) with the aid of Sec. 6.02 reduces to

$$\sigma = \frac{4}{\pi}\left(\frac{4^{1/2n}}{w_{3\text{-db}}}\right) \tag{6.15-7}$$

where $w_{3\text{-db}}$ in Eq. (6.15-7) is the 3-db fractional bandwidth; while for Tchebyscheff transformers,

$$\sigma = \frac{8}{\pi}\left(\frac{\mathcal{E}_r^{1/2n}}{w}\right) . \tag{6.15-8}$$

Similarly it can be shown[33] for maximally flat time-delay filters, that

$$\left.\begin{aligned}\sigma &= 8\left[\frac{2(n!)}{(2n)!}\right]^{1/n} f_0(t_d)_0 \\ &= 4\left[\frac{2}{1.3.5.7.\ \ldots\ .(2n-1)}\right]^{1/n} f_0(t_d)_0\end{aligned}\right\} \tag{6.15-9}$$

and that for equal-element filters (corresponding to periodic filters),

$$\sigma = \frac{4}{\pi}\,\frac{\omega_1'}{w}\,g . \tag{6.15-10}$$

It can be deduced from Eq. (6.09-2) that the attenuation characteristics are independent of bandwidth or the value of R when plotted against x, defined by Eq. (6.15-5). Similarly, it follows from Eqs. (6.15-1) and (6.09-2) that the time delay should be plotted as

$$y = \frac{f_0 t_d}{\sigma} \tag{6.15-11}$$

so that it should become independent of bandwidth and the quantity R (still supposing small bandwidth, large R).

By using Eq. (6.15-7) through (6.15-10) to obtain σ, the curves in Figs. 6.15-1 through 6.15-10 can be used also for lumped-constant filters.

These curves are useful not only for predicting the group delay, but also for predicting the dissipation loss and (less accurately) the power-handling capacity in the pass band, when the values of these quantities at midband are already known [as, for instance, by Eq. (6.14-6) or (6.14-15)].

The following filter types are presented: maximally flat; Tchebyscheff (0.01 db ripple, 0.1 db ripple and 1.0 db ripple); maximally flat time delay; and periodic filters. The last-named are filters in which $V_1^2 = V_i = V_{n+1}^2$ for $i = 2, 3, \ldots, n$. [They correspond to low-pass prototype filters in which all the g_i ($i = 1, 2, \ldots, n$) in Fig. 4.04-1 are equal to one another. For large R and small bandwidth periodic filters give minimum band-center dissipation loss[12, 31] and greatest power-handling capacity[34] for a given selectivity.]

The figures go in pairs, the first plotting the attenuation characteristics, and the second the group delay. Figures 6.15-1 and 6.15-2 are for three periodic filters. The case $n = 1$ cannot be labelled, as it belongs to all types. The case $n = 2$ periodic is also maximally flat. The case $n = 3$ periodic is equivalent to a Tchebyscheff filter of about 0.15 db ripple.

Figures 6.15-3 to 6.15-8 are for $n = 4$, $n = 8$, and $n = 12$ sections, respectively, and include various conventional filter types. Figures 6.15-9 and 6.15-10 are for several periodic filters, showing how the characteristics change from $n = 4$ to $n = 12$ sections.

Example 2—Calculate the dissipation loss at band-edge of the filter in Example 1 of Sec. 6.14.

It was shown in that example that the band-center dissipation loss for that filter is 2.29 db. Since this is a Tchebyscheff 0.01-db ripple filter with $n = 4$, we see from Fig. 6.15-4 that the ratio of band-edge to band-center dissipation loss is approximately 0.665/0.535 = 1.243. Therefore the band-edge dissipation loss is approximately $2.29 \times 1.243 = 2.85$ db.

The application of the universal curves to the power-handling capacity of filters is discussed in Section 15.03.

REFERENCES

1. S. B. Cohn, "Optimum Design of Stepped Transmission-Line Transformers," *IRE Trans. PGMTT*-3, pp. 16-21 (April 1955).

2. R. E. Collin, "Theory and Design of Wide-Band Multisection Quarter-Wave Transformers," *Proc. IRE* 43, pp. 179-185 (February 1955).

3. H. J. Riblet, "General Synthesis of Quarter-Wave Impedance Transformers," *IRE Trans. PGMTT*-5, pp. 36-43 (January 1957).

4. Leo Young, "Tables for Cascaded Homogeneous Quarter-Wave Transformers," *IRE Trans. PGMTT*-7, pp. 233-237 (April 1959), and *PGMTT*-8, pp. 243-244 (March 1960).

5. Leo Young, "Optimum Quarter-Wave Transformers," *IRE Trans. PGMTT*-8, pp. 478-482 (September 1960).

6. Leo Young, "Inhomogeneous Quarter-Wave Transformers of Two Sections," *IRE Trans. PGMTT*-8, pp. 645-649 (November 1960).

7. S. B. Cohn, "Direct-Coupled-Resonator Filters," *Proc. IRE* 45, pp. 187-196 (February 1957).

8. G. L. Matthaei, "Direct-Coupled Band-Pass Filters with $\lambda/4$ Resonators," IRE National Convention Record, Part 1, pp. 98-111 (March 1958).

9. Leo Young, "The Quarter-Wave Transformers Prototype Circuit," *IRE Trans. PGMTT*-8, pp. 483-489 (September 1960).

10. Leo Young, "Synchronous Branch Guide Directional Couplers for Low and High Power Applications," *IRE Trans. PGMTT*-10, pp. - (November 1962).

11. Leo Young, "Synthesis of Multiple Antireflection Films over a Prescribed Frequency Band," *J. Opt. Soc. Am.* 51, pp. 967-974 (September 1961).

12. Leo Young, "Prediction of Absorption Loss in Multilayer Interference Filters," *J. Opt. Soc. Am.*, 52, pp. 753-761 (July 1962).

13. J. E. Holte and R. F. Lambert, "Synthesis of Stepped Acoustic Transmission Systems," *J. Acoust. Soc. Am.* 33, pp. 289-301 (March 1961).

14. Leo Young, "Stepped Waveguide Transformers and Filters," Letter in *J. Acoust. Soc. Am.* 33, p. 1247 (September 1961).

15. Leo Young, "Inhomogeneous Quarter-Wave Transformers," *The Microwave Journal*, 5, pp. 84-89 (February 1962).

16. IRE Standards on Antennas and Waveguides, *Proc. IRE* 47, pp. 568-582 (1959). See especially, p. 581.

17. G. C. Southworth, *Principles and Application of Waveguide Transmission* (D. Van Nostrand Co., Inc., New York City, 1950).

18. C. L. Dolph, "A Current Distribution for Broadside Arrays Which Optimizes the Relationship Between Beam Width and Side-Lobe Level," *Proc. IRE* 34, pp. 335-348 (June 1946). See also Discussion in *Proc. IRE* 35, pp. 489-492 (May 1947).

19. L. B. Brown and G. A. Sharp, "Tchebyscheff Antenna Distribution, Beamwidth and Gain Tables," NAVORD Report 4629 (NOLC Report 383), Naval Ordnance Laboratory, Corona, California (28 February 1958).

20. M. L. Reuss, Jr., "Some Design Considerations Concerning Linear Arrays Having Dolph-Tchebyscheff Amplitude Distributions," NRL Report 5240, ASTIA Number AD 212 621 (12 February 1959).

21. G. J. Van der Maas, "A Simplified Calculation for Dolph-Tchebyscheff Arrays," *J. Appl. Phys.* 24, p. 1250 (September 1953).

22. J. R. Whinnery, H. W. Jamieson, and Theo Eloise Robbins, "Coaxial Line Discontinuities," *Proc. IRE* 32, pp. 695-709 (November 1944).

23. N. Marcuvitz, *Waveguide Handbook*, MIT Rad. Lab. Series, Vol. 10 (McGraw-Hill Book Co., Inc., New York City, 1951).

24. C. G. Montgomery, R. H. Dicke, and E. M. Purcell, *Principles of Microwave Circuits*, MIT Rad. Lab. Series Vol. 9 (McGraw-Hill Book Co., Inc., New York City, 1948).

25. E. A. Ohm, "A Broad-Band Microwave Circulator," *IRE Trans. PGMTT*-4, pp. 210-217 (October 1956).

26 B. Bramham, "A Convenient Transformer for Matching Coaxial Lines," *Electronic Engineering* 33, pp. 42-44 (January 1961).

27. G. L. Ragan, *Microwave Transmission Circuits*, MIT Rad. Lab. Series, Vol. 9, pp. 29-36 (McGraw-Hill Book Co., Inc., New York City, 1946).

28. K. D. Mielenz, "Use of Chebychev Polynomials in Thin Film Computations," *J. Res. Nat. Bur. Stand.*, 63A, pp. 297-300 (November-December 1959). [There is a misprint in Eq. (17b): the lower left element in the matrix should be $S_{n-1}a_{21}$.]

29. F. Abelès, "Sur l'élévation à la puissance *n* d'une matrice carrée a quatre éléments à l'aide des polynomes de Tchébychev," Comptes Rendus 226, pp. 1872-1874 (1948) and "Transmission de la lumière à travers un système de lames minces alternées," Comptes Rendus, 226, pp. 1808-1810 (1948).

30. Leo Young, "Q-Factors of a Transmission Line Cavity," *IRE Trans. PGCT*-4, pp. 3-5 (March 1957).

31. S. B. Cohn, "Dissipation Loss in Multiple-Coupled-Resonator Filters," *Proc. IRE* 47, pp. 1342-1348 (August 1959).

32. Leo Young, "Analysis of a Transmission Cavity Wavemeter," *IRE Trans. PGMTT*-8, pp. 436-439 (July 1960).

33. Leo Young, "Suppression of Spurious Frequencies," Sec. III, Quarterly Progress Report 1, SRI Project 4096, Contract AF 30(602)-2734, Stanford Research Institute, Menlo Park, California (July 1962).

34. S. B. Cohn, "Design Considerations for High-Power Microwave Filters," *IRE Trans. PGMTT*-7, pp. 149-153 (January 1959).

NOTE: The material for this chapter is largely derived from:

35. Leo Young and G. L. Matthaei, "Microwave Filters and Coupling Structures," Quarterly Progress Report 4, SRI Project 3527, Contract DA 36-039 SC-87398, Stanford Research Institute, Menlo Park, California (January 1962)

Sections 6.01 through 6.07 and Sections 6.09 and 6.10 are mostly contained in:

36. Leo Young, "Stepped Impedance Transformers and Filter Prototypes," *IRE Trans. PGMTT*-10, pp. 339-359 (September 1962).

CHAPTER 7

LOW-PASS AND HIGH-PASS FILTERS USING SEMI-LUMPED ELEMENTS OR WAVEGUIDE CORRUGATIONS

SEC. 7.01, PROPERTIES OF THE FILTERS DISCUSSED IN THIS CHAPTER

Unlike most of the filter structures to be discussed in later chapters, the microwave filters treated in this chapter consist entirely of elements which are small compared to a quarter-wavelength (at pass-band frequencies). In the cases of the TEM-mode filters treated, the design is carried out so as to approximate an idealized lumped-element circuit as nearly as possible. In the cases of the corrugated and waffle-iron low-pass waveguide filters discussed, the corrugations are also small compared to a quarter-wavelength. Such filters are a waveguide equivalent of the common series-L, shunt-C, ladder type of low-pass filter, but due to the waveguide nature of the structure, it is more difficult to design them as a direct approximation of a lumped-element, low-pass filter. Thus, in this chapter the waveguide filters with corrugations are treated using the image method of design (Chapter 3).

In Sec. 7.02 will be found a discussion of how lumped elements may be approximated using structures which are practical to build for microwave applications. In later sections the design of filters in specific common types of construction are discussed, but using the principles in Sec. 7.02 the reader should be able to devise additional forms of construction as may be advantageous for special situations.

Figure 7.01-1(a) shows a coaxial form of low-pass filter which is very common. It consists of short sections of high-impedance line (of relatively thin rod or wire surrounded by air dielectric) which simulate series inductances, alternating with short sections of very-low-impedance line (each section consisting of a metal disk with a rim of dielectric) which simulate shunt capacitances. The filter shown in Fig. 7.01-1(a) has tapered lines at the ends which permit the enlarging of the coaxial region at the center of the filter so as to reduce dissipation loss. However, it is more common to build this type of filter with the outer conductor consisting of a uniform, cylindrical metal tube. The popularity

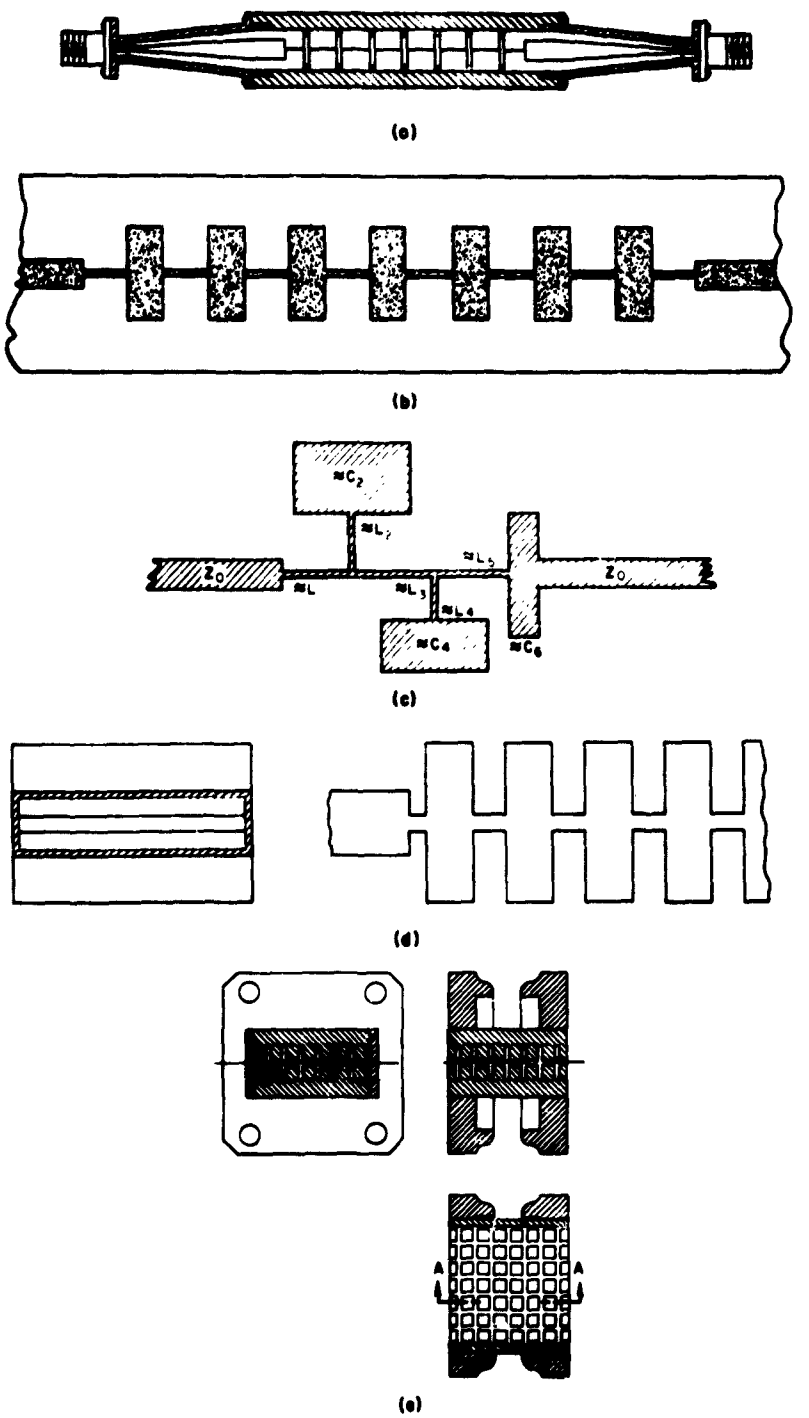

FIG. 7.01-1 SOME SPECIFIC LOW-PASS FILTER STRUCTURES DISCUSSED IN THIS CHAPTER

of this type of low-pass filter results from its simplicity of fabrication and its excellent performance capabilities. Its first spurious pass band occurs, typically, when the high-impedance lines are roughly a half-wavelength long. It is not difficult with this type of filter to obtain stop bands which are free of spurious responses up as far as five times the cutoff frequency of the filter. Filters of this type are commonly built with cutoff frequencies ranging from a few hundred megacycles up to around 10 Gc. A discussion of their design will be found in Sec. 7.03.

Figure 7.01-1(b) shows a printed-circuit, strip-line filter which is equivalent to the filter in Fig. 7.01-1(a) in most respects, but which has somewhat inferior performance characteristics. The great advantage of this type of filter is that it is unusually inexpensive and easy to fabricate. It usually consists primarily of two sheets of low-loss dielectric material with a photo-etched, copper-foil, center-conductor [shown in Fig. 7.01-1(b)] sandwiched in between, and with copper foil or metal plates on the outer surfaces of the dielectric pieces to serve as ground planes. When this type of circuit is used the dissipation loss is generally markedly higher than for the filter in Fig. 7.01-1(a) because of the presence of dielectric material throughout the circuit. Also, when this type of construction is used it is generally not possible to obtain as large a difference in impedance level between the high- and low-impedance line sections as is readily feasible in the construction shown in Fig. 7.01-1(a). As a result of this, the attenuation level at frequencies well into the stop band for filters constructed as shown in Fig. 7.01-1(b) is generally somewhat lower than that for filters constructed as shown in Fig. 7.01-1(a). Also, spurious responses in the stop band generally tend to occur at lower frequencies for the construction in Fig. 7.01-1(b). Filters using this latter construction can also be used in the 200-Mc to 10-Gc range. However, for the high portion of this range they must be quite small and they tend to have considerable dissipation loss. A discussion of the design of this type of filter will be found in Sec. 7.03.

Figure 7.01-1(c) shows another related type of printed-circuit low-pass filter. The symbols L_1, L_2, C_2, etc., indicate the type of element which different parts of the circuit approximate. Elements L_2 and C_2 in series approximate an L-C branch which will short-circuit transmission at its resonant frequency. Likewise for the part of the circuit which approximates L_4 and C_4. These branches then produce peaks of high attenuation at frequencies above the cutoff frequency and fairly close to it,

and by so doing, they increase the sharpness of the cutoff characteristic. This type of filter is also easy to fabricate in photo-etched, printed-circuit construction, but has not been used as much as the type in Fig. 7.01-1(b), probably because it is somewhat more difficult to design accurately. This type of filter can also be designed in coaxial or coaxial split-block form so as to obtain improved performance, but such a filter would, of course, be markedly more costly to build. Discussion of the design of filters such as that in Fig. 7.01-1(c) will be found in Sec. 7.03.

The filter shown in Fig. 7.01-1(d) is a waveguide version of the filters in Figs. 7.01-1(a) and (b). In this case the low- and high-impedance sections of line are realized by raising and lowering the height of the guide, which has led to the name "corrugated waveguide filter" by which it is commonly known. It is a low-pass filter in its operation, but since the waveguide has a cutoff frequency, it cannot operate, of course, to DC as do most low-pass filters. This type of filter can be made to have very low pass-band loss because of its waveguide construction, and it can be expected to have a higher power rating than equivalent TEM-mode filters. However, this type of filter has disadvantages compared to, say, the coaxial filter in Fig. 7.01-1(a) because (1) it is larger and more costly to build, (2) the stop bands cannot readily be made to be free of spurious responses to as high a frequency even for the normal TE_{10} mode of propagation, and (3) there will be numerous spurious responses in the stop-band region for higher-order modes, which are easily excited at frequencies above the normal TE_{10} operating range of the waveguide. Due to the presence of the corrugations in the guide, modes having variations in the direction of the waveguide height will be cut off up to very high frequencies. Therefore, TE_{n0} modes will be the only ones that need be considered. If the waveguide is excited by a probe on its center line, the TE_{20}, TE_{40}, and other even-order modes will not be excited. In this case, the first higher-order mode that will be able to cause trouble is the TE_{30} mode which has a cutoff frequency three times that of the TE_{10} mode. In typical cases the TE_{30} mode might give a spurious response at about 2.5 times the center frequency of the first pass band. Thus, if the TE_{20} mode is not excited, or if a very wide stop band is not required, corrugated waveguide filters will frequently be quite satisfactory. The only limitations on their useful frequency range are those resulting from considerations of size and ease of manufacture. Filters of this type (or

the waffle-iron filters discussed below) are probably the most practical forms of low-pass filters for frequencies of 10 Gc or higher. This type of filter is discussed in Sec. 7.04.

Figure 7.01-1(e) shows a waffle-iron filter which in many respects is equivalent to the corrugated waveguide filter in Fig. 7.01-1(d), but it includes a feature which reduces the problem of higher-order modes introducing spurious responses in the stop band. This feature consists of the fact that the low-impedance sections of the waveguide are slotted in the longitudinal direction so that no matter what the direction of the components of propagation in the waveguide are, they will see a low-pass filter type of structure, and be attenuated. Filters of this type have been constructed with stop bands which are free of spurious responses up to three times the cutoff frequency of the filter. The inclusion of longitudinal slots makes them somewhat more difficult to build than corrugated waveguide filters, but they are often worth the extra trouble. Their characteristics are the same as those of the corrugated waveguide filter, except for the improved stop band. This type of filter is discussed in Sec. 7.05.

Figure 7.01-2 shows a common type of high-pass filter using coaxial split-block construction. This type of filter is also designed so that its elements approximate lumped elements. In this case the short-circuited coaxial stubs represent shunt inductances, and the disks with Teflon spacers represent series capacitors. This type of filter has

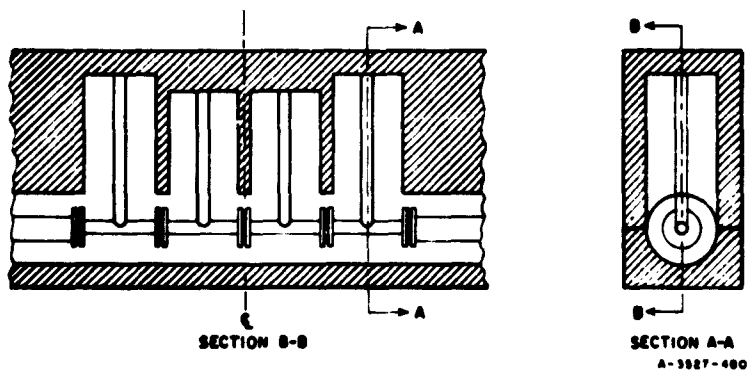

FIG. 7.01-2 A HIGH-PASS FILTER IN SPLIT-BLOCK COAXIAL CONSTRUCTION

excellent cutoff characteristics since for a design with n reactive elements there is an nth-order pole of attenuation (Sec. 2.04) at zero frequency. Typical filters of this sort have a low-attenuation, low-VSWR pass band extending up about an octave above the cutoff frequency, with relatively low attenuation extending up to considerably higher frequencies. The width of the pass band over which the filter will simulate the response of its idealized, lumped prototype depends on the frequency at which the elements no longer appear to be sufficiently like lumped elements. To achieve cutoffs at high microwave frequencies, structures of this type have to be very small, and they require fairly tight manufacturing tolerance. This makes them relatively difficult to construct for high microwave frequency applications. For this reason they are used most often for cutoffs in the lower microwave frequency range (200 to 2000 Mc) where their excellent performance and compactness has considerable advantage, but they are also sometimes miniaturized sufficiently to operate with cutoffs as high as 5 or 6 Gc. Usually at the higher microwave frequency ranges the need for high-pass filters is satisfied by using wideband band-pass filters (see Chapters 9 and 10). The type of high-pass filter in Fig. 7.01-2 has not been fabricated in equivalent printed-circuit form much because of the difficulties in obtaining good short-circuits on the inductive stubs in printed circuits, and in obtaining adequately large series capacitances.

SEC 7.02, APPROXIMATE MICROWAVE REALIZATION OF LUMPED ELEMENTS

A convenient way to realize relatively wide-band filters operating in the frequency range extending from about 100 Mc to 10,000 Mc is to construct them from short lengths of coaxial line or strip line, which approximate lumped-element circuits. Figure 7.02-1 illustrates the exact T- and π-equivalent circuits of a length of non-dispersive TEM transmission line. Also shown are the equivalent reactance and susceptance values of the networks when their physical length l is small enough so that the electrical length $\omega l/v$ of the line is less than about $\pi/4$ radians. Here we have used the symbol ω for the radian frequency and v for the velocity of propagation along the transmission line.

For applications where the line lengths are very short or where an extremely precise design is not required, it is often possible to represent a short length of line by a single reactive element. For example, inspection of Fig. 7.02-1 shows that a short length of high-Z_0 line terminated at both ends by a relatively low impedance has an effect equivalent to that

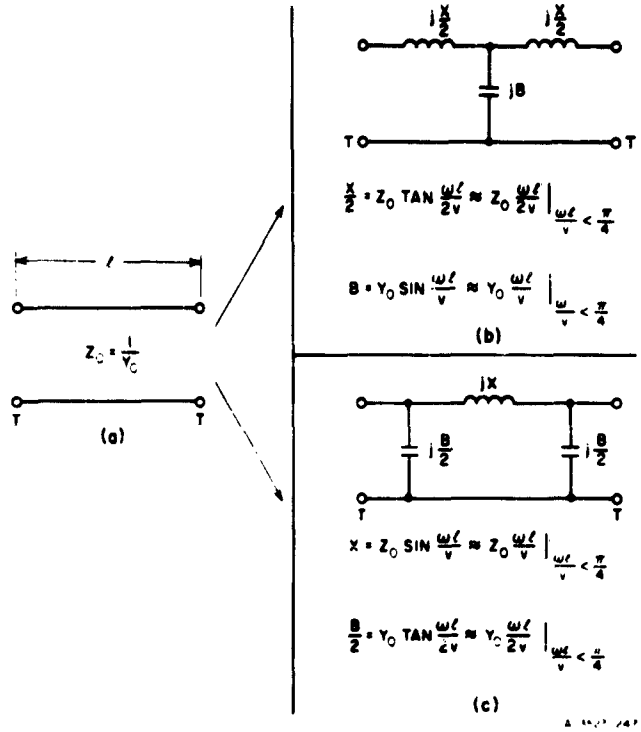

FIG. 7.02-1 TEM-LINE EQUIVALENT CIRCUITS

of a series inductance having a value of $L = Z_0 l/v$ henries. Similarly, a short length of low-Z_0 line terminated at either end by a relatively high impedance has an effect equivalent to that of a shunt capacitance $C = Y_0 l/v = l/Z_0 v$ farads. Such short sections of high-Z_0 line and low-Z_0 line are the most common ways of realizing series inductance and shunt capacitance, respectively, in TEM-mode microwave filter structures.

A lumped-element shunt inductance can be realized in TEM transmission line in several ways, as illustrated in Fig. 7.02-2(a). The most convenient way in most instances is to employ a short length of high-Z_0 line, short-circuited to ground at its far end, as shown in the strip-line example. For applications where a very compact shunt inductance is required, a short length of fine wire connected between the inner and outer conductors can be used, as is illustrated in the coaxial line example in Fig. 7.02-2(a).

Also, a lumped element series capacitance can be realized approximately in TEM transmission lines in a variety of ways, as illustrated in Fig. 7.02-2(b). Often the most convenient way is by means of a gap in the center conductor.[1] Where large values of series capacitance are required in a coaxial system a short length of low-Z_0, open-circuited line, in series with the center conductor can be used. Values of the series capacitance of overlapping strip lines are also shown in Fig. 7.02-2(b). Section 8.05 presents some further data on capacitive gaps.

A lumped-element, series-resonant, shunt circuit can be realized in strip line in the manner shown in Fig. 7.02-2(c). It is usually necessary when computing the capacitive reactance of the low-impedance (Z_{01}) line in Fig. 7.02-2(c) to include the fringing capacitance at the end of the Z_{01} line and at the step between lines. The end fringing capacitance can be accounted for as follows. First, compute the per-unit-length capacitance

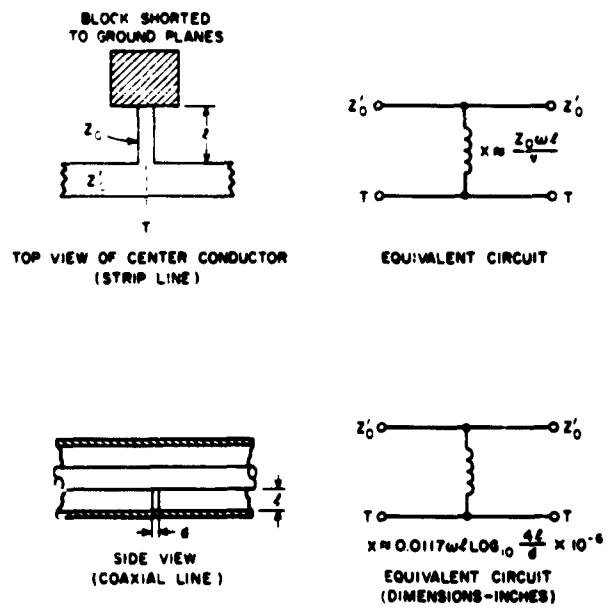

(a) SHUNT INDUCTANCES

A 3527 A248

FIG. 7.02-2 SEMI-LUMPED-ELEMENT CIRCUITS IN TEM TRANSMISSION LINE

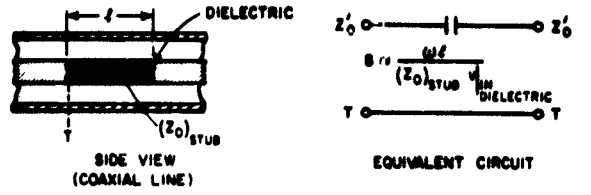

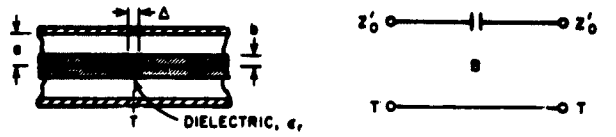

$$B \approx \omega \left[0.706 \epsilon_r \frac{b^2}{\Delta} + 0.442 b \ln \left(\frac{2a - 2b}{\Delta} \right) \right] \times 10^{-12}$$

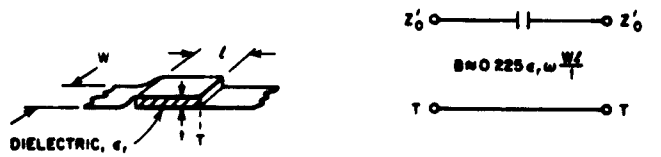

(b) SERIES CAPACITANCES

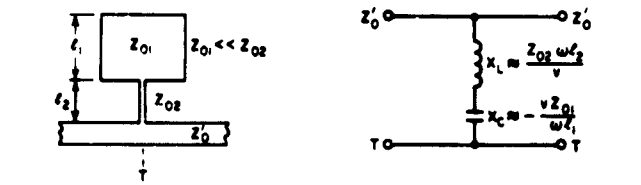

(c) SERIES-RESONANT SHUNT CIRCUIT

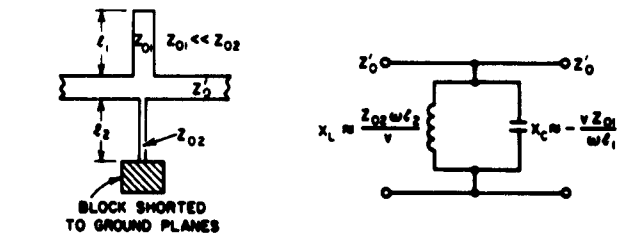

(d) PARALLEL-RESONANT SHUNT CIRCUIT

FIG. 7.02-2 Concluded

$$C_{01} = \frac{84.73\sqrt{\epsilon_r}}{Z_{01}} \ \mu\mu f/\text{inch} \qquad (7.02\text{-}1)$$

for the Z_{01} line, where ϵ_r is the relative dielectric constant. Then the effect of the fringing capacitances at the ends of the line can be accounted for, approximately, by computing the total effective electrical length of the Z_{01} line as the measured length plus a length

$$\Delta l = \frac{0.450\ w\epsilon_r}{C_{01}}\left(\frac{C_f'}{\epsilon}\right) \text{ inches} \qquad (7.02\text{-}2)$$

added at each end. In Eqs. (7.02-1) and (7.02-2), w is the width of the strip in inches, and C_f'/ϵ is obtained from Fig. 5.07-5. A further refinement in the design of resonant elements such as that in Fig. 7.02-2(c) can be made by correcting for the junction inductance predicted by Fig. 5.07-3; however, this correction is usually quite small.

A lumped-element parallel-resonant shunt circuit can be realized in the manner shown in Fig. 7.02-2(d). Here too it is necessary, when computing the capacitive reactance of the low-impedance (Z_{01}) line, to include the fringing capacitance at the end of the open-circuited line.

The series-resonance and parallel-resonance characteristics of the lumped elements of Figs. 7.02-2(c) and 7.02-2(d) can also be approximated over limited frequency bands by means of quarter-wavelength lines, respectively, open-circuited or short-circuited at their far ends. Formulas for computing the characteristics of such lines are given in Fig. 5.08-1.

Series circuits having either the characteristics of lumped series-resonant circuits or lumped parallel-resonant circuits are very difficult to realize in semi-lumped-form TEM transmission lines. However, they can be approximated over limited frequency bands, in coaxial lines, by means of quarter wavelength stubs in series with the center conductor, that are either open-circuited or short-circuited at their ends, respectively. Such stubs are usually realized as lines within the center conductor in a manner similar to the first example in Fig. 7.02-2(b).

SEC. 7.03, LOW-PASS FILTERS USING SEMI-LUMPED ELEMENTS

The first step in the design of filters of this type is to select an appropriate lumped-element design (usually normalized), such as those in the tables of low-pass prototypes in Secs. 4.05 to 4.07. The choice of the type of the response (for example, the choice between a 0.1- or 0.5-db ripple Tchebyscheff response) will depend on the requirements of a specific application. Also, the number n of reactive elements will be determined by the rate of cutoff required for the filter. For Tchebyscheff and maximally flat series-L, shunt-C, ladder low-pass filters the required value of n is easily determined from the normalized attenuation curves in Sec. 4.03.

Having obtained a suitable lumped-element design, the next step is to find a microwave circuit which approximates it. Some examples will now be considered.

An Example of a Simple L-C Ladder Type of Low-Pass Filter—It is particularly advantageous to design low-pass filters in coaxial- or printed-circuit form using short lengths of transmission line that act as semi-lumped elements. In order to illustrate the design procedure for this type of filter the design of a 15-element filter is described in this section. The design specifications for this filter are 0.1-db equal-ripple insertion loss in the pass band extending from zero frequency to 1.971 Gc, and at least 35-db attenuation at 2.168 Gc. A photograph of the filter constructed from coaxial elements using the "split-block" coaxial line construction technique is shown in Fig. 7.03-1.

The form of the 15-element low-pass prototype chosen for this filter has a series inductance as the first element, as illustrated in the schematic of Fig. 7.03-2(a). At the time this filter was designed the element values in Table 4.05-2(b) were not available, but the element values for filters containing up to 10 elements as listed in Table 4.05-2(a) were available. Therefore, the 15-element prototype was approximated by using the nine-element prototype in Table 4.05-2(a), augmented by repeating three times each of the two middle elements of the nine-element filter. Comparison of these values with the more recently obtained exact values from Table 4.05-2(b) shows that the end elements of the filter are about 1.2 percent too small and that the error in the element values increases gradually toward the center of the filter so that the center element is about 4.2 percent too small. These errors are probably too

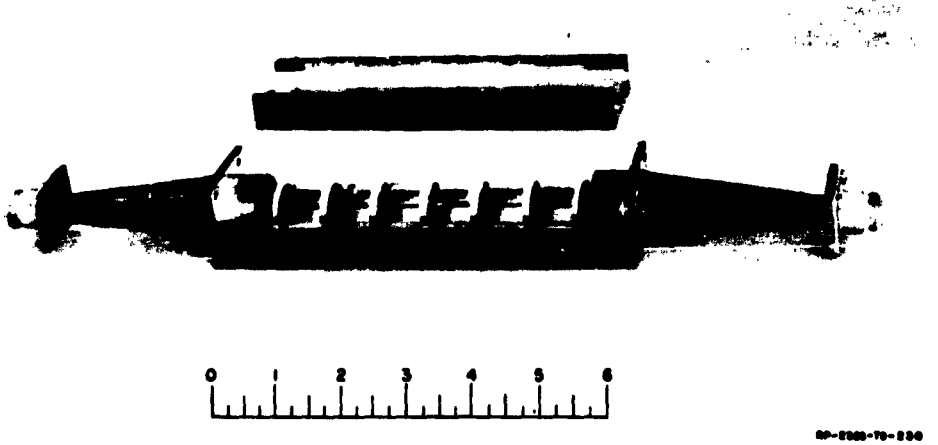

FIG. 7.03-1 A MICROWAVE LOW-PASS FILTER

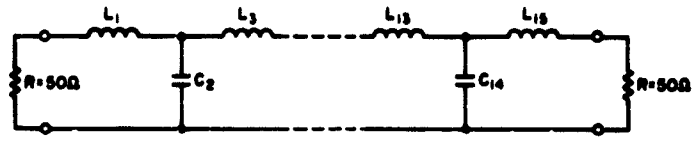

$L_1 = L_{15} = 4.826 \times 10^{-9}$ henries
$C_2 = C_{14} = 2.329 \times 10^{-12}$ farads
$L_3 = L_{13} = 8.616 \times 10^{-9}$ henries
$C_4 = C_6 = C_8 = C_{10} = C_{12} = 2.610 \times 10^{-12}$ farads
$L_5 = L_7 = L_9 = L_{11} = 8.902 \times 10^{-9}$ henries

SCHEMATIC OF LUMPED CONSTANT PROTOTYPE

(a)

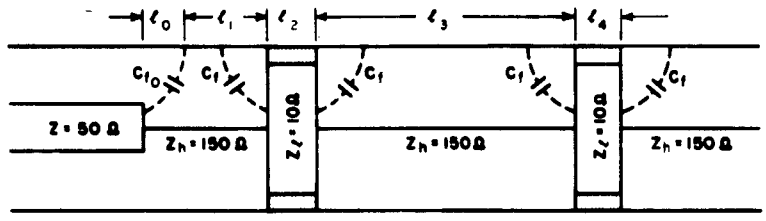

SEMI-LUMPED REALIZATION OF A PORTION OF THE LOW-PASS FILTER

(b)

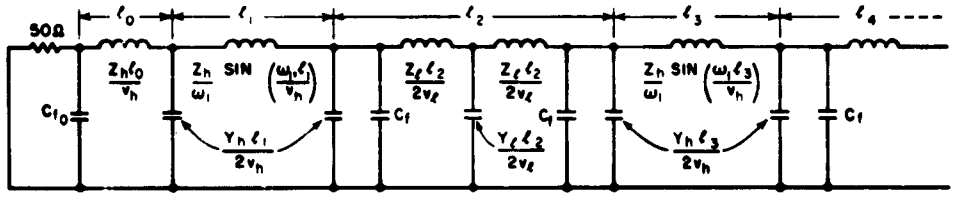

EQUIVALENT CIRCUIT OF A PORTION OF THE SEMI-LUMPED LOW-PASS FILTER

(c)

8-3527-249

FIG. 7.03-2 STEPS IN THE REALIZATION OF A MICROWAVE LOW-PASS FILTER

small to be of significance in most applications. It should be noted that since tables going to $n = 15$ are now available, good designs for even larger n's can be obtained by augmenting $n = 14$ or $n = 15$ designs, in the above manner.

The schematic of the lumped-constant prototype used in the design of the actual filter is shown in Fig. 7.03-2(a). This filter is scaled to operate at a 50-ohm impedance level with an angular band-edge frequency ω_1 of 12.387×10^9 radians per second. The values of the inductances and capacitances used in the lumped-constant circuit are obtained from the low-pass prototype by means of Eqs. (4.04-3) and (4.04-4). That is, all inductances in the low-pass prototype are multiplied by $50/(12.387 \times 10^9)$ and all capacitances are multiplied by $1/(50 \times 12.387 \times 10^9)$. Sometimes, instead of working with inductance in henries and capacitance in farads, it is more convenient to work in terms of reactance and susceptance. Thus, a reactance $\omega_1' L_k'$ for the prototype becomes simply $\omega_1 L_k = (\omega_1' L_k')(R_0/R_0')$ for the actual filter, where R_0' is the resistance of one of the prototype terminations and R_0 is the corresponding resistance for the scaled filter. Also, the shunt susceptances $\omega_1' C_k'$ for the prototype become $\omega_1 C_k = (\omega_1' C_k')(R_0'/R_0)$ for the scaled filter. This latter approach will be utilized in the numerical procedures about to be outlined.

The semi-lumped realization of a portion of the filter is shown in Fig. 7.03-2(b). It is constructed of alternate sections of high-impedance ($Z_h = 150$ ohms) and low-impedance ($Z_l = 10$ ohms) coaxial line, chosen so that the lengths of the high-impedance line would be approximately one-eighth wavelength at the equal-ripple band-edge frequency of 1.971 Gc. The whole center conductor structure is held rigidly aligned by dielectric rings ($\epsilon_r = 2.54$) surrounding each of the low-impedance lengths of line. The inside diameter of the outer conductor was chosen to be 0.897 inch so that the 2.98-Gc cutoff frequency of the first higher-order mode* that can propagate in the low-impedance sections of the filter is well above the 1.971-Gc band-edge frequency of the filter. The values of the inductances and capacitances in the lumped-constant circuit, Fig. 7.03-2(a), are realized by adjusting the lengths of the high- and low-impedance lines respectively.

* As discussed in Sec. 5.03, the first higher mode can occur when $f \geq 7.51(b + d)/\sqrt{\epsilon_r}$, where f is in Gc and b and d are the outer and inner diameters in inches.

The exact equivalent circuit of the semi-lumped realization of the first three end elements of the filter are shown in Fig. 7.03-2(c). In this figure C_{f0} is the fringing capacity at the junction of the 50-ohm terminating line and the 150-ohm line representing the first element in the filter, as determined from Fig. 5.07-2. Similarly, C_f is the fringing capacitance at each junction between the 10-ohm and 150-ohm lines in the filter. It is also determined from Fig. 5.07-2, neglecting the effect on fringing due to the dielectric spacers in 10-ohm lines. The velocity of propagation v_h of a wave along the 150-ohm line is equal to the velocity of light in free space while the velocity of propagation v_l along the 10-ohm line is $v_h/\sqrt{\epsilon_r}$.

Some of the 150-ohm lines in this filter attain electrical lengths of approximately 50 electrical degrees at the band-edge frequency ω_1. For lines of this length it has been found that the pass-band bandwidth is most closely approximated if the reactances of the lumped-constant inductive elements at frequency ω_1 are matched to the exact inductive reactance of the transmission line elements at frequency ω_1 using the formulas in Fig. 7.02-1. The inductive reactance of the 10-ohm lines can also be included as a small negative correction to the lengths of the 150-ohm lines. Following this procedure we have

$$\omega_1 L_1 = Z_h \sin\left(\frac{\omega_1 l_1}{v_h}\right) + \frac{Z_l l_2 \omega_1}{2v_l} \quad \text{ohms} \qquad (7.03\text{-}1)$$

$$\omega_1 L_3 = Z_h \sin\left(\frac{\omega_1 l_3}{v_h}\right) + \frac{Z_l l_2 \omega_1}{2v_l} + \frac{Z_l l_4 \omega_1}{2v_l}$$

etc.

The capacitance of each shunt element in the low-pass filter in Fig. 7.03-2(a) is realized as the sum of the capacitance of a short length of 10-ohm line, plus the fringing capacitances between the 10-ohm line and the adjacent 150-ohm lines, plus the equivalent 150-ohm-line capacitance as lumped at the ends of the adjacent 150-ohm lines. Thus, we can determine the lengths of the 10-ohm lines by means of the relations

$$\omega_1 C_2 = \frac{Y_l l_2 \omega_1}{v_l} + 2C_f\omega_1 + \frac{Y_h l_1 \omega_1}{2v_h} + \frac{Y_h l_3 \omega_1}{2v_h} \quad \text{mhos} \qquad (7.03\text{-}2)$$

$$\omega_1 C_4 = \frac{Y_l l_4 \omega_1}{v_l} + 2C_f\omega_1 + \frac{Y_h l_3 \omega_1}{2v_h} + \frac{Y_h l_5 \omega_1}{2v_h}$$

etc.

In Eqs. (7.03-1) above, the first term in each equation on the right is the major one, and the other terms on the right represent only small corrections. Thus, it is convenient to start the computations by neglecting all but the first term on the right in each of Eqs. (7.03-1), which makes it possible to solve immediately for preliminary values of the lengths l_1, l_3, l_5, etc., of the series-inductive elements. Having approximate values for l_1, l_3, l_5, etc., it is then possible to solve each of Eqs. (7.03-2) for the lengths l_2, l_4, l_6, etc., of the capacitive elements. Then, having values for l_2, l_4, l_6, etc., these values may then be used in the correction terms in Eqs. (7.03-1), and Eqs. (7.03-1) can then be solved to give improved values of the inductive element lengths l_1, l_3, l_5, etc.

The iterative process described above could be carried on to insert the improved values of l_1, l_3, l_5, etc., in Eq. (7.03-2) in order to recompute the lengths l_2, l_4, l_6, etc. However, this is unnecessary because the last two terms on the right in each of Eqs. (7.03-2) are only small correction terms themselves, and a small correction in them would have negligible effect on the computed lengths of the capacitor elements.

The reactance or susceptance form of Eqs. (7.03-1) and (7.03-2) is convenient because it gives numbers of moderate size and avoids the necessity of carrying multipliers such as 10^{-12}. The velocity of light is $v = 1.1803 \times 10^{10}/\sqrt{\epsilon_r}$ inches per second, so that the ratios ω_1/v_h and ω_1/v_h are of moderate size.

The effect of the discontinuity capacitances C_{f0} and $Y_h l_1/2v_h$ at the junction between the 50-ohm lines terminating the filter and the 150-ohm lines comprising the first inductive elements of the filter can be minimized by increasing the length of the 150-ohm lines by a small amount l_0 to simulate the series inductance and shunt capacitance of a

short length of 50-ohm line. The necessary line length l_0 can be determined from the relation

$$Z_0 = 50 = \sqrt{\frac{\frac{Z_h l_0}{v_h}}{C_{f0} + \frac{Y_h l_1}{2v_h}}} = \sqrt{\frac{\text{Series Inductance}}{\text{Shunt Capacitance}}} \quad .$$

Solving for l_0 gives

$$l_0 = Z_0^2 \left[\frac{(\omega_1 C_{f0}) v_h}{Z_h \omega_1} + \frac{l_1}{2Z_h^2} \right] \quad . \qquad (7.03\text{-}3)$$

Figure 7.03-3(a) shows the dimensions of the filter determined using the above procedures, while Fig. 7.03-3(b) shows the measured response of the filter. It is seen that the maximum pass-band ripple level as determined from VSWR measurements is about 0.12 db over most of the pass band while rising to 0.2 db near the edge of the pass band. It is believed that the discrepancy between the measured pass-band ripple

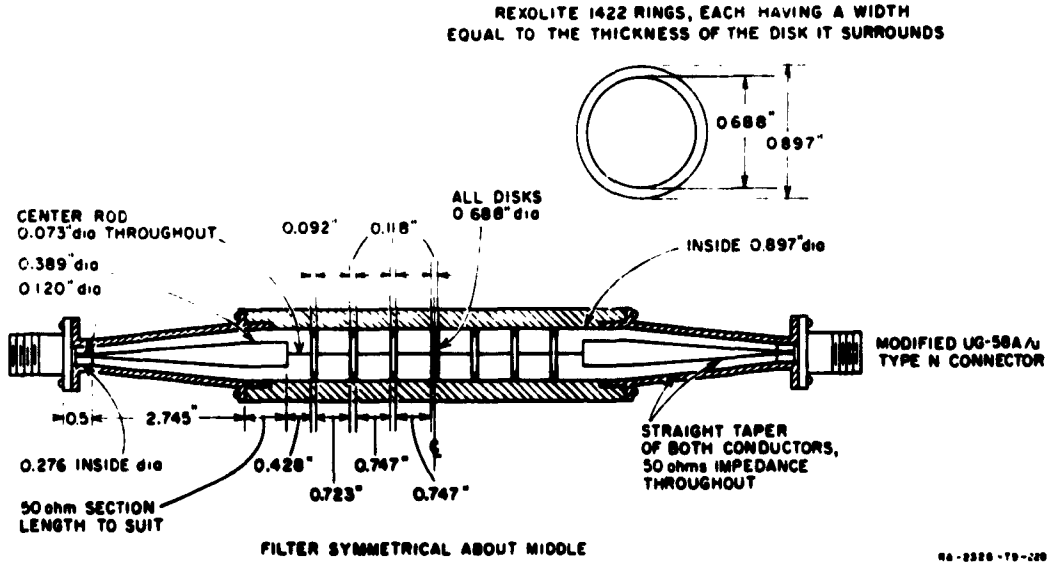

FIG. 7.03-3(a) DIMENSIONS OF THE FILTER IN FIG. 7.03-1

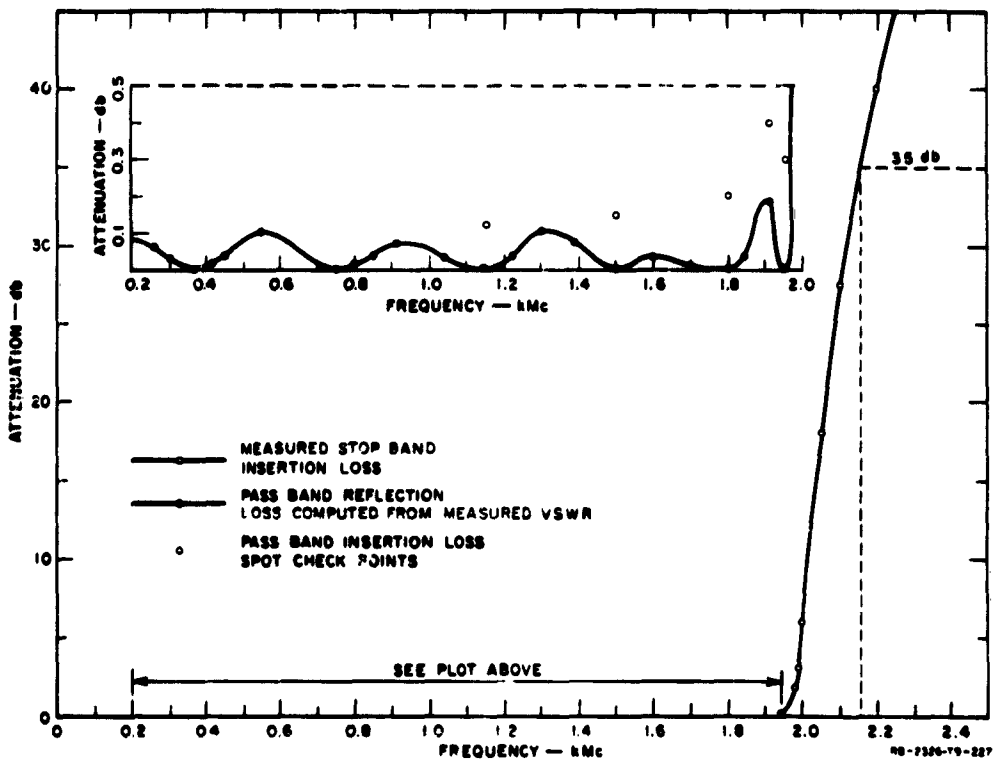

FIG. 7.03-3(b) MEASURED RESPONSE OF THE FILTER IN FIG. 7.03-1

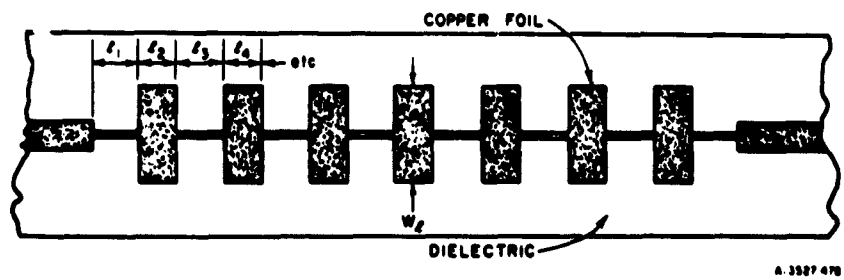

FIG. 7.03-3(c) A POSSIBLE PRINTED-CIRCUIT VERSION OF THE LOW-PASS FILTER IN FIG. 7.03-3(a)

level and the theoretical 0.1-db level is caused primarily by the fact that the approximate prototype low-pass filter was used rather than the exact prototype as given in Table 4.05-2(b). The actual pass-band attenuation of the filter, which includes the effect of dissipation loss in the filter, rises to approximately 0.35 db near the edge of the pass band. This behavior is typical and is explained by the fact that $d\phi/d\omega'$, the rate of change of phase shift through the low-pass prototype filter as a function of frequency, is more rapid near the pass-band edge, and this leads to increased attenuation as predicted by Eq. (4.13-9). A more complete discussion of this effect is contained in Sec. 4.13.

This filter was found to have some spurious responses in the vicinity of 7.7 to 8.5 Gc, caused by the fact that many of the 150-ohm lines in the filter were approximately a half-wavelength long at these frequencies. No other spurious responses were observed, however, at frequencies up through *X*-band. In situations where it is desired to suppress these spurious responses it is possible to vary the length and the diameter of the high-impedance lines to realize the proper values of series inductance, so that only a few of the lines will be a half-wavelength long at any frequency within the stop band.

The principles described above for approximate realization of low-pass filters of the form in Fig. 7.03-2(a) can also be used with other types of filter constructions. For example, Fig. 7.03-3(c) shows how the filter in Fig. 7.02-3(a) would look if realized in printed-circuit, strip-line construction. The shaded area is the copper foil circuit which is photo-etched on a sheet of dielectric material. In the assembled filter the photo-etched circuit is sandwiched between two slabs of dielectric, and copper foil or metal plates on the outside surfaces serve as the ground planes. The design procedure is the same as that described above, except that in this case the line impedances are determined using Fig. 5.04-1 or 5.04-2, and the fringing capacitance C_f in Eqs. (7.03-2) is determined using Fig. 5.07-5. It should be realized that C_f' in Fig. 5.07-5 is the capacitance per unit length from one edge of the conductor to one ground plane.* Thus, C_f in Eqs. (7.03-2) is $C_f = 2C_f'W_t$, where W_t is the width of the low-impedance line sections [Fig. 7.03-3(c)]. The calculations then proceed exactly as described before. The relative

* If in computing C_f' from C_f'/ϵ in Fig. 5.07-5, $\epsilon = 0.255\epsilon_r \times 10^{-12}$ is used, then C_f' will have the units of farads/inch.

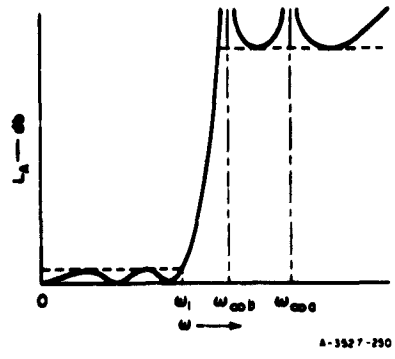

FIG. 7.03-4 TCHEBYSCHEFF FILTER CHARACTERISTIC WITH INFINITE ATTENUATION POINTS AT FINITE FREQUENCIES

advantages and disadvantages of printed-circuit *vs.* coaxial construction are discussed in Sec. 7.01.

Low-Pass Filters Designed from Prototypes Having Infinite Attenuation at Finite Frequencies—The prototype filters tabulated in Chapter 4 all have their frequencies of infinite attenuation (see Secs. 2.02 to 2.04) at $\omega = \infty$. The corresponding microwave filters, such as the one just discussed in this section, are of a form which is very practical to build and commonly used in microwave engineering. However, it is possible to design filters with an even sharper rate of cutoff for a given number of reactive elements, by using structures giving infinite attenuation at finite frequencies. Figure 7.03-4 shows a Tchebyscheff attenuation characteristic of this type, while Fig. 7.03-5 shows a filter structure which can give such a characteristic. Note that the filter structure has series-resonant branches connected in shunt, which short out transmission at the frequencies ω_{∞_a} and ω_{∞_b}, and thus give the corresponding infinite attenuation points shown in Fig. 7.03-4. In addition this structure has a second-order pole of attenuation at $\omega = \infty$ since the ω_{∞_a} and ω_{∞_b} branches have no effect at that frequency, and the inductances L_1, L_3, and L_5 block transmission by having infinite

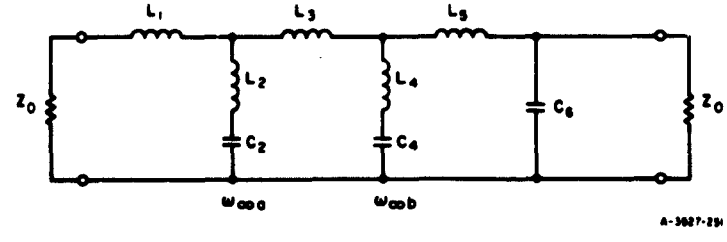

FIG. 7.03-5 A FILTER STRUCTURE WHICH IS POTENTIALLY CAPABLE OF REALIZING THE RESPONSE IN FIG. 7.03-4

series reactance, while C_6 shorts out transmission by having infinite shunt susceptance (see Sec. 2.04).

Filters of the form in Fig. 7.03-5 having Tchebyscheff responses such as that in Fig. 7.03-4 are mathematically very tedious to design. However, Saal and Ulbrich[2] have tabulated element values for many cases. If desired, of course, one may obtain designs of this same general class by use of the classical image approach discussed in Secs. 3.06 and 3.08. Such image designs are sufficiently accurate for many less critical applications.

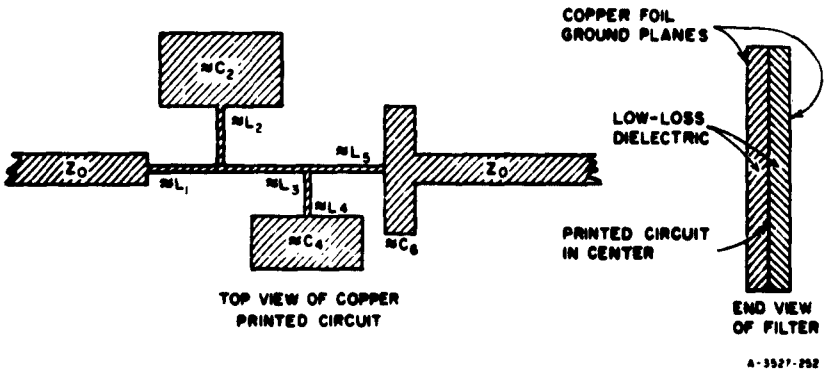

FIG. 7.03-6 A STRIP-LINE PRINTED-CIRCUIT FILTER WHICH CAN APPROXIMATE THE CIRCUIT IN FIG. 7.03-5

Figure 7.03-6 shows how the filter in Fig. 7.03-5 can be realized, approximately, in printed-circuit, strip-line construction. Using this construction, low-loss dielectric sheets are used, clad on one or both sides with thin copper foil. The circuit is photo-etched on one side of one sheet, and the printed circuit is then sandwiched between the first sheet of dielectric and a second sheet, as shown at the right in the figure. Often, the ground planes consist simply of the copper foil on the outer sides of the dielectric sheets.

The L's and C's shown in Fig. 7.03-6 indicate portions of the strip-line circuit which approximate specific elements in Fig. 7.03-5. The various elements are seen to be approximated by use of short lengths of high- and low-impedance lines, and the actual dimensions of the line

elements are computed as discussed in Sec. 7.02. In order to obtain best accuracy, the shunt capacitance of the inductive line elements should be compensated for in the design. By Fig. 7.02-1(c) the lengths of the inductive-line-elements can be computed by the equation

$$l_k = \frac{v}{\omega_1} \sin^{-1} \frac{\omega_1 L_k}{Z_k},$$

and the resulting equivalent capacitive susceptance *at each end* of the pi-equivalent circuit of inductive-line-element k is then

$$\omega_1 (C_\pi)_k = \frac{1}{Z_k} \tan \frac{\omega_1 l_k}{2v} \qquad (7.03\text{-}4)$$

where ω_1 is the cutoff frequency, Z_k is the characteristic impedance of inductive-line-element k, l_k is the length of the line element, and v is again the velocity of propagation. Now, for example, at the junction of the inductive line elements for L_1, L_2, and L_3 in Fig. 7.03-6 there is an unwanted total equivalent capacitive susceptance of $\omega_1 C_L = \omega_1 (C_\pi)_1 + \omega_1 (C_\pi)_2 + \omega_1 (C_\pi)_3$ due to the three inductance line elements. The unwanted susceptance $\omega_1 C_L$ can be compensated for by correcting the susceptance of the shunt branch formed by L_2 and C_2 so that

$$B_2 = \omega_1 C_L + B_2^c \qquad (7.03\text{-}5)$$

where B_2 is the susceptance at frequency ω_1 of the branch formed by L_2 and C_2 in Fig. 7.03-5, and B_2^c is the susceptance of a "compensated" shunt branch which has L_2 and C_2 altered to become L_2^c and C_2^c in order to compensate for the presence of C_L. Solving Eq. (7.03-5) for $\omega_1 C_2^c$ and $\omega_1 L_2^c$ gives

$$\omega_1 C_2^c = \omega_1 C_2 - \omega_1 C_L \left[1 - \left(\frac{\omega_1}{\omega_{\infty_c}}\right)^2\right] \qquad (7.03\text{-}6)$$

$$\omega_1 L_2^c = \frac{1}{\omega_1 C_2^c} \left(\frac{\omega_1}{\omega_{\infty_c}}\right)^2 \qquad (7.03\text{-}7)$$

where

$$\left(\frac{\omega_1}{\omega_{\infty_a}}\right)^2 = \omega_1 L_2 \omega_1 C_2 \quad . \tag{7.03-8}$$

Then the shunt branch is redesigned using the compensated values L_2^c and C_2^c which should be only slightly different from the original values computed by neglecting the capacitance of the inductive elements.

In filters constructed as shown in Fig. 7.03-6 (or in filters of any analogous practical construction) the attenuation at the frequencies ω_{∞_a} and ω_{∞_b} (see Fig. 7.03-4) will be finite as a result of losses in the circuit. Nevertheless, the attenuation should reach high peaks at these frequencies, and the response should have the general form in Fig. 7.03-4, at least up to stop-band frequencies where the line elements are of the order of a quarter-wavelength long.

Example—One of the designs tabulated in Ref. 2 gives normalized element values for the circuit in Fig. 7.03-5 which are as follows:

$Z_0' = 1.000$		$L_4' = 0.7413$	
$L_1' = 0.8214$		$C_4' = 0.9077$	
$L_2' = 0.3892$		$L_5' = 1.117$	
$C_2' = 1.084$		$C_6' = 1.136$	
$L_3' = 1.188$		$\omega_1' = 1.000$	

This design has a maximum pass-band reflection coefficient of 0.20 (0.179 db attenuation) and a theoretical minimum stop-band attenuation of 38.1 db which is reached by a frequency $\omega' = 1.194\ \omega_1'$. As an example of how the design calculations for such a filter will go, calculations will be made to obtain the dimensions of the portions of the circuit in Fig. 7.03-6 which approximate elements L_1 to L_3. The impedance level is to be scaled so that $Z_0 = 50$ ohms, and so that the un-normalized cutoff frequency is $f_1 = 2$ Gc or $\omega_1 = (2\pi)2 \times 10^9 = 12.55 \times 10^9$ radians/sec.

A printed-circuit configuration with a ground-plane spacing of $b = 0.25$ inch using dielectric with $\epsilon_r = 2.7$ is assumed. Then, for the input and output line $\sqrt{\epsilon_r} Z_0 = 1.64\ (50) = 82$, and by Fig. 5.04-1, $W_0/b = 0.71$, and a width $W_0 = 0.71\ (0.25) = 0.178$ inch is required.

Now $v = 1.1803 \times 10^{10}/\sqrt{\epsilon_r}$ inches/sec

so

$$\frac{v}{\omega_1} = \frac{1.1803 \times 10^{10}}{(1.64)(12.55 \times 10^9)} = 0.573 \quad .$$

For inductor L_1, $\omega_1 L_1 = \omega_1' L_1' (Z_0/Z_0') = 1(0.8214)(50)/1 = 41.1$ ohms. Assuming a line impedance of $Z_1 = 118$ ohms, $\sqrt{\epsilon_r} Z_1 = 193$, and Fig. 5.04-1 calls for a line width of $W_1 = 0.025$ inch. Then the length of the L_1-inductive element is

$$l_1 = \frac{v}{\omega_1} \sin^{-1} \frac{\omega_1 L_1}{Z_1} = 0.573 \sin^{-1} \frac{41.1}{118} = 0.204 \quad \text{inch} \quad .$$

The effective, unwanted capacitive susceptance at each end of this inductive line is

$$\omega_1 (C_\pi)_1 = \frac{1}{2} \left(\frac{\omega_1}{v}\right) \frac{l_1}{Z_1} = \frac{0.204}{2(0.573)118} = 0.0015 \quad \text{mho} \quad .$$

After some experimentation it is found that in order to keep the line element which realizes L_2 from being extremely short, it is desirable to use a lower line impedance of $Z_2 = 90$ ohms, which gives a strip width of $W_2 = 0.055$ inch. Then $\omega_1 L_2 = \omega_1' L_2' (Z_0/Z_0') = 19.95$ and

$$l_2 = \frac{v}{\omega_1} \sin^{-1} \frac{\omega_1 L_2}{Z_2} = 0.573 \sin^{-1} \frac{19.95}{90} = 0.128 \quad \text{inch} \quad .$$

Even a lower value of Z_2 might be desirable in order to further lengthen l_2 so that the large capacitive piece realizing C_2 in Fig. 7.03-6 will be further removed from the L_1 and L_2 lines. However, we shall proceed with the sample calculations. The effective unwanted capacitance susceptance at each end of l_2 is

$$\omega_1 (C_\pi)_2 = \frac{1}{2} \frac{\omega_1}{v} \frac{l_2}{Z_2} = \frac{0.128}{2(0.573)90} = 0.0012 \quad \text{mho} \quad .$$

Similar calculations for L_3 give $l_3 = 0.302$ inch and $\omega_1(C_\pi)_3 = 0.0022$ mho, where Z_3 is taken to be 118 ohms as was Z_1. Then the net unwanted susceptance due to line capacitance at the junction of L_1, L_2, and L_3 is

$$\omega_1 C_L = \omega_1(C_\pi)_1 + \omega_1(C_\pi)_2 + \omega_1(C_\pi)_3 = 0.0049 \text{ mho} .$$

Now $\omega_1 C_2 = \omega_1' C_2'(Z_0'/Z_0) = 1(1.084)/50 = 0.0217$ mhos. Then by Eq. (7.03-8)

$$\left(\frac{\omega_1}{\omega_{\infty_e}}\right)^2 = 19.45(0.0217) = 0.422 ,$$

and by Eq. (7.03-6) the compensated value for $\omega_1 C_2$ is

$$\omega_1 C_2^e = 0.217 - 0.0049\,[1 - 0.422] = 0.0189 \text{ mho} .$$

Now the compensated value for $\omega_1 L_2$ is

$$\omega_1 L_2^e = \left(\frac{\omega_1}{\omega_{\infty_e}}\right)^2 \frac{1}{\omega_1 C_2^e} = 22.3 \text{ ohms} .$$

Then the compensated value for the length l_2 of the line for L_2 is

$$l_2 = 0.573 \sin^{-1} \frac{22.3}{90} = 0.144 \text{ inch} .$$

To realize C_2 we assume a line of impedance $Z_{C_2} = 30.5$ ohms which calls for a strip width of $W_{C_2} = 0.362$ inch. This strip should have a capacitive susceptance of $\omega_1 C_2^e - \omega_1(C_\pi)_2 = 0.0189 - 0.0012 = 0.0177$ mho. Neglecting end-fringing, this will be obtained by a strip of length

$$l_{C_2} = [\omega_1 C_2^e - \omega_1(C_\pi)_2]\, Z_{C_2} \frac{v}{\omega_1}$$

$$= 0.0177(30.5)(0.573) = 0.309 \text{ inch} .$$

To correct for the fringing capacitance at the ends of this strip we first use Eq. (7.02-1) to obtain the line capacitance

$$C = \frac{84.73\sqrt{\epsilon_r}}{Z_{C_2}} = \frac{84.73(1.64)}{30.5} = 4.55 \ \mu\mu f \text{ per inch} \quad .$$

Then by Fig. 5.07-5, $C_f'/\epsilon = 0.45$, and by Eq. (7.02-2) we need to subtract about

$$\Delta l = \frac{0.450 W \epsilon_r}{C} \left(\frac{C_f'}{\epsilon}\right)$$

$$= \frac{0.450(0.362)}{4.55} (2.7)(0.45) = 0.0435 \quad \text{inch}$$

from each end of the capacitive strip, realizing C_2^e in order to correct for end-fringing. The corrected length of the strip is then $l_{C_2} - 2\Delta l = 0.222$ inch. This calculation ignores the additional fringing from the corners of the C_2 strip (Fig. 7.03-6), but there appear to be no satisfactory data for estimating the corner-fringing. The corner-fringing will be counter-balanced in some degree by the loss in capacitance due to the shielding effect of the line which realizes L_2.

In this manner the dimensions of the portions of the circuit in Fig. 7.03-6 which are to realize L_1, L_2, C_2, and L_3 in Fig. 7.03-5 are fixed. It would be possible to compensate the length of the line realizing L_1 so as to correct for the fringing capacitance at the junction between L_1 and Z_0 (Fig. 7.03-6), but in this case the correction would be very small and difficult to determine accurately.

SEC. 7.04, LOW-PASS CORRUGATED-WAVEGUIDE FILTER

A low-pass* corrugated-waveguide filter of the type illustrated schematically in Fig. 7.04-1 can be designed to have a wide, well-matched

* That is the filter is low-pass in nature except for the cutoff effect of the waveguide.

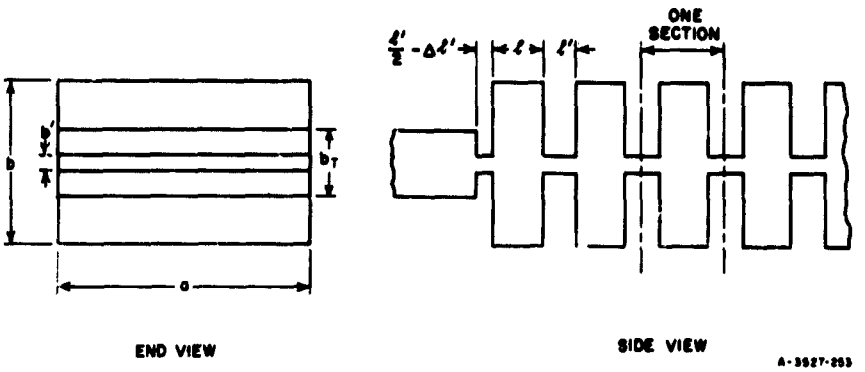

SOURCE: Proc. IRE (See Ref. 4 by S. B. Cohn)

FIG. 7.04-1 A LOW-PASS CORRUGATED WAVEGUIDE FILTER

pass band and a wide, high-attenuation stop band, for power propagating in the dominant TE_{10} mode. Because the corrugations are uniform across the width of the waveguide the characteristics of this filter depend only on the guide wavelength of the TE_{n0} modes propagating through the filter, and not on their frequency. Therefore, while this type of filter can be designed to have high attenuation over a particular frequency band for power propagating in the TE_{10} mode, it may offer little or no attenuation to power incident upon it in the TE_{20} or TE_{30} modes in this same frequency band, if the guide wavelengths of these modes falls within the range of guide wavelengths which will give a pass band in the filter response.

A technique for suppressing the propagation of the higher-order TE_{n0} modes, consisting of cutting longitudinal slots through the corrugations, thus making a "waffle-iron" filter, is described in Sec. 7.05. However, the procedure for designing the unslotted corrugated waveguide filter will be described here because this type of filter is useful in many applications, and an understanding of design techniques for it is helpful in understanding the design techniques for the waffle-iron filter.

The design of the corrugated waveguide filter presented here follows closely the image parameter method developed by Cohn.[3,4] When $b \leq l$ the design of this filter can be carried out using the lumped-element prototype approach described in Sec. 7.03; however, the present design applies for unrestricted values of b. Values of l' are restricted, however, to

be greater than about $b'/2$ so that the fringing fields at either end of the line sections of length l' will not interact with each other.

Figure 7.04-2 illustrates the image parameters of this type of filter as a function of frequency. The pass band extends from f_c, the cutoff frequency of the waveguide, to f_1, the upper cutoff frequency

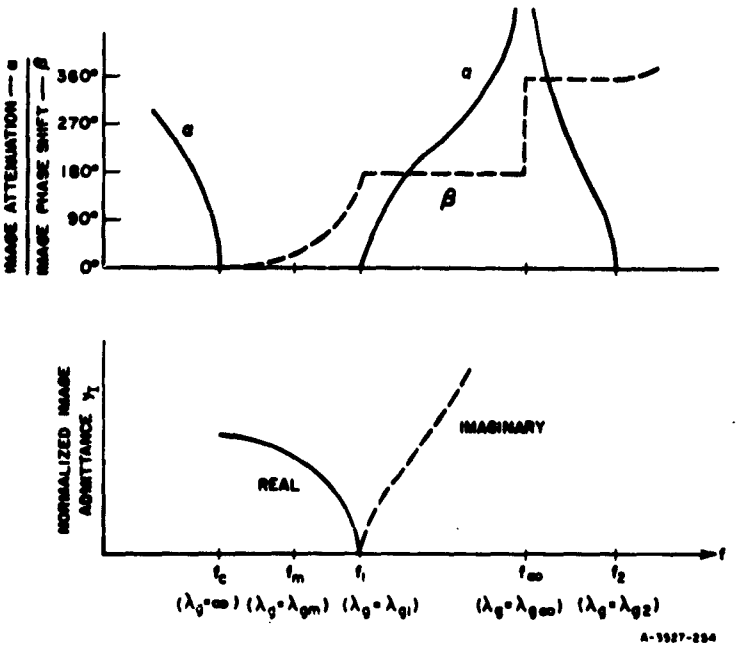

FIG. 7.04-2 IMAGE PARAMETERS OF A SECTION OF A CORRUGATED WAVEGUIDE FILTER

of the first pass band of the filter. At the infinite attenuation frequency, f_∞, the image phase shift per section changes abruptly from 180 to 360 degrees. The frequency f_2 is the lower cutoff frequency of the second pass band. The *normalized* image admittance y_I of the filter is maximum at f_c (where the guide wavelength $\lambda_g = \infty$) and zero at f_1 (where $\lambda_g = \lambda_{g1}$).

The equivalent circuit of a single half-section of the filter is illustrated in Fig. 7.04-3. *For convenience all admittances are normalized with respect to the waveguide characteristic admittance of the portions of*

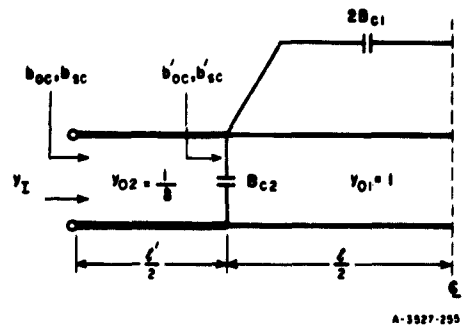

FIG. 7.04-3 NORMALIZED EQUIVALENT CIRCUIT OF A WAVEGUIDE CORRUGATED FILTER HALF-SECTION
y_{01} and y_{02} are normalized characteristic admittances and y_1 is the normalized image admittance

the filter of height b and width a. Thus, the normalized characteristic admittance of the terminating lines are b/b_T, where b and b_T are defined in Fig. 7.04-1.

The half-section open- and short-circuit susceptances are given by

$$b_{oc} = \frac{1}{\delta} \tan\left[\frac{\pi l'}{\lambda_g} + \tan^{-1}(\delta b'_{oc})\right] \qquad (7.04\text{-}1)$$

$$b_{sc} = \frac{1}{\delta} \tan\left[\frac{\pi l'}{\lambda_g} + \tan^{-1}(\delta b'_{sc})\right] \qquad (7.04\text{-}2)$$

where

$$b'_{oc} = \tan\left(\frac{\pi l}{\lambda_g}\right) + B_{c2} \qquad (7.04\text{-}3)$$

$$b'_{sc} = -\cot\left(\frac{\pi l}{\lambda_g}\right) + B_{c2} + 2B_{c1} \qquad (7.04\text{-}4)$$

and

$$\delta = b'/b \quad .$$

The susceptances marked *oc* are evaluated with the ends of the wires on the right in Fig. 7.04-3 left open-circuited, while the susceptances marked *sc* are evaluated with the ends of the wires on the right all shorted together at the center line.

When $\delta \leq 0.15$, the shunt susceptance B_{e2} is given accurately by the equation

$$B_{e2} = \frac{2b}{\lambda_g}\left\{ ln\,\frac{1}{\delta} - 0.338 + \sum_{k=1}^{\infty}\left[\frac{\tanh\dfrac{k\pi lF}{b}}{F} - 1\right]\right\} - 0.09\,\frac{b}{\lambda_g} \qquad (7.04\text{-}5)$$

and the series susceptance B_{e1} has the value

$$B_{e1} = \frac{2b}{\lambda_g}\sum_{k=1}^{\infty}\frac{\operatorname{csch}\dfrac{2\pi k lF}{b}}{F} \qquad (7.04\text{-}6)$$

where

$$F = \sqrt{1 - \left(\frac{b}{k\lambda_g}\right)^2} \quad .$$

The normalized image admittance $y_I = \sqrt{y_{oc}y_{sc}}$ is

$$y_I = j\,\frac{\cot\dfrac{\theta'}{2}}{\delta}\sqrt{\frac{\left(b'_{oc} + \dfrac{\tan\dfrac{\theta'}{2}}{\delta}\right)\left(b'_{sc} + \dfrac{\tan\dfrac{\theta'}{2}}{\delta}\right)}{\left(b'_{sc} - \dfrac{\cot\dfrac{\theta'}{2}}{\delta}\right)\left(b'_{oc} - \dfrac{\cot\dfrac{\theta'}{2}}{\delta}\right)}} \qquad (7.04\text{-}7)$$

and the image propagation constant for a *full section* is

$$\gamma = \alpha + j\beta = 2\tanh^{-1}\sqrt{\frac{y_{oc}}{y_{sc}}}$$

or

$$\gamma = 2 \tanh^{-1} \sqrt{\frac{\left(b'_{oe} + \frac{\tan \frac{\theta'}{2}}{\delta}\right)\left(b'_{oe} - \frac{\cot \frac{\theta'}{2}}{\delta}\right)}{\left(b'_{oe} - \frac{\cot \frac{\theta'}{2}}{\delta}\right)\left(b'_{oe} + \frac{\tan \frac{\theta'}{2}}{\delta}\right)}} \qquad (7.04\text{-}8a)$$

where $\theta' = 2\pi l'/\lambda_g$ is the electrical length of the low-impedance lines of length l'.*

The attenuation per section of a corrugated filter can be computed by use of Eq. (7.04-8a) (for frequencies where the equivalent circuit in Fig. 7.04-3 applies). However, once the image cutoff frequency of the sections has been determined, with its corresponding guide wavelength λ_{g1}, the approximate formula

$$\alpha = 17.372 \cosh^{-1} \frac{\lambda_{g1}}{\lambda_g} \quad \text{db/section} \qquad (7.04\text{-}8b)$$

is convenient, where λ_g is the guide wavelength at a specified stop-band frequency. Equation (7.04-8b) is based on Eq. (3.06-7) which is for lumped-element filters. Thus, Eq. (7.04-8b) assumes that the corrugations are small compared to a wavelength. Note that a section of this filter is defined as the region from the center of one tooth of the corrugation to the center of the next tooth. The approximate total attenuation is, of course, α times the number of sections.

Equations (7.04-7) and (7.04-8a) can be interpreted most easily with the aid of Fig. 7.04-4, which shows a sketch of the quantities in these equations as a function of reciprocal guide wavelength. It is seen that the image cutoff frequency f_1 at which $y_I = 0$, is determined by the condition that

$$b'_{oe} + \frac{\tan \frac{\theta'}{2}}{\delta} = 0 \quad . \qquad (7.04\text{-}9)$$

* The equations used here for y_I and γ are essentially the same as equations which can be found in Table 3.03-1. Their validity for the case in Fig. 7.04-3, where there are more than two terminals on the right, can be proved by use of Bartlett's Bisection Theorem.[5]

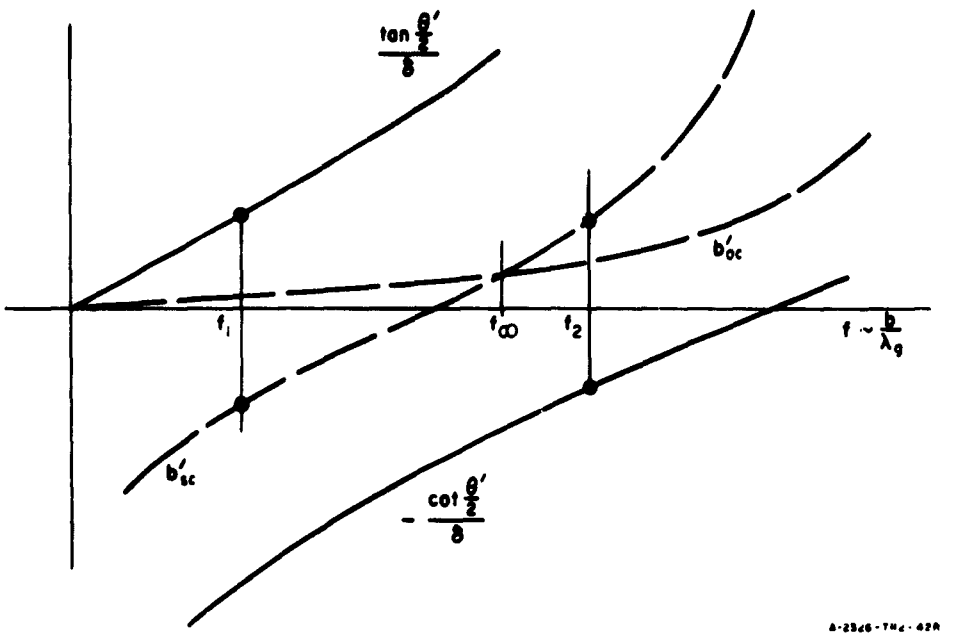

FIG. 7.04-4 GRAPH OF QUANTITIES WHICH DETERMINE CRITICAL FREQUENCIES IN CORRUGATED-WAVEGUIDE FILTER RESPONSE

The infinite attenuation frequency f_∞ is determined by the condition that

$$b'_{sc} = b'_{oc} \quad . \tag{7.04-10}$$

Finally, the image cutoff frequency f_2 at the upper edge of the first stop band is determined from the condition that

$$b'_{sc} - \frac{\cot \dfrac{\theta'}{2}}{\delta} = 0 \quad . \tag{7.04-11}$$

Design Procedure—One can design corrugated waveguide filters by means of Eqs. (7.04-1) to (7.04-11), using computed values of b'_{sc} and b'_{oc} or the values plotted by Cohn[3] for $l/b = 1/\pi$, $1/2\pi$, and $1/4\pi$. Alternatively one can use the values of b'_{sc} and b'_{oc} derived from the equivalent circuit of a waveguide E-plane T-junction as tabulated by Marcuvitz[6] for $l/b' \leq 1.0$. However, it is generally easier to use the design graphs

(Figs. 7.04-5, 7.04-6, and 7.04-7) prepared by Cohn,[7] which are accurate to within a few percent for $\delta \leq 0.20$.* In using these graphs the first step is to specify f_c, f_1, and f_∞. The width a is then fixed, since

$$a = \frac{5.9}{(f_c)_{Gc}} \tag{7.04-12}$$

where a is measured in inches and $(f_c)_{Gc}$ in gigacycles. Values of λ_{g1} and $\lambda_{g\infty}$ measured in inches are then calculated in the usual way from the relation

$$\lambda_{gn} = \frac{11.8}{\sqrt{(f_n)^2_{Gc} - (f_c)^2_{Gc}}} \tag{7.04-13}$$

using $n = 1$ and $n = \infty$.

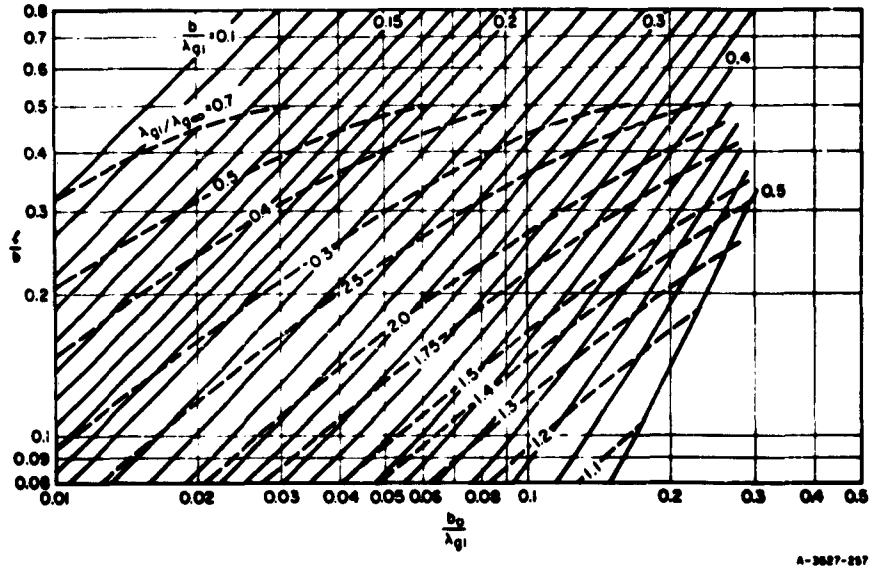

SOURCE: Proc. IRE (See Ref. 7 by S. B. Cohn)

FIG. 7.04-5 DESIGN GRAPH GIVING THE PARAMETER b USED IN SEC. 7.04

* It will be noted that use of Cohn's graphs bypasses the use of Eqs. (7.04-5) and (7.04-6), which were accurate for $\delta \leq 0.15$.

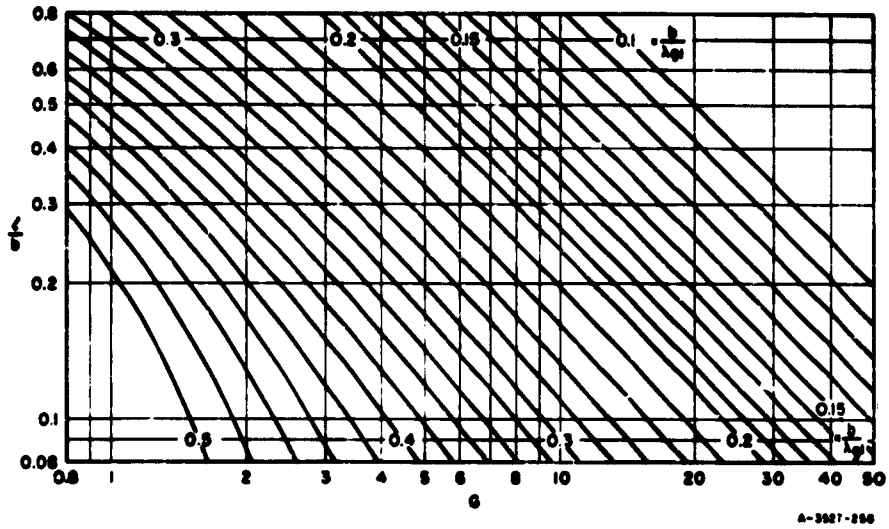

SOURCE: Proc. IRE (See Ref. 7 by S. B. Cohn)

FIG. 7.04-6 DESIGN GRAPH GIVING THE PARAMETER G USED IN SEC. 7.04

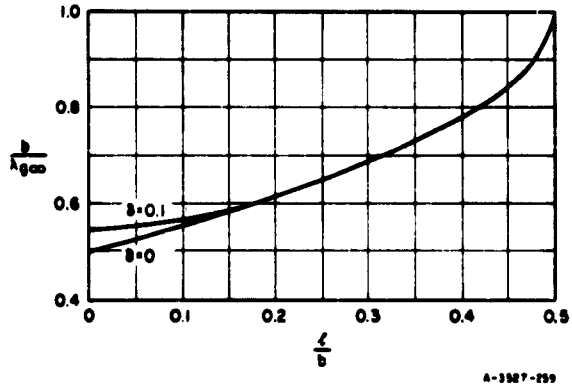

SOURCE: Proc. IRE (See Ref. 7 by S. B. Cohn)

FIG. 7.04-7 INFINITE-ATTENUATION-WAVELENGTH CURVE

The next step in the filter design is to choose a convenient value of l/b. Using this value of l/b and the value of $\lambda_{g1}/\lambda_{g\infty}$ one then enters Fig. 7.04-5 and determines b/λ_{g1} and b_0/λ_{g1}, thus fixing the values of b, b_0, and l. Here b_0 is the terminating guide height which will match the filter as λ_g approaches infinity. Then one determines the design parameter G from Fig. 7.04-6 in terms of l/b and b/λ_{g1}. Finally, one assumes a value of $\delta \leq 0.20$ and calculates l' from the relation

$$\tan \frac{\pi l'}{\lambda_{g'}} = \pi\delta \frac{b}{\lambda_{g1}} \left[G - \frac{2}{\pi} \ln \frac{1}{\delta} + 0.215 \right] . \qquad (7.04\text{-}14)$$

If l'/b' is less than 0.5, a different value of δ should be used.

The image admittance in the pass band of the filter, normalized to a guide of height b, is given to very good approximation by

$$y_I = \frac{b}{b_0} \sqrt{1 - \left(\frac{\lambda_{g1}}{\lambda_g}\right)^2} \qquad (7.04\text{-}15)$$

where λ_{g1} is the guide wavelength at frequency f_1. In order that a perfect match to the filter be achieved at some frequency f_a (for which $\lambda_g = \lambda_{ga}$), the height b_T of the terminating guide may be adjusted so that

$$b_T = \frac{b_0}{\sqrt{1 - \left(\frac{\lambda_{g1}}{\lambda_{ga}}\right)^2}} . \qquad (7.04\text{-}16)$$

If $b_0 = 0.7\ b_T$ a fairly good over-all match in the pass band is obtained. The amount of mismatch can be estimated by use of Eq. (7.04-15) and Fig. 3.07-2, where the abscissa of Fig. 3.07-2 is $a = y_I b_T/b$. A superior alternative for achieving a wide-band match is to use transforming end sections as described in Sec. 3.08. In this case, one sets $b_0 = b_T$, both for the internal sections and for the transforming end sections. However, the internal sections are designed to have a cutoff at λ_{g1}, while the transforming end sections are designed to have their cutoff at about $\lambda_{g1}/1.3$.

An explicit relation for $b/\lambda_{g\infty}$ in terms of l/b is also presented in Fig. 7.04-7, which is often useful in design work.

Unfortunately Cohn's[7] simplified design procedure does not enable one to specify f_2. However, it is generally found that f_2 is only about 20% higher in frequency than f_∞. Therefore, it is wise in any design situation to place f_∞ quite near the upper edge of the prescribed stop band.

The length $l'/2$ of the low-impedance line of height b', connecting to the terminating line of height b_T, must be reduced by an amount $\Delta l'$ to account for the discontinuity susceptance B of the junction. This is illustrated in Fig. 7.04-1. The amount of $\Delta l'$ that the line should be decreased in length is given by the expression

$$\Delta l' = \frac{b'}{2\pi}\left[\frac{\lambda_g}{b_T}\frac{B}{Y_0}\right] \qquad (7.04\text{-}17)$$

where Y_0 is the characteristic admittance of the terminating line. The appropriate value of $[(\lambda_g/b_T)(B/Y_0)]$ is easily determined from Fig. 5.07-11.

Two examples of this procedure as applied to the design of waffle-iron filters will be presented in the next section.

SEC. 7.05, LOW-PASS WAFFLE-IRON FILTERS HAVING VERY WIDE STOP BANDS

This section describes the design of low-pass corrugated waveguide filters containing longitudinal slots cut through the corrugations.* These types of filter, known as waffle-iron filters, have wide, well matched pass bands and wide, high-attenuation stop bands which can be made to be free of spurious responses for all modes. Several specific designs will be discussed.

Figure 7.05-1 is a drawing of a waffle-iron filter, illustrating the metal islands, or bosses (from which it derives its name) lying between the longitudinal and transverse slots. In these filters it is essential that the center-to-center spacing of the bosses be no greater than a half of a free-space wavelength at the highest required stop-band frequency. Under these conditions the waffle-iron structure is essentially isotropic and has the same characteristics, at a given frequency, for TEM waves

* This type of filter was originated by S. B. Cohn.

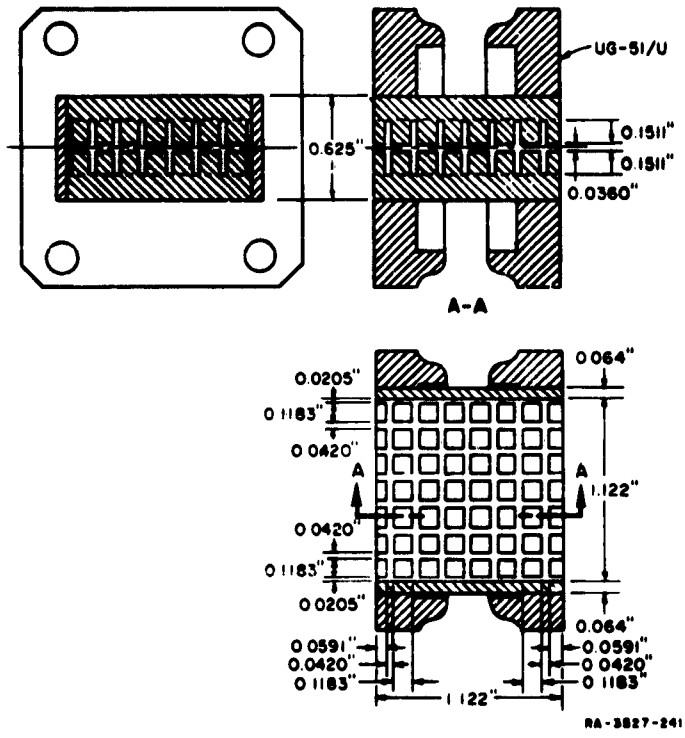

FIG. 7.05-1 DETAILS OF A TYPICAL WAFFLE-IRON FILTER

propagating through it in any direction. Thus, since any TE_{a0} mode can be resolved into TEM waves traveling in different directions through the filter it is seen that the properties of the waffle-iron filter for TE_{a0} modes are functions of frequency only. This is in contrast to the unslotted corrugated waveguide filters described in Sec. 7.04, whose response properties involve guide dimensions and mode numbers also, and are functions of guide wavelength.

Incident modes having horizontal components of electric field can excite slot modes that will propagate through the longitudinal slots in the filter at frequencies where the slot height b is greater than one half a free-space wavelength. Usually these modes are troublesome only at the highest stop-band frequencies. However, when unslotted step transformers are used to match the waffle-iron filters to waveguide of the standard

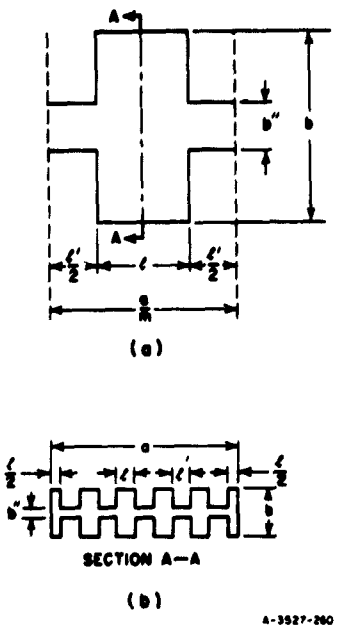

FIG. 7.05-2 A SINGLE-FILTER SECTION OF A WAFFLE-IRON FILTER

height, the reduced height of the stepped transformers effectively suppresses the incident modes with horizontal components of electric field which could otherwise excite slot modes in the filters.

Design Utilizing Cohn's Corrugated Filter Data—Waffle-iron filters can be designed approximately using the technique described in Sec. 7.04 *if the guide wavelength* λ_g *used there is everywhere replaced by the free-space wavelength* λ_1. As an illustration we will consider the design of Waffle-Iron-Filter-I, used with WR-650 waveguide of width $a = 6.5$ inches. We use the notation in Sec. 7.04 and that shown in Fig. 7.05-2, and choose $f_1 = 2.02$ Gc ($\lambda_1 = 5.84$ inches), $f_\infty = 5.20$ Gc ($\lambda_\infty = 2.27$ inches), so that $\lambda_1/\lambda_\infty = 2.57$. Letting $l/b = 0.318 = 1/\pi$, we find from Fig. 7.04-5 that $b_0/\lambda_1 = 0.077$, and $b/\lambda_1 = 0.275$, so that $b_0 = 0.450$ inch, $b = 1.607$ inches and $l = 0.511$ inch. Referring to Fig. 7.04-6 we find the design parameter G to be 3.85. Now, we make the assumption that we want five bosses across the $a = 6.5$-inch width of the filter so that $l + l' = 6.5/5 = 1.3$ inches and $l' = 0.789$ inch. From various trial designs, it has been found that for a 3:1 stop-band width, five bosses is about optimum in terms of giving convenient dimensions. For narrower stop-band widths more bosses can be used. Substituting the values of G and l' into Eq. (7.04-16) we find that $\delta = b'/b = 0.176$ and since $b = 1.607$ inches, $b' = 0.282$ inch.

The presence of the longitudinal slots through the filter has the effect of decreasing the capacitance per unit length of the low-impedance lines. This decrease in capacitance can be compensated for by decreasing the dimension b' for an unslotted filter to b''. The ratio b''/b' is given approximately by

$$\frac{b''}{b'} = \frac{l'}{l+l'} + \frac{2}{\pi}\frac{l}{(l+l')}\left[\tan^{-1}\left(\frac{b''}{b'}\frac{b'}{l}\right) + \frac{\ln\sqrt{1+(lb'/b'b'')^2}}{\frac{l}{b'}\frac{b'}{b''}}\right] . \qquad (7.05\text{-}1)$$

Solving the above equation gives $b''/b' = 0.81$. However, the filter described here has the edges of the bosses rounded with a 0.0625-inch radius to increase its power-handling capacity, and this rounding further decreases the capacitance of the low-impedance lines. Therefore, b''/b' was chosen to be 0.75, yielding a value of $b'' = 0.210$ inch.

The height of the unslotted terminating guide b_T necessary to match this filter at some pass-band design frequency f_a is related to b_0, the height to give a match when $\lambda_g \to \infty$, by

$$b_T = \frac{b_0}{\sqrt{1 - \left(\frac{f_a}{f_1}\right)^2}} \quad . \tag{7.05-2}$$

In order to maintain a reasonably good match across the band, f_a should not be too close to f_1; typically, $f_a \lesssim 0.7\, f_1$ is desirable. For the best wide-band match, matching end sections should be used, as will be described in a following example. Using $f_a = 1.3$ Gc, Eq. (7.05-2) predicts $b_T = 0.555$ inch. Step transformers were used at each end to match t. .s guide of height b_T to standard guide.

The attenuation per section in the stop-band region just above the pass band can be estimated by use of Eq. (7.04-8b), with λ_g and λ_{g1} replaced by λ and λ_1.

Figure 7.05-3 shows the measured insertion loss of this filter in the stop band. It is seen to be everywhere greater than 60 db from 2.2 to 5.7 Gc. The VSWR in the 1.25-to-1.40-Gc required pass band of this filter was less than 1.08 and the attenuation was less than 0.1 db. As will be discussed at the end of this section, a broader band of good impedance match could have been obtained if the filter had been constructed to start and end in the center of a boss [*i.e.*, at plane *A-A* in Fig. 7.05-2(a)] instead of in the center of a row of teeth [*i.e.*, in the plane of one of the dotted lines in Fig. 7.05-2(a)].

Design Using the T-Junction Equivalent Circuit of Marcuvitz—Though the method described above is usually easier, waffle-iron filters can also be designed using the equivalent circuit of a waveguide *T*-junction as given by Marcuvitz[6] when $l/b' \lesssim 1$, for arbitrary values of $\delta = b'/b$,

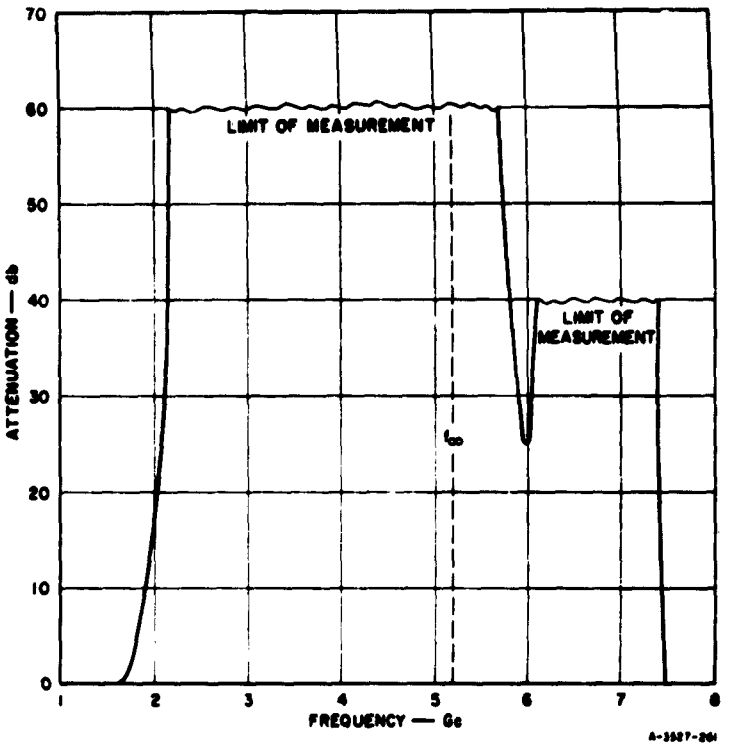

SOURCE: Technical Note 2, Contract AF 30(602)-2392, SRI (See Ref. 8 by Eugene Sharp)

FIG. 7.05-3 MEASURED INSERTION LOSS OF WAFFLE-IRON FILTER I

so long as $l'\ b'$ is greater than about 0.5. Cohn's graphs apply only when $l/b' > 1$, so if $l/b' < 1$, the use of Marcuvitz's data is the most convenient. In order to illustrate this procedure we will now describe the design of Waffle-Iron-Filter-II, used with WR-112 waveguide of width $a = 1.122$ inch. It has a pass band extending from 7.1 to 8.6 Gc and a stop band with greater than 40-db attenuation extending from 14 to 26 Gc. This filter could also be designed by the technique described above but the alternate procedure is presented here for completeness.

Figure 7.05-4 illustrates the bottom half of a single section of the waffle-iron filter together with its equivalent circuit. The part of the equivalent circuit representing the junction of the series stub with the main transmission line of characteristic impedance Z_0 is taken from Marcuvitz's Fig. 6.1-2. (The parameter labeled b/λ_g on Marcuvitz's

curves[6] in his Figs. 6.1-4 to 6.1-14 should in reality be $2b/\lambda_g$.) The normalized image impedance of a filter section is

$$\frac{Z_I}{Z_0} = \frac{1}{Z_0}\sqrt{Z_{se}Z_{oe}} = \frac{1}{2}\sqrt{\frac{1 + \cot\frac{\phi}{2}\left(\frac{X}{Z_0} + n^2\frac{Z_0'}{Z_0}\tan\phi'\right)}{1 - \tan\frac{\phi}{2}\left(\frac{X}{Z_0} + n^2\frac{Z_0'}{Z_0}\tan\phi'\right)}} \qquad (7.05\text{-}3)$$

while the image attenuation constant $\gamma = \alpha + j\beta$ per section is related to the bisected section open- and short-circuit impedance Z_{oe} and Z_{se} by

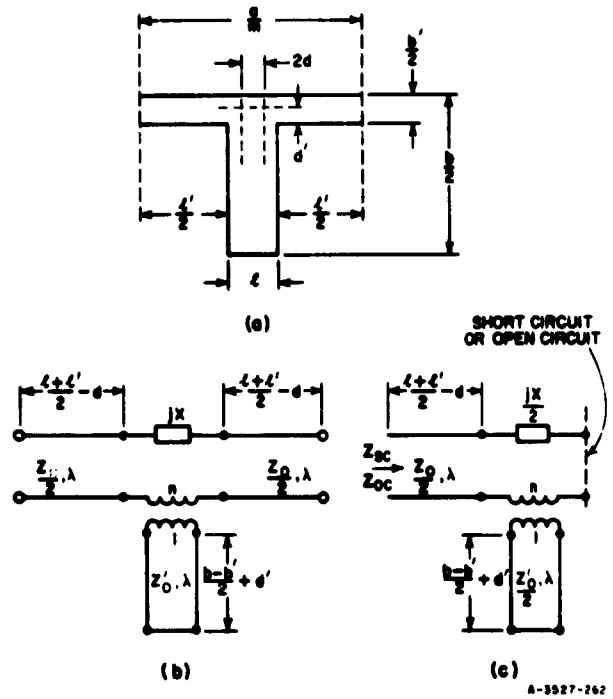

FIG. 7.05-4 FULL-FILTER SECTION – CROSS SECTION OF WAFFLE-IRON FILTER AND EQUIVALENT CIRCUIT
At (c) the equivalent circuit has been bisected

$$\tanh \frac{(\alpha + j\beta)}{2} = \sqrt{\frac{Z_{se}}{Z_{oe}}} = \sqrt{\frac{\frac{X}{Z_0} + n^2 \frac{Z_0'}{Z_0} \tan \phi' + \tan \frac{\phi}{2}}{\frac{X}{Z_0} + n^2 \frac{Z_0'}{Z_0} \tan \phi' - \cot \frac{\phi}{2}}} \qquad (7.05\text{-}4)$$

where

$$\frac{\phi}{2} = \frac{2\pi}{\lambda}\left[\frac{l + l'}{2} - d\right], \qquad (7.05\text{-}5)$$

$$\phi' = \frac{2\pi}{\lambda}\left[\frac{b - b'}{2} + d'\right], \qquad (7.05\text{-}6)$$

and the remaining parameters are as indicated in Fig. 7.05-4. In applying Eqs. (7.05-3) and (7.05-4) it has been found that $\phi/\phi' = 1$ is nearly optimum. Values of $\phi/\phi' \approx 2$ are to be avoided because they cause the filter to have a narrow spurious pass band near the infinite attenuation frequency f_∞.

The design of this filter proceeded by a trial and error technique using Eq. (7.05-4) to determine the dimensions to yield approximately equal attenuations at 14 and 26 Gc. In this design the curves for the equivalent-circuit element values for series T-junctions in Marcuvitz[6] were extrapolated to yield equivalent-circuit parameters for $l'/b = 1.17$, and λ_g was replaced by λ. The choice of dimensions was restricted to some extent in order to have an integral number, m, of bosses across the width of the guide. The value of m was chosen to be 7. The calculated attenuation per section was calculated to be 7.6 db at 14 Gc and 8.8 db at 26 Gc. The total number of sections along the length of the filter was chosen to be 7 in order to meet the design specifications. Reference to Eq. (7.05-1) showed that b'' was within 5 percent of b', so $b'' = b'$ was used. The final dimensions of the filter obtained by this method are those shown in Fig. 7.05-1.

The normalized image impedance Z_I/Z_0 of the filter was computed from Eq. (7.05-3) to be 2.24 at 7.9 Gc. Thus, it is expected that the height b_T of the terminating guide should be

$$b_T = b'' \frac{Z_I}{Z_0} \qquad (7.05\text{-}7)$$

or $0.036 \times 2.24 = 0.080$ inch. Experimentally, it was determined that the optimum value for b_T is 0.070 inch at 7.9 Gc.

This filter was connected to standard WR-112 waveguide by means of smooth tapered transitions which had a VSWR of less than 1.06 over the frequency band from 7.1 to 8.6 Gc, when they were placed back-to-back. The measured insertion loss of the filter and transitions in the stop band was less than 0.4 db from 6.7 to 9.1 Gc while the VSWR was less than 1.1 from 7 to 8.6 Gc. The measured stop-band attenuation of the filter is shown in Fig. 7.05-5, and it is seen to agree quite closely with the theoretical analysis.

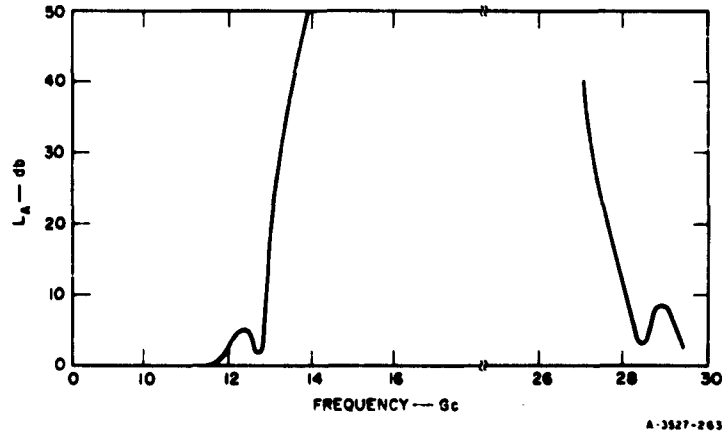

FIG. 7.05-5 STOP-BAND ATTENUATION OF WAFFLE-IRON FILTER II

No spurious responses were measured on either of the above described filters in the stop band when they were terminated by centered waveguides. However, if the terminating waveguides are misaligned at each end of the filter, it is found that spurious transmissions can occur when $\lambda < 2b$. These spurious responses are caused by power propagating through the longitudinal slots in the filter in a mode having a horizontal component of electric field. Thus, it is seen to be essential to accurately align the waveguides terminating waffle-iron filters if maximum stop-band width is desired.

A Third Example with Special End-Sections to Improve Impedance Match—As a final example, the design of a low-pass waffle-iron filter

having integral longitudinally slotted step transformers will be described. This filter is designed to be terminated at either end with WR-51 waveguide. The pass band of the filter extends from 15 to 21 Gc and the stop band which has greater than 40-db attenuation, extends from 30 to 63 Gc. A photograph of this filter is shown in Fig. 7.05-6, illustrating the split-block construction, chosen so that the four parts of the filter would be easy to machine.

The longitudinal slots in the stepped transformers necessitate that the design of this filter be different than those described previously. This occurs because these slots allow modes incident on the transformers such as the TE_{11} or TM_{11} to set up the previously described slot modes, having horizontal electric fields, which propagate through the filter when $b \gtrsim \lambda/2$. Thus, it is necessary in the design of this filter to choose $b \lesssim \lambda/2$ at the highest stop-band frequency of 63 Gc. In the design presented here, $b = 0.0803$ and $f_1 = 24.6$ Gc ($\lambda_1 = 0.480$ inch). It was decided to use 5 bosses across the width of the guide with $l = 0.0397$ inch and $l' = 0.0623$ inch. Referring to Fig. 7.04-5 we find $b_0 = 0.021$ inch, and from Fig. 7.04-6 we find the design parameter $G = 7$. Substituting in Eq. (7.04-16) we find $\delta = 0.139$ or $b' = 0.0113$ inch. We find the reduction in gap height due to the presence of the longitudinal slots from Eq. (7.05-1), which predicts $b''/b' = 0.77$ or $b'' = 0.0087$ inch.

The height b_T of a parallel-plate terminating guide that will give a match at 18 Gc is determined from Eq. (7.04-16) to be 0.031 inch. The actual height of the longitudinally slotted lines used in this design is $b_T = 0.030$ inch.

In order to further improve the match of this filter over the operating band, transforming end sections were used at either end having the same values of b, b'', and l, but with l' reduced from 0.0623 inch to 0.040 inch. This reduction in the value of l' causes the end sections to have a low-frequency image admittance about 14 percent lower than that of the middle sections and an image cutoff frequency about 14 percent higher than that of the middle sections. Figure 7.05-7 shows a sketch of the image admittance of the middle and end sections of the filter normalized to the admittance of a parallel-plate guide of height $b = 0.0803$ inch. The image phase shift of the end sections is 90 degrees at 21 Gc (the upper edge of the operating band) and not greatly different from 90 degrees over the rest of the operating band. The approximate admittance level of the

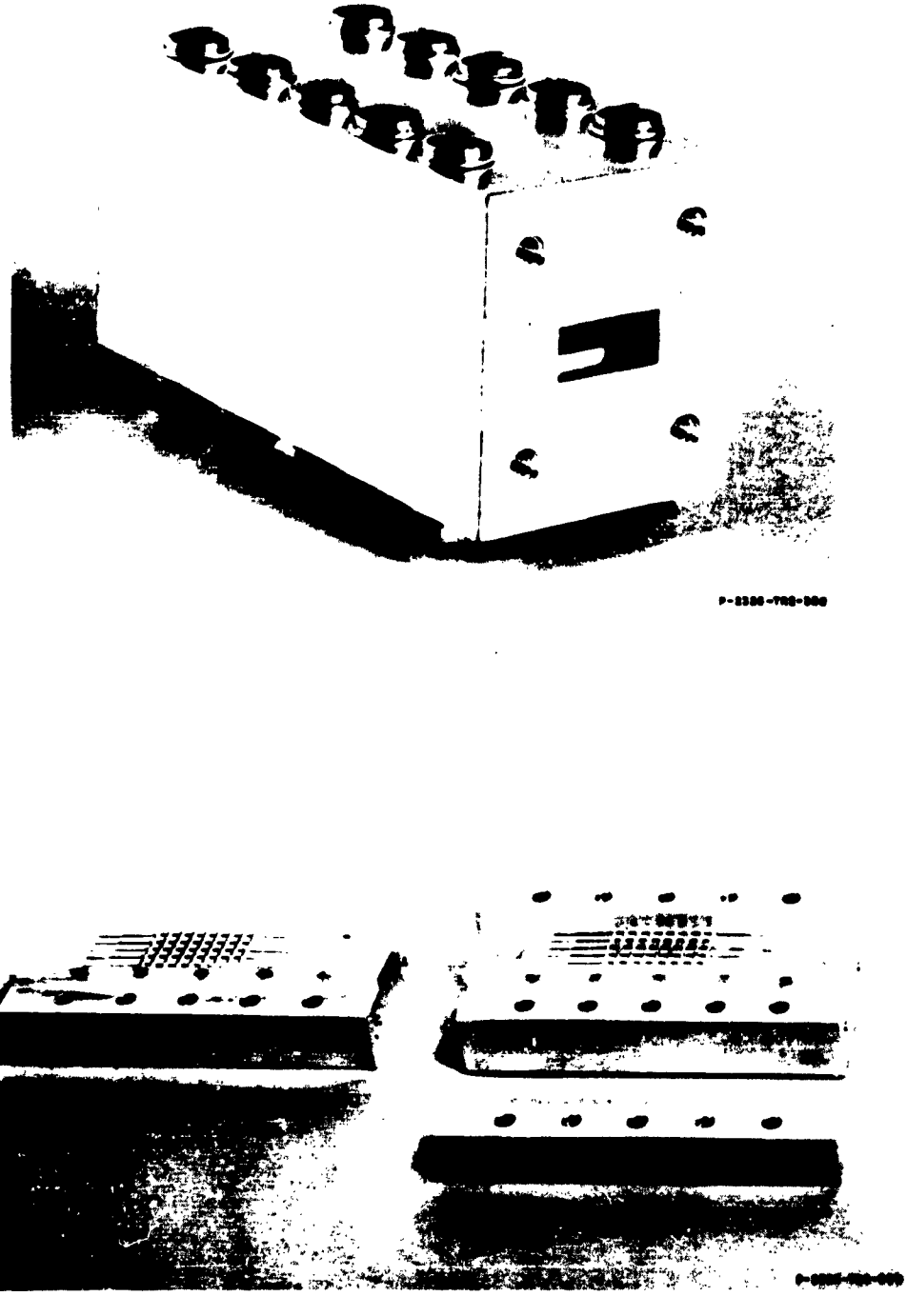

FIG. 7.05-6 PHOTOGRAPHS OF WAFFLE-IRON FILTER III HAVING 15-to-21-Gc PASS BAND AND 30-to-63-Gc STOP BAND

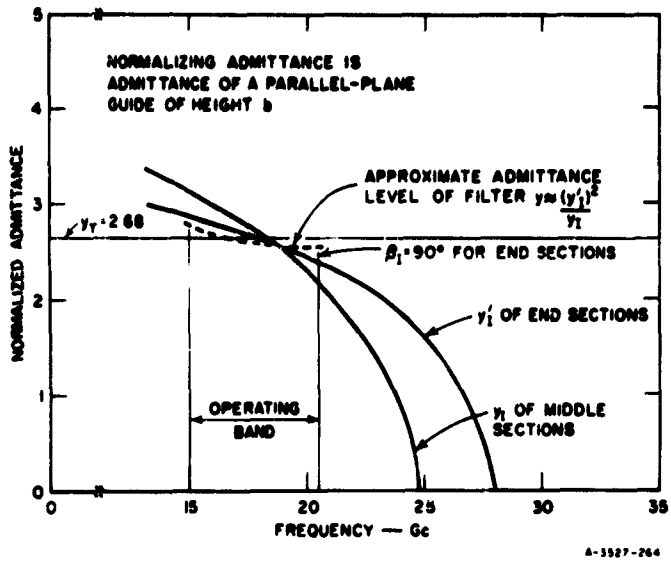

FIG. 7.05-7 SKETCH OF NORMALIZED IMAGE ADMITTANCE vs. FREQUENCY OF MIDDLE- AND END-SECTIONS OF WAFFLE-IRON FILTER III

filter is transformed to closely approximate the normalized terminating admittance $y_T = 2.68$ over the operating band, as indicated in the figure. A more general discussion of this matching technique is presented in Sec. 3.08.

The discontinuity capacity at the junction between each end section and the terminating line was compensated for by reducing the length of each end section by 0.004 inch as predicted by Eq. (7.04-17).

Quarter-Wave Transformers with Longitudinal Slots—Quarter-wave transformers, some of whose sections contained longitudinal slots, were designed for Waffle-Iron Filter III using the methods presented in Chapter 6. If there were no longitudinal slots in any of the steps of the transformers the appropriate transformation ratio to use in the design of the transformers would be the ratio of the height of the terminating guide, which is 0.255 inch, to the height of the guide which properly terminates the filter, which in this case is 0.030 inch. Thus, the transformation ratio would be 0.255/0.030 = 8.5.

If the filters and the step transformers are made from the same piece of material it is difficult to machine longitudinal slots in the main body of the filter without machining them in the step transformers at the end also. However, this difficulty can be avoided if the step transformers are made as inserts or as removable sections. Alternately, the step transformers can be designed to include longitudinal slots.

The presence of the longitudinal slots would tend to increase the transformation ratio about 8 percent since the impedance of a slotted transformer step is slightly lower than that of an unslotted step. The procedure used to calculate the impedance of a slotted waveguide is explained in detail later in this section. Qualitatively, however, it can be seen that the impedance of a slotted waveguide tends to be increased because the capacity between the top and bottom of the waveguide is reduced. On the other hand, the slots also reduce the guide wavelength which tends to *decrease* the waveguide impedance. Ordinarily it is found that the net result of these two competing effects is that the impedance of a longitudinally slotted waveguide is less than that for an unslotted waveguide.

The present design was carried out including the presence of the slots; however, it is believed that in future designs they may well be neglected in the design calculations.* The ratio of guide wavelengths at the lower and upper edge of the operating band of the transformers was chosen to be 2.50, which allowed ample margin to cover the 2.17 ratio of the guide wavelengths at the lower and upper edges of the operating band of the filter. The maximum theoretical pass-band VSWR is 1.023, and five $\lambda_g/4$ steps were used.

The procedure used to account for the presence of the longitudinal slots in the step transformers is as follows:

One assumes that the impedance Z_{0_g} of the longitudinally slotted guide is

$$Z_{0_g} = Z_0(\infty) \Big/ \sqrt{1 - \left(\frac{\lambda}{\lambda_g}\right)^2} \qquad (7.05\text{-}8)$$

* Calculations have shown that at least in some cases the corrections for the presence of the slots is quite small.

where $Z_0(\infty)$ is the impedance of the slotted waveguide at infinite frequency and λ_c is the cutoff wavelength of the slotted waveguide. Both $Z_0(\infty)$ and λ/λ_c are functions of the guide height h_i, which is taken as the independent variable for the purpose of plotting curves of these quantities. [If Fig. 7.05-2(b) is interpreted as a cross section of the longitudinally slotted transformers, h_i corresponds to b''.]

First $Z_0(\infty)$ is calculated for several values of $h < b$ [where b is again as indicated in Fig. 7.05-2(b)] by considering TEM propagation in the longitudinal direction. Since the line is uniform in the direction of propagation

$$Z_0(\infty) = \frac{84.73\ 10^{-12}}{C_0} \quad \text{ohms} \tag{7.05-9}$$

where C_0 is the capacitance in farads per inch of length for waveguide a inches wide. The capacitance C_0 can be expressed as

$$C_0 = C_{pp} + C_d \quad . \tag{7.05-10}$$

Here the total parallel-plate capacitance C_{pp} of the longitudinal ridges of the waveguide of width a is given approximately by

$$C_{pp} = 0.225 \times 10^{-12} \left(\frac{l'}{l' + l}\right) \frac{a}{h_i} \quad \text{farads/inch} \quad . \tag{7.05-11}$$

The total discontinuity capacitance C_d of the $2n$ step discontinuities across the width of the guide is given approximately by

$$C_d = (2n) \frac{4}{\pi} \frac{l}{h_i} \times 0.225 \times 10^{-12} \left[\tan^{-1} \frac{h_i}{l} + \frac{ln\ \sqrt{1 + l^2/h_i^2}}{l/h_i}\right] \quad \text{farads/inch} \quad . \tag{7.05-12}$$

The cutoff wavelength, λ_c, of a rectangular waveguide with longitudinal slots is then calculated from the condition of transverse resonance for the values of h_i used above. For this calculation it is necessary to consider the change in inductance as well as the change in capacitance

for waves propagating in a direction perpendicular to the longitudinal slots, back and forth across the guide of width a.

We will use static values of capacitance and inductance, and to be specific, consider that the waves propagating back and forth across the width of the guide are bounded by magnetic walls transverse to the longitudinal axis of the guide and spaced a distance w inches apart. The capacitance per slice w wide, per inch of guide width (transverse to the longitudinal axis of the guide), is

$$\frac{C_0 w}{a} \quad \text{farads/inch} \quad . \tag{7.05-13}$$

The inductance per inch of the same slice is approximately

$$L_0 = 0.032 \times 10^{-6} \frac{(lb + l'b')}{w(l + l')} \quad \text{henries/inch} \tag{7.05-14}$$

where all dimensions are in inches. A new phase velocity in the transverse direction is then calculated to be

$$v_p = \frac{1}{\sqrt{L_0 C_0 \frac{w}{a}}} \quad \text{inches/second} \quad . \tag{7.05-15}$$

The new cutoff wavelength is now

$$\lambda_c = 2a \left(\frac{v}{v_p} \right) \quad \text{inches} \tag{7.05-16}$$

where v is the plane-wave velocity of light in air—*i.e.*, 1.1803×10^{10} inches/second.

A graph of Z_{0_g} *vs.* h is then made using Eq. (7.05-8), and from this graph the guide height, h_i, is obtained for each Z_i of the stepped transformer, and also for the optimum filter terminating impedance, all as previously calculated. Finally, new values of step length are calculated at the middle of the pass band for each slotted step using the values of λ_g computed from the new values of λ_c by means of the relation

$$\lambda_g = \frac{\lambda}{\sqrt{1 - \left(\frac{\lambda}{\lambda_c}\right)^2}} \quad . \qquad (7.05\text{-}17)$$

Figure 7.05-8 shows a dimensioned drawing of the filter. The lengths of the terminating guides at each end of the filter were experimentally adjusted on a lower-frequency scale model of this filter for best pass-band match. By this procedure a maximum pass-band VSWR of 1.4, and a maximum pass-band attenuation of 0.7 db was achieved. The stop-band attenuation of this filter as determined on the scale model is shown in Fig. 7.05-9. The circled points within the stop band represent spurious transmission through the filter when artificially generated higher-order modes are incident upon it. These higher-order modes were generated by twisting and displacing the terminating waveguides. The freedom from spurious responses over most of the stop band in Fig. 7.05-9, even when higher-order modes were deliberately excited, shows that this waffle-iron filter does effectively reflect all modes incident upon it in its stop band.

A Simple Technique for Further Improving the Pass-Band Impedance Match—In the preceding examples step transformers were used to match standard waveguide into waveguide of the proper height needed to give a reasonably good match into the waffle-iron filter structure. In Waffle-Iron Filter III, besides a step transformer, additional end sections designed by the methods of Sec. 3.08 were used to further improve the impedance match. As this material is being prepared for press an additional design insight has been obtained, and is described in the following paragraphs. This insight can improve pass-band performance even more, when used in conjunction with the previously mentioned techniques.

Waffle-iron filters starting with half-capacitances (half-teeth) at either end, as used in the examples so far, are limited in the bandwidth of their pass band. The reason for this is the change of image impedance with frequency. This variation is shown in Fig. 3.05-1 for Z_{IT} and $Z_{I\pi}$. The waffle-iron with half-teeth presents an image impedance $Z_{I\pi}$, whose value increases with frequency. (The image admittance then decreases with frequency, as indicated in Fig. 7.05-7.) However, the characteristic impedance Z_0 of rectangular waveguide decreases with frequency as

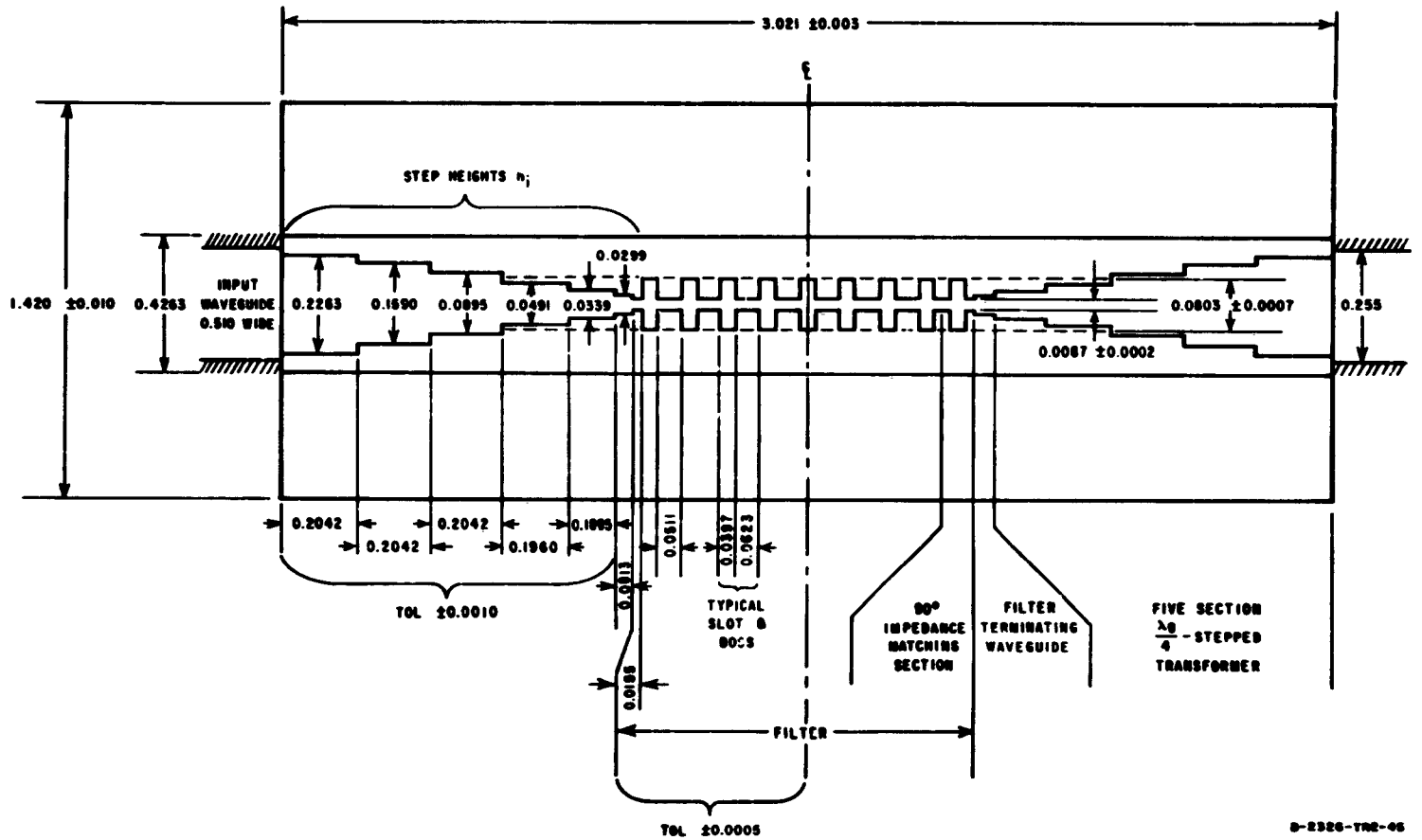

FIG. 7.05-8 SKETCH OF WAFFLE-IRON FILTER III GIVING DIMENSIONS

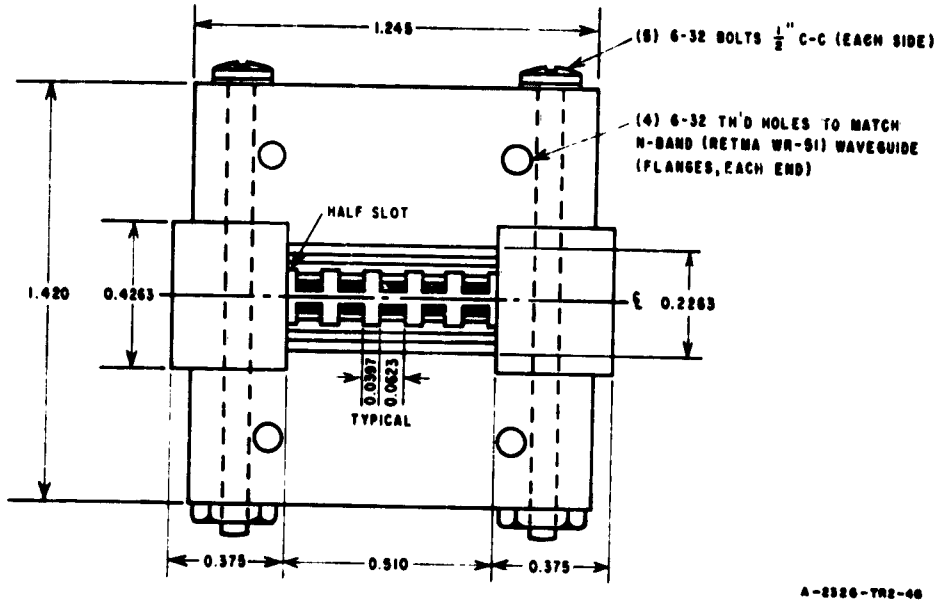

FIG. 7.05-8 Concluded

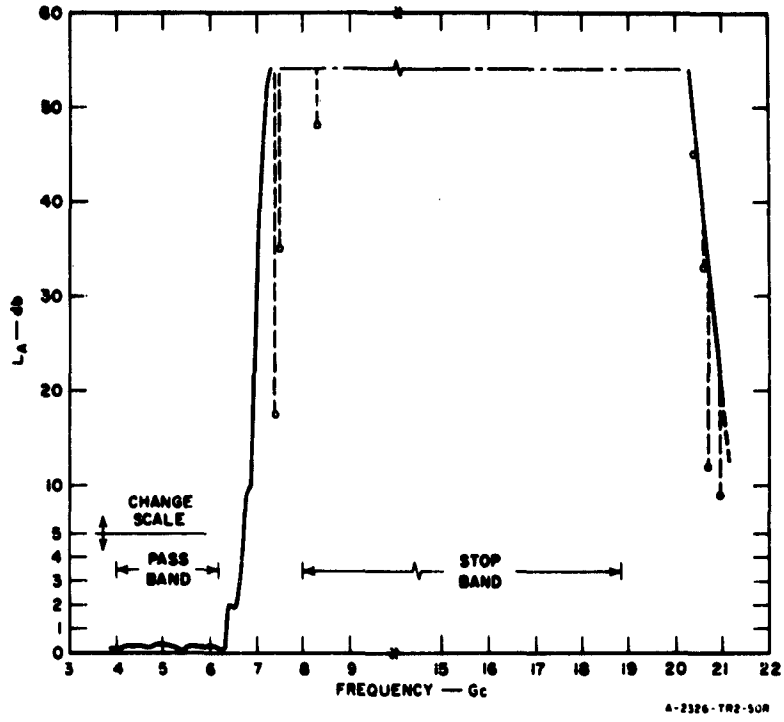

FIG. 7.05-9 MEASURED PERFORMANCE OF SCALE MODEL OF WAFFLE-IRON FILTER III SHOWING EFFECT OF ARTIFICIALLY GENERATED HIGHER MODES
The scale factor was 3.66

indicated by $Z_0 \approx \sqrt{1 - (f_c/f)^2}$ where f_c is the cutoff frequency of the waveguide. Thus, while it is possible to match the image impedance $Z_{I\pi}$ of the filter to the characteristic impedance Z_0 of the waveguide at one frequency, $Z_{I\pi}$ and Z_0 diverge rapidly with frequency, resulting in a relatively narrow pass band.

By terminating the filter with a half T-section, the image impedance Z_{IT} (Fig. 3.05-1) runs parallel to the waveguide impedance Z_0 over a substantial frequency band; then by matching Z_{IT} to Z_0 at one frequency, they stay close together over a relatively wide frequency band. Such a filter[8] has been built and is shown in Fig. 7.05-10. This L-band, five-section filter has circular (instead of square) teeth to improve the power-handling capacity by an estimated factor[8] of 1.4. The dimensions of this filter, using the notation of Fig. 7.05-2, were: b = 1.610 inches,

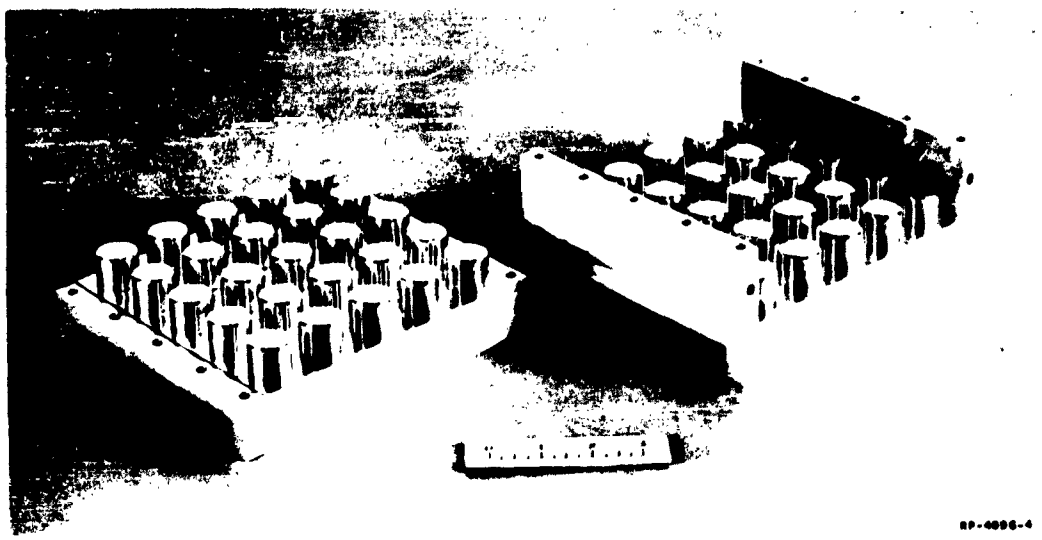

SOURCE: Quarterly Progress Report 1, Contract AF 30(602)-2734
(See Ref. 9 by Leo Young)

FIG. 7.05-10 EXPLODED VIEW OF WAFFLE-IRON FILTER WITH ROUND TEETH AND HALF-INDUCTANCES AT THE ENDS

b'' = 0.210 inch, a = 6.500 inches, center-to-center spacing = 1.300 inches, tooth diameter = 0.893 inch, edge radius of the rounded teeth is R = 0.063 inch. This filter is in fact based on the Waffle-Iron Filter I design, whose stop-band performance is shown in Fig. 7.05-3.

The new filter (Fig. 7.05-10) had a stop-band performance which almost duplicates Fig. 7.05-3 (after allowance is made for the fact that it has five rather than ten sections), showing that neither the tooth shape (round, not square), nor the end half-sections (half-T, not half-π) affect the stop-band performance.

In the pass band, the filter (Fig. 7.05-10) was measured first with 6.500-inch-by-0.375-inch waveguide connected on both sides. The VSWR was less than 1.15 from 1200 to 1640 megacycles. (It was below 1.08 from 1250 to 1460 megacycles). The same filter was then measured connected to 6.500-inch-by-0.350-inch waveguide, and its VSWR remained below 1.20 from 1100 to 1670 megacycles (as compared to 1225 to 1450 megacycles for 1.2 VSWR or less with Waffle-Iron Filter I). Thus the VSWR remains low over almost the whole of L-band.

The estimated power-handling capacity of the filter[8] in Fig. 7.05-10 is over two megawatts in air at atmospheric pressure. This power-handling capacity was later quadrupled by paralleling four such filters (Chapter 15).

SEC. 7.06, LOW-PASS FILTERS FROM QUARTER-WAVE TRANSFORMER PROTOTYPES

This section is concerned with the high-impedance, low-impedance short-line filter, which is the most common type of microwave low-pass filter, and which has been treated in Sec. 7.03 in terms of an approximately lumped-constant structure (Fig. 7.03-1). Such an approximation depends on:

(1) The line lengths being short compared to the shortest pass-band wavelength

(2) The high impedances being very high and the low ones very low—*i.e.*, the impedance steps should be large.

There is then a close correspondence between the high-impedance lines of the actual filter and series inductances of the lumped-constant prototype, on the one hand, and the low-impedance lines and shunt capacitances, on the other.

There is another way of deriving such a transmission-line low-pass filter, which is exact when:

(1) All line lengths are equal (and not necessarily vanishingly short)

(2) When the step discontinuity capacities are negligible.

When either of these, or both, are not satisfied, approximations have to be made, as in the design from the lumped-constant prototype. Which one of the two prototypes is more appropriate depends on which of the two sets of conditions (1) and (2) above are more nearly satisfied. Whereas the lumped-constant prototype (Sec. 7.03) is usually the more appropriate design procedure, the method outlined in this section gives additional insight, especially into the stop-band behavior, and into the spurious pass bands beyond.

This second way of deriving the short-line low-pass filter can best be understood with reference to Fig. 7.06-1. In Fig. 7.06-1(a) is shown a quarter-wave transformer (Chapter 6) with its response curve. Each section is a quarter-wave long at a frequency inside the first pass band,

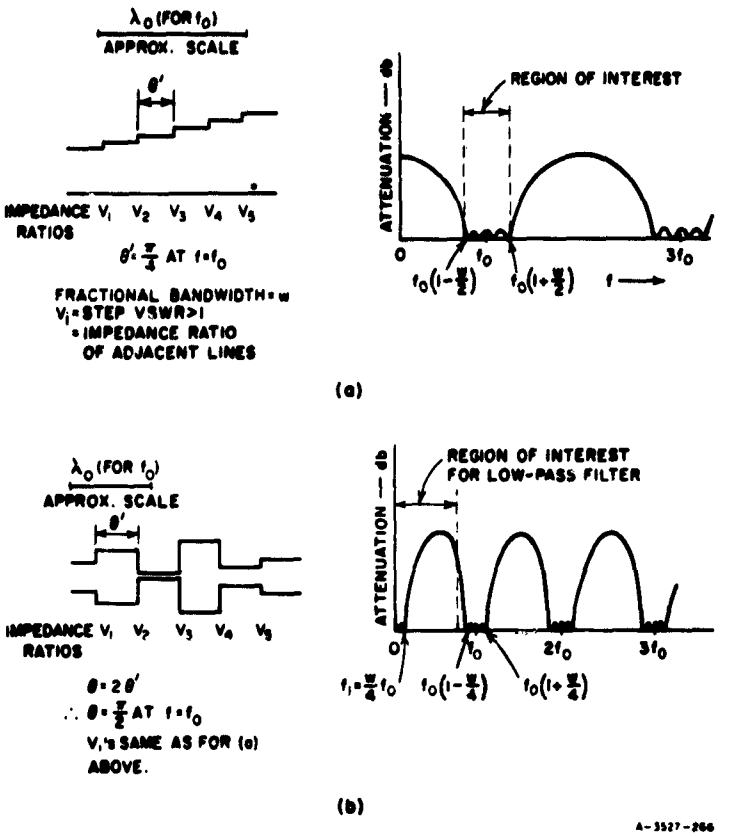

FIG. 7.06-1 CONNECTION BETWEEN QUARTER-WAVE TRANSFORMERS (a) AND CORRESPONDING LOW-PASS FILTERS (b)

called the band center, f_0. The "low-pass filter" is sketched in Fig. 7.06-1(b). Its physical characteristics differ from the quarter-wave transformer in that the impedance steps are alternately up and down, instead of forming a monotone sequence; it is essentially the same structure as the "half-wave filter" of Chapter 9. Each section is a half-wave long at a frequency f_0 at the center of the first band-pass pass band. However, note that there is also a low-pass pass band from $f = 0$ to f_1, and that the stop band above f_1 is a number of times as wide as the low-pass pass band. The fractional bandwidth of the spurious pass band at f_0 for the low-pass filter has half the fractional pass-band bandwidth, w, of the quarter-wave transformer. The VSWRs V_i of the corresponding steps in the step-transformer and in the low-pass filter

are the same for both structures, the VSWRs here being defined as equal to the ratio (taken so as to be greater than one) of the impedances of adjacent lines.

Low-pass filters are generally made of non-dispersive lines (such as strip lines or coaxial lines), will be treated as such here. If waveguides or other dispersive lines are used, it is only necessary to replace normalized frequency f/f_0 by normalized reciprocal guide wavelength λ_{g0}/λ_g. Since the low-pass filter sections are a half-wavelength long at $f = f_0$, the over-all length of a low-pass filter of n sections is at most $n\pi/8$ wavelengths at any frequency in the (low-pass) pass band, this being its length at the low-pass band-edge, $f_1 = \pi f_0/4$. Note that the smaller π for the step-transformer is chosen to be, the larger the size of the stop band above f_1 will be for the low-pass filter, relative to the size of the low-pass pass band.

Exact solutions for Tchebyscheff quarter-wave transformers and half-wave filters have been tabulated up to $n = 4$ (Sec. 6.04); and for maximally flat filters up to $n = 8$ (Sec. 6.05); all other cases have as yet to be solved by approximate methods, such as are given in Secs. 6.06 to 6.09.

The low-pass filter (as designed by this method) yields equal line lengths for the high- and low-impedance lines. When the impedance steps, V_i, are not too large (as in the wide-band examples of Sec. 6.09), then the approach described in this section can be quite useful.* Corrections for the discontinuity capacitances can be made as in Sec. 6.08 If large impedance steps are used, as is usually desirable, the discontinuity effects become dominant over the transmission-line effects, and it is usually more straightforward to use lumped-element prototypes as was done for the first example in Sec. 7.03.

SEC. 7.07, HIGH-PASS FILTERS USING SEMI-LUMPED ELEMENTS

High-pass filters, having cutoff frequencies up to around 1.5 or possibly 2.0 Gc can be easily constructed from semi-lumped elements. At frequencies above 1.5 or 2.0 Gc the dimensions of semi-lumped high-pass

* It should be noted that small impedance steps imply a relatively limited amount of attenuation. Thus, small steps will be desired only in certain special situations.

filters become so small that it is usually easier to use other types of structures. The wide-band band-pass filters discussed in Chapters 9 and 10 are good candidates for many such applications.

In order to illustrate the design of a semi-lumped-element high-pass filter we will first describe the general technique for designing a lumped-element high-pass filter from a lumped-element low-pass prototype circuit. Next we will use this technique to determine the dimensions of a split-block, coaxial-line high-pass microwave filter using semi-lumped elements.

Lumped-Element High-Pass Filters from Low-Pass Prototype Filters—The frequency response of a lumped-element high-pass filter can be related to that of a corresponding low-pass prototype filter such as that shown in Fig. 4.04-1(b) by means of the frequency transformation

$$\omega' = -\frac{\omega_1\omega_1'}{\omega} \quad . \tag{7.07-1}$$

In this equation ω' and ω are the angular frequency variables of the low- and high-pass filters respectively while ω_1' and ω_1 are the corresponding band-edge frequencies of these filters. It is seen that this transformation has the effect of interchanging the origin of the frequency axis with the point at infinity and the positive frequency axis with the negative frequency axis. Figure 7.07-1 shows a sketch of the response, for positive frequencies, of a nine-element low-pass prototype filter together with the response of the analogous lumped-element high-pass filter obtained by means of the transformation in Eq. (7.07-1).

Equation (7.07-1) also shows that any inductive reactance $\omega'L'$ in the low-pass prototype filter is transformed to a capacitive reactance $-\omega_1\omega_1'L'/\omega = -1/(\omega C)$ in the high-pass filter, and any capacitive susceptance $\omega'C'$ in the low-pass prototype filter is transformed into an inductive susceptance $-\omega_1\omega_1'C'/\omega = -1/(\omega L)$ in the high-pass filter.

Thus, any inductance L' in the low-pass prototype filter is replaced in the high-pass filter by a capacitance

$$C = \frac{1}{\omega_1\omega_1'L'} \quad . \tag{7.07-2}$$

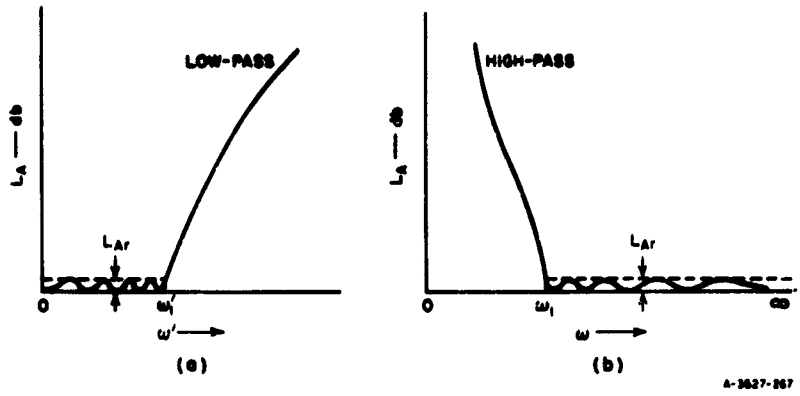

FIG. 7.07-1 FREQUENCY RESPONSE OF A LOW-PASS PROTOTYPE AND OF A CORRESPONDING HIGH-PASS FILTER

Likewise any capacitance C' in the low-pass prototype is replaced in the high-pass filter by an inductance

$$L = \frac{1}{\omega_1 \omega_1' C'} \quad . \tag{7.07-3}$$

Figure 7.07-2 illustrates the generalized equivalent circuit of a high-pass filter obtained from the low-pass prototype in Fig. 4.04-1(b) by these methods. A dual filter with an identical response can be obtained by applying Eqs. (7.07-2) and (7.07-3) to the dual low-pass prototype in Fig. 4.04-1(a). The impedance level of the high-pass filter may be scaled as discussed in Sec. 4.04.

Design of a Semi-Lumped-Element High-Pass Filter—In order to illustrate the technique for designing a semi-lumped-element high-pass filter we will consider the design of a nine-element high-pass filter with a pass-band ripple L_{Ar} of 0.1 db, a cutoff frequency of 1 Gc ($\omega_1 = 2\pi \times 10^9$), that will operate between 50-ohm terminations. The first step in the design is to determine the appropriate values of the low-pass prototype elements from Table 4.05-2(a). It should be noted that elements in this table are normalized so that the band-edge frequency $\omega_1' = 1$ and the termination element $g_0 = 1$. The values of the inductances and capacitances for the high-pass filter operating between 1-ohm terminations are then

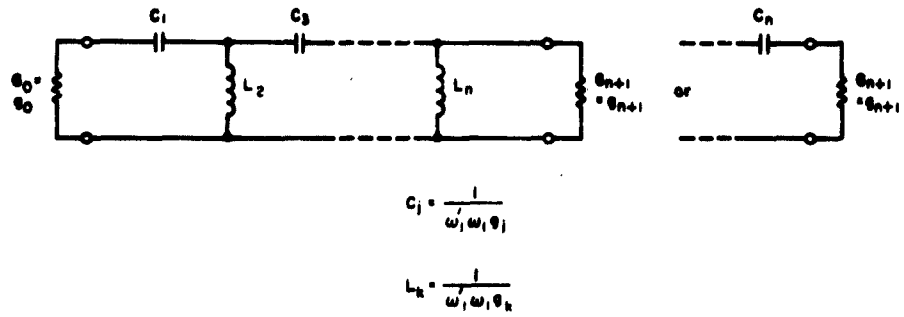

FIG. 7.07-2 HIGH-PASS FILTER CORRESPONDING TO THE LOW-PASS PROTOTYPE IN FIG. 4.04-1(b)
Frequencies ω_1' and ω_1 are defined in Fig. 7.07-1. A dual form of this filter corresponding to the low-pass filter in Fig. 4.04-1(a) is also possible

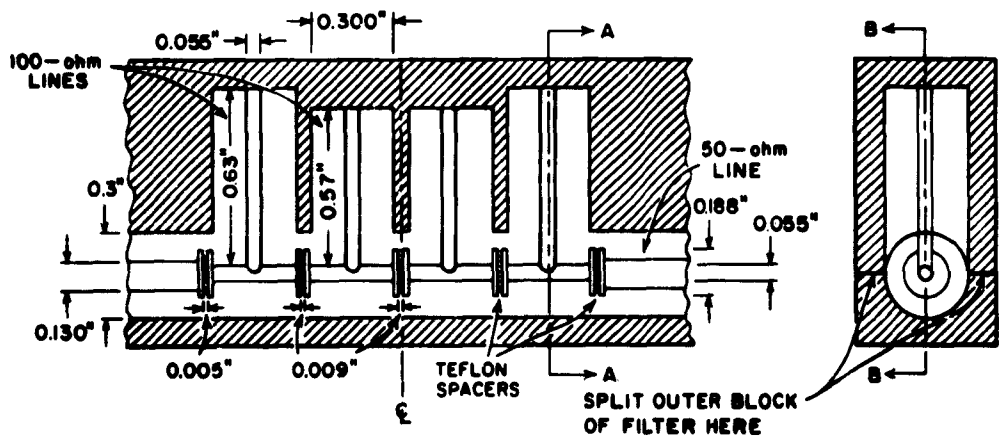

FIG. 7.07-3 DRAWING OF COAXIAL LINE HIGH-PASS FILTER CONSTRUCTED FROM SEMI-LUMPED ELEMENTS USING SPLIT-BLOCK CONSTRUCTION

determined using the formulas in Fig. 7.07-2, upon setting $\omega_1' = 1$, $\omega_1 = 2\pi \times 10^9$, and using the g_k values selected from Table 4.05-2(a). In order to convert the above design to one that will operate at a 50-ohm impedance level it is necessary to divide all the capacitance and conductance values obtained by 50 and to multiply all the inductance values obtained by 50. When this procedure is carried through we find that $C_1 = C_9 = 2.66$ $\mu\mu$f, $L_2 = L_8 = 5.51$ mμh, $C_3 = C_7 = 1.49$ $\mu\mu$f, $L_4 = L_6 = 4.92$ mμh, and $C_5 = 1.44$ $\mu\mu$f.

A sketch showing a possible realization of such a filter in coaxial line, using split-block construction, is shown in Fig. 7.07-3. Here it is seen that the series capacitors are realized by means of small metal disks utilizing Teflon ($\epsilon_r = 2.1$) as dielectric spacers. The shunt inductances are realized by short lengths of $Z_0 = 100$-ohm line short-circuited at the far end. In determining the radius r of the metal disks, and the separation s between them, it is assumed that the parallel-plate capacitance is much greater than the fringing capacitance, so that the capacitance C of any capacitor is approximately

$$C \approx \epsilon_r \, 0.225 \, \frac{\pi r^2}{s} \qquad \mu\mu f \tag{7.07-4}$$

where all dimensions are measured in inches. The lengths l of the short-circuited lines were determined by means of the formula

$$L = 0.0847 \, Z_0 l \qquad m\mu h \tag{7.07-5}$$

where Z_0 is measured in ohms and l is measured in inches. Equation (7.07-4) is adapted from one in Fig. 7.02-2(b), while Eq. (7.07-5) is adapted from one in Fig. 7.02-1(a).

The dimensions presented in Fig. 7.07-3 must be regarded as tentative, because a filter having these particular dimensions has not been built and tested. However, the electrical length of each of the lines in the filter is very short—even the longest short-circuited lines forming the shunt inductors have an electrical length of only 19.2 degrees at 1 Gc. Therefore, it is expected that this semi-lumped-constant filter will have very close to the predicted performance from low frequencies up to at least 2.35 Gc, where two of the short-circuited lines are an eighth-wavelength

long and have about 11 percent higher reactance than the idealized lumped-constant design. Above this frequency some increase in pass-band attenuation will probably be noticed (perhaps one or two db) but not a really large increase. At about 5 Gc when the short-circuited lines behave as open circuits, the remaining filter structure formed from the series capacitors and the short lengths of series lines has a pass band, so that the attenuation should be low even at this frequency. However, somewhere between 5 Gc and 9 Gc (where the short-circuited lines are about 180 degrees long) the attenuation will begin to rise very rapidly.

SEC. 7.08, LOW-PASS AND HIGH-PASS IMPEDANCE-MATCHING NETWORKS

Some microwave loads which can be approximated by an inductance and a resistance in series, or by a capacitance and a conductance in parallel, can be given a satisfactory broadband impedance match by use of low-pass matching networks. Having L and R, or C and G to represent the load, the decrement

$$\delta = \frac{R}{\omega_1 L} \quad \text{or} \quad \frac{G}{\omega_1 C} \tag{7.08-1}$$

is computed, where ω_1 is the pass-band cutoff frequency above which a good impedance match is no longer required. Though the prototype filter to be used in designing the matching network may have a considerably different impedance level and cutoff frequency ω_1', it must have the same decrement δ. Thus, having computed δ from the given microwave load elements and required cutoff frequency ω_1, an appropriate impedance-matching-network prototype filter can be selected from the computed value of δ and the charts of prototype element values in Sec. 4.09. Having selected a satisfactory prototype filter, the impedance-matching network can be designed by scaling the prototype in frequency and impedance level and by using the semi-lumped-element realization techniques discussed in Sec. 7.03. As was illustrated in Fig. 4.09-1, the microwave load to be matched provides the microwave circuit elements corresponding to the prototype elements g_0 and g_1, the microwave impedance-matching network corresponds to the prototype elements g_2 through g_n, and the microwave driving-source resistance or conductance corresponds to g_{n+1}.

Though low-pass microwave impedance-matching structures are quite practical for some applications, they do, nevertheless, have some inherent disadvantages compared to the band-pass impedance-matching networks discussed in Secs. 11.08 to 11.10. One of these disadvantages is that a good impedance match all the way from dc up to microwave frequencies is rarely really necessary. As was discussed in Sec. 1.03, allowing energy to be transmitted in frequency bands where energy transmission is not needed will detract from the efficiency of transmission in the band where good transmission is really needed. Thus if the decrement computed using Eq. (7.08-1) is found to be so small that Fig. 4.09-3 indicates an unacceptable amount of pass-band attenuation, the possibility of using a band-pass matching network instead should be considered. If a band-pass transmission characteristic is usable, better performance can be obtained.

Another disadvantage of low-pass impedance-matching networks is that the designer is not free to choose the driving source resistance. For a given R-L or G-C load circuit and a given cutoff frequency ω_1, the charts in Sec. 4.09 will lead to matching networks which must use the driving source resistances (or conductances) specified by the charts, if the predicted performance is to be obtained. In many microwave applications, adjustments of the driving-source impedance level will not be convenient. In such cases the use of band-pass impedance-matching networks is again recommended since in the case of band-pass filters, impedance-level transformations are easily achieved in the design of the filter, without affecting the transmission characteristic.

High-pass impedance-matching networks have basically the same disadvantages as low-pass impedance-matching networks. Nevertheless they are of practical importance for some applications. Loads which can be approximated by a capacitance and resistance in series, or by an inductance and conductance in parallel can be given a high-pass impedance match by using the methods of this book. In this case the decrement is computed by use of the formula

$$\delta = \omega_1 CR \quad \text{or} \quad \omega_1 LG \tag{7.08-2}$$

where in this case ω_1 is the cutoff frequency for the desired high-pass matching characteristic. Knowing δ, the $(L_A)_{max}$ values for various numbers of matching elements are checked and a prototype is then selected, as discussed in Sec. 4.09. [Again, if the values of $(L_A)_{max}$ for the computed

value of δ are too large, the possibility of band-pass matching should be considered.] The low-pass prototype is then transformed to a high-pass filter as discussed in Sec. 7.07, and its frequency scale and impedance level are adjusted so as to conform to the required ω_1 value and the specified microwave load. If the cutoff frequency ω_1 is not too high, it should be practical to realize the microwave impedance-matching structure by use of the semi-lumped-element high-pass filter techniques discussed in Sec. 7.07.

SEC. 7.09, LOW-PASS TIME-DELAY NETWORKS

Most of the primary considerations in the design of low-pass time-delay networks have been previously discussed in Secs. 1.05, 4.07, and 4.08. The maximally flat time-delay networks tabulated in Sec. 4.07 were seen to give extremely flat time-delay* characteristics, but at the expense of having an attenuation characteristic which varies considerably in the operating band. Maximally flat time-delay networks also are unsymmetrical, which makes their fabrication more difficult. In Sec. 4.08 it was noted that Tchebyscheff filters with small pass-band ripple should make excellent time-delay networks for many practical applications. As was discussed in Sec. 1.05, the amount of time delay can be increased considerably for a given circuit complexity by using, where possible, a band-pass rather than a low-pass structure for the delay network (see Secs. 1.05 and 11.11). High-pass delay networks are also conceivable, but they would not give much delay, except, possibly, near cutoff.

Example—As an example of the initial steps in the design of a low-pass time-delay network, let us suppose that a time delay of about 7.2 nanoseconds is required from frequencies of a few megacycles up to 200 Mc. From considerations such as those discussed in Sec. 4.08, let us further suppose that it has been decided to use a 0.1-db ripple Tchebyscheff filter with a cutoff of $f_1 = 250$ Mc, as the delay network. From Eq. (4.08-3), the low-frequency time delay of a corresponding normalized prototype filter with a cutoff of $\omega_1' = 1$ radian/sec is

$$t'_{do} = t_{do}\frac{\omega_1}{\omega_1'} = \frac{7.2(10^{-9})2\pi(0.25)10^9}{1} = 11.3 \text{ seconds} .$$

* More time delay is assumed to imply group time delay (Sec. 1.05).

By Eq. (4.08-2) and Fig. 4.13-2, this nominal time delay will be achieved by a 0.10-db ripple filter having $n = 13$ reactive elements. Hence, an $n = 13$, $L_{ar} = 0.10$ db prototype should be selected from Table 4.05-2(b). The actual microwave filter is then designed from the prototype as discussed in Sec. 7.03. If desired, this filter could be designed to be a few inches long, while it would take approximately 7 feet of air-filled coaxial line to give the same time delay.

REFERENCES

1. N. Marcuvitz, *Waveguide Handbook*, p. 178 (McGraw Hill Book Company, New York, N.Y., 1951).
2. R. Saal and E. Ulbrich, "On the Design of Filters by Synthesis," *Trans. IRE*, PGCT-5, pp. 284-327 (December 1958). The same tables and many more will be found in the book, R. Saal, *Der Entwurf von Filtern mit Hilfe des Kataloges normierter Tiefpasse*, Telefunken GMBH, Backnang, Wurttemburg, Germany (1961).
3. S. B. Cohn, "A Theoretical and Experimental Study of a Waveguide Filter Structure," Cruft Laboratory Report 39, ONR Contract N50 RI-76, Harvard University (April 1948).
4. S. B. Cohn, "Analysis of a Wide-Band Waveguide Filter," *Proc. IRE* 37, 6, pp. 651-656 (June 1949).
5. E. A. Guillemin, *Communication Networks, Vol. 2*, p. 439 (John Wiley and Sons, New York, N.Y., 1935).
6. N. Marcuvitz, *op. cit.*, p. 336-350.
7. S. B. Cohn, "Design Relations for the Wide-Band Waveguide Filter," *Proc. IRE* 38, 7, pp. 799-803 (July 1950).
8. Eugene Sharp, "A High-Power Wide-Band Waffle-Iron Filter," Tech. Note 2, SRI Project 3478, Contract AF 30(602)-2392, Stanford Research Institute, Menlo Park, California (January 1962).
9. Leo Young, "Suppression of Spurious Frequencies," Quarterly Progress Report 1, SRI Project 4096, Contract AF 30(602)-2734, Stanford Research Institute, Menlo Park, California (July 1962).

CHAPTER 8

BAND-PASS FILTERS
(A GENERAL SUMMARY OF BAND-PASS FILTERS, AND A VERSATILE DESIGN TECHNIQUE FOR FILTERS WITH NARROW OR MODERATE BANDWIDTHS)

SEC. 8.01, A SUMMARY OF THE PROPERTIES OF THE BAND-PASS OR PSEUDO HIGH-PASS FILTERS TREATED IN CHAPTERS 8, 9, AND 10

This chapter is the first of a sequence of four chapters concerning band-pass filter design. Chapters 8, 9, and 10 deal with the design theory and specific types of microwave filters, while Chapter 11 discusses various experimental and theoretical techniques which are generally helpful in the practical development of many kinds of band-pass filters and impedance-matching networks. This present chapter (Chapter 8) utilizes a design point of view which is very versatile but involves narrow-band approximations which limit its usefulness to designs having fractional bandwidths typically around 0.20 or less. The design procedure utilized in Chapter 9 makes use of step transformers as prototypes for filters, and the procedures given there are useful for either narrow or wide bandwidths. Chapter 10 uses yet another viewpoint for design, and the method described there is also useful for either narrow or wide bandwidths. The procedures in Chapter 9 are most advantageous for filters consisting of transmission lines with lumped discontinuities placed at intervals, while the methods in Chapter 10 are most advantageous when used for filters consisting of lines and stubs or of parallel-coupled resonators.

In this chapter the general design point of view is first described in a qualitative way, then design equations and other data for specific types of filters are presented, and finally the background details of how the design equations for specific filters were derived are presented. Chapters 9 and 10 also follow this pattern as far as is possible.

It is recognized that some designers may have little interest in filter design theory, and that they may only wish to pick out one design for one given job. To help meet this need, Table 8.01-1 has been prepared. It summarizes the more significant properties of the various types of filters discussed in Chapters 8, 9, and 10, and tells the reader in which sections design data for a given type of filter can be found.

Table 8.01-1

SUMMARY OF BAND-PASS AND PSEUDO HIGH-PASS FILTERS IN CHAPTERS 8, 9, AND 10

Symbols

ω_0 = pass-band center frequency

ω_{SPB} = center frequency of second pass band

$(L_A)_{USB}$ = peak attenuation (in db) in upper stop band (between ω_0 and ω_{SPB})

L_{Ar} = peak attenuation (in db) in pass band

w = fractional bandwidth

λ_0 = wavelength at ω_0

λ_g = guide wavelength

$\lambda_{g0}, \lambda_{g1}, \lambda_{g2}$ = guide wavelengths at ω_0 and at lower and upper pass-band-edge frequencies

$w_\lambda = \frac{\lambda_{g1} - \lambda_{g2}}{\lambda_{g0}}$ = guide-wavelength fractional bandwidth

STRIP-LINE (OR COAXIAL) AND SEMI-LUMPED-ELEMENT FILTERS

Typical Resonator or Section	Filter Properties
1 ★ 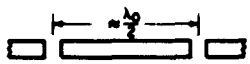 STRIP LINE	$\omega_{SPB} \approx 2\omega_0$. $(L_A)_{USB}$ decreases with increasing w. $(L_A)_{USB}$ is usually sizeable for $w = 0.20$ or less, but it is usually only 5 or 10 db for $w = 0.70$. Has first-order pole of attenuation at $\omega = 0$. Dielectric support required for resonators. Coupling gaps may become quite small for w much larger than 0.10, which presents tolerance considerations. See Sec. 8.05 for designs with w about 0.20 or less. See Chapter 9 for designs having larger w, or for designs with very small L_{Ar} (0.01 db, for example), or for designs for high-pass applications. Coaxial filters of this type are widely used as pseudo high-pass filters.
2 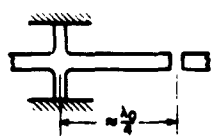 STRIP LINE	$\omega_{SPB} \approx 3\omega_0$. $(L_A)_{USB}$ decreases with increasing w, but for given w and ω_0, $(L_A)_{USB}$ will be larger than for Filter 1 above. Has multiple-order pole of attenuation at $\omega = 0$. Inductive stubs can provide mechanical support for resonator structure so that dielectric is not required. For given w and ω_0 capacitive coupling gaps are larger than for Filter 1 above. See Sec. 8.08 for designs with $w \lesssim 0.30$. See Chapter 9 for designs having larger w, or for designs with very small L_{Ar} (0.01 db, for example), or for designs for high-pass applications.
3 ★ 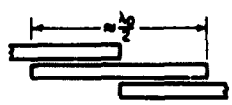 STRIP LINE	$\omega_{SPB} = 3\omega_0$. Has first-order pole of attenuation at $\omega = 0$ and at $\omega = 2\omega_0$. However, is prone to have narrow spurious pass bands near $2\omega_0$ due to slightest mistuning. Dielectric support material required. Very attractive structure for printed circuit fabrication, when $w \lesssim 0.15$. See Sec. 8.09-1 for $w \lesssim 0.15$. See Sec. 10.02 for designs having larger w, or for designs for high-pass applications.

Table 8.01-1 *Continued*

STRIP-LINE (OR COAXIAL) AND SEMI-LUMPED ELEMENT FILTERS	
Typical Resonator or Section	**Filter Properties**
4 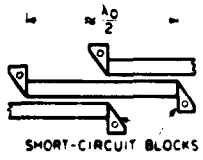 STRIP LINE	$\omega_{SPB} = 3\omega_0$. Has first-order pole of attenuation at $\omega = 0$ and at $\omega = 2\omega_0$. However, is prone to narrow spurious pass bands near $2\omega_0$ due to slightest mistuning. Short-circuit blocks provide mechanical support for resonators. Suitable for values of w from around 0.01 to 0.70 or more. See Sec. 10.02.
5 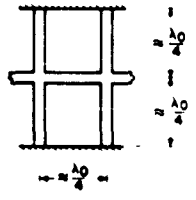 STRIP LINE	$\omega_{SPB} = 3\omega_0$. Has first-order pole of attenuation at $\omega = 0$ and at $\omega = 2\omega_0$. However, is prone to narrow spurious pass bands near $2\omega_0$ due to slightest mistuning. Short-circuits at ends of stubs provide mechanical support for structure. Suitable for values of w from around 0.40 to 0.70 or more. See Sec. 10.03. Also see Sec. 10.05 for case where series stubs are added at ends to give poles of attenuation at additional frequencies.
6 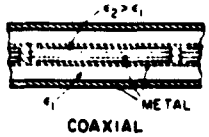 COAXIAL	Structure in coaxial form with series stubs fabricated within center conductor of main line. $\omega_{SPB} = 3\omega_0$. Has first-order pole of attenuation at $\omega = 0$ and at $\omega = 2\omega_0$. However, is prone to narrow spurious pass bands near $2\omega_0$ due to slightest mistuning. Structure requires dielectric support material. Suitable for values of w around 0.60 or more. See Sec. 10.03.
7 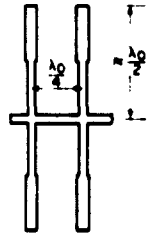 STRIP LINE	$\omega_{SPB} = 2\omega_0$, and also has a pass band around $\omega = 0$. Has poles of attenuation above and below ω_0 at frequencies ω_∞ and $(2\omega_0 - \omega_\infty)$, where ω_∞ may be specified. Requires dielectric material for support. Can conveniently be fabricated by printed circuit means. Little restriction on w if ω_∞ can be chosen appropriately. See Sec. 10.04.

Table 8.01 *Continued*

STRIP-LINE (OR COAXIAL) AND SEMI-LUMPED-ELEMENT FILTERS	
Typical Resonator or Section	**Filter Properties**
8 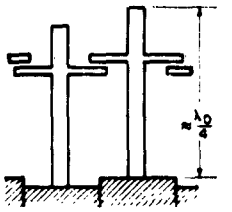 STRIP LINE	ω_{SPB} can be made to be as high as $5\omega_0$ or more. Has multiple-order poles of attenuation at $\omega = 0$. Short-circuited ends of resonators provide mechanical support so that dielectric material is not required. Structure is quite compact. See Sec. 8.12 for design data suitable for designs with $w \lesssim 0.10$.
9 ★ 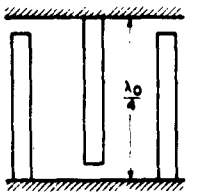 STRIP LINE	Interdigital Filter. $\omega_{SPB} = 3\omega_0$. Has multiple-order poles of attenuation at $\omega = 0$ and $\omega = 2\omega_0$. Can be fabricated without using dielectric support material. Spacings between resonator elements are relatively large which relaxes mechanical tolerances. Structure is very compact. See Secs. 10.06 and 10.07 for equations for designs with w ranging from small values up to large values around 0.70 or more.
10 ★ 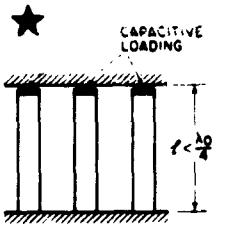 STRIP LINE	Comb-line filter. Resonator length l depends on amount of capacitive loading used. $\omega_{SPB} \gtrsim \omega_0 \lambda_0/(2l)$ so filter can be designed for very broad upper stop band. Poles of attenuation at $\omega = 0$ and $\omega = \omega_0 \lambda_0/(4l)$. Extremely compact structure which can be fabricated without dielectric support material. Unloaded Q's of resonators somewhat less than those for Filter 9 for some strip-line cross-section. See Sec. 8.13 for designs having w up to about 0.15.
11 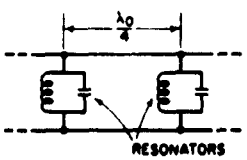 LUMPED ELEMENTS	Filter with quarter-wave-coupled resonators. Resonators may be cavities, resonant irises, or lumped-element resonators. See Sec. 8.08 for design data useful when w is around 0.05 or less.

Table 8.01-1 *Concluded*

Typical Resonator or Section	Filter Properties
STRIP-LINE (OR COAXIAL) AND SEMI-LUMPED-ELEMENT FILTERS	
12 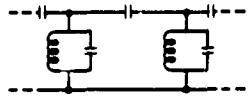 LUMPED ELEMENTS	Lumped-element circuit for use as a guide for design of semi-lumped-element microwave filters. See Sec. 8.11 for designs with $w \lesssim 0.20$.
13 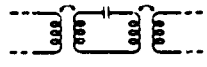 LUMPED ELEMENTS	Lumped-element circuit for use as a guide for design of semi-lumped-element microwave filters. See Sec. 8.11 for designs with $w \lesssim 0.20$.
WAVEGUIDE AND CAVITY FILTERS	
14 ★ 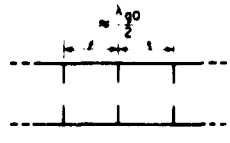 WAVEGUIDE	ω_{SPB} occurs when λ_g is about $\lambda_{g0}/2$; however, when higher-order modes can propagate, the upper stop band and second pass band may be disrupted. $(L_A)_{USB}$ decreases with increasing w_λ. Waveguide resonators give relatively low dissipation loss for given w_λ. See Secs. 8.06 and 8.07 for designs with w_λ about 0.20 or less. See Chapter 9 for designs having larger w_λ, or for designs with very small L_{Ar} (0.01 db, for example), or for designs for high-pass applications.
15 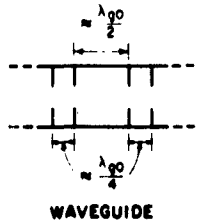 WAVEGUIDE	Use of $\lambda_{g0}/4$ couplings gives irises which are all nearly the same. If a disassembly joint is placed in the middle of each $\lambda_{g0}/4$ coupling region, resonators may be easily tested individually. ω_{SPB} occurs when λ_g is about $\lambda_{g0}/2$; however, when higher-order modes can propagate the upper stop band and second pass band may be disrupted. $(L_A)_{USB}$ decreases with increasing w_λ. Waveguide resonators give relatively low dissipation loss for given w_λ. Satisfactory for designs having w_λ about 0.05 or less. See Sec. 8.08.

The filters whose properties are summarized in Table 8.01-1 are suitable for a wide range of applications. Some are suitable for either narrow- or wide-band band-pass filter applications. Also, since it is difficult, if not impossible, to build a microwave high-pass filter with good pass-band performance up to many times the cutoff frequency, pseudo high-pass filters, which are simply wideband band-pass filters, provide some of the most practical means for fabricating filters for microwave high-pass applications. Thus, many of the filters in Table 8.01-1 should also be considered as potential microwave high-pass filters.

Although most of the filters in Table 8.01-1 are pictured in strip-line form, many of them could be fabricated equally well in coaxial form or in split-block coaxial form (Fig. 10.05-3). One of the filter properties which is of interest in selecting a particular type of band-pass filter structure is the frequency at which the second pass band will be centered. In Table 8.01-1, this frequency is designated as ω_{SPB}, and it is typically two or three times ω_0, the center frequency of the first pass band. However, in the case of Filter 8 in Table 8.01-1, ω_{SPB} can be made to be as much as five or more times ω_0. Filter 10 is also capable of very broad stop bands.

All of the filters in Table 8.01-1 have at least one frequency, ω, where they have infinite attenuation (or where they would have infinite attenuation if it were not for the effects of dissipation loss). These infinite attenuation points, known as poles of attenuation (see Sec. 2.04), may be of first order or of multiple order; the higher the order of the pole of attenuation, the more rapidly the attenuation will rise as ω approaches the frequency of the pole. Thus, the presence of first-order or multiple-order poles of attenuation at frequencies ω are noted in Table 8.01-1 as a guide towards indicating what the relative strength of the stop band will be in various frequency ranges. Four of the filters in Table 8.01-1 (Filters 1, 2, 14, and 15) have no poles of attenuation in the stop-band region above the pass-band center ω_0, and the attenuation between the first and second pass-bands levels off at a value of $(L_A)_{USB}$ decibels. As is mentioned in Table 8.01-1, the values of $(L_A)_{USB}$ will in such cases be influenced by the fractional bandwidth w of the filter. Also, it should be noted that the filters which have a first-order pole of attenuation in the stop band above ω_0 may be liable to spurious responses close to this pole if there is any mistuning.

Another consideration in choosing a type of filter for a given job is the unloaded Q's obtainable with the resonator structures under consideration. Waveguide or cavity resonators will, of course, give the best unloaded Q's, and hence will result in filters with minimum insertion loss for a given fractional

bandwidth. However, waveguide resonators have the disadvantages of being relatively bulky and of being useful over only a limited frequency range because of the possibility of higher-order modes. Thus, where wide pass bands or wide stop bands are required, strip-line, coaxial, or semi-lumped-element filters are usually preferable. If strip-line or coaxial constructuions are used, the presence of dielectric material, which may be required for mechanical support of the structure, will tend to further decrease the resonator Q's obtainable. For this reason, it is in many cases noted in Table 8.01-1 whether or not the specific structure can be fabricated without the use of dielectric support material.

The filter structures marked with stars in Table 8.01-1 are filter types which represent attractive compromise choices for many applications. However, they are by no means necessarily the best choices in all respects, and special considerations may dictate the use of some of the unstarred types of filters listed in the table.

Filter 1 in Table 8.01-1 was starred because, in coaxial form, it provides a very rugged and convenient way for manufacturing pseudo high-pass filters. Commercial coaxial high-pass filters are most commonly of this form.

Filter 3 in Table 8.01-1 has been starred because it is extremely easy to design and fabricate in printed-circuit construction when the fractional bandwidth is around 0.15 or less. However, its stop-band characteristics and its resonator Q's are inferior to those that can be obtained with some of the other types of strip-line or coaxial filters in the table.

Filter 9 was starred because it is easy to design for anywhere from small to large fractional bandwidths, it is compact, and it has strong stop bands on both sides of ω_0.

Filter 10 was starred because of its compactness and ease of design, and because it is capable of a very broad upper stop band.

Filter 14 was starred because it is the simplest and most commonly used type of waveguide filter. Within the single-mode frequency range of the waveguide, such filters generally give excellent performance.

SEC. 8.02, GENERAL PRINCIPLES OF COUPLED-RESONATOR FILTERS*

In this section we will discuss the operation of coupled-resonator filters in qualitative terms. For the benefit of those readers who are concerned

---

* The point of view used herein is that due to S. B. Cohn.[1] However, herein his point of view has been restated in more general terms, and it has been applied to additional types of filter structures not treated by Cohn. Some other points of view and earlier contributions are listed in References 2 to 8.

primarily with practical design, rather than with theory, this qualitative discussion will be followed by design data for specific types of filters. Details of the derivation of the design equations will be found in Sec. 8.14.

In the design procedures of this chapter, the lumped-element prototype filter designs discussed and tabulated in Chapter 4 will be used to achieve band-pass filter designs having approximately the same Tchebyscheff or maximally flat response properties. Thus, using a lumped-element prototype having a response such as the Tchebyscheff response shown in Fig. 8.02-1(a), the corresponding band-pass filter response will also be Tchebyscheff as shown in Fig. 8.02-1(b). As suggested in Fig. 8.02-1(b), the multiple resonances inherent in transmission-line or cavity resonators generally give band-pass microwave filters additional pass bands at higher frequencies.

Figure 8.02-2(a) shows a typical low-pass prototype design, and Fig. 8.02-2(b) shows a corresponding band-pass filter design, which can be obtained directly from the prototype by a low-pass to band-pass transformation to be discussed in Sec. 8.04. In the equations for the band-pass filter element values, the g_j are the prototype filter element values, ω' and ω'_1 are for the prototype filter response as indicated in Fig. 8.02-1(a) for a typical Tchebyscheff case, and ω, ω_0, ω_1, and ω_2 apply to the corresponding band-pass filter response as indicated in Fig. 8.02-1(b). Of course, the filter in Fig. 8.02-2(b) would not have the higher frequency pass bands suggested in Fig. 8.02-1(b) because it is composed of lumped elements.

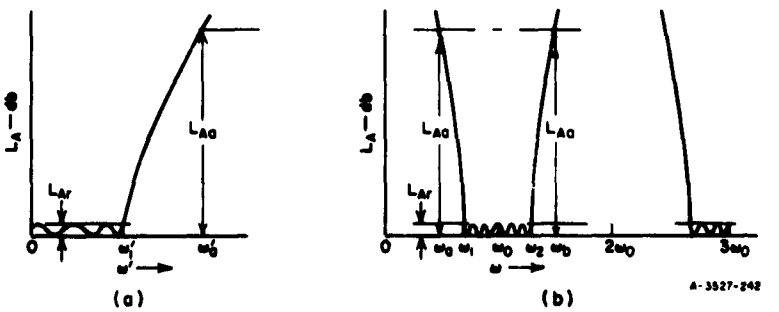

FIG. 8.02-1 LOW-PASS PROTOTYPE RESPONSE AND CORRESPONDING BAND-PASS FILTER RESPONSE

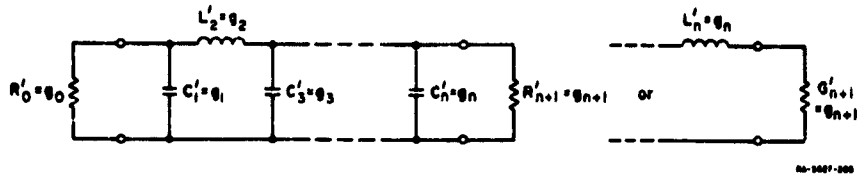

FIG. 8.02-2(a) A LOW-PASS PROTOTYPE FILTER

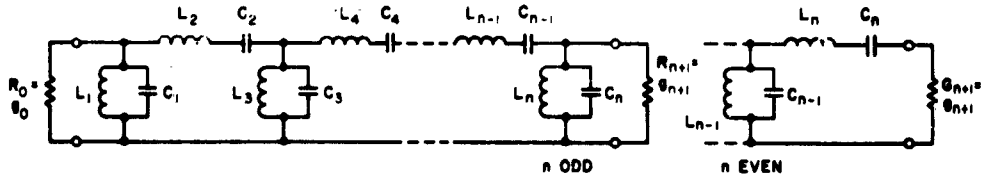

A-3527-184

FOR SHUNT RESONATORS:

$$b_j = \omega_0 C_j = \frac{1}{\omega_0 L_j} = \frac{\omega'_1 g_1}{w} = \text{susceptance slope parameter} \qquad (1)$$

FOR SERIES RESONATORS:

$$x_k = \omega_0 L_k = \frac{1}{\omega_0 C_k} = \frac{\omega'_1 g_1}{w} = \text{reactance slope parameter} \qquad (2)$$

$$w = \frac{\omega_2 - \omega_1}{\omega_0}$$

$$\omega_0 = \sqrt{\omega_1 \omega_2}$$

FIG. 8.02-2(b) BAND-PASS FILTERS AND THEIR RELATION TO LOW-PASS PROTOTYPES
Frequencies ω'_1, ω_1, and ω_2 are defined in Fig. 8.02-1, ang $g_0, g_1, \ldots, g_{n+1}$ are defined in Fig. 8.02-2(a)

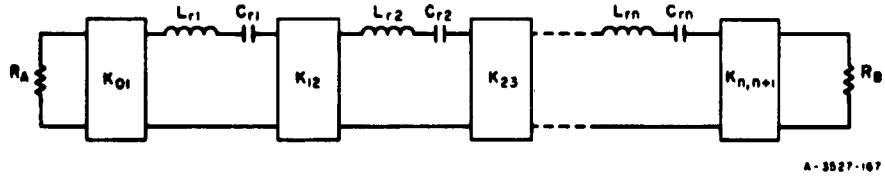

A-3527-187

NOTE: Adapted from Final Report, Contract DA-36-039 SC-64625, SRI; reprinted in *Proc. IRE* (see Ref. 1 by S. B. Cohn).

FIG. 8.02-2(c) THE BAND-PASS FILTER IN FIG. 8.02-2(b) CONVERTED TO USE ONLY SERIES RESONATORS AND IMPEDANCE INVERTERS

The filter structure in Fig. 8.02-2(b) consists of series resonators alternating with shunt resonators, an arrangement which is difficult to achieve in a practical microwave structure. In a microwave filter, it is much more practical to use a structure which approximates the circuit in Fig. 8.02-2(c), or its dual. In this structure all of the resonators are of the same type, and an effect like alternating series and shunt resonators is achieved by the introduction of "impedance inverters," which were defined in Sec. 4.12, and are indicated by the boxes in Fig. 8.02-2(c). The band-pass filter in Fig. 8.02-2(c) can be designed from a low-pass prototype as in Fig. 8.02-2(a) by first converting the prototype to the equivalent low-pass prototype form in Fig. 4.12-2(a) which uses only series inductances and impedance inverters in the filter structure. Then a low-pass to band-pass transformation can be applied to the circuit in Fig. 4.12-2(a) to yield the band-pass circuit in Fig. 8.02-2(c). Practical means for approximate realization of impedance inverters will be discussed in Sec. 8.03 following.

Since lumped-circuit elements are difficult to construct at microwave frequencies, it is usually desirable to realize the resonators in distributed-element forms rather than the lumped-element forms in Figs. 8.02-2(b), (c). As a basis for establishing the resonance properties of resonators regardless of their form it is convenient to specify their *resonant frequency* ω_0 and their *slope parameter*. For any resonator exhibiting a series-type resonance (case of zero reactance at ω_0) the *reactance slope parameter*

$$\alpha = \frac{\omega_0}{2} \left.\frac{dX}{d\omega}\right|_{\omega_0} \quad \text{ohms} \tag{8.02-1}$$

applies, where X is the reactance of the resonator. For a simple series L-C resonator, Eq. (8.02-1) reduces to $\alpha = \omega_0 L = 1/(\omega_0 C)$. For any resonator exhibiting a shunt-type resonator (case of zero *susceptance* at ω_0) the *susceptance slope parameter*

$$b = \frac{\omega_0}{2} \left.\frac{dB}{d\omega}\right|_{\omega_0} \quad \text{mhos} \tag{8.02-2}$$

applies where B is the susceptance of the resonator. For a shunt L-C resonator, Eq. (8.02-2) reduces to $b = \omega_0 C = 1/(\omega_0 L)$. Note that in Fig. 8.02-2(b) the properties of the lumped resonators have been defined in terms of susceptance and reactance slope parameters. The slope parameters of certain transmission-line resonators were discussed in Sec. 5.08 and are summarized in Fig. 5.08-1. Any resonator having a series-type resonance with a reactance slope parameter α and series resistance R has a Q of

$$Q = \frac{\alpha}{R} \quad . \tag{8.02-3}$$

Likewise, any resonator having a shunt-type resonance with a susceptance slope parameter b and a shunt conductance G has a Q of

$$Q = \frac{b}{G} \quad . \tag{8.02-4}$$

Figure 8.02-3(a) shows a generalized circuit for a band-pass filter having impedance inverters and series-type resonator characteristics as indicated by the resonator-reactance curve in Fig. 8.02-3(b). Let us suppose that a band-pass filter characteristic is desired like that in Fig. 8.02-1(b), and the filter is to be designed from a low-pass prototype having a response like that in Fig. 8.02-1(a) and having prototype parameters g_0, g_1, ..., g_{n+1}, and ω_1'. The resonator slope parameters α_1, α_2, ..., α_n for the band-pass filter may be selected arbitrarily to be of any size corresponding to convenient resonator designs. Likewise, the terminations R_A, R_B, and the fractional bandwidth w may be specified as desired. The desired shape of response is then insured by specifying the impedance-inverter parameters K_{01}, K_{12}, ..., $K_{n,n+1}$ as required by Eqs. (2) to (4) in Fig. 8.02-3. If the resonators of the filter in Fig. 8.02-3(a) were each comprised of a lumped L and C, and if the impedance inverters were not frequency sensitive, the equations in Fig. 8.02-3 would be exact regardless of the fractional bandwidth w of the filter. However, since the inverters used in practical cases are frequency sensitive (see Sec. 8.03), and since the resonators used will generally not be lumped, in practical cases the equations in Fig. 8.02-3 represent approximations which are best for narrow bandwidths. However, in some cases good results can be obtained for bandwidths as great as

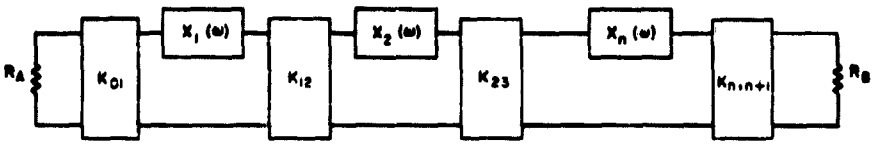

(a) A GENERALIZED, BAND-PASS FILTER CIRCUIT USING IMPEDANCE INVERTERS

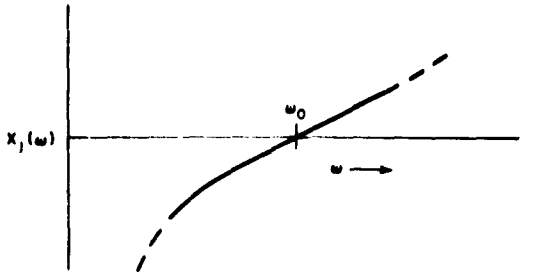

8-3527-165

(b) REACTANCE OF jth RESONATOR

$$x_j = \frac{\omega_0}{2}\frac{dX_j(\omega)}{d\omega}\bigg|_{\omega=\omega_0} \quad \text{ohms} \tag{1}$$

= Reactance Slope Parameter

$$K_{01} = \sqrt{\frac{R_A x_1 w}{g_0 g_1 \omega_1'}} \tag{2}$$

$$K_{j,j+1}\Big|_{j=1 \text{ to } n-1} = \frac{w}{\omega_1'}\sqrt{\frac{x_j x_{j+1}}{g_j g_{j+1}}} \tag{3}$$

$$K_{n,n+1} = \sqrt{\frac{R_B x_n w}{\omega_1' g_n g_{n+1}}} \tag{4}$$

$$w = \text{fractional bandwidth} = \frac{\omega_2 - \omega_1}{\omega_0} \text{ or} \approx \tag{5}$$

where ω_1', ω_0, ω_1, and ω_2 are defined in Fig. 8.02-1, and g_0, g_1, ... g_{n+1} are as defined in Sec. 4.04 and Fig. 8.02-2(a).

For Experimental Determination of Couplings (As Discussed in Chapter 11)

External Q's are:

$$(Q_e)_A = \frac{x_1}{(K_{01}^2/R_A)} = \frac{g_0 g_1 \omega_1'}{w} \tag{6}$$

$$(Q_e)_B = \frac{x_n}{(K_{n,n+1}^2/R_B)} = \frac{\omega_1' g_n g_{n+1}}{w} \tag{7}$$

Coupling coefficients are:

$$k_{j,j+1}\Big|_{j=1 \text{ to } n-1} = \frac{K_{j,j+1}}{\sqrt{x_j x_{j+1}}} = \frac{w}{\omega_1'\sqrt{g_j g_{j+1}}} \tag{8}$$

FIG. 8.02-3 GENERALIZED EQUATIONS FOR DESIGN OF BAND-PASS FILTERS FROM LOW-PASS PROTOTYPES
Case of filters with resonators having series-type resonances. The K-inverters represent the couplings

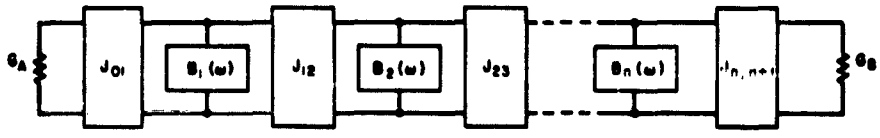

(a) A GENERALIZED, BAND-PASS FILTER CIRCUIT USING ADMITTANCE INVERTERS

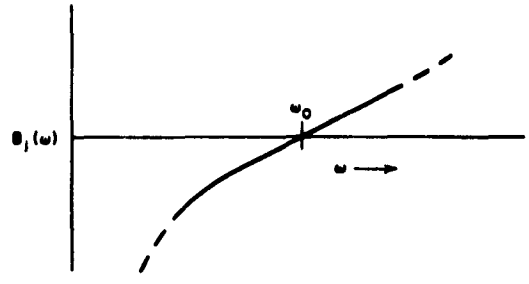

(b) SUSCEPTANCE OF jth RESONATOR

A-5527-106

$$b_j = \frac{\omega_0}{2}\frac{dB_j(\omega)}{d\omega}\bigg|_{\omega=\omega_0} \quad \text{mhos} \tag{1}$$

= Susceptance Slope Parameter

$$J_{01} = \sqrt{\frac{G_A b_1 w}{g_0 g_1 \omega_1'}} \tag{2}$$

$$J_{j,j+1}\Big|_{j=1 \text{ to } n-1} = \frac{w}{\omega_1'}\sqrt{\frac{b_j b_{j+1}}{g_j g_{j+1}}} \tag{3}$$

$$J_{n,n+1} = \sqrt{\frac{G_B b_n w}{\omega_1' g_n g_{n+1}}} \tag{4}$$

$$w = \text{fractional bandwidth} = \frac{\omega_2 - \omega_1}{\omega_0} \tag{5}$$

where ω_1', ω_0, ω_1 and ω_2 are defined in Fig. 8.02-1, and g_0, g_1, ..., g_{n+1} are as defined in Sec. 4.04 and Fig. 8.02-2(a).

For Experimental Determination of Couplings (As Discussed in Chapter 11)

External Q's are:

$$(Q_e)_A = \frac{b_1}{(J_{01}^2/G_A)} = \frac{g_0 g_1 \omega_1'}{w} \tag{6}$$

$$(Q_e)_B = \frac{b_n}{(J_{n,n+1}^2/G_B)} = \frac{\omega_1' g_n g_{n+1}}{w} \tag{7}$$

Coupling coefficient are:

$$k_{j,j+1}\Big|_{j=1 \text{ to } n-1} = \frac{J_{j,j+1}}{\sqrt{b_j b_{j+1}}} = \frac{w}{\omega_1'\sqrt{g_j g_{j+1}}} \tag{8}$$

FIG. 8.02-4 GENERALIZED EQUATIONS FOR DESIGN OF BAND-PASS FILTERS FROM LOW-PASS PROTOTYPES
Case of filters having resonators with only shunt-type resonances. The J-inverters represent the couplings

20 percent when half-wavelength resonators are used, and when quarter-wavelength resonators are used, good results can be obtained in some cases for bandwidths approaching 40 percent.

Equations (6) to (8) in Fig. 8.02-3 are forms which are particularly convenient when the resonator couplings are to be adjusted by experimental procedures discussed in Chapter 11. The external Q, $(Q_e)_A$, is the Q of Resonator 1 coupled by the Inverter K_{01} to the termination R_A. The external Q, $(Q_e)_B$ is the corresponding Q of resonator n coupled by $K_{n,n+1}$ to R_B. The expression for the coupling coefficients $k_{j,j+1}$ is a generalization of the usual definition of coupling coefficient. For lumped-element resonators with inductive couplings $k_{j,j+1} = M_{j,j+1}/\sqrt{L_j L_{j+1}}$ where L_j and L_{j+1} are self inductances and $M_{j,j+1}$ is the mutual inductance. By specifying the coupling coefficients between resonators and the external Q's of the end resonators as indicated in Eqs. (6) to (8) in Fig. 8.02-3, the response of the filter is fixed. Equations (2) to (4) and Eqs. (6) to (8) are equivalent.

The band-pass filter in Fig. 8.02-4(a) uses *admittance inverters* and *shunt-type* resonator characteristics as indicated by the resonator-*susceptance* curve in Fig. 8.02-4(b). Admittance inverters are in principle the same as impedance inverters, but for convenience they are here characterized by an admittance parameter, $J_{j,j+1}$, instead of an impedance parameter, $K_{j,j+1}$ (see Sec. 4.12). The equations in Fig. 8.02-4 are duals of those in Fig. 8.02-3, and the same general principles discussed in the preceding paragraphs apply.

In the discussions to follow K-inverter impedance parameters will be used whenever the resonators have a series-type resonance, and J-inverter admittance parameters will be used whenever the resonators have a shunt-type resonance.

SEC. 8.03. PRACTICAL REALIZATION OF K- AND J-INVERTERS

One of the simplest forms of inverters is a quarter-wavelength of transmission line. Observe that such a line obeys the basic impedance-inverter definition in Fig. 4.12-1(a), and that it will have an inverter parameter of $K = Z_0$ ohms where Z_0 is the characteristic impedance of the line. Of course, a quarter-wavelength of line will also serve as an admittance inverter as can be seen from Fig. 4.12-1(b), and the admittance inverter parameter will be $J = Y_0$ where Y_0 is the characteristic admittance of the line.

Although its inverter properties are relatively narrow-band in nature, a quarter-wavelength line can be used satisfactorily as an impedance or admittance inverter in narrow-band filters. Thus, if we have six identical cavity resonators, and if we connect them by lines which are a quarter-wavelength long at frequency ω_0, then by properly adjusting the coupling at each cavity it is possible to achieve a six resonator Tchebyscheff response such as that in Fig. 8.02-1(b). Note that if the resonators all exhibit, say, series-type resonances, and if they were connected together directly without the impedance inverters, they would simply operate like a *single* series resonator with a slope parameter equal to the sum of the slope parameters of the individual resonators. Some sort of inverters between the resonators are essential in order to obtain a multiple-resonator response if all of the resonators are of the same type, *i.e.*, if all exhibit a series-type resonance or all exhibit a shunt-type resonance.

Besides a quarter-wavelength line, there are numerous other circuits which operate as inverters. All necessarily give an image phase (see Sec. 3.02) of some odd multiple of ±90 degrees, and many have good inverting properties over a much wider bandwidth than does a quarter-wavelength line. Figure 8.03-1 shows four inverting circuits which are of special interest for use as *K*-inverters (*i.e.*, inverters to be used with series-type resonators). Those shown in Figs. 8.03-(a),(b) are particularly useful in circuits where the negative *L* or *C* can be absorbed into adjacent positive series elements of the same type so as to give a resulting circuit having all positive elements. The inverters shown in Figs. 8.03-1(c),(d) are particularly useful in circuits where the line of positive or negative electrical length ϕ shown in the figures can be added to or subtracted from adjacent lines of the same impedance. The circuits shown at (a) and (c) have an over-all image phase shift of −90 degrees, while those at (b) and (d) have an over-all image phase shift of +90 degrees. The impedance-inverter parameter *K* indicated in the figure is equal to the image impedance (see Sec. 3.02) of the inverter network and is analogous to the characteristic impedance of a transmission line. The networks in Fig. 8.03-1 are much more broadband inverters than is a quarter-wavelength line.*

* In the cases of Figs. 8.03-1(c),(d), this statement assumes that $|X/Z_0| \ll 1$ which is usually the case in the practical application of these circuits.

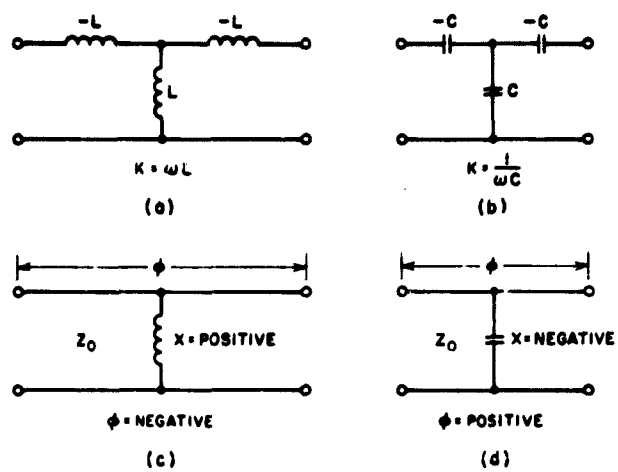

For both cases (c) and (d)

$$K = Z_0 \tan \left| \frac{\phi}{2} \right| \quad \text{ohms}$$

$$\phi = -\tan^{-1} \frac{2X}{Z_0} \quad \text{radians}$$

$$\left| \frac{X}{Z_0} \right| = \frac{\frac{K}{Z_0}}{1 - \left(\frac{K}{Z_0}\right)^2}$$

A-3527-107

FIG. 8.03-1 SOME CIRCUITS WHICH ARE PARTICULARLY USEFUL AS K-INVERTERS (Inverters To Be Used with Series-Type Resonators)

Figure 8.03-2 shows four inverting circuits which are of special interest for use as *J*-inverters (*i.e.*, inverters to be used with shunt-type resonators). These circuits will be seen to be the duals of those in Fig. 8.03-1, and the inverter parameters *J* are the image admittances of the inverter networks.

Figure 8.03-3 shows two more circuits which operate as inverters. These circuits are useful for computing the impedance-inverting properties of certain types of discontinuities in transmission lines. Examples will be cited in Secs. 8.05 and 8.06. Figure 8.03-4 shows yet another form of inverter composed of transmission lines of positive and negative

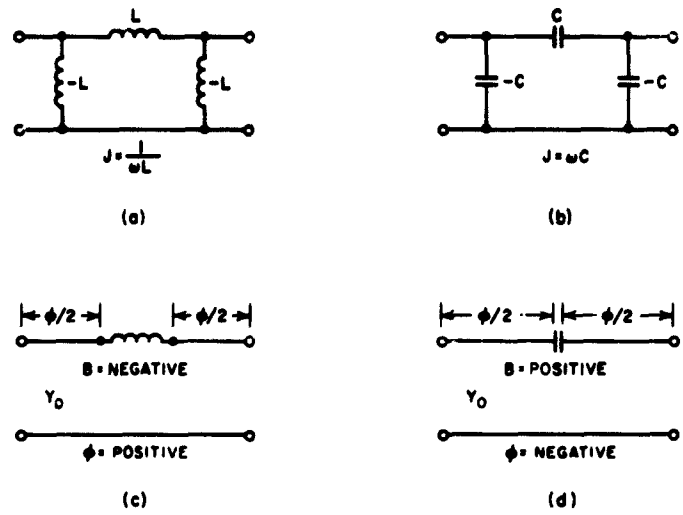

For both cases (c) and (d):

$$J = Y_0 \tan\left|\frac{\phi}{2}\right| \quad \text{mhos}$$

$$\phi = -\tan^{-1}\frac{2B}{Y_0} \quad \text{radians}$$

$$\left|\frac{B}{Y_0}\right| = \frac{\frac{J}{Y_0}}{1-\left(\frac{J}{Y_0}\right)^2}$$

A-3527-100

FIG. 8.03-2 SOME CIRCUITS WHICH ARE PARTICULARLY USEFUL AS J-INVERTERS (Inverters to be Used with Shunt-Type Resonators)

characteristic admittance. The negative admittances are in practice absorbed into adjacent lines of positive admittance.

Numerous other circuits will operate as impedance or admittance inverters, the requirements being that their image impedance be real in the frequency band of operation, and that their image phase be some odd multiple of $\pm\pi/2$. For any symmetrical inverter, these conditions will be satisfied if

$$(X_{1/2})_{oc} = -(X_{1/2})_{sc} \qquad (8.03\text{-}1)$$

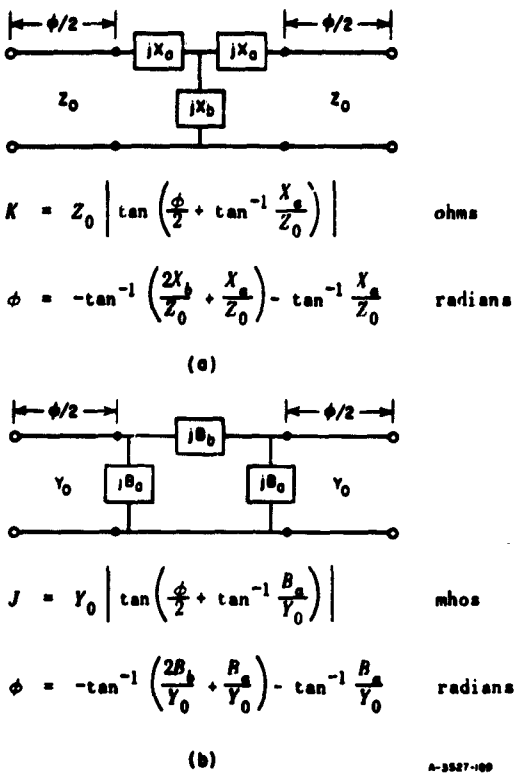

FIG. 8.03-3 TWO CIRCUITS WHICH ARE USEFUL FOR REPRESENTING THE INVERTER PROPERTIES OF CERTAIN DISCONTINUITIES IN TRANSMISSION LINES

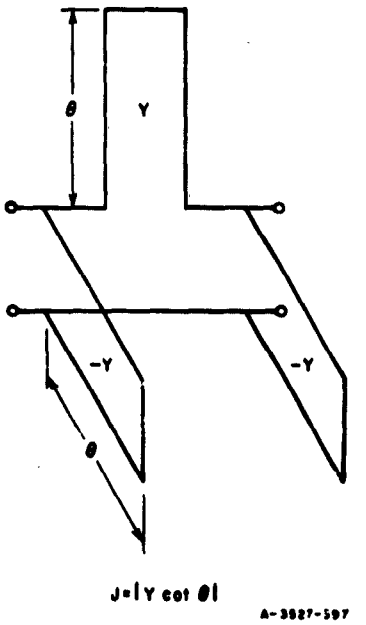

FIG. 8.03-4 AN ADMITTANCE INVERTER FORMED FROM STUBS OF ELECTRICAL LENGTH θ

where $(X_{1/2})_{oc}$ is the input reactance of the circuit when cut in half and the cut wires are left open-circuited, while $(X_{1/2})_{sc}$ is the corresponding reactance when the cut wires are shorted together.

SEC. 8.04, USE OF LOW-PASS TO BAND-PASS MAPPINGS

The response of a low-pass prototype circuit such as either of those in Fig. 4.04-1 can be related *exactly* to the response of a corresponding band-pass filter as shown in Fig. 8.02-2(b) by a well known *low-pass to band-pass mapping*

$$\frac{\omega'}{\omega_1'} = \frac{1}{w}\left(\frac{\omega}{\omega_0} - \frac{\omega_0}{\omega}\right) \qquad (8.04\text{-}1)$$

where w is the fractional bandwidth

$$w = \frac{\omega_2 - \omega_1}{\omega_0} \quad , \tag{8.04-2}$$

$$\omega_0 = \sqrt{\omega_2 \omega_1} \quad , \tag{8.04-3}$$

and ω' and ω_1' refer to the low-pass filter response as indicated in Fig. 8.02-1(a) while ω, ω_0, ω_1, and ω_2 refer to the corresponding band-pass filter response as shown in Fig. 8.02-1(b). Mappings of this sort are particularly useful in determining the number of resonators needed to meet given attenuation requirements. For example, suppose that an audio-frequency filter of the form in Fig. 8.02-2(b) was desired with a 1.0-db Tchebyscheff ripple from $f_1 = 2$ kc to $f_2 = 4$ kc and with at least 50-db attenuation at 1.5 kc. It is then desired to know how many resonators will be required to do the job. Using the mapping Eq. (8.04-1)

$$w = \frac{\omega_2 - \omega_1}{\sqrt{\omega_2 \omega_1}} = \frac{f_2 - f_1}{\sqrt{f_2 f_1}} = \frac{4 - 2}{\sqrt{(4)(2)}}$$

$$= 0.707 \quad .$$

Now

$$\frac{\omega'}{\omega_1'} = \frac{1}{w}\left(\frac{\omega}{\omega_0} - \frac{\omega_0}{\omega}\right) = \frac{1}{w}\left(\frac{f}{f_0} - \frac{f_0}{f}\right) \quad ,$$

$f_0 = \sqrt{f_2 f_1} = 2.825$ kc, and we wish, 50-db attenuation or more at $f = 1.5$ kc. Then the low-pass prototype must have at least 50-db attenuation for

$$\frac{\omega'}{\omega_1'} = \frac{1}{0.707}\left(\frac{1.5}{2.825} - \frac{2.825}{1.5}\right) = -1.914 \quad .$$

The minus sign in the above result occurs because, mathematically, the portion of the band-pass filter response below ω_0 in Fig. 8.02-1(b) maps to negative values of the low-pass filter frequency variable ω', while, mathematically, the low-pass filter response in Fig. 8.02-1(a) for

negative values of ω' is a mirror image of its response for positive values of ω. For our present purposes we may ignore the minus sign. The chart shown in Fig. 4.03-8 shows the cutoff characteristics of filters with 1.0-db Tchebyscheff ripple. Using this chart we see that an $n = 6$ reactive element prototype will give 54.5 db attenuation for $|\omega'/\omega_1'| = 1.914$ (*i.e.*, $|\omega'/\omega_1'| - 1 = 0.914$) as required, and $n = 5$ elements will give only 43 db attenuation. Thus, the corresponding bandpass filter with $f_1 = 2$ kc and $f_2 = 4$ kc will require $n = 6$ resonators in order to meet the attenuation requirement at $f = 1.5$ kc.

The various microwave filter structures about to be discussed approximate the performance of the filter in Fig. 8.02-2(b) very well for narrow bandwidths, but their rates of cutoff will differ noticeably from that for the filter in Fig. 8.02-2(b) when the bandwidth becomes appreciable (more than five percent or so). However, in most cases in this chapter, approximate mappings will be suggested which are more accurate than Eq. (8.04-1) for the given structure. In many cases the suggested mappings give very accurate results for filters with bandwidths as great as 20 percent or somewhat more. Though the mapping functions will be somewhat different from Eq. (8.04-1), they are used in exactly the same way for determining the required number of resonators for a given application.

SEC. 8.05, CAPACITIVE-GAP-COUPLED TRANSMISSION LINE FILTERS

Figure 8.05-1 presents design relations for coupled-resonator filters consisting of transmission-line resonators which are approximately a half-wavelength long at the midband frequency ω_0, and which have series-capacitance coupling between resonators. In this case the inverters are of the form in Fig. 8.03-2(d). These inverters tend to reflect high impedance levels to the ends of each of the half-wavelength resonators, and it can be shown that this causes the resonators to exhibit a shunt-type resonance (see Sec. 8.14). Thus, the filters under consideration operate like the shunt-resonator type of filter whose general design equations were shown in Fig. 8.02-4.

If the capacitive gaps operate like purely series capacitances, then the susceptance of the capacitive couplings can be computed by use of Eqs. (1) to (4) in Fig. 8.05-1, and the electrical distance between the series capacitance discontinuities is obtained by Eq. (5). However, in

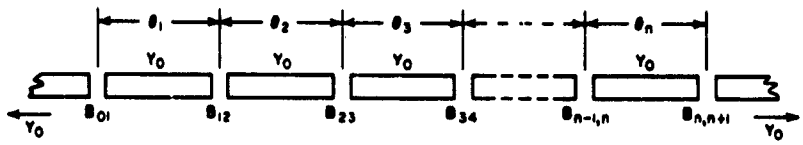

A-3827-190

$$\frac{J_{01}}{Y_0} = \sqrt{\frac{\pi}{2}\frac{w}{g_0 g_1 \omega_1'}} \qquad (1) \qquad \frac{J_{j,j+1}}{Y_0}\Bigg|_{j=1 \text{ to } n-1} = \frac{\pi w}{2\omega_1'}\frac{1}{\sqrt{g_j g_{j+1}}} \qquad (2)$$

$$\frac{J_{n,n+1}}{Y_0} = \sqrt{\frac{\pi w}{2 g_n g_{n+1} \omega_1'}} \qquad (3)$$

where $g_0, g_1, \ldots, g_n$ are as defined in Fig. 4.04-1, ω' is defined in Fig. 8.02-1(a), and w is the fractional bandwidth defined below. The $J_{j,j+1}$ are admittance inverter parameters and Y_0 is the characteristic admittance of the line.

Assuming the capacitive gaps act as perfect, series-capacitance discontinuities of susceptance $B_{j,j+1}$ as in Fig. 8.03-2(d)

$$\frac{B_{j,j+1}}{Y_0} = \frac{\frac{J_{j,j+1}}{Y_0}}{1 - \left(\frac{J_{j,j+1}}{Y_0}\right)^2} \qquad (4)$$

and

$$\theta_j = \pi - \frac{1}{2}\left[\tan^{-1}\left(\frac{2B_{j-1,j}}{Y_0}\right) + \tan^{-1}\left(\frac{2B_{j,j+1}}{Y_0}\right)\right] \quad \text{radians} \qquad (5)$$

where the $B_{j,j+1}$ and θ_j are evaluated at ω_0.

For the construction in Figs. 8.05-3(a),(b); determine the gap spacings Δ from the $J_{j,j+1}/Y_0$ values and Figs. 8.05-3(a),(b); determine the $\phi_{j,j+1}$ values from the Δ's and Fig. 8.05-3(c); then

$$\theta_j\Big|_{j=1 \text{ to } n} = \pi + \frac{1}{2}\left[\phi_{j-1,j} + \phi_{j,j+1}\right] \quad . \qquad (6)$$

where the $\phi_{j,j+1}$ will usually be negative.

To map low-pass prototype filter response to corresponding band-pass filter response use the approximation

$$\frac{\omega'}{\omega_1'} = \frac{2}{w}\left(\frac{\omega - \omega_0}{\omega}\right) \qquad (7)$$

where

$$w = 2\left(\frac{\omega_2 - \omega_1}{\omega_2 + \omega_1}\right) \quad , \quad (8) \qquad \omega_0 = \left(\frac{2\omega_2\omega_1}{\omega_2 + \omega_1}\right) \quad , \quad (9)$$

where ω' and ω_1' are as defined in Fig. 8.02-1(a); and ω, ω_0, ω_1, and ω_2 are defined in Fig. 8.02-1(b).

FIG. 8.05-1 DESIGN EQUATIONS FOR CAPACITIVE-GAP-COUPLED TRANSMISSION-LINE FILTERS

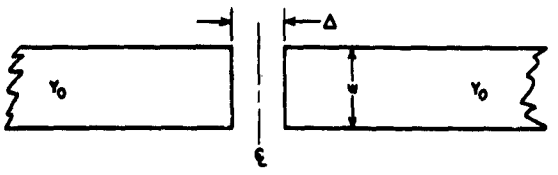

(a)

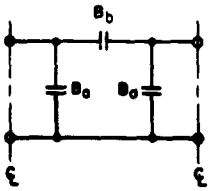

(b)

$$\frac{B_a}{Y_0} = -\frac{2b}{\lambda} \ln\left[\cosh\left(\frac{\pi\Delta}{b}\right)\right] \qquad (1)$$

$$\frac{B_b}{Y_0} = \frac{b}{\lambda} \ln\left[\coth\ \frac{\pi\Delta}{2b}\right] \qquad (2)$$

A-3827-101

FIG. 8.05-2 GAP EQUIVALENT CIRCUIT, AND OLINER'S EQUATIONS[9,10] FOR CAPACITIVE-GAP SUSCEPTANCES FOR THIN STRIP LINE
Parameter b is the ground-plane spacing, and λ is the wavelength in media of propagation, in same units. Equations are most accurate for w/b ≈ 1.2 or more and t/b ≈ 0, where t is the strip thickness.

many practical situations the capacitive gaps between resonators will be so large that they cannot be treated as simple series capacitances. Consider, for example, the capacitive gap in a strip transmission line shown in Fig. 8.05-2(a). If the length of each resonator is defined as extending from the *centerline* of one capacitive gap to the *centerline* of the next gap (as is done in Fig. 8.05-1), then an equivalent circuit for the gap, *as referred to the centerline of the gap*, will include series capacitance and some *negative* shunt capacitance to account for the fact that the gap reduces the shunt capacitance in the vicinity of the centerline. Figure 8.05-2(b) shows such an equivalent circuit for the gap, and also shows some equations due to Oliner[9] which give approximate values for the susceptances, for the case of strip line of nearly zero thickness. (Altschuler and Oliner[10] point out that these equations are reasonably accurate if w/b is fairly large as is the case for a 50-ohm strip line having nearly zero thickness and air dielectric. However, if w/b is small the error is considerable.) Having reasonably accurate values for the susceptances in Fig. 8.05-2(b), the corresponding admittance inverter parameters for a given gap size can be computed by use of Fig. 8.03-3(b). The gap sizes must be chosen to give the $J_{j,j+1}/Y_0$ values called for by Eqs. (1) to (3) in Fig. 8.05-1, and the corresponding values of ϕ obtained from Fig. 8.03-3(b) are then used with Eq. (6) in Fig. 8.05-1 in order to obtain the proper electrical distance between the centerlines

of the coupling gaps. It should be noted that all susceptances and electrical distances are to be evaluated at the midband frequency ω_0.

Figures 8.05-3(a) to (c) present data for capacitive-gap filters which were obtained by experimental procedures[11] (see Chapter 11). These data are for the particular rectangular-bar strip line construction shown in Fig. 8.05-3(a). Figures 8.05-3(a),(b) give data to be used for determining the proper gap spacing Δ in inches to give a specified J/Y_0 value, while Fig. 8.05-3(c) is for use in determining the proper negative line length to be associated with the inverter. A simple numerical example will clarify the use of these charts.

Suppose that a filter is desired with a 0.5-db ripple Tchebyscheff pass band from f_1 = 3.0 Gc to f_2 = 3.20 Gc and that 30-db attenuation

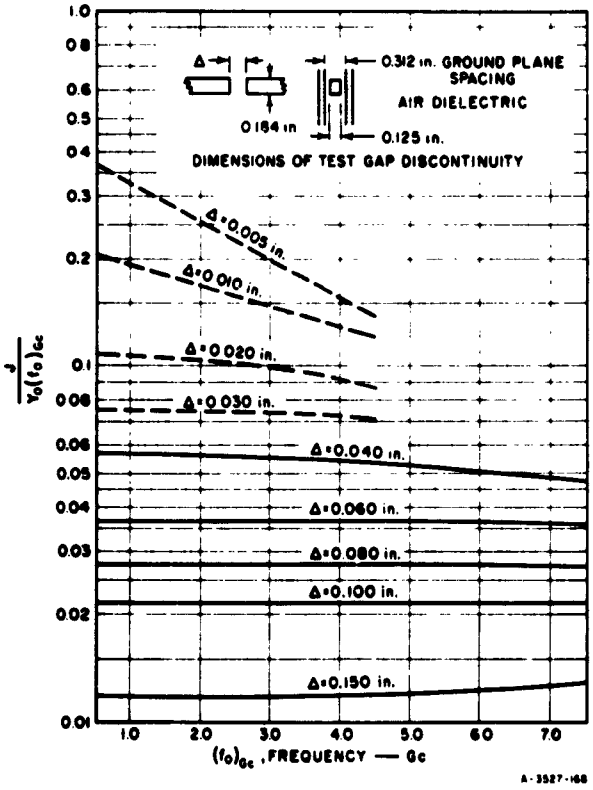

SOURCE: Reference 11, by G. L. Matthaei. (By courtesy of the Ramo-Wooldridge Div. of the Thompson-Ramo-Wooldridge Corp.)

FIG. 8.05-3(a) $J/[Y_0(f_0)_{Gc}]$ vs. $(f_0)_{Gc}$ FOR CAPACITIVE-GAP J-INVERTERS IN BAR TRANSMISSION-LINE CONSTRUCTION
The characteristic impedance of the transmission lines is $Z_0 = 1/Y_0 = 50$ ohms and $(f_0)_{Gc}$ is the band center frequency of the filter in Gc

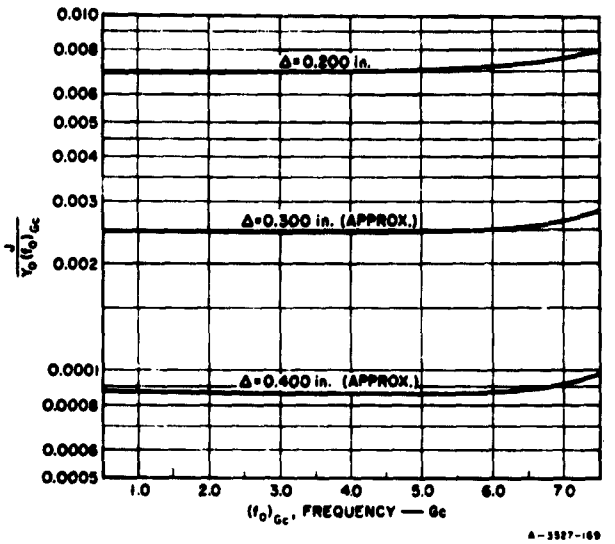

SOURCE: Reference 11, by G. L. Matthaei. (By courtesy of the Ramo-Wooldridge Div. of the Thompson-Ramo-Wooldridge Corp.)

FIG. 8.05-3(b) CONTINUATION OF FIG. 8.05-3(a)

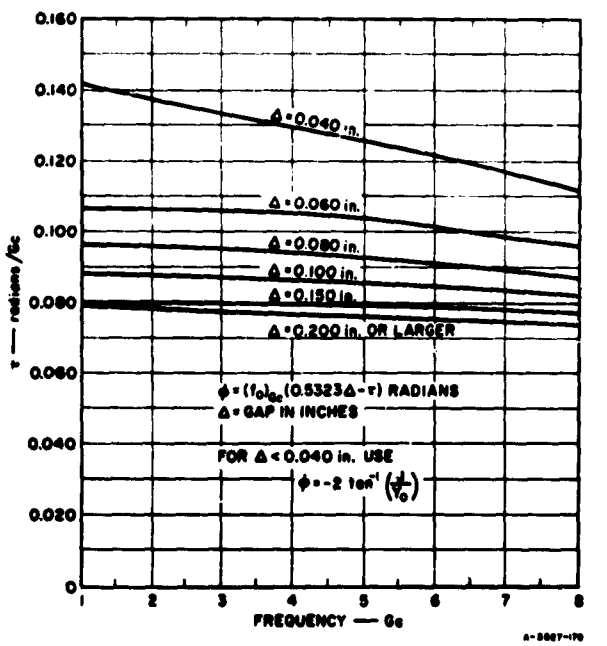

SOURCE: Reference 11, by G. L. Matthaei. (By courtesy of the Ramo-Wooldridge Div. of the Thompson-Ramo-Wooldridge Corp.)

FIG. 8.05-3(c) PARAMETER ϕ FOR THE J-INVERTER DISCONTINUITY IN FIG. 8.05-3(a) IN TERMS OF AN AUXILIARY PARAMETER τ

is required at $f_a = 2.50$ Gc and at $f_b = 3.50$ Gc. By Eqs. (7) to (9) in Fig. 8.05-1

$$w = 2\left(\frac{\omega_2 - \omega_1}{\omega_2 + \omega_1}\right) = 2\left(\frac{f_2 - f_1}{f_2 + f_1}\right) = 0.0645 \quad ,$$

$$f_0 = \frac{2f_2 f_1}{f_2 + f_1} = 3.10 \text{ Gc} \quad ,$$

$$\frac{\omega'}{\omega_1'} = \frac{2}{w}\left(\frac{f - f_0}{f}\right)$$

which for $f_a = 2.5$ Gc gives $\omega'/\omega_1' = -7.45$, while for $f_b = 3.5$ Gc it gives $\omega'/\omega_1' = 3.55$. Since ω'/ω_1' has the smaller magnitude for $f = 3.5$ Gc, the restriction at that frequency controls the design. Using Fig. 4.03-7 and the procedure discussed in Sec. 8.04, for $L_{Ar} = 0.5$ db we find that for a three-resonator design, L_A should be about 35 db at 3.5 Gc, and it should be about 55 db at 2.5 Gc. Thus, three resonators will be sufficient.

By Table 4.05-2(a), the element values for an $n = 3$ reactive element 0.5 db-ripple Tchebyscheff prototype are $g_0 = 1$, $g_1 = 1.5963$, $g_2 = 1.0967$, $g_3 = 1.5963$, and $g_4 = 1.000$. By Eqs. (1) to (3) in Fig. 8.05-1, $J_{01}/Y_0 = J_{34}/Y_0 = 0.252$, $J_{12}/Y_0 = J_{23}/Y_0 = 0.0769$.* Since $f_0 = 3.1$ Gc, $J_{01}/Y_0(f_0)_{Gc} = 0.252/3.1 = 0.0813$ and $J_{12}/Y_0(f_0)_{Gc} = 0.0769/3.1 = 0.0248$. Using Fig. 8.05-3(a) a plot of Δ *vs.* $J/Y_0(f_0)_{Gc}$ for $f_0 = 3.1$ Gc is made for purposes of interpolation, and from this plot the required gaps are found to be $\Delta_{01} = \Delta_{34} = 0.027$ inch, and $\Delta_{12} = \Delta_{23} = 0.090$ inch.

Using Fig. 8.05-3(c) for determining the $\phi_{j,j+1}$, since $\Delta_{01} < 0.040"$ we use

$$\phi_{01} = \phi_{34} = -2 \tan^{-1}\left(\frac{J_{01}}{Y_0}\right) = -2 \tan^{-1}(0.252) = -0.494 \quad \text{radian} \, .$$

For the $\Delta_{12} = 0.090$-inch gap we use the chart to get $\tau = 0.090$ radian/Gc for $f_0 = 3.1$ Gc. Then

* Filters designed using Fig. 8.05-1 and any symmetrical or antimetrical prototype such as those in Tables 4.05-1(a),(b), or 4.05-2(a),(b) will always be symmetrical.

$$\phi_{12} = \phi_{23} = (f_0)_{Ge}(0.5323\,\Delta - \tau) = -0.130 \quad \text{radian} .$$

By Eq. (6) in Fig. 8.05-1

$$\theta_1 = \theta_3 = \pi + \frac{1}{2}[-0.494 - 0.130] = 2.830 \quad \text{radians}$$

and

$$\theta_2 = \pi + \frac{1}{2}[-0.130 - 0.130] = 3.012 \quad \text{radians} .$$

For propagation in air, $\lambda = 3.810$ inches at 3.10 Gc, and the distances between the *centerlines* of the capacitive gaps is $l_1 = l_3 = \theta_1\lambda/2\pi = 1.715$ inches for Resonators 1 and 3, and $l_2 = \theta_2\lambda/2\pi = 1.825$ inches for Resonator 2. The resonator bars may be supported by Polyfoam or by thin horizontal slabs of dielectric passing through the sides of the bars. Of course, some correction in resonator bar dimensions will be required to compensate for the effect of the dielectric supporting material on the velocity of propagation and line impedance. In order to tune the filter precisely tuning screws may be used as described in Sec. 11.05, or alternately the resonant frequency of the various resonators may be checked by testing them individually or in pairs as is also described in Secs. 11.03 to 11.05.

Figure 8.05-4(a) shows a filter constructed using the design charts in Fig. 8.05-3(a) to (c). This is a four-resonator filter designed for a 1.0-percent bandwidth maximally flat response centered at $f_0 = 6.120$ kMc. In this filter the resonators are supported by 0.062-inch-thick Rexolite 2200 dielectric slabs which pass through the sides of the resonator bars, the slabs being held by clamp strips at the sides of the filter. The four bars in the interior of the filter are resonators while the bar at each end is a 50-ohm input or output line. The resonant frequencies of the resonators were checked by testing them in pairs as discussed in Sec. 11.04. These tests indicated small errors in the lengths of the resonator bars, and the required corrections were made. Figure 8.05-4(b) shows the resulting measured response obtained after the filter was assembled without tuning screws.[11]

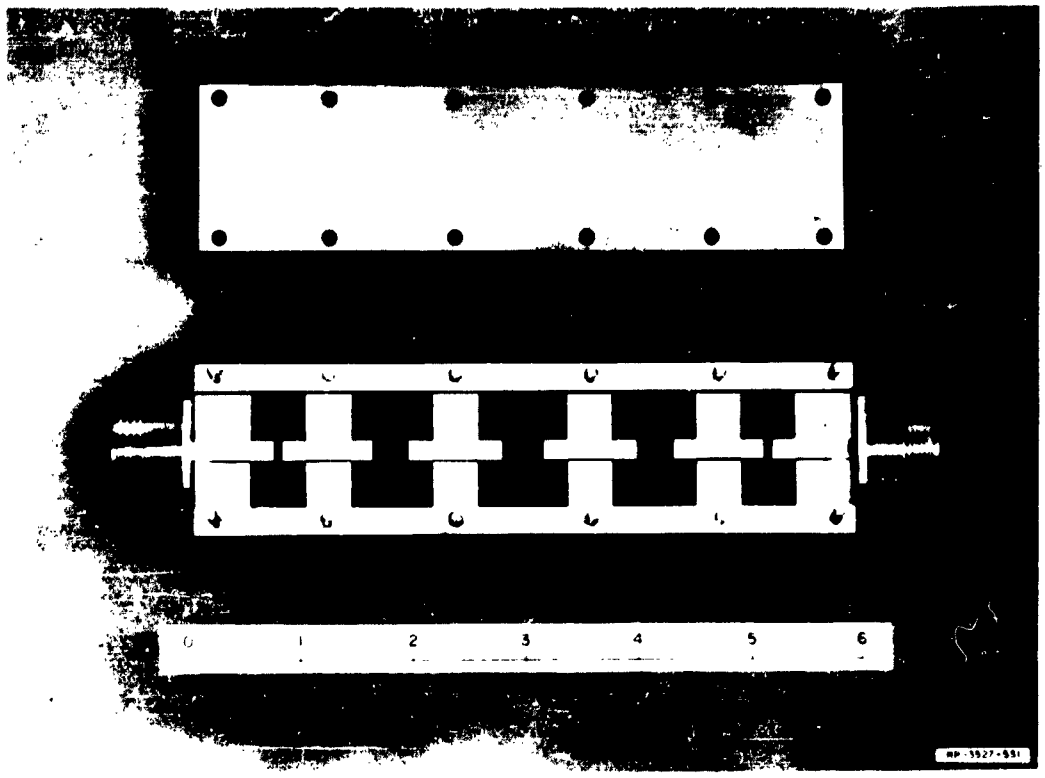

SOURCE: Reference 11, by G. L. Matthaei. (By courtesy of the Ramo-Wooldridge Div. of the Thompson-Ramo-Wooldridge Corp.)

FIG. 8.05-4(a) A FILTER WITH 0.9% BANDWIDTH CENTERED AT 6.120 Gc AS SHOWN IN FIG. 8.05-4(b)
As is seen from the photograph, this filter uses four, $\lambda_0/2$ resonators in bar construction

Figure 8.05-5 shows the measured response of a six-resonator filter in similar construction.[12] This filter was designed for 1-db Tchebyscheff ripple and 20 percent bandwidth. The x's show the measured data while the circles show points mapped from the low-pass prototype using the mapping in Eqs. (7) to (9) of Fig. 8.05-1. As can be seen, even for bandwidths as large as 20 percent the design procedure and the mapping give good accuracy. However, the bandwidth for which this procedure is accurate depends somewhat on the pass-band ripple tolerance. For ripples as small as 0.01 db, this design procedure will not meet the design objectives for as large bandwidths as it will when the ripples are, say, 0.5 or 1.0 db. For bandwidths of around 15 percent or more and very

small pass-band ripples, the procedures in Chapter 9 are recommended for this type of filter.

Observe that, the wider bandwidth filter response in Fig. 8.05-5 shows less dissipation loss than does the narrow-band response in Fig. 8.05-4(b). The unloaded Q for resonators in this construction has been found to be typically about 1000 to 1300 at S band.

Other considerations in the practical design and application of filters of this type are that the second pass band of the filter will be centered at roughly twice the center frequency of the first pass band, and that the attenuation in the stop band between the first and second

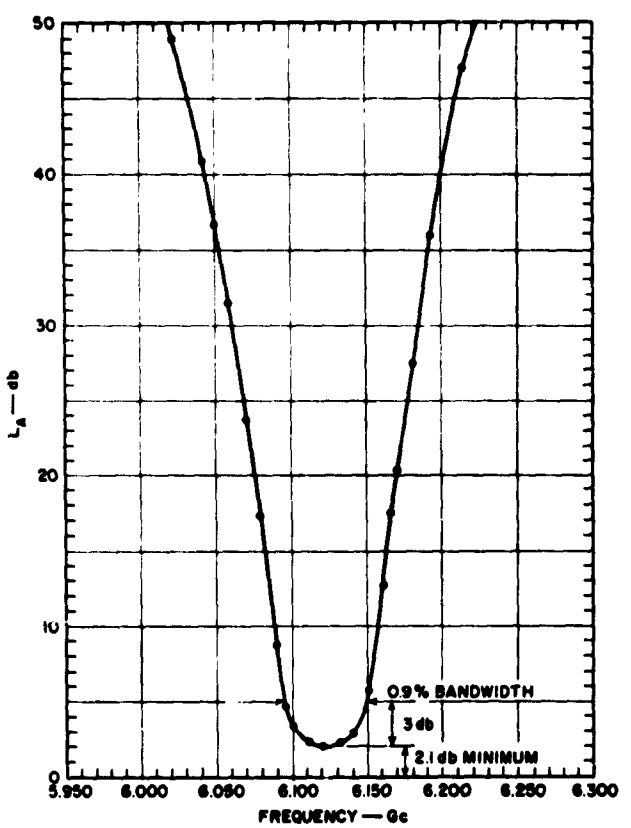

SOURCE: Reference 11, by G. L. Matthaei. (By courtesy of the Ramo-Wooldridge Div. of the Thompson-Ramo-Wooldridge Corp.)

FIG. 8.05-4(b) THE ATTENUATION CHARACTERISTIC OF THE FILTER IN FIG. 8.05-4(a)

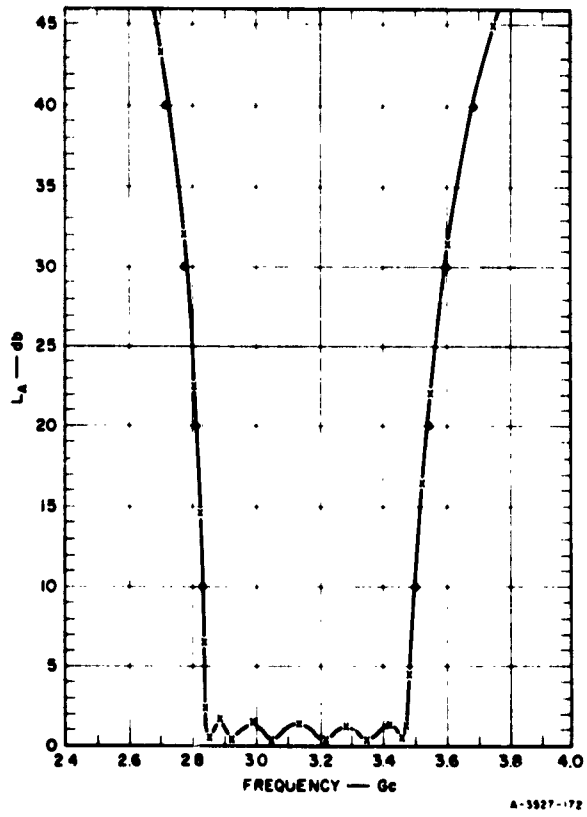

SOURCE: Reference 12, by G. L. Matthaei. (By courtesy of the Ramo-Wooldridge Div. of the Thompson-Ramo-Wooldridge Corp.)

FIG. 8.05-5 THE ATTENUATION CHARACTERISTIC OF A 6-RESONATOR FILTER
The x's indicated measured attenuation while the circles are theoretical points calculated using the mapping in Eqs. (7) to (9) of Fig. 8.05-1

pass band will level off to some peak finite value of $(L_A)_{USB}$ decibels, which occurs at about $\omega = 3\omega_0/2$. The size of this maximum attenuation in the upper stop band can be estimated by use of the formula

$$(L_A)_{USB} = 20 \log_{10}\left[\frac{1}{\left(\frac{B_{01}}{Y_0}\right)\left(\frac{B_{12}}{Y_0}\right) \cdots \left(\frac{B_{n,n+1}}{Y_0}\right)}\right] - (n+1)3.53 - 6.02 \quad \text{db} \tag{8.05-1}$$

where the $B_{j,j+1}/Y_0$ are computed from the $J_{j,j+1}/Y_0$ by use of Eq. (4) in Fig. 8.05-1. The stop band below the pass band has a first-order pole of attenuation (Sec. 2.04) at $\omega = 0$. Thus, in the case of the lower stop band the attenuation continues to grow as the frequency goes lower, and the attenuation approaches an infinite value as ω approaches zero.

If sizeable attenuation in the upper stop band is required for a given application, $(L_A)_{USB}$ should be computed. The attenuation predicted by Eqs. (7) to (9) in Fig. 8.05-1 for upper-stop-band frequencies near the pass band, will be reasonably accurate only so long as the computed attenuation values are around 20 db or more below $(L_A)_{USB}$.

In the case of the three-resonator numerical example discussed above, $J_{01}/Y_0 = J_{34}/Y_0 = 0.252$, and $J_{12}/Y_0 = J_{23}/Y_0 = 0.0769$. By Eq. (4) in Fig. 8.05-1, $B_{01}/Y_0 = B_{34}/Y_0 = 0.269$, and $B_{12}/Y_0 = B_{23}/Y_0 = 0.077$. Then by Eq. (8.05-1), $(L_A)_{USB} \approx 54$ db. Thus, the 35-db value computed for 3.5 Gc by use of the mapping should be reasonably accurate since the 35-db value is about 19 db below $(L_A)_{USB}$.

It will be found that $(L_A)_{USB}$ *decreases* rapidly as the fractional bandwidth increases, but at the same time $(L_A)_{USB}$ *increases* rapidly as the number of resonators is increased. Thus, if $(L_A)_{USB}$ is found to be too small, it can be increased by adding more resonators.

SEC. 8.06, SHUNT-INDUCTANCE-COUPLED, WAVEGUIDE FILTERS

The waveguide filter in Fig. 8.06-1 is in most respects the dual of the capacitive-gap coupled filter in Fig. 8.05-1. In this case, the inverters are of the type in Fig. 8.03-1(c) and the structure operates like the filter with series resonators shown in Fig. 8.02-3. The low-pass to band-pass transformation in Eqs. (6) to (8) in Fig. 8.06-1 for the waveguide filter is the same as that in Eqs. (7) to (9) for the capacitive-gap coupled filter if both transformations are expressed in terms of guide wavelength. However, since the guide wavelength for waveguide varies with frequency in a different way from the guide wavelength in a TEM-mode structure, the frequency responses will be somewhat different for the two types of filters. In particular, for a given range of guide wavelength, the waveguide-type of filter will have narrower frequency bandwidth because of the more rapid change in guide wavelength for non-TEM modes of propagation.

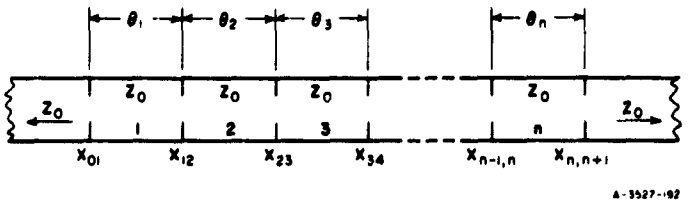

$$\frac{K_{01}}{Z_0} = \sqrt{\frac{\pi}{2}\frac{w_\lambda}{g_0 g_1 \omega_1'}} \tag{1}$$

$$\left.\frac{K_{j,j+1}}{Z_0}\right|_{j=1 \text{ to } n-1} = \frac{\pi w_\lambda}{2\omega'}\frac{1}{\sqrt{g_j g_{j+1}}} \tag{2}$$

$$\frac{K_{n,n+1}}{Z_0} = \sqrt{\frac{\pi}{2}\frac{w_\lambda}{g_n g_{n+1}\omega_1'}} \tag{3}$$

where $g_0, g_1, \ldots, g_{n+1}$ are as defined in Fig. 4.04-1, ω_1' is defined in Fig. 8.02-1(a), and w_λ is the guide-wavelength fractional bandwidth defined below. The $K_{j,j+1}$ are impedance inverter parameters and Z_0 is the guide impedance.

For purely lumped-inductance discontinuities having shunt reactance $X_{j,j+1}$,

$$\frac{X_{j,j+1}}{Z_0} = \frac{\frac{K_{j,j+1}}{Z_0}}{1-\left(\frac{K_{j,j+1}}{Z_0}\right)^2} \tag{4}$$

and

$$\theta_j = \pi - \frac{1}{2}\left[\tan^{-1}\left(\frac{2X_{j-1,j}}{Z_0}\right) + \tan^{-1}\left(\frac{2X_{j,j+1}}{Z_0}\right)\right] \quad \text{radians}. \tag{5a}$$

For discontinuities with more complicated equivalent circuits use Fig. 8.03-3 and

$$\theta_j = \pi + \frac{1}{2}\left[\phi_{j-1,j} + \phi_{j,j+1}\right] \quad \text{radians}, \tag{5b}$$

where the ϕ's will usually be negative.

(Continued on p. 448)

FIG. 8.06-1 DESIGN EQUATIONS FOR SHUNT-INDUCTANCE-COUPLED WAVEGUIDE FILTERS

To map low-pass filter response to corresponding band-pass filter response use

$$\frac{\omega'}{\omega_1'} = \frac{2}{w_\lambda}\left(\frac{\lambda_{g0} - \lambda_g}{\lambda_{g0}}\right) \tag{6}$$

where

$$w_\lambda = \left[\frac{\lambda_{g1} - \lambda_{g2}}{\lambda_{g0}}\right] = \left(\frac{\lambda_{g0}}{\lambda_0}\right)^2 \left(\frac{\omega_2 - \omega_1}{\omega_0}\right) , \tag{7}$$

$$\lambda_{g0} = \frac{\lambda_{g1} + \lambda_{g2}}{2} , \tag{8}$$

λ_{g0}, λ_{g1}, λ_{g2}, and λ_g are the guide wavelengths at frequencies ω_0, ω_1, ω_2, and ω as defined in Fig. 8.02-1(b); ω' and ω_1' are as defined in Fig. 8.02-1(a); and λ_0 is the wavelength of a plane wave at frequency ω_0 in the medium of the guide.

FIG. 8.06-1 Concluded

Assuming that the waveguide propagates the TE_{10} mode of propagation and that all higher-order modes are cut off, the procedure for using the equations in Fig. 8.06-1 is very similar to that for the equations in Fig. 8.05-1. Figures 8.06-2 and 8.06-3(a),(b) present inductive iris and inductive post coupling discontinuity data from Marcuvitz.[13] The reactances plotted relate to the equivalent circuit in Fig. 8.06-4. Since for a very thin iris, $X_a \approx 0$, Eqs. (4) and (5) in Fig. 8.06-1 which assume a simple, shunt, lumped-inductance discontinuity may be used. For the

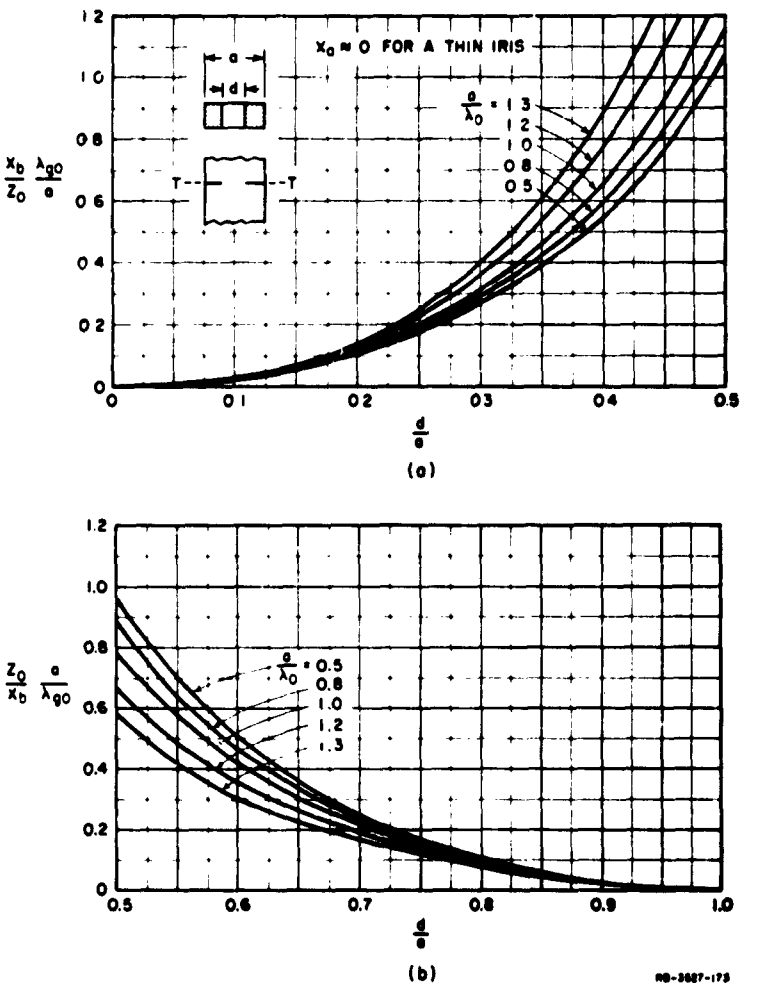

SOURCE: *Waveguide Handbook* edited by N. Marcuvitz.[13]

FIG. 8.06-2 SHUNT REACTANCE OF SYMMETRICAL INDUCTIVE WINDOW IN RECTANGULAR GUIDE
Fig. 8.06-4 shows the equivalent circuit for this discontinuity

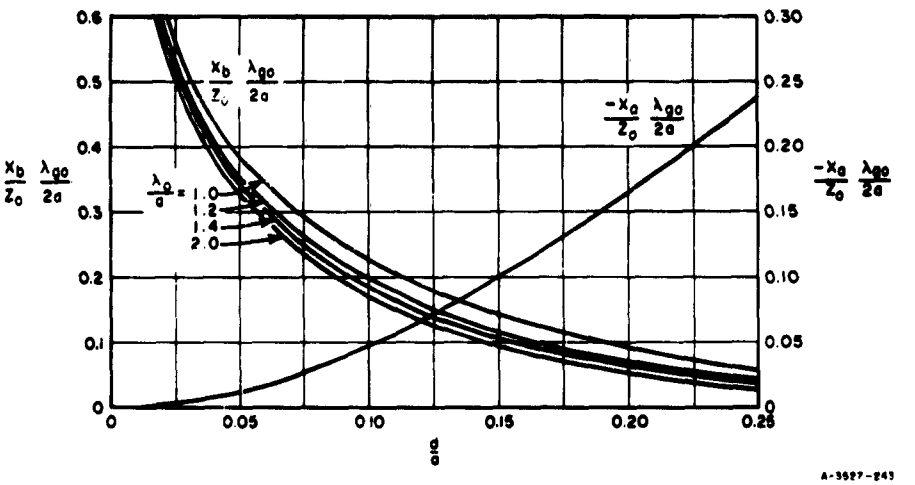

SOURCE: *Waveguide Handbook* edited by N. Marcuvitz.[13]

FIG. 8.06-3(a) CIRCUIT PARAMETERS OF CENTERED INDUCTIVE POST IN RECTANGULAR GUIDE
The guide wavelength at midband is λ_{g0} while λ_0 is the corresponding free-space wavelength

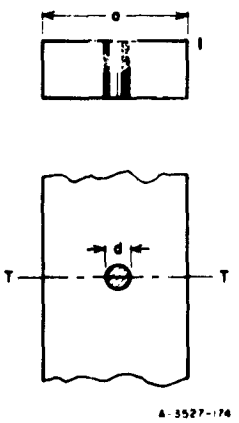

FIG. 8.06-3(b) DEFINITION OF THE DIMENSIONS IN FIG. 8.06-3(a)

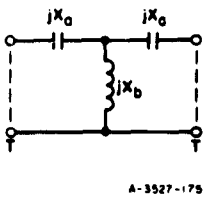

FIG. 8.06-4 EQUIVALENT CIRCUIT FOR THE SHUNT-INDUCTIVE DISCONTINUITIES IN FIG. 8.06-2 AND 8.06-3(a), (b)
Note that $X_a \approx 0$ for case of Fig. 8.06-2

case of the inductive post (or a thick iris), X_s is not negligible and it should be accounted for in the design process. This can be done for the case of inductive posts by first computing the required normalized inverter parameter values $K_{j,j+1}/Z_0$ by use of Eqs. (1) to (3) in Fig. 8.06-1. Then, using the data in Fig. 8.06-3(a) along with Fig. 8.03-3(a), a plot is made of K/Z_0 and ϕ *vs.* d/a, for the desired midband guide wavelength λ_{g0}, corresponding plane-wave wavelength λ_0, and waveguide width a. From this chart the post diameters d which will give the normalized impedance inverting parameters $K_{j,j+1}/Z_0$ can be determined, and also the corresponding values of $\phi_{j,j+1}$. Then, paralleling the analogous case for Fig. 8.05-1, the electrical distance between the centers of the posts at each end of Resonator j is

$$\theta_j = \pi + \frac{1}{2}\left[\phi_{j-1,j} + \phi_{j,j+1}\right] \quad \text{radians} \quad . \qquad (8.06\text{-}1)$$

Except possibly for the case of large posts, the $\phi_{j,j+1}$ should be negative. The distance between post centers for Resonator j is then

$$l_j = \frac{\lambda_{g0}\theta_j}{2\pi} \quad . \qquad (8.06\text{-}2)$$

This design procedure should give good accuracy for designs having guide-wavelength fractional bandwidths w_λ [see Eq. (7) in Fig. 8.06-1] of 20 percent,[1] with diminishing accuracy for larger bandwidths.

Analogously to the strip-line filter in Sec. 8.05, this waveguide filter will have for TE_{10}-mode propagation a second pass band centered approximately at the frequency for which $\lambda_g = \lambda_{g0}/2$. This frequency would be somewhat less than $2\omega_0$ because of the manner in which λ_g and the $X_{j,j+1}$ vary with frequency. Also, the attenuation between the first and second pass bands for TE_{10}-mode propagation will level off with a peak value of $(L_A)_{USB}$, which can be estimated by use of the equation

$$(L_A)_{USB} = 20 \log_{10}\left[\frac{1}{\left(\frac{X_{01}}{Z_0}\right)\left(\frac{X_{12}}{Z_0}\right)\cdots\left(\frac{X_{n,n+1}}{Z_0}\right)}\right] - (n+1)3.53 - 6.02 \quad \text{db} \qquad (8.06\text{-}3)$$

where the $X_{j,j+1}/Z_0$ are computed from the $K_{j,j+1}/Z_0$ by use of Eq. (4) in Fig. 8.06-1. Equation (8.06-1) is the dual of Eq. (8.05-1), and some further ramifications concerning its use are discussed at the end of Sec. 8.05.

As for the type of filter in Sec. 8.05, the waveguide filter in Fig. 8.06-1 will have monotonically increasing attenuation for frequencies varying from the pass-band frequency downward. Thus, the attenuation in the lower stop band rises to an infinite value at $\omega = 0$, due to the attenuating effects of the irises, and due to the cutoff of the waveguide.

It should be noted that the discussion above assumes that only the TE_{10} mode is present. If other modes are also present (as is likely to happen for frequencies which are around 1.5 or more times ω_0), the performance can be greatly disrupted. This disruption arises because higher-order modes have different guide wavelengths than that for the TE_{10} mode. As a result the pass and stop bands for energy in the higher modes will occur at quite different frequencies than for the TE_{10} mode. Thus, the possible effects of higher-order modes should be kept in mind when this or any other type of waveguide filter is to be used.

In order to clarify the differences between strip-line and waveguide filter design, a waveguide filter design example will now be considered which is closely related to the strip-line filter example in Sec. 8.05. Let us suppose that a pass band with 0.5-db Tchebyscheff ripple is desired from $f_1 = 3.047$ to $f_2 = 3.157$ Gc, and that at least 30-db attenuation is required at the frequencies $f_a = 2.786$ Gc and $f_b = 3.326$ Gc. Let us suppose that WR-284 waveguide is to be used. The design calculations are those outlined in Table 8.06-1.

In Part (a) of Table 8.06-1, guide wavelengths are computed that correspond to the various frequencies of importance. In Part (b), w_λ and $w = (f_2 - f_1)/f_0$ are computed, and it should be noted that w_λ, the guide-wavelength fractional bandwidth, is nearly twice as large as the frequency fractional bandwidth w. Also, normalized prototype frequencies ω'/ω_1' are computed corresponding to f_a and f_b for the waveguide filter, and the attenuation is predicted by use of the chart in Fig. 4.03-7. It will be noted that $w_\lambda = 0.0645$ for this example, which corresponds exactly to $w = 0.0645$ for the example in Sec. 8.05. Also, the ratios $\lambda_{g0}/\lambda_{ga} = 5.130/6.361 = 0.806$ and $\lambda_{g0}/\lambda_{gb} = 5.130/4.544 = 1.129$ correspond exactly

Table 8.06-1

OUTLINE OF A WAVEGUIDE FILTER DESIGN CALCULATION

Part (a)

Assume WR-284 guide. Width = a = 2.840 inches

Height = b = 1.340 inches

$$\lambda_g = \frac{1}{\sqrt{(0.08472f)^2 - \left(\frac{1}{2a}\right)^2}} \text{ inches} \qquad (1)$$

where a is in inches and f is in Gc.

f_1 = 3.047 Gc , λ_{g1} = 5.296 inches

f_2 = 3.157 Gc , λ_{g2} = 4.965 inches

$\lambda_{g0} = \frac{\lambda_{g1} + \lambda_{g2}}{2}$ = 5.130 inches (f_0 = 3.100 Gc)

λ_0 = (Plane wavelength at f_0) = 3.807 inches

f_a = 2.786 Gc , λ_{ga} = 6.361 inches

f_b = 3.326 Gc λ_{gb} = 4.544 inches

Part (b)

$$w_\lambda = \frac{\lambda_{g1} - \lambda_{g2}}{\lambda_{g0}} = 0.0645 \quad , \quad w = \frac{f_2 - f_1}{f_0} = 0.0355$$

Alternately:

$$w_\lambda = \left(\frac{\lambda_{g0}}{\lambda_0}\right)^2 w = \left(\frac{5.130}{3.807}\right)^2 (0.0355) = 0.0645$$

$$\frac{\omega'}{\omega_1'} = \frac{2}{w_\lambda}\left(\frac{\lambda_{g0} - \lambda_g}{\lambda_{g0}}\right) \qquad (2)$$

For $f = f_a$ = 2.786 Gc , $\lambda_g = \lambda_{ga}$ and $\frac{\omega'}{\omega_1'}$ = - 7.45

For $f = f_b$ = 3.326 Gc , $\lambda_g = \lambda_{gb}$ and $\frac{\omega'}{\omega_1'}$ = 3.55

By Fig. 4.03-7, for a 0.5-db ripple n = 3 design:

For $f = f_a$ $\left(|\omega'/\omega_1'| = 7.5\right)$, L_A = 55 db.

For $f = f_b$ $\left(|\omega'/\omega_1'| = 3.55\right)$, L_A = 35 db.

Table 8.06-1 *Continued*

Part (c)

For $n = 3$, 0.5-db ripple Tchebyscheff prototype, by Table 4.05-2(a): $g_0 = 1$, $g_1 = 1.5963$, $g_2 = 1.0967$, $g_3 = 1.5963$, $g_4 = 1.0000$, and $\omega_1' = 1$.

$$\frac{K_{01}}{Z_0} = \sqrt{\frac{\pi}{2}\frac{w\lambda}{g_0 g_1 \omega_1'}} = \frac{K_{34}}{Z_0} = 0.252$$

$$\frac{K_{12}}{Z_0} = \frac{\pi w\lambda}{2\omega_1'}\frac{1}{\sqrt{g_1 g_2}} = \frac{K_{23}}{Z_0} = 0.0769$$

$$\frac{X_{j,j+1}}{Z_0} = \frac{\frac{K_{j,j+1}}{Z_0}}{1-\left(\frac{K_{j,j+1}}{Z_0}\right)^2} \qquad (3)$$

$$\frac{X_{01}}{Z_0} = \frac{X_{34}}{Z_0} = 0.269$$

$$\frac{X_{12}}{Z_0} = \frac{X_{23}}{Z_0} = 0.0774$$

$$\frac{X_{01}}{Z_0}\frac{\lambda_{g0}}{a} = \frac{X_{34}}{Z_0}\frac{\lambda_{g0}}{a} = \frac{0.269(5.130)}{2.840} = .486$$

$$\frac{X_{12}}{Z_0}\frac{\lambda_{g0}}{a} = \frac{X_{23}}{Z_0}\frac{\lambda_{g0}}{a} = \frac{0.0774(5.130)}{2.840} = 0.140$$

By Fig. 8.06-2, with $a/\lambda_0 = 2.840/3.807 = 0.746$:

For X_{01} and X_{34}, $d/a = 0.37$ and $d = 1.050$ inches

For X_{12} and X_{23}, $d/a = 0.22$ and $d = 0.625$ inch

Part (d)

$$\theta_j = \pi - \frac{1}{2}\left[\tan^{-1}\frac{2X_{j-1,j}}{Z_0} + \tan^{-1}\frac{2X_{j,j+1}}{Z_0}\right] \qquad (4)$$

$\theta_1 = \theta_3 = 2.819$ radians, $\theta_2 = 2.989$ radians

the spacing between irises is:

$$l_1 = l_3 = \frac{\theta_1\lambda_{g0}}{2\pi} = 2.302 \text{ inches}$$

$$l_2 = \frac{\theta_2\lambda_{g0}}{2\pi} = 2.441 \text{ inches}$$

to the $f_a/f_0 = 2.5/3.10 = 0.806$ and $f_b/f_0 = 3.5/3.10 = 1.129$ ratios for the example of Sec. 8.05. The attenuations are seen to be the same for these corresponding ratios. In fact, using λ_{g0}/λ_g as a normalized frequency variable, the response of the waveguide filter would be identical to that of the strip-line filter example in Sec. 8.05, plotted *vs.* f/f_0. But note that the waveguide filter response plotted as a function of frequency will be quite different. As is seen from the calculations, an $n = 3$ design gives an adequate rate of cutoff, and over 30-db attenuation at both f_a and f_b.

In Part (c) of the table the dimensions of the coupling irises are determined with the aid of the chart in Fig. 8.06-2, and in Part (d) the spacings between irises are determined. The iris data in Fig. 8.06-2 are for thin irises, and if the iris is, say, 0.020-inch thick, the error due to thickness should not be serious for most purposes, since the main effect will be on the resonant frequency of the cavities. There are presently no data available which give an accurate thickness correction for irises of the form in Fig. 8.06-2 with holes as large as are to be used in this filter. A suggested procedure is to measure the resonator lengths l_1, l_2, and l_3 from the *centerline* of one iris to the *centerline* of the next. This should make the resonant frequencies of the resonators a trifle high, so that they can be tuned down to the correct frequency using tuning screws and the alternating short- and open-circuit method discussed in Sec. 11.05. If a precision design without tuning screws is desired, the single- or double-resonator test procedures described in Secs. 11.03 to 11.05 are recommended for precision determination of the iris sizes and resonator tunings.

The peak attenuation $(L_A)_{USB}$ between the first and second pass bands will be about 54 db just as for the example in Sec. 8.05. However, it should be recalled that this holds only if the TE_{10} mode alone is present.

SEC. 8.07, NARROW-BAND CAVITY RESONATOR FILTERS COUPLED BY SMALL IRISES

The design of cavity resonator filters coupled by small irises can be carried out in a general fashion by means of Bethe's small-aperture theory (see Sec. 5.10). For most of the filters discussed in this chapter, it will be convenient to carry out the design in terms of the resonator slope parameters α_j or b_j and the inverter parameters $K_{j,j+1}$ or $J_{j,j+1}$.

However, in this section it will be more convenient to use the entirely equivalent approach which deals in terms of the external Q's, $(Q_e)_A$ and $(Q_e)_B$ of each end resonator loaded by its adjacent termination, and the coupling coefficients $k_{j,j+1}$ for the coupling between adjacent resonators. These matters were introduced in Sec. 8.02, and equations for the external Q's and coupling coefficients are given in Eqs. (6) to (8) of Figs. 8.02-3 and 8.02-4.

Figure 8.07-1 presents formulas for the external Q's of a rectangular cavity coupled to a terminated waveguide in any of various ways. In the equations and in the discussion below λ is the free-space wavelength, λ_g and λ_{g1} are the guide wavelengths

$$\lambda_g = \frac{\lambda}{\sqrt{1 - \left(\frac{\lambda}{2a}\right)^2}} \quad \text{and} \quad \lambda_{g1} = \frac{\lambda}{\sqrt{1 - \left(\frac{\lambda}{2a_1}\right)^2}} \quad , \quad (8.07\text{-}1)$$

s is the number of half guide-wavelengths in the l_1 dimension of the cavity, M_1 is the magnetic polarizability of the iris, and the quantities a, b, a_1, b_1, and t_1 are dimensions defined in the figures. Having computed the required values of $(Q_e)_A$ and $(Q_e)_B$ from Eqs. (6) and (7) of Figs. 8.02-3 or 8.02-4, the appropriate equation in Fig. 8.07-1 can be used to solve for the required magnetic polarizability M_1. Then, by use of Figs. 5.10-4(a),(b), the dimensions of the coupling iris can be obtained. It should be noted that M_1 has dimensions of (length)^3 which is consistent with the equations in Fig. 8.07-1, and with the normalization of the ordinates in Figs. 5.10-4(a),(b).

Figure 8.07-2 shows formulas for the coupling coefficient k for two rectangular resonators coupled by a small iris in either the end or side wall. The significance of the other parameters in the equations is the same as for Fig. 8.07-1. The required coupling coefficient values for the couplings between the various adjacent resonators of a filter can be computed by use of Eq. (8) of Fig. 8.02-3 or Fig. 8.02-4. Then, by use of the appropriate formula in Fig. 8.07-2, the magnetic polarizability M_1 of the various coupling irises can be solved for. As for the end irises, the dimensions of the internal irises can be determined with the aid of Fig. 5.10-4(a),(b).

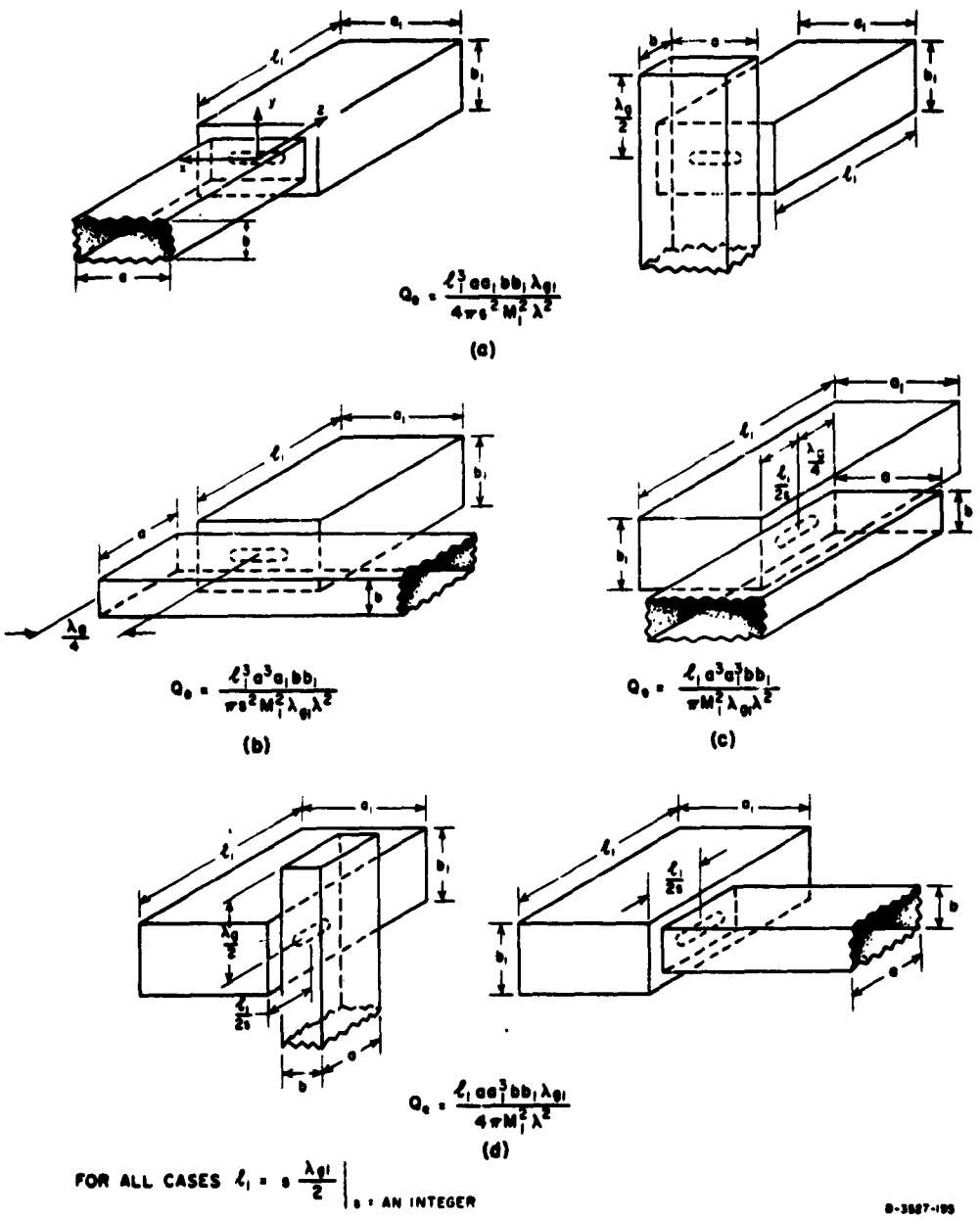

FIG. 8.07-1 EXTERNAL Q, Q_e, OF A RECTANGULAR CAVITY COUPLED TO A TERMINATED WAVEGUIDE BY A SMALL IRIS IN VARIOUS WAYS

For narrow-band filters such as those discussed in this section, the low-pass to band-pass mapping

$$\frac{\omega'}{\omega_1'} = \frac{2}{w}\left(\frac{f - f_0}{f_0}\right) \qquad (8.07\text{-}2)$$

where

$$w = \frac{\omega_2 - \omega_1}{\omega_0}$$

and

$$\omega_0 = \frac{\omega_2 + \omega_1}{2}$$

should give satisfactory accuracy.

As an example of the use of this method we consider the design of a three-cavity direct-coupled filter having a 0.01-db pass-band ripple to operate at a center frequency of 10 Gc in WR-90 waveguide (a = 0.900 inch, b = 0.400 inch). We choose the bandwidth to be 50 Mc (w = 0.005) and choose $l_1 = \lambda_{g1}/2$ = 0.7815 (s = 1). The elements of the low-pass prototype

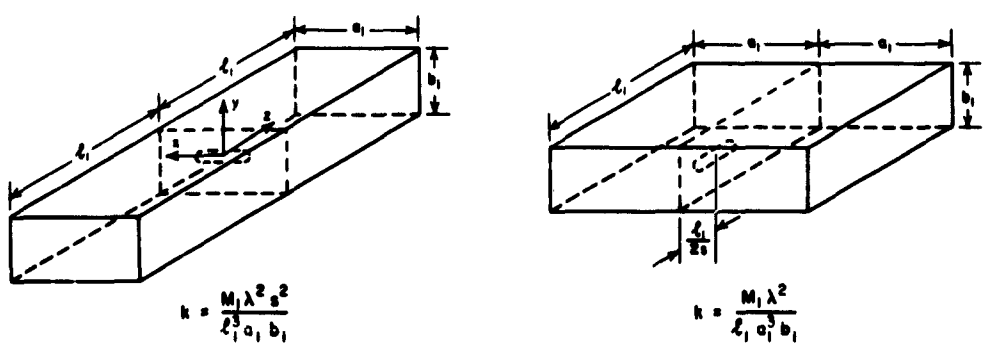

FIG. 8.07-2 COUPLING COEFFICIENT k FOR RECTANGULAR CAVITIES COUPLED BY A SMALL IRIS IN THE END WALL OR SIDE WALL

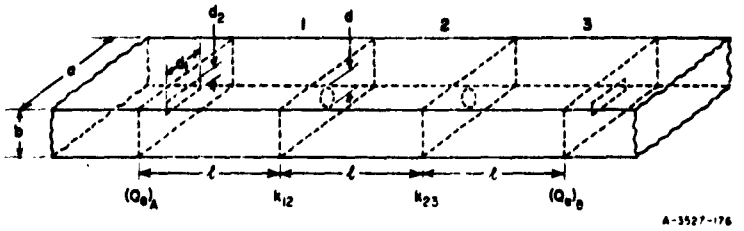

FIG. 8.07-3 REALIZATION OF NARROW-BAND DIRECT-COUPLED FILTER USING SMALL IRISES

filter are determined from Table 4.05-2(a) to be $g_0 = g_4 = 1.000$, $g_1 = g_3 = 0.6291$, and $g_2 = 0.9702$. Figure 8.07-3 illustrates the realization of this filter. We determine from Fig. 8.02-3 that $(Q_e)_A = (Q_e)_B = g_0 g_1 \omega_1'/w = 125.8$ and that $k_{12} = k_{23} = w/(\omega_1' \sqrt{g_1 g_2}) = 0.0064$. Using Figs. 8.07-1(a) and 8.07-2(a) we find the polarizabilities M_1 for the external and internal apertures to be 6.62×10^{-3} and 0.79×10^{-3} respectively. For the rectangular end irises we choose $d_2/d_1 = 0.5$ (see Fig. 8.07-3). Referring to Fig. 5.10-4(a), we find from the curve for rectangular irises, an initial value of $d_2 = 0.344$ inch. However, d_2 is an appreciable fraction of $\lambda = 1.18$ inches, so that we use Eq. (5.10-3) to determine an approximate correction and find as final values $d_2 = 0.31$ inch and $d_1 = 0.155$ inch. For the circular middle irises we find $d = (6M_1)^{1/3} = 0.168$ inch (see Sec. 5.10). If the thickness of the irises is 0.005 inch or less, the thickness correction of Eq. (5.10-5) is negligible. However, for greater thickness this correction should be applied.

The presence of the apertures will have the effect of lowering the resonant frequencies of the resonators slightly from what they were before the apertures were added. If desired, a small correction in the lengths of the resonators in Fig. 8.07-3 could be made by applying Eq. (5) of Fig. 8.06-1. For this example the normalized reactances $X_{j,j+1}/Z_0$ can be obtained from Fig. 5.10-5, which for the centered irises in Fig. 8.07-3 gives

$$\left.\frac{X_{j,j+1}}{Z_0}\right|_{j=0 \text{ to } 3} = \frac{4\pi (M_1)_{j,j+1}}{ab\lambda_{g1}} \quad , \qquad (8.07\text{-}3)$$

where X_{01}/Z_0 and X_{34}/Z_0 are for the irises at the ends.

The design method of this section is based on Bethe's small-aperture theory and is very versatile. However, it does rely on the assumption that the coupling irises are relatively small, which also implies that the fractional bandwidth w of the filter is small (say, of the order of 0.01 or less). Some discussion of the derivation of the equations in Figs. 8.07-1 and 8.07-2 will be found in Sec. 8.14.

SEC. 8.08, FILTERS USING TWO-PORT, QUARTER-WAVELENGTH RESONATORS

The filters discussed in Sec. 8.05 use J-inverters of the type in Fig. 8.03-2(d) along with half-wavelength resonators, and their design equations can be derived from Fig. 8.02-4 as will be outlined in Sec. 8.14. The filters discussed in Sec. 8.06 use K-inverters of the type in Fig. 8.03-1(c) along with half-wavelength resonators, and their design equations can be derived from Fig. 8.02-3. If quarter-wavelength resonators are used in an analogous way, they themselves have an inverting effect so that if at one end of each resonator they behave like the series resonators in Fig. 8.02-3, at their other ends they will operate like the shunt resonators in Fig. 8.02-4. In this manner it can be shown that filters can be constructed using two-port, quarter-wavelength resonators if they are coupled alternately by K- and J-inverters.[14]

Though other types of construction and other types of K- and J-inverters may also be used, Fig. 8.08-1 gives design data for a TEM-mode type of filter using quarter-wavelength resonators with capacitive-gap J-inverters, and shunt inductance K-inverters. Except for the use of two different kinds of inverters and other minor differences which result from the fact that the resonators are a quarter-wavelength rather than a half-wavelength long, the design procedure is much the same as for the preceding cases. Using the st ·p-line construction shown in Fig. 8.05-3(a), the J-inverter capacitive-gap spacing and the electrical length ϕ can be determined by use of the data in Figs. 8.05-3(a),(b), and (c). Figures 8.08-2(a) to 8.08-4(b) show data for inductive-stub K-inverters. Note that the ordinates on these graphs are normalized with respect to frequency in Gc, and that due to the junction effect the ϕ values are not always negative in this case.

Figure 8.08-5(a) shows a filter with six quarter-wavelength resonators designed using the charts just discussed.[11] The construction is

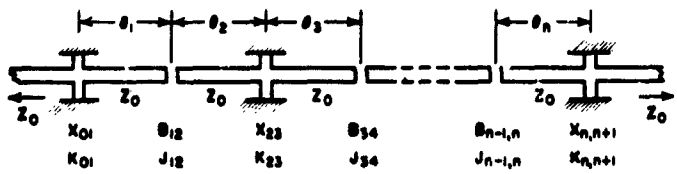

$$\frac{K_{01}}{Z_0} = \sqrt{\frac{\pi w}{4 g_0 g_1 \omega_1'}} \tag{1}$$

$$\frac{J_{j,j+1}}{Y_0} \text{ or } \frac{K_{j,j+1}}{Z_0} \quad {\scriptstyle j=1 \text{ to } n-1} = \frac{\pi w}{4\omega_1'} \frac{1}{\sqrt{g_j g_{j+1}}} \tag{2}$$

$$\frac{K_{n,n+1}}{Z_0} = \sqrt{\frac{\pi w}{4 g_n g_{n+1} \omega_1'}} \tag{3}$$

where g_0, g_1, ..., g_n are as defined in Fig. 4.04-1, ω_1' is defined in Fig. 8.02-1(a), and w is the fractional bandwidth defined below. In this structure, impedance inverters (with parameters $K_{j,j+1}$) alternate with admittance inverters (with parameters $J_{j,j+1}$), and $Z_0 = 1/Y_0$ is the characteristic impedance of the line between inverters.

Using $K_{j,j+1}$ inverters of the form in Fig. 8.03-1(c) and $J_{j,j+1}$ inverters of the form in Fig. 8.03-2(d), the $X_{j,j+1}$, $B_{j,j+1}$, and $\phi_{j,j+1}$ values can be computed from the equations in those figures. Then

$$\theta_j = \frac{\pi}{2} + \frac{1}{2}\left[\phi_{j-1,j} + \phi_{j,j+1}\right] \quad \text{radians} \tag{4}$$

where the $\phi_{k,k+1}$ are negative.

Using the construction shown in Figs. 8.08-5(a), the gap spacings Δ and the ϕ values for the $J_{j,j+1}$ inverters may be determined by Figs. 8.05-3(a), (b), (c). The stub lengths and ϕ values for the $K_{j,j+1}$ inverters may be determined by Figs. 8.08-2(a) to 8.08-4(b).

To map low-pass prototype filter response to corresponding band-pass filter response use the approximation

$$\omega' = \frac{2\omega_1'}{w}\left(\frac{\omega - \omega_0}{\omega}\right), \tag{5}$$

where

$$w = 2\left(\frac{\omega_2 - \omega_1}{\omega_2 + \omega_1}\right), \tag{6}$$

and

$$\omega_0 = \frac{2\omega_2\omega_1}{\omega_2 + \omega_1}. \tag{7}$$

FIG. 8.08-1 DESIGN EQUATIONS FOR FILTERS WITH TWO-PORT, QUARTER-WAVELENGTH RESONATORS

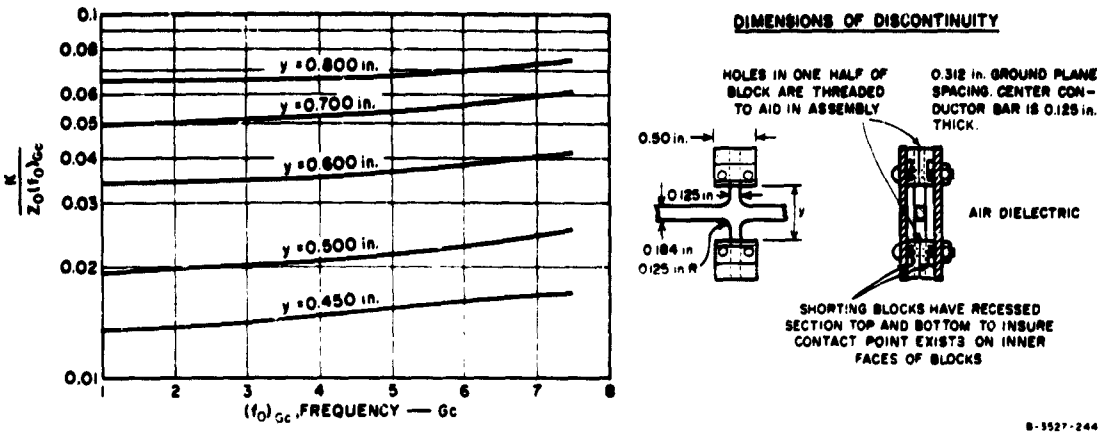

SOURCE: Reference 11, by G. L. Matthaei. (By courtesy of the Ramo-Wooldridge Div. of the Thompson-Ramo Wooldridge Corp.)

FIG. 8.08-2(a) $K/[Z_0(f_0)_{Gc}]$ vs. $(f_0)_{Gc}$ FOR DOUBLE-STUB, SHUNT INDUCTANCE K-INVERTERS IN BAR TRANSMISSION-LINE CONSTRUCTION
The characteristic impedance of the resonator transmission line is $Z_0 = 1/Y_0 = 50$ ohms, and $(f_0)_{Gc}$ is the resonant frequency in Gc

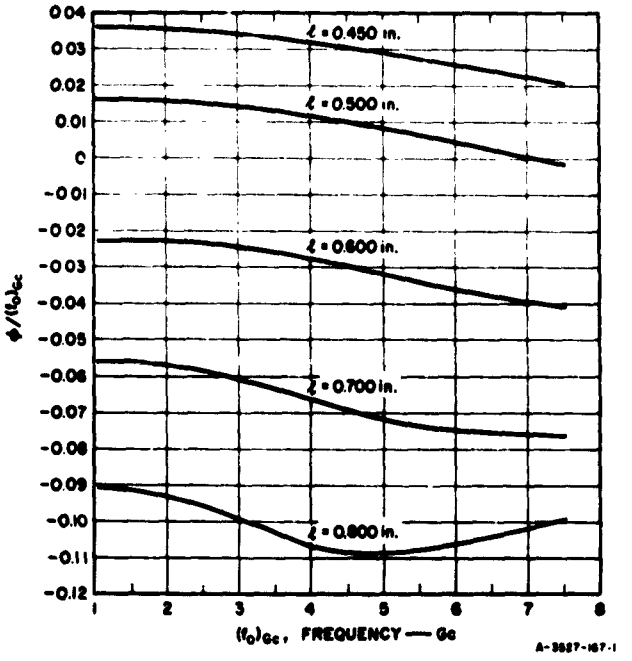

SOURCE: Reference 11, by G. L. Matthaei. (By courtesy of the Ramo-Wooldridge Div. of the Thompson-Ramo-Wooldridge Corp.)

FIG. 8.08-2(b) $\phi/(f_0)_{Gc}$ vs. $(f_0)_{Gc}$ vs. $(f_0)_{Gc}$ FOR THE DOUBLE-STUB K-INVERTER IN FIG. 8.08-2(a)

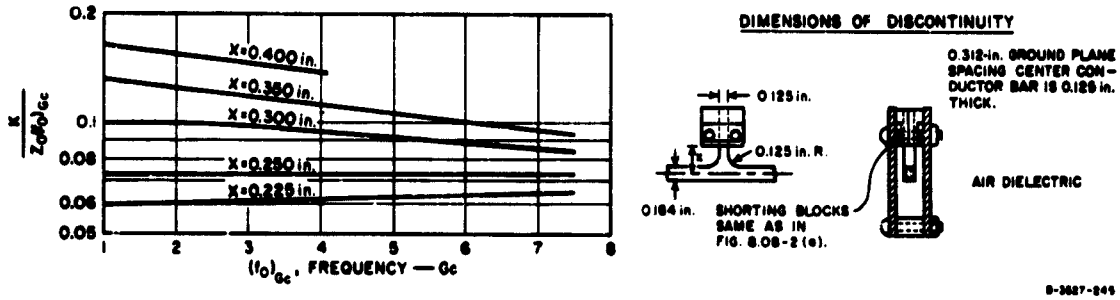

SOURCE: Reference 11, by C. L. Matthaei. (By courtesy of the Ramo-Wooldridge Div. of the Thompson-Ramo-Wooldridge Corp.)

FIG. 8.08-3(a) $K/[Z_0(f_0)_{Gc}]$ vs. $(f_0)_{Gc}$ FOR A SINGLE-STUB, SHUNT INDUCTANCE K-INVERTER IN BAR TRANSMISSION-LINE CONSTRUCTION
The characteristic impedance of the resonator transmission line is $Z_0 = 1/Y_0 = 50$ ohms, and $(f_0)_{Gc}$ is the resonant frequency in Gc

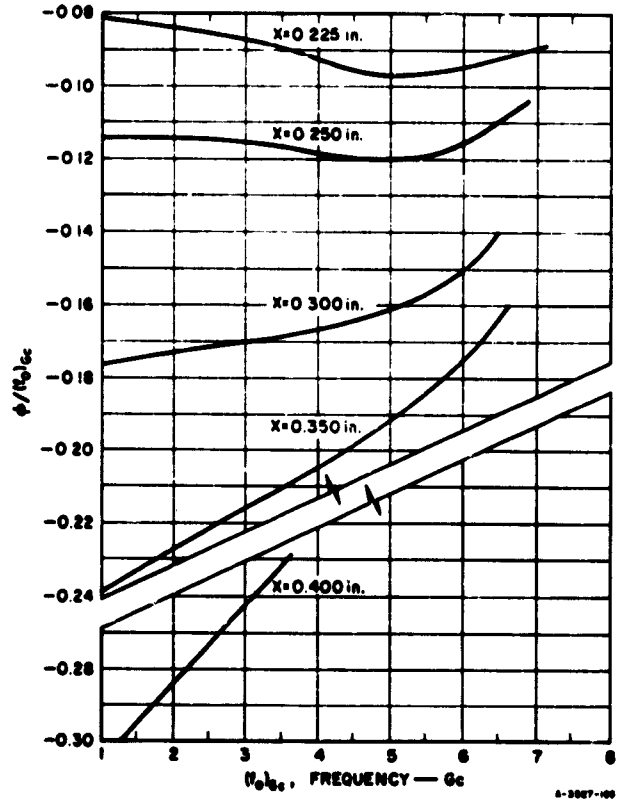

SOURCE: Reference 11, by G. L. Matthaei. (By courtesy of the Ramo-Wooldridge Div. of the Thompson-Ramo-Wooldridge Corp.)

FIG. 8.08-3(b) $\phi(f_0)_{Gc}$ vs. $(f_0)_{Gc}$ FOR THE SINGLE-STUB K-INVERTER IN FIG. 8.08-3(a)

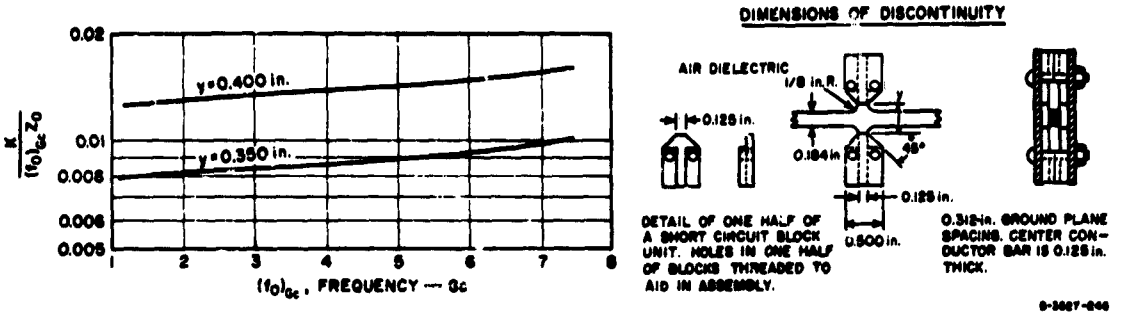

SOURCE: Reference 11, by G. L. Matthaei. (By courtesy of the Ramo-Wooldridge Div. of the Thompson-Ramo Wooldridge Corp.)

FIG. 8.08-4(a) $K/[Z_0(f_0)_{Gc}]$ vs. $(f_0)_{Gc}$ FOR A SHUNT INDUCTANCE K-INVERTER DESIGNED TO PERMIT RELATIVELY LOOSE COUPLINGS IN BAR TRANSMISSION LINE

The characteristic impedance of the resonator transmission line is $Z_0 = 1/Y_0 = 50$ ohms, and $(f_0)_{Gc}$ is the resonant frequency in Gc

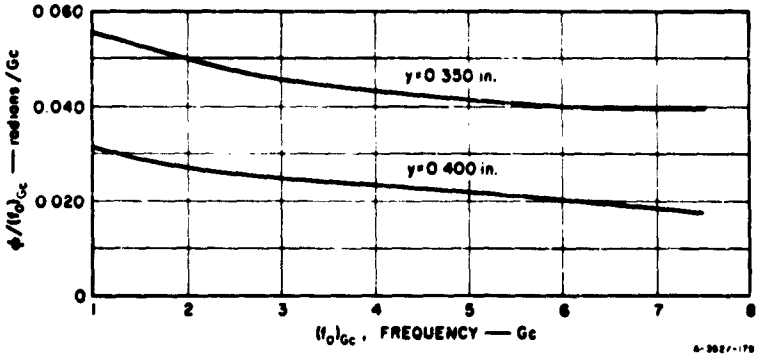

SOURCE: Reference 11, by G. L. Matthaei. (By courtesy of the Ramo-Wooldridge Div. of the Thompson-Ramo-Wooldridge Corp.)

FIG. 8.08-4(b) $\phi/(f_0)_{Gc}$ vs. $(f_0)_{Gc}$ FOR THE K-INVERTER IN FIG. 8.08-4(a)

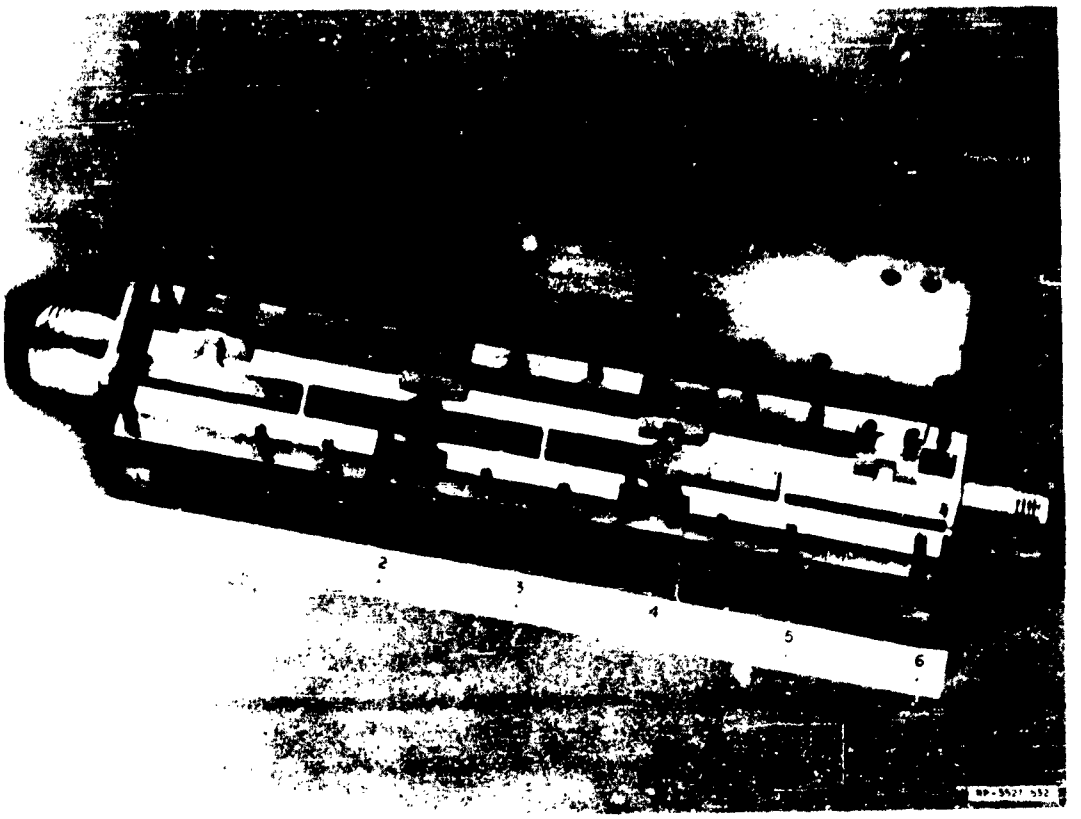

SOURCE: Reference 11, by G. L. Matthaei. (By courtesy of the Ramo-Wooldridge Div. of the Thompson-Ramo-Wooldridge Corp.)

FIG. 8.08-5(a) A FILTER WITH SIX, $\lambda_0/4$ RESONATORS IN BAR CONSTRUCTION
The response is shown in Fig. 8.08-5(b)

quite rugged, and no dielectric support material is required. The resonators in this filter were tested in pairs by the methods described in Secs. 11.04 and 11.05 to insure that their tuning was correct. The design pass band was from 2.6 to 3.4 Gc, and as can be seen from Fig. 8.08-5(b), this was achieved with good accuracy. The mapping defined in Eqs. (5) to (7) in Fig. 8.08-1 is not quite as accurate, however, for this type of filter as for the type in Fig. 8.05-1. In this case, the predicted attenuation at 2.4 Gc is about 40 db, which is only about 2 db more than was measured; however, the predicted attenuation at 3.7 Gc is about 37 db as against a measured attenuation of 32 db.

This type of filter has several advantages over analogous filters using half-wavelength resonators.[14] The quarter-wavelength resonators are, of course, shorter which gives a smaller filter for a given number of resonators. A filter with half-wavelength resonators equivalent to the filter in Fig. 8.08-5(a) would have a second pass band centered at about twice the center frequency of the first pass band, or at about 6 kMc. However, in this quarter-wavelength-resonator type of filter, the second pass band is centered roughly three times the band center of the first pass band, or at about 9 kMc in this case. This particular filter has about 61.5 db attenuation at 6 kMc.

Quarter-wavelength resonators of the type described have an additional advantage in that their reactance or susceptance slope parameters are half as large as for corresponding half-wavelength resonators.

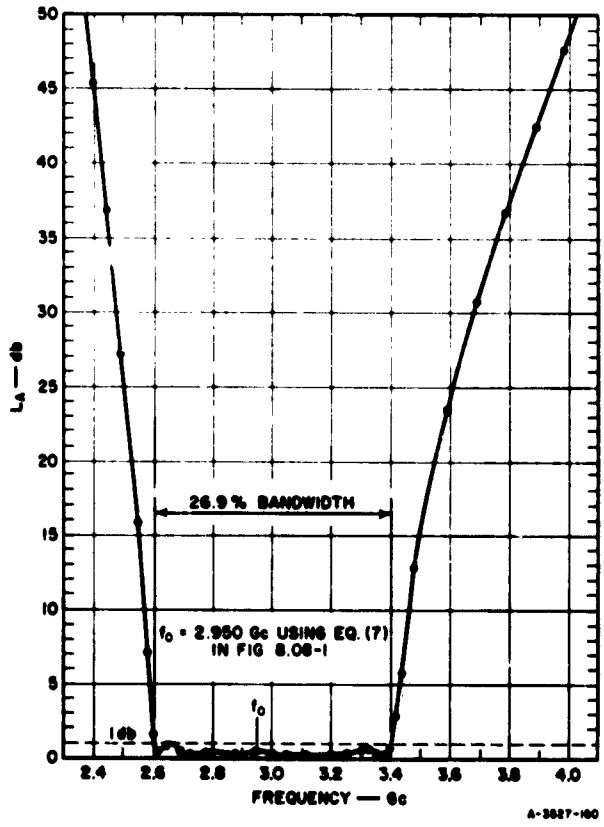

SOURCE: Reference 11, by G. L. Matthaei. (By courtesy of the Ramo-Wooldridge Div. of the Thompson-Ramo-Wooldridge Corp.)

FIG. 8.08-5(b) THE ATTENUATION CHARACTERISTIC OF THE FILTER IN FIG. 8.08-5(a)

Because of this, for a given bandwidth and pass-band shape the couplings are considerably looser for the quarter-wavelength than for the half-wavelength resonator types of filters. This calls for larger capacitive gaps so that tolerances are less of a problem, and it also results in considerably higher maximum attenuation $(L_A)_{USB}$ in the stop band above the pass band. Also, because of the shorter resonators and looser couplings the circuit is more nearly lumped, and as a result, the design equations in Fig. 8.08-1 will be found to give filters with specified pass-band characteristics accurately for greater bandwidths. They should give good results for many filters having bandwidths as large as 30 percent. As in the preceding cases, the equations are more accurate for larger bandwidths if the pass-band ripple tolerance is 0.5 to 1.0 db than if a very small tolerance such as 0.01 db is called for.

For this type of filter, the maximum attenuation between the first and second pass band is always finite (just as for the filters in Secs. 8.05, 8.06, and 8.07), but in this case, the attenuation levels off to a maximum value near $\omega = 2\omega_0$. This maximum upper-stop-band attenuation can be estimated by use of the formula

$$(L_A)_{USB} = 20 \log_{10}\left[\frac{1}{\left(\frac{X_{01}}{Z_0}\right)\left(\frac{B_{12}}{Y_0}\right)\cdots\left(\frac{B_{n-1,n}}{Y_0}\right)\left(\frac{X_{n,n+1}}{Z_0}\right)}\right] - (n+1)6.02 - 6.02 \quad \text{db} \tag{8.08-1}$$

where

$$\frac{X_{j,j+1}}{Z_0} = \frac{\frac{K_{j,j+1}}{Z_0}}{1 - \left(\frac{K_{j,j+1}}{Z_0}\right)^2}, \tag{8.08-2}$$

$$\frac{B_{j,j+1}}{Y_0} = \frac{\frac{J_{j,j+1}}{Y_0}}{1 - \left(\frac{J_{j,j+1}}{Y_0}\right)^2}, \tag{8.08-3}$$

and the $K_{j,j+1}/Z_0$ and $J_{j,j+1}/Y_0$ are computed by use of Eq. (1) to (3) in Fig. 8.08-1. An n-resonator filter of this type will have an $(n + 1)$-order pole of attenuation (Sec. 2.04) at $\omega = 0$. For that reason, this type of filter will have a very fast rate of cutoff below the pass band, as can be seen in the case of the response in Fig. 8.08-5(b).

SEC. 8.09, FILTERS WITH PARALLEL-COUPLED STRIP-LINE RESONATORS

Figure 8.09-1 presents design equations (which are a modified form of equations due to Cohn[15]) for filters using half-wavelength strip-line resonators, positioned so that adjacent resonators parallel each other along half of their length. This parallel arrangement gives relatively large coupling for a given spacing between resonator strips, and thus, this construction is particularly convenient for printed-circuit filters up to about 10 or 15 percent bandwidth.[15] For larger bandwidths the resonators can be constructed from bars having a rectangular cross section (which permits tighter coupling), and for that case the wide-band filter equations in Chapter 10 are recommended.

The use of the equations in Fig. 8.09-1 is best illustrated by use of an example. Let us suppose that a low VSWR in the pass band is desired so that a 0.01-db ripple, Tchebyscheff prototype is to be used in the design. The desired fractional bandwidth is assumed to be $w = 0.10$, and the design center frequency is to be $f_0 = 1207$ Mc. We shall assume that 25-db attenuation is required at $f = 1100$ Mc. Then, by mapping Eqs. (6) to (8) in Fig. 8.09-1 for $f = 1100$ Mc,

$$\frac{\omega'}{\omega_1'} = \frac{2}{w}\left(\frac{\omega - \omega_0}{\omega_0}\right) = \frac{2}{w}\left(\frac{f - f_0}{f_0}\right)$$

$$= \frac{2}{0.10}\left(\frac{1100 - 1207}{1207}\right) = -1.77 \quad .$$

By Fig. 4.03-4 it is found that an $n = 6$ design has 29 db attenuation for $|\omega'/\omega_1'| - 1 = 0.77$ while an $n = 5$ design has $L_A = 18.5$ db. Thus, $n = 6$ is required. By Table 4.05-2(a), the desired $n = 6$ prototype parameters are $g_0 = 1$, $g_1 = 0.7813$, $g_2 = 1.3600$, $g_3 = 1.6896$, $g_4 = 1.5350$, $g_5 = 1.4970$, $g_6 = 0.7098$, $g_7 = 1.1007$, and $\omega_1' = 1$.

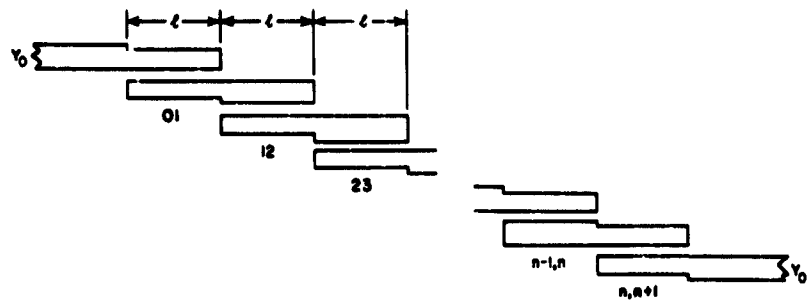

$$\frac{J_{01}}{Y_0} = \sqrt{\frac{\pi w}{2g_0 g_1}} \tag{1}$$

$$\left.\frac{J_{j,j+1}}{Y_0}\right|_{j=1 \text{ to } n-1} = \frac{\pi w}{2\omega_1'} \frac{1}{\sqrt{g_j g_{j+1}}} \tag{2}$$

$$\frac{J_{n,n+1}}{Y_0} = \sqrt{\frac{\pi w}{2g_n g_{n+1}}} \tag{3}$$

where $g_0, g_1, \ldots, g_{n+1}$ are as defined in Fig. 4.04-1, ω_1' is as defined in Fig. 8.02-1(a), and w is the fractional bandwidth defined below. The $J_{j,j+1}$ are admittance inverter parameters and Y_0 is the characteristic admittance of the terminating lines. The even- and odd-mode impedances of the strips are

$$\left.(Z_{oe})_{j,j+1}\right|_{j=0 \text{ to } n} = \frac{1}{Y_0}\left[1 + \frac{J_{j,j+1}}{Y_0} + \left(\frac{J_{j,j+1}}{Y_0}\right)^2\right] \tag{4}$$

$$\left.(Z_{oo})_{j,j+1}\right|_{j=0 \text{ to } n} = \frac{1}{Y_0}\left[1 - \frac{J_{j,j+1}}{Y_0} + \left(\frac{J_{j,j+1}}{Y_0}\right)^2\right] \tag{5}$$

and the strip dimensions can be determined by use of Sec. 5.05.

To map the low-pass prototype response to the band-pass filter response use the approximation

$$\frac{\omega'}{\omega_1'} = \frac{2}{w}\left(\frac{\omega - \omega_0}{\omega_0}\right) \tag{6}$$

where

$$w = \frac{\omega_2 - \omega_1}{\omega_0} \tag{7}$$

$$\omega_0 = \frac{\omega_2 + \omega_1}{2} \tag{8}$$

and ω_1 and ω_2 are as defined in Fig. 8.02-1(b).

FIG. 8.09-1 DESIGN EQUATIONS FOR FILTERS WITH PARALLEL-COUPLED RESONATORS

Table 8.09-1

DESIGN PARAMETERS FOR EXPERIMENTAL PARALLEL-COUPLED STRIP-LINE-RESONATOR FILTER

j	$J_{j,j+1}/Y_0$	$(Z_{oe})_{j,j+1}$	$(Z_{oo})_{j,j+1}$	$W_{j,j+1}$	$s_{j,j+1}$	$d_{j,j+1}$
0	0.449	82.5 ohms	37.6 ohms	0.236 inch	0.021 inch	0.073 inch
1	0.1529	58.8 ohms	43.5 ohms	0 346 inch	0.110 inch	0.084 inch
2	0.1038	55.7 ohms	45.3 ohms	0.360 inch	0.158 inch	0.085 inch
3	0.0976	55.4 ohms	45.6 ohms	0.361 inch	0.163 inch	0.085 inch

SOURCE: Final Report, Contract DA 36-039 SC-64625, SRI; reprinted in *IRE Trans. PGMTT* (see Ref. 15 by S. B. Cohn).

Table 8.09-1 shows the $J_{j,j+1}/Y_0$, $(Z_{oe})_{j,j+1}$, and $(Z_{oo})_{j,j+1}$ values as computed from the equations in Fig. 8.09-1. This filter was constructed[15] using polystyrene dielectric with a relative dielectric constant ϵ_r of 2.55. Using a 0.5-inch ground plane spacing and copper-foil resonators of negligible thickness, by use of Figs. 5.05-3(a),(b) the dimensions of the strip widths $W_{j,j+1}$, and the gaps $s_{j,j+1}$, were obtained and they are as is also shown in Table 8.09-1. The significance of these dimensions is further illustrated in Fig. 8.09-2.

The dimensions $d_{j,j+1}$ indicated in Table 8.09-1 and Fig. 8.09-2 are resonator length corrections to account for the fringing capacitance from

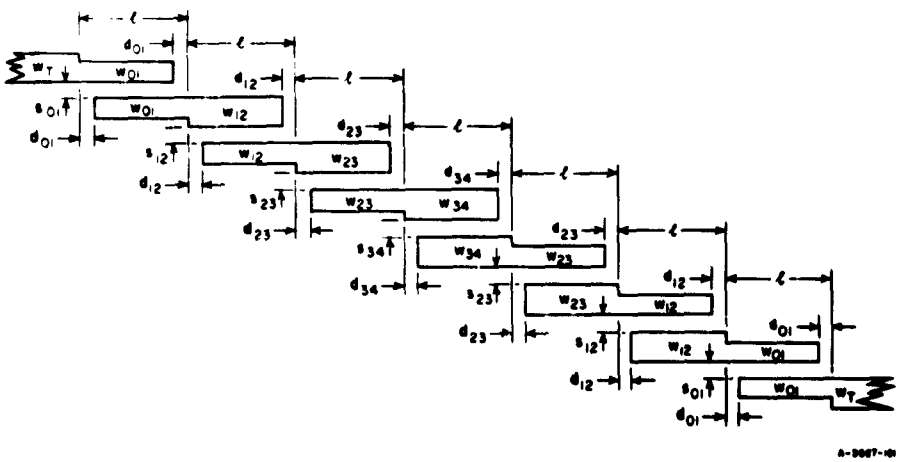

SOURCE: Final report, Contract DA 36-039 SC-64625, SRI; reprinted in *IRE Trans., PGMTT* (see Ref. 15 by S. B. Cohn).

FIG. 8.09-2 LAYOUT OF PARALLEL-COUPLED-RESONATOR FILTER

the end of each strip. The basic length l indicated in the Fig. 8.09-2 is a quarter-wavelength at frequency ω_0 in the medium of propagation, while the actual strip lengths are shortened by the amount $d_{j,j+1}$. Although Table 8.09-1 indicates some variation in the $d_{j,j+1}$ values, Cohn[15] has found that a constant correction of $d_{j,j+1} = 0.165b$ (where b is the ground-plane spacing) is apparently satisfactory.

As a result of the filter being designed from an antimetric prototype filter (see Sec. 4.05), the resulting parallel-coupled microwave filter has symmetry about its center. For that reason only the dimensions of half the filter are shown in Table 8.09-1. The input and output lines are of 50 ohms impedance which requires that they be $w_1 = 0.372$ inch wide as determined from Fig. 5.04-1 with $b = 0.50$, $t = 0$, and $\epsilon_r = 2.55$. Figure 8.09-3 shows the manner in which the input and output strips were beveled to give a low-reflection transition from the printed-circuit strip line to coaxial line.

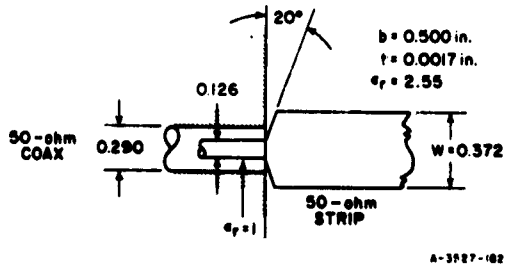

FIG. 8.09-3 COAXIAL-LINE TO STRIP-LINE JUNCTION

Figure 8.09-4 shows a photograph of the completed printed-circuit filter with its upper half removed. The circles in Fig. 8.09-5 show measured attenuation values while the solid curve shows the theoretical attenuation as computed from the low-pass prototype attenuation with the aid of the mappings in Eqs. (6) to (8) of Fig. 8.09-1. As can be seen from the figure, the agreement is very good. Of course, as a result of dissipation loss, the pass-band attenuation is considerably above the 0.01 db theoretical value for a lossless filter. Working back from the measured attenuation using Eqs. (4.13-2), (4.13-8), and Fig. 4.13-2, the Q of the resonators in this filter is estimated to be roughly 600.

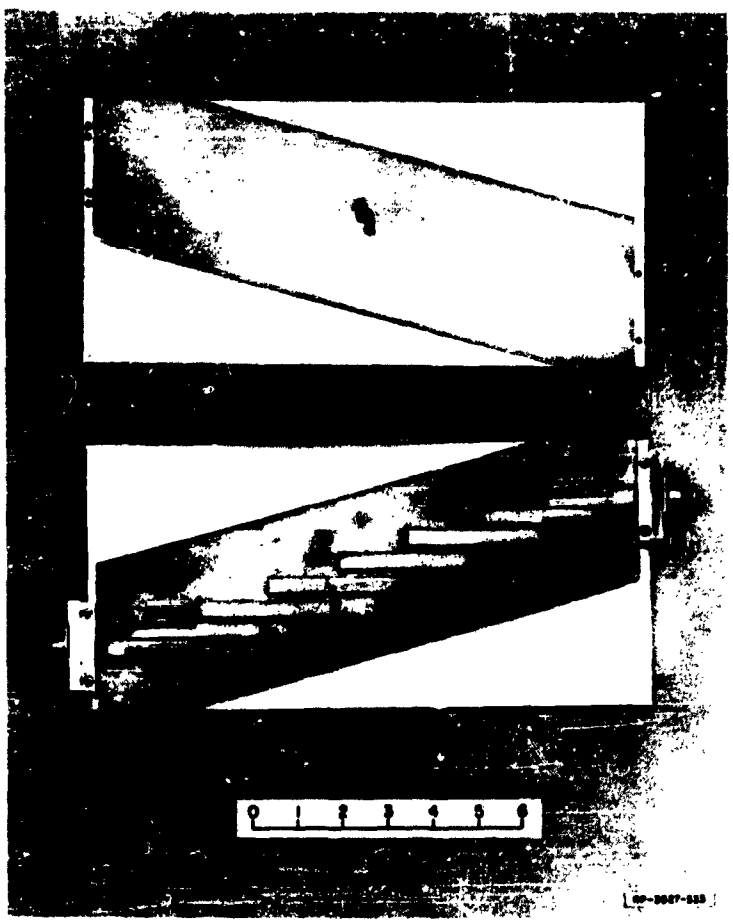

SOURCE: Final Report, Contract DA 36-039 SC-64625, SRI; reprinted in *IRE Trans., PGMTT* (see Ref. 15 by S. B. Cohn).

FIG. 8.09-4 PHOTOGRAPH OF THE EXPERIMENTAL PARALLEL-COUPLED FILTER WITH ITS COVER PLATE REMOVED

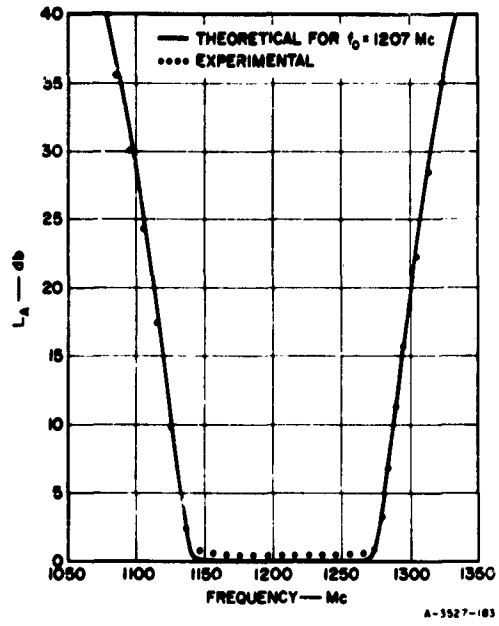

SOURCE: Final report, Contract DA 36-039 SC-64625, SRI; reprinted in *IRE Trans., PGMTT* (see Ref. 15 by S. B. Cohn).

FIG. 8.09-5 THEORETICAL AND MEASURED ATTENUATION FOR THE FILTER IN FIG. 8.09-4

SEC. 8.10, FILTERS WITH QUARTER-WAVELENGTH COUPLINGS

As has been previously mentioned, quarter-wavelength lines can be used satisfactorily as K- or J-inverters in narrow-band filters (*i.e.*, filters with bandwidths of the order of a few percent or less). Figure 8.10-1 shows a filter with quarter-wavelength lines for inverters and presents the appropriate design equations. The $\pi/4$ and $\pi/2$ terms in the equations for the normalized resonator susceptance slope parameters b_j/Y_0 represent correction terms for the added selectivity introduced by the quarter-wavelength lines.[4] The particular structure shown gives perfect transmission at the midband frequency ω_0, hence, it is only applicable for achieving responses that have this property (*i.e.*, no reflection loss at ω_0). Therefore, the data given is valid for use with the maximally flat low-pass prototypes in Tables 4.05-1(a),(b), having any value of n, but only for Tchebyscheff prototypes in Tables 4.05-2(a), (b), having an *odd* number of reactive elements n.*

* Tchebyscheff responses corresponding to n even can also be achieved with this type of filter if the coupling lines are allowed to have Y_0 values different from that of the terminations. In Fig. 8.10-1, the lines are all the same, for simplicity.

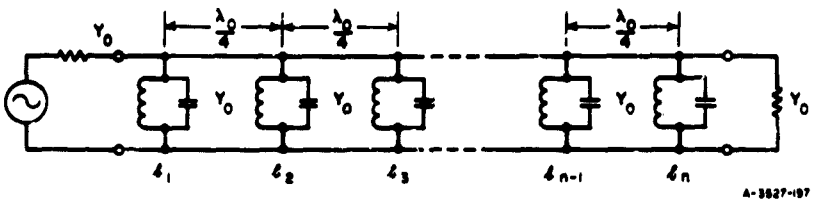

For maximally flat filters with n even or odd, or Tchebyscheff filters with n odd:

$$\frac{b_1}{Y_0} = \frac{\omega_1' g_1 g_0}{w} - \frac{\pi}{4} \tag{1}$$

$$\left.\frac{b_j}{Y_0}\right|_{j=\text{even}<n} = \frac{\omega_1' g_j}{w g_0} - \frac{\pi}{2} \tag{2}$$

$$\left.\frac{b_j}{Y_0}\right|_{j=\text{odd}<n} = \frac{\omega_1' g_j g_0}{w} - \frac{\pi}{2} \tag{3}$$

$$\frac{b_n}{Y_0} = \frac{b_1}{Y_0} \tag{4}$$

where the $g_0, g_1, \ldots, g_{n+1}$ are as defined in Fig. 4.04-1, ω_1' is defined in Fig. 8.02-1(a), the b_j are susceptance slope parameters defined in Fig. 8.02-4, w is as defined below, λ_0 is the propagation wavelength at the midband frequency ω_0, and Y_0 is the admittance of the transmission line connecting the resonators.

To map low-pass filter response to corresponding band-pass filter response use (for narrow-band designs):

$$\frac{\omega'}{\omega_1'} = \frac{2}{w}\left(\frac{\omega - \omega_0}{\omega_0}\right) \tag{5}$$

where

$$w = \left(\frac{\omega_2 - \omega_1}{\omega_0}\right) , \tag{6}$$

$$\omega_0 = \left(\frac{\omega_2 + \omega_1}{2}\right) , \tag{7}$$

and ω_0, ω_1, and ω_2 are as defined in Fig. 8.02-1(b).

FIG. 8.10-1 DESIGN EQUATIONS FOR FILTERS WITH QUARTER-WAVELENGTH COUPLINGS

The resonators for filters of this type can be formed from semi-lumped elements, cavities with loop couplings, resonant irises,[5] and other means. One common way of realizing the desired resonators is illustrated in Fig. 8.10-2.[4] In this case, the resonator used is a half-wavelength resonator with a K-inverter at each end, as indicated at (b) in the figure. The K-inverters tend to reflect low-impedance levels to the ends of the half-wavelength line section which, it can be shown, will make it operate like a series resonator (see Sec. 8.14). However, this series resonance operation when viewed from the outside through the K-inverters looks like a shunt resonance equivalent to that of the shunt-tuned circuit shown in Fig. 8.10-2(a). Using waveguide and inductive irises of shunt reactance X_j to realize the K_j inverters, the resulting quarter-wavelength-coupled waveguide filter takes the form shown in Fig. 8.10-3. Note that the half-wavelength resonators are corrected for the electrical length Φ_j associated with the K-inverters, and that the quarter-wavelength coupling lengths should be corrected in a similar way.

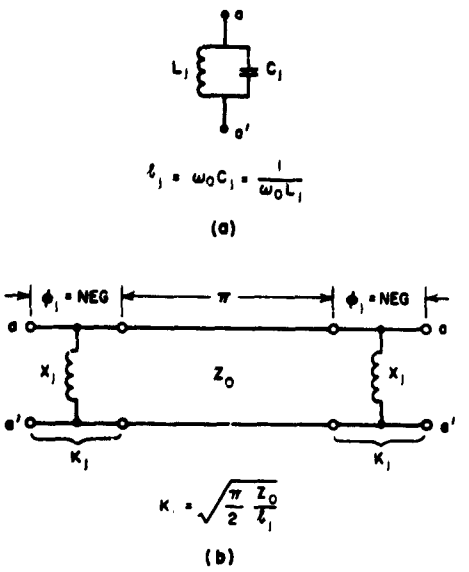

FIG. 8.10-2 REPLACEMENT OF A SHUNT RESONATOR BY A HALF-WAVELENGTH RESONATOR WITH TWO K-INVERTERS
The K-Inverters shown are of the type defined in Fig. 8.03-1(c)

The main advantage of this type of filter appears to be that the resonators are easily tested individually. If a waveguide joint is placed in the center of each quarter-wavelength coupling, the filter can easily be disassembled and each resonator checked by itself. Each resonator should, of course, resonate at ω_0, and if Fig. 8.10-1 calls for a susceptance slope parameter of b_j for the jth resonator, then if the resonator is connected to matched source and load waveguides of the same dimensions (and characteristic admittance Y_0), the resonator should exhibit a doubly loaded Q of

$$Q_j = \frac{b_j}{2Y_0} = \frac{f_0}{f_b - f_a} \qquad (8.10\text{-}1)$$

where f_b and f_a are the 3-db points of the transmission through the resonator.

To summarize the procedure for the design of a quarter-wavelength coupled waveguide filter of the type in Fig. 8.10-3, the number of resonators and the value for w_λ and the required number n of resonators should be determined by use of Eqs. (6) to (8) in Fig. 8.06-1, as discussed in Sec. 8.04.* Then w_λ should be used to replace w in Eqs. (1) to (4) in Fig. 8.10-1 (since guide-wavelength variation controls the bandwidth in this case) and the normalized susceptance slope parameters b_j, Y_0 should be determined using the desired lumped-element prototype parameters. By Fig. 8.10-2

$$\frac{K_j}{Z_0} = \sqrt{\frac{\pi}{2}\frac{Y_0}{b_j}} \qquad (8.10\text{-}2)$$

since $Z_0 = 1/Y_0$. Having values for the K_j, Z_0, the dimensions of the discontinuities and their corresponding b_j values can be determined as previously discussed in Sec. 8.06. The radian electrical spacings θ_j and

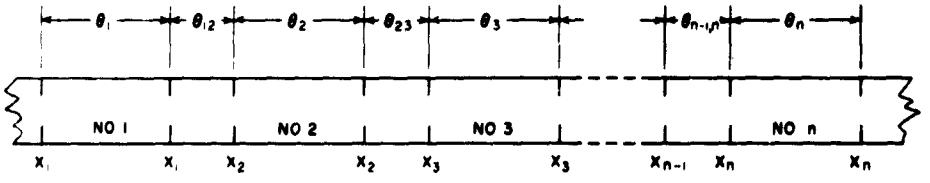

$$\theta_j = \pi + \phi_j$$

$$\theta_{j,j+1} = \frac{\pi}{2} + \frac{1}{2}(\phi_j + \phi_{j+1})$$

A-3527-199

FIG. 8.10-3 WAVEGUIDE FILTER USING SHUNT-INDUCTIVE IRISES AND QUARTER-WAVELENGTH COUPLINGS
The Φ_j are as indicated in Figs. 8.10-2 and 8.03-1(c)

* See Sec. 8.14 for discussion of the use of λ_{g0}/λ_g as a frequency parameter in design of waveguide filters.

$\theta_{j,j+1}$ (with respect to guide wavelength) of the discontinuities are then determined as indicated in Fig. 8.10-3.

SEC. 8.11, LUMPED-ELEMENT, COUPLED-RESONATOR FILTERS

At the lower microwave frequencies it may be possible to use semi-lumped elements, and analysis in terms of the lumped-element structures in Fig. 8.11-1 or 8.11-2 may be helpful. The structure in Fig. 8.11-1 approximates that in Fig. 8.02-4 using lumped, shunt resonators $B_j(\omega)$ and lumped J-inverters of the form in Fig. 8.03-2(b). In Fig. 8.11-1 the capacitances C_{rj} are the effective capacitances for determining the resonant frequency and susceptance slope parameters of the resonators. But, the actual shunt-capacitor elements used are smaller than the C_{rj}, as indicated in Eqs. (8) to (10). This is because the negative shunt capacitance of the J-inverters must be subtracted from the positive resonator capacitance to give the net shunt capacitance actually inserted in the circuit. The end coupling capacitances C_{01} and $C_{n,n+1}$ are treated in a somewhat different manner, as discussed in Sec. 8.14, in order to prevent having to deal with a negative shunt capacitance next to the terminations G_A and G_B. Note that G_A, G_B, and the C_{rj} may be given any values desired.

The circuit in Fig. 8.11-2(b) is the exact dual of that in Fig. 8.11-1 if L_{r0} and $L_{r,n+1}$ are chosen to equal M_{01} and $M_{n,n+1}$, respectively, which will make L_0 and L_{n+1} zero. The equations are slightly modified from those in Fig. 8.11-1, however, in order to also accommodate the circuit form in Fig. 8.11-2(a).

The low-pass to band-pass mappings shown in Figs. 8.11-1 and 8.11-2 are accurate for narrow bandwidths only; however, Cohn[1] has shown that the approximate mapping

$$\frac{\omega'}{\omega_1'} = \left| \frac{2 - \frac{\omega_0}{\omega} - \frac{1}{2 - \frac{\omega_0}{\omega}}}{2 - \frac{\omega_0}{\omega_2} - \frac{1}{2 - \frac{\omega_0}{\omega_2}}} \right| \tag{8.11-1}$$

where

$$\omega_0 = \omega_1 + \omega_2 - \sqrt{(\omega_2 - \omega_1)^2 + \omega_1\omega_2} \tag{8.11-2}$$

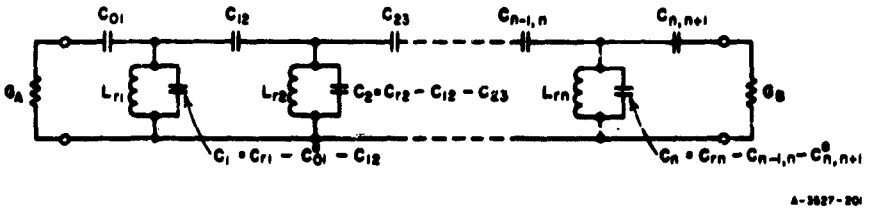

For definitions of the g_j, ω_1', ω_0, ω_1, ω_2, and the $J_{j,j+1}$; see Figs. 4.04-1, 8.02-1(a), (b), 8.02-4, and 8.03-2(b).

Choose values for G_A, C_{r1}, C_{r2}, ..., C_{rn}, and G_B. Then:

$$L_{rj}\big|_{j=1 \text{ to } n} = \frac{1}{C_{rj}\omega_0^2} \tag{1}$$

$$J_{01} = \sqrt{\frac{G_A \omega_0 C_{r1} w}{g_0 g_1 \omega_1'}} \tag{2}$$

$$J_{j,j+1}\big|_{j=1 \text{ to } n-1} = \frac{w\omega_0}{\omega_1'}\sqrt{\frac{C_{rj}C_{rj+1}}{g_j g_{j+1}}} \tag{3}$$

$$J_{n,n+1} = \sqrt{\frac{G_B \omega_0 C_{rn} w}{g_n g_{n+1} \omega_1'}} \quad , \tag{4}$$

where w is defined below.

The coupling capacitances are:

$$C_{01} = \frac{J_{01}}{\omega_0\sqrt{1 - \left(\frac{J_{01}}{G_A}\right)^2}} \tag{5}$$

$$C_{j,j+1}\big|_{j=1 \text{ to } n-1} = \frac{J_{j,j+1}}{\omega_0} \tag{6}$$

$$C_{n,n+1} = \frac{J_{n,n+1}}{\omega_0\sqrt{1 - \left(\frac{J_{n,n+1}}{G_B}\right)^2}} \quad . \tag{7}$$

FIG. 8.11-1 DESIGN FORMULAS FOR CAPACITIVELY COUPLED LUMPED-ELEMENT FILTERS

The net shunt capacitances are:

$$C_1 = C_{r1} - C'_{01} - C_{12} \tag{8}$$

$$C_j\big|_{j=2 \text{ to } n-1} = C_{rj} - C_{j-1,j} - C_{j,j+1} \tag{9}$$

$$C_n = C_{rn} - C_{n-1,n} - C'_{n,n+1} \tag{10}$$

where the $C_{j,j+1}$ are given by Eqs. (5) to (7) and

$$C'_{01} = \frac{C_{01}}{1 + \left(\frac{\omega_0 C_{01}}{G_A}\right)^2} \tag{11}$$

$$C'_{n,n+1} = \frac{C_{n,n+1}}{1 + \left(\frac{\omega_0 C_{n,n+1}}{G_B}\right)^2} \quad . \tag{12}$$

For mapping low-pass prototype response approximately to band-pass response use, if $\omega_2/\omega_1 \leq 1.05$,

$$\omega' = \frac{\omega'_1}{w}\left(\frac{\omega}{\omega_0} - \frac{\omega_0}{\omega}\right) \tag{13}$$

where

$$\omega_0 = \sqrt{\omega_1 \omega_2} \tag{14}$$

$$w = \frac{\omega_2 - \omega_1}{\omega_0} \quad . \tag{15}$$

For $\omega_2/\omega_1 > 1.05$ see text for a suitable mapping and definition of w and ω_0

FIG. 8.11-1 Concluded

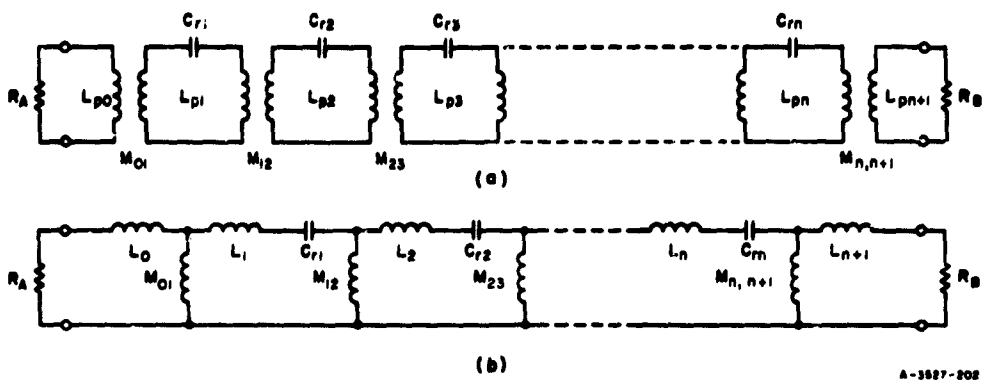

For definitions of the g_j, ω_1', ω_0, ω_1, ω_2, and the $K_{j,j+1}$: see Figs. 4.04-1, 8.02-1(a),(b), and 8.03-1(a).

Choose values for R_A, R_B, L_{r0}, L_{r1}, ..., L_{rn}, L_{rn+1} where the L_{rj} are related to the L_{pj} as indicated in Eqs. (15) to (19) below.

$$C_{rj}\Big|_{j=1 \text{ to } n} = \frac{1}{L_{rj}\omega_0^2} \tag{1}$$

$$K_{01} = \sqrt{\frac{R_A \omega_0 L_{r1} w}{g_0 g_1 \omega_1'}} \tag{2}$$

$$K_{j,j+1}\Big|_{j=1 \text{ to } n-1} = \frac{w\omega_0}{\omega_1'}\sqrt{\frac{L_{rj}L_{rj+1}}{g_j g_{j+1}}} \tag{3}$$

$$K_{n,n+1} = \sqrt{\frac{R_B \omega_0 L_{rn} w}{g_n g_{n+1} \omega_1'}} \tag{4}$$

where w is as defined below.

The mutual couplings are:

$$M_{01} = \frac{K_{01}}{\omega_0}\sqrt{1 + \left(\frac{\omega_0 L_{r0}}{R_A}\right)^2} \tag{5}$$

$$M_{j,j+1}\Big|_{j=1 \text{ to } n-1} = \frac{K_{j,j+1}}{\omega_0} \tag{6}$$

$$M_{n,n+1} = \frac{K_{n,n+1}}{\omega_0}\sqrt{1 + \left(\frac{\omega_0 L_{rn+1}}{R_B}\right)^2} \quad . \tag{7}$$

The series inductances drawn at (b) above are

$$L_0 = L_{r0} - M_{01} \tag{8}$$

FIG. 8.11-2 DESIGN FORMULAS FOR INDUCTIVELY COUPLED, LUMPED-ELEMENT FILTERS

$$L_1 = L_{r1} - M^e_{01} - M_{12} \tag{9}$$

$$L_j\Big|_{j=2 \text{ to } n-1} = L_{rj} - M_{j-1,j} - M_{j,j+1} \tag{10}$$

$$L_n = L_{rn} - M_{n-1,n} - M^e_{n,n+1} \tag{11}$$

$$L_{n+1} = L_{rn+1} - M_{n,n+1} \tag{12}$$

where

$$M^e_{01} = \frac{M_{01} + \dfrac{(L_{r0} - M_{01})\omega_0^2 M_{01} L_{p0}}{R_A^2}}{1 + \left(\dfrac{\omega_0 L_{r0}}{R_A}\right)^2} \tag{13}$$

$$M^e_{n,n+1} = \frac{M_{n,n+1} + \dfrac{(L_{rn+1} - M_{n,n+1})\omega_0^2 M_{n,n+1} L_{pn+1}}{R_B^2}}{1 + \left(\dfrac{\omega_0 L_{rn+1}}{R_B}\right)^2} \tag{14}$$

For form shown at (a) above, the L_{pj} are the total loop inductances and

$$L_{p0} = L_{r0} \tag{15}$$

$$L_{p1} = L_{r1} + M_{01} - M^e_{01} \tag{16}$$

$$L_{pj}\Big|_{j=2 \text{ to } n-1} = L_{rj} \tag{17}$$

$$L_{pn} = L_{rn} + M_{n,n+1} - M^e_{n,n+1} \tag{18}$$

$$L_{pn+1} = L_{rn+1} \tag{19}$$

For mapping low-pass response approximately to band-pass response, if $\omega_2/\omega_1 \leq 1.05$ use

$$\omega' = \frac{\omega'_1}{w}\left(\frac{\omega}{\omega_0} - \frac{\omega_0}{\omega}\right) \tag{20}$$

where

$$\omega_0 = \sqrt{\omega_1 \omega_2} \tag{21}$$

$$w = \frac{\omega_2 - \omega_1}{\omega_0} \tag{22}$$

For $\omega_2/\omega_1 > 1.05$, see text for a suitable mapping and definition of w and ω_0.

FIG. 8.11-2 Concluded

gives good results to bandwidths around 20 percent. A definition* of w for use in such cases is[1]

$$w = \left(\frac{\omega_0}{\omega_1} - \frac{\omega_0}{\omega_2}\right) \quad . \tag{8.11-3}$$

SEC. 8.12, BAND-PASS FILTERS WITH WIDE STOP BANDS[16]

All of the filter structures discussed so far that involve transmission lines tend to have additional pass bands at frequencies which are multiples of their first pass-band frequencies, or at least at frequencies which are odd multiples of their pass-band frequency. Figure 8.12-1 shows a filter structure which when properly designed can be made to be free of higher-order pass bands up to quite high frequencies. The shunt capacitances C_j' in Fig. 8.12-1 are not necessary to the operation of the device, but are stray capacitances that will usually be associated with the coupling capacitances $C_{j,j+1}$. At the pass-band center frequency of the filter, each resonator line is somewhat less than a quarter-wavelength long, as measured from its short-circuited end to its open-circuited end. (They would all be exactly a quarter-wavelength long, if it were not for the capacitive loading due to the C_j' and the $C_{j,j+1}$.) As seen from the connection points at which the resonator lines are attached, at midband the short-circuited portion of each line looks like a shunt inductance, while the open-circuited portion looks like a shunt capacitance, so the circuit is very similar to that in Fig. 8.11-1.

The circuit in Fig. 8.12-1 will tend to have additional pass bands when the length of the transmissions line resonators is roughly an odd multiple of a quarter-wavelength long. However, it can be seen that such pass bands can be suppressed if, when a line is resonant, the length from the short-circuited end of the line to the connection point is exactly one-half wavelength or a multiple thereof, while the electrical distance from the open-circuited end to the connection point is exactly an odd multiple of one-quarter wavelength. Under these conditions the connection point of such a resonator is at a voltage null, and the resonance looks like a series resonance which short-circuits the signal to ground, instead

* The definition of w used here differs from the w' that Cohn[1] uses for this case, by a factor of ω_0/ω_1'. This fact is consistent with the equations used herein and gives the same end result. The w defined here is fractional bandwidth, while Cohn's w' is not.

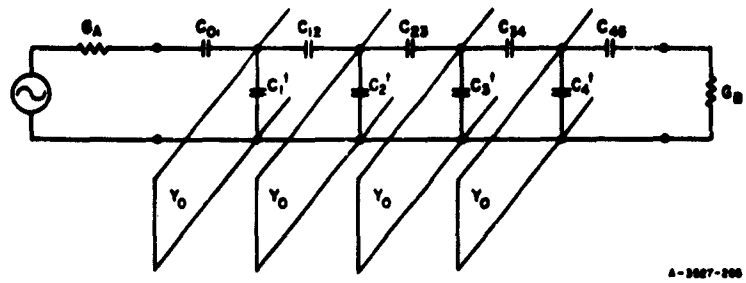

For definitions of the g_j, ω_1', ω_0, ω_1, ω_2, and the $J_{j,j+1}$; see Figs. 4.04-1, 8.02-1(a),(b), 8.02-4, and 8.03-2(b).

Choose values for G_A, G_B, and Y_0 and estimate:

$$B_1^J = \left(\frac{\omega_0 C_{01}}{1 + \left(\frac{\omega_0 C_{01}}{G_A} \right)^2} + \omega_0 C_1' + \omega_0 C_{12} \right) \qquad (1)$$

$$B_j^J\Big|_{j=2 \text{ to } n-1} = (\omega_0 C_{j-1,j} + \omega_0 C_j' + \omega_0 C_{j,j+1}) \qquad (2)$$

$$B_n^J = \left(\omega_0 C_{n-1,n} + \omega_0 C_n' + \frac{\omega_0 C_{n,n+1}}{1 + \left(\frac{\omega_0 C_{n,n+1}}{G_B} \right)^2} \right) . \qquad (3)$$

Obtain slope parameters b_j from the B_j^J, Y_0, and Fig. 8.12-2 or Fig. 8.12-3 or Eq. (8.12-4).

$$J_{01} = \sqrt{\frac{G_A b_1 w}{g_0 g_1 \omega_1'}} \qquad (4)$$

$$J_{j,j+1}\Big|_{j=1 \text{ to } n-1} = \frac{w}{\omega_1'} \sqrt{\frac{b_j b_{j+1}}{g_j g_{j+1}}} \qquad (5)$$

$$J_{n,n+1} = \sqrt{\frac{G_B b_n w}{g_n g_{n+1} \omega_1'}} \qquad (6)$$

(Continued on p. 484)

FIG. 8.12-1 DATA FOR BAND-PASS FILTERS WITH WIDE STOP BANDS

where w is given by (11) below.

$$\omega_0 C_{01} = \frac{J_{01}}{\sqrt{1 - \left(\frac{J_{01}}{G_A}\right)^2}} \tag{7}$$

$$\omega_0 C_{j,j+1}\Big|_{j=1 \text{ to } n-1} = J_{j,j+1} \tag{8}$$

$$\omega_0 C_{n,n+1} = \frac{J_{n,n+1}}{\sqrt{1 - \left(\frac{J_{n,n+1}}{G_B}\right)^2}} \; . \tag{9}$$

For mapping low-pass prototype response approximately to band-pass response use

$$\omega' = \frac{2\omega_1'}{w}\left(\frac{\omega - \omega_0}{\omega}\right) \tag{10}$$

where

$$w = 2\left(\frac{\omega_2 - \omega_1}{\omega_2 + \omega_1}\right) \tag{11}$$

and

$$\omega_0 = \frac{2\omega_2\omega_1}{\omega_2 + \omega_1} \tag{12}$$

FIG. 8.12-1 Concluded

of a shunt resonance which passes the signal. Since for this higher resonance the connection point has zero voltage, the C_j^t and the $C_{j,j+1}$ have no effect on the higher resonant frequency. By designing the various resonators to suppress different pass bands, it should be possible to make the stop band extend very far without any spurious pass bands.

The B_j^J in Eqs. (1) to (3) in Fig. 8.12-1 are susceptances which account for effects of the C_j^t and $C_{j,j+1}$ on the tuning of the resonators and on their susceptance slope parameters at the midband frequency ω_0. The total susceptance of the jth resonator is then

$$B_j(\omega) = Y_0 \tan\left(\frac{\theta_{aj}\omega}{\omega_0}\right) - Y_0 \cot\left(\frac{\theta_{bj}\omega}{\omega_0}\right) + \frac{\omega}{\omega_0} B_j^J \qquad (8.12\text{-}1)$$

where Y_0 is the characteristic admittance of the resonator line, θ_{aj} is the electrical length of the open-circuited portion of the resonator line at frequency ω_0, and θ_{bj} is the electrical length of the short-circuited portion at the same frequency. At frequency ω_0 we require that $B_j(\omega_0) = 0$ which calls for

$$\frac{B_j^J}{Y_0} = \cot\theta_{bj} - \tan\theta_{aj} \quad . \qquad (8.12\text{-}2)$$

In order to short-circuit pass bands at $3\omega_0$ or $5\omega_0$, etc., it is only necessary that $\theta_{aj} = \theta_{bj}/2$, or $\theta_{aj} = \theta_{bj}/4$, etc., respectively, as previously discussed. Having related θ_{aj} and θ_{bj}, one may solve Eq. (8.12-2) for the total electrical length required at frequency ω_0 in order to give resonance in the presence of the susceptance B_j^J. If l_j is the resonator length, then

$$\frac{l_j}{\lambda_0/4} = \frac{\theta_{aj} + \theta_{bj}}{\pi/2} \qquad (8.12\text{-}3)$$

where λ_0 is the wavelength in the medium of propagation at the frequency ω_0. Applying Eq. (1) of Fig. 8.02-4 to Eq. (8.12-1) gives, for the susceptance slope parameter b_j normalized with respect to Y_0,

$$\frac{b_j}{Y_0} = \frac{1}{2}\left[\frac{\theta_{aj}}{\cos^2 \theta_{aj}} + \frac{\theta_{bj}}{\sin^2 \theta_{bj}} + \frac{B_j^J}{Y_0}\right] . \qquad (8.12\text{-}4)$$

Figure 8.12-2 shows a plot of $l_j/(\lambda_0/4)$ and b_j/Y_0 *vs.* B_j^J/Y_0 for resonators which are to suppress transmission at the $3\omega_0$ pass band. Figure 8.12-3 shows corresponding data for resonators designed to suppress the pass band in the vicinity of $5\omega_0$.

When using the design data in Figs. 8.12-1 to 8.12-3, some iteration in the design calculations will be necessary if high accuracy is desired.

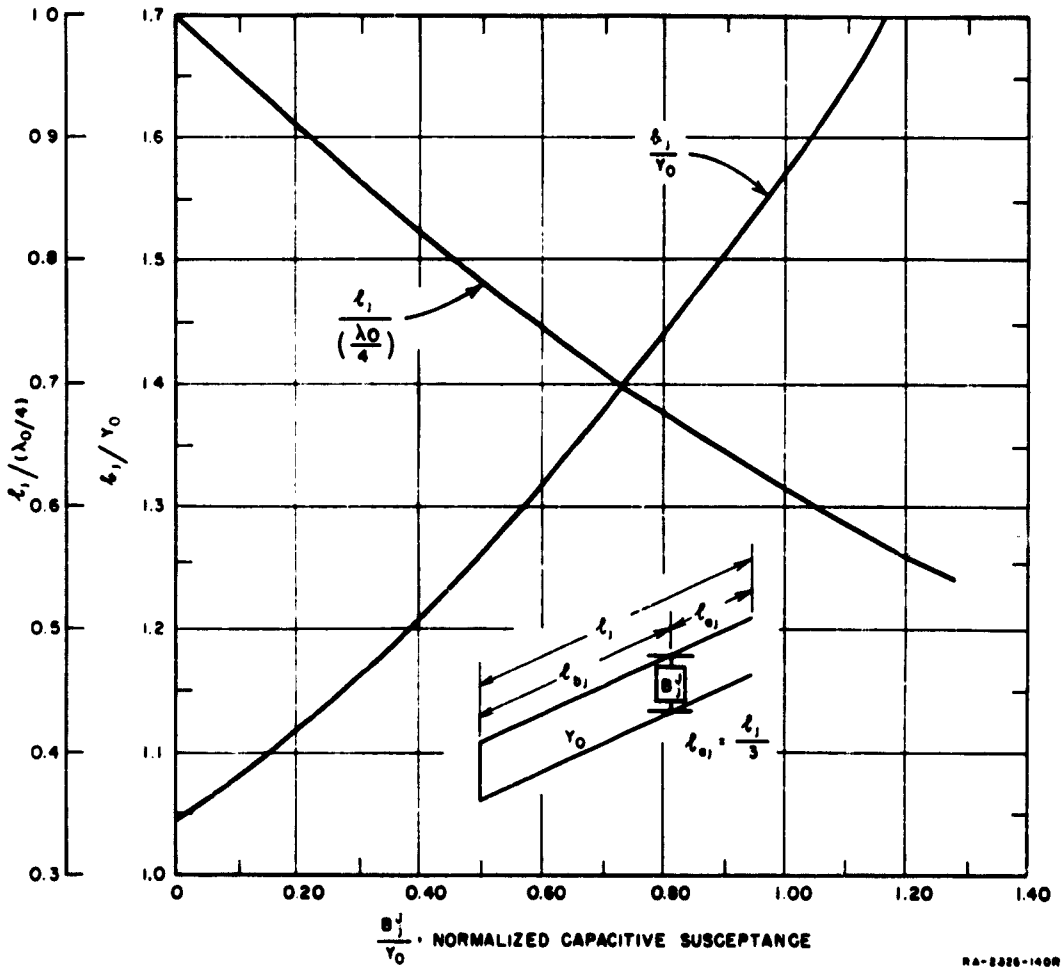

FIG. 8.12-2 CHART FOR DESIGN OF RESONATORS TO SUPPRESS THE SPURIOUS PASS BAND IN THE VICINITY OF $3\omega_0$

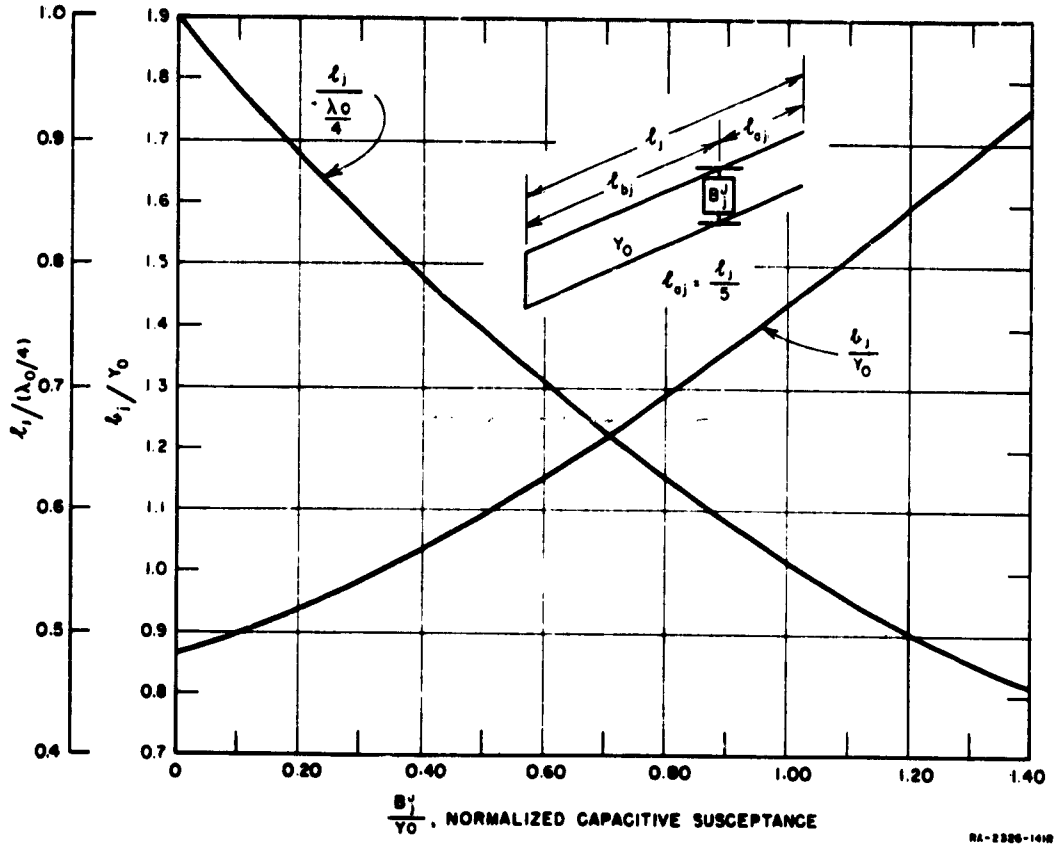

FIG. 8.12-3 CHART FOR DESIGN OF RESONATORS TO SUPPRESS THE SPURIOUS PASS BAND IN THE VICINITY OF $5\omega_0$

This is because the B_j^J must be known in order to compute the coupling capacitances $C_{j,j+1}$ (and usually the C_j^t) accurately, while in turn the $C_{j,j+1}$ and C_j^t must be known in order to determine the B_j^J accurately. However, since the B_j^J generally have a relatively minor influence on the coupling capacitance values $C_{j,j+1}$ required, the calculations converge quickly and are not difficult. First the B_j^J are estimated and corresponding values of the $C_{j,j+1}$ and C_j^t are obtained. Then improved values for the B_j^J are computed, and from them improved values for the $C_{j,j+1}$ and $\ell_j/(\lambda_0/4)$ are obtained. These latter values should be sufficiently accurate.

Figure 8.12-4 shows a possible form of construction for the filters under consideration. The resonators are in 50-ohm (Y_0 = 0.020 mhos)

rectangular-bar strip-transmission-line form, with small coupling tabs between the resonator bars. The spacing between resonators has been shown to give adequate isolation between resonators as evidenced by tests on trial, two-resonator and four-resonator designs.[16] Figure 8.12-5(a) shows a plot of estimated coupling capacitance $C_{j,j+1}$ *vs.* gap spacing y for various amounts of coupling tab overlap x. The similar data in Fig. 8.12-5(b) are for the shunt capacitance to ground $C^s_{j,j+1}$ of an individual tab in the $j,j+1$th coupling. Using the data in Fig. 8.12-5(b), the junction capacitance C^t_j for the jth junction is

$$C^t_j = C^s_{j-1,j} + C^s_{j,j+1} + C^* \qquad (8.12\text{-}5)$$

where C^* introduces an additional junction shunt susceptance like that for the T-junctions in Sec. 5.07. Calculations from measurements on the two-resonator filter mentioned above suggest that C^* should be taken as

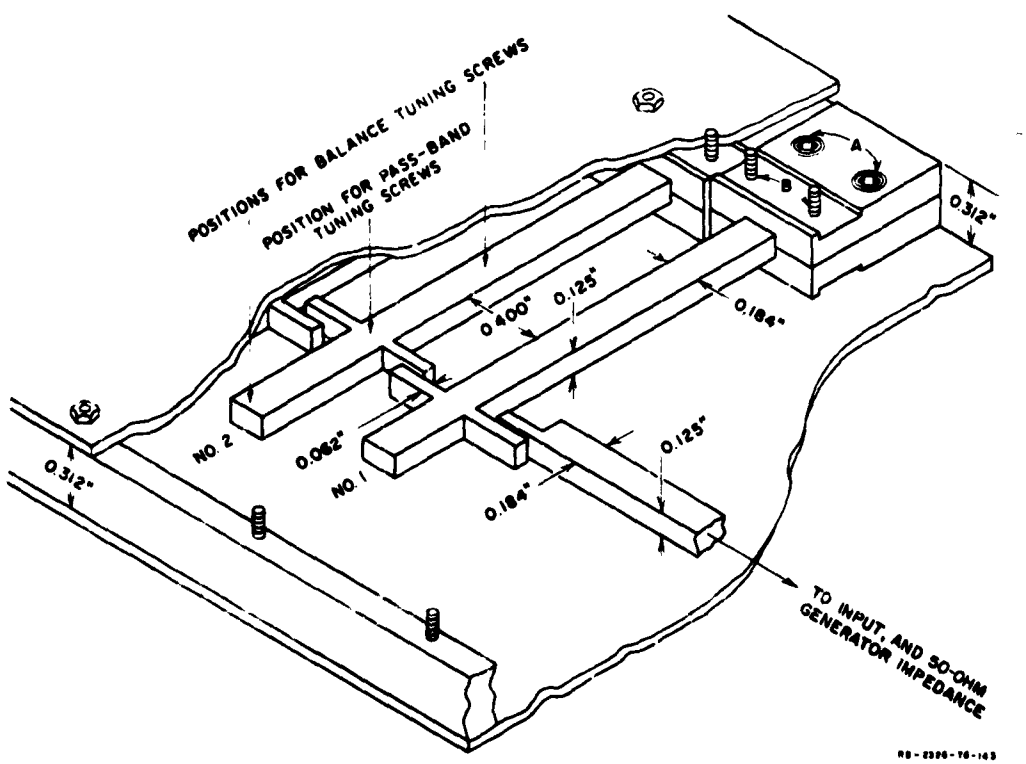

FIG. 8.12-4 A BAR TRANSMISSION LINE CONSTRUCTION FOR THE FILTER IN FIG. 8.12-1

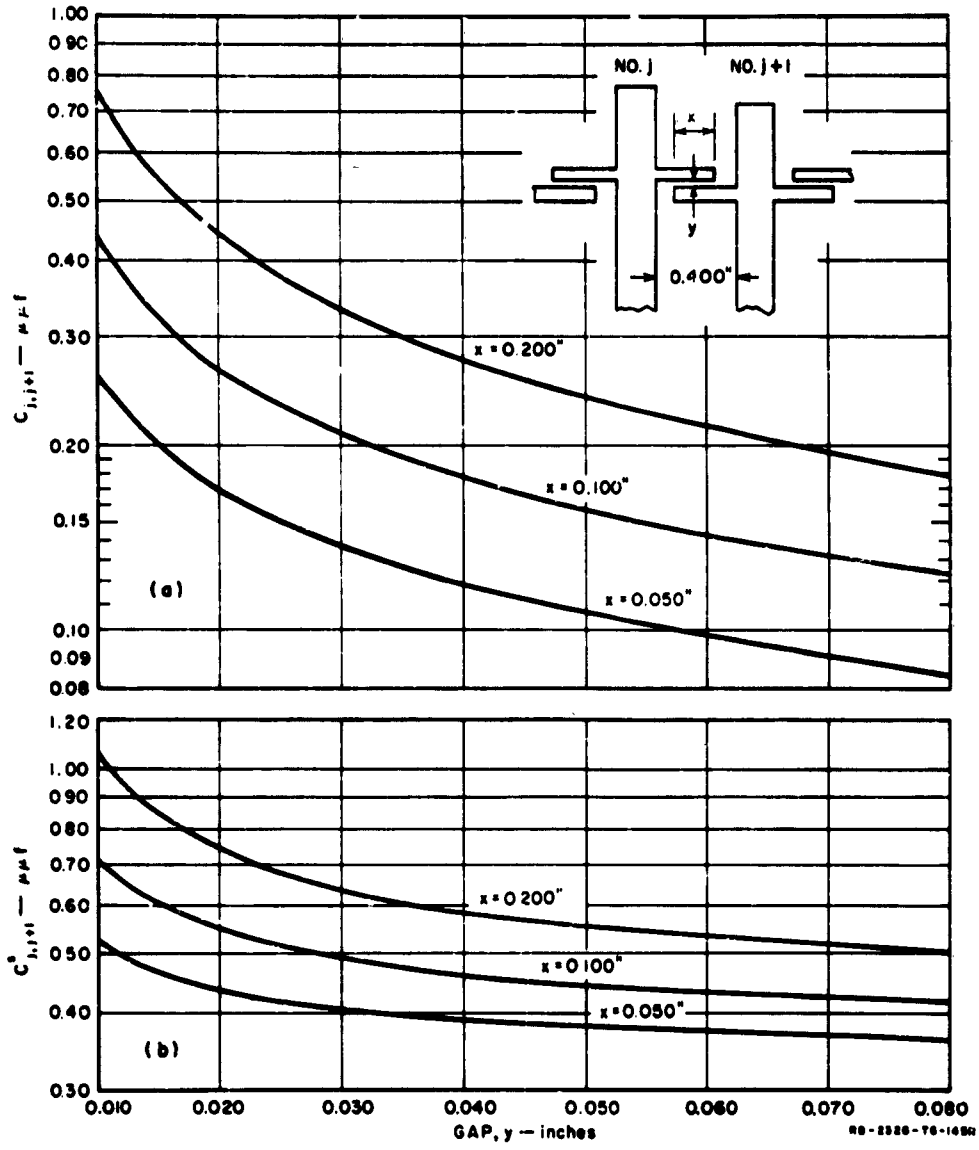

FIG. 8.12-5 CHARTS OF ESTIMATED VALUES OF THE CAPACITANCES ASSOCIATED WITH THE COUPLINGS FOR THE CONSTRUCTION IN FIG. 8.12-4

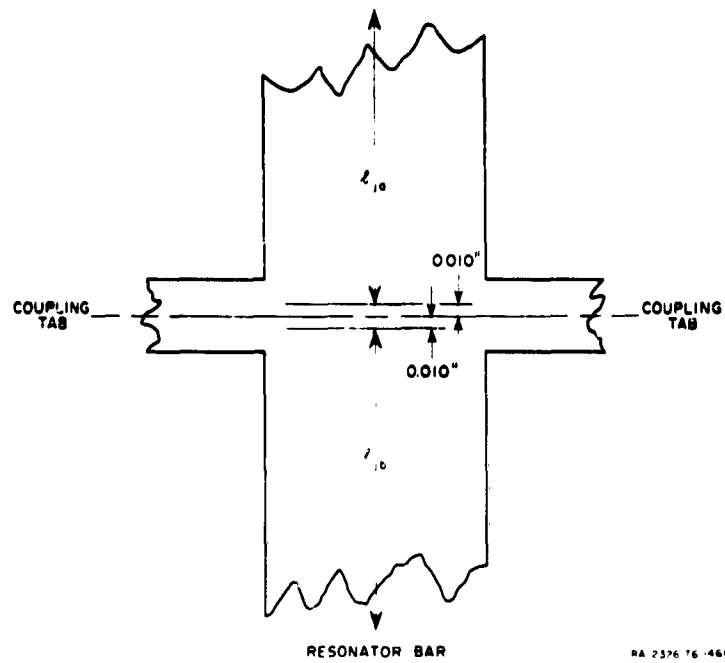

FIG. 8.12-6 DEFINITION OF THE JUNCTION REFERENCES PLANES FOR THE CONSTRUCTION IN FIG. 8.12-4

about -0.10 inf.* Approximate reference planes for fixing the lengths of the open- and short-circuited sides of the resonator are shown in Fig. 8.12-6. In fixing the length of the open-circuited end, allowance must be made for the fringing capacitance from the end of the bar. It is estimated that, in order to correct for this capacitance, the length $l_{a)}$ (see Figs. 8.12-2, -3, -6) should be reduced by about 0.055 inch.

The two-resonator filter built in the construction in Fig. 8.12-4 was intended to suppress the 3% pass band, but at first did not do so. The reason was that the open- and short-circuited sides of the resonators did not reflect short-circuits to the connection points at exactly the same frequencies, as they must for high attenuation. To correct this, "balance" tuning screws were added at two points on each resonator indicated by the arrows in Fig. 8.12-4. In addition, pass-band tuning screws were placed directly over the coupling-tab junction of each resonator.

* The negative sign merely indicates that with the junction reference planes being used, some capacitance must be subtracted in order to represent the junction.

The balance screws were adjusted first to give high attenuation in the vicinity of $3\omega_0$ and then the pass-band tuning screws were adjusted using the procedure discussed in Sec. 11.05. Since the pass-band tuning screws are at a voltage null point for the resonance in the vicinity of $3\omega_0$, the adjustment of the pass-band tuning screws will not affect the balance tuning adjustment of the resonators. However, it should be noted that the balance adjustment must be made before the pass-band tuning adjustment since the setting of the balance tuning screws will affect the pass-band tuning.

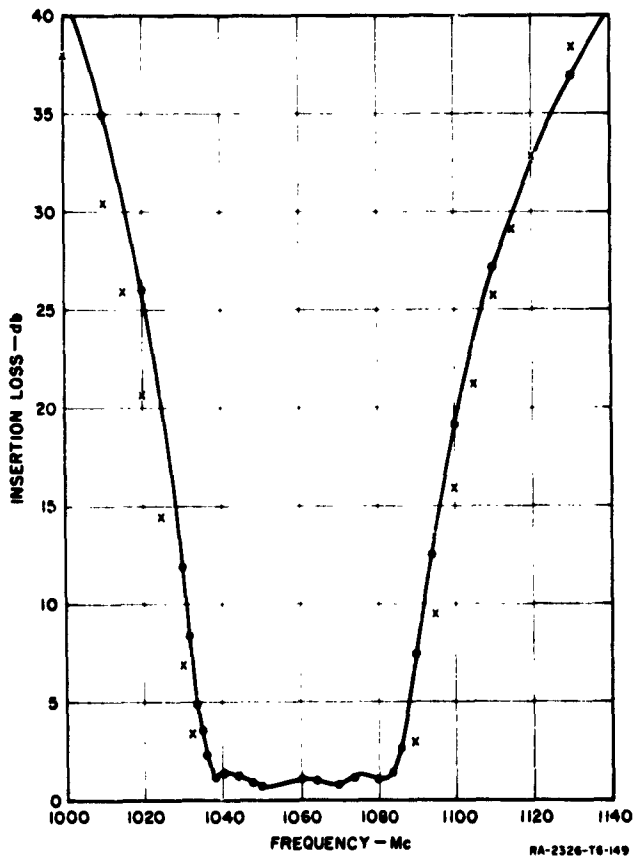

FIG. 8.12-7 THE MEASURED RESPONSE OF A FOUR-RESONATOR FILTER OF THE FORM IN FIG. 8.12-4
The solid line is the measured response while the x's represent attenuation values mapped from the low-pass prototype using Eq. (10) in Fig. 8.12-1

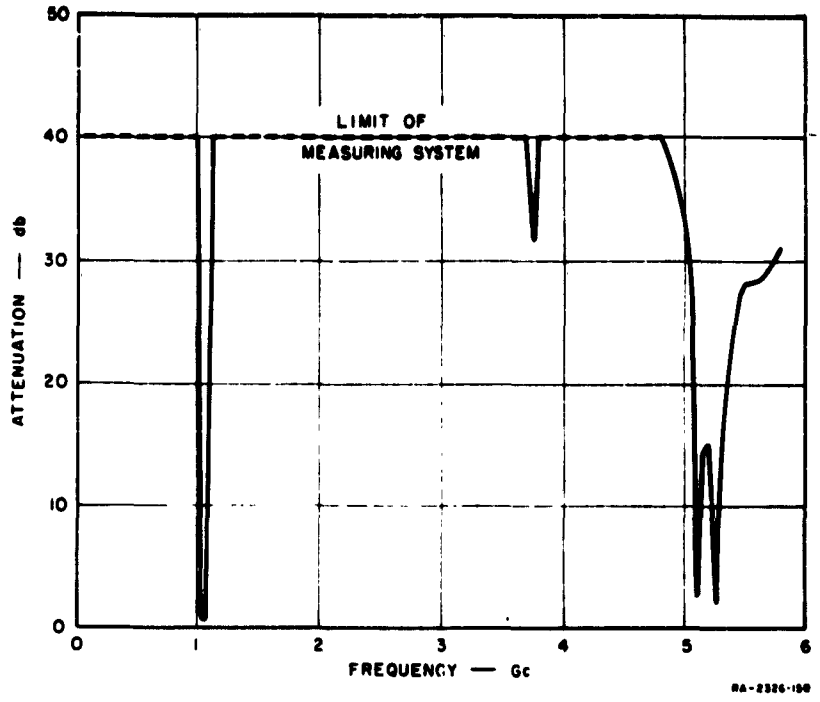

FIG. 8.12-8 THE STOP-BAND RESPONSE OF A FOUR-RESONATOR FILTER OF THE FORM IN FIG. 8.12-4

Figures 8.12-7 and 8.12-8 show the measured response of a four-resonator filter constructed in the form in Fig. 8.12-4 using the design data discussed above. As can be seen from Fig. 8.12-7, the bandwidth is about 10 percent narrower than called for by the points mapped from the low-pass prototype (which are indicated by x's). This is probably due largely to error in the estimated coupling capacitances in Fig. 8.12-5. If desired, this possible source of error can be compensated for by using values of w which are 10 percent larger than actually required. The approximate mapping used is seen to be less accurate on the high side of the response in Fig. 8.12-7 than on the low side for this type of filter.

The four-resonator filter discussed above was designed using one pair of resonators to suppress the $3\omega_0$ resonance and a second pair to suppress the $5\omega_0$ resonance. Since the two sets of resonators had their higher resonances at somewhat different frequencies it was hoped that balance tuning would be unnecessary. This was practically true for the $3\omega_0$ resonance since high attenuation was attained without balance tuning of the

resonators intended to suppress that resonance. However, there was a small dip in attenuation at about 3.8 kMc (see Fig. 8.12-8) which probably could easily have been removed by balance tuning.

The pass band near $5\omega_0$ would not disappear in this case no matter how the balance screws were adjusted on the resonators meant to suppress that pass band. Some experimentation with the device suggested that this was due to a resonance effect in the coupling tabs, which was greatly aggravated by the fact that the resonators involved were the end resonators (which have relatively large coupling capacitances). This difficulty can probably be avoided by putting the resonators to suppress pass bands near $5\omega_0$ or higher in the interior of the filter and putting the resonators to suppress the pass band near $3\omega_0$ at the ends of the filter. Also, keeping the coupling tabs as short as possible should help.

SEC. 8.13. COMB-LINE, BAND-PASS FILTERS

Figure 8.13-1(a) shows a comb-line band-pass filter in strip-line form and Fig. 8.13-1(b) presents design equations for this type of filter. The resonators consist of line elements which are short-circuited at one end, with a lumped capacitance C_j^s between the other end of each resonator line element and ground. In Fig. 8.13-1(a) Lines 1 to n, along with their associated lumped capacitances C_1^s to C_n^s comprise resonators, while Lines 0 and $n + 1$ are not resonators but simply part of impedance-transforming

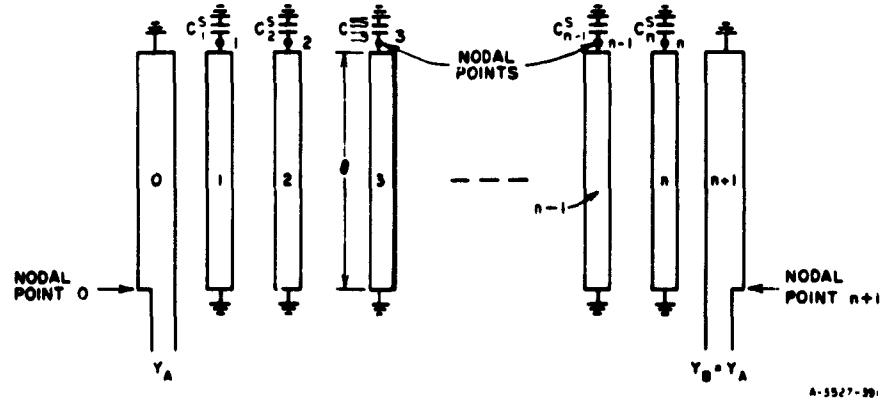

FIG. 8.13-1(a) A COMB-LINE, BAND-PASS FILTER
These nodal points are defined for use in the design equation derivations discussed in Sec. 8.14

Choose the normalized characteristic admittances Y_{ej}/Y_A so as to give good resonator unloaded Q's. (See text.) Then compute:

$$\left.\frac{b_j}{Y_A}\right|_{j=1 \text{ to } n} = \frac{Y_{ej}}{Y_A}\left(\cot\theta_0 + \frac{\theta_0 \csc^2\theta_0}{2}\right) \tag{1}$$

where θ_0 is the electrical length of the resonator elements at the mid-band frequency ω_0.

Compute:

$$\frac{G_{T1}}{Y_A} = \frac{w\frac{b_1}{Y_A}}{g_0 g_1 \omega_1'} \tag{2}$$

$$\left.\frac{J_{j,j+1}}{Y_A}\right|_{j=1 \text{ to } n-1} = \frac{w}{\omega_1'}\sqrt{\frac{(b_j/Y_A)(b_{j+1}/Y_A)}{g_j g_{j+1}}} \tag{3}$$

$$\frac{G_{Tn}}{Y_A} = \frac{w\left(\frac{b_n}{Y_A}\right)}{g_n g_{n+1}\omega_1'} \tag{4}$$

where w is the fractional bandwidth defined below.

The normalized capacitances per unit length between each line and ground are

$$\frac{C_0}{\epsilon} = \frac{376.7\,Y_A}{\sqrt{\epsilon_r}}\left(1 - \sqrt{\frac{G_{T1}}{Y_A}}\right)$$

$$\frac{C_1}{\epsilon} = \frac{376.7\,Y_A}{\sqrt{\epsilon_r}}\left(\frac{Y_{e1}}{Y_A} - 1 + \frac{G_{T1}}{Y_A} - \frac{J_{12}}{Y_A}\tan\theta_0\right) + \frac{C_0}{\epsilon}$$

$$\left.\frac{C_j}{\epsilon}\right|_{j=2 \text{ to } n-1} = \frac{376.7\,Y_A}{\sqrt{\epsilon_r}}\left(\frac{Y_{ej}}{Y_A} - \frac{J_{j-1,j}}{Y_A}\tan\theta_0 - \frac{J_{j,j+1}}{Y_A}\tan\theta_0\right) \tag{5}$$

$$\frac{C_n}{\epsilon} = \frac{376.7\,Y_A}{\sqrt{\epsilon_r}}\left(\frac{Y_{en}}{Y_A} - 1 + \frac{G_{Tn}}{Y_A} - \frac{J_{n-1,n}}{Y_A}\tan\theta_0\right) + \frac{C_{n+1}}{\epsilon}$$

$$\frac{C_{n+1}}{\epsilon} = \frac{376.7\,Y_A}{\sqrt{\epsilon_r}}\left(1 - \sqrt{\frac{G_{Tn}}{Y_A}}\right)$$

FIG. 8.13-1(b) DESIGN EQUATIONS FOR COMB-LINE FILTERS

where ϵ is the absolute dielectric constant of the medium of propagation, and ϵ_r is the relative dielectric constant.

The normalized mutual capacitances per unit length between adjacent lines are:

$$\frac{C_{01}}{\epsilon} = \frac{376.7\ Y_A}{\sqrt{\epsilon_r}} - \frac{C_0}{\epsilon}$$

$$\left.\frac{C_{j,j+1}}{\epsilon}\right|_{j=1 \text{ to } n-1} = \frac{376.7\ Y_A}{\sqrt{\epsilon_r}} \left(\frac{J_{j,j+1}}{Y_A} \tan \theta_0\right) \tag{6}$$

$$\frac{C_{n,n+1}}{\epsilon} = \frac{376.7\ Y_A}{\sqrt{\epsilon_r}} - \frac{C_{n+1}}{\epsilon} \quad .$$

The lumped capacitances C_j^s are:

$$\left.C_j^s\right|_{j=1 \text{ to } n} = Y_A\left(\frac{Y_{oj}}{Y_A}\right) \frac{\cot \theta_0}{\omega_0} \quad . \tag{7}$$

A suggested low-pass to band-pass transformation is

$$\frac{\omega'}{\omega_1'} = \frac{2}{w}\left(\frac{\omega - \omega_0}{\omega_0}\right) \tag{8}$$

where

$$w = \frac{\omega_2 - \omega_1}{\omega_0} \tag{9}$$

and

$$\omega_0 = \frac{\omega_2 + \omega_1}{2} \quad . \tag{10}$$

FIG. 8.13-1(b) Concluded

sections at the ends. Coupling between resonators is achieved in this type of filter by way of the fringing fields between resonator lines. With the lumped capacitors C_j^s present, the resonator lines will be less than $\lambda_0/4$ long at resonance (where λ_0 is the wavelength in the medium of propagation at midband), and the coupling between resonators is predominantly magnetic in nature. Interestingly enough, if the capacitors C_j^s were not present, the resonator lines would be a full $\lambda_0/4$ long at resonance, *and the structure would have no pass band!*[17] This is so because, without some kind of reactive loading at the ends of the resonator line elements, the magnetic and electric coupling effects cancel each other out, and the comb-line structure becomes an all-stop structure.*

For the reasons described above, it is usually desirable to make the capacitances C_j^s in this type of filter sufficiently large that the resonator lines will be $\lambda_0/8$ or less, long at resonance. Besides having efficient coupling between resonators (with sizeable spacings between adjacent resonator lines), the resulting filter will be quite small. In this type of filter, the second pass band occurs when the resonator line elements are somewhat over a half-wavelength long, so if the resonator lines are $\lambda_0/8$ long at the primary pass band, the second pass band will be centered at somewhat over four times the frequency of the center of the first pass band. If the resonator line elements are made to be less than $\lambda_0/8$ long at the primary pass band, the second pass band will be even further removed. Thus, like the filter in Sec. 8.12, comb-line filters also lend themselves to achieving very broad stop bands above their primary pass bands.

Since the coupling between the resonators is distributed in nature, it is convenient to work out the design of the resonator lines in terms of their capacitance to ground C_j per unit length, and the mutual capacitances $C_{j,j+1}$ per unit length between neighboring lines j and $j + 1$. These capacitances are illustrated in the cross-sectional view of the line elements shown in Fig. 8.13-2. Fringing capacitance effects beyond nearest neighbors will be neglected. Figure 8.13-2 also defines various dimensions for the case where the resonator lines are to be constructed in rectangular-bar strip line. Using the design formulas in Fig. 8.13-1(b), the distributed line capacitances will be computed in normalized form to

* However, if every other unloaded, $\lambda_0/4$ resonator were turned end for end so that the structure had open- and short-circuited ends alternating, the band-stop structure would become a band-pass structure. The resulting configuration is that of the interdigital filters discussed in Secs. 10.06 and 10.07.

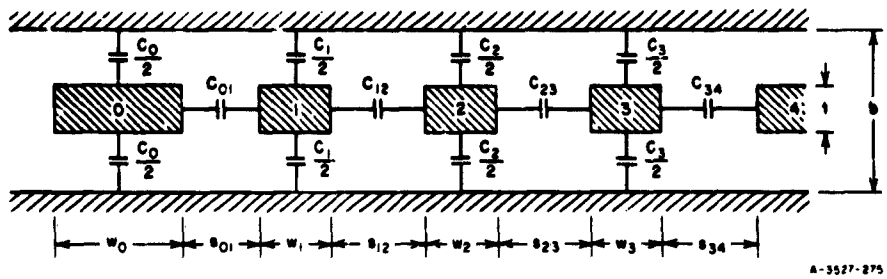

FIG. 8.13-2 DEFINITIONS OF THE LINE CAPACITANCES AND SOME OF THE DIMENSIONS INVOLVED IN COMB-LINE FILTER DESIGN

give C_j/ϵ and $C_{j,j+1}/\epsilon$ values, where ϵ is the absolute dielectric constant of the medium of propagation. Then by use of the charts and formulas in Sec. 5.05 the corresponding rectangular-bar line dimensions w_j and $s_{j,j+1}$ in Fig. 8.13-2 can be determined for specified t and b.

To carry out the design of a comb-line filter by use of Fig. 8.13-1(b), the low-pass prototype filter parameters g_0, g_1, ..., g_{n+1} and ω_1' are selected in the usual manner (Secs. 8.02 and 8.04). The low pass to band-pass mapping indicated in Eqs. (8) to (10) is a commonly used, simplified, narrow-band mapping, but unfortunately it is not outstandingly accurate for this type of filter when the bandwidth is as large as 10 percent or so. From the trial design described below, the largest error is seen to occur on the high side of the pass band where the narrow-band mapping does not predict as large a rate of cutoff as actually occurs. The reason that the actual rate of cutoff tends to be unusually large on the high-frequency side of the pass band is that the structure has infinite attenuation (theoretically) at the frequency for which the resonator lines are a quarter-wavelength long. Thus, the steepness of the attenuation characteristic on the high side will depend to some extent upon the choice of θ_0, the electrical length of the resonator lines at the pass-band center frequency. Although the simplified mapping in Eqs. (8) to (10) of Fig. 8.13-1(b) cannot account for these more subtle effects in the response of this type of filter, it is sufficiently accurate to serve as a useful guide in estimating the number of resonators required for a given application.

Next the terminating line admittance Y_A, the midband electrical length θ_0 of the resonator lines, the fractional bandwidth w, and the normalized line admittances Y_{oj}/Y_A must all be specified. As indicated above, it is

usually desirable to make $\theta_0 = \pi/4$ radians or less. The choice of the resonator line admittances Y_{aj} fixes the admittance level within the filter, and this is important in that it influences the unloaded Q's that the resonators will have. At the time of this writing the line characteristic admittances to give optimum unloaded Q's for structures of this type have not been determined. However, choosing the Y_{aj} in Eq. (1) of Fig. 8.13-1(b) to correspond to about 0.0143 mho (*i.e.*, about 70 ohms), appears to be a reasonable choice. [The admittance Y_{aj} in Fig. 8.13-1(b) is interpreted physically as the admittance of Line j with the adjacent Lines $j - 1$ and $j + 1$ grounded.] The remainder of the calculations procced in a straightforward manner as presented in the figure. As mentioned above, having the C_j/ϵ and $C_{j,j+1}/\epsilon$, the required line dimensions are obtained from the data in Sec. 5.05.

Table 8.13-1 summarizes various parameters used and computed in the design of a trial four-resonator, comb-line filter designed for a fractional bandwidth of $w = 0.10$, and 0.1-db Tchebyscheff ripple. Due to a misprint in the table of prototype-filter element values which were used for the design of this filter, the g_1 element value is, unfortunately, off by about 10 percent. However, a computed response for this filter revealed that this error should not have any sizeable effect on the shape of the response. In this design $\theta_0 = \pi/4$ radians so that the resonator lines are $\lambda_0/8$ long at the midband frequency, which was to be 1.5 Gc.

Table 8.13-1

VARIOUS PARAMETERS WHICH WERE SPECIFIED OR COMPUTED IN THE DESIGN OF THE TRIAL, FOUR-RESONATOR, COMB-LINE FILTER

j	$\frac{J_{j,j+1}}{Y_A}$	$\frac{C_{j,j+1}}{\epsilon}$	$s_{j,j+1}$ (inches)	j	$\frac{C_j}{\epsilon}$	w_j (inches)
0 and 4		2.130	0.116	0 and 5	5.404	0.362
1 and 3	0.0730	0.550	0.337	1 and 4	3.022	0.152
2	0.0572	0.431	0.381	2 and 3	4.119	0.190

$g_0 = 1$	$g_3 = 1.7703$	$w = 0.10$	$\theta_0 = \pi/4$ radian
$g_1 = 1.0880^*$	$g_4 = 0.8180$	$Y_A = 0.020$ mho	$b = 0.625$ inch
$g_2 = 1.3061$	$g_5 = 1.3554$	$b_j/Y_A = 0.870$	$t = 0.188$ inch
	$\omega_1' = 1$	$Y_{aj}/Y_A = 0.677$ $j=1$ to 4	

* This value should have been $g_1 = 1.1088$ for a true 0.1-db ripple prototype.

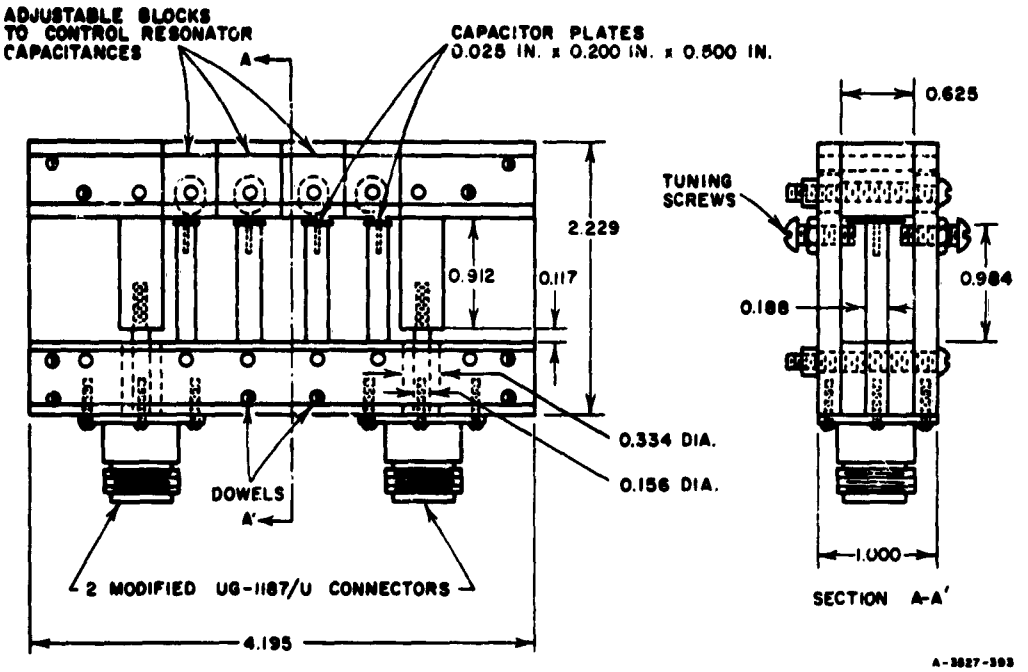

FIG. 8.13-3 DRAWING OF THE TRIAL, FOUR-RESONATOR, COMB-LINE FILTER
Additional dimensions of electrical importance are given in Table 8.13-1

Note that $Y_{ej}/Y_A = 0.677$ which with $Y_A = 0.020$ mho makes $Y_{ej} = 0.0135$ mho, or $1/Y_{ej} = 74$ ohms. The electrically important dimensions of this filter are summarized in Table 8.13-1 along with Figs. 8.13-2 and 3. Figure 8.13-4 shows the completed filter with its cover plate removed.

The filter was tuned using a slotted line and the alternating short-circuit and open-circuit procedure described in Sec. 11.05. To adjust the capacitance of an individual resonator, first its sliding block (shown in Fig. 8.13-3) was adjusted to give slightly less than the required resonator capacitance, and then the tuning screws on the resonator were used to bring the resonator to the exact desired frequency. In this case the bandwidth was sufficiently large so that the alternating short-circuit and open-circuit procedure did not give entirely satisfactory results as evidenced by some lack of symmetry in the pass-band response. However, it was found that this could be easily corrected by readjusting the tuning screws on the end resonators* while using a sweep-generator and recording-reflectometer

* Since the end resonators have adjacent couplings which are quite different from those of the interior resonators, it is usually the end resonators that cause tuning difficulties when using the alternating short-circuit and open-circuit procedure.

set-up. After the tuning was completed, the measured input VSWR was as shown in Fig. 8.13-5 and the measured attenuation as shown in Fig. 8.13-6.

The VSWR characteristic in Fig. 8.13-5 corresponds to roughly a 0.2-db Tchebyscheff ripple rather than a 0.1-db ripple. The discrepancy is believed to be due to the fact that coupling effects beyond nearest-neighbor lines have been neglected in the design procedure in Fig. 8.13-1. If a smaller ripple were necessary, this could be achieved by small adjustment of the spacings s_{01} and s_{45} between the input line and the first

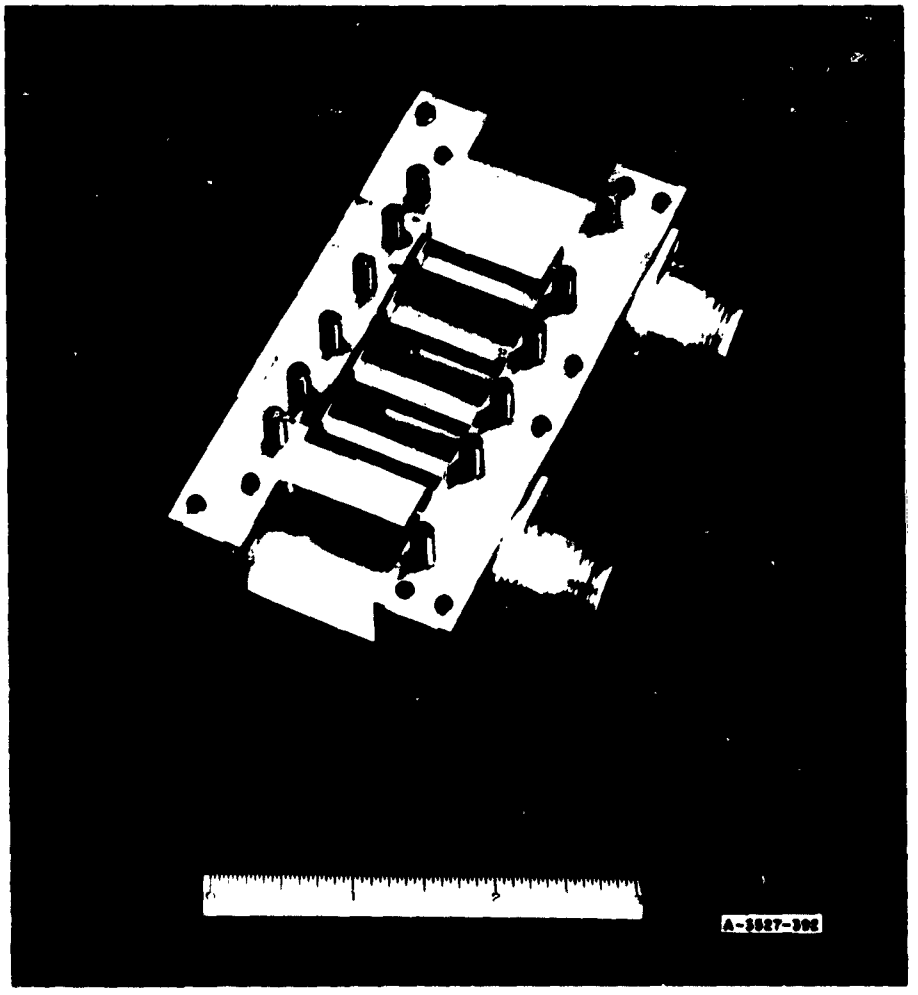

FIG. 8.13-4 A FOUR-RESONATOR COMB-LINE FILTER WITH ITS COVER PLATE REMOVED

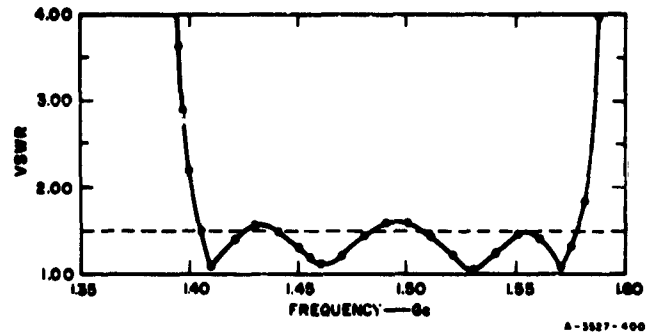

FIG. 8.13-5 MEASURED VSWR OF THE FILTER IN FIG. 8.13-4

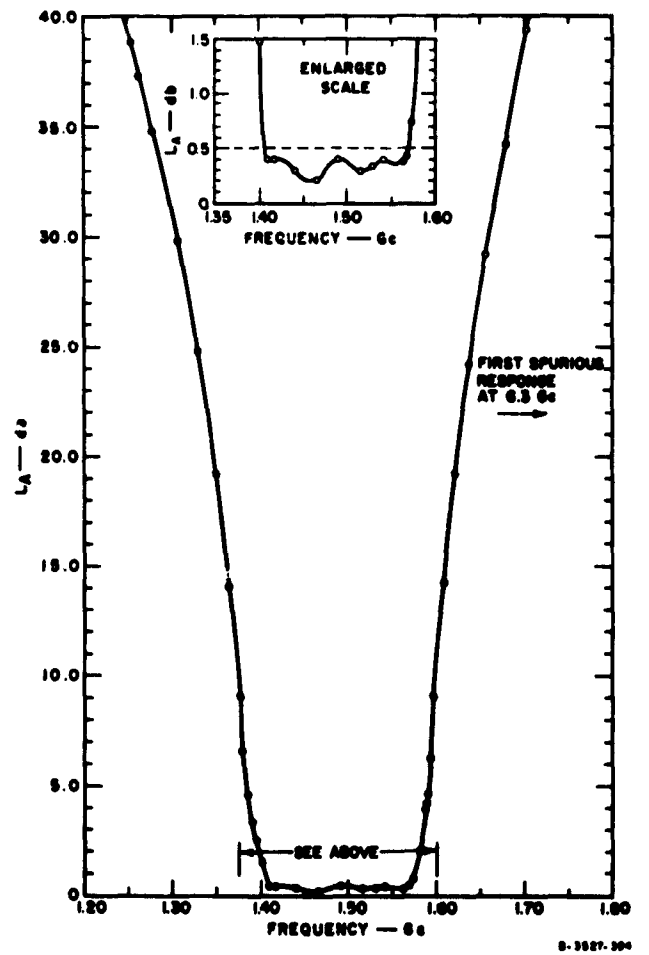

FIG. 8.13-6 MEASURED ATTENUATION OF THE FILTER IN FIG. 8.13-4

resonator, and between Resonator 4 and the output line. A similar phenomenon occurred in the interdigital line filter example discussed in Sec. 10.06. In that case the size of the ripples was easily reduced by decreasing the sizes of end-gap spacings s_{01} and $S_{n,n+1}$. In the case of Fig. 8.13-5, the ripples were not considered to be sufficiently oversized to warrant expenditure of time on additional adjustments.

From the VSWR characteristic in Fig. 8.13-5 the measured fractional bandwidth at the equal-VSWR-ripple level is found to be $w = 0.116$ instead of the specified $w = 0.100$. This somewhat oversize bandwidth may also be due to coupling effects beyond nearest neighbor line elements, which were neglected in the derivation of the design equations in Fig. 8.13-1(b). Table 8.13-2 compares attenuation values computed by use of the mapping Eqs. (8) to (10) of Fig. 8.13-1(b) as compared to the actual measured values. Conditions A are for the original specifications while Conditions B are for the $w = 0.116$ fractional bandwidth and approximately 0.2-db ripple indicated by the VSWR characteristic in Fig. 8.13-5. Note that in either case the attenuation predicted by the mapping for $f = 1.25$ Gc (f below f_0) has come out close to being correct, while the attenuation predicted by the mapping for $f = 1.70$ Gc (f above f_0) is somewhat low, for reasons previously discussed.

Table 8.13-2

COMPARISON OF ATTENUATION VALUES OBTAINED BY MAPPING AND BY MEASUREMENT

	MAPPING CONDITIONS	f (Gc)	L_A BY MAPPING (db)	L_A MEASURED (db)
A	Original Specifications, $w = 0.10$, 0.10-db Tchebyscheff Ripple, $f_0 = 1.491$ Gc	1.25	41.5	39
		1.70	36.5	39
B	Measured Specifications, $w = 0.116$, 0.20-db Tchebyscheff Ripple, $f_0 = 1.491$ Gc	1.25	39.5	39
		1.70	34.0	39

SEC. 8.14, CONCERNING THE DERIVATION OF SOME OF THE PRECEDING EQUATIONS

For convenience in using the preceding sections for practical filter design, some background theoretical matters have been delayed until this section. Let us first note how the design equations for the general, coupled-series-resonator case in Fig. 8.02-3 are derived.

In Sec. 4.12 it was shown that the lumped-prototype circuit in Fig. 8.02-2(a) can be converted to the form in Fig. 4.12-2(a) (where R_A, R_B, and the L_{ej} may be chosen arbitrarily), and the same transmission

response will result. This low-pass circuit may be transformed to a corresponding lumped-element band-pass circuit by use of the transformation

$$\omega' = \frac{\omega_1'}{w}\left(\frac{\omega}{\omega_0} - \frac{\omega_0}{\omega}\right) \tag{8.14-1}$$

where

$$w = \frac{\omega_2 - \omega_1}{\omega_0} , \tag{8.14-2}$$

$$\omega_0 = \sqrt{\omega_2\omega_1} , \tag{8.14-3}$$

and ω', ω_1', ω, ω_0, ω_1, and ω_2 are as indicated in Figs. 8.02-1(a), (b) for the case of Tchebyscheff filters. Then the series reactances $\omega' L_{aj}$ in Fig. 4.12-2(a) transform as follows:

$$\omega' L_{aj} = \frac{\omega_1'}{w}\left(\frac{\omega}{\omega_0} - \frac{\omega_0}{\omega}\right) L_{aj} \tag{8.14-4}$$

$$= L_{rj}\omega - \frac{1}{C_{rj}\omega} \tag{8.14-5}$$

where

$$L_{rj} = \frac{\omega_1' L_{aj}}{w\omega_0} \quad \text{and} \quad C_{rj} = \frac{w}{\omega_1' L_{aj}\omega_0} . \tag{8.14-6}$$

This reasoning may then be used to convert the low-pass circuit in Fig. 4.12-2(a) directly into the band-pass circuit in Fig. 8.02-2(c). To derive the corresponding general equations in Fig. 8.02-3 we can first use the function

$$X_j(\omega) = L_{rj}\omega - \frac{1}{C_{rj}\omega} \tag{8.14-7}$$

for the resonator reactances in Fig. 8.02-2(c) in order to compute the resonator slope parameters

$$x_j = \frac{\omega_0}{2} \left. \frac{dX_j(\omega)}{d\omega} \right|_{\omega=\omega_0} = L_{rj}\omega_0 = \frac{1}{C_{rj}\omega_0} \quad . \qquad (8.14\text{-}8)$$

Then by Eqs. (8.14-6) and (8.14-8)

$$L_{aj} = \frac{x_j'\omega}{\omega_1'} \quad . \qquad (8.14\text{-}9)$$

Substitution of this result in the equations in Fig. 4.12-2(a) yields Eqs. (2) to (4) in Fig. 8.02-3.

Equations (6) and (7) in Fig. 8.02-3 can be derived by use of Eq. (8.14-8), Fig. 4.12-1, and the fact that the external Q of each end resonator is simply $\omega_0 L_{r1}$ or $\omega_0 L_{rn}$ divided by the resistive loading reflected through the adjacent impedance inverter. The basis for Eq. (8) in Fig. 8.02-3 can be seen by replacing the idealized impedance inverters in Fig. 8.02-2(c) by inverters of the form in Fig. 8.03-1(a), yielding a circuit similar to that in Fig. 8.11-2(b) with the equivalent transformer-coupled form shown in Fig. 8.11-2(a). Then the coupling coefficients of the interior resonators of the filter are

$$k_{j,j+1}\Big|_{j=1 \text{ to } n-1} = \frac{\omega_0 M_{j,j+1}}{\sqrt{\omega_0 L_{pj}\omega_0 L_{pj+1}}} \quad . \qquad (8.14\text{-}10)$$

Equation (8) in Fig. 8.02-3 will be seen to be a generalized expression for this same quantity. For example, for Fig. 8.11-2, $K_{j,j+1} = \omega_0 M_{j,j+1}$, and the $x_j = \omega_0 L_{pj}$. If these quantities are substitutes in Eq. (8.14-10), Eq. (8) of Fig. 8.02-3 will result.

The derivations of the equations in Fig. 8.02-4 follow from Fig. 4.12-2(b) in exactly the same manner, but on the dual basis. The equations for the K- or J-inverter parameters for the various filter structures discussed in this chapter are obtained largely by evaluation of the reactance or susceptance slope parameters x or b for the particular resonator structure under consideration, and then inserting these quantities in the equations in Fig. 8.02-3 or 8.02-4. *Thus the derivations of the design equations for the various types of filters discussed in this chapter rest largely on the general design equations in Figs. 8.02-3 and 8.02-4.*

The Capacitively-Coupled Filters of Sec. 8.05—Let us now derive the resonator, susceptance slope parameters for the capacitive-gap-coupled transmission-line filter in Fig. 8.05-1. In this case, the resonator lines are roughly a half-wavelength long in the pass band of the filter, and if Z_L is the impedance connected to one end of a resonator line the impedance looking in at the other end will be

$$Z_{in} = Z_0\left[\frac{Z_L + jZ_0 \tan \frac{\pi\omega}{\omega_0}}{Z_0 + jZ_L \tan \frac{\pi\omega}{\omega_0}}\right] \qquad (8.14\text{-}11)$$

$$= Z_0\left[\frac{Z_L + jZ_0\pi\left(\frac{\omega - \omega_0}{\omega_0}\right)}{Z_0 + jZ_L\pi\left(\frac{\omega - \omega_0}{\omega_0}\right)}\right]_{\omega \text{ near } \omega_0} . \qquad (8.14\text{-}12)$$

Filters of the form in Fig. 8.05-1 which have narrow or moderate bandwidth will have relatively small coupling capacitances. It can be shown that because of this each resonator will see relatively large impedances at each end. Applying this condition to Eq. (8.14-12), $|Z_L| >> Z_0$, and at least for frequencies near ω_0 Eq. (8.14-12) reduces to

$$Z_{in} = \frac{1}{Y_L + jB(\omega)} , \qquad (8.14\text{-}13)$$

where

$$B(\omega) = Y_0\pi\left(\frac{\omega - \omega_0}{\omega_0}\right) , \qquad (8.14\text{-}14)$$

$$Y_L = 1/Z_L \quad \text{and} \quad Y_0 = 1/Z_0 . \qquad (8.14\text{-}15)$$

Thus, Z_{in} looking into the line looks like the load admittance Y_L in parallel with a resonator susceptance function $B(\omega)$. Applying Eq. (1) of Fig. 8.02-4, to Eq. (8.14-14) for the jth transmission line resonator gives, for the susceptance slope parameter

$$b_j = \frac{\pi}{2} Y_0 . \qquad (8.14\text{-}16)$$

Since all of the lines in Fig. 8.05-1 have the same characteristic admittance Y_0, all of the b_j are the same in this case. Inserting Eq. (8.14-16) in Eqs. (2) to (4) in Fig. 8.02-3 yields Eqs. (1) to (3) of Fig. 8.05-1. It is interesting to note that filters of the type in Fig. 8.05-1 can also be constructed using resonators which are nominally n half-wavelengths long at the desired pass-band center frequency ω_0. In that case the susceptance slope parameters become

$$b_j = \frac{n\pi}{2} Y_0 \quad . \tag{8.14-17}$$

The Waveguide Filters in Sec. 8.06—The waveguide filter in Fig. 8.06-1 with shunt-inductance couplings is the dual of the capacitively-coupled filter in Fig. 8.05-1 except for one important factor. This factor is that the additional frequency effect due to the dispersive variation of the guide wavelength λ_g in the waveguide must also be accounted for. It can be shown that the response of the waveguide filter in Fig. 8.06-1 will have the same form as that of an equivalent strip line filter as in Fig. 8.05-1 if the waveguide filter response is plotted with $1/\lambda_g$ as a frequency variable instead of ω. Thus, the equations in Fig. 8.06-1 are simply the duals of those in Fig. 8.05-1 with frequency ratios ω/ω_0, ω_1/ω_0 and ω_2/ω_0 replaced by corresponding guide-wavelength ratios λ_{g0}/λ_g, $\lambda_{g0}/\lambda_{g1}$, and $\lambda_{g0}/\lambda_{g2}$, where λ_{g0} is the guide wavelength at midband. The half-wavelength resonators in this case have a series-type resonance with slope parameter

$$a_j = \frac{\pi}{2} Z_0 \quad . \tag{8.14-18a}$$

Equation (8.14-18a) applies to waveguide resonators *only if the frequency variable is in terms of reciprocal guide wavelength* (*or* λ_{g0}/λ_g); however, it applies to TEM-mode resonators on *either* a frequency or reciprocal-guide-wavelength basis. If radian frequency ω is to be used as the frequency variable of a waveguide filter, the slope parameter must be computed including the additional effects of λ_g as a function of frequency. Using ω as the frequency variable, the slope parameter

$$a_j = \frac{\pi}{2} Z_0 \left(\frac{\lambda_{g0}}{\lambda_0}\right)^2 \tag{8.14-18b}$$

discussed in Sec. 5.08 must be used. In an actual filter design the difference between the slope parameters given by Eqs. (8.14-18a) and (8.14-18b) is compensated for by the fact that the fractional bandwidth w in terms of frequency will be different from the fractional bandwidth w_λ in terms of guide wavelength by the factor $(\lambda_{g0}/\lambda_0)^2$, at least for narrow-band cases. [See Eq. (7) of Fig. 8.06-1.] The reciprocal guide wavelength approach appears to be the most natural for most waveguide cases, though either may be used.

Insertion of Eq. (8.13-18a), $R_A = R_B = Z_0$, and w_λ (in place of w) in Eqs. (2) to (4) of Fig. 8.02-3 gives Eqs. (1) to (3) of Fig. 8.06-1.

The Narrow-Band, Cavity Filters of Sec. 8.07—As an example of the derivation of the equations in Sec. 8.07, consider the case of Fig. 8.07-1(a) which shows a cavity connected to a rectangular waveguide propagating the TE_{10} mode by a small iris with magnetic polarizability M_1 (see Sec. 5.10). The fields within the cavity in MKS units are

$$E_{y1} = jH_1 \sqrt{\frac{\mu_0}{\epsilon_0}} \frac{2l_1}{s\lambda} \cos\frac{\pi x}{a_1} \sin\frac{s\pi z}{2l_1}$$

$$H_{x1} = H_1 \cos\frac{\pi x}{a_1} \cos\frac{s\pi z}{2l_1} \qquad (8.14\text{-}19)$$

$$H_{z1} = \frac{H_1 l_1}{s a_1} \sin\frac{\pi x}{a_1} \sin\frac{s\pi z}{2l_1} \quad .$$

In these equations $\sqrt{\mu_0/\epsilon_0} = 376.6$ ohms (the intrinsic impedance of free space), λ is free space wavelength and s is the number of field variation along the length, l_1, of the cavity. The normal mode fields in the waveguide are

$$E_y = H \sqrt{\frac{\mu_0}{\epsilon_0}} \frac{\lambda_g}{\lambda} \cos\frac{\pi x}{a} e^{j[\omega t + (2\pi/\lambda_g)z]}$$

$$H_x = H \cos\frac{\pi x}{a} e^{j[\omega t + (2\pi/\lambda_g)z]} \qquad (8.14\text{-}20)$$

$$H_z = -jH \frac{\lambda_g}{2a} \sin \frac{\pi x}{a} e^{j[\omega t + (2\pi/\lambda_g)z]} \qquad (8.14\text{-}20)_{\text{Cont.}}$$

where λ_g is given by Eq. (8.07-1). We define Q_e as

$$Q_e = \frac{\omega W}{P_L} \qquad (8.14\text{-}21)$$

where $\omega = 2\pi f$ is the angular resonance frequency, W is stored energy within the cavity and P_L is the average power lost through the iris to the terminating guide.

The stored energy within the cavity is

$$W = \frac{1}{2}\epsilon_0 \iiint |E_{y1}|^2 \, dx \, dy \, dz = \frac{\mu_0 H_1^2 a_1 b_1 l_1^3}{2s^2 \lambda^2} \qquad (8.14\text{-}22)$$

where we have used Eq. (8.13-19).

The power lost through the iris is

$$P_L = \frac{|A_e|^2 S_e}{2} \qquad (8.14\text{-}23)$$

where A_e, the amplitude of the normal mode fields excited in the terminating guide, is given by

$$A_e = \frac{\omega \mu_0 M_1 H H_1}{S_e} \qquad (8.14\text{-}24)$$

The amplitude of the tangential normal-mode magnetic field in the terminating waveguide at the center of gravity of the window is H, and H_1 is the amplitude of the tangential magnetic field in the cavity at the center of gravity of the window. The quantity S_e is the peak power of the normal mode in the rectangular waveguide or

$$S_e = \iint a \sqrt{\frac{\mu_0}{\epsilon_0}} \frac{\lambda_g}{\lambda} H^2 \cos^2 \frac{\pi x}{a} \, dx \, dy$$

$$= \sqrt{\frac{\mu_0}{\epsilon_0}} \frac{\lambda_g}{\lambda} H^2 \frac{ab}{2} \qquad (8.14\text{-}25)$$

Substituting Eqs. (8.14-24) and (8.14-25) into Eq. (8.14-23) we find

$$P_L = \sqrt{\frac{\mu_0}{\epsilon_0}} \frac{4\pi^2 M_1^2 H_1^2}{ab\lambda_g \lambda} \quad . \tag{8.14-26}$$

When Eq. (8.14-26) and Eq. (8.14-22) are substituted in Eq. (8.14-21) we find

$$Q_e = \frac{a_1 b_1 ab l_1^3 \lambda_g}{4\pi s^2 M_1^2 \lambda^2} \tag{8.14-27}$$

as given in Fig. 8.07-1(a).

When two resonant cavities are connected together by a small iris as shown in Fig. 8.07-2(a) they will have two natural resonant frequencies ω_r and $\omega_r - \Delta\omega$. When the tangential magnetic fields are pointing in the same direction on either side of the iris the cavities will oscillate at frequency ω_r, which is the natural resonant frequency of a cavity with no iris. When the tangential magnetic fields are pointing in opposite directions on either side of the window, the natural resonant frequency is $\omega_r - \Delta\omega$. When $\Delta\omega$ is small the coupling coefficient k can be defined as

$$k = \frac{\Delta\omega}{\omega_r} = \frac{M_1 \mu_0 H_1^2}{\epsilon_0 \iiint |E_{y1}|^2 \, dx \, dy \, dz} \quad . \tag{8.14-28}$$

Substituting Eq. (8.13-19) into Eq. (8.13-28) we find

$$k = \frac{M_1 \lambda^2 s^2}{l_1^3 a_1 b_1} \quad . \tag{8.14-29}$$

as for Fig. 8.07-2(a).

The Quarter-Wavelength-Resonator Filter of Sec. 8.08—As discussed in Sec. 8.08, the filter structure in Fig. 8.08-1 looks like the filter type in Fig. 8.02-3 when observed from its K-inverters, but looks like the filter type in Fig. 8.02-4 when observed from its J-inverters. Thus, at one end of each quarter-wavelength resonator a reactance slope parameter applies, while at the other end a susceptance slope parameter applies.

By analysis similar to that in Eqs. (8.14-11) to (8.14-16) it can be shown that for quarter-wavelength resonators exhibiting series resonance

$$\alpha_j = \frac{\pi}{4} Z_0 \quad . \tag{8.14-30}$$

and when exhibiting shunt resonance

$$\beta_j = \frac{\pi}{4} Y_0 \quad . \tag{8.14-31}$$

Insertion of these equations in the appropriate equations in Figs. 8.02-3 and 8.02-4 gives Eqs. (1) to (3) of Fig. 8.08-1.

The Parallel-Coupled Filters of Sec. 8.09—The equations presented in Fig. 8.09-1 can be derived by showing that for narrow or moderate bandwidths each of the parallel-coupled sections $j, j+1$ of length l in Fig. 8.09-1 is equivalent to a J-inverter with a length of line on each side, the lines being a quarter-wavelength long at frequency ω_0. A complete derivation of the equations in Fig. 8.09-1 (in somewhat different form) can be found in Ref. 15.

The Quarter-Wavelength-Coupled Filters of Sec. 8.10—The design equations (1) to (4) in Fig. 8.10-1 can be derived from those in Fig. 8.02-4 by setting G_A, G_B, and the inverter parameters $J_{j,j+1}$ all equal to Y_0, and then solving for the β_j/Y_0. As previously discussed in Sec. 8.10, the $\pi/4$ and $\pi/2$ terms were introduced in these equations to account for the added selectivity introduced by the quarter-wavelength lines.[4] The correction is $\pi/4$ for the end resonators which have only one, quarter-wavelength line adjacent to them, and is twice as large for the interior resonators which have a quarter-wavelength line on each side. Note that the $\pi/4$ correction per quarter-wavelength line corresponds to the β_j/Y_0 values for the quarter-wavelength resonators discussed in connection with Eq. (8.14-31).

The Lumped-Element Filters of Sec. 8.11—The resonator susceptance slope parameters for the capacitively-coupled, lumped-element filter in Fig. 8.11-1 are simply

$$\beta_j = \omega_0 C_{rj} \tag{8.14-32}$$

and these values inserted in Eqs. (2) to (4) of Fig. 8.02-4 yield Eqs. (2) to (4) in Fig. 8.11-1. The J-inverters in this case are of the form in Fig. 8.03-2(b). The negative shunt capacitances required for these inverters are lumped with the resonator capacitances C_{rj} to yield the somewhat smaller net shunt capacitance actually used in constructing the filter. However, in the case of the inverters between the end resonators and the terminations, this procedure does not work since there is no way of absorbing the negative capacitance that would appear across the resistor termination. This difficulty in analysis can be avoided by analyzing the end couplings in a somewhat different way.

Looking from Resonator 1 in Fig. 8.11-1 out toward C_{01} and G_A in series, the admittance is

$$Y = \frac{1}{\frac{1}{jB_{01}} + \frac{1}{G_A}} = \frac{\left(\frac{B_{01}^2}{G_A}\right)}{1 + \left(\frac{B_{01}}{G_A}\right)^2} + \frac{jB_{01}}{1 + \left(\frac{B_{01}}{G_A}\right)^2} \qquad (8.14\text{-}33)$$

where $B_{01} = \omega_0 C_{01}$. Meanwhile, looking left from Resonator 1 in Fig. 8.02-4 into the J_{01} inverter the conductance

$$G = \frac{J_{01}^2}{G_A} \qquad (8.14\text{-}34)$$

is seen. Equating G in Eq. (8.14-34) to the real part of Y in Eq. (8.14-33) and solving for C_{01} gives Eq. (5) in Fig. 8.11-1, and ensures that the conductance loading on Resonator 1 will be the same as that called for by the general equations in Fig. 8.02-4. The imaginary part of Y in Eq. (8.14-33) can be dealt with satisfactorily by replacing it by a shunt capacitive susceptance $\omega_0 C'_{01}$ of the same size which then leads to Eq. (11) in Fig. 8.11-1. Since C'_{01} effectively increases the shunt capacitance of Resonator 1, this amount should be subtracted from C_{r1} as indicated in Eq. (8) in Fig. 8.11-1 when computing the net shunt capacitance to be used in constructing Resonator 1. Of course, the same reasoning applies for design of the $C_{n,n+1}$ coupling at the other end of the filter.

It should be noted why the procedure discussed above is necessary for the lumped-element circuit in Fig. 8.11-1 when it was not necessary for the

circuits with

8.08-1. In t

length of li

is negativ

ained

as simply r

generator a

that their

filter. I

the termina

load termir

The de

Fig. 8.11-

The end co

general ap

The

equations

filter in

Sec. 8.12

resonator

Therefore,

slope-para

J-inverter

correspon

the reson

shunt sus

The

equation

wire-li

indicat

The ci

with

to t

Poi

transmission-line resonators in Figs. 8.05-1, 8.06-1, e

ese latter cases, the inverters used involved a negativ

(rather than a negative capacitance or inductance).

length of line had a characteristic impedance equal to the

the terminations, the negative line lengths can be regarded

ducing the length of the matched lines connected to the

d load impedance. These terminating lines are matche

engt has no effect on the attenuation characteristics of the

s, in this manner, the inverter negative lines adjace to

tions can, effectively, be absorbed into the generator and

tions.

ivation of the design equations for the filter str ure in

follows reasc essentially the dual of th Fig. 8.11-1.

plines in this ly more co he same

oach applies.

ide-Stop-Band Fi f the design

for the filter in at for the

ig. 8.11-1 except discussed in

Note that in this duce the net

unt capacitance as of Fig. 8.11-1.

ior purposes of compu and susceptance

ers. The negative sh ated with the

o interior of the nsated for by a

n, the increase in positive ttributed to

ces. This is why it wa duce the positive

ceptances equal to $-\omega_0 C_{j,j}$ of Fig. 8.12-1.

Comb-Line Structures of Sec. filter design

s in Fig. 8.13-1(b) were der approximate, open-

e representation in Fig. 8.1 nodal points are

d which corresponds to total ted in Fig. 8.13-1(a).

uitry in Fig. 1 between nd 1 was specified

he aid of the equivalences in s to correspond

e parallel-coupled strip lines in (a) between Nodal

ts 0 and 1. The circuitry between Nodal ints 1 and 2, 2 and 3,

n − 1 and *n*, was specified with the a of the equivalences in

gs. 5.09-4(a) and (b) so as to correspo the pairs of parallel-

oupled sections formed by the strip line nected to Nodal Points 1

and 2, 2 and 3, etc. Note that the line admittances in Fig. 8.14-1 are defined in terms of the line capacitances per unit length C_j and $C_{j,j+1}$ as defined in Fig. 8.13-2, times the velocity of propagation (which gives the dimensions of admittance). This representation of a comb-line filter is approximate, and neglects the effects of fringing capacitances beyond nearest neighbors.[17]

The design equations in Fig. 8.13-1(b) are based on the general equations in Fig. 8.02-4. In order to modify the circuit in Fig. 8.14-1 to a form such that the data in Fig. 8.02-4 can be easily applied, the series stubs between Nodal Points 1 and 2, 2 and 3, etc., in Fig. 8.14-1 were incorporated into J-inverters of the form in Fig. 8.03-4, which gave the result shown in Fig. 8.14-2. Since each of the inverters $J_{j,j+1}$ consists of a pi configuration of a series stub of characteristic admittance Y, and two shunt stubs of characteristic admittance $-Y$, it was necessary to increase the characteristic admittances of the actual shunt stubs on each side in order to compensate for the negative admittances ascribed to the inverters. This is why the shunt stubs 2 to $n-1$ in Fig. 8.14-2 now have the admittances $Y_{aj} = v\,(C_j + C_{j-1,j} + C_{j,j+1})$ instead of just $v\,C_j$. The portion of the circuit in Fig. 8.14-1 between Nodal Points 0 and 1 has been converted to the form shown in Fig. 8.14-2 by use of a simplifying constraint which brings about the properties summarized in Fig. 5.09-3(a).

When applying the general relations in Fig. 8.02-4 to the circuit in Fig. 8.14-2 to derive design equations for comb-line filters, the admittance-inverter parameters $J_{j,j+1}$ are, of course, evaluated at midband, and the resonator slope parameters are computed from the resonator circuits consisting of the lines of admittance Y_{aj} shunted by the lumped capacitances C_j^s. The terminating admittance G_{T1} in Fig. 8.14-2 is specified so that $G_{T1} = J_{01}^2/Y_A$, where the value of J_{01} is as given in Fig. 8.02-4.

REFERENCES

1. S. B. Cohn, "Direct-Coupled-Resonator Filters," *Proc. IRE*, Vol. 45, pp. 187-196 (February 1957).

2. W. L. Pritchard, "Quarter Wave Coupled Filters," *J. Appl. Phys.*, Vol. 18, pp. 862-872 (October 1947).

3. R. M. Fano and A. W. Lawson, "Microwave Filters Using Quarter-Wave Couplings," *Proc. IRE*, Vol. 35, pp. 1318-1323 (November 1947).

4. W. W. Mumford, "Maximally Flat Filters in Waveguide," *Bell System Tech. J.*, Vol. 27, pp. 648-714 (October 1948).

5. G. L. Ragan, *Microwave Transmission Circuits*, McGraw-Hill Book Co., Inc., New York City, 1948. Chapters 9 and 10, by R. M. Fano and A. W. Lawson.

6. G. C. Southworth, *Principles and Applications of Waveguide Transmission*, D. Van Nostrand Co., Inc., New York City, 1950, pp. 285-293.

7. J. Reed, "Low Q Microwave Filters," *Proc. IRE*, Vol. 38, pp. 793-796 (July 1950).

8. H. J. Riblet, "A Unified Discussion of High-Q waveguide Filter Design Theory," *IRE Trans. PGMTT*, Vol. MTT-6, pp. 359-368 (October 1958).

9. A. A. Oliner, "Equivalent Circuits for Discontinuities in Balanced Strip Transmission Line," *IRE Trans. PGMTT*, Vol. MTT-3, pp. 134-143 (March 1955).

10. H. M. Altschuler and A. A. Oliner, "Discontinuities in the Center Conductor of Symmetric Strip Transmission Line," *IRE Trans. PGMTT*, Vol. MTT-8, pp. 328-339 (May 1960).

11. G. L. Matthaei, "Final Report on Microwave Filter and Ferrite Device Research," Report ERL-123, Electronics Research Laboratory, Ramo-Wooldridge Division of T-R-W Corp., Canoga Park, California (20 August 1958).

12. G. L. Matthaei, "Theory, Design, and Special Applications of Direct-Coupled Strip Transmission Line, Band-Pass Filters," Report ERL-115, Electronics Research Laboratory, Ramo-Wooldridge Division of T-R-W Corp., Canoga Park, California (18 December 1957).

13. N. Marcuvitz, *Waveguide Handbook*, McGraw-Hill Book Co., New York City, 1951, Chapter 5.

14. G. L. Matthaei, "Direct-Coupled-Band-Pass Filters with $\lambda_0/4$ Resonators," *1958 IRE National Convention Record*, Part 1, pp. 98-111.

15. S. B. Cohn, "Parallel-Coupled Transmission-Line-Resonator Filters," *IRE Trans. PGMTT*, Vol. MTT-6, pp. 223-231 (April 1958).

16. G. L. Matthaei, *et al.*, "Design Criteria for Microwave Filters and Coupling Structures," Final Report, Chapter 16, SRI Project 2326, Contract DA 36-039 SC-74862, Stanford Research Institute, Menlo Park, California (January 1961).

17. J. T. Bolljahn and G. L. Matthaei, "A Study of the Phase and Filter Properties of Arrays of Parallel Conductors Between Ground Planes," *Proc. IRE*, Vol. 50, pp. 299-311 (March 1962).

STANFORD
RESEARCH
INSTITUTE

MENLO PARK
CALIFORNIA

Regional Offices and Laboratories

Southern California Laboratories
820 Mission Street
South Pasadena, California

Washington Office
808 17th Street, N.W.
Washington 5, D.C.

New York Office
270 Park Avenue, Room 1770
New York 17, New York

Detroit Office
The Stevens Building
1025 East Maple Road
Birmingham, Michigan

European Office
Polikenstrasse 37
Zurich 1, Switzerland

Representatives

Honolulu, Hawaii
Finance Factors Building
195 South King Street
Honolulu, Hawaii

London, Ontario, Canada
85 Wychwood Park
London 14, Ontario, Canada

London, England
15 Abbotsbury Close
London W. 14, England

Milan, Italy
Via Macedonio Melloni 40
Milano, Italy

Tokyo, Japan
911 Iino Building
22, 2-chome, Uchisaiwai-cho, Chiyoda-ku
Tokyo, Japan